THE EFFECT OF CLIMATE CHANGE ON DURABILITY OF EXISTING CONCRETE STRUCTURES: A COMPARISON BETWEEN THE UNITED KINGDOM AND IRAQ

Abbas Salim Abbas AL-Ameeri

A thesis submitted in partial fulfillment of the requirements of the University of Brighton for the degree of Doctor of Philosophy

2019

School of Environment and Technology

University of Brighton

United Kingdom

DECLARATION

I declare that the research contained in this thesis, unless otherwise formally indicated within text, is the original work of the author. The thesis has not been previously submitted to this or any other University for a degree and does not incorporate any material already submitted for a degree.

Signature: Date: /10/ 2019

Abbas Salim Abbas AL-Ameeri

DEDICATION

I dedicate my dissertation to,

My wife ……I am proud of her patience

My Sons and Daughter ……..... My love

My Father and Mother …… I am grateful to them

My Brothers and Sisters ……..... My love and respect

Abbas S.A. AL-Ameeri

ACKNOWLEDGEMENT

All praise be to the Lord of the world, who is the Owner of the glory, might, favours and bounties and prayer be upon our Prophet. I would like to thank all who contributed from Great Iraq in giving me this opportunity to complete my Ph.D. study.

I am extremely thankful to my supervisor Dr. M. I. Rafiq for his positive attitude, patience, sound guidance and valuable advice enabling me to complete this study. I feel very proud to have worked under his guidance and consider it a special blessing of God. Due to his kind support and able coaching, I have now successfully finished this study and it is a great privilege to acknowledge his guidance. Also, I would like to thank the other supervisors, Dr.Ourania Tsioulou and Dr. Oyuna Rybdylova for their continuous cooperation and valuable guidance in the completion of this research.

I would like to thank the staff of the Concrete and Geochemical laboratory for their cooperation in the successful completion of the research. I would like to take this opportunity to thank the administrative staff of the University of Brighton in general and that of the Civil Engineering Department and School of Environment and Technology in particular for extending their full cooperation and help in completing the administrative requirements for this study.

I am extremely thankful to Professor Lars-Olof Nilsson, Professor Leon Black and Charles Fentiman for their positive attitude and valuable advice to complete this study. I am extremely thankful to the examiners Dr. Monower Sadique from Liverpool John Moores University of and Dr. Kevin Stone from Brighton University, for spending their positive attitude and valuable time.

I would especially like to thank my wife, Mrs. Nawal Ali and my sons, Ali and Mohammed, and my daughter, Elaf for their unwavering love, support, faith, and encouragement. Finally, I would like to extend my heartfelt thanks to my family and friends, especially Hussam Kuttar, Bashar Ali and Haider AL-Baghdadi for being a continuous source of encouragement to finish my study.

Abbas S. A. AL-Ameeri

ABSTRACT

A vast majority of scientists agree that the greenhouse gases (GHG), in terms of CO_2 emissions generated by human activity, cause a "greenhouse effect" which affects the planet's temperature. GHG controls radiation impacting the climate system, creating global warming or climate change. Hence, by increasing the atmospheric CO_2 emissions is likely to increase the average maximum temperature and reduce the relative humidity (RH). These changes in CO_2 concentration, temperature and RH have considerable impacts on the durability of existing concrete structures, as they affect the carbonation rate, the chloride penetration and the corrosion rate.

The fundamental aim of this study is to investigate the potential impact of the global climate change on the structures and their durability, with special emphasis on the existing concrete structures in the UK and Iraq. Climate change can accelerate the deterioration processes in concrete and as a result, this can affect the safety and serviceability of concrete structures.

The present study is divided into two parts: The first part consists of the experimental work that includes the casting of two groups of concrete samples (reinforced & unreinforced) with different water-cement ratio (w/cm ratio) and partial replacement of ordinary Portland cement with supplementary cementitious materials such as pulverized fuel ash (PFA) and ground granulated blast furnace slag (GGBS). Each group was tested under controlled environmental conditions representing both the environmental conditions in the UK and Iraq. These samples were exposed to the variables of climate change, such as; changes in temperature, carbon dioxide concentration, and humidity level. The depth of carbonation (DoC), depth of chloride penetration (d_{Cl^-}) and chloride concentration profile were measured and in the post corrosion stage, the study investigates the effect of such climate change parameters on the rate of corrosion of concrete structures.

The second part of the study consists of an integrated analytical and numerical investigation of the effect of the climate changes and materials' properties on the durability of concrete structures (cracked and un-cracked) under different climate scenarios of the Inter-governmental Panel of Climate Change reports (IPCC 2014) and the UKCP'09 climate projection models. These models were also calibrated and validated using the experimental results.

The results have indicated that:

(i): The depth of carbonation increased by increasing the w/cm ratio. In addition, there is a considerable influence of crack width, carbon dioxide concentration, relative humidity and relative increase of temperature on the depth of carbonation. X-ray powder diffraction analysis (XRD) and pH tests have confirmed these results.

(ii): The chloride migration coefficient (D_{nssm}) is affected by the w/cm ratio, porosity, supplementary cementitious materials and mechanical properties of concrete. The chloride penetration rate and the chloride concentration along the depth of the specimen were significantly affected by the carbonation, and the reduction in pH level, the exposure temperature, the crack width, the supplementary cementitious materials, and the w/cm ratio in concrete samples.

(iii): The half-cell potential and linear polarization resistance (LPR) in reinforced concrete specimens pointed to corrosion activity in reinforced concrete samples, influenced considerably by carbonation and reduction in pH level, exposure temperature, increasing crack width, increases in the chloride concentration with an increase in depth and w/cm ratio in concrete samples.

(iv): Integrated deterioration models (chloride concentration profile and carbonation depth) have been developed that are a function of both material properties and environmental factors (change in CO_2, temperature and relative humidity). The analytical investigations of these models indicated that chloride ingress and carbonation depth are highly influenced by changing weather conditions in the surrounding environment due to climate change. Also, the results revealed an acceleration in the deterioration rate of structures that can reduce the effective service life of structures.

TABLE OF CONTENTS

LIST OF TABLES

LIST OF FIGURES

List of Abbreviations

TERM	DEFINITION
ϵ	porosity of media
$\propto_l$ & β_l	Langmuir Isotherm constants
$\emptyset_{paste}$	porosity of capillary and gel pores in cement paste
$\propto_H$	hydration rate
a_i	atomic mass of iron (55.8 g/mol)
γ	electrical resistivity of the concrete
Δ	enthalpy constant
λ_{ion}	ion conductivity ($S.m^2/mol$)
λ_{25}	ion conductivity at temperature 25 °C
ρ	density
ρ_d	dry density
α	constant value, 0.25 (year $^{-1}$) of Kassir and Ghosn (2002)
β	constant value (0.685) of Song et al. (2008).
γ	electrical resistivity of the concrete
μ	gas dynamic viscosity at 20°C +/- 2°C (Pa.s)
ρ_c	density of cement
ρw	density of water
ρ_p	density of supplementary cementitious materials
A_s	surface area of steel bar
a	amount of CO_2 uptake to complete carbonation by Fick's Second Law
a_1	amount of CO_2 uptake to complete carbonation by Fick's first Law
a_t	average distance between the line of fracture and the nearest support
b	average width of specimen
B	Stern–Geary constant

TERM	DEFINITION
CO_3^{-2}	carbonate ion
$Ca\ (OH)_2$	calcium hydroxide
$C_{Cl}(x,t)$	concentration of chloride ions at depth, x with time, t
$CO_{2(aq)}$	aqueous *concentration of* carbon dioxide
$Ca(OH)_{2(aq)}$	aqueous *concentration of* calcium hydroxide
Cl_f	free chloride in % by mass of binder
Cl_t	total chloride in % by mas s of the binder, is, and
C	cement content (kg) per m^3
c	the concentration of the species (mole/m^3)
$C(x, t)$	chloride concentration at depth with time
$C(x,y,z,t)$	chloride concentration for point (x,y,z) at the time
C_2S	dicalcium silicate
C_3S	tricalcium silicate
Ca^{2+}	calcium ion
$CaCO_3$	calcium carbonate
C-A-H	calcium aluminates hydrates
CaO	calcium oxide
C_{CH}	$Ca(OH)_2$ content
C_{Cl}	total concentration of chloride ions
C_{CO2}	carbon dioxide concentration
$C_{CO2}(x, t)$	carbon dioxide concentration at depth and time
C_d	color change boundary
CH	calcium hydroxide
C_i	initial chloride concentration (% mass of concrete)
$C_i(x)$	the concentration of ionic species *i* as a function of location *x*
Cl^-	chloride ion
C_o	max. value of chloride (5.343 kg/m^3)
CO_2	carbon dioxide
$CO_{2(gas)}$	carbon dioxide in air

TERM	DEFINITION
COV	coefficient of variation
C_s	surface concentration of chloride
$C_s(t)$	surface chloride concentration at time *t*
CSE	copper-copper sulfate electrode
C-S-H	calcium silicate hydrates
C^*_{O2}	concentration of O_2 (mole/m^3)
C_{si}:	surface chloride at the standard time (3.0431%) of Song et al. (2008)
D	chloride diffusion coefficient
d	total depth concrete sample
D(x,t)	diffusion coefficient for *x* direction with time
D_a	chloride diffusion coefficient
d_a	cylinder diameter
D_a	diffusion coefficients
$D_{a,ref}$	diffusion coefficient of chloride at reference condition
D_{aex}	apparent diffusion at t_{ex}
D_{app}	apparent diffusion coefficient of chloride
d_C	concrete cover
D_{Cl}	diffusion coefficient of chloride in pore solution (free space)
d_{cl^-}	chloride penetration depth
Dco_2	carbone dioxide diffusion coefficient
d_{crack}	crack depth
d_d	average depth of specimen
D_e	effective diffusion coefficient
D_{eff}	effective chloride diffusion coefficient
D_i	diffusion coefficient of species
D_{nssm}	chloride ions migration coefficient (non-steady state migration)
DoC	depth of carbonation
DoC_a	depth of carbonation tested in accelerated condition
$DoC_{n,t}$	depth of carbonation tested in natural environments

TERM	DEFINITION
D_s	diffusion coefficient of species
D_{O2}	efficient diffusion coefficient of O_2 in concrete (m^2/s)
E	voltage or potential
$E(x)$	the applied voltage as a function of x
E_a	the activation energy for free pore fluid (17.6×10^3 (J/mol))
E_C	modulus of elasticity
E_{corr}	corroded potential
$erfc$	complementary error function
F	Faraday's constant
f	molarity of $AgNO_3$
$f_{c1}(RH)$	factor of effective diffusivity
f_{cf}	flexural tensile strength
f_{cu}	compressive strength
FE	finite elements
F_{galv}	galvanic interactions between different parts of the steel bar
F_{O2}	oxygen in pore water in contact
F_{oxide}	oxide (rust) layer formation on corrosion rate
f_{st}	splitting tensile strength
$GGBS$	Ground Granulated Blast Furnace Slag
GHG	greenhouse gases
H	Henry's constant
H_2CO_3	carbonic acid
h_c:	critical humidity level (hc=0.75)
HCl	hydrochloric acid
HCP	half-cell potential
H_{ref}	reference Henry's Constant
I	current
i	valence of ionic species i
i_{corr}	corrosion current density ($\mu A/cm^2$).

TERM	DEFINITION
ICP	inductively coupled plasma
IPCC	Intergovernmental Panel on Climate Change
ITZ	interfacial transition zone
J	quantity of a component or species
K	carbonation rate
k_p	efficiency factor for resisting against carbonation
K_1	carbonation rate
K_2	carbonation rate
k_c	constant of reaction rate
KCl	Potassium chloride
K_{O2}	kinetic constant of oxygen reduction
k_p	efficiency factor for resisting against carbonation
l	cylinder length
L	thickness of the specimen
LPR	linear polarization resistance
l_s	span length
l_t	thickness of the sample
m	ageing factor (diffusivity reduction factor)
M	atomic weight
m_a	component or species
m_i	mass of iron per area dissolved at the anode (g/m^2)
m_t	mass of the concrete powder, g
M_{CO_2}	molar weight carbon dioxide
M_{CaO}	molar weight calcium oxide
NaCl	sodium chloride
N_K	Knudsen number
OCP	open circuit potential
OH^-	hydroxide ion
P	amount of supplementary cementitious materials

TERM	DEFINITION
$P(t)$	penetration attack function
P_p	atmospheric pressure
P_a	max. applied load
PFA	pulverized Fuel Ash
pH	acid indicator
R	gas constant (8.314 J/ mol. K)
r	specific resistance of metal
R^2	correlation coefficient
R_a	ratio of total area to the cracked area
R_c	reaction rate expression for the species (mole/(m^3·s))
R_{CO}	ohmic resistance of the concrete cover
R_{Cl}	bound chloride due to react chloride with cement compounds
RCPT	rapid chloride permeability test
RH	relative humidity
R_m	electrical resistance of an alloy element or metal
Rp	polarisation resistance
S	degree of saturation of porous media
S_1	surface chloride concentration coefficient
SCE	saturated calomel electrode
SCMs	supplementary cementitious materials
SO_2	sulfur dioxide
T	temperature
t	time
Tc	thermal conductivity
T_{cr}	travel time around the crack
t_{ex}	initial exposure time (may be 28 days or 1 years)
TGA	thermogravimetric analysis
T_{ref}	reference temperature (298 K)
T_s	surface travel time through sound concrete

TERM	DEFINITION
Tp	tafel plot
u_D	coefficient of Darcy Law
U	reaction activation energy (40,000 J/mol K)
u	velocity vector (m/s)
UKCP'09	UK Climate change projections
U_C	diffusion activation energy of chloride
U_v	the absolute value of applied voltage
V_1	volume of the NH_4SCN used in the titration, ml;
V_2	volume of the NH_4SCN used in the blank titration, ml
V_a	aggregate weight / concrete weight ratio
V_{corr}	corrosion rate
$v_i(x)$	convection velocity of *i*
w	water content
w/b	water - binder ratio
w/c	water-cement ratio
w/cm	water-cementitious material ratio
Wt_1	weight of the sample is dry at 105°C for 24 hours
Wt_2	weight of the sample is saturated and surface dry
Wt_3	weight of the sample is immersion in water
x	depth of concrete
$x(t)$	carbonation depth at time
$x_{d:}$	average value of penetration of chloride with time
X_f	carbonation front
X_p	depth of fully carbonation zone
XRD	X-Ray Diffraction
Z	number of ion equivalents exchanged
Z_{Cl}	electric charge of the chloride ion (-1C)

CHAPTER I: INTRODUCTION

1.1 General

The impact of human activities on the climate system is unequivocal. Recent research has shown that anthropogenic emission of greenhouse gases (GHS) is the highest in history (IPCC, 2014). Currently, climate change has had widespread influences on natural systems, and on human as well as civil infrastructure. Since the 1950s, the increase of carbon dioxide concentration and warming of the climate system is clear, and many of the observed changes are recorded over the last two decades (Letcher, 2015; IPCC,2007) Atmospheric temperature is increasing, causing ice to melt and as a result sea level is increasing and relative humidity is decreasing. The increase of anthropogenic emissions of greenhouse gases has mainly grown due to the economic and population growth and they are today higher than ever. The climate Change 2014 Synthesis Report (AR5) of IPCC(2014) reported that anthropogenic emissions of greenhouse gases have controlled to atmospheric concentrations of carbon dioxide and other gases that are unprecedented in at least the last 800,000 years. Their impacts, together with those of other anthropogenic drivers, have been noticed throughout the climate system and are extremely likely to have been the dominant cause of the observed warming since the mid-20^{th} century.

In this context, nowadays there is a deep universal worry about the impact of climate change, the global warming and GHS emissions on the durability of concrete structures and the properties of engineering materials, which are the major section of the infrastructure exposed to the environment (Valdez *et al.*, 2010). Future climate change and its potential influence on the performance of the existing structures is also an issue which concerns more and more countries (Fifer *et al.*, 2014).

These changes, in particular the increase of carbon dioxide and temperature, and decrease of relative humidity have a considerable impact on the climate system. Hence, these changes have a significant impact on structures, particularly in the microstructure

of concrete structures (Talukdar *et al.*, 2012 a). These variations in the microstructure can also affect the durability of existing concrete structures.

1.2 Problem Definition

The industrial developments provided huge opportunities for the evolution of human life throughout the whole world. However, these developments were not free from negative influence on the environment. Greenhouse gas emissions (GHG) including CO_2 are considerable contributors to pollution. Carbon dioxide gas (CO_2) is one of the principal anthropogenic GHGs forming about 78% of total GHGs emissions in 2010 (IPCC, 2014). The increasing concentration of CO_2 in the Earth's atmosphere has raised concerns about global warming, climate change, and their subsequent effects on its inhabitants. According to the worst scenario (RCP 8.5) of Intergovernmental Panel on Climate Change (IPCC, 2014), the CO_2 concentration in the global atmosphere is likely to exceed 1000 ppm and the average temperature is predicted to increase by about 4.3°C in 2100. GHGs including CO_2, cause a change in the environmental system (Letcher, 2009). At the same time, CO_2 affects the properties and durability of concrete structures (Tarun and Rakesh, 2010). As a result, increasing atmospheric CO_2 emissions will likely accelerate carbonation of concrete, chloride penetration and the corrosion rate of steel reinforcement in concrete structures (Wang *el at*., 2010; Bertolini *et al.*, 2013) which are considered as important factors affecting the durability of concrete structures (ACI 201.2R: 2008).

Climate change or atmospheric aggressive conditions tend to affect the environment for a longer term, by accelerating the deterioration processes in concrete and therefore by decreasing the resistance, safety and serviceability of reinforced concrete structures that lead to shorter expected service life (Stewart *et al*., 2012). In addition, the demand to carry out maintenance of deteriorated structures increases exponentially (Kamaitis, 2008). The impacts of global climate changes on the durability of concrete infrastructure have been picked up only been recently as an area requiring further research (Talukdar *et al*., 2012 a). There are no integrated models that can appropriately account for both the environment factors (or climate change parameters) as well as the materials' properties in order to predict the depth of carbonation, chloride penetration and corrosion rate as a function of time. In the present study, integrated models considering the impact of climate change parameters on the durability of concrete structures such as chloride penetration

and carbonation depth are proposed. These models can be of great importance as those can predict future phenomena and as a result, maintenance and rehabilitation of structures can be done in advance to protect the structures and reduce the cost.

1.3 Research Significance

Environmental factors play a vital role in the deterioration of concrete structures over their lifetime. Climate change has complicated the matter further through a potential increase in carbon dioxide and temperature, and a potential reduction in the relative humidity. The weather patterns have changed with warmer and prolonged summer periods accompanied by the shorter but colder winter periods. The frequency and intensity of extreme weather conditions have increased. The combined effect of these phenomena would accelerate the deterioration rate of the concrete structures and may lead to premature failure in service. Within this context, the concrete structures are primarily exposed to both chloride and carbonation that induce corrosion of the steel rebar embedded in the concrete. Key factors affecting carbonation and chloride impact within the context of climate change are CO_2 concentration, temperature, relative humidity and increase in use of de-icing salt.

Moreover, the existing concrete structures suffer from cracking due to service loading and environmental factors. These cracks vary in size and distribution but are not significant to endanger structural safety or stability, however, affects their durability. Hence, these structures need to resist two effects, the external impact resulting from the climate system and its changes and the internal impact resulting from the performance of cracking and properties of the material. These effects are a challenge and threaten the durability of cracked concrete structures. Hence, this study will focus on addressing the main points as the follows:

- The impact of the change in CO_2 concentration, temperature and relative humidity on the carbonation rate in concrete structures cracked under service loads.
- The impact of the change in CO_2 concentration, temperature and relative humidity on the chloride penetration in concrete structures cracked under service loads.

- The impact of the carbonation in concrete(due to the increase in CO_2 concentration) on the chloride penetration in concrete structures.
- The impact of the change in CO_2 concentration, temperature and relative humidity on the rate of corrosion in concrete structures cracked under service loads.
- Models accounting the effect of climate change parameters, and properties of the material and cracking on the carbonation rate and chloride penetration induced deterioration of reinforced concrete structures will be proposed**.**

Experimental data is used to calibrate the developed models in order to predict the impact of climate changes on the durability of concrete structures (carbonation depth and chloride penetration) in the UK and Iraqi cities. This research (experimental works and integrated models) will contribute to development of guidelines which will be used to assist engineers to investigate, monitor and manage the maintenance decision to concrete structures.

1.4 Aims and Objectives of the Study

1.4.1 Aims of the Investigation

The main aim of this study is the identification and investigation of the potential impact of global climate change on infrastructure with special emphasis on durability of the existing reinforced concrete structures in the UK and Iraq. In particular, this study investigates the effect of a potential increase in CO_2 concentration, temperature and variation of relative humidity on the carbonation and chloride attack, and the associated tendency of corrosion-induced deterioration in reinforced concrete structures that are subjected to service loads related cracking. Another key aim is to develop integrated models taking into account the influence of climate change and the microstructure of concrete on the carbonation rate and chloride penetration in existing concrete structures in the UK and Iraqi cities. These models are underpinned by phenomenological basis and are calibrated by experimental results.

Geographically highlighting the impact of potential climate change on the durability of existing reinforced concrete structures based on metrological data and climate change predictions available in the IPCC, 2014 and the UKCP'09 and models

have been developed in this study in order to investigate, monitoring and maintenance decisions which have been taken.

1.4.2 Objectives

In order to achieve the above aims, a number of specific objectives have been identified;

- To investigate the impact of the change in temperature on the chloride penetration depth of cracked reinforced concrete structures.
- To investigate the effects of change in temperature on chloride-induced corrosion initiation.
- To investigate the influence of change in temperature, CO_2 concentration and relative humidity on the depth of carbonation of cracked concrete structures.
- To improve the existing model for the carbonation in existing concrete structures incorporating factors affected by the climate changes such as carbon dioxide concentration, temperature and relative humidity and internal factors such as strength and microstructure of concrete and service load induced cracks.
- To investigate the effects of permeability of concrete on the depth of carbonation, chloride penetration depth and chloride concentration profile in the reinforced concrete structures.
- To develop an integrated model for the penetration of chloride in existing concrete structures incorporating factors affected by climate changes such as carbon dioxide concentration, temperature and internal factors such as microstructure of concrete and cracks.

1.5 Thesis Organization

The thesis consists of eight chapters as follows:

Chapter 1: The introduction, problem definition, research significance of the study and fundamental aims and objectives of the study are defined and highlighted.

Chapter 2: Information available in literature on the durability of concrete structures under different environmental conditions, is reviewed. The carbonation depth, chloride attack and corrosion are explored, including a wide-ranging set of variables with a focus on the effect of properties of concrete and

environmental conditions on the durability of concrete structures. Current experimental protocols and standard codes of monitoring of carbonation depth, chloride penetration and corrosion rate are reviewed, allowing for the development of a detailed experiment programme. On the other hand, the current models and theoretical basis of these models of chloride penetration, carbonation depth and corrosion rate are reviewed as well.

Chapter 3: The methodology, experimental variables of the study and procedures are explained in detail, environmental exposure conditions, designing of specimens used and the set up for tests of the sections of study. The properties of the material and mix proportions, testing and monitoring method used in the study are set out. Experimental work also includes chloride diffusion and migration, carbonation depth and corrosion rate through a range of crack widths and concretes properties with multiple exposures (temperature, relative humidity and CO_2)

Chapter 4: Results of experimental works are presented, discussed and clarified. In particular, the results of the concrete properties of mixes used, fresh, physical and mechanical to use in the assessment of the impacts of these properties and major environmental conditions on the depth of carbonation and chloride penetration and corrosion rate.

Chapter 5: Results obtained through experimental programmes, highlighting key observations and exploring a theoretical basis to explain how observed results are reported. In this chapter, investigations are carried out into the depth of carbonation through a range of concrete properties and crack widths in numerous exposures of environmental conditions, using different methods of testing.

Chapter 6: Investigations are carried out into the chloride penetration and corrosion rate through a range of concrete properties and crack widths with several exposures of environmental conditions using a different method of testing. Results obtained through experimental programmes, highlighting key observations and exploring a theoretical basis to explain observed results

are presented in order to use in a deterioration model (chloride concentration profile).

Chapter 7: Impacts of temperature, relative humidity, carbon dioxide and crack widths on carbonation depth and chloride penetration are considered and simulated using integrated and developed models. This chapter includes a comparison of the modelling results with experimental data from chapters (four, five and six) to calibrate and validate these models. This chapter also investigates the variation of the impacts of climate change on the durability of reinforced concrete structures for the UK and Iraq. Conclusions are drawn on the depth of carbonation and chloride penetration, and methods for investigating the remaining effective service life of concrete structures.

Chapter 8: This chapter draws overall conclusions from the presented experimental and modelling works, highlighting a number of contradictory findings and setting out a number of recommendations for further studies and experimental program. Continuation of a number of the experiments undertaken for this study will be described and set out for future research studies in order to develop the further experimental and theoretical aspects.

CHAPTER II: LITERATURE REVIEW

2.1 Introduction

In this chapter, the effect of climate change parameters on the durability of concrete, in particular carbonation, chloride penetration and corrosion rate are reviewed. Particularly, impacted factors, examining and predicting the carbonation rate, chloride concentration profile, the rate of corrosion and durability of concrete structures will be presented.

Carbon dioxide (CO_2) is the main parameter affecting climate change, which is a major threat to the environment, and as a result, affect, the durability of concrete structures, as well. The following sections will firstly review climate change and its impact on the environment and secondly, the effect of climate change on the durability of concrete structures in terms of carbonation rate, chloride penetration, and corrosion rate.

2.2 Impact of Carbon Dioxide Emissions on Climate Change

Climate change is defined as: " any change in climate over time, whether due to natural variability or as a result of human activity" (IPCC, 2007). The increase in CO_2 emissions plays a vital role in the climate system changes by affecting the global atmosphere (IPCC, 2014). According to IPCC (2007), the concentration of CO_2 in the global atmosphere has increased from 280 ppm in 1775 to 379 ppm in 2005. In Iraq, the territorial emissions of CO_2 increased from 8.26 $MtCO_2$ in 1960 to 138.21 $MtCO_2$ in 2013. Whilst, in the UK, CO_2 emissions reduced from 583.82 $MtCO_2$ in 1960 to 471.26 $MtCO_2$ in 2013 (Global Carbon Atlas, 2014). It is generally agreed that greenhouse gases (GHG) in terms of CO_2 emissions is the main contributor to global warming (Letcher, 2015). GHG also controls radiation, forcing the climate system into global warming or climate change.

Global warming causes an increase in air, surface and seawater temperatures which in turn could cause glaciers to melt and sea level to rise. For example, the average

temperature in central England has increased by 1ºC since the 1970s and is likely to rise more as a result of the influence of human activities (anthropogenic GHGs) on the environment (UKCP'09, 2010).

IPCC (2007) and UKCP'09 (2010) propose climate projections (scenarios) for the 21st century and beyond. According to these scenarios, there is an increase in CO_2 concentrations and temperature and drop in relative humidity over this period. As an example, UKCP'09(2010) models (projections) forecast the increase in mean summer temperature in parts of southern England of up to 4.2°C by 2080. Also, relative humidity is expected to be reduced by around 9% in the same period. Whereas, in the Scottish islands, the expectation is that the temperature will increase by up to 2.5°C. IPCC (2007) and UKCP'09(2010) considered, A1F1 scenario to be the worst changes in temperature and CO_2 concentration. The average concentration of CO_2 in this scenario would approach 710 ppm. While, the worst exceptions scenario of IPCC (2014) is RCP8.5 which forecasts that carbon dioxide emissions may exceed 1000 ppm (see Figure 2.1-a) and the mean increase in temperature will be higher than A1F1 scenario for IPCC (2007). RCP8.5 scenario of IPCC (2014) predicted the increase in temperature between 2.8 to 5.75°C as shown in Figure 2.1-b. The Assessment Report 5 of IPCC (2014 AR-5) has suggested four Representative Concentration Pathways, RCPs (lines), RCP 2.6, RCP 4.5, RCP 6.0 and RCP 8.5 of emissions of carbon dioxide (CO_2) and temperature, as shown in Figure 2.1. Global average surface temperature and emissions of carbon dioxide change from 2006 to 2100 are determined by multi-model simulations and all changes are relative to 1986–2005. Time series of projections, RCPs and a measure of uncertainty (shading) are illustrated for scenarios (e.g., RCP 2.6 (blue) and RCP8.5 (red)) as shown in Figure 2.1.

To date the researchers, who have dealt with the impact of climate change on the durability of concrete, depended mainly on the expectations of the previous scenario of the Inter-governmental Panel on Climate Change report in 2007(IPCC-2007), in particular, CO_2 concentration, average temperature, and relative humidity. Whilst here, the new scenarios of the (IPCC 2014-AR5) will be employed in the experimental programme of this study.

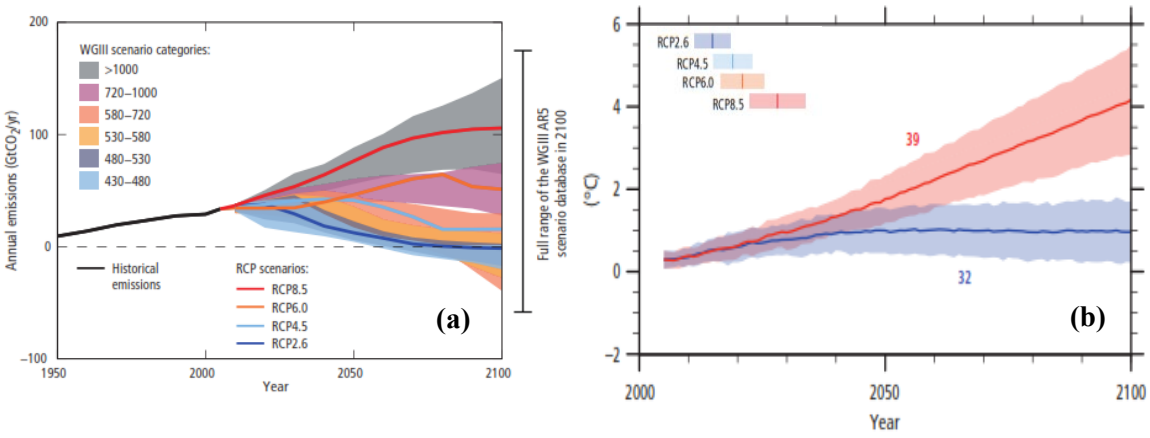

Figure 2.1: IPCC scenarios (a) annual CO_2 emissions (b) Global average surface temperature change (relative to 1986 -2005) (IPCC, 2014)

In Iraq, there are limited studies on climate change, so the prediction of the changes in CO_2 concentration, temperature's mean, and relative humidity will be based on IPCC (2014) scenarios in terms of AR5 report.

In summary, the increase in atmospheric CO_2 concentration is a significant factor in global warming of the environment, which causes an increase in temperature and sea level and a decrease in the relative humidity. The previously listed information related to CO_2 concentration, temperature, relative humidity, and their changes, will be the main parameters utilized in the research methodology of this study.

2.3 Effect of Climate Change on the Durability of Concrete Structures

The durability of concrete is "defined by its capability to resist mechanical action, chemical attack, or any other progression of degradation to retain its basic quality, shape, and ability to be serviceable and safe when exposed to aggressive conditions" (ACI 201.2R, 2014). Climate change may change this environment, especially in the long term, causing an acceleration of deterioration processes and consequently influencing the safety and serviceability of concrete infrastructure. The deterioration or durability of concrete structures can be affected directly or indirectly by climate change, in association with the change in CO_2 concentration, temperature and relative humidity (Wang *et al.,* 2010). The climate-related deterioration of concrete structures is mostly caused by the infiltration of deleterious substances from the environment, for example, CO_2 and chloride penetration, which cause corrosion of reinforcement in concrete structures (Tuutti, 1982; Chen and Mahadevan, 2008). The temperature in concrete due to environment exposure is the main

factor influencing durability of concrete structures carbonation, chloride penetration and the corrosion rate of steel bars in the concrete. The temperature response of the concrete illustrates obvious hysteresis features compared with the climate temperature variations due to the thermal properties of the concrete. Therefore, to predict the temperature response in concrete in a natural climate environment, Yuan and Jiang (2011) proposed a model based on the behaviour of the concrete's thermal conduction.

The major challenges of concrete durability involve the corrosion of steel embedded in concrete, destructive chemical exposure and abrasion. Carbon dioxide and chloride ions attack seems to be the major factors influencing the durability of concrete structures (ACI 201.2R, 2014). Furthermore, the temperature and relative humidity affect the penetration of chloride and CO_2 in concrete structures. The CO_2 and chloride penetration have a significant impact on the corrosion rate (Tuutti, 1982; Hussain *et al*., 1995). Also, the durability of reinforced concrete structures in a chloride environment exposed to an increase in CO_2 concentration and temperature is of a great interest to researchers, infrastructure owners, design engineers and maintainers (Shi *et al*., 2012).

Premature deterioration of concrete structures currently is a major global concern for the construction industry throughout the world (Hussain *et al*., 1995). Therefore, many requirements have been proposed by the codes to maintain the durability of concrete structures in terms of chloride attack, carbonation, and corrosion for the construction of new buildings. On the other hand, code recommendations for existing concrete structures focus on the evaluation and monitoring of these structures by non-destructive testing to investigate the deterioration in order to repair and rehabilitate (ACI 201.2R, 2014; ACI 222R, 2001; CEB-FIP.2013). The main issues of durability or deterioration of concrete structures are presented in the following sections.

2.4 Carbonation in Concrete Structures

2.4.1 Mechanism of Carbonation in Concrete

Carbonation is the chemical reaction between carbonic acid (H_2CO_3), resulting from the combination of atmospheric carbon dioxide (CO_2) with water, and calcium ions (Ca^{2+}) from dissolution of hydrated cement products, such as calcium hydroxide ($Ca(OH)_2$), calcium silicate hydrates (C-S-H) and calcium aluminates hydrates(C-A-H). This results in the formation of calcium carbonate ($CaCO_3$), as shown in Equation 2.1 (Neville,

2011; Tarun and Rakesh, 2010). The sources of CO_2 which can induce carbonation are either in the atmosphere or as dissolved CO_2 in water (rain or groundwater) (ACI 201.2R-2008; Chi *et al*., 2002).

$$\left.\begin{aligned} &CO_2(gas) + H_2O = H_2CO_3 \\ &Ca(OH)_2 + H_2CO_3 = CaCO_3 + 2H_2O \\ &3CaO.2SiO_2.3H_2O + 3H_2CO_3 = 3CaCO_3 + 2SiO_2 + 3H_2O \\ &4CaO.Al_2O_3.13H_2O + 3H_2CO_3 = 4CaCO_3 + 2Al(OH)_3 + 10H_2O \end{aligned}\right\} \quad (2.1)$$

The mechanisms of carbonation that will occur in the water phase depend on the solubility and speed of diffusion (Dyer, 2014; Lagerblad, 2005). Diffusion is controlled by the concentration gradient. Thus, the diffusion processes and the effect on the structure of the carbonated layer must be considered in carbonation mechanisms. It is a process with inward diffusion of carbon dioxide gas and carbonate ions (CO_3^{2-}) dependent on the humidity and porosity in the concrete. The diffusion processes of carbon dioxide gas in a pore of a carbonating concrete is shown in Figure 2.2.

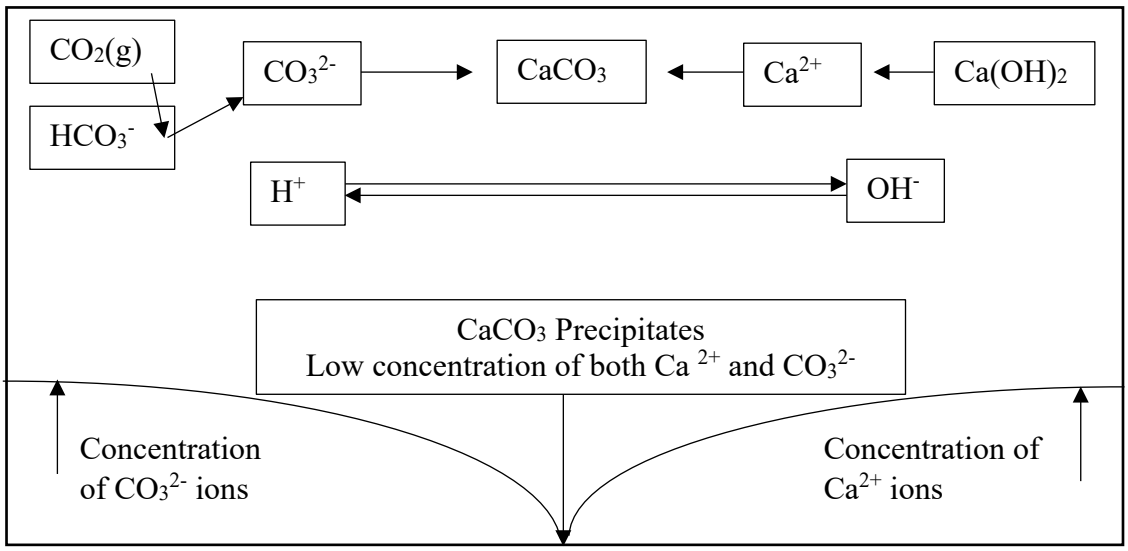

Figure 2.2: Schematic illustration of diffusion processes in a pore of a carbonating concrete (Lagerblad, 2005).

It is, however, a two-way diffusion. The carbonation process will lower the content of Ca^{2+} ions in the pore solution, which in turn will activate dissolution of $Ca(OH)_2$ and Ca^{2+} diffusion from the interior of the concrete to the carbonation front

where the concentration of both components will be at a low point due to the low solubility of calcium carbonate. The point of $CaCO_3$ precipitation depends on the concentration gradient of both components (Ca^{2+} and CO_3^{2-}). The carbonate may precipitate on the surface of the $Ca(OH)_2$ if the concentration of CO_3^{2-} is high but it may also precipitate in the pore solution or on other phases if the Ca^{2+} concentration is high. This will affect the porosity. Where the precipitation occurs will depend on the speed of diffusion of both $Ca^{2+}$and CO_3^{2-} to the point of calcite precipitation where the concentration of both components is low (Lagerblad, 2005) as shown in Figure 2.2.

The carbonation of concrete has both positive and negative impacts on concrete properties. The strength (compressive and tensile) and electrical resistivity of concrete tend to improve slightly due to carbonation (Chi *et al*., 2002). The main reason for the enhanced properties is the densification, and the reduction in porosity, of concrete due to a reduction in average pore size by the carbonation products and sedimentation of $CaCO_3$ crystals in pores of concrete (Dyer, 2014).

On the other hand, carbon dioxide penetration and reaction with hydrated cement-based materials often lead to carbonation shrinkage in concrete structures. It is a physio-chemical change in concrete that causes an increment in weight and shrinking in volume (increment in density). This type of shrinkage is likely to generate narrow and shallow cracks on the concrete surface, however, may have a limited impact on the strength of concrete (Neville and Brooks, 2010).

Moreover, carbonation negatively affects the concrete alkalinity and reduces the pH of concrete pores solution from 13 to 9 (Neville, 2011), which is a considerable factor accelerating the chloride penetration as well as the corrosion of reinforced concrete structures (Dyer, 2014; Broomfield, 2007).

2.4.2 Factors Affecting Carbonation of Concrete Structures

The parameters influencing the rate of concrete carbonation can be classified as external and internal. The external factors include the concentration of atmospheric CO_2, the temperature and the relative humidity (Neville, 2011; Dyer, 2014). Whilst, the internal factors are related to the concrete composition.

2.4.2.1 External Factors Influencing Carbonation of Concrete Structures

The external factors that affect the carbonation rate of concrete are carbon dioxide concentration, temperature and relative humidity (Dyer, 2014). A rise in CO_2 concentration (50,75 and 100%) increases depth of carbonation, DoC in concrete as concluded through accelerated carbonation experiments in a relatively short time of 28 days. There is a linear correlation between the increase in the CO_2 concentration and the increase in the DoC (Chi *et al*., 2002). The higher concentration of CO_2 will yield a higher rate of reaction to form carbonation, $CaCO_3$ (Dyer, 2014).

As mentioned in the previous section, the IPCC (2014) predicted climate change atmospheric CO_2 concentrations for emission scenarios RCP 8.5 will reach 1000 ppm by 2100 due to climate change as shown (see Figure 2.1) and this increase in CO_2 maybe affect DoC (Wang *et al*., 2010) and initiation of corrosion may happen when the carboantion reaches reinforcement bar surface (Yoon *et al.,* 2007).

A significant increase in the DoC has been observed when relative humidity (RH) ranges between 52-75% (Roy *et al*. (1999). However, it reduces as the relative humidity increases beyond this range up to 84% and increased again between 84% and 92% RH (Roy *et al*. (1999). The maximum DoC in different mixes used in the study was acheived at the relative humidity level of 92%. It seems that the causes of this abnormal behaviour at a higher humidity level were unknown at that time. Because (Lagerblad, 2005) reported that in fully water saturated concrete only carbonate ions can move, and carbonation is slow. Alongside this, Russell *et al*. (2001) confirmed that the peak of carbonation rate is reached at a relative humidity range of 55-65%. This propagation of carbonation rate slows down when the concrete pores are fully water-saturated due to the diffusion of CO_2 and reactions of carbonate ions with hydrated cement products hardly react (Kropp and Hilsdorf, 2005). In lower moisture content below 50%, or dry concrete, the carbon dioxide can penetrate deeply but there is insufficient moisture for the carbonation reaction to take place. Thus, the carbonation rate reduces when there is a lower content of water owing to the inadequate amount of water in the pores (Tarun and Rakesh, 2010; Lagerblad, 2005).

In another study, Talukdar *et al*. (2012 a) pointed out that the change in temperature has a considerable impact on the diffusion of carbonate ions into concrete, due to amplified molecular activity and an increase in the reaction rate between carbonate ions CO_3^{2-} and Ca^{2+} in the pore water of concrete. The carbonation rate in concrete

structures may also be affected by the severity and frequency of the environmental conditions which are on the increase due to climate change.

Finally, Drouet *et al*. (2019) tested two hardened cement pastes using 100% CO_2 at different temperature and relative humidity (RH) levels and concluded that the impact of temperature on carbonation rate is dependent on the types of cement. It was also concluded that the decrease in RH causes an increase in DoC. The changes in the mineralogy of cement products due to carbonation is not the same in high concentration CO_2 environment (10-100%). The results in a microstructure are not like those corresponding to natural carbonation at 0.03% of CO_2 (Castellote *et al*., 2009).

In summary, the external factors, atmospheric carbon dioxide concentration, temperature, and relative humidity have affected the DoC and the change in these factors due to climate change (as mentioned in section 2.2) have a significant impact on the durability of concrete structure, carbonation. Where, (Talukdar *et al*., 2012 a) reported there are limited studies which have been carried out on the impacts of climate change on the infrastructure of concrete, essentially because the concern has been recently taken into consideration.

2.4.2.2 Internal Factors Affecting Carbonation of Concrete Structures

As mentioned in the mechanism of carbonation, the speed of carbonation depends mainly on the humidity in the concrete, i.e. how filled with liquid the connective pore system is. Where this optimum is dependent on the porosity of the carbonated layer in concrete and the water blockade diffusion of CO_2 (Lagerblad, 2005). Thus, carbonation rate in concrete is also influenced by variation of the material composition of concrete, such as type and quantity of cement, water-cement ratio (w/c), curing period, type and dosage of chemical admixtures (AL-Khaiat *et al*., 2004; Neville, 2011) and these parameters have a significant impact on concrete strength. According to Roy *et al*. (1999), the DoC is proportional to the strength^{-1}. On the other hand, Neville (2011) reported: "The fundamental factor controlling carbonation is the diffusivity of the hardened cement paste, which is a function of the pore system of the hardened cement paste during the period when the diffusion of CO_2 takes place". More porous concrete seems to have an optimum at a higher degree of water saturation than more dense concrete (Lagerblad, 2005).

The pores in concrete structures have a direct impact on the permeability of concrete. The permeability is defined as the property that controls the flow rate of a fluid (liquids or gases) into a porous media. The concrete permeability mainly depends on the amount and type of cementitious materials, the degree of hydration, the w/c ratio, size, type, and aggregates grading, curing conditions and the degree of compaction (Neville, 2011). Consequently, the higher DoC of concrete is achieved in concrete with higher permeability (Atis, 2004). A lower w/c ratio and long-term curing in water caused a slower rate of carbonation, due to the enhanced microstructure of concrete (Sulapha *et al*., 2003).

2.4.3 Monitoring and Testing the Depth of Carbonation

The measurement of DoC is underpinned by the mineralogical and concentration changes of $Ca(OH)_2$ and *C-S-H* in cementitious material due to exposure to CO_2 environment (Chang and Chen, 2004). Several methods have been used to investigate the DoC as the following:

2.4.3.1 Phenolphthalein Indicator

The phenolphthalein solution is the pH indicator or alkalinity of concrete samples. The main sources of alkalinity of cementitious materials are $Ca(OH)_2$ and C-S-H. This indicator used is a solution of phenolphthalein, ethanol, and water (BS EN 12390-10:2018). After splitting the concrete specimens, the freshly split surface is cleaned and sprayed with a phenolphthalein pH indicator. In the noncarbonated parts of the specimen, where the concrete is still highly alkaline (pH > 9), a purple-red colour is obtained. In the carbonated parts of the specimen where the alkalinity of concrete is reduced (pH ≤ 9), no colouration occurred. The average depth of carbonation, DoC (X_p) of the colourless phenolphthalein region is measured from different points, perpendicular to the two edges of the split face, both immediately after spraying the indicator and at 24 hrs later. Figure 2.3 is presenting the colourless region shown after using the phenolphthalein pH indicator, and the mean DoC, X_p can be calculated by Equation 2.2. This method of measuring DoC has been well documented, and it is the most commonly used method to investigate the full carbonation depth. On the other hand, pH-value, carbonation degree or partial carbonation cannot be determined by phenolphthalein pH indicator (Thiery *et al*., 2007). This method cannot be used to measure the reduction in pH-value due to

exposure to another acidic result from gases such as SO_2, HCl. However, this method is used by BS EN 13295:2004 and CEN/TS 12390-10:2007 to measure the DoC in concrete structures.

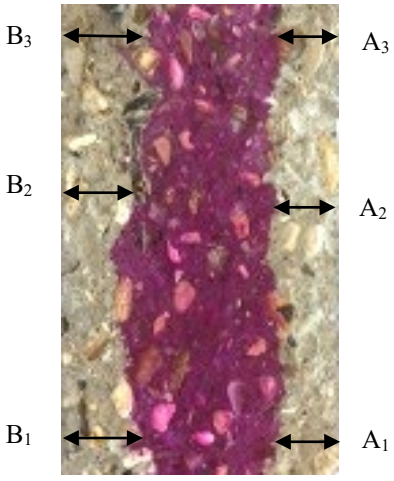

Figure 2.3 Cross-section of split concrete specimens after using Phenolphthalein pH indicator to measure DoC

$$X_p = \frac{A_1+A_2+A_3+B_1+B_2+B_3}{6} \quad (2.2)$$

where:

X_p is the depth of fully carbonated concrete, A_1, A_2, A_3, B_1, B_2 and B_3 are individual measurements of DoC.

2.4.3.2 Thermogravimetric Analysis (TGA) Method

This method is based on computing the molar concentrations of $Ca(OH)_2$ and $CaCO_3$ in powder concrete samples exposed to carbonation. The molar concentrations of these compounds were computed based on the thermogravimetric curve determined from the thermogravimetric analysis test for concrete specimens subjected to various periods of accelerated carbonation, and also from the rate of weight loss indicated by the thermogravimetric curve which included the dehydration of $Ca(OH)_2$ and thermal decomposition of $CaCO_3$ as shown in Equation 2.3 and 2.4.

$$CaCO_{3(s)} = CaO_{(s)} + CO_{2(g)} \quad (2.3)$$

$$Ca(OH)_{2(s)} = CaO_{(s)} + H_2O_{(g)} \quad (2.4)$$

Based on the above facts, changes in the amounts of calcium carbonate in concrete specimens under various periods of carbonation could be analysed (Chang and

Chen, 2004). In this method, a thermogravimetric analysis instrument is used to cause the dehydration of $Ca(OH)_2$ and thermal decomposition of $CaCO_3$ by increasing temperature at a 20 ºC/min rate to reach to 1000 ºC.

Based on the percentage loss in weight of $Ca(OH)_2$ and $CaCO_3$ due to the applied temperature and the Equations 2.3 and 2.4, the proportions by weight of calcium hydroxide and calcium carbonate in the sample can be determined with the depth of concrete surface as shown in Figure 2.4. In this Figure, it is clearly shown that as the degree of carbonation increases, more $CaCO_3$ progresses while more $Ca(OH)_2$ is consumed. If the area in which the phenolphthalein indicator is colourless is defined as the depth, X_p of full carbonation, and the transition point where the concentration distribution of $Ca(OH)_2$ and $CaCO_3$ approaches the horizontal as the carbonation front depth, X_f, then X_p is approximately half of the X_f as shown in Figure 2.4 and Equation 2.5.

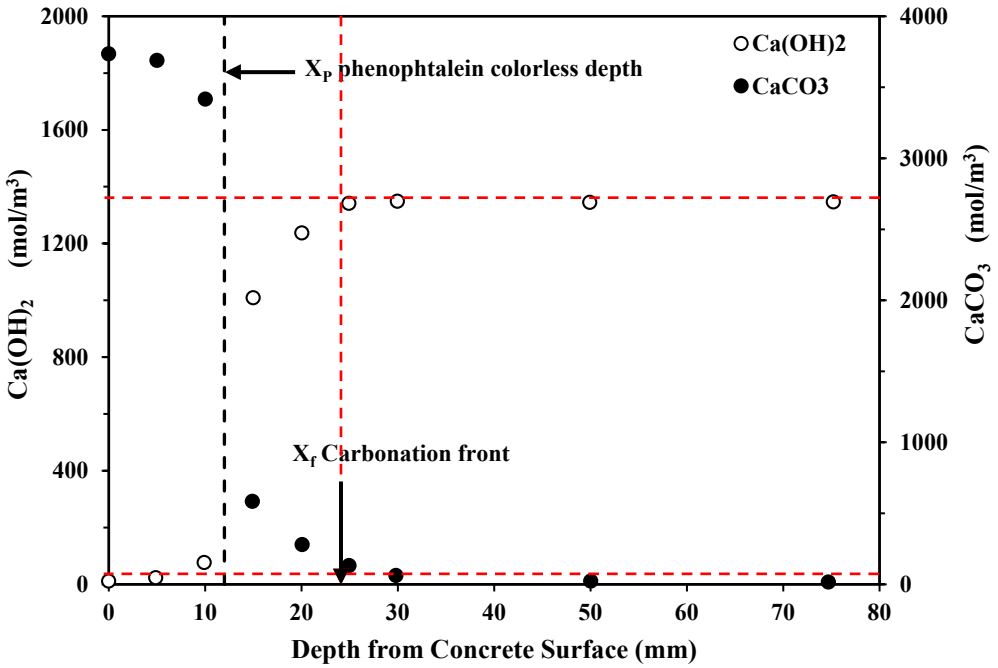

Figure 2.4: The concentrations of $Ca(OH)_2$ and $CaCO_3$ with the depth of concrete by TGA and phenolphthalein colourless depth by Chang and Chen (2004)

$$X_f \approx 2\,X_p \qquad (2.5)$$

On the other hand, Park (2008) found that the *pH* of concrete drops to 9 at 50% consumption of $Ca(OH)_2$ in the concrete mix. Therefore, he confirmed the location of the carbonation front, X_f at the location where 50% of the $Ca(OH)_2$ is consumed as shown in Figure 2.5.

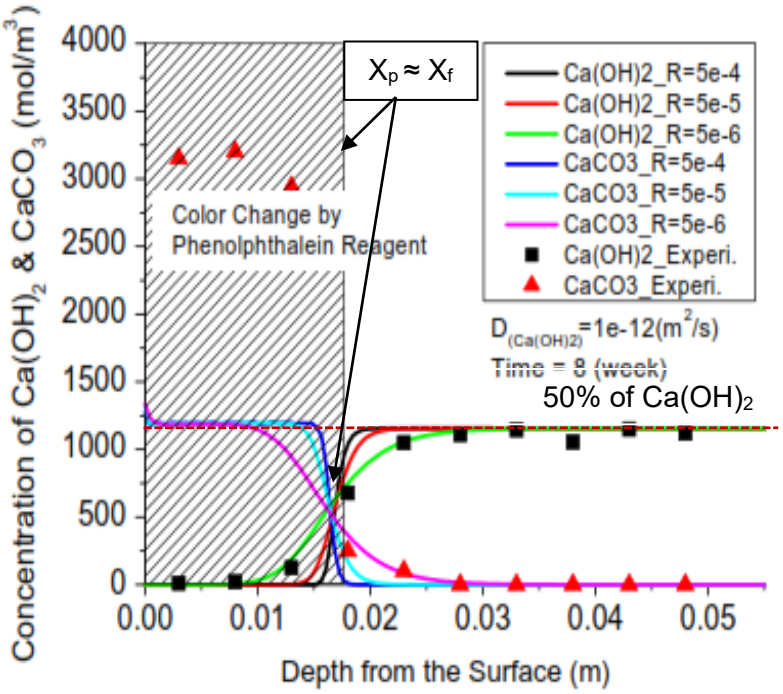

Figure 2.5: Concentration distribution of *Ca(OH)₂* and *CaCO₃* to determine carbonation front depth, according to Park (2008)

2.4.3.3 XRDA Method

X-Ray Diffraction Analysis indicates major crystalline components in the concrete specimen namely; feldspar, quartz, *CaCO₃* and *Ca(OH)₂*. The first and second component comes from the aggregates. While, $CaCO_3$ and *Ca(OH)₂* are produced from cement hydration and vary with the time of carbonation in the concrete specimens (Neville, 2011). Chang and Chen (2006) observed the concrete exposed to 8 weeks of accelerated carbonation; the concrete surfaces had not yet been fully carbonated; *CaCO₃* and *Ca(OH)₂* were both observed in varying intensities of X-Ray diffraction. While the $Ca(OH)_2$ content (relative intensity of XRD) increases from the surface of the concrete to interior, the $CaCO_3$ content (relative intensity of XRD) reduces with depth from the concrete surface. Due to carbonation, the *Ca(OH)₂* intensities are more at the interior than the surface (more detail in section 3.3.4.6-c). The carbonation front depth for sound concrete samples, X_f is the transition point of distribution of relative intensity for *CaCO₃* and *Ca(OH)₂* approaching to be horizontal. The X_f is approximately twice of the X_p as shown in Figure 2.6.

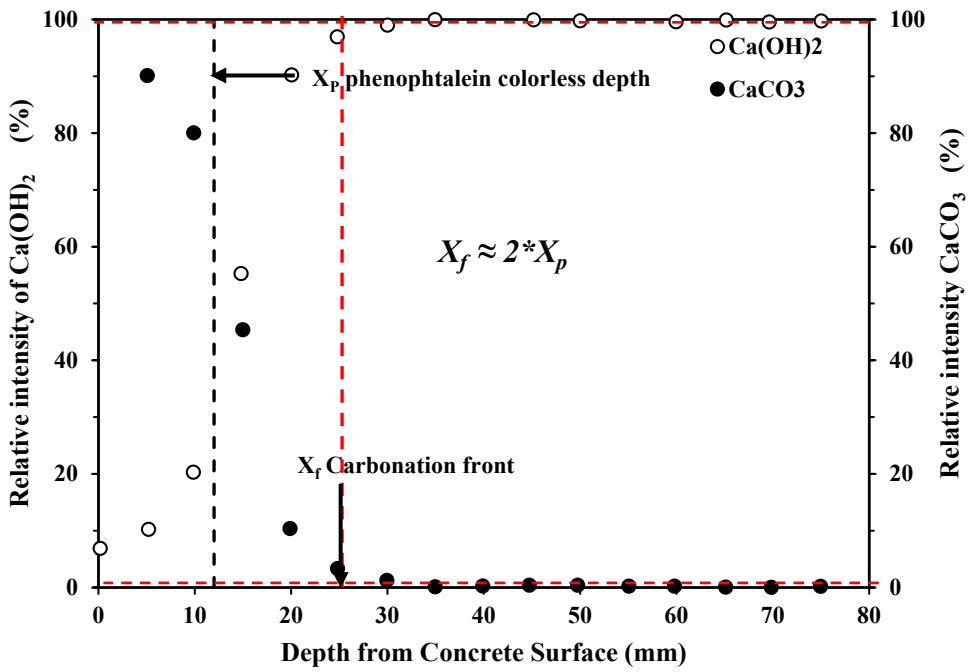

Figure 2.6: The $Ca(OH)_2$-$CaCO_3$ concentration distribution by XRDA with the depth of concrete and phenolphthalein colourless depth for accelerated carbonation (Chang and Chen, 2004)

2.4.3.4 Apparent pH and Consumed OH^- Method

This method is based on measuring the apparent pH of concrete pore solution and concentration of $[OH^-]$ as shown in Equation 2.6 (Li *et al.*, 1999; Suryavanshi and Swamy, 1996)

$$pH = 14 - log[OH^-] \qquad (2.6)$$

Apparent *pH* of concrete can be measured by dissolving the concrete powder in deionized water (McPolin *et al.*, 2007; Wang *et al.*, 2016). The method proposed is used to establish the consumption of $[OH^-]$ due to carbonation of un-carbonated powder. According to this procedure, a typical profile of consumed $[OH^-]$ ions concentration with the depth of concrete is shown in Figure 2.7. This profile can be divided into three zones based on the consumption of $[OH^-]$ ions: fully carbonated, partially carbonated and non-carbonated zone. Where, X_p is the boundary between fully carbonated and partially carbonated zone, and X_f is the boundary between partially carbonated and non-carbonated zone (indicating the carbonation front). Graphically, it can be determined as the boundary between the first and second zones, it is named X_p, while the boundary between partial

carbonation and the non-carbonated zone is called carbonation front depth, X_f as shown in Figure 2.7. The method proposed by (McPolin *et al*., 2007; Wang *et al*., 2016) does not determine the relationship between fully carbonated depth, X_p and carbonation front depth, X_f.

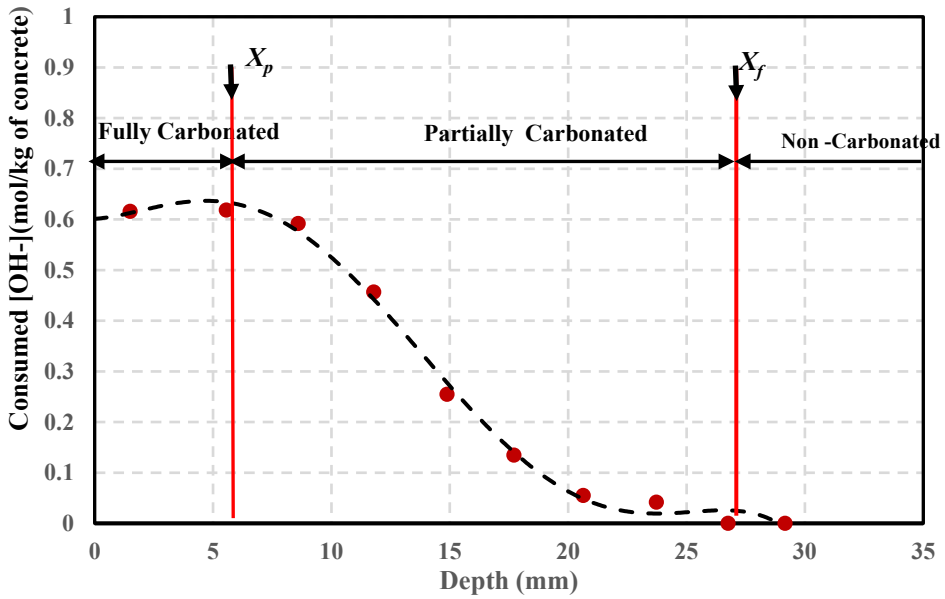

Figure 2.7: Analysis of the profile of consumed OH^- (Wang *et al*., 2016)

2.4.3.5 Summary of Testing Methods of Carbonation

Finally, Table 2.1 is presented to summarize noticeable differences between the carbonation - testing techniques used throughout literature and three of these methods (phenolphthalein indicator, XRDA, and apparent pH and consumed of OH^-) were used in this study.

Table 2.1: Summarized characteristics of carbonation monitoring techniques

Criteria	Phenolphthalein indicator	TGA method	XRDA method	PH and consumed of OH^- method
Basic hypothesis	the alkalinity of concrete, (pH)	chemical – analysis of $CaCO_3$, $Ca(OH)_2$	Intensities of crystalline components $CaCO_3$ & $Ca(OH)_2$	Alkalinity of concrete
Measurement Parameter	Colorless the depth has PH < 9	Concentration of $CaCO_3$, $Ca(OH)_2$	Intensities peak of $CaCO_3$, $Ca(OH)_2$	pH and OH^-
Results indication	fully carbonation depth X_p	fully, partial and no carbonated depth, X_p, X_f	fully, partial and no carbonated depth, X_p, X_f	fully, partial and no carbonated depth, X_p, X_f
Relationship achieved from literature	Find carbonation depth X_p	Find X_f , Xp And $X_f = 2\ X_p$	Find X_f , Xp And $X_f = 2\ X_p$	Find X_p and X_f without any connected Relationship
Field versus laboratory application	Field and laboratory	Take the specimen and test in the laboratory	Take the specimen and test in the laboratory	Take the specimen and test in the laboratory
Advantages	It is to measure full carbonation	It is possible to measure extremely low carbonation	It is possible to measure extremely low carbonation	It is possible to measure extremely low carbonation
Simplicity (equipment required and method of the test) or disadvantage	Simple	Difficult and complicated	Difficult and complicated	Simple

2.4.4 Modelling of Carbonation Depth in Concrete Structures

A number of models which have been proposed to simulate the DoC in concrete are based on the properties of concrete and a given exposure condition. The CO_2 diffusivity models are those chemical-empirical models based on Fick's laws in order to predict DoC as the following.

2.4.4.1 Carbonation Depth in Concrete Based on Fick's First Law

Concrete can carbonate whenever carbon dioxide and some water are available. The speed of carbonation depends on how the CO_2 and /or the CO_3^{2-} can penetrate the concrete and react with cement hydration products. In the normal case, however, CO_2 is

available, and it can be assumed to be a constant amount of diffusion through the surface of the concrete with time. In this case, the diffusion is mass transportation of CO_2 down a concentration gradient. The diffusion of CO_2 and /or the CO_3^{2-} follows Fick's First Law, which is based on the steady state of diffusion of carbonate ions in porous materials (Lagerblad, 2005; Broomfield, 2007; Tarun and Rakesh, 2010). Other assumptions of applying this law are in general consistent only for isotropic medium, whose structure and diffusion properties in the neighbourhood of any point are the same relative to all directions. Because of this symmetry, the flow of diffusing substance at any point is along the normal to the surface of constant concentration through the point (Crank, 1975). Fick's law of diffusion has been applied to describe the depth of carbonation as a function of time (Lagerblad, 2005; Broomfield, 2007; Tarun and Rakesh, 2010). Based on Fick's First Law of diffusion, the amount of a component, m_a of CO_2 and Cl^- diffusing through a concrete layer is given by:

$$J = D\frac{dc}{dx} \tag{2.7}$$

$$J = \frac{m_a}{A_c\, t} \tag{2.8}$$

$$m_a = D_{CO2}\, A_c \frac{C_1 - C_2}{x}\, t \tag{2.9}$$

where:

J is a quantity of a component (m_a) passing through the unit area (A_c) per unit of time (t), i.e. it is, in this case, the net transport rate of CO_2 or the CO_3^{-2} through the unit area, D is a diffusion coefficient, D_{CO2} is a diffusion coefficient of CO_2, $\frac{dc}{dx}$ is the concentration gradient / slope of molar concentration with depth (x) and c_1 and c_2 are the CO_2 concentration of external and at carbonation front depth respectively.

At the carbonation front depth, the penetrated CO_2 reacts with the alkaline compounds available in a given depth. For the carbonation of these alkaline compounds contained in a unit volume of concrete an amount of CO_2 (a_1) is required, and gives the mass of CO_2 required to increase the depth of carbonation by an increment dx.

$$m_a = a_1\, A_c\, dx \tag{2.10}$$

Inserting Equation 2.10, Equation 2.9 may be rewritten as:

$$a_1\, A_c\, dx = D_{CO2}\, A_c \frac{C_1 - C_2}{x}\, t \tag{2.11}$$

$$x\,dx = \frac{D_{CO2}}{a_1}\,(c_1 - c_2)\,t \qquad (2.12)$$

Integrate the Equation finally yields:

$$x^2 = \frac{2D_{CO2}}{a_1}\,(c_1 - c_2)\,t \qquad (2.13)$$

$$x = \sqrt{\frac{2D_{CO2}}{a_1}\,(c_1 - c_2)}\;\sqrt{t} \qquad (2.14)$$

Kropp and Hilsdorf (2005) assumed *K* (carbonation rate) ($mm/\sqrt{y}$);

$$K = \sqrt{\frac{2D_{CO2}}{a_1}\,(c_1 - c_2)} \qquad (2.15)$$

$$x = K\sqrt{t} \qquad (2.16)$$

Roy *et al*. (1999), Al-khaiat *et al*. (2004) and Chi *et al*. (2002) used this model to predict the DoC (in mm) and this Equation is the most commonly used.

Approximate values of carbonation rate, *K* were proposed depending on the experimental data of studies as shown in Table 2.2. These values of *K* are based on the properties of concrete and a given environmental exposure conditions (Tarun and Rakesh, 2010).

This model of the DoC does not adequately consider external and internal factors, such as pore structure of the concrete, quantity of $Ca(OH)_2$ (Talukdar *et al*., 2012 b) and uses of supplementary cementitious materials (SCMs) in concrete (Lea 1971). On the other hand,the diffusion of CO_2 or the CO_3^{2-} through the unit area of concrete is not constant or non-steady state (Dyer, 2014). The *K* values for cases in which the CO_2 concentrations are higher than 10%, do not actually present the normal environmental conditions allowing us to predict the DoC in concrete in the future. The results in a microstructure are not like those corresponding to natural carbonation at 0.03% of CO_2 (Castellote *et al*., 2009).

Table 2.2: Carbonation rate for some researchers with different environment exposure and properties of concrete

Research	CO_2 Concentration	The exposure time of the test	Carbonation rate K ($\frac{mm}{\sqrt{y}}$)	
			Min. Value	Max. Value
Russell *et al.* (2001)	5%	6 weeks	10	79
Chi *et al.* (2002)	50-100%	28 days	6	51
Huang *et al*. (2012)	Atmospheric CO_2	35 years	2.4 1.09	2.7 1.3
Khunthongkeaw *et al.* (2006)	0.0225-0.0625 %	24 months	1.7	9.2
Roy *et al*. (1999)	6%	7- 42 days	10.89	16.9
Al-khaiat *et al*. (2004)	Atmospheric CO_2	8.6 years	2.1	7.8
Lagerblad (2005)	Atmospheric CO_2	Did not notice	0.5	15

2.4.4.2 Carbonation Depth in Concrete Based on Fick's Second Law

The concentration of carbon dioxide in the atmosphere affects carbonation in concrete in two ways; firstly, the movement of carbon dioxide into concrete is a result of diffusion, a higher concentration gradient between the exterior and interior of concrete will lead to a greater rate of diffusion. Secondly, higher concentration of CO_2 will yield a higher rate of reaction to form carbonation, $CaCO_3$ (Dyer, 2014).

The diffusion and concentration of CO_2 changes both with the depth of concrete exposure to environment CO_2 and with time due to changes in the atmospheric CO_2 concentration and the amount of CO_2 consumed in carbonation. That is called the non-steady state of diffusion; therefore, Fick's Second Law can be applied where the concentration of CO_2 alters with time and location factor, ∂x and ∂t respectively as shown in Equation 2.17. Fick's Second Law gives a depth of alteration /carbonation and not the amount of material that is being altered (Lagerblad, 2005).

$$\frac{\partial}{\partial t}(C_{CO_2}) = D_{CO_2}\frac{\partial^2}{\partial x^2}(C_{CO_2}) \qquad (2.17)$$

Several solutions for Equation 2.17 have been proposed to compute carbonation depth, *x*, or carbonation rate; *K* as follows:

CEB-FIP (2013); Yoon *et al*.(2007) proposed Equation 2.18 to compute the depth of carbonation in concrete. This equation is a function of diffusivity and concentration of carbon dioxide in concrete and is based on the quantity of CO_2 uptake by CaO due to carbonation.

$$x = \sqrt{\frac{2D_{CO_2}(C_{CO_2}/100)}{a}\,t} \qquad (2.18)$$

(Lagerblad, 2005) assumed $K_1 = \sqrt{\frac{2D_{CO_2}(C_{CO_2}/100)}{a}}$ (2.19)

Then, $x(t) = K_1\sqrt{t}$ (2.20)

where:

The D_{CO2} is the CO_2 diffusion coefficient, C_{CO2} is the atmospheric CO_2 concentration %, *a* is the amount of CO_2 uptake to complete carbonation is calculated by Equation 2.21, K_1 is the rate of carbonation in ($mm/\sqrt{y}$) and this is the slope of the curve of the relationship between $x(t)$ and $\sqrt{t}$.

$$a = 0.75 * C * CaO * \propto_H \frac{M_{CO_2}}{M_{CaO}} \qquad (2.21)$$

This modification assumes the 0.75 of *CaO* will be carbonated, *C* is unit content of cement (kg/m^3), *CaO* is content of *CaO* (calcium oxide, 0.65), $\propto_H$ is the hydration rate (0.85), and M_{CO_2} , M_{CaO}, are molar wethe ight of CO_2= 44 and *CaO*= 56 respectively (Yoon *et al*., 2007).

Papadakis and Tsimas (2002) proposed carbonation rate, K_1, involving the weight of total cementitious materials (cement + supplementary cement materials) to be more comprehensive for all cementitious materials by:

$$K_1 = \sqrt{\frac{2D_{CO_2}(C_{CO_2}/100)}{0.218\,(C+k_pP)}} \qquad (2.22)$$

where:

k_p is an efficiency factor for resisting against carbonation of 0.5 to 0.7 (Papadakis and Tsimas, 2002) and *P* is the quantity of SCMs.

Huang *et al*. (2012) applied the Laplace transformation to Equation 2.23, the analytical solution of this Equation is achieved by assuming the diffusion coefficient and surface concentration of CO_2 are constant.

$$C_{CO2}(x,t) = C_s erfc\left(\frac{x}{\sqrt{4D_{CO2}t}}\right) \quad (2.23)$$

Huang *et al*. (2012) assumed $K_2 = \sqrt{4D_{CO2}}\ erfc^{-1}\left(\frac{C_{CO2}(x,t)}{C_s}\right)$ (2.24)

Then, $x(t) = K_2\sqrt{t}$ (2.25)

where:

$C_{CO2}(x, t)$ is the CO_2 concentration at depth (x) and time t; C_s is the surface CO_2 concentration; D_{CO2} is the diffusion coefficient of CO_2 (m^2/sec); *erfc* is the complementary error function; $x(t)$ is carbonation depth at time *t*, K_2 is carbonation rate ($mm/\sqrt{y}$) is the slope of curve of relationship between $x(t)$ and $\sqrt{t}$.

Equation 2.24 illustrates carbonation rate depends on carbon dioxide diffusion coefficient and concentration of CO_2 at ($C_{CO2}(x,t)$) to the concentration of CO_2 at concrete surface. Consequently, Huang *et al.* (2012) did not consider the minimum concentration of CO_2 to precipitate $CaCO_3$ in concrete.

Finally, Talukdar *et al*. (2012a) have proposed a model based on a group of partial differential equations of diffusion of $CO_{2(aq)}$ and $Ca(OH)_{2(aq)}$. These are based on Fick's Second Law to find the concentration of $CO_{2(aq)}$ and $Ca(OH)_{2(aq)}$ in the depth of concrete, x and the time, *t* by using the numerical solution of these equations. Talukdar *et al*. (2012a) depended on one-dimensional diffusion of CO_2 and $Ca(OH)_2$ to find the concentration at *x* and *t*, as shown in Equation 2.26 and 2.27.

$$\frac{\partial}{\partial t}[CO_{2(aq)}] = D_{CO_2}\frac{\partial^2}{\partial x^2}[CO_{2(aq)}] - k_c[CO_{2(aq)}][Ca(OH)_{2(aq)}] \quad (2.26)$$

$$\frac{\partial}{\partial t}[Ca(OH)_{2(aq)}] = D_{Ca(OH)_2}\frac{\partial^2}{\partial x^2}[Ca(OH)_{2(aq)}] - k_c[CO_{2(aq)}][Ca(OH)_{2(aq)}] \quad (2.27)$$

where:

$CO_{2(aq)}$, $Ca(OH)_{2(aq)}$ are aqueous concentration of CO_2 and $Ca(OH)_2$ respectively, k_c is the rate constant of reaction and *x* is the depth of concrete and time *t.*

Talukdar *et al.* (2012a) tested one mix of concrete (w/c ratio, 0.5) with different temperature and relative humidity (change with exposure time) and they used the

numerical solution of these equations simultaneously to determine $Ca(OH)_2$ *(aq)* and CO_2 *(aq)* concentration at a given point with respect to time. They did not determine the minimum concentration of CO_2 and $Ca(OH)_2$ to forms $CaCO_3$ and find the DoC. Talukdar *et al*. (2012 a) assumed that the CO_2 *(aq)* is consumed by $Ca(OH)_2$ *(aq)* only as shown in the second term of Equation 2.26 and 2.27. Actually, one half of CO_2 *(aq)* is consumed in concrete by reacting with $Ca(OH)_2$ *(aq)* and the second half of CO_2 *(aq)* is depleted by *C-S-H* (Yoon *et al*., 2007; Park, 2008).

As mentioned previously, the diffusion coefficient of carbon dioxide in concrete (D_{CO2}) is considered in these models to find DoC. The diffusion coefficient D_{CO2} is a variable that depends on the microstructures of concrete (connective porosity) and microclimate condition especially the temperature and the RH inside the cement paste in concrete (Lagerblad, 2005; Talukdar *et al*., 2012) as well as crack in concrete samples (Kwon and Na, 2011). Thus, the calculation of CO_2 uptake due to carbonation must to a large extent rely on laboratory data, empirical data, and measurements on real concrete structures. D_{CO2} values of the most important types of concrete must be estimated to find accurate values of DoC (for more details see section 7.6.2).

As mentioned above, the diffusion coefficient of CO_2 is a major factor in simulating the models to predict carbonation depth. Therefore, this study aims to develop an integrated model for the diffusion coefficient of CO_2 in existing concrete structures incorporating factors affected by climate parameters such as carbon dioxide concentration, temperature, and relative humidity, in addition to the properties of concrete and width of crack. In order to predict carbonation depth, essentially because the climate change (change in CO_2 concentration, temperature, and relative humidity) has only been recently identified and there is limited research that has been carried out on the impacts of global climate change which may influence concrete infrastructure (Talukdar *et al*., 2012 a). Moreover, carbonation becomes observable to be potentially unsafe, particularly in climatic conditions of high temperature- humidity regions (Haque and Al-Khaiat, 1997; Talukdar and Banthia, 2013) such as case study (Iraq).

2.5 Chloride Penetration in Concrete Structures

2.5.1 Mechanism for Chloride Penetration in Concrete and Chloride Forms

Chloride attack is one of the greatest threats for the reinforced concrete structures. Chloride ions maybe penetrate into concrete from different sources, external sources such as de-icing salt, seawater and groundwater, and internal sources through contaminants in concrete composition such as, aggregate or sea water brackish water, or by chemical admixtures containing chloride content (Neville, 2011; Dyer, 2014).

The transportation of chloride ions in aqueous solutions into concrete occur mainly through pore spaces in the cement paste matrix or micro-cracks (Ishida *et al*., 2014). A variety of different physical and/or chemical mechanisms may govern the transport of chloride ions into the concrete. Chloride ingress in concrete depends on the chloride ions flowing and their local concentration, the environmental conditions (temperature and relative humidity), the pore water structure of concrete, the pore radius or width of micro-cracks and the degree of saturation of the pore system (Kropp and Hilsdorf, 2005).

Considering the wide range of pore sizes and a varying moisture concentration in the concrete as a function of the climatic exposure conditions, the transportation of chloride ions into concrete in most cases is not due to one single mechanism. However, several mechanisms may act simultaneously. Chloride transportation into concrete can be a combination of the concentration gradient of chloride ions, the pressure gradient and capillary sorption making the flow of chloride through pores by combined transport methods such as diffusion, permeation and capillary sorption (Morocous and Lounis, 2005; Dyer, 2014).

Chloride ions can be present in concrete in various forms such as (Katwan, 1988):
- Dissolved chloride or free ions in the pore solution of concrete.
- Chloride ions physically bound with hydrates of calcium silicate (C_2S, C_3S).
- Chloride ions chemically bound with hydrates of calcium aluminates (C_3A).

The total chloride ions in concrete are the sum of these components as shown in Equation 2.28 and Figure 2.8.

$$Chloride_{(total)} = Chloride_{(dissolved\ or\ free)} + Chloride_{(bound)} \qquad (2.28)$$

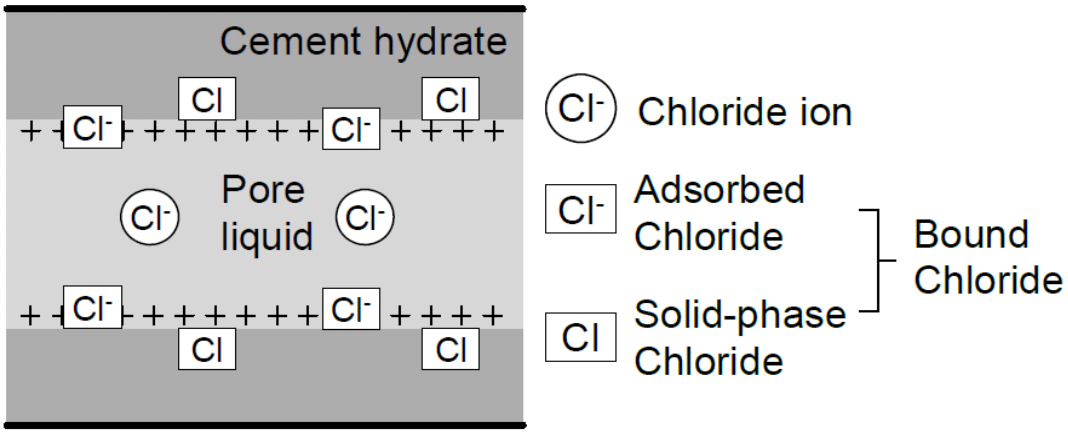

Figure 2.8*:* Classification and definition of chloride in hardened cement pastes (Maruya *et al*., 1998)

The dissolved chloride ions are in a freely transportable form in the pore liquid in concrete. On the other hand, the bound chlorides, apparently cannot move at normal concentration gradients or in normal advective environments. Bound chlorides can be further classified into constituents of hydrates, chemically bound as Friedel's salt ($C_3A.CaCl_2.10H_2O$) and physically bound as chlorides adsorbed into the pore walls as shown in Figure 2.8 (Maruya *et al*., 1998).

Under normal circumstances, the contribution of bound chloride in corrosion is negligibly small (Markeset and Myrdal, 2008). However, the bound chloride starts to dissolve in the pore solution with a reduction in pH of the pore water of concrete due to carbonation. Wan *et al*. (2013) found that the bound chloride in the cement mortar sample decreased by 27%- 54% when the sample pH value reduced from 13.2 to 8 due to carbonation. Various factors affect the dissolved chloride concentration such as pH, temperature, relative humidity and the chloride binding capacity of cement components (Neville, 2011; Zibara, 2001). In the next sections, some of the factors will be analytically reviewed.

There are a few studies, which focused on the impact of carbonation (reduction in pH) on the binding of chloride in the concrete samples (Yuan *et al*., 2009). The pore structure of hydrated cement in the concrete sample is quite different from that of cement mortar (Mehta and Monteiro, 2006). In addition, it is necessary to focus on the impact of carbonation on the binding of chloride owing to the importance of effect of them on corrosion rate (Markeset and Myrdal, 2008).

Finally, available studies have carried out on cement paste samples and in simulated concrete pore solutions. According to Angst *et al*. (2009), these techniques are correlated with doubts and might at least partly be responsible for the inconsistency between the general assumption that bound chlorides are rendered harmless and experimental results in literature.

As mentioned in the reasons above, this proposal is an in-depth research using a real concrete samples in order to study the effect of carbonation (reduction in pH) on cocncrte structures. Due to the climate change effect, an increase in CO_2 concentration and temperature and reducing the relative humidity on the penetration of chlorides and binding in the concrete sample,one should consider evaluating the diffusion coefficient of chloride in concrete.

Regarding the combined mechanisms of penetration of CO_3^{2-} and Cl^- ions in concrete, on one hand, it has been proved that carbonation influences the ingress of Cl^-. It can be summarised as follows: at the early stage of carbonation, densification of concrete due to the formation of $CaCO_3$ slows down the ingress of Cl^- (Wang *et al*., 2016); on the other hand, the carbonation process works to reduce the chloride binding capacity of cement paste and promotes the chloride ingress to a certain extent (Dyer, 2014). With the progress of carbonation, micro-cracks resulting from carbonation may be created on the surface of the concrete leading to a decrease in the resistance of chloride penetration.

2.5.2 Factors Affecting Chloride Penetration in Concrete

The chloride ions concentration, C_{Cl} in the pore water in the concrete-steel interface is affected by some parameters as shown in Equation 2.29 (Markeset and Myrdal, 2008) by:

$$C_{(Cl)} = f(Total\ chloride, C_3A - content, pH, Temperature, Relative\ humidity) \quad (2.29)$$

The external concentration of chloride has a significant impact on the diffusion of chloride in concrete and is transported due to a variation in concentration and pressure. However, the effect of external chloride concentration on the rate of chloride penetration is rather more complex. The chloride diffusion coefficient decreases by increasing the external concentration (Tang, 1997) due to a greater interaction between ions at higher concentrations, which holds back their movement. This decline in diffusion coefficient at

higher concentrations is an important phenomenon, which needs to be examined independently. Although the rate of transport of chloride ions into the concrete reduces with the lower chloride diffusion coefficient, however, the total quantity of chloride that has arrived in the depth of concrete is still much greater than the higher external concentration (Maruya *et al*., 1998) as shown in Figure 2.9.

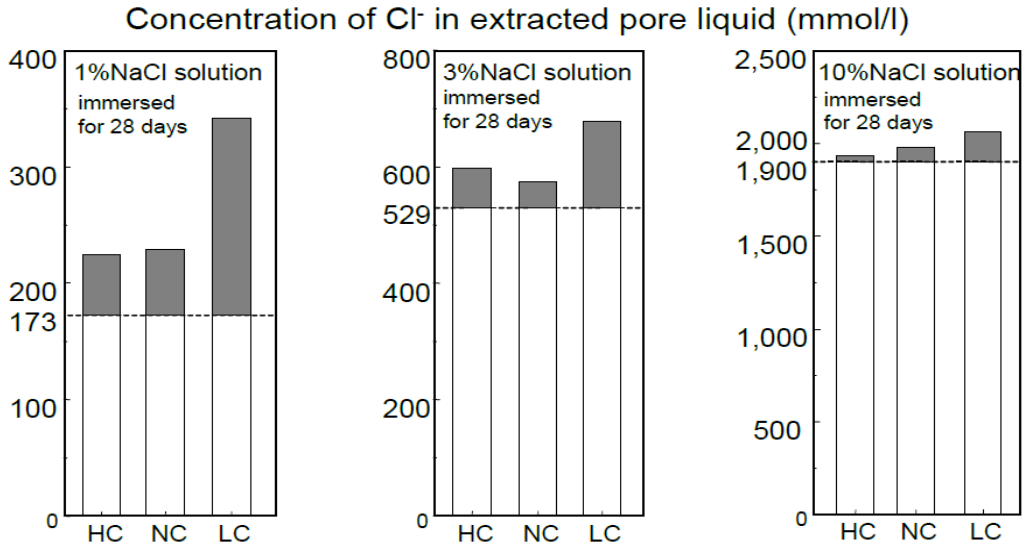

Figure 2.9: Concentration of chloride ions in pore liquid extracted from test concrete (different strength of concrete, high, normal and low strength) (Maruya *et al*.,1998)

The Second-factor affecting chloride ions concentration, C_{Cl} is C_3A content in cement. The increment of C_3A content in cement decreases the dissolved chloride content within pore water solution due to chemical binding of the chloride, however, the optimum content of C_3A has not been found (Gjorv, 1979).

The chloride bound, calcium chloroaluminate, becomes unstable when carbonation happens which tends to liberate the waves of chloride ions (Wan *et al*., 2013). Furthermore, the carbonation in concrete plays a significant role in the reduction of pH of concrete pore solution (McPolin *et al*., 2007). Essentially, the pH of pore water in concrete depends on the type of cement and binder but maybe change at a later stage as the result of carbonation and leaching. It is recognized as a major factor affecting chloride threshold early by inhibiting the impact of (OH^-) against (Cl^-) induced corrosion (Shi *et al*., 2012). Consequently, Gouba (1970) cited by (Angst *et al*., 2009) found increasing [Cl^-/OH^-] ratio with an increase in pH of the pore water solution. Otherwise, Katwan

(1988) claimed that it is commonly recognized that chlorides ions have a negligible impact on pH of pore water in concrete.

As previously noticed, climate change affects the temperature and relative humidity. Firstly, Hussain *et al*. (1995) demonstrated a significant impact of the temperature of curing cement paste on the threshold chloride content for the three plain cements with variable C_3A contents of 2.43, 7.59 and 14%. Exposure temperature has a very strong influence on threshold chloride values. Increase in temperature from 20° to 70°C, threshold chloride contents are reduced by at least five times for all three cements tested in this investigation. Also, Hussain *et al*. (1995) claim that the threshold of chloride content [Cl^-/OH^-] ratio activity is 0.4 according to their experimental tests and this view disagreed with the suggestion of Hausmann (1967) employing probability consideration to suggest [Cl^-/OH^-] ratio activity is 0.6.

There should be two reasons to study the impact of temperature on chloride concentration in existing concrete structures. First, there is not available research on the effect of temperature on chloride penetration in the cracked concrete samples. Page *et al*. (1981) studied the effect of the increase of temperature on chloride diffusion coefficient in the cement paste. As noticed previously, the properties of concrete such as the porosity and permeability are different from the cement paste properties, which are key factors affecting the transport of aggressive agents, i.e. chloride ions (Mehta and Monteiro, 2006). In concrete, interfacial transition zone (ITZ) exists between the cement paste and aggregate particles. This (ITZ) contains micro-cracks due to aggregate restrained shrinkage (Grassl *et al*., 2008; Hobbs, 1974) and hence contributes to the permeation properties of concrete (Dyer, 2014). Also, the aggregates also have altered the permeation properties (Neville, 2011).

The second climate change factor, the relative humidity or moisture content is the one important factor which influences the chloride penetration and increases the chloride concentration in concrete structures. Where, pore water transports the chloride ion and oxygen to concrete-steel interface zone. In other words, moisture content controls the movement of chloride and oxygen to the steel surface (Markeset and Myrdal, 2008). Angst *et al*. (2009) pointed out that the quantity of water in the concrete pores may affect the distribution between bound and free chloride and therefore determines the free chloride concentration in pore liquid.

Finally, chloride concentration in concrete may be influenced by the presence of cracks in concrete; they have a significant impact on diffusion and permeation of chloride ions in concrete as well as permeable pores (Sheo -Feng *et al*., 2011). Park *et al*. (2012) found the chloride diffusion coefficient in concrete increases 24 times for crack width of 0.1 mm and 145 times for crack width of 0.4mm, when compared with un-cracked concrete. These results are not completely consistent with the results obtained by Kwon et al. (2009); Sheo -Feng *et al*. (2011) that are shown in Figure 2.10. It is clear, there are big differences in the results of the researchers, which may result from the natural formation of cracks in the sample or from the method of measuring the diffusion coefficient of chloride.

Marsavina *et al*. (2009) utilized notch tip in concrete specimens and found the chloride diffusion coefficient increases with an increase in notch depth. Also, the influence of the notch width was not clear on the penetration of chloride, and more research should be carried out to clarify the effect of the notch width on the penetration of chloride in concrete. This representation of cracks maybe make crack width a constant.

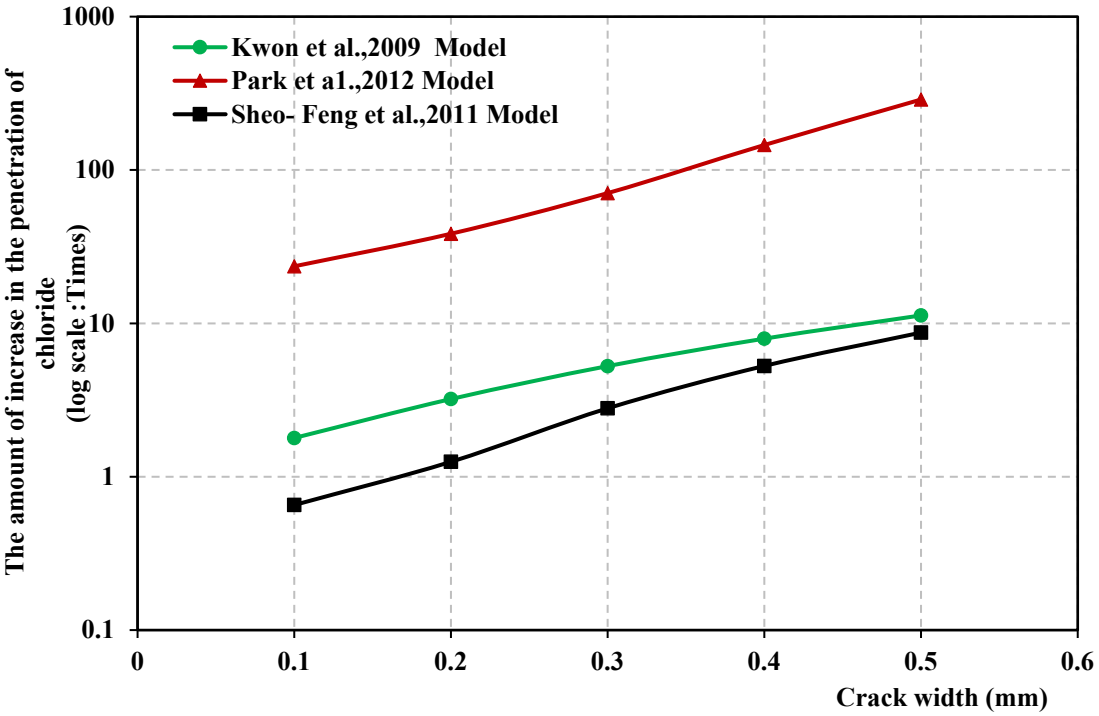

Figure 2.10: Effect of cracks width on chloride penetration in cracked concrete samples from different literature sources

In Iraq, the soil and material which is used to produce concrete suffers from an increase in sulfates and chlorides content. The results of groundwater analysis prepared

by the Iraqi National Centre for Geological Survey cited by (Tawfiq, 1992) show that the chloride ions concentration is between 2% to 4%, while the sulfate ions concentrations range is between (0.5-0.7) %. As mentioned above, these concentrations of chloride and sulfate are very high according to literature summaries by Santhanam *et al*. (2002). Hence, their high concentration has negatively affected on both the chemical and the physical binding capacity of chloride in concrete. Furthermore, chloride and sulfates form aggressive agents to corrode reinforcing rebar in concrete especially at low chloride content 0.1M (Zibara, 2001). Also, the high sulfates concentration in the surrounding environment of concrete helps to attack and form gypsum and Ettringite which is created an additional risk to concrete (Neville, 2011).

Finally, the changes in temperature and humidity (due to climate change) should require a new investigation of the effect of these parameters on chloride penetration and chlorides binding in the cracked concrete sample. Secondly, one must determine the accurate relationship between chloride penetration and diffusion coefficient with crack width for cracked concrete samples.

2.5.3 Impact of Carbonation on the Chloride Penetration in Concrete

Carbonation has the potential to reduce the pH of the pore water in concrete. The reduction in the pH can also break down the chloride binding (calcium chloroaluminate). It is a result of the reaction between one of the cement components, namely tricalcium aluminate (C_3A) and the chloride salt that is in pore water in concrete (Broomfield, 2007). Carbonation is a significant factor in reducing the pH and liberation of bound chlorides in cement mortar sample (Wan *et al*., 2013).

The properties of concrete are different from the properties of cement mortar, particularly the permeability which is a considerable factor affecting the penetration of both aggressive agents, carbon dioxide and chloride (Mehta and Monteiro, 2006). The presence of a small amount of chloride in carbonated concrete accelerates the corrosion rate due to reducing the water solution pH of concrete pores (Neville, 2011). Additionally, reinforced concrete structures are more vulnerable to corrosion by the combined impact of chloride and carbonation than those with only one of the two sources (Broomfield, 2007). The carbonation in concrete structures marks the onset of chemical and physical

processes toward their deterioration and creates an appropriate environment with the chloride ions to initiate the corrosion in the steel bar in concrete structures.

2.5.4 Monitoring and Testing Chloride Penetration in Concrete Structures

Previous studies and standards have proposed common methods of measuring chloride penetration, regarding the natural diffusion of chloride ions and the migration of chloride ions. Each method has some frequently employed experimental techniques to find the steady-state and non-steady chloride migration or diffusion coefficients through concrete samples. Castellote and Andrade (2006) reported the results of the participation of twenty-seven research laboratories in round-robin testing on the penetration of chloride test methods. This study showed that the process of chloride penetration is very complex.

2.5.4.1 Natural Diffusion

Natural diffusion methods of chloride penetration tests are commonly used. These methods depend on the standards code such as ASTM specification, EN BS and NT Build (Nord test method). Concrete samples from existing structures and laboratory samples cab be tested by using these methods. They are based on diffusion of chloride ions in concrete. Where, the diffusion is the movement of ions or molecules under a gradient of chloride concentration, which is the transport of chloride ions from a higher concentration zone to a lower concentration zone (BS EN 12390-11: 2015). So, the used concentration of chlorides in this testing is higher than practiced in common environments to accelerate the test. However, these methods are still comparatively time-consuming procedures for finding apparent diffusion coefficients (D_a).

Owing to find the bulk transport properties of the concrete mixes it is necessary to cut the surface of concrete samples as well as to predict the lifespan of concrete structures as accurately as possible, additionally, the effect of skin and concrete properties should be accounted for measuring chloride penetration. The data on the diffusion of chloride can be provided by exposing the cast surface of the concrete to the penetration of chloride. The recommended procedures for sampling concrete in natural diffusion methods are drilling or profile grinding and dry cutting and crushing (Vennesland *et al*., 2013).

2.5.4.1.1 BS EN 12390 Part 11 (2015) and ASTM C 1556 – 11a (2016)

British Standards Institution, 12390 -11: 2015 and ASTM C 1556-11a: 2016 gives an approach of clear plans on a natural diffusion method test of chloride. The samples are exposed to 1M of NaCl solution for three months by ponding, inversion or immersion as shown in Figure 2.11. After exposure time to chloride, a minimum of eight slices of concrete samples are cut and ground to determine the acid-soluble chloride content of these layers by titration according to BS EN 14629:2007 or ASTM C 1152:2012 + ASTM C114:2015 or RILEM TC 178-TMC-2003. An apparent chloride diffusion coefficient, D_{app} is obtained by regression of results of chloride profile and curve fitting of Crank's solution of diffusion law (Fick's Second Law). Accepting the proper value for surface chloride concentration is essential, as the obtained D_{app}, could be significantly affected by the use of incorrect results.

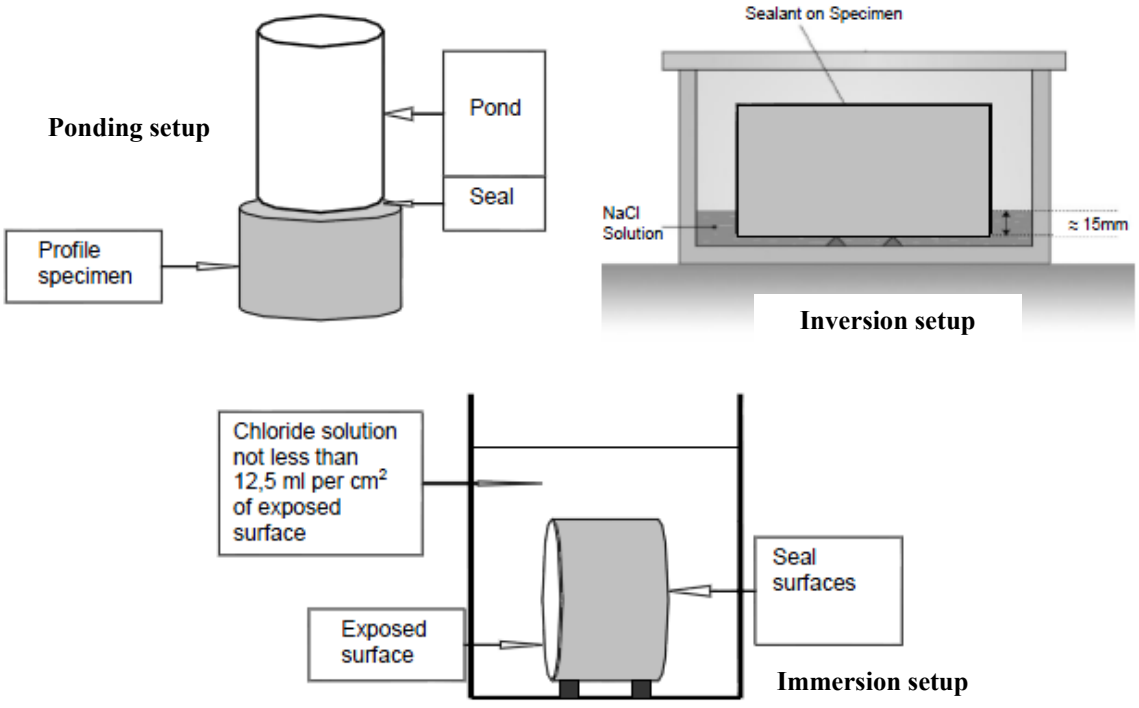

Figure 2.11: Inversion, ponding and immersion setups according to BS EN 12390-11: 2015

2.5.4.1.2 NT Build 443

In Nordtest method, (1995), one face of the concrete specimen is exposed to vacuum-saturated 2.8 M of sodium chloride solution for five weeks. Profile crushing and titration according to NT Build 208:1996 is used to determine the chloride content at

predetermined depths from the exposed surface within the concrete specimen to determine the surface concentration, C_s and effective diffusion coefficient, D_e by using non-linear regression analysis on the obtained concentrations of chloride with depth. Expected accuracy of variation coefficients in this method are: D_e = 15% and C_s = 20%. Also, Tang and Sørensen (2001) stated the repeatability coefficient of variation, COV to be between 8 to 14%, with the reproducibility of COV between 16 to 23%. However, owing to the complications with titration measurements and profile grinding, differences of results obtained from this test technique may be estimated to be higher (Song, 2014).

Consequently, Vallini and Aldred (2003) did a comparison study between results obtained from exposed beams in natural conditions and this testing method. The results illustrated the diffusion coefficients obtained from Nordtest methods were between 5 to 178 times higher than those for exposed beams in natural conditions.

2.5.4.2 Chloride Migration

The chloride migration method is based on an applied potential to accelerate the chloride ions through the concrete, either for a specific period or until a steady state is reached. The applied voltage or currents can be a reason to change the results when compared with the actual state of structures. However, a migration test is more accepted due to being faster in the determination of transport properties in concrete. Nernst-Planck equation governs the movement of chloride ions in an electric field (Andrade, 1993) as shown in Equation 2.30.

$$-J = D_i \frac{\partial C_i(x)}{\partial x} + \frac{zF}{RT} D.C_i \frac{\partial E(x)}{\partial x} + C_i v_i(x) \qquad (2.30)$$

where:

J is the flux of the ionic species i, $C_i(x)$ is the concentration of ionic species i as a function of location x, D_i is the diffusion coefficient of species, i is the valence of ionic species i, R is gas constant, F is Faraday's constant, $E(x)$ is the applied voltage as a function of x, $v_i(x)$ is the convection velocity of i and T is the temperature.

2.5.4.2.1 AASHTO T277 and ASTM C1202

This method called the “Rapid Chloride Permeability Test” (RCPT), measures the current (charge) passed through concrete specimen of a 100mm diameter and 50 mm thick

core and relates this to the permeability of chloride ions. The concrete samples are subjected to 60 V applied from DC voltage supplier for 6 hrs by using the device shown in Figure 2.12. Current is scheduled overtime periods at least 30 minutes long and then summarized to find the charge passed. Table 2.4 shows this charge passed through concrete sample related to chloride ion permeability. This method have received criticism because the applied potential prompts the movement of all ions and not just ions of chloride through the concrete sample. It, also, does not measure the permeability but rather, ionic movement.

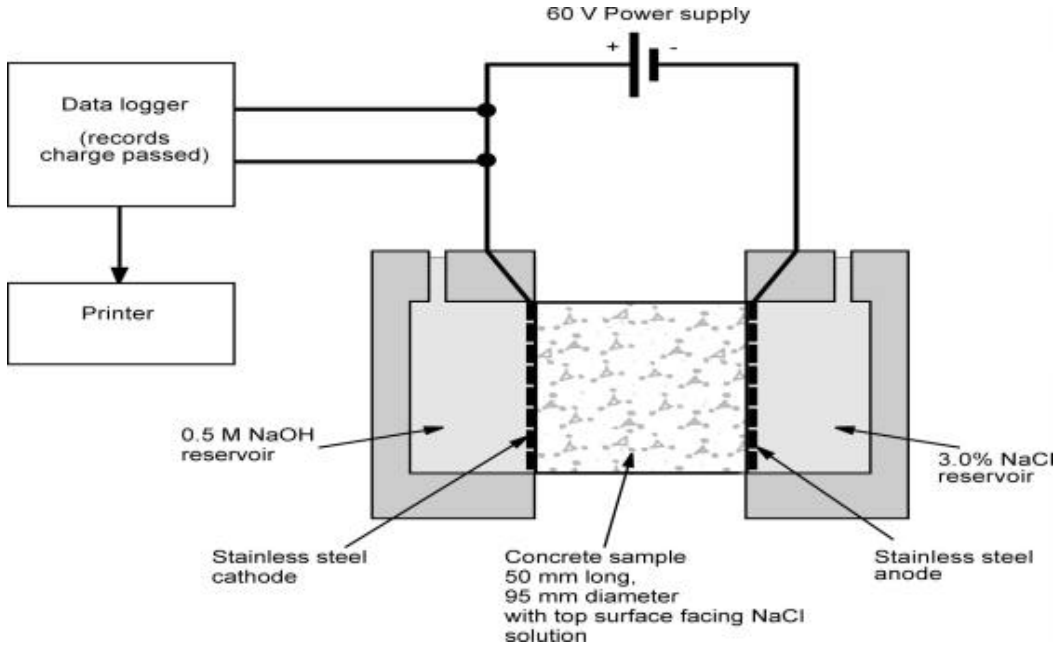

Figure 2.12: ASTM C1202 and AASHTO T277 test setup

Consequently, Grace Construction Products (2006) reported this method might produce a difference in results by up to 42%, 51% with round-robin testing when two tests carried out on the same concrete mix by the same operator.

Table 2.3: RCPT ratings according to ASTM C1202:2012

Charge passed, Coulombs	Chloride ion permeability
4,000	High
2,000 – 4,000	Moderate
1,000 – 2,000	Low
100 – 1,000	Very low
< 100	Negligible

2.5.4.2.2 Multi-Regime (MR)

The methodology of the MR method is based on the applied potential difference, 12V, to accelerate chloride ions through a sliced sample of concrete (Castellote *et al*., 2001; Castellote and Andrade, 2006). There are two compartments; a 1M NaCl solution is applied to one compartment and distilled water into the other. A positively charged bar is placed into the distilled water; while a negatively charged steel bar is inserted into the NaCl solution. The negative charge of chloride ions is pulled to the positive steel rod. Figure 2.13 shows an overview of the setup of MR.

Results of the MR test are based on the conductivity of solution 'downstream' at the anode and the drop-in potential across the sample as well as measuring the temperature at this time of measurement because the conductivity of the solution is affected by temperature. Then, coefficients of diffusion of both states (steady, non-steady) can be computed by measuring the rise in conductivity over time. The use of artificial seawater has negatively charged sulfate ions as well as chloride ions. The former would also be pulled through the concrete slice and dissolved into the positive solution. Therefore, the results are expressed on conductivity 'downstream' of a solution of both ions; then a diffusion coefficient may be greater than that which happens naturally.

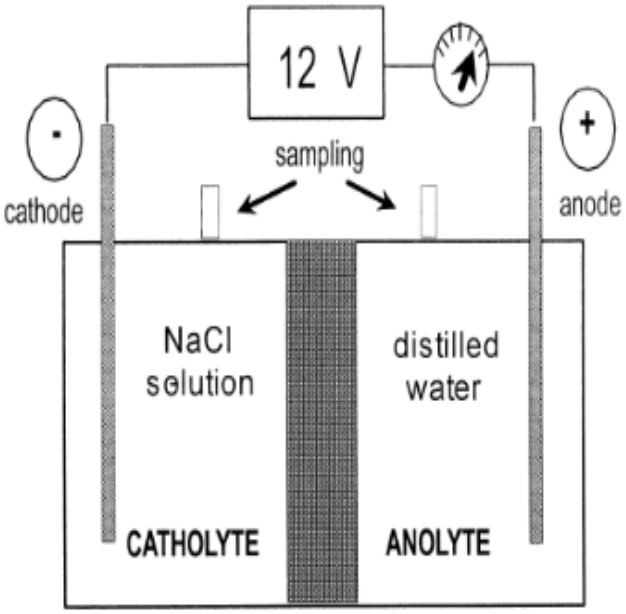

Figure 2.13: Multi-Regime (MR) setup (Castellote *et al*., 2001)

2.5.5.2.3 NT Build 492

The migration cell of NT Build 492 (1999) is set up with a concrete specimen 50 mm thick, 100 mm in diameter, and applied potential DC about (30-60 V) according to the type of concrete, as illustrated in Figure 2.14. In this method, the $AgNO_3$ spray is easily visually assessed when on the chloride penetration ion reach a sufficient concentration. The NT Build 492 standard determines the coefficient of variation of reproducibility is 13%, and the coefficient of variation of repeatability is 9%, meaning that NT Build 443 has a slightly lower reproducibility value. However, comparison of the precisions of experimental results will achieve an approximation of differences which may be employed in probabilistic prediction of service life.

Mentioned chloride concentrations at the colour change boundary differ between 0.28% to 1.69% mass of cement (He *et al*., 2012; Yuan *et al*., 2008). In order to further information on the OH^- concentration, tests of the pH of the pore concrete solution, may be provided with an indicator of the actual concentration of chloride in the concrete sample at the penetration front (He *et al*., 2011).

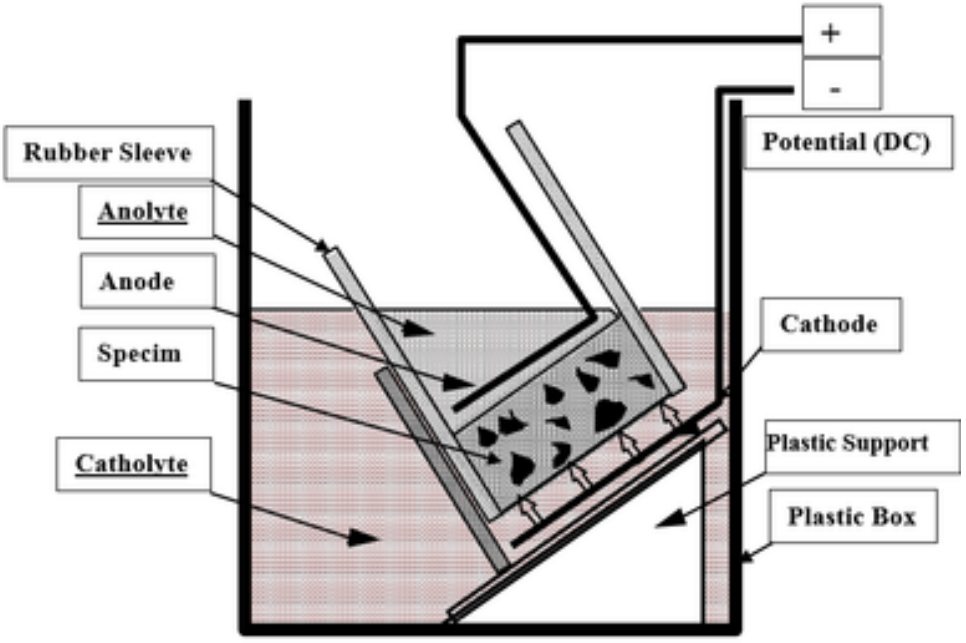

Figure 2.14: NT Build 492 (1999) setup

2.5.4.3 Summary of Testing Methods of Chloride Penetration

In summary, although several methods use similar procedures, results differ between each experimental design. However, the summarised methods in Table 2.4 are

appropriate for characteristics between the resistance to chloride penetration of different concrete mixes, using data from the test in short-term chloride diffusion to forecast modelling for the long-term.

Table 2.4: Summary of experimental methods used in determinations of the chloride penetration in concrete

Method	Type of chloride penetration	Comments	Reference
BS EN 12390:11	Natural diffusion	28 days curing and 90 days of chloride exposure, it is similar to real the exposure to chloride, and it needs a long time.	BS Institution:2015
NT Build 443	Natural diffusion	Immersion in chloride solution about 35 days it is an accelerated method to the penetration of chloride by vacuum, and the results are achieved in a short time	NORDTEST, NT Build 443:1995
ASTM & AASHTO227	Migration	Test period 6 hours reported repeatability of COV in results up to 51%, it is a relatively inaccurate method, and it gives a range of permeability, not a specific value.	Grace Construction Products,2006
Multi regime (MR)	Migration	Test period up to a month, potential to gain non-steady and steady state coefficient, the diffusion coefficient for both states can be achieved and the time of test is longer than the method NT Build 492.	Castellote, *et al*., 2001; Castellote and Andrade, 2006

Method	Type of chloride penetration	Comments	Reference
NT Build 492	Migration	24 hours rapid test, it is an accelerated method to get the diffusion coefficient, and it is accurate.	NORDTEST, NT Build 492, 1999

2.5.5 Modelling for Chloride Penetration in Concrete Structures

The service life and durability should be factors with the main significance of rational design and maintenance of them. In facilitating the forecast of the predicted service life of new concrete structures, service life estimation models are now proving to be vital tools. Furthermore, the prediction of the residual service life is critical when developing efficient repair strategies and the cost of the deteriorated concrete structures. The service life models are classified into different groups based on different standards: (i) probabilistic and deterministic models, and (ii) mechanical and empirical models (Song, 2014). The chloride penetration models discussed in this study are those empirical models based on Fick's laws.

Generally, the empirical models of chloride penetration are underpinned by the theories of diffusion or Fick's laws, and connected with wide-ranging empirical results from the laboratory works or field studies of existing reinforced concrete structures. These were developed from a simple element to complexity, by using the consideration of a single component of the multi-elements.

2.5.5.1 Principle Diffusion Equations

In order to apply the laws of diffusion, the concrete structures should be based on some assumptions such as,

- Concrete is an homogenous and isotropic material.
- The semi-infinite medium of penetration of chloride ions.
- Chloride concentrations are uniform throughout the surfaces of concrete.
- Non-reactive material exposed to the chloride diffusion process.

There are two cases of diffusion or flow, the first case is the steady state flow, where the average transport of chloride ions throughout a sectional unit area of concrete per unit time(*J*) is constant and proportional to the concentration gradient of the chloride ions (Pack *et al*.,2010; Stanish and Thomas, 2003 ; Marchand and Samson, 2009). This is Fick's First Law of diffusion, as shown in Equation 2. 7. Poulsen and Mejlbro (2006) pointed out the first applied of Fick's Laws of diffusion was in concrete through the project of Mario Collepardi in the 1970s.

Chloride ions into concrete are a non-steady state process (changeable with time and space). Fick's Second Law of diffusion can designate the non-steady state diffusion processes and is used in this case (Crank, 1975; Frederiksen *et al.*, 2008; Song, 2014), as shown in Equation 2.31:

$$\frac{\partial C_{(x,y,z,t)}}{\partial t} = \frac{\partial}{\partial x}\left\{D(x,t)\ \frac{\partial^2 C_x}{\partial x}\right\} + \frac{\partial}{\partial y}\left\{D(y,t)\ \frac{\partial^2 C_y}{\partial y}\right\} + \frac{\partial}{\partial z}\left\{D(z,t)\ \frac{\partial^2 C_z}{\partial z}\right\} \qquad (2.\ 31)$$

where:

C(x,y,z,t) is the chloride concentration for point *(x,y,z)* at the time t, *D(x,t) ,D(y,t)* and *D(z,t)* are the diffusion coefficient for *x, y* and *z* direction respectively with time.

In almost all the available studies, the chloride diffusion in concrete has been studied in one- dimensional diffusion flow and it could be summarized in Equation 2.32. This model is widely employed to estimate the chloride diffusion profile as a function of time (Andrade *et al*., 1996).

$$\frac{\partial C_{(x,t)}}{\partial t} = \frac{\partial}{\partial x}\left\{D(x,t)\ \frac{\partial^2 C_{(x,t)}}{\partial x^2}\right\} \qquad (2.32)$$

where:

C(x, t) is the chloride concentration at depth *(x)* with time t, *D(x,t)* is the diffusion coefficient for *x*-direction with the time, *t*.

There are several assumptions that have been made to solve the Equation 2.32 depending on the diffusivity of chloride ingress and it is time-dependent surface concentration, C_s, and time-dependent diffusion of chloride coefficient, $D_{(x,t)}$.
Some of the solutions have been proposed to solve this Equation as follows:

2.5.5.2 Error Function Based Model with Constant C_s and D_a

With simple assumptions such as:

- The diffusion coefficient of chloride ions D_a and surface concentration C_s are constant in space with time.
- The initial concentration throughout the medium is zero.
- Diffusion occurs only in one direction (along with the depth).
- *x* will never be greater than the sample thickness.

The Equation 2.32 or Fick's Second Law has been formulated with the error function complement solution and proposed model as shown in Equation 2.33 (Collepardi *et al*., 1972 and Crank, 1975), to forecast the chloride ingress in concrete, providing the chloride profile in concrete at a given duration of chloride exposure.

$$C(x,t) = C_i + (C_S - C_i)\left[1 - erf\left(\frac{x}{2\sqrt{D_a \cdot t}}\right)\right] \qquad (2.33)$$

where:

C (x, t) is the chloride concentration at depth (*x*) with time t; C_i is initial chloride concentration (% mass of concrete); C_s is the surface chloride concentration (% mass of concrete); D_a is the diffusion coefficient of chlorides (m^2/sec); *erf* is the error function for solution of partial equation.

This has been considered the main model for almost 25 years (Song, 2014) and employed by many researchers (Vu and Stewart, 2000; Morcous and Lounis, 2005; Shi *et al*., 2012, Amey *et al.*, 1998) and used by EN BS and ATSM standards to simulate the chloride concentration profiles in concrete.

2.5.5.3 Time-Dependent Diffusion Coefficient, $D_a(t)$

The diffusion coefficient of chloride ($D_a(t)$) varies according to the micro-structure of concrete, the permeability of concrete which is influenced by w/c ratio, cement type, curing time temperature and relative humidity and exposure time (Vu and Stewart, 2000). This coefficient decreases with time and this reduction is rapid in the first five years of exposure and after that may be a constant value (Bamforth *et al*., 1997).

The dependency of this coefficient $D_a(t)$ on the exposure period t, Takewaka and Mastumoto (1988) was first established and proposed as an empirical formula which designates the reduction of diffusion coefficient with time, that is, $D_a(t)$ is proportional to t^{m} by:

$$D_a(t) = \frac{1}{t-t_{ex}} \int_{t_{ex}}^{t} D_a(\tau)d\tau = D_{aex} \left\{\frac{t_{ex}}{t}\right\}^{m}, \; t>t_{ex} \; , \; 0 \leq m \leq 1 \qquad (2.34)$$

where:

t_{ex} is initial exposure time (may be 28 days or 1 years), t: specific time , D_{aex} is an apparent diffusion at t_{ex} , m is ageing factor(diffusivity reduction factor), depending on development of strength of concrete and type of used binding material in mortar /concrete such as cement, silica fume, fly ash and GGBS micro environmental conditions. CEB-FIP (2010); ACI Committee 365(2008); Wang *et al*. (2016) reported the ageing factor is likely to be between 0.2 and 0.8.

The original formula was modified by Tang and Nilsson (1993) to incorporate mathematical time-dependent equations, from observation in rapid diffusivity test that the determined diffusion coefficient in premature concrete dramatically was reduced with the age. This was further improved by Tang and Joost (2007), by using the essential difference between $D_a(t)$ and D_a as shown in Equation 2.35, and validating the application of the D_a result after time integration from the beginning to the completion of the test, instead of the constant $D_a(t)$ achieved by a short-term diffusion test, D_a is much more precise.

$$D_a = D_a(t).\frac{1}{1-n}.\left[\left(1+\frac{t_{ex}}{t}\right)^{1-n} - \left(\frac{t_{ex}}{t}\right)^{1-n}\right] \qquad (2.35)$$

2.5.5.4 Time-Dependent Model for Surface Concentration, $C_s(t)$

The surface concentration of chloride in concrete (C_s) considers a significant factor affecting chloride transport in concrete. Previous studies observed the concentration of chloride on the surface of concrete is time dependent. Where the relationship between chloride surface concentrations C_s and exposure time were proposed using different models based on type exposure environments and cement types (Pack *et al*., 2010). Ann *et al*. (2009) stated that expression of the build-up of C_s in concrete invariant models marks in different descriptions of the solution to the Fick's Second Law, providing to the different form of chloride diffusion profile.

The ERF model is not effective when challenged with time-dependent *Cs(t)*, in its place ψ_p function was presented by simply substituting the *ERF* function in the chloride-ingress equation, getting the correct solution in Equation 2.37 (Mejlbro, 1996).

$$C(x,t) = C_s(t_{ex}, t).\psi_p\left(\frac{x_{cr}}{2\sqrt{D_c.\ t}}\right) \qquad (2.36)$$

There are two assumptions of C_s for the environmental conditions of chloride exposure in terms of a de-icing salt and marine environmental conditions.

a. C_s Time- dependent

Initially, concrete is a heterogeneous material that is frequently exposed to time-variant surface chloride concentration (Arteaga *et al.,* 2010). The C_s in concrete increases with the time and it is significantly affected by the mix proportion of the concrete, the air void content, type of exposure condition, the curing method and the climate condition. Therefore, numerous researchers have proposed that models based on the assumption that C_s is time dependent as shown in Equation 2.37 (Uji *et al.*, 1990, Amey *et al.*, 1998):

$$C_S(t) = S_1\sqrt{t} \qquad (2.37)$$

where:

$C_s(t)$ is surface chloride concentration at time t (% by mass of concrete or cement); S_1 is the surface chloride concentration coefficient.

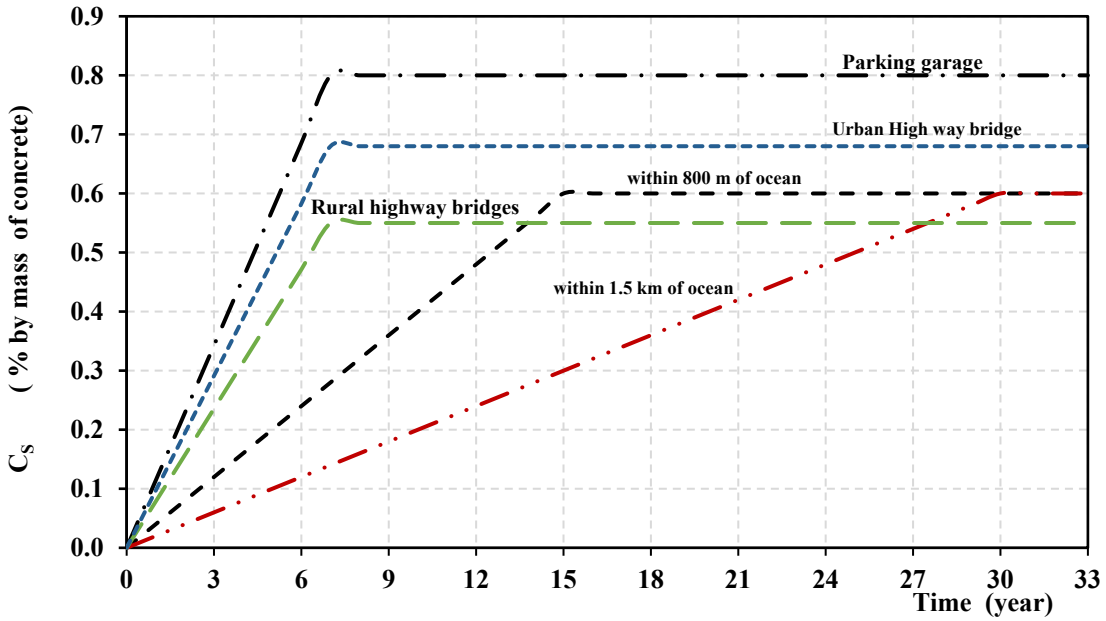

Figure 2.15: Surface chloride concentration with time according to ACI 365-2018 Scenarios

This model does not consider an initial build-up of chlorides on the surface of the cover concrete, where concrete is exposed to a salt environment at an early age (Song *et al*., 2008). In addition, the increase of C_s may be continuous with time. While, ACI 365-2000 demonstrated other models for C_s increasing with time were considered and the C_s becomes a constant at a specific time according to the type of exposure condition, type of structures and location of the structure as shown in Figure 2.15.

b. C_s is a Constant with Time

On the other hand, Hoffman and Weyers (1994) & Hoffman and Weyers (1996) assume C_s is a constant, and they claimed that C_s is the most practical and realistic approach. A literature review has addressed a large amount of data of in-situ results for C_s on samples due to the exposure to de-icing salts as shown in Fig 2.16 for groups of bridges (mean values) or individual bridges. This data of C_s and diffusion coefficients, D_a resulted from curve-fitting to Fick's Second Law and based on equilibrium with the concentration of chlorides.

The C_s may be impacted by the amount of de-icing salts applied to a bridge deck (i.e. geographical location), quality of expansion or construction joints, the efficiency of drainage, etc. This helps clarify the high variability of C_s shown in Figure 2.16 that presents data of Hoffman and Weyers (1994); Hetek(1997), it is observed that most of the results are below 5 kg/m^3. Hoffman and Weyers (1994) categorized this data comprising samples taken from 321 concretes is in broad agreement with other data shown in Figure 2.16. Thus, the mean and coefficient of variation bridge decks in the US seem to be the most comprehensive to date and its mean of 3.5 kg/m^3 (0.15% by mass of concrete by using concrete density about 2350 kg/m^3).

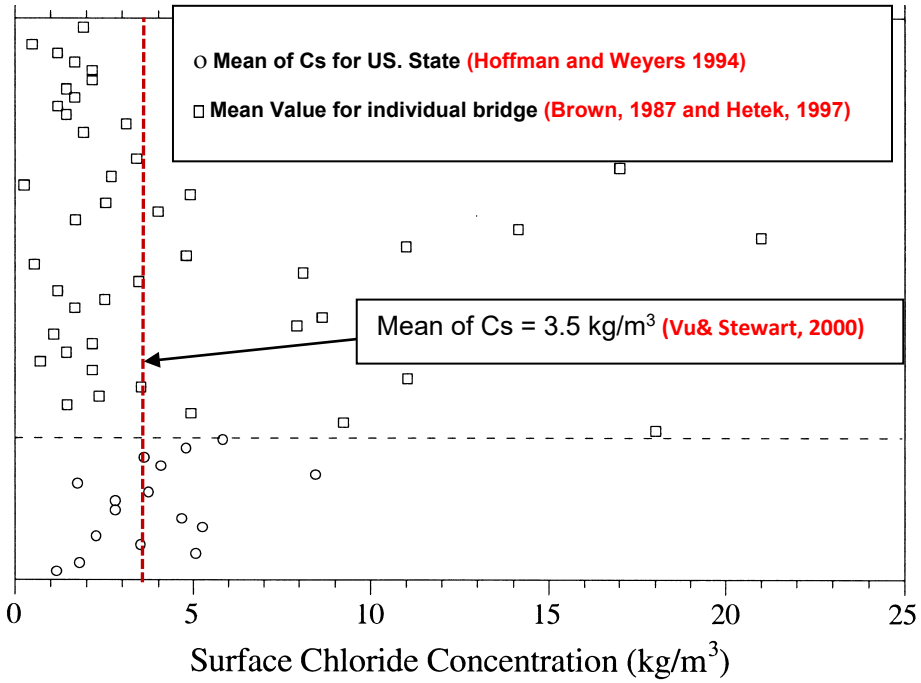

Figure 2.16: Surface chloride concentrations of concrete exposed to de-icing salts Vu and Stewart (2000).

Stewart *et al*., (1998) and Vu and Stewart (2000) adopted this assumption (C_s does not accumulate with time) in prediction of the time-dependence on the deterioration of reinforced concrete bridges. They provided clarification of C_s as a constant (averaged over a year) because C_s is in equilibrium with the concentration of chlorides in the saturated de-icing salt solution, so, C_s is a constant.

Also, Tikalsky (2016) demonstrated a study based on an in-situ investigation on bridges in the US exposed to de-icing salt for 13 years to simulate chloride diffusion in concrete. In this study, C_s was taken to be a typical constant value equal to 0.6% by mass of cement.

Consequently, Val and Trapper (2008); Lin *et al.* (2010); Czarnecki and Woyciechowski (2013) established their studies on the constant value of C_s in order to investigate the effect of other parameters on the durability of concrete structures due to chloride penetration.

2.5.5.5 Numerical Solutions of Fick's Second Law Model

As mentioned previously, chloride ingress into the concrete structures is non-steady state due to changes in the diffusion of chloride with exposure time that lead to

surface concentrations and diffusion coefficients of chloride are variable with time (Frederiksen *et al*., 2008). So, when we combine the ideas of Takewaka and Matsumoto (1988) and Uji *et al.* (1990), the new case is described by:

$$\frac{\partial C}{\partial t} = D(t)\frac{\partial^2 C}{\partial x}, \qquad x > 0,\ t \geq t_{ex} \tag{2.38}$$

$$C(0,t) = C_s(t), \qquad t \geq t_{ex} \tag{2.39}$$

$$C(x,t_{ex}) = C_i, \qquad x > 0 \tag{2.40}$$

This model of time-dependent surface chloride concentration and diffusion chloride coefficient was numerically solved by Mejlbro (1996). Considerable developments have taken place in numerical analysis and in the construction of efficient computer programmes to obtain numerical solutions (Crank, 1975).

The numerical models (Petcherdchoo, 2013; Lin *et al*., 2010) have illustrated influential ability in solving the partial differential diffusion equations numerically (in space as boundary-condition values and in time as an initial value). They are not only considering the time-dependent parameters of $C_s(t)$ and $D_a(t)$.

The solution of Fick's Second Law, as illustrated in Equations 2.38-2.40 with any time dependence of the surface chloride concentration and the diffusion coefficients may easily be solved numerically. There are some numerical methods used to find a numerical solution by finite difference approaches such as the Crank-Nicolson, explicit method and implicit method.

2.6 Corrosion Rate in Concrete Structures

2.6.1 Introduction

Corrosion rate represents the most significant factor on corrosion operation of a reinforcing bar that affects structures safety and treatment process. The corrosion rate varies depending greatly on the diffusing reactants, including chloride, oxygen, carbon dioxide and the moisture at the surrounding concrete of the reinforcing bar surface. Environmental factors such as temperature, relative humidity and pH of the concrete will also affect the rate of corrosion (Broomfield, 2007). Corrosion reaction in zones of a concrete member will likely occur at different rates and times, depending upon variations

in environmental exposure and electrochemical interaction between the regions (Katwan, 1988).

2.6.2 Mechanism and Effect of Corrosion of Steel Reinforcement in Concrete Structures

Chloride attack is a major factor affecting the initiation period of corrosion, in which the reinforcement is in a passive state, but this phenomenon can lead to loss of passivity of reinforcement. The presence of reinforcement steel bar embedded in concrete with high alkalinity of pores solution (pH 12-13) creates the passive protective film (PPF) spontaneously. This film, which is self-generated soon after the hydration of cement has started.It consists of γ-Fe2O3 tightly adhering to the steel. PPF is a thin and dense oxide film, not exceeding a few nanometers thick (Broomfield, 2007; Neville, 2011). It protects the steel surface from corrosion because it slows down its oxidation rate and the chloride ions and carbonation are destroyed PPF (Bertolini *et al*., 2013). The microstructure and permeation properties of concrete play a vital role in penetrating the chloride ions and carbon dioxide to initiate corrosion of steel in concrete (Dyer, 2014; Wang *et al*., 2016). The chloride ions transport to the location of preferential gathering and later by adaptable the flux of ions out and in of the pit (Silva, 2013).

The corrosion is an electrochemical or chemical interaction between steel and its environment (Revie and Uhlig, 2008). The chloride generates corrosion in three stages. The depassivation happens when the chloride ions concentration dissolved in the pore water in the surrounding environment with the steel achieves a threshold value. There are many different threshold values reported. Reported threshold values are high and it is not always clear for which reason or which is the major reason regarding a specific threshold value for a given concrete structure or part of the structure (Angst and Vennesland, 2008). According to Angst *et al*. (2009) the chloride threshold value ranges between 0.04 % and 8.34% by weight of cement. That is a wide range of chloride concentration. The first step, chloride ions penetrate and break down the depassivation of steel in concrete as the pH of the pore water of concrete falls lower than 11(Broomfield, 2007; Neville and Brook, 2010). This phase of corrosion is called ‘Corrosion Initiation stage’. Where chloride ions initiate the depassivation of steel in concrete.

Pre- corrosion of the reinforcement stage involves the corrosion initiation and absorption of the chlorides. Whilst, the third stage is in post corrosion stage. The hydroxyl ions work with chlorides to interact with ferrous ions with appearance of corrosion products when chloride concentration exceeds 0.6 of hydroxyl ions (Broomfield, 2007). Then, the formation of ferric chloride compound spreads away from the surface of steel propagating the PPF breakdown. This phase of corrosion is called 'Corrosion Propagation stage'. The chlorides also form a significant factor in the second phase which is corrosion propagation that begins when the steel is depassivated (Bertolini *et al*., 2013). These stages are shown in Figure 2.17.

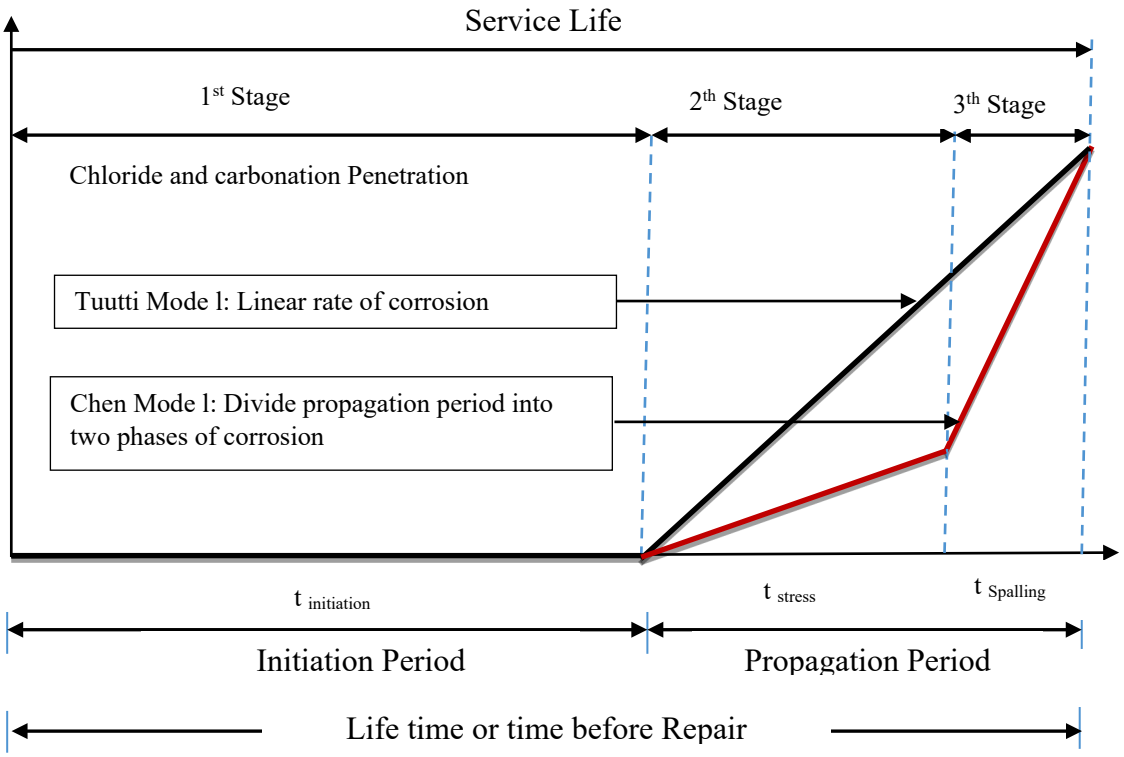

Figure 2.17: Modified chloride –induced corrosion models (Tuutti, 1982; Chen and Mahadevan, 2008)

Recently, some researchers have used a variety of experimental techniques which propose the concept of critical chloride content (chloride threshold level for corrosion of steel in concrete). Some evidence has been investigated indicating that the hydroxyl ions concentrations affect this critical chloride content. Venu *et al*. (1964) cited in (Angst *et al*., 2009) has suggested the [Cl^-/OH^-] form an express critical chloride threshold. The [Cl^-/OH^-] ratio has usually been considered to be a more common and reliable indicator than chloride concentration alone, it is apparently not a constant value and is often

considered as the most accurate way to express a critical chloride threshold (Angst *et al*., 2009).

The passive layer around reinforcement in concrete starts to dissolve, as soon as, corrosion begins to appear on rebar surface. The same chemical reaction can be noticed in chloride and carbonation corrosion, where anodes crumble in pore water solution and impart electrons (Broomfield, 2007):

$$Fe \rightarrow 2Fe^{2+} + 2e^{-} \quad (2.41)$$

The electrons produced from anodes will be consumed in order to continue the electrical process. In another words, it cannot receive a high electricity charge when it is in the same portion of the re-bar. So, another process, the cathodic reaction will occur and consume water and oxygen as shown in Equation 2.42 and Figure 2.18- a:

$$2e^{-} + H_2O + \frac{1}{2}O_2 \rightarrow 2OH^{-} \quad (2.42)$$

The (OH^{-}) ions are created in cathodic reaction. Oxygen and water are required at the cathode for the corrosion process to occur. The OH^{-} ions raise the local pH, and successively steel passivity at the cathode. Figure (2.18- a) and the Equations 2.43 - 2.45 are represented by the reactions of hydroxyl (OH^{-}) ions with ferrous (Fe^{2+}) characterizing the initial step in the corrosion process (Broomfield, 2007).

$$Fe^{2+} + 2OH^{-} \rightarrow Fe(OH)_2 \quad (2.43)$$

$$2Fe(OH)_2 + O_2 + H_2O \rightarrow 4Fe(OH)_3 \quad (2.44)$$

$$2Fe(OH)_3 \rightarrow Fe_2O_3.2H_2O \quad (2.45)$$

Ferrous hydroxide, $Fe(OH)_2$ will be produced from this reaction, then it will react still with oxygen and water to form ferric hydroxide ($Fe(OH)_3$). The last component becomes hydrated (rust) again by reacting with oxygen and water. Graphically, Figure (2.18-b) illustrates these reactions (El-Reedy, 2008).

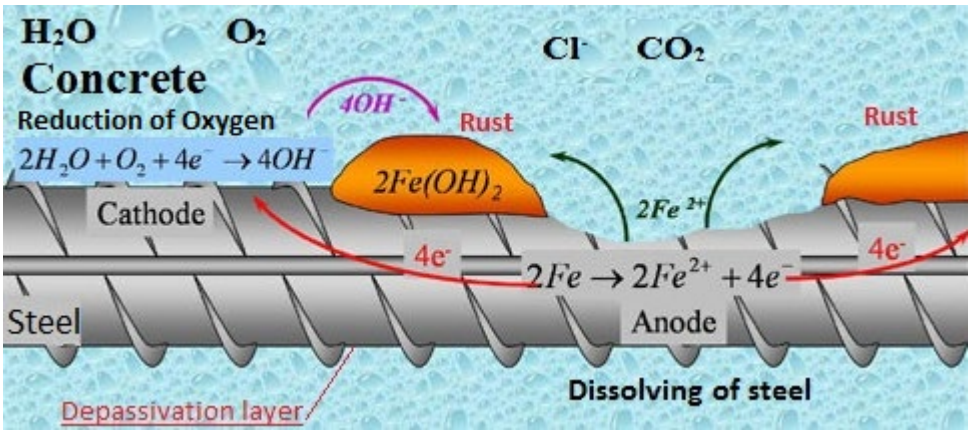

(a)

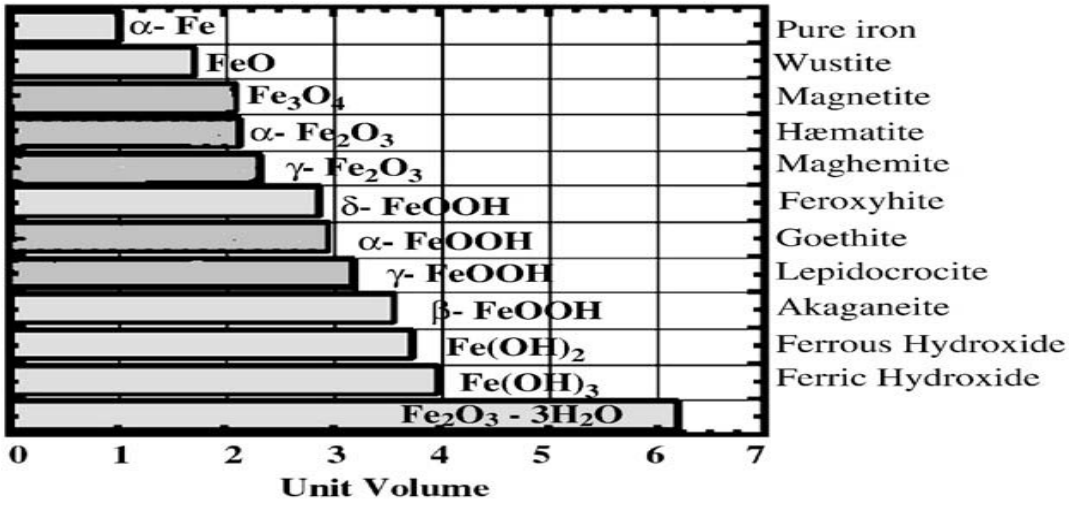

(b)

Figure 2.18: (a) Corrosion mechanism of reinforcement in concrete (Broomfield, 2007), (b) Volume increment produced by corrosion of steel (Yu and Bull , 2006)

As stated previously that, as the corrosion process continues, the volume of corrosion products in steel bar increases by up to 2 to 6 times the original metal volume, depending on the oxidation level (Broomfield, 2007). Therefore, these volumetric increments in steel reinforcement in concrete structures will produce internal stress in concrete when they have exceeded the tensile strength of the concrete, cracking will occur. Such cracking will start from the reinforcement to the nearest surface, and a direct path is created for further ingress of chloride, oxygen and water to the steel surface.

As further amounts of corrosion products accumulate, the crack will evolve into a delaminating or spalling, resulting in the effective or actual loss of concrete cover, and leaving the steel directly exposed to the source of reactants, the environment (Brown, 1999) as shown in Figure 2.19.

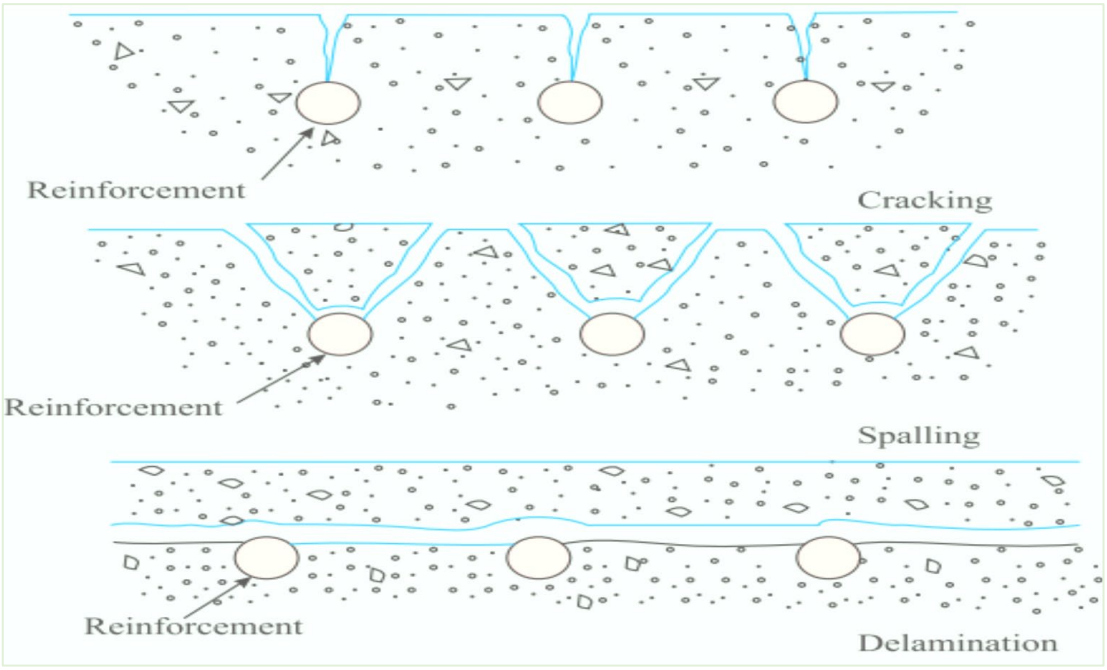

Figure 2.19: Corrosion damage on cracking spalling concrete structures (Shetty, 2005; Neville, 2011)

The precise mechanism by which depassivation occurs is still a subject of contention (ACI 222R: 2001). Either the chloride ions convert the insoluble iron- oxide to soluble iron- chloride which diffuses away and destroys the passive film, or the chloride ions are absorbed on the metal surface and promote the hydration and dissolution of metal ions (Katwan, 1988).

Although, the microstructure of the concrete-steel interface and the surface finish of the steel are generally identified as affecting the initiation of corrosion. No systematic analysis has been carried out concerning the distributions of chloride at the pit location and their relationship with the chloride content in the surrounding concrete (Ahlstron, 2013).

The corrosion in steel bar is likely to reduce the mechanical strength of the reinforcing steel bar as well as a decrease in load carrying capacity of concrete structures totally (Bertolini *et al*., 2013). Moreover, the bond strength between steel bar and concrete tends to decline according to the corrosion level (Bilcik and Holly, 2013; Zhao and Lin, 2018). The decrease in bond strength is likely to start when corrosion level exceeds 1.74% (Elbusaefi, 2014).

2.6.3 Factors Affecting Corrosion Rate in Reinforced Concrete Structures

Once a sufficient amount of aggressive agents have reached the steel reinforcing bars to depassivate the bars and initiate corrosion, factors influencing the corrosion rate of steel reinforcing bars embedded in concrete are included in Equation 2.46 (Markeset and Myrdal, 2008):

$$V_{corr} = f\left(T, F_{O2}, RH, C_{cl}, PH, \gamma, F_{galv}, F_{oxide}\right) \quad (2.46)$$

where:

V_{corr} is the corrosion rate, T is temperature, F_{O2} is a supply of oxygen to the pore water in contact with the cathodic area of the steel surface, RH is the relative humidity in the concrete pores (or the degree of pore water saturation), C_{Cl} is the concentration of dissolved chloride ions in the pore water in contact with the anodic areas of the steel surface, pH is the alkalinity, or the concentration of OH^- ions in the pore water in contact with the steel surface, γ is the electrical resistivity of the concrete, F_{galv} is the galvanic interactions between different parts of the steel reinforcement and F_{oxide} is the effect of oxide (rust) layer formation on corrosion rate.

The factors associated with climate change and concrete micro-structure will be reviewed only because of relationship to the objectives of the study as follows:

Firstly, the temperature is an important factor affecting corrosion stages. According to Živca (2003); Stewart *et al*., (2011), the increase in temperature may influence corrosion rate, indirectly by increasing the carbonate ions penetration and chloride ions diffusion due to decreases in the pH and the amount of bound chloride respectively (Tuutti, 1982) (as mentioned in previous reports). In addition, it has significant impacts on concrete resistivity (Liu and Weyers, 1998). A higher temperature causes the resistivity to reduce and vice versa (for a constant relative humidity) (Broomfield, 2007). This is caused by changes in the ions' mobility in the pore solution and by changes in the ion-solid interaction in the cement paste (Bertolini *et al*., 2013). It also affects the RH in the concrete, lowering it when temperature increases and therefore introducing an opposite effect.

These events occur at the pre corrosion stage and achieve an appropriate environment for next stage of corrosion. Moreover, increases in temperature raise corrosion rate directly. The rate of the oxidation reaction is affected by the amount of heat energy available to drive the reaction (Broomfield, 2007). Berke (2006) claimed that the reaction rate is doubled for each 10°C rise in temperature. Also, Živica (2002) studied the significance and influence of the ambient temperature as a rate factor of steel reinforcement corrosion in cement mortar samples. The effects of ambient temperature on the rate of chloride-induced corrosion were: (i) acceleration of the rate when the ambient temperature increased to about 40 °C, and (ii) inhibition of the rate when the ambient temperature is increased over the given value of the temperature. The main reason for reduction of the corrosion rate is caused by insufficiency of oxygen (the oxygen solubility decreases with rising temperature) (Markeset and Myrdal, 2008; Neville, 2011).

Secondly, the relative humidity (RH) or moisture content is a significant factor affecting the corrosion rate of reinforced concrete structures. The concrete has different kinds of pores according to its type and state. These pores are partially filled with water, depending on contacted materials such as water or soil (groundwater) in addition to the moisture in the environment. So, the water filled pores tend to transform to carbonate ion, chloride ion and oxygen in concrete. Consequently, the steel is exposed to high relative humidity; the corrosion rate may be lower because of decreased transportation rate of oxygen (Broomfield, 2007). Conversely, totally dry concrete cannot corrode due to the absence of water. However, highly water saturated structures can corrode rapidly without signs of cracking. This is due to the limited amount of oxygen available as the iron ions (Fe^{2+}) stays in solution without forming solid rust that expands and cracks the concrete (Broomfield, 2007). There is an argument as to which is the optimum relative humidity that causes a higher corrosion rate. Ahlstron (2013) found the 97% RH gave the highest corrosion rate of steel in cement mortar. On the other hand, Tuutti (1982) indicated that the 95% of RH provided the highest rate of corrosion. Whilst, Neville and Brooks (2010) claimed that the 70 to 80 % is the optimum percentage of RH which creates the higher corrosion rate.

A full analysis of the corrosion process showed that the decrease of oxygen content and water in the pores of the corroding system (concrete – steel), is a result of the above two effects. Also, there is disagreement in which is the optimum percentage RH

leading to a higher corrosion rate. Then, there are the other parameters that may affect corrosion rate besides that of relative humidity that controls the optimum percentage RH. The moisture content in the pore water solution in concrete has a significant impact on the resistivity of concrete. Where, the higher moisture content beside higher ionic strength due to dissolve the salts (e.g. Cl^-) leads to reduce the resistivity of concrete, increase the migration ions and development of corrosion pits (Markeset and Myrdal, 2008). Also, the cathode/anode area ratio may become very large.

Thirdly, the microstructure and permeation properties of concrete play a vital role on pitting corrosion of steel at an early stage of depassivation, the permeability is the property that manages the flow rate of a fluid (liquids and gases) into a porous solid. It depends essentially on the water-cement ratio, mineral additives and cement type. The chloride ions transport to the location of preferential gathering and later by adapting the flux of ions out of and into the pit (Silva, 2013). Elbusaefi (2014) demonstrated that the permeability of concrete directly influences the corrosion rate, the concretes have lower permeability, create a lower corrosion rate. The concretes that contain fly ash have lower permeability values and rate of corrosion compared with other mixes at the same water-cement ratio. He reported the reduction in the permeability of paste within the concrete was the main reason for these results.

In existing concrete structures, micro-cracks already exist due to the inevitable differences in mechanical properties between the coarse aggregate and the hydrated cement paste, coupled with shrinkage or thermal movement (Neville, 2011). Some other cracks develop when concrete is exposed to environmental gradients or service loads (Montes *et al*., 2004). Cracks can be induced in concrete by the load, volumetric change due to the plastic settlement, high curing temperature, various types of shrinkage, creep, and deteriorating mechanisms such as frost and alkali-aggregate reaction (Jacobsen *et al*.,1998). Cracks may reduce the corrosion initiation time by providing a preferential path for the penetration of carbonation or chlorides at first stage and develop to the propagation of corrosion at second stage. Experiments with section steel bars in intentionally cracked concrete beams have shown that the depassivation time decreases as the crack width increases (Schiessl and Raupach, 1997).On the other hand, the generally accepted mechanism whereby reinforcement corrosion occurs at concrete cracks involves a macro-cell where steel is exposed at the crack tip and immediately

becomes an anode and actively corrodes once the critical chloride concentration is exceeded here with the adjacent passive rebar serving as a cathode for oxygen reduction (Hartt, 2009). .

Schiessl and Raupach (1997); Otieno *et al.* (2009) performed corrosion studies on mechanically cracked concrete specimens. They observed that, while corrosion initiated the wider the crack sooner and concluded that the microstructure of concrete cover was "much more" important and sensitive in controlling corrosion of steel at cracks than was the crack width. Quero and Garcia (2010) reported that the effect of crack width for ordinary Portland cement concrete, in w/c ratios ranging between 0.3 and 0.4 is significant on corrosion; however, the existence of cracking for 0.5 and 0.6 w/c ratios is less important because the effect of an increase of permeability of concrete due to an increase w/c ratios (Otieno *et al*., 2008).

Finally, the casting of concrete in hot weather and lower relative humidity such as in Iraq accelerates the hydration of cement and decreases setting time as well as the lower long-term strength of concrete due to the slowing down of hydration of cement happening at an early time. Consequently, the drying shrinkage takes place faster because the tensile strength of concrete is unable to resist the stresses owing to shrinkage and restraint of concrete (Neville and Brooks, 2010). As a result, the shrinkage cracking will be induced in concrete surfaces. Increase in crack width and length permits the chloride to penetrate and diffuse more speedily in concrete. Thus, the chloride ingress, oxygen and water are on the surface of the steel and tend to cause a quicker initiation and propagation of corrosion of reinforcing rebar steel (Sosdean *et al*., 2014). This is an example of the severity of the climate condition in Iraq and its effect on the performance of concrete particularly in penetration of chloride and carbon dioxide and causing corrosion.

In summary, temperature, relative humidity microstructure of concrete and presence of cracks affect corrosion initiation and propagation in reinforced concrete structures. Many researchers have studied these parameters separately. There is no studies in literature has investigated these parameters together and the existing concrete structures are actually affected by combined effects of these parameters. In addition, similar research is very limited and almost non- existent in Iraq and does not consider the risk of the issue of the service life of concrete structures. This proposal will investigate the effect of climate change parameters (change in CO_2 concentration, temperature and

relative humidity) on corrosion rate for concrete samples cracked under service load. Secondly, these data will be used to construct and calibrate a model to predict the corrosion rate in existing concrete structures.

2.6.4 Monitoring and Testing of Corrosion in Reinforced Concrete Structures

Numerous methods are employed for observing the corrosion process in concrete structures according to corrosion stages, including: visual inspection involving delamination surveys and cracking; spalling survey; measurement of carbonation depth ;determination chloride ions ,Cl^- content; measurement of the depth of concrete cover; corrosion rate tests; measuring the loss of steel cross-section; testing of resistivity of concrete and relative humidity of concrete; determination of concrete pH and corrosion product; and drawing the map of corrosion potential (ACI 222.3R: 2003). While, the opportunity of a corrosion reaction happening can be forecast theoretically because the kinetics of this reaction in the particle, the rate of its progress, due to its nature, is less foreseeable and can only be found empirically.

Several monitoring techniques have been utilized in order to help in the prediction or assessment of the corrosion process on a structures in-situ. These techniques can be classified into four comprehensive sets which are (Kutwan, 1988):

- Use of coupons of specific material.
- Analytical measurements.
- Electrical Resistance Method.
- Electrochemical Techniques.

2.6.4.1 Use of Coupons

This method includes employing coupons of known weight, made of the materials which the corrosion rate is to be measured, for a period of time in the corrosive environment, these coupons are then removed, cleaned of the rust product and re-weighed. The difference in weight is computed and employed into appropriate units of corrosion. This method gives the average of corrosion over exposure time rather than the instantaneous corrosion rate.

If the differences in rate are wanted, it is necessary to use numerous coupons and eliminate them at steady intervals (Feitler, 1970). Using one sample irregularly removed

for weight change readings often influences the subsequent corrosion rate upon re-exposure to the environment (Stern and Weisert, 1959).

This method is comparatively simple and cheap but generally needs considerable time to get data. This is mainly so when studying extremely low rates (Bandy, 1980) in which case large sample sizes or long exposure times should be used to get reasonable accuracy (Kutwan,1988).

2.6.4.2 Analytical Measurements

This method depends on the chemical analysis of the surrounding solution by measuring the metal ion concentration created by the rusting metal. Other factors which can affect the corrosion process such as temperature, pH and oxygen concentration may also be checked as a part of the overall monitoring method. This method also presents problems (Chandler, 1985) mainly when rust products are insoluble or when the rate changes obviously with time (Stern and Weisert, 1959). Generally, this method is not adequately sensitive and is only applicable to specific conditions, as it is unlikely to be completely quantitative (Kutwan, 1988).

2.6.4.3 Electrical Resistance Method

This method depends on the principle that the electrical resistance of metal may change directly with the change in its cross-sectional area. In this method based on the resistance of the probe, it contains a strip or wire of the metal being checked, which is measured by the specific electrical circuit and then converted into penetration parts. The principles of operation of this method are based on the electrical resistance of an alloy element or metal (R_m) is given by:

$$R_m = r.\frac{l}{A_c} \qquad (2.47)$$

where:

l is the element length, A_c is the cross-sectional area and r is the specific resistance of metal

Temperature compensation for combined into the probe by protected from the environment resistance change is a reference electrode. This method may be used in any

environment and is able to make continuous readings. It has been commonly (Chandler,1985) employed in multi-stage flash distillation plants and oil-refineries. The main inadequacy (Stern and Weisert, 1957) in the application of this method, however, is that it is only quantitative if the corrosion process creates a very uniform attack.

Electrical Resistance of Portland cement concrete is affected by many factors such as moisture, chloride and sulfate contamination (Saleem *et al*., 1996). There are numerous authors such as Browne (1982); Hussain *et al*., (1995) who have proposed a relationship between electrical resistivity and corrosion rate as follows in Table 2.5.

Table 2.5: Corrosion risk based on resistivity Browne (1982)

Resistivity (Ohm.cm^2)	Corrosion Risk
> 20000	Negligible
10000-20000	Low
5000-10000	High
< 5000	Very high

2.6.4.4 Electrochemical Methods

Many electrochemical and non-destructive techniques have been developed for monitoring corrosion rate of reinforcement steel in concrete structures. Rebar corrosion on existing concrete structures can be assessed by different techniques (Song and Saraswathy, 2007). Three of the most used techniques which have been utilized for monitoring in this research are described below.

a. Open circuit potential (OCP) or Half-cell potential measurements.

b. Tafel extrapolation

c. Linear polarization resistance (LPR) measurement

a. Corrosion Potential (Half Cell Potential)

Half-cell potential is a widely accepted non-destructive technique, a simple and practical test which can be employed to get large amounts of data regarding the corrosion activity of the bridge deck (Babaei, 1986). It is also used to predict the corrosion of reinforcement steel in a concrete structure qualitatively (Kim *et al.*, 2014). The principle involved in this technique is essentially a measurement of corrosion potential of rebar with respect to a standard reference electrode (half-cell) and reinforcement steel

embedded in concrete (half-cell). There are many types of a standard reference electrode such as copper/copper sulfate electrode (CSE), saturated calomel electrode (SCE), silver/ silver chloride electrode, etc. When active corrosion is present, current flows through the concrete between the anodic and cathodic locations due to the migration of ions, and this current is accompanied by an electrical potential field surrounding the corroding rebar.

Also, once the used metals for the half-cell electrodes such as (silver, mercury, or copper) have a more positive standard potential than iron, the external electrode will be the cathode in the circuit (Mancio *et al*., 2005) as shown Figure 2.20. So, if the bar is corroded, the excess electrons in the bar will tend to flow from this rebar (anode) to the half-cell (cathode). Because of the way the terminals of the voltmeter are connected, the voltmeter shows a negative voltage. A more negative voltage reading is interpreted to mean that the embedded bars have more excess electrons and, therefore, there is a higher probability that the bar is corroding (Mancio *et al*., 2005). According to ASTM C 876-15 standard, Table 2.6 illustrates the likelihood of reinforcement corrosion according to half-cell potential measurements for SCE and CSE (Song and Saraswathy, 2007).

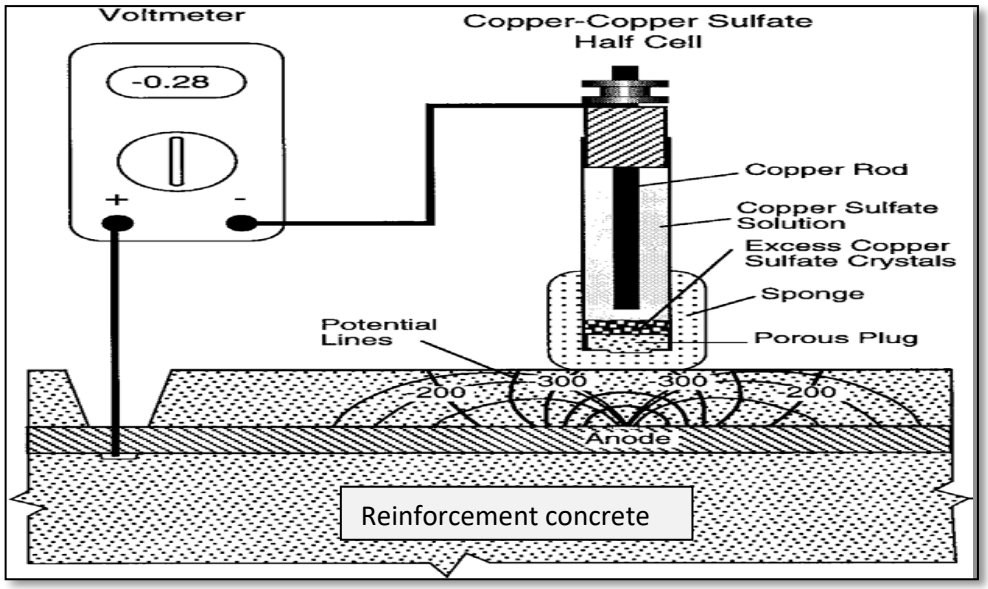

Figure 2.20: Schematic of Half-cell potential measurement (Mancio *et al*., 2005)

Table 2.6: Probability of Corrosion condition according to half-cell potential (HCP) measurements (Song and Saraswathy, 2007)

Half-Cell Potential measurements		Corrosion Activity
Copper-copper sulfate electrode, CSE ,mV	Saturated calomel electrode, SCE, ,mV	
> - 200	> -125	Low (10 %) risk of corrosion
-200 to 350	- 125 to - 275	Intermediate corrosion risk
< - 350	< -276	High (< 90%) risk of corrosion
< - 500	< - 426	Severe corrosion

b. Extrapolation Method or Tafel plot Tp

This method is called full polarization technique, it includes polarising the electrodes whose corrosion rate is tested both anodically and cathodically for comparatively high over-potentials and simultaneously finding the current (Fontana, 2005). The extrapolation of the linear region of the isolated cathodic and anodic plots to the potential of corrosion ought to provide a common value of the corrosion current which may be adapted to corrosion rate by using Faraday's Law (Kutwan, 1988).

In addition, the slopes of the linear regions of the plots give the values of the anodic and cathodic Tafel constants, B_a and B_c as shown in an idealized Tafel plot in Figure 2.21. The main difference between these two methods is that the change in potential must be kept to less than ± 25 mV for the LPR technique, while the change of potential can go up to ± 250 mV for the *Tp* technique (Song and Saraswathy, 2007). The basic apparatus utilized is shown in Figure 2.22(Mancio *et al*., 2005).

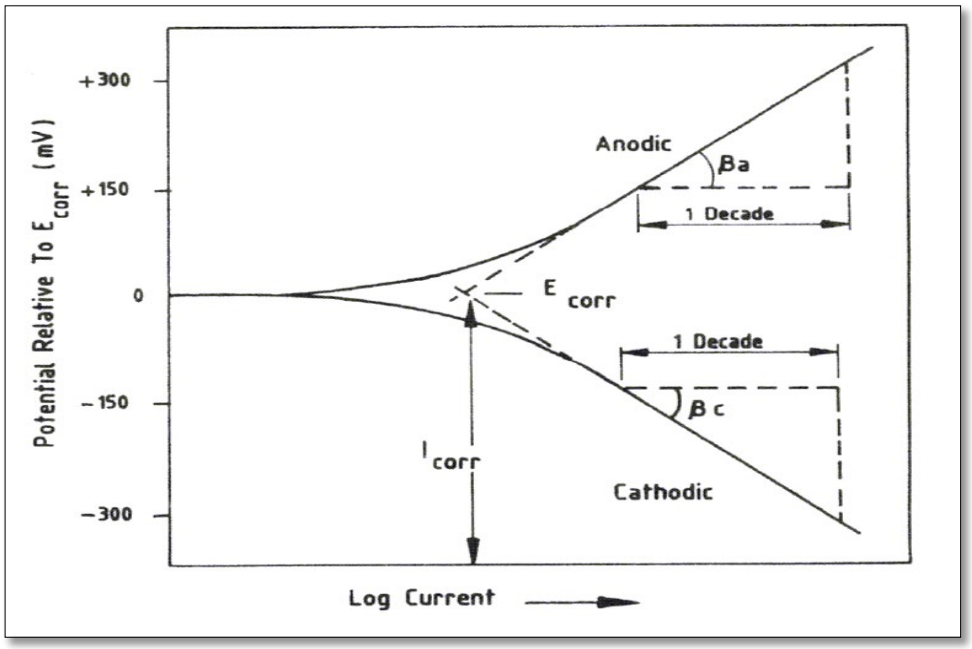

Figure 2.21: Idealized Tafel plot (Al-Tayyib and Khan,1988)

The readings can be determined either potentio - dynamically with an appropriate sweep rate, which is frequently employed for high to moderate corrosion rate systems or potentio-statically where the potential is supplied in steps and the system permitted to give the equilibrium at each step before the current is gauged. This method is more suitable for systems corroding at low corrosion rate such as passivated steel state in reinforcement steel in concrete. The main limitations of this technique are, firstly: the supplied current is usually several times the current of corrosion and thus the nature of the surface may alter considerably, particularly during polarizating the anodic with subsequent alteration in the rate of corrosion. Secondly, in certain systems the linear Tafel behaviour cannot be achieved because of the influences of concentration polarization and resistance (Bandy, 1980). Thirdly, the simple devices are such that they can be slow to operate but more importantly they do not define the area of measurement accurately (Grantham, 2003)

Some guidelines have been proposed to establish a relationship between corrosion current density and corrosion state, as listed in Table 2.7 (Mancio *et al*., 2005).

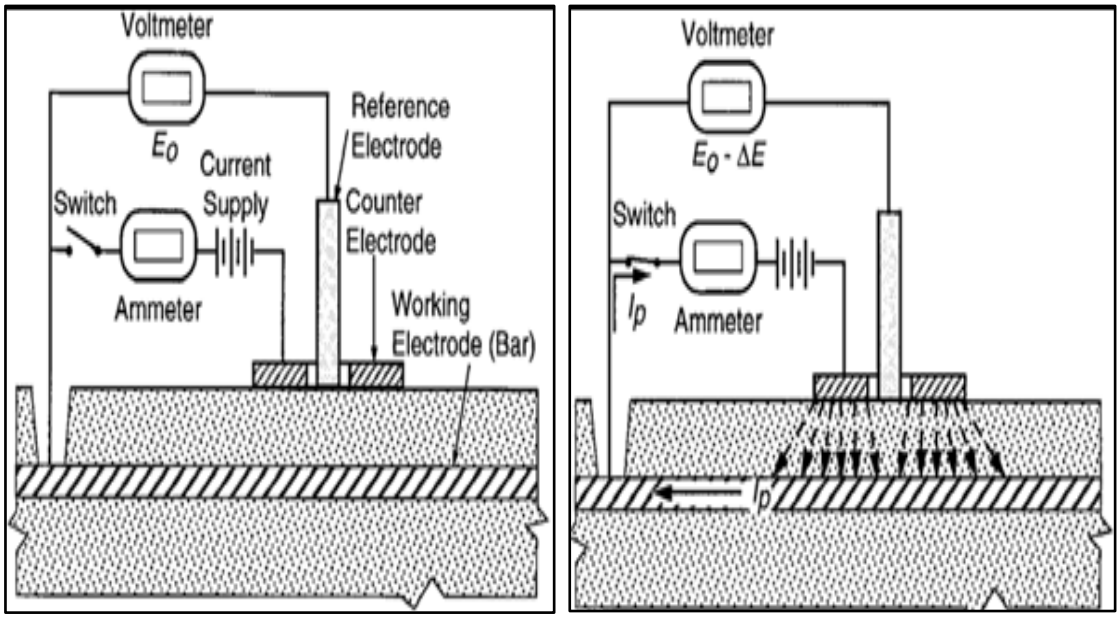

(a)Measurement of the open-circuit potential (half-cell potential)

(b) Current applied to the counter electrode to produce a small change in voltage ΔE

Figure 2.22: Three- electrode Linear Polarization Resistance method (Mancio *et al*., 2005).

Table 2.7: Relationship between corrosion current and corrosion state (Song and Saraswathy, 2007)

Corrosion current density (μA/cm^2) *	Corrosion state
< 0.1	Negligible
0.1 – 0.5	Low
0.5 – 1.0	Moderate
> 1.0	High

*Measurements made with a guard electrode device.

c. Linear Polarization Resistance (LPR)

This method is based on perturbing a small amount from its equilibrium potential. This can be achieved potentiostatically by altering the potential of the reinforcement steel by applying a fixed amount of potential, *ΔE*, and checking the current decay, *ΔI*, after a specific time. Alternatively, it may be done galvanostatically by supplying a small constant current, *ΔI*, to the reinforcement steel and checking the potential change, ΔE, after a specific time as shown in Figure 2.23. In each case, the conditions are designated such that the alteration in potential, *ΔE* reduces within the linear Stern–Geary range of 10–30 mV.

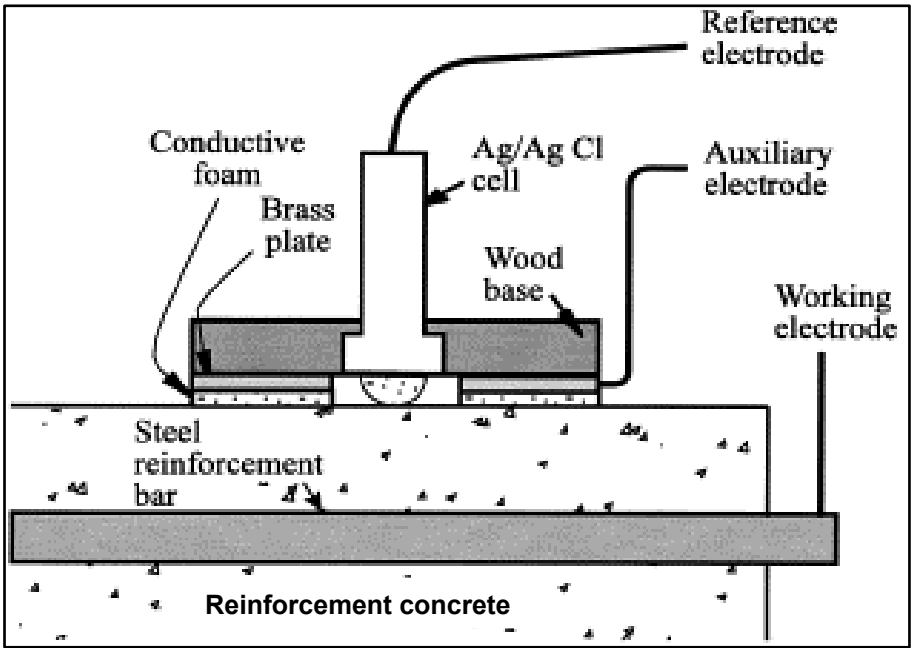

Figure 2.23: Schematic of Linear polarization resistance techniques (Mancio *et al*., 2005)

The linear polarization resistance, Rp, of the steel is then computed by Equation 2.48 as shown in Figure 2.24:

$$R_P = \frac{\Delta E}{\Delta I} \tag{2.48}$$

From which the corrosion current, I_{corr}, can then be computed.

$$I_{corr} = \frac{B}{R_P} \tag{2.49}$$

where:

B is the Stern–Geary constant.

Although many studies in the literature apply 26 mV as the B value, a more recent study indicates that calculating this value from the measured E_{corr} values can provide better estimates and better correlations with weight loss measurements (Trejo *et al*., 2008; Kutwan, 1988).

$$B = \frac{Ba*Bc}{2.3(Ba+Bc)} \tag{2.50}$$

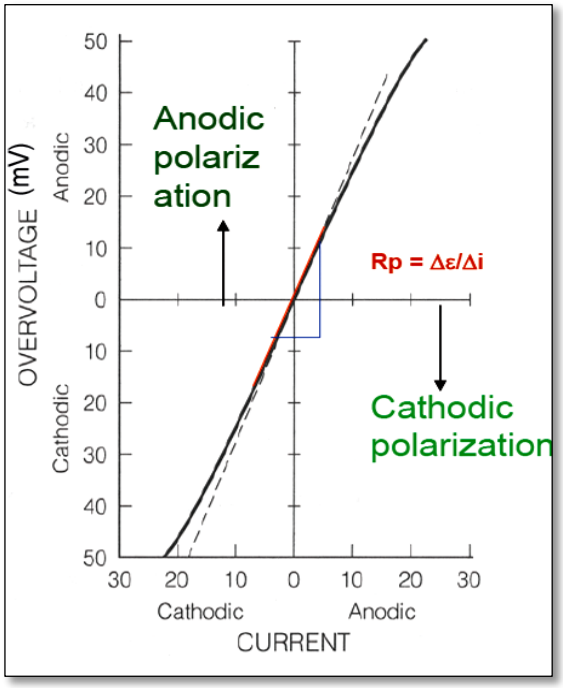

Figure 2.24 :Linear polarization resistance plot

In order to determine the corrosion current density, i_{corr}, the surface area of steel bars (A_s) that has been polarized needs to be accurately known:

$$i_{corr} = \frac{I_{corr}}{A_s} \qquad (2.51)$$

In Equation 2.50, *Ba* and *Bc* are the anodic and the cathodic Tafel constants, respectively, expressed in mV/decade of the current. It is seen here that for the determination of I_{corr} in this technique, *Ba* and *Bc* are prerequisites that are determined from the Tafel plot (Al-Tayyib and Khan, 1988).

The current density values are converted to corrosion rate, r, using Faraday's Law as shown in Equation 2.52 (Kutwan, 1988).

$$Corrosion\ Rate(r) = \frac{i_{corr}\, M}{ZFD} \qquad (2.52)$$

where:

M is the atomic weight, (for iron=55.84), *Z* is the number of ion equivalents exchanged, (for iron=2), *F* is the Faraday's constant (96500 amp-sec/equivalent), and *D* is the density of metal(for iron 7.87 gm/cm^3)

Equation 2.52 becomes Equation 2.53 when appropriate values are substituted for atomic weight, equivalence number, Faraday's constant, and the density of the metal as follows:

$$Corrosion\ Rate\ (r) = \propto i_{corr} \qquad (2.53)$$

where

r = corrosion rate in μm/yr

$\propto$ { 11.59 For conventional reinforcement; 14.98 For galvanized reinforcement

i_{corr} = current density in μA/cm^2.

Finally, Table 2.8 is presented to summarize noticeable differences between the corrosion- monitoring techniques used throughout this research, which are based on a literature survey.

Table 2.8: Summarized characteristics of corrosion monitoring techniques (Song and Saraswathy, 2007)

Criteria	Corrosion monitoring technique	
	Half-cell technique	Polarization measurement (Tafel plot and linear polarization resistance)
Simplicity (equipment required and method of the test)	Simple	Difficult and complicated
Measurement Parameter	Probability of corrosion	Indicative of corrosion rate
Cost	Not expensive	Expensive
Field versus laboratory application	Field and laboratory	Field and laboratory
Limitations	-Not applicable to epoxy coated bars -Not indicative of corrosion rate	Testing and interpretation must be done by experienced personnel
Advantages	It can be used for continuous monitoring without disturbing the sample	It is possible to measure extremely low corrosion rates

2.6.5 Modelling of Corrosion Rate in Reinforced Concrete Structures

Numerous models have been proposed for predicting the onset and the rate of corrosion of steel reinforcement in concrete exposed to chlorides and carbonation. Maruya *et al*. (2003) refer to three types of approaches used in modelling the corrosion rate in the propagation period:

2.6.5.1 Models Based on Electrochemistry

It is well known that the corrosion rate may vary with time. Accordingly, a penetration attack function, $P(t)$, representing the loss of rebar diameter at time t, has been developed (DuraCrete, 2000):

$$P(t) = \int_{t_i}^{t} V\,(\tau\,)d\tau \qquad (2.54)$$

By using Faraday's law of electrochemical equivalence, the corrosion rate in terms of the amount of steel dissolving and forming hydroxide/oxide may be calculated from the electric current:

$$m_i = \frac{i*t*a_i}{n*F} \qquad (2.55)$$

where:

m_i is the mass of iron per area dissolved at the anode (g/m^2), i is the electric current density (A/m^2), t is the time (s), a_i is the atomic mass of iron (55.8 g/mol), n is the number of electrons liberated in the anodic reaction (2)and F is the Faraday's constant (96487 As/mol). Assuming the mass density of iron to be 7.87 kg/dm^3 and the Faraday's law can be expressed as:

$$V_{corr} = 11.6 i_{corr} \qquad (2.56)$$

where:

V_{corr} is the corrosion rate (μm/year) and i_{corr} is the corrosion current density ($\mu A/cm^2$).

In other words, a corrosion current density of 1 $\mu A/cm^2$ corresponds to 11.6μm steel section losses per year.

2.6.5.2 Models Related to a Diffusion-Limited Access of Oxygen

This type deals with the modelling of the cathodic reaction that is one of the main mechanisms of steel rebar corrosion. This model takes into account oxygen reduction and oxygen diffusion through a diffusion barrier (iron oxide and/or carbonated concrete) as a function of water saturation degree (Huet *et al.*, 2007).

This model is dependent on the limiting current density and may be calculated by combining Faraday's Law (electrochemistry) and Fick's First Law of diffusion (mass transport):

$$\frac{i}{n.F} = -D_{O2}\left[\frac{dC^*_{O2}}{dx}\right] \qquad (2.57)$$

where:

i is the cathodic current density (μA/cm2), n is the number of electrons transferred in the cathodic reaction (=4), F is the Faraday's constant (96487 A s/mole), D_{O2} is the efficient diffusion coefficient of O_2 in concrete (m^2/s), C^*_{O2} is the concentration of O_2 (mole/m^3) and x is the distance (m).

(Huet *et al*., 2007) modified this model in Equation 2.59 shown as.

$$i_{O2} = \frac{C^*_{O2}}{\left\{\left(\frac{1}{k_{O2}} + \frac{d_c}{D_{O2}}\right)\right\}} \qquad (2.58)$$

where:

k_{O2} is the kinetic constant of oxygen reduction depending on several parameters like porosity and diffusion coefficient, d_c is the concrete cover, and i_{O2} is the oxygen diffusion path.

2.6.5.3 Models in the Form of Empirical Relations

For example, these models based on electrical resistivity of the concrete. Corrosion rates may also be predicted using empirical models. One basic approach to empirical modelling has been proposed by (DuraCrete, 2000):

$$V_{Corr} = \frac{m_o}{\gamma(t)} * F_{Cl} * F_{Galv} * F_{O2} * F_{oxide} \qquad (2.59)$$

where:

m_o is the factor given by the corrosion rate versus electrical resistivity; γ is the electrical resistivity of the concrete; the factors F_{Cl}, F_{galv}, F_{O2} and F_{oxide} are the chloride corrosion rate factor, the galvanic effect factor, the oxygen availability factor and the oxide (rust) factor respectively.

Also, Liu and Weyers (1998) suggested an empirical model incorporating (Temperature, Ohmic resistance, Chloride content and Exposure time). In this model based on experimental works, the following non-linear regression model was found:

$$ln\,1.08\,V_{corr} = 7.89 + 0.7771ln1.69C_{cl} - \frac{3006}{T} - 0.000116R_{co} + 2.24\,t^{-0.215} \quad (2.60)$$

where:

V_{corr} is corrosion rate ($\mu A/cm^2$), C_{Cl} is chloride content (kg/m3 concrete), T is the temperature at the depth of steel surface (Kelvin), R_{CO} is ohmic resistance of the concrete cover and t is the time since the start of corrosion (years).

2.7 Concluding Remarks

In summary, the main key to climate change phenomenon is the increase of the greenhouse gases (GHG) in terms of CO_2 emissions, it is the major contributor to global warming in the world. The most prominent impacts of the increase the (GHG) emissions are that the ocean and atmosphere have warmed; amounts of ice and snow are reduced, there is a decrease in relative humidity, as well as a rise in sea level.

The durability of existing concrete structures in terms of carbonation depth, chloride penetration and corrosion rate of concrete structure is depending considerably on internal factors (microstructures of concrete and crack) and external environmental conditions, CO_2 concentration, temperature and humidity.

The key mechanisms for the durability of concrete structures in this study are carbonation, chloride penetration and corrosion of steel embedded in concrete. Chloride and carbonic ions inducing corrosion in reinforced concrete structures are the leading phenomenon for the deterioration in many countries such as the UK and Iraq.

Most of the predictive models available for carbonation and chloride penetration are based on Fick's laws. These laws have been most commonly employed in practice to forecast the initiation of corrosion in concrete structures whereas its propagation is constructed on basic corrosion section loss relationships.

Finally, this study is for existing concrete structures. These structures are already loaded and cracked. There is a need to explore a new knowledge by investigating the effect of temperature on chloride penetration, chlorides binding in the concrete structures cracked under service loads. Secondly, it should demonstrate an accurate relationship between diffusion coefficients of chloride and width of cracks in concrete cracked under loads. Thirdly; it should also consider the effect of carbonation in concrete with chloride penetration and diffusion. Furthermore, the combined impact of carbonation and dissolved chloride on corrosion rates will be investigated. Fourthly, improve an integrated model for the diffusion coefficient of chloride and CO_2 to account for the global climate change parameters as well as the effect of (presence of cracks) on chloride concentration profile and carbonation depth respectively.

Chapter III: Methodology and Experimental Programme

3.1 Introduction

In this Chapter, the methodology of the study and the experimental programmes are described and presented to achieve the expected objectives of the study. Methodology of study involves, the parts for investigation (carbonation, chloride penetration and corrosion rate), environmental exposure conditions, specimen design and environmental exposure conditions of specimens tested in the experimental work. While, the experimental programme covers the properties of materials used in the study, concrete mixture design, types of specimens and their design, selection of environmental exposure conditions and types of tests that were carried out in the study.

The main aims of the experimental programme of study are to investigate the impacts of climate parameters on characteristics of the durability of concrete structures, in particular the effect of increased temperature and concentration of carbon dioxide, and the decrease in relative humidity, on carbonation, chloride penetration and rate of corrosion. After the concrete had been cast and cured; compressive strength, splitting tensile strength and flexural strength tests were conducted in order to find the respective properties of the concrete. Consequently, carbonation depth, chloride penetration depth, and corrosion rate were also studied, and tests carried out using different methods to create a database to verify and support modelling and simulation work.

3.2 Methodology

In this study, carbonation, chloride penetration and rate of corrosion were investigated. These properties have a significant impact on the durability of concrete structures. The outline of the methodology and experimental programme of the study are listed in Figure 3.1 and the aims and the main objectives of this study are also presented as well. Accordingly, the design of samples used in the test and the exposure environmental conditions were considered and described in the following sections.

3.2.1 Environmental Exposure Conditions of Study

This study focuses on concrete structures in two different countries, the UK and Iraq. The meteorological data, temperature, the relative humidity for the UK and Iraq cities are the major factors of current weather. The Met office and Iraqi meteorological organization and Seismology supplied the data for the main cities of the UK and Iraq respectively, as shown in Figure 3.2. The prediction of climate change data in the UK and Iraq cities are dependent on IPCC-2014 and UKCP'09 scenarios.

The data of temperature and relative humidity of major places in the UK and Iraq in the last ten years from beginning of this study, 2004-2014 which is shown in Figures. 3.3 to 3.8) were considered in the design of the environmental exposure conditions of experimental and modelling works. The range of the average temperature and humidity during this period was 1 to 47.5 ºC and 17.7to 90 % respectively. According to the IPCC-2014 scenario, the carbon dioxide concentrations may be expected to rise from 400 ppm to 1000 ppm in the year 2100. On the other hand, IPCC-2014 and UKCP'09 scenarios projections of climate change in the change in temperature (T), CO_2, and relative humidity (RH) are considered in the experimental and the modelling programmes as shown in Table 3.1.

Table 3.1: IPCC-2014 and UKCP'09 (2010) scenarios projections of climate change in the change in T, CO_2, and RH in the UK and Iraq

Case	Maximum temperature change (°C)	Relative humidity change (%)	CO_2 Concentration ppm
UK	2.9 (1.3 - 4.5) for north of UK * 4.5 (2.0 -7.1) for south of UK*	9 (20-0) *	1000**
Iraq	4.3(2.8 -5.75) **	No information	1000**

* This data is from UKCP'09 (2010)

** This data is from IPCC-2014

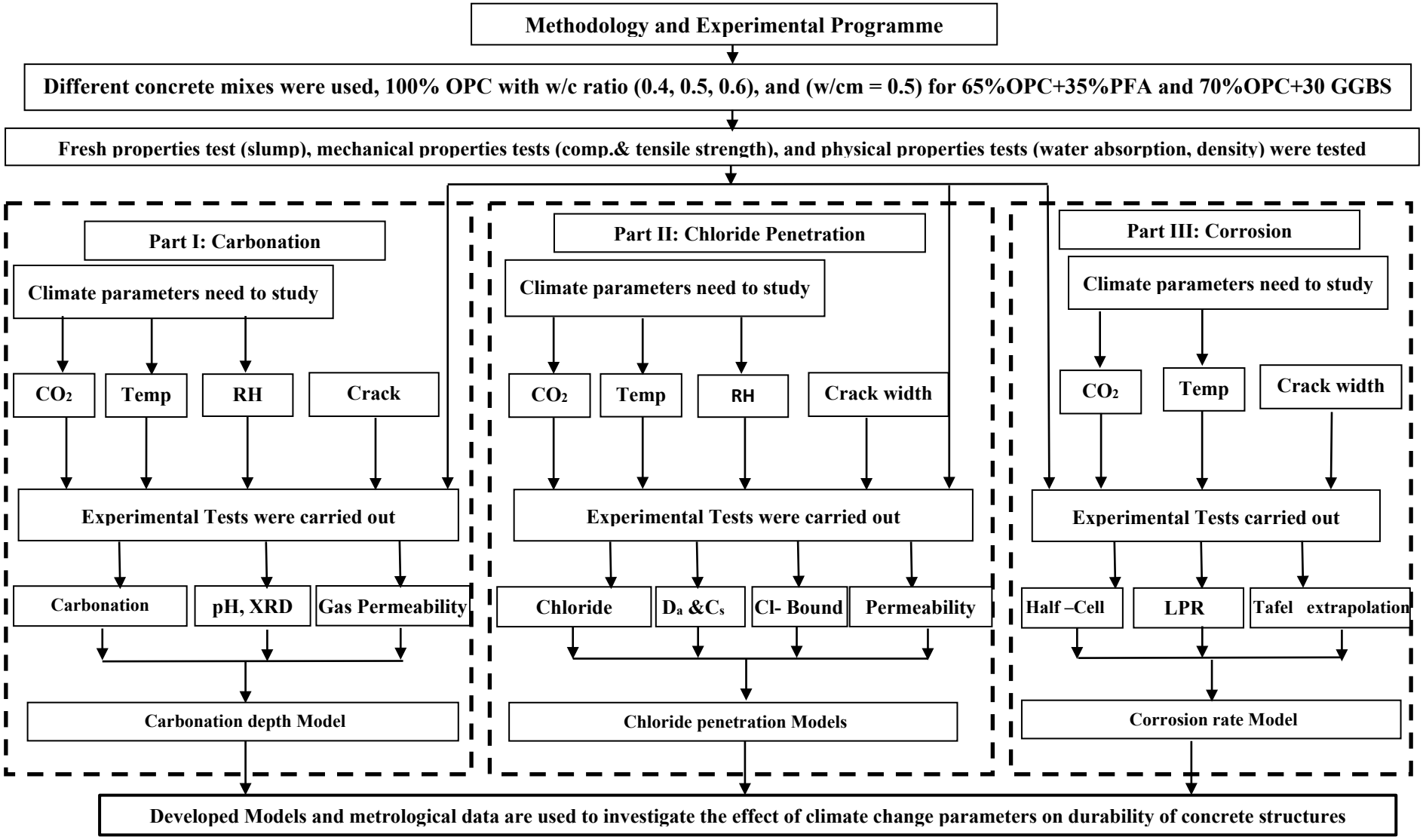

Figure 3.1: Schematic of Methodology and Experimental Programme of Study

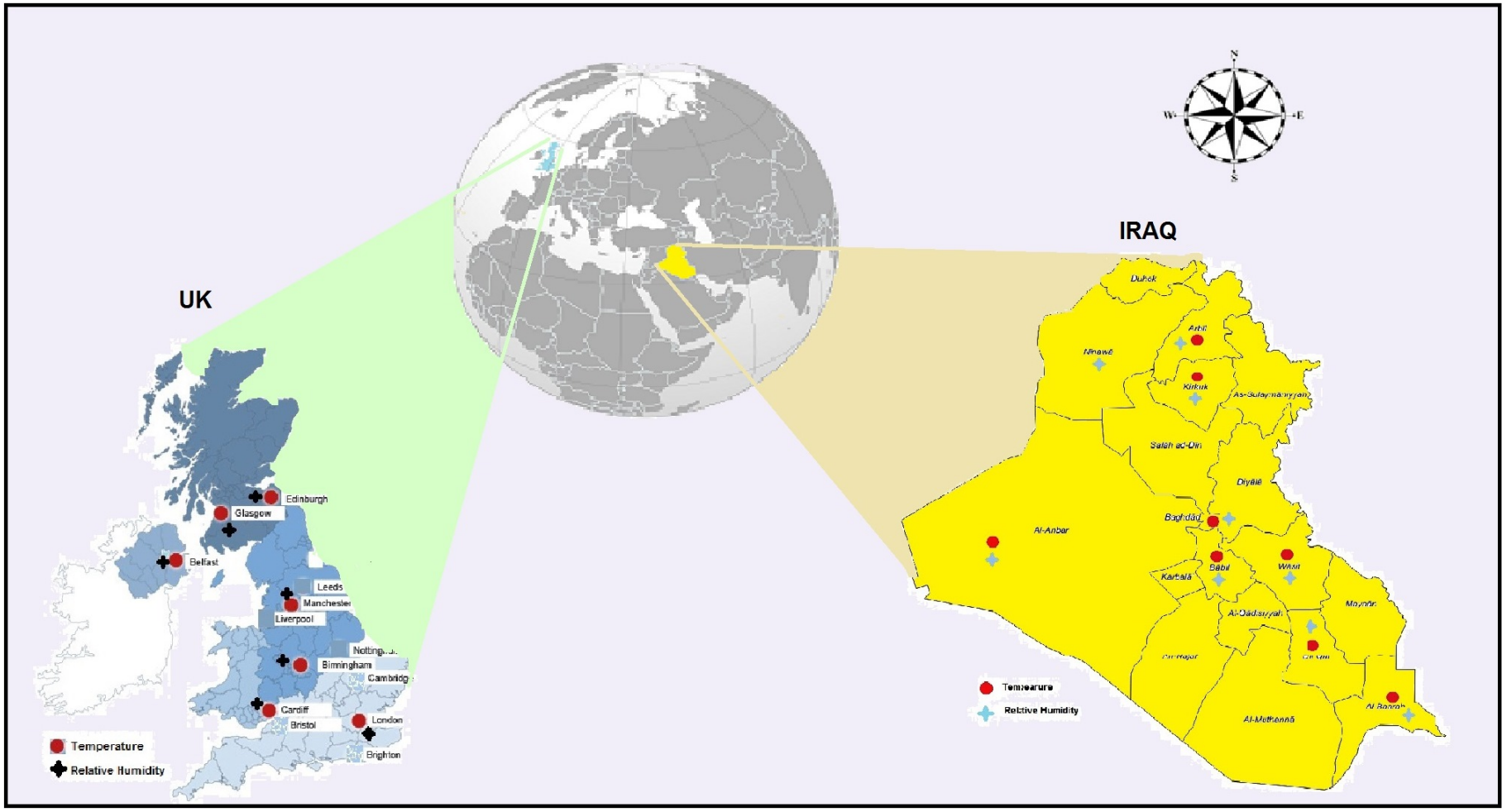

Figure 3.2: Schematic representation of the main cities in the UK and Iraq, where the temperature and relative humidity were measured

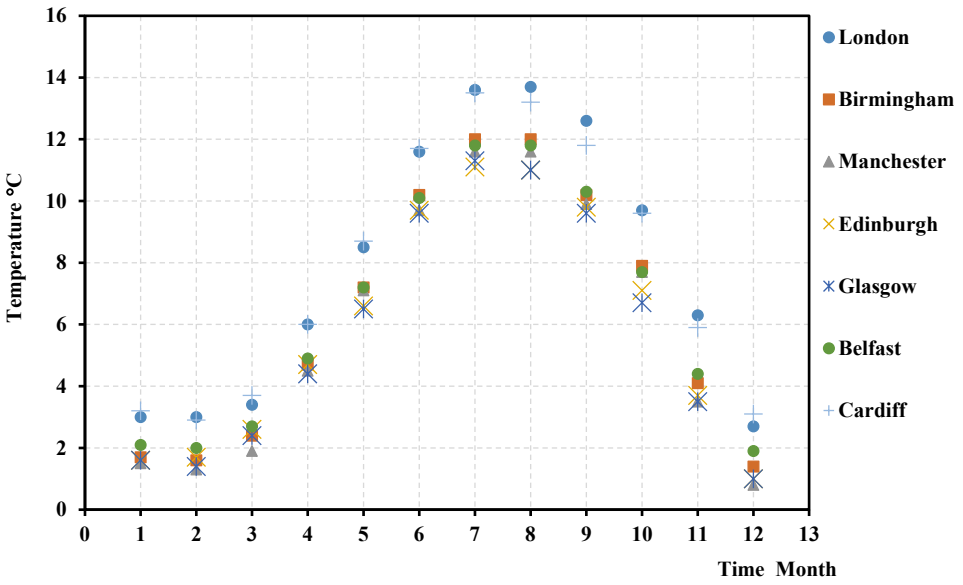

Figure 3.3: Mean minimum temperature throughout a year in the main cities of the UK during period (2004-2014)

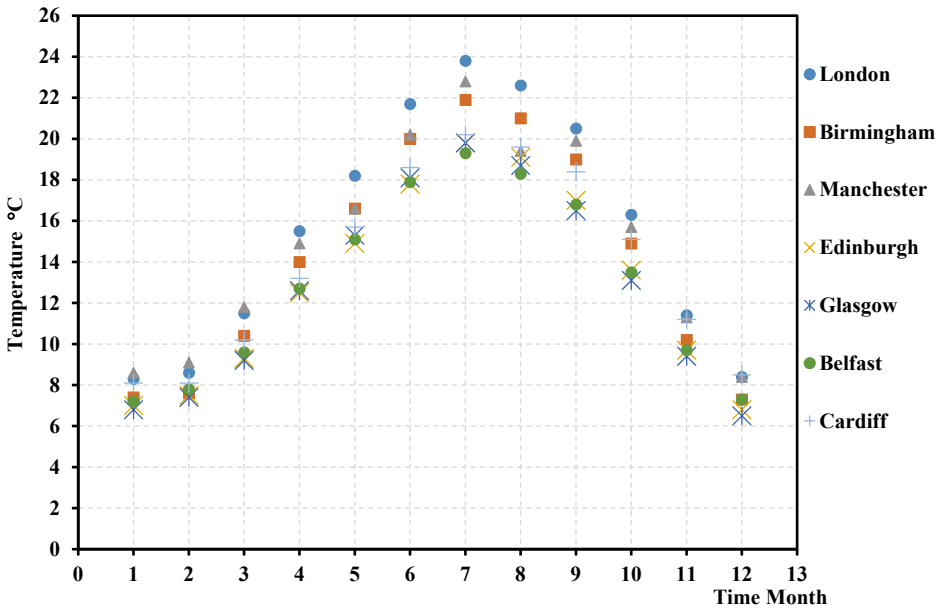

Figure 3.4: Mean maximum temperature throughout a year in the main cities of the UK during period (2004-2014)

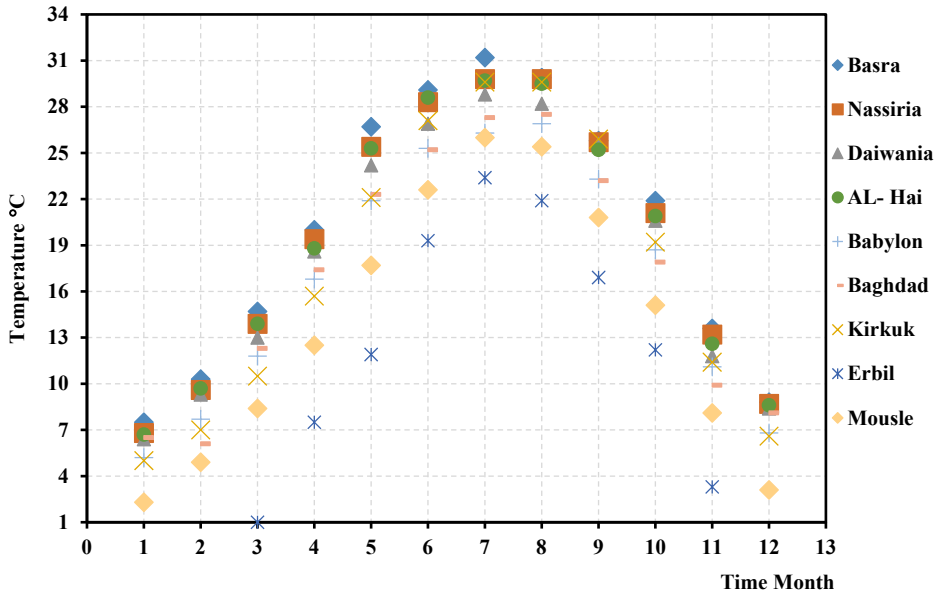

Figure 3.5: Mean minimum temperature throughout a year in the main cities of Iraq for period (2004-2014)

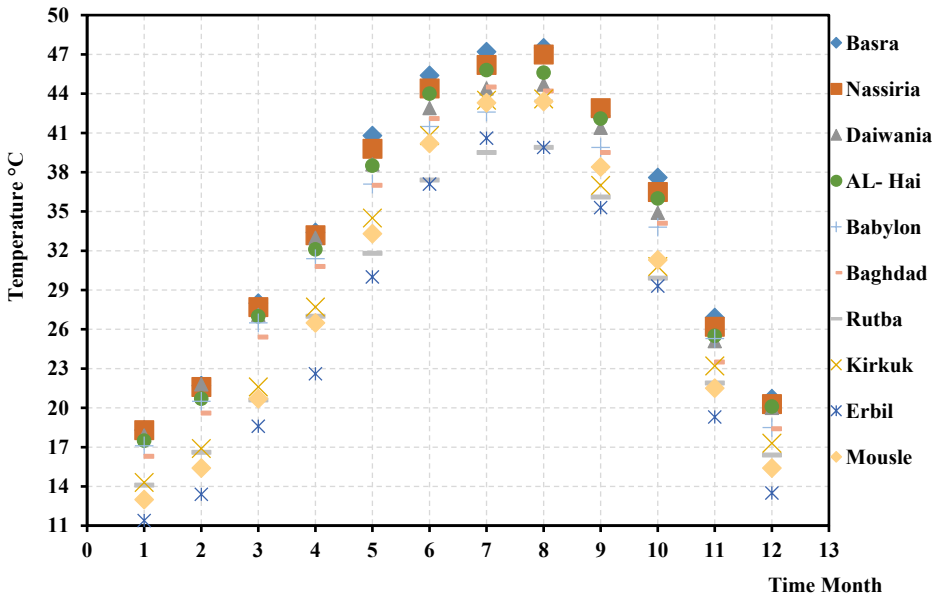

Figure 3.6: Mean maximum temperature throughout a year in the main cities of Iraq for period (2004-2014)

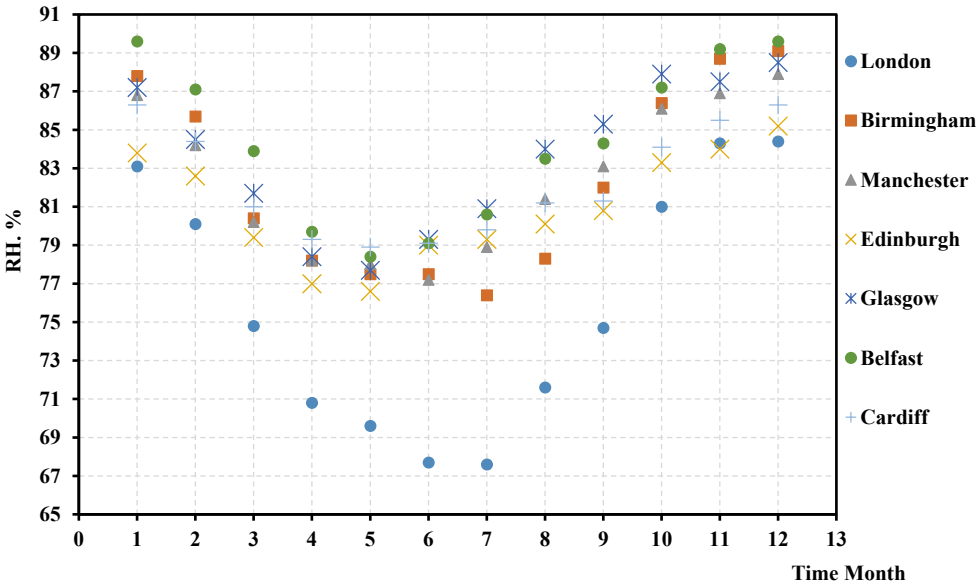

Figure 3.7: Mean Relative Humidity throughout a year in the main cities of the UK during period (2004-2014)

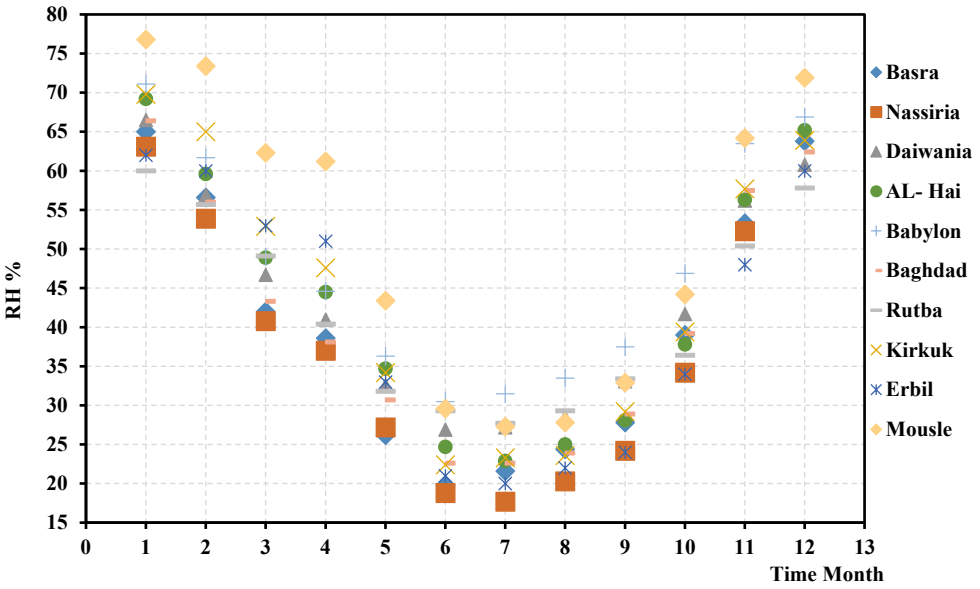

Figure 3.8: Mean Relative Humidity throughout a year in the main cities of Iraq for period (2004-2014)

3.2.3 Specimens Conditioning

The main objectives of the present study are to investigate the impact of the climate parameters on carbonation and chloride penetration and the corrosion rate of cracked concrete structures. Therefore, the cracked concrete specimens were designed and exposed to these parameters. There are three different methods that can be used to induce the cracks in concrete samples. This can be done by a flexural test, a notch tips method or by a splitting test as shown in Figure 3.9 (a, b and c). The first and second method were used in the investigation of carbonation depth, chloride penetration and corrosion rate according to the status and requirements of these tests.

In this study, the flexural method was used to induce the cracks in concrete prisms with the dimensions of 100*100*500 mm as shown in Figure (3.9- a). Deformed steel bars (8mm diameter) at a cover depth of 2 cm was used to reinforce the concrete prisms (see Figure 3.10) to induce the major cracks and achieve the controlled crack width within the samples and to investigate the corrosion. The depth of cover (2 cm) has been considered according to calculation of design of reinforced prism to create the crack. In addition to the control samples (no cracks), three different crack width ranges, (0.05-0.15mm, 0.15-0.25mm and 0.25-0.35mm) were examined. The crack width was measured by a microscope meter with an accuracy of 0.01 mm, and the crack depth, D_{crack} was computed by measuring the time of transfer of pulse velocity for the ultrasonic devices (see section 3.3.4.4). In Figures 3.11 and 3.12, the measuring methods for crack width and crack depth are illustrated respectively.

For the second method, notch tips, cubic or plain concrete prisms with specific plate thickness (0.1mm,0.25mm, and 0.35mm) were used and cut by a core machine with the required width and depth as shown in Figure (3.9- b). Using the last method (see Figure (3.9- c)), splitting of the cylinder or cube, it is difficult to create the cracks with specific width because the concrete is brittle and the failure may occur suddenly with no control on crack width and depth.

a: Flexural method for cracking in the prism samples

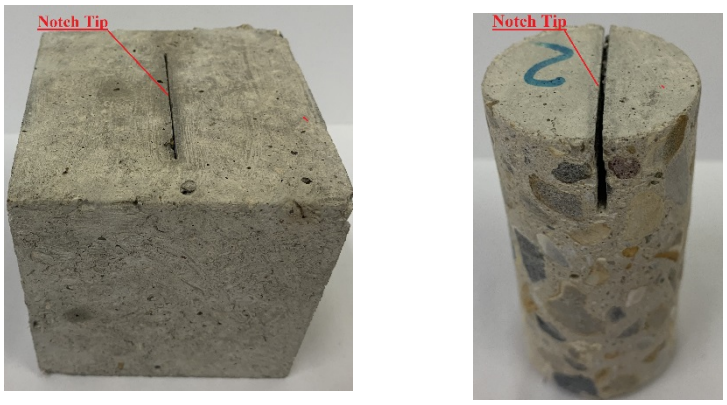

b: The notch tips method

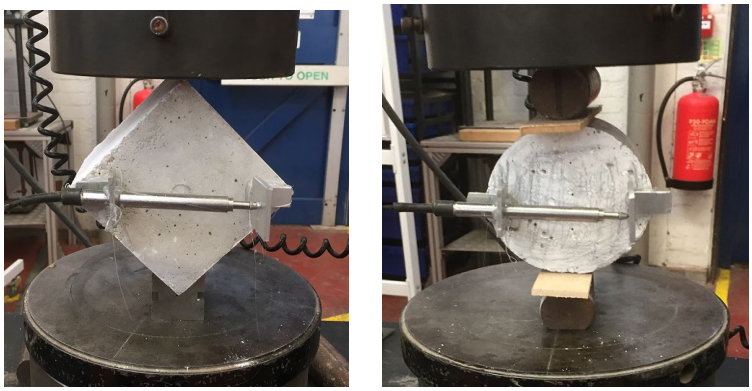

c: The crack by splitting test

Figure 3.9: Method of creating the crack in a concrete sample

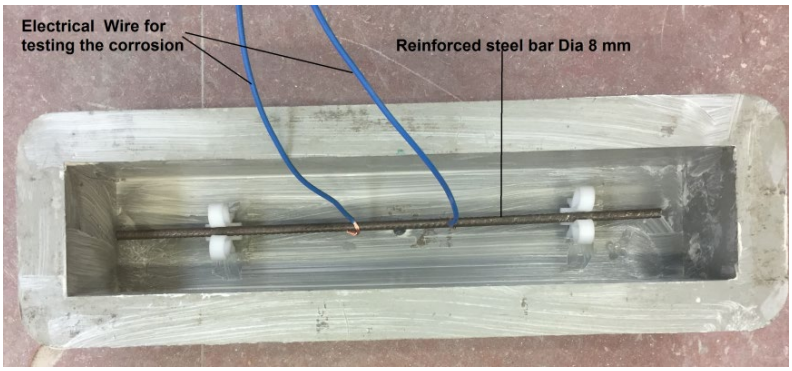

Figure 3.10: Mould with a steel bar for casting reinforced concrete prism

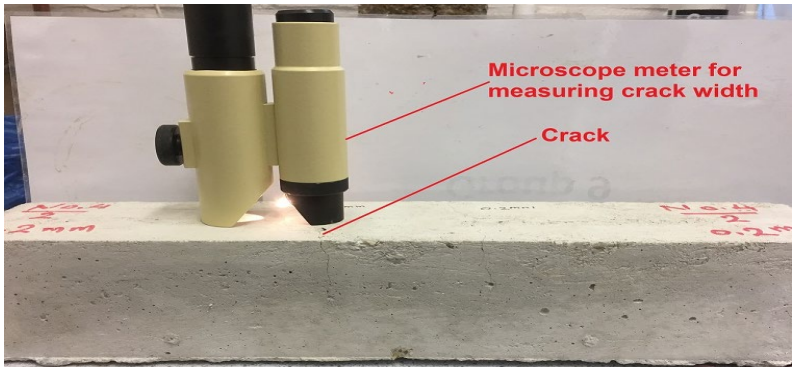

Figure 3.11: Measuring the width of the crack by microscope meter

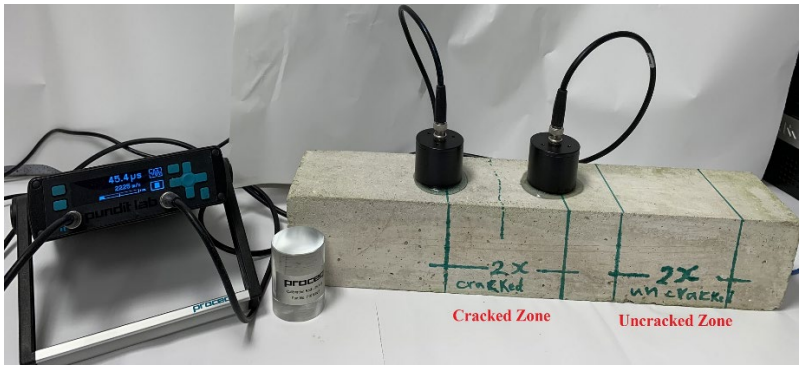

Figure 3.12: Measuring the crack depth by pulse velocity of the ultrasonic devices

3.2.4 Environmental Exposure Conditions of Experimental Test

Specimens were exposed to two conditions:

(i) Main factors of recent climate and forecasted climate conditions for the UK and Iraq cities are presented in Figures 3.3 to 3.8 and in Tables 3.1 according to the meteorological data from the UK and Iraq.

(ii) Type of the target test.

The environmental exposure conditions of the sample consisted of two cases:

3.2.4.1 Carbonation Part (I)

The main factors for part I are the; temperatures (1 to 47.5 ºC), degree of humidity (17.7-90 %) (Met office (UK) and meteorological organization and Seismology (Iraq)) and the carbon dioxide concentrations (400 - 1000 ppm) (IPCC, 2014). This data has been considered with respect to the environmental exposure conditions of the experimental work which were simulated to be as accurate as possible with equipment and time were available. An accelerated environmental test programme of CO_2 environment has been used on concrete samples by utilizing a carbon dioxide incubator (see Figure 3.13) to minimize the time and simulate the CO_2 exposure conditions (Russell *et al*., 2002; Talukdar *et al.,* 2012 a). Temperature and relative humidity were also considered in the experimental and modelling works.

Figure 3.13: The exposure conditions CO_2 concentration, temperature and relative humidity was considered in the incubator

Three scenarios of environmental exposure conditions of the specimen were utilized in this part of study to investigate the impact of the external factors such as CO_2, temperature(T), and relative humidity (RH) and internal parameters, properties of

concrete and crack width on the depth of carbonation, DoC. For external factors, three levels for T, RH and CO_2 have been utilized to simulate these influences on DoC. For example, three concentration of CO_2 ,1.5%,3% and 5%, and temperature and humidity 25 °C and 65% respectively are listed in Scenario a. The DoC was tested for three samples in each case, after 8 weeks of CO_2 exposure (Roy *et al*., 2000; Russell *et al*., 2002). The scenarios of environmental exposure conditions of this part are presented in Table 3.2 (simulating the effect of climate change).

Table 3.2: Scenario of environmental exposure conditions of part I of the experimental programme

Scenarios	Series No.	Environmental exposure condition			Duration of exposure (weeks)
		CO_2 (%)	Temperature (°C)	Humidity (%)	
Scenario a	7	1.5	25	65	8
	6	3	25	65	8
	5	5	25	65	8
Scenario b	5	5	25	65	8
	3	5	35	65	8
	1	5	45	65	8
Scenario c	5	5	25	65	8
	4	5	25	75	8
	2	5	25	85	8

The experimental programme was built in order to study the effect of changing one factor while keeping other factors constant in order to investigate these changes in predicting some relationship to use in the modelling work. On the other hand, the DoC is the reflection of CO_2 penetration in concrete and change in the mineralogical structures and alkalinity of concrete (McPolin *et al*., 2007). Consequently, the DoC can be used in predicting the risk of CO_2 penetration by initiating the corrosion of the steel bar in reinforced concrete structures and determining the service life of reinforced concrete structures.

In the experimental work of this part, the carbonation depth was measured using different methods. Phenolphthalein indicator is used to measure fully carbonated depth,

X_p. Whilst, the apparent pH and consumed OH^- and intensities of crystalline phases of $Ca(OH)_2$ and $CaCO_3$ by using XRD are used to find the carbonation front depth, X_f. The last two methods, this profile of consumed OH^- and relative intensities of crystalline phases of $Ca(OH)_2$ and $CaCO_3$ can be used to divide the conditioned samples into three zones based on the consumption of $[OH^-]$ ions and relative intensities of $Ca(OH)_2$: fully carbonated, partially carbonated and non-carbonated zones. Where, X_p is the boundary between the fully carbonated and partially carbonated zone. X_f is the boundary between the partially carbonated and non-carbonated zone (indicating the carbonation front) (McPolin *et al*., 2007; Chang and Chen, 2006).

3.2.4.2 Chloride Penetration Part (II) and Corrosion Part (III)

Cyclic corrosion test chamber (CCT) was utilized to simulate the exposure conditions of these parts in particular chloride concentration and temperature. An accelerated environmental test programme of chloride environment was applied by using cycles of wetting and drying to measure the chloride penetration and corrosion rate. Cyclic chloride spraying, aeration, and drying were applied to accelerate the chloride penetration. This is because the chloride can be quickly permeated the concrete to initiate the corrosion (Broomfield, 2007). Three temperature levels were used to investigate the influence of the temperature on chloride penetration and corrosion rate (simulating the effect of climate change). The duration of the cycle of wetting (spraying), aeration and drying was set as shown in Figure 3.14. For a period of 360 minutes, a solution with NaCl of 5% content was sprayed for wetting phase; the content then went through 20 minutes of aeration, and the drying time took a further 340 minutes. The chamber and reinforced concrete prisms are illustrated in Figure 3.15.

Two scenarios of environmental exposure conditions of the specimen were utilized in these parts of the project in order to study the influence of the external factors of CO_2, temperature and internal factors, properties of concrete and crack width on the depth of chloride penetration (McPolin *et al*., 2005) and corrosion rate (Bertolini *et al.*, 2013). For external factors, three levels of temperature (20ºC,30 ºC, and 40ºC) and one series was exposed to a cycle of (chloride-CO_2- chloride) environmental condition, were used (see Table 3.3) to simulate the effect of temperature and carbonation on chloride penetration and corrosion rate. These chloride exposure conditions included the maximum temperatures in Iraq and the UK cities, simulated to be as accurate as possible

using the equipment available. The chloride penetration and corrosion rate were investigated for three samples in each case, after 15 weeks of chloride exposure (Song *et al*., 2008; Chalee *et al*., 2009). These scenarios of environmental exposure conditions of these parts are presented in Table 3.3.

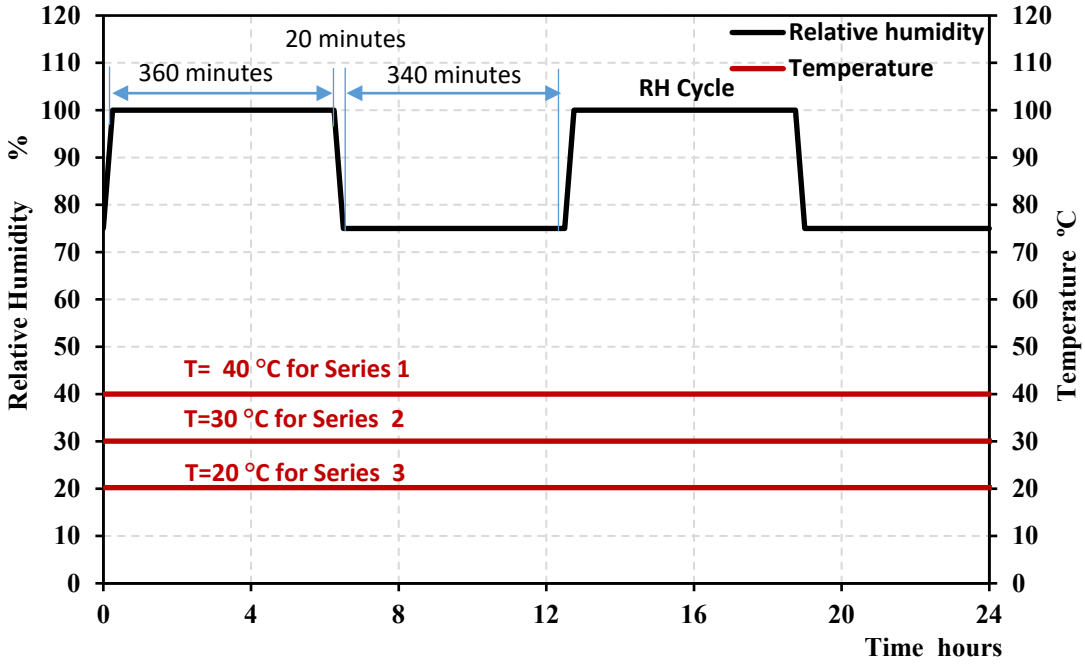

Figure 3.14: Cyclic wetting, aeration, and drying for chloride chamber

Figure 3.15: CCT Chamber for accelerating the chloride penetration and corrosion

In the experimental work of these parts, the chloride penetration and corrosion tests were measured using different methods. For chloride, the silver nitrate colorimetric method was used to measure the chloride penetration depth (d_{Cl^-}) and color change boundary (C_d). Whilst, the chloride concentration (total and free) was determined by the acid and water-soluble chlorides test method respectively. The total chloride concentration profile, apparent diffusion coefficient, D_a and surface concentration, C_s were all determined according to BS EN 12390-11:2015 and ASTM C 1556-11a: 2016.

The D_a and C_s can be determined by the least square difference between the experimental results of chloride concentration profile and the non-linear best fitting of Fick's Second Law of Equation 2.33, as shown in Figure 3.16.

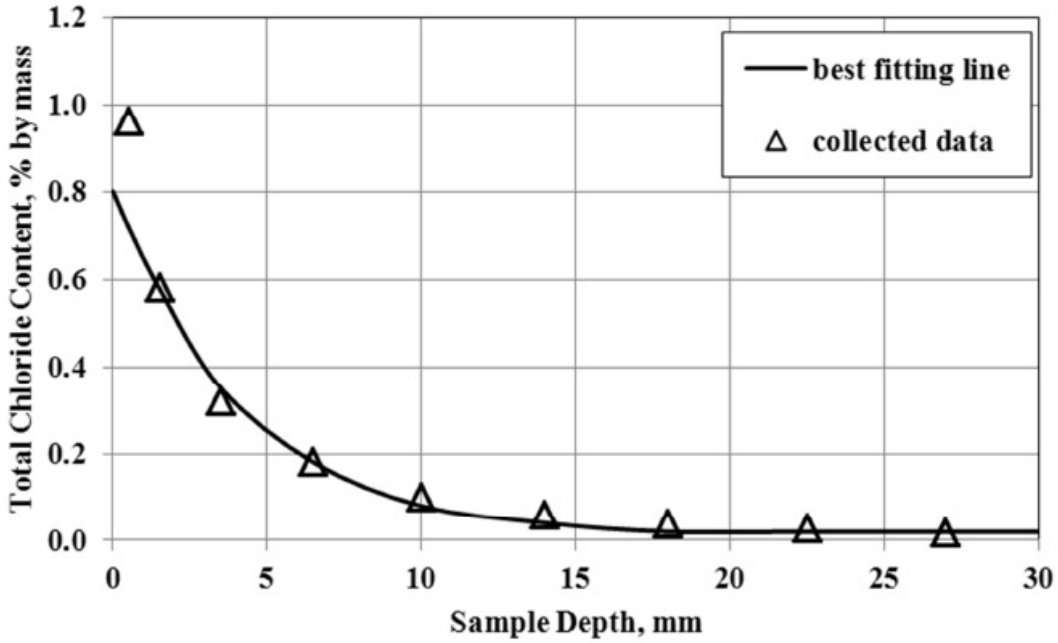

Figure 3.16: The chloride profile with fitted curves for surface chloride content BS EN 12390-11:2015

The D_a and C_s can be used to predict the risk of chloride by initiating the corrosion of the steel bar in reinforced concrete structures by exposure to chloride and CO_2 environmental conditions (Tuutti, 1982; Chen and Mahadevan, 2008). On the other hand, the D_a is the movement of ions where the fluxes are measured per unit area of the porous medium and the average concentration in the material (Marriaga and Claisse, 2009). Thus, D_a and C_s can be used to forecast the service life of reinforced concrete structures.

In the other sections, the methods of corrosion monitoring were non-destructive techniques, and these techniques have been utilized to assess the corrosion activity and determine the corrosion rate of reinforced concrete samples.

Table 3.3: Scenario of environment exposure condition of part II and III of the experimental programmes

Scenarios	Series No.	Environmental exposure condition			Duration of exposure (weeks)
		CO_2 (%)	Temperature (°C)	Humidity (%)	
Scenario a	3	Atmosphere	20	No meter	15
	2	Atmosphere	30	No meter	15
	1	Atmosphere	40	No meter	15
Scenario b *	3-1	Atmosphere	20	No meter	8 for Cl^-
		5	25	65	5 for CO_2
		Atmosphere	20	No meter	7 for Cl^-

* Scenario b includes three sequences of exposure (Cl^- - CO_2 - Cl^-)

3.2.5 Modelling and Simulation of Carbonation Depth and Chloride Penetration

The methodology of the study is based on the two sections, an experimental programme, and modelling or theoretical work. Firstly, the different microstructure and crack width in concrete specimens, CO_2, temperature, and relative humidity, and the changes they underwent due to climate change on the DoC, chloride penetration and corrosion rate were investigated experimentally. Secondly, the data of these tests are used to verify the proposed modelling in order to achieve the objectives and purposes of the study in phases by:

a- Using the experimental data to propose some of the empirical formula related to carbonation depth and chloride penetration, such as proposing the relationship of the effect of temperature or crack width on the diffusion coefficient of chloride or carbon dioxide.

b- Proposing the relationship of the effect of external and internal factors on the main parameters in the models used in predicting the DoC and chloride penetration or Cl^- concentration profile. For example, the effect of temperature, relative

humidity, crack width and time on the diffusion coefficient of chloride or carbon dioxide.

c- Developing integrated deterioration models (chloride concentration profile and carbonation depth) that take into consideration both internal and external factors, material properties, crack width, and environmental conditions (change in CO_2, temperature and relative humidity) to predict the DoC on Cl^- concentration profile.

d- Using the experimental and literature data to validate and verify the empirical formula and developed modelling of DoC and Cl^- concentration profile to calibrate these models which can be used to predict DoC in future climate change scenarios.

e- The meteorological data and the IPCC-2014 and UKCP'09 scenario projections of climate change for the UK and Iraqi cities is considered alongside the properties of concrete and crack width in the proposed models to forecast and investigate the DoC and Cl^- concentration profile in the future.

3.3 Experimental Programme

In this section of chapter three, the properties of materials used, the design of concrete mixes and, fresh and hardened concrete tests are presented. The methods of tests for materials and concrete samples and standards used in these tests are described in the following sections.

3.3.1 Material

3.3.1.1 Cement

Portland Limestone cement (CEM II/A-LL 32,5R) from Hanson Cement is used in this study. Chemical analysis and physical properties of the cement satisfied BS EN 197-1: 2011 and Tables 3.4 and 3.5 are illustrated respectively.

Table 3.4: Chemical composition & main compounds of cement (CEM II/A-LL 32,5R)*

Compound composition	Chemical formula	Mass fraction %	Limits of (Reference standard BS EN 197-1:2011)
Limestone	$CaCO_3$	14.8	6-20 %
Calcium Oxide	CaO	65.02	-
Silicon Dioxide	SiO_2	17.56	-
Aluminum Oxide	Al_2O_3	4.42	-
Ferric Oxide	Fe_2O_3	2.63	-
Sulphur Trioxide	SO_3	3.01	≤ 3.5 %
Sodium Oxide	Na_2O	0.69	-
Potassium Oxide	K_2O	0.19	-
Magnesium Oxide	MgO	0.97	≤ 5 %
Chloride	Cl^-	0.05	≤ 0.1
Free lime	Free CaO	0.5	-
Loss on ignition	L.O.I.	3.41	≤ 5%
Insoluble residue	I.R	0.91	≤ 5%
Lime saturation factor	L.S.F	0.86	-

Main compounds (Bogue's Eqs.)	Mass Fraction %	Limits of (Reference standard BS EN 197-1: 2011)
Tricalcium silicate (C_3S)	65.3	-
Dicalcium silicate (C_2S)	18	-
Tricalcium aluminate (C_3A)	8	-
Tetracalcium aluminoferrite (C_4AF)	9.7	-

* Hanson Cement Company carried out the chemical tests.
(-) It denotes no limitation in the specification.

Table 3.5: Physical and mechanical properties of cement*

Properties	Test results	Limits of (Reference standard BS EN 197-1: 2011)
Setting time (Vicat's Method)		
Initial, min	145	≥ 75 min
Final, hrs: min	4:00	-
Fineness (Blaine Method), m^2/kg	405	-
Expansion (mm)	0.5	10
H_2O/Standard Consistency	0.25	-
Compressive strength, MPa		
1 day	13.1	-
2 days	23.7	≥ 10 MPa
7 days	35.9	-
28 days	45.4	≥ 32.5 MPa
Particle density kg/m^3	3070	-

* Hanson Cement Company carried out the physical tests.

3.3.1.2 Ground Granulated Blast Furnace Slag (GGBS)

Ground granulated blast furnace slag, GGBS was produced by Hanson Cement, chemical analysis and physical properties of the GGBS, satisfied BS EN 15167-1: 2006, and Tables 3.6 and 3.7 are illustrated respectively.

Table 3.6: Chemical composition & main compounds of (GGBS)*

Compound composition	Chemical formula	Mass fraction %	Limits of (Reference standard BS EN 15167-1: 2006)
Calcium Oxide	CaO	38.94	-
Silicon Dioxide	SiO_2	34.40	-
Aluminum Oxide	Al_2O_3	13.26	-
Ferric Oxide	Fe_2O_3	0.43	-
Sulphur Trioxide	SO_3	0.29	≤ 2.5%
Sodium Oxide	Na_2O	0.38	-
Potassium Oxide	K_2O	0.59	-
Magnesium Oxide	MgO	8.82	≤ 18%
Chloride	Cl^-	0.011	≤ 0.1%
Loss on ignition	L.O.I.	1.17	≤3%
Insoluble residue	I.R	0.41	-
Glass Content	-	98	-
Moisture	-	0.11	≤ 1%

* Hanson Cement Company carried out the chemical tests.

Table 3.7: Physical and mechanical properties of GGBS*

Properties	Test results	Limits of (Reference standard BS EN 15167-1: 2006)
Setting time (Vicat's Method) Initial, min	190	≥ 150 min
Fineness (Blaine Method) , m^2/kg	456	≥ 275 m^2/kg
Expansion (mm)	0.5	-
H_2O/Standard Consistency	0.30	-
Activity Index (%) at		
7day	65	≥ 50%
28 days	90	≥ 50%

* Hanson Cement Company carried out the physical tests.

3.3.1.3 Pulverized Fuel Ash (PFA)

Pulverized fuel ash (PFA) was obtained from CEMEX UK, chemical analysis of this PFA is fulfilled to BS EN 450-1: 2012, is illustrated in Table 3.8.

Table 3.8: Chemical composition & main compounds of PFA

Compound composition	Chemical composition	Percentage by weight	Limits of (Reference guide (BS EN 450-1: 2012)
Calcium Oxide*	CaO	2.38	≤ 10 %
Silicon Dioxide*	SiO_2	59	$SiO_2 \geq 25\%$ And $SiO_2 + Al_2O_3 + Fe_2O_3 \geq 70\%$
Aluminum Oxide*	Al_2O_3	23	
Ferric Oxide*	Fe_2O_3	8.8	
Sulphur Trioxide*	SO_3	0.27	≤ 3 %
Sodium Oxide**	Na_2O	0.74	$Na_2O + 0.658\ K_2O \leq 5\%$
Potassium Oxide	K_2O	2.81	
Magnesium Oxide*	MgO	1.39	≤ 4 %
Chloride**	Cl^-	0.0	0.1%
Loss on ignition **	L.O.I.	4	≤ 5%
Moisture **	-	0.2	≤ 1 %

* Chemical tests were obtained from manufacture company (CEMEX UK).
** These tests were carried out in the School of Environment and Technology labs /Brighton University.

3.3.1.4 Fine Aggregate

In this study, natural sand was used as fine aggregate (particle size < 5mm). The grain size distribution, chloride, and sulfate content were tested according to BS EN 933-1:1997, BS EN 1744-1:2009 and BS EN 1744-1:2009+A: 2012 respectively are presented in Figure 3.17 and Table 3.9. Fineness modulus of fine aggregate is 3.23. Accordingly, results of the tested sand are harmonious with BS EN 12620:2002+A1:2008, Zone C.

Table 3.9: Physical and chemical properties of fine aggregate*

Sieve size (mm)	Cumulative passing %	Limits of the Reference standard BS EN 12620:2002+A1:2008/(C)
4.75	100	-
2.36	78	60-100
1.18	52	30-90
0.6	35	15-54
0.3	11	5- 40
0.15	1	-
Physical properties	**Test Result**	**Limits of Reference standard BS EN 12620:2002+A1:2008**
Specific gravity	2.60	-
Chloride content %	0.006	0.06%
Sulfate content %	0.29	-
Absorption	1.5	-
Fineness modulus	3.23	-

* These tests were carried out in School of Environment and Technology labs /Brighton University according to BS EN 933-1:1997, BS EN 1744-1:2009 and BS EN 1744-1:2009+A:2012.

3.3.1.5 Coarse Aggregate

Coarse aggregate was used in the form of crushed gravel with a size range of 5-14 mm. Grain sieve analysis and chemical contaminated chloride and sulfate were tested according to BS EN 933-1:1997, BS EN 1744-1:2009 and BS EN 1744-1:2009+A:2012 respectively, results of the tested coarse aggregate are illustrated in Figure 3.18 and Table 3.10. This gravel is in accordance with BS EN 12620:2002+A1:2008.

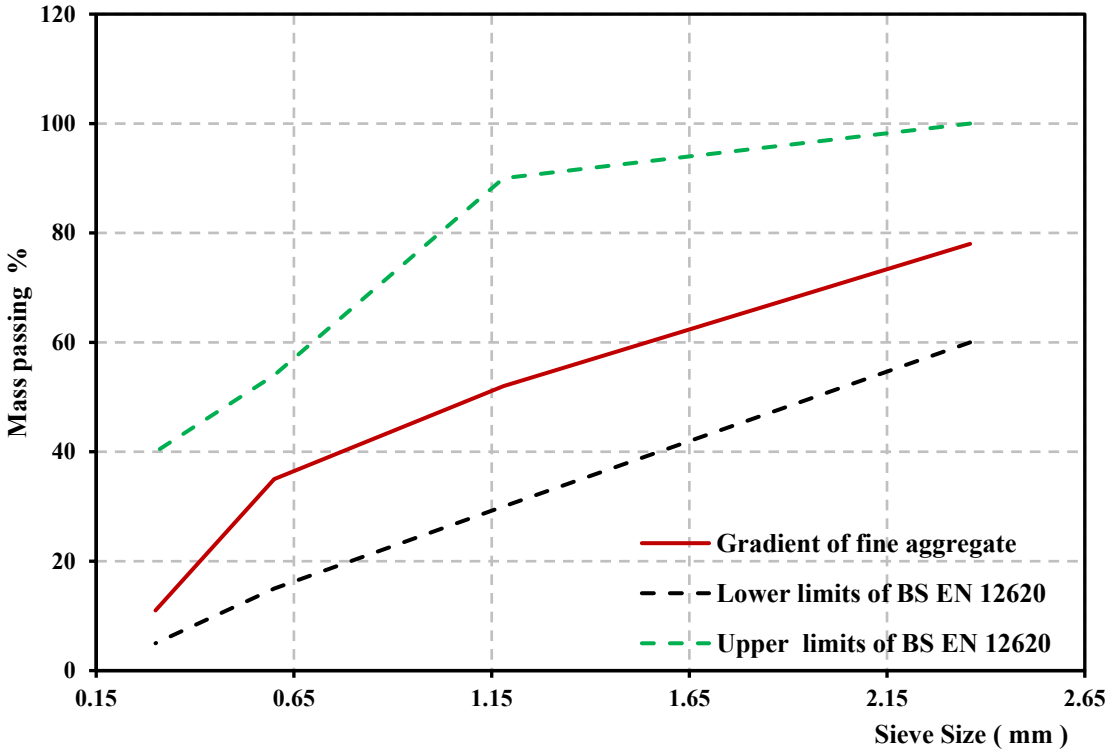

Figure 3.17: The curve of fine aggregate gradient comparing with limits of BS EN 12620:2002+A1:2008

Table 3.10: Physical and chemical properties of coarse aggregate*

Sieve size (mm)	Cumulative passing%	Limits of Reference guide BS.882:1983/(5-14 mm)
20	100	100
14	95	90-100
10	80	50-85
5	8	0-10
Physical properties	**Test Result**	**Limits of Reference guide BS 882:1983**
Specific gravity	2.60	-
Bulk density	1630	-
Chloride content %	0.008	0.06
Sulfate content %	0.17	-
Absorption %	2.8	-

* These tests were carried out in School of Environment and Technology labs /Brighton University according to BS EN 933-1:1997, BS EN 1744-1:2009 and BS EN 1744-1:2009+A:2012.

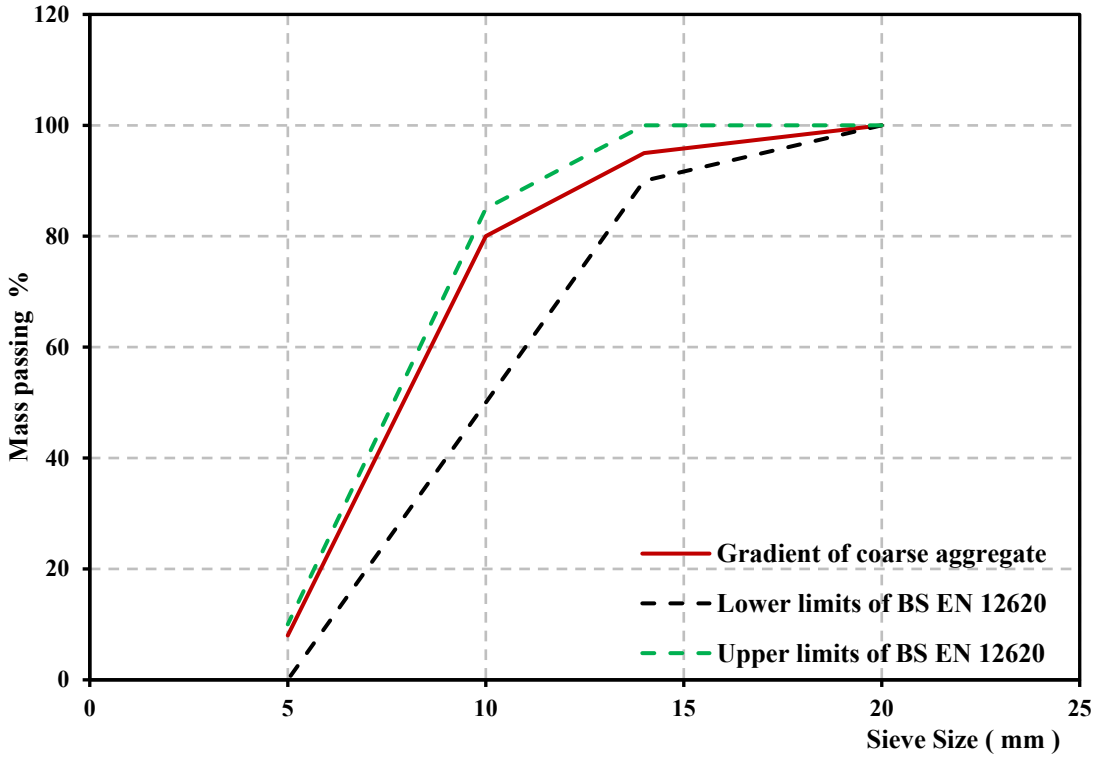

Figure 3.18: The curve of coarse aggregate gradient comparing with limits of BS EN 1744-1:2009+A:2012

3.3.1.6 Steel Reinforcement

Deformed or ribbed steel (B500A) (8mm) used longitudinal reinforcement in the concrete specimens for corrosion samples. Mechanical properties of steel are the average of three samples and in compliance with requirements of British standard, BS 4449:2005+A2:2009, shown in Table 3.11.

Table 3.11: Mechanical properties of the steel reinforcement used

Property	Result	Limitation of BS 4449: 2005+A2: 2009
Yield stress (MPa)	525	485 ≤ Yield stress ≤ 650
Tensile stress (MPa)	580	Tensile stress ≥ 514.1
Elongation (%)	2.5	Elongation ≥ 2.0

* Test was carried out by the laboratory of Brighton University according to British standard, BS 4449: 2005+A2: 2009.

3.3.1.7 Water

Tap water was used in concrete mixes works, casting concrete and curing of specimens.

3.3.2 Concrete Mix Design

In this study, different mixes of concrete were used to achieve the various properties of concrete. This variation in properties was determined by designing concrete mixes with different water/cementitious materials, w/cm ratio and different cementitious materials such as ground granulated blast furnace slag (GGBS) and pulverized fly ash (PFA) used as a partial substitution for cement. The GGBS and PFA have the ability to change the microstructure and strength of concrete. The Research Establishment method (1988) or the British method was used to design mixes that were used in this study as shown in Table 3.12.

Table 33.12: Concrete mixes designs used in this study

Mix symbol	$\frac{w}{cm}$	Content per unit volume of concrete (m^3)						$\frac{Agg}{cm}$
		Cementitious materials kg			Water kg	Aggregate (Agg)		
		Cement	PFA	GGBS		Sand kg	Gravel kg	
M 0.4	0.4	513	-	-	205	653	980	3.23
M 0.5	0.5	410	-	-	205	711	1023	4.22
M 0.6	0.6	350	-	-	205	711	1041	5.00
M 0.5+0.35 PFA	0.5	266	144	-	205	711	1023	4.22
M 0.5+ 0.30 GGBS	0.5	287	-	123	205	711	1023	4.22

3.3.3 Concrete Mixing, Casting and Curing the Specimens

The mixing method is important to obtain the required workability and homogeneity of the concrete mix. Mechanical mixing was used following ASTM C192:2016a and BS EN 12390-2: 2009 in the mixing of concrete. The concrete mixing stages are presented in section A-1 (Appendix A).

Plastic moulds were used for cube and prisms specimens, while the steel moulds were utilized in casting cylinder samples as shown in Figure 3.19.

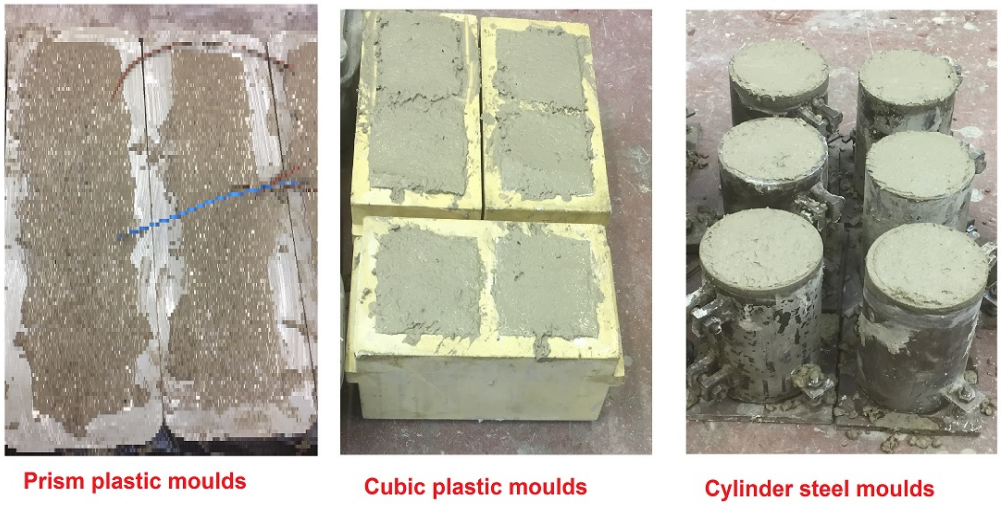

Figure 3.19: Types of used moulds in the casting of concrete

Reinforced concrete samples (prisms) have been used for two purposes. Firstly, they were used to induce the major cracks by the flexural method as shown in Figure (3.9-a). Secondly, they were used to investigate the corrosion. Reinforced concrete prisms were used by fixing reinforcement in moulds with a concrete cover 2 cm as shown in Figure 3.10. All moulds were prepared for casting by painting oil along the interior surfaces of the moulds to prevent adhesion with concrete after hardening.

Samples were cast in two layers. Each layer was vibrated using an electrical vibrating device to achieve the homogenous concrete and avoid the segregation of concrete. The specimens were demoulded and cured using tap water until the time of testing, or exposure to the CO_2 or chloride environment condition at the age of 28 days.

Finally, the method of filling and preparation of moulds, compaction and levelling the surface of concrete, curing and transporting of samples were carried out according to BS EN 12390-2: 2009.

3.3.4 Experimental Tests for Concrete Samples

Several tests were carried out in order to achieve some of the objectives of the study and collect experimental data about properties of concrete mixes and the main tests (e.g DoC) in order to investigate the effect of the main parameters of (external such as climate parameters) according to the parts of the study as the following:

Firstly, the characteristics of the fresh state of concrete are important in investigating the properties of the microstructure of concrete. These tests can be carried out to give an indication of the quality of the concrete. There are various test methods used to show the fresh properties of concrete. In this study, a slump test was used; it is the simplest and most widely used test method to determine the workability and flowability of concrete. The test procedure and apparatus used were given in BS EN 12350-2: 2009.

Secondly, several hardened concrete tests were carried out to ascertain the mechanical and physical properties of concrete and the main tests of the study; carbonation depth, chloride penetration and corrosion rate are presented in the following sections.

3.3.4.1 Compressive Strength Test

The compressive strengths were tested according to BS EN 12390- 3: 2009. Cubes of (100×100×100) mm were tested using a hydraulic compression machine of 1800 kN capacity, at a loading rate of 0.6 N/mm^2 sec. The sample was carefully aligned at the centre of thrust of the upper bearing block and loading was applied continuously until failure.

3.3.4.2 Splitting Tensile Strength Test

The splitting tensile strength was carried out according to BS EN 12390 - 6: 2000 using cylinders (100 mm diameter and 200mm length). Two thin plywood strips were placed between the specimen and both the upper and the lower bearing blocks of the testing machine. The test consisted of applying a diametric compressive force along the length of a cylindrical concrete specimen at a rate of 0.04N /mm^2.sec until failure. The splitting tensile strength is computed by BS EN 12390- 6: 2000:

$$f_{st} = \frac{2P_a}{\pi d_a l} \qquad (3.1)$$

where:

f_{st} is Splitting tensile strength, (MPa), P_a is max. applied load indicated by the testing machine, (N), d_a is Cylinder diameter, (mm) and l is Cylinder length, (mm).

3.3.4.3 Flexural Strength Test

The flexural strength was measured using the results obtained from a simple beam with a two-point loading test according to BS EN 12390-5: 2009, using prisms measuring (100×100×500 mm). A hydraulic compression machine was used for the test at a rate of loading of 0.04N/mm^2 sec. The flexural strength is calculated as follows according to BS EN 12390-5: 2009:

1. If the fracture initiates in the tension surface within the middle third of the span length, then

$$f_{cf} = \frac{P_a l_s}{b d_d^2} \quad (3.2)$$

where:

f_{cf} is flexural tensile strength, MPa, P_a is maximum applied load, N, b is the average width of the specimen, mm, d_d is the average depth of specimen, mm and l_s is span length, mm

2. If the fracture occurred in the tension surface outside the middle third of the span length by not more than 5% of the span length, then:

$$f_{cf} = \frac{3 P_a a_t}{b d_d^2} \quad (3.3)$$

where:

a_t is the average distance between the line of fracture and the nearest support measured on the tension surface of the prism, in mm (Neville, 2011).

3.3.4.4 Ultrasonic Pulse Velocity Test (UPV)

The UPV is a method to determine the velocity of propagation of ultrasonic pulses of longitudinal waves in hardened concrete. This test can be used in several applications. It is a non-destructive test method, applied to assess the homogeneity and quality of concrete and it can be used to measure crack depth (Al-Samaraai and Raouf, 1999) by measuring the velocity of ultrasonic waves passing through the concrete with and without a crack. This test was carried out in accordance with BS EN 12504- 4: 2004 and ASTM C 597: 2002. Ultrasonic pulse velocity was measured on concrete prisms using PUNDIT device in an indirect transmission of the pulse. Measurements were made in one direction

on the surface of the prism. The transducers were smeared with gel to give good contact, and the device setting was checked frequently using a reference bar supplied with the device. The crack depth, d_{crack} was computed by measuring the time of transfer of pulse velocity for the ultrasonic devices according to Equation 3.4 as shown in Figure 3.12 (Al-Samaraai and Raouf, 1999).

$$d_{crack} = x\sqrt{\frac{T_{cr}^2}{T_s^2} - 1} \qquad (3.4)$$

where:

2x is the path length without crack; T_{cr} is travel time around the crack and T_s is surface travel time through sound concrete without a crack (*2*x).

3.3.4.5 Permeability Test

The permeability is an indication of permeable voids in the concrete and the internal microstructure of concrete. This characteristic is important when studying the durability of concrete, in particular, carbon dioxide diffusion and chloride penetration in concrete. This test can be carried out by many methods, in this study it was determined by:

a. Water Permeability by Water Absorption and Volume of Concrete

This test was carried out on 100 mm cubes at ages of 28, 60, 90 and 150 days to find the percentage of the permeable pore structure of concrete and its impact on the diffusion of carbonate ions and chloride penetration. This method was used according to ASTM C642: 2013 and BS EN 12390-7: 2000. This method is based on the weight of specimens at the different states, dry, saturated surface dry and the weight of specimen immersed in water. The permeable pores can be computed by:

$$Volume\ of\ permeable\ pores\ space\ \% = \frac{Wt_2 - Wt_1}{Wt_2 - Wt_3} * 100 \qquad (3.5)$$

where:

Wt_1 is the weight of the sample is dry at 105°C for 24 hours, Wt_2 is the weight of the sample is saturated and surface dry and Wt_3 is the weight of the sample when immersed in water.

b. Chloride Ions Migration (Diffusion) by NT Build 492-1999

This method is used to find the chloride migration coefficient by the impact of an electrical field on two different solutions, NaCl and NaOH, to accelerate the chloride penetration. This test is to measure the resistance of tested concrete to the penetration of chloride in a non-steady state. The cylinder concrete specimens with a diameter of 100 mm and a length of 50 mm were tested according to NT Build 492:1999 and this equipment is shown in Figure 3.20. Chloride ions migration coefficient, D_{nssm} (*10^{-12} m^2/s) is computed by the modified Nernst Planck's equation in Equation 3.6.

$$D_{nssm} = \frac{0.0239(273+T)l_t}{(U_v-2)t}\left(x_d - 0.0238\sqrt{\frac{(273+T)l_t\, x_d}{U_v-2}}\right) \qquad (3.6)$$

where:

T is the average value of the initial and final temperature in the anolyte solution (NaOH), l_t is the thickness of the sample (mm), x_d is the average value of penetration of chloride, with time, t and U_v *is* the absolute value of applied voltage in V.

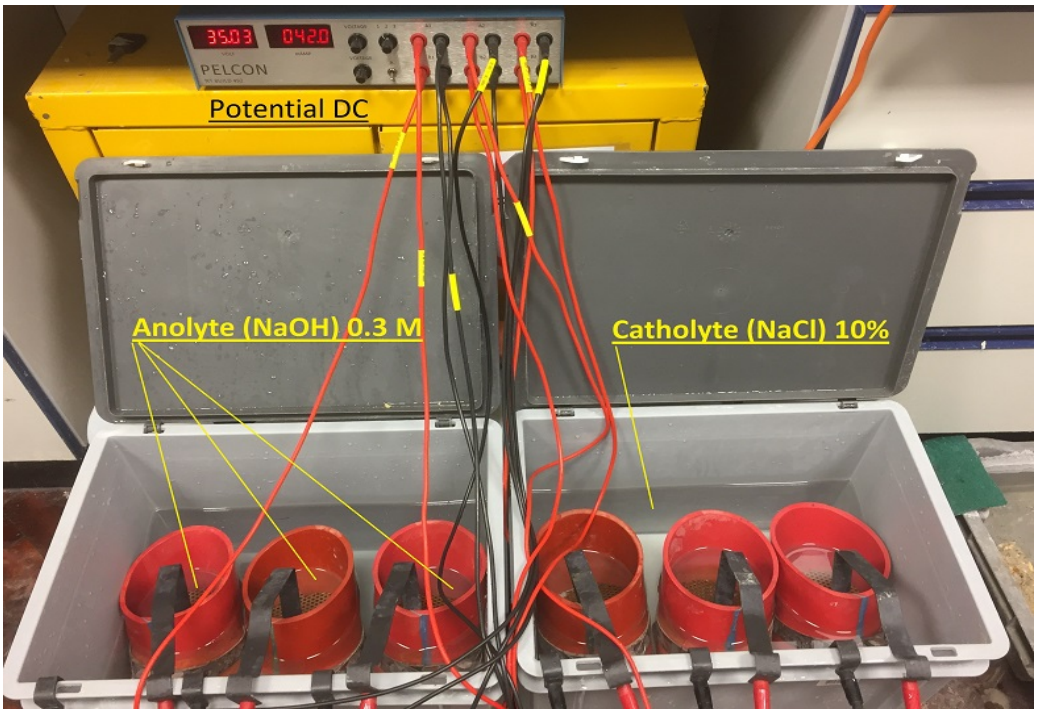

Figure 3.20: The device for testing chloride migration by an applied potential direct current with NaCl and NaOH solution to measure (D_{nssm})

c. Gas Permeability

This technique covers the measurement of the gas (N_2) permeability in hardening concrete samples confined by gas (O_2). This procedure can be used in plain concrete marks of structural applications in addition to similar cement-based materials utilized in construction. The cylinder concrete specimens with a diameter of 35 mm and a length of 70 mm were tested according to a method of RILEM TC 116-PCD:1999 to measure the gas permeability coefficient, K_i , which is computed by the modified Darcy's equation in Equation 3.7. Figure 3.21 shows the gas permeability equipment.

$$K_i = \frac{2P_p\, Q_i L\, \mu}{A_c(P_i^2 - P_p^2)} \qquad (3.7)$$

where:

K_i is gas permeability coefficient at pressure stage i, A_c is a cross-section of the specimen (m^2), D is the diameter of the specimen (m), L denotes the thickness of the specimen (m), P_p is atmospheric pressure in absolute(Pa), P_i is applied test pressure in absolute (Pa), Q_i denotes flow rate at pressure stage i (m^3/s) and μ is gas dynamic viscosity at 20°C $\pm$ 2°C (Pa.s).

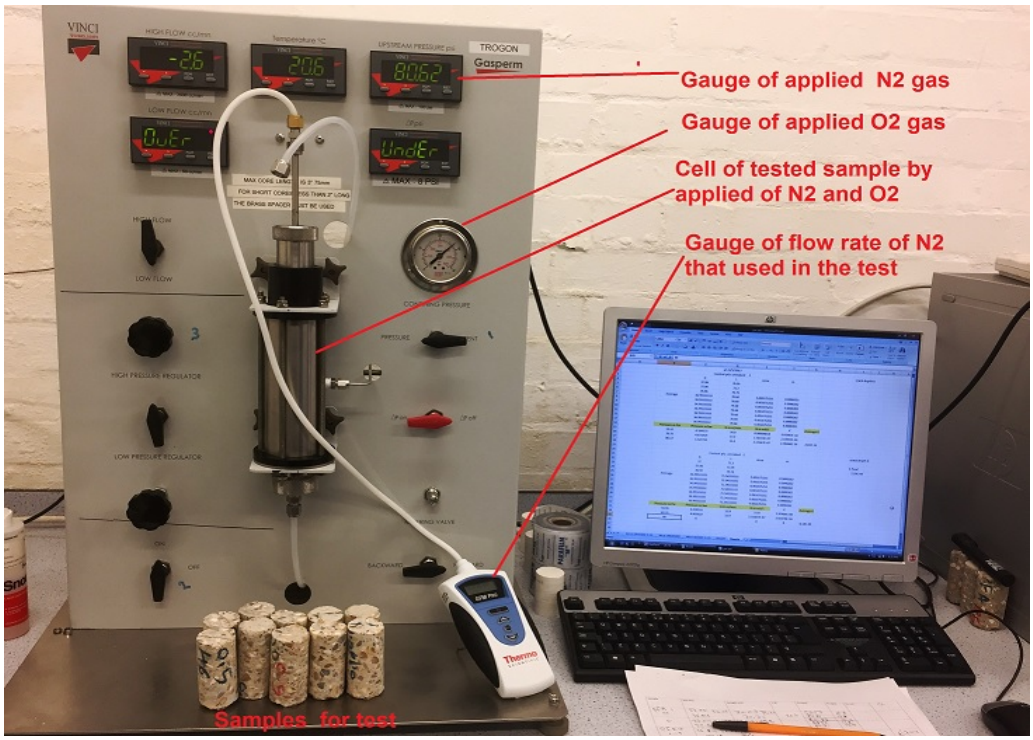

Figure 3.21: The device for testing gas permeability by applied O_2 gas confining the sample and N_2 to find the gas permeability coefficient, K_i

3.3.4.6 Depth of Carbonation

The carbonation test measures the diffusivity of carbon dioxide and the reaction with hydrated cement products to form the calcium carbonate that leads to change concrete alkalinity by reducing the pH of concrete pore solution from 13 to 9. In this study, the specimens were exposed to a carbon dioxide environment condition for 8 weeks (Roy *et al*., 2000; Russell *et al*., 2002).

The conditioned samples were split open into two parts. The first part was sprayed with phenolphthalein solution with 1% concentration to establish the DoC, X_p. The second part of the sample was drilled (at the crack location) in order to collect concrete powder samples to find apparent pH and crystalline phases, XRD at eight different depths from the exposed surface, namely 0-6 mm, 6-12 mm, 12-18 mm, 18-24 mm, 24-30 mm, 30-36 mm, 36-42 mm and 42-48 mm using dry drilling equipment as illustrated in Figure 3.23. The powder was sieved by a 150 micro-meter sieve to reduce the amount of coarse grain particles resulting from aggregate, then dried in an oven at 50°C for 24 hours and kept in sealed plastic bags until tested to measure the apparent pH and crystalline phases of $CaCO_3$ and $Ca(OH)_2$.

The carbonation test can be measured using different methods, and as mentioned in chapter 2, this study was focused on three methods as follows:

a. Phenolphthalein Indicator

This method uses phenolphthalein solution with one gram of phenolphthalein powder dissolved into a solution of 70 ml and 30 ml of ethanol and deionized water respectively according to (BS EN 12390-10: 2018). This technique is based on the change of color due to the reduced pH of concrete from 13 to 8 that provides an adequately pure color change in a sample of concrete to distinguish the neutralized zone, e.g. thymolphthalein. In this method, the spraying of a solution of phenolphthalein on the freshly split concrete sample as designated by Al-Amoudi *et al*. (1991) is to establish the DoC. The colourless concrete refers to DoC, X_p and the pH $\leq$ 9 and the purple color refers to the alkalinity of concrete and the pH $\geq$ 9. This test method is based on BS EN 12390-10: 2018; BS 1881-210: 2013.

b. pH and Consumed OH^- Method

This technique is based on determining the apparent pH of concrete pore solution and concentration of [OH^-] as Equation 2.6 (Li *et al*., 1999; Suryavanshi and Swamy, 1996) (see section 2.4.3.4). Apparent pH of concrete was measured by dissolving 1g of the concrete powder in deionized water. This mixture (powder and water) was rotated for about 30 seconds and then stood about 24 hours (McPolin *et al*., 2007; Wang *et al*., 2016) as shown in Figure 3.22. Then, the apparent pH of concrete was measured using pH meter according to BS EN ISO 10523: 2012. The apparent a pH can be used to compute the concentration of [OH^-] for carbonated and uncarbonated sample (control) using Equation 2.6 (Li *et al*., 1999; Suryavanshi and Swamy, 1996).

The method proposed in (McPolin *et al*., 2007; Wang *et al.*, 2016) was used to establish the consumption of [OH^-] (mol/kg of concrete) due to carbonation of uncarbonated powder. According to this procedure, a typical profile of consumed [OH^-] ions concentration with the depth of concrete is shown in Figure 2.7. This profile can be divided into three zones based on the consumption of [OH^-] ions: fully carbonated, partially carbonated and non-carbonated zones. Where, X_p is the boundary between the fully carbonated and partially carbonated zone, and X_f is the boundary between the partially carbonated and non-carbonated zone (indicating the carbonation front).

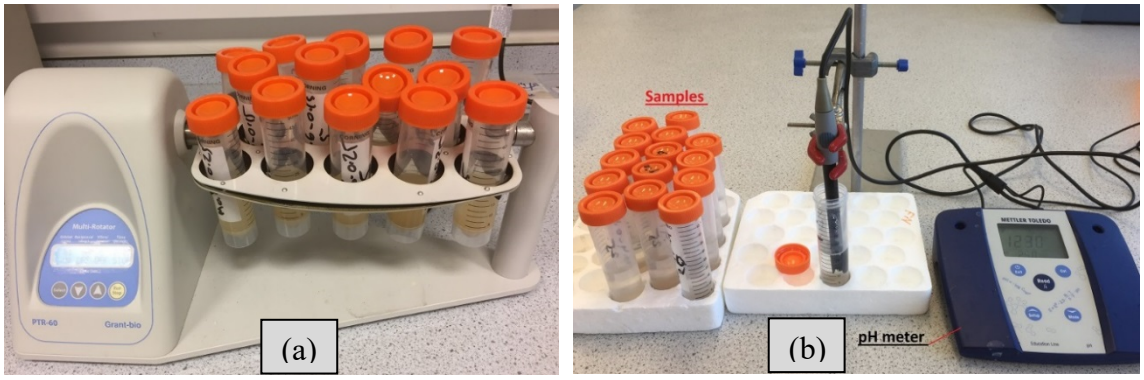

Figure 3.22: (a) rotator to shake the solution, (b) PH meter to measure the apparent pH of the concrete sample

c. XRD Method

This instrumental technique is based on the detection of the crystalline phases of materials and minerals. In the carbonation phase, calcium carbonate $CaCO_3$ and calcium hydroxide $Ca(OH)_2$ were identified to investigate the profile of the change in relative intensities of crystalline phases of $Ca(OH)_2$ and $CaCO_3$ (Chang and Chen, 2006) due to the penetration of CO_2 to establish the carbonation front depth, X_f as shown in Figure 3.23. On one hand, the quantity of chloride bound or Friedel's salt (chloride part) was also

identified to investigate the presence of this type of salt in concrete due to chloride penetration. The intensity or main peaks of $Ca(OH)_2$ are noticed at angles of diffraction (2θ) 18.1° and 34.1° (International Centre for Diffraction Data, ICDD). It reduces or disappears as the degree of carbonation increases in the samples. On the other hand, the intensity of the $CaCO_3$ phase for the main peak can be detected at the angle of diffraction (2θ) 29.39°, which increases in the samples with the increase in carbonation depth. The intensity of the Friedel's salt can be identified at (2θ) between 11.18° to11.26° in the solid phase (Talero *et al*., 2011).

the PANalytical type device was used in the analysis and the current and voltage applied are 40 mA, 40kV respectively. A target or anode material of the device was made from copper (CU) as shown in Figure 3.24. The scan programme used to analyse the concrete powder (grain size = 75 µm) is listed in Table 3.13 (for more detail see Appendix C-2).

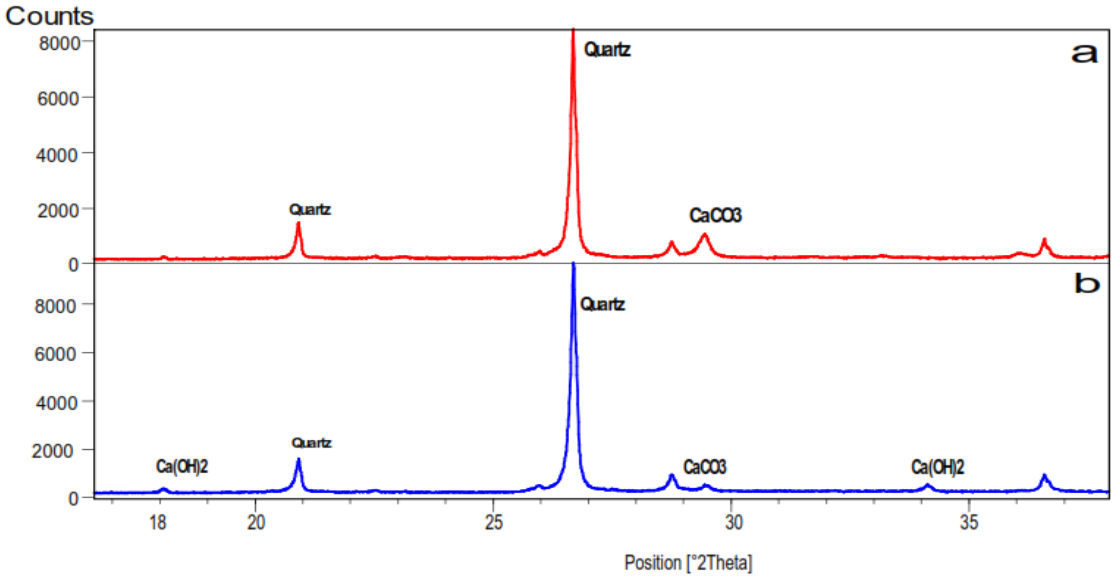

Figure 3.23: Carbonation front depth was investigated by XRD,(a) Sample is taken from the surface,(b) samples are taken from an un-carbonated depth

Table 3.13: The scan programme used in powder XRD test

Properties	Value
Start Position (°2Th.)	5.0052
End Position (°2Th.)	69.9892
Step Size (°2Th.)	0.008
Scan Step Time (s)	10.16
Specimen Length or diameter (mm)	10
Scan Type	Continuous

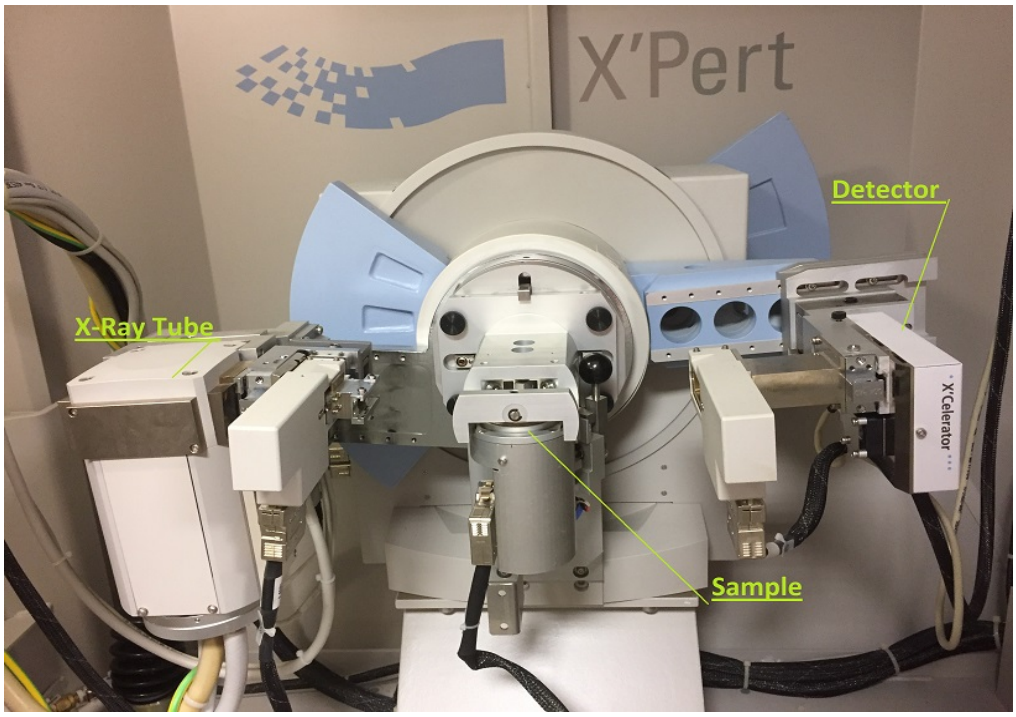

Figure 3.24: XRD -Ray instrument set –up

3.3.4.7 Chloride Content and Chloride Penetration

The diffusion of chloride in concrete is a non-steady state. BS EN 12390-11: 2015 was used to determine the chloride concentration for concrete samples at a specified age also to determine the quality of concrete by comparative testing. The conditioned samples were split open into two parts as shown in Figure 3.25. The first part was sprayed with silver nitride $AgNO_3$ with a concentration of 0.1 N to establish the chloride penetration depth, d_{Cl^-} and color change boundary, c_d using silver nitrate colorimetric due to a chemical reaction between Cl^- with Ag^+ (Yuan *et al*., 2008; He *et al.*, 2012). The second part of the sample was drilled (at the crack location) in order to collect concrete powder samples to find the chloride content (chloride profile concentration) at seven different depths from the exposed surface, namely 0-6 mm, 6-12 mm, 12-18 mm, 18-24 mm, 24-30 mm, 30-36 mm and 36-42 mm using dry drilling equipment as illustrated in Figure 3.26. The powder was sieved by a 150 micro-meter sieve to reduce the amount of coarse

grain particles resulting from aggregate, then dried in oven at 50°C for 24 hours and kept in sealed plastic bags until tested.

Figure 3.25: The steps of collecting powder from concrete to measure chloride concentration in concrete specimen

Figure 3.26: Dry drilling of the concrete sample to collect the powder of concrete

Concrete powder obtained from concrete samples was used to measure the following:

a. Total Chloride

Acid soluble chloride according to BS EN 14629: 2007 was used to measure ion concentration, free and bound. 1 g of the powder was weighed to the nearest ± 0.001 g and dispersed in 20 ml of distilled water by stirring to achieve separation of the particles of concrete powder. 10 ml of nitric acid was added to the solution with continuous stirring, and then 50 ml of hot distilled water added. The mixture was boiled for approximately 3 minutes. This mixture was left to cool for about one hour until it reached ambient temperature. The solution was filtrated using medium-textured paper and the beaker, stirrer and the residue on the filter rinsed with 1 % nitric acid at least two times. The distilled water was added to the extracted solution until it reached 100 ml. Then, 1 ml of saturated ammonium ferric-sulfate solution, $NH_4Fe(SO_4)_2$ x 12 H_2O) and 2–3 ml benzyl alcohol (C_7H_8O)were added to the solution as indicators. 10 ml of silver nitrate was added to the mixture and stirred very vigorously until the silver nitrate separated and then the remaining amount of silver nitrate titrated using the ammonium thiocyanate solution NH_4SCN, 0.1 N. The solution was then stirred vigorously when the endpoint was near. The titration at a slower rate was continued by continuous intensive mixing until the solution attained a permanent, faint red-brown colour. The set-up of titration of the solution is shown in Figure 3.27 and the concentration of chlorides, Cl^- (% by mass of sample) is then calculated according to the following formula (BS EN 14629: 2007):

$$C_{cl}\% = \frac{3.545\, f\, (V_2 - V_1)}{m_t} \qquad (3.8)$$

where:

f is the molarity of $AgNO_3$, V_1 is the volume of the NH_4SCN used in the titration in ml, V_2 is the volume of the NH_4SCN used in the blank titration in ml and m_t is the mass of the concrete powder in g.

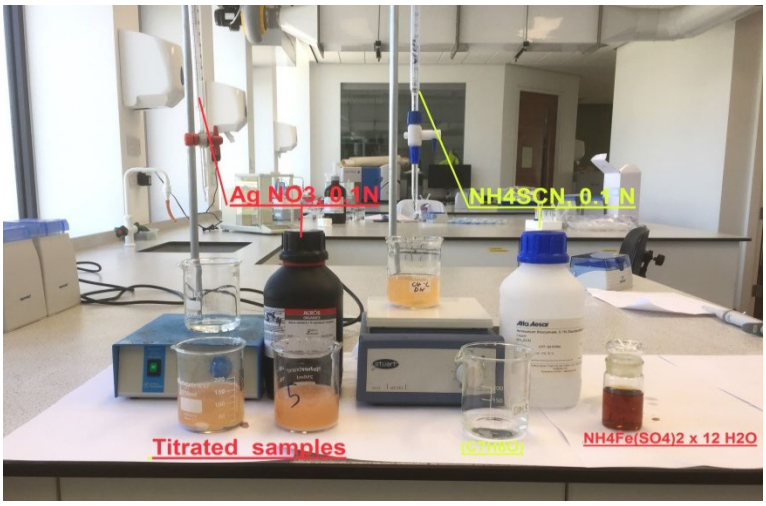

Figure 3.27: Volhard's Method was used to determine the total chloride in concrete samples

b. Free Chloride

Water-soluble chlorides as described by Zuquan *et al.* (2007) tested ion concentration. A 1 g of the powder was weighed to the nearest ± 0.001 g and dispersed in 20 ml of distilled water. This mixture (powder and water) was continuously rotated for approximately 1 minute and stood for about 24 hours. Then, the solution was filtered by a fast grade paper filter and 1 ml of the extracted solution was taken to test. Ion chromatography system type (DIONEX ICS-1100) was used (as shown in Figure 3.28) to separate and measure ion concentration such as chloride ions and sulfate ions by a chromatography process based on their similar ions exchange. The chloride ion concentration was determined according to standard solutions of chloride ions.

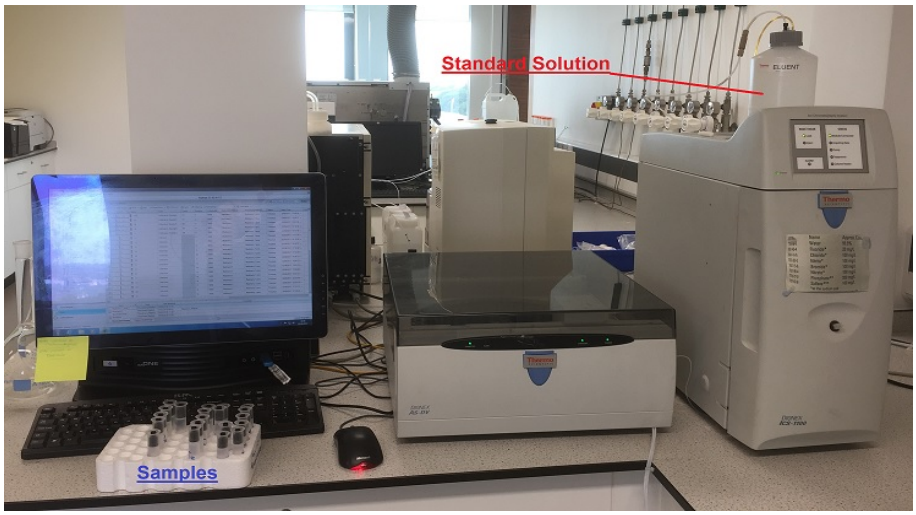

Figure 3.28: Ion chromatography set-up

3.3.4.8 Corrosion Monitoring Techniques

Two of the most used electrochemical techniques were used for monitoring corrosion of steel in concrete namely: half-cell potential and Linear Polarization Resistance, LPR.

a. Corrosion Potential (Half Cell Potential)

The electrical half-cell, E_{corr} potential is used to assess and monitor the un-coated steel rebar in the laboratory or in the field. In addition, the corrosion activity of the reinforcing steel can be discovered. The reference electrode was a saturated calomel electrode with KCl and was used to measure the corrosion potential of the steel rebar in concrete relatively according to the ASTM C876: 2015. Corrosion potentials of the reinforced concrete specimens were measured twice monthly during the exposure of samples to chloride in the chamber. The E_{corr} of the rebar from each specimen was monitored versus time and E_{corr} value was obtained after 10 minutes (achieved stability) (Bouteiller *et al*., 2012). The half-cell potential readings are interpreted according to ASTM C 876: 2015 as shown in Table 3.14. Figure 3.29 shows the half-cell potential test set –up.

Table 3.14: Probability of Corrosion condition according to half-cell potential (HCP) measurements (Song and Saraswathy, 2007)

Half-Cell Potential measurements		Corrosion Activity
Copper-copper sulfate electrode, CSE ,mV	Saturated calomel electrode, SCE, mV	
> - 200	> -126	Low (10 %) risk of corrosion
-200 to - 350	- 126 to - 276	Intermediate corrosion risk
< - 350	< -276	High (< 90%) risk of corrosion
< - 500	< - 426	Severe corrosion

b. Linear Polarization Resistance

The open circuit potential (OCP), linear polarization resistance (LPR) is used to the monitoring of corrosion activity. LPR was carried out using a potentiostat (ACM Instruments model, see Figure 3.30) connected to a computer. The reference and auxiliary electrode used a saturated calomel electrode with KCl and stainless-steel rod respectively.

The test was conducted over 15 weeks of environmental exposure to the spraying of saline solution with 5% NaCl. The LPR of the rebar from each specimen was monitored versus time and an LPR value was obtained following every two weeks of environmental exposure to chloride.

The LPR measurements were performed using a potential shift of 10 mV in both anodic and cathodic directions (around E_{corr}) with a 10 mV/minute scan rate. No compensation for ohmic drop effect was considered because in a wet and chlorinated medium this parameter was assumed to be negligible compared to the R_p resistance. Therefore, the values of polarisation resistance (R_p) were used to estimate the corrosion current density (i_{corr} in μA/cm^2) using the Stern and Geary equation with B taken as constant as shown in Equation 3.9 (Andrade and González, 1978; Bouteiller *et al*., 2012).

The set –up of the test is shown in Figure 3.30. The exposure area, (*A*) of steel bar embedded in concrete was computed (diameter of the bar in cm*π* length of the bar in cm = area in cm^2). The polarization resistance *Rp (ΔE/ΔI)* is obtained from the slope of the polarization current curve near E_{corr} in the cathodic and anodic direction (Stern and Geary, 1957). In addition, the corrosion current, i_{corr} was achieved by applying the Stern-Geary Equation (Andrade and González, 1978; Bouteiller *et al*., 2012).

$$i_{corr} = \frac{B}{R_P} \qquad (3.9)$$

where:

B is the Stern–Geary constant.

B is often estimated as 52 mV for passive conditions and 26 mV for active corrosion. Bouteiller *et al*., (2012) used in all cases of the transition phase from active to passive corrosion, the *B* constant was 26 mV for all cases.

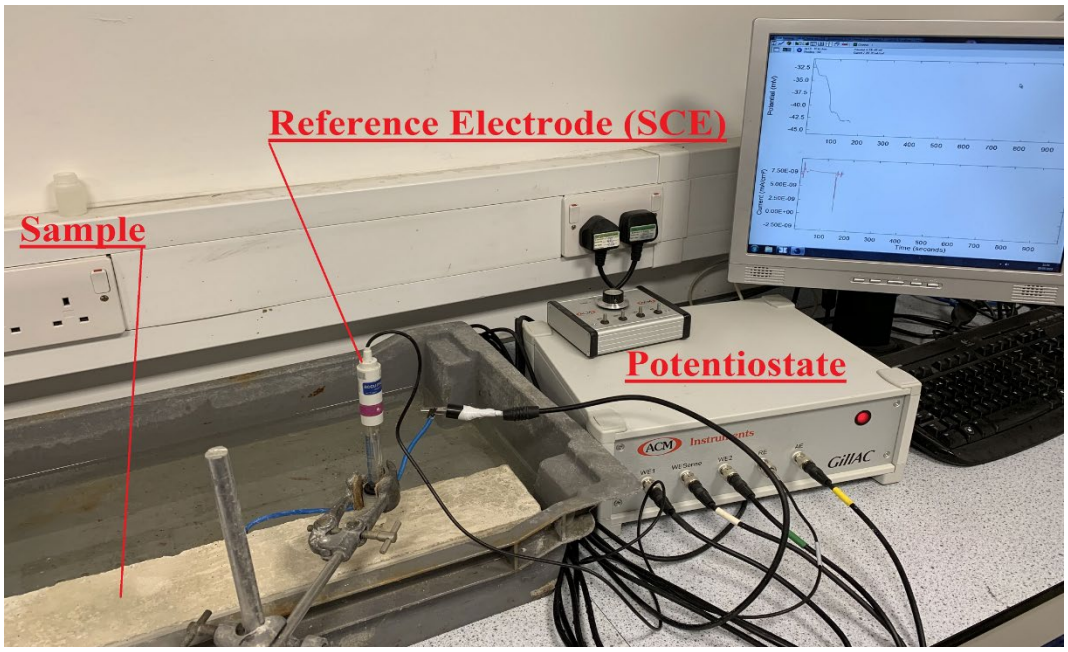

Figure 3.29: Half -cell instrument set –up

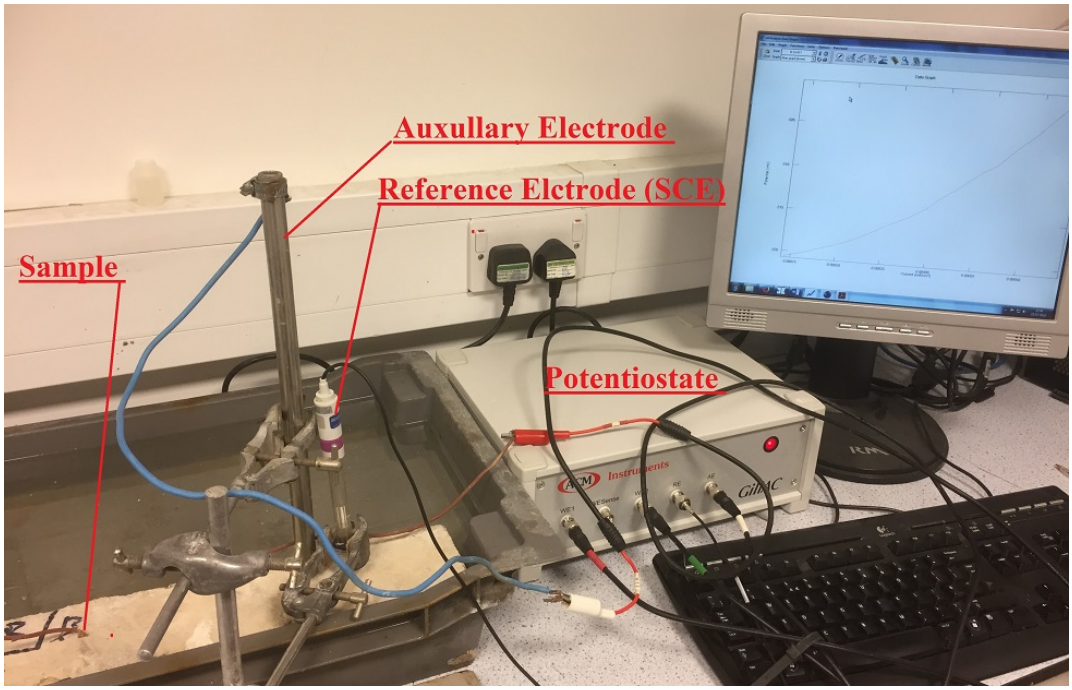

Figure 3.30: LPR instrument set –up

CHAPTER IV: PROPERTIES OF CONCRETE MIXES

4.1 Introduction

In this chapter, the experimental results of fresh, physical and mechanical properties of concrete mixes are presented and discussed. The results and discussion mainly focus on the impact of water/cementitious material (w/cm) ratio and supplementary cementitious materials (SCMs) on the fresh, physical and mechanical properties.

In total five mix designs are examined, which are then used subsequently for carbonation and chloride penetration, and corrosion rate measurements. Three of these are Ordinary Portland Cement, OPC based mixes with three different water/ cementitious material ratios (w/cm) ratios (0.4, 0.5 and 0.6) and the remaining two have the same w/cm ratio (0.5) but OPC has been partially replaced by supplementary cementitious materials (SCMs) such as PFA and GGBS in order to get the variety of properties and microstructure of concrete.

Standard test and investigation methods have been used to measure the fresh, physical and mechanical properties

4.2 Fresh Properties of Concrete

The flowing ability of fresh concrete (workability) is tested using the slump (Abrams cone) method. It is a measurement of deformability of mixes under their own weight. The results in Figure 4.1 shows that the higher workability of concrete was achieved for mixes, M 0.6 (w/cm ratio 0.6) and M 0.5+GGBS (w/cm ratio 0.5 + 0.3% GGBS). The mixes M 0.4 (0.4 w/cm ratio) and M 0.5+PFA (w/cm ratio 0.5+0.35 PFA) were less workable as can be seen in Figure 4.1 and in Table A.1 (Appendix A). Segregation and bleeding were visually checked during the slump flow test and were not observed in any of the mixtures.

As expected, increasing the w/cm ratio in concrete increased the slump flow values of mixes due to higher water content with respect to cement.

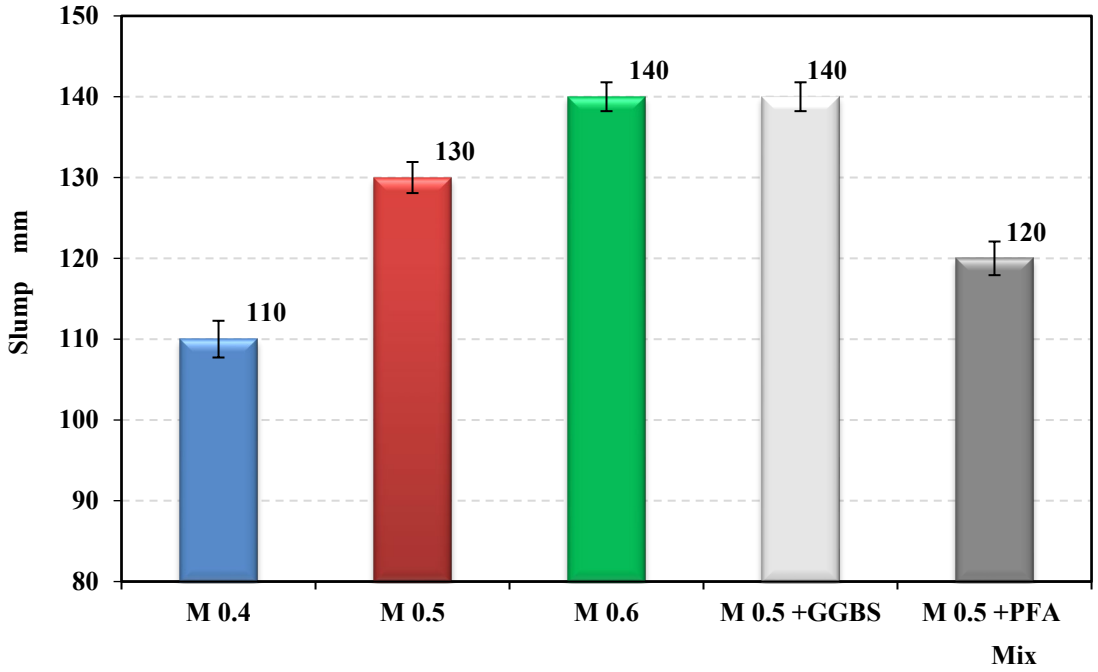

Figure 4.1: Effect of water/ cementitious material ratio on a slump of concrete used in the study

Comparing the three mixes with a w/cm ratio equal to 0.5 in mixes (M 0.5, M0.5+GGBS and M0.5+PFA), it can be seen that mix M0.5+GGBS increase the slump of the mix by 7% while, the PFA decreases it at the same rate.

The improvement in a slump for mixes without SCMs can be accounted for due to an increase of the water quantity with respect to a decrease of cement content, hence, the consumption of water was relatively less, due to the amount of water required for complete hydration of cement being lower, therefore making concrete mixtures workable. Accordingly, the yield stress value might decrease causing the increased flowability (Mehta and Monteiro, 2006). The improvement in a slump for M 0.5 +GGBS being since the particle surface of GGBS is smooth, and a result there is a reduction of the hydration speed and consumption of water. Because of this material needs the $Ca(OH)_2$ which is produced from cement hydration to break down its external layers firstly, then GGBS starts in hydrated with water (Meusel and Rose, 1983). Whilst, the slump of a M 0.5+ PFA was less than the reference mix, due to size, shape and quality of the surface of particle of PFA. These results were compatible with the results that were achieved by Archuleta *et al*. (1986).

Finally, the slump test results are a measurement of workability and fresh properties of concrete mixes (consistency and uniformity of mix). These results with other parameters (content and type of cement and curing period etc.) affect the physical and mechanical properties of concrete.

4.3 Hardened Properties of Concrete

4.3.1 Water Permeability and Porosity of Concrete

The micro- pore structure of concrete, continuous porosity is one of the principal factors affecting the durability of concrete. The porosity for both types of concrete (with and without supplementary cementitious materials, SCMs) is presented in Table A.1 (Appendix A) and Figure 4.2. The results demonstrated that the porosity of concrete slightly increases with an increase of the w/cm ratio at the different age (see Figure 4.3 and Table 4.1) and the effect of SCMs on the porosity of concrete samples varied with curing age due to the hydration of these materials as mentioned previously.

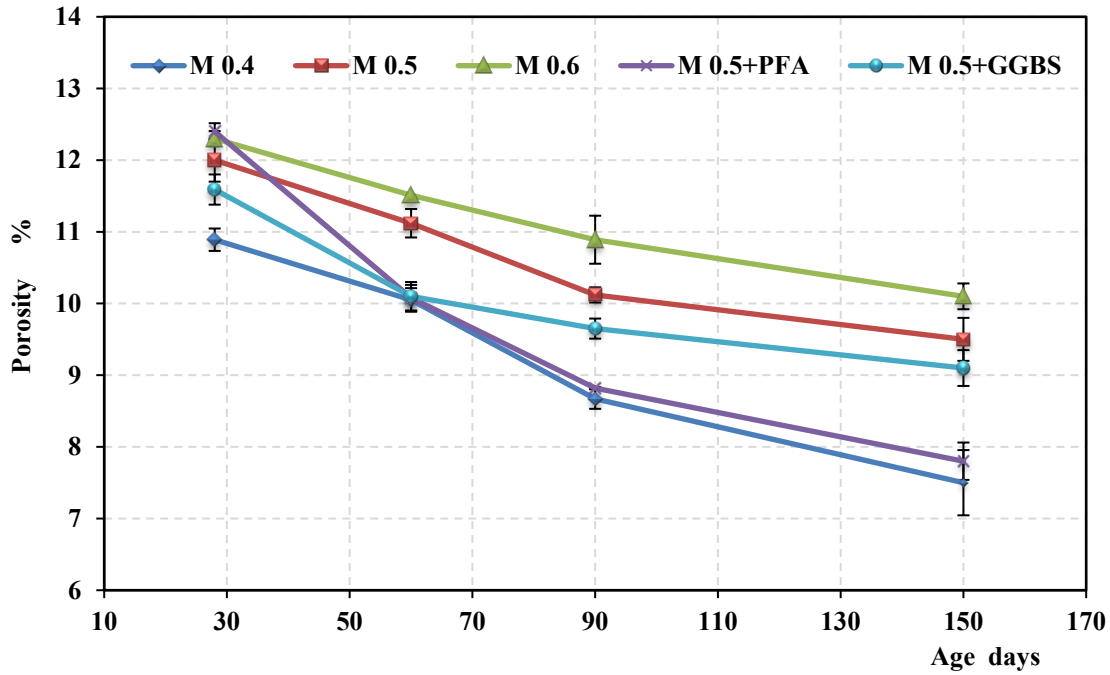

Figure 4.2: Change in porosity of concrete with age

The results showed that the porosity of concrete slightly reduces as hydration progresses with age. The cement content and the increase of hydration production of cement due to the hydration progresses with age was the main reason for development pore structure commensurate that led to the decrease in the porosity for all specimens mixes at 150 days. Thus, the reduction in porosity is a decrease in the volume of micro-

pore structure of concrete. The hydration products act as a gelling material that fills the concrete pores and creates an impermeable structure (gel/ space) that reduces the porosity and water absorption of concrete (Mehta and Monteiro, 2006; Neville, 2011).

The main reason of an increase the porosity due to an increase w/cm ratio of concrete as is the demand of cement for water to hydrate is less than what is currently available, above that amount will be over demand of cement hydration. Hence, extra water or moisture that is unbound by hydrated compounds (free moisture) may evaporate leaving voids inside the structure of the concrete mass (Neville, 2011).

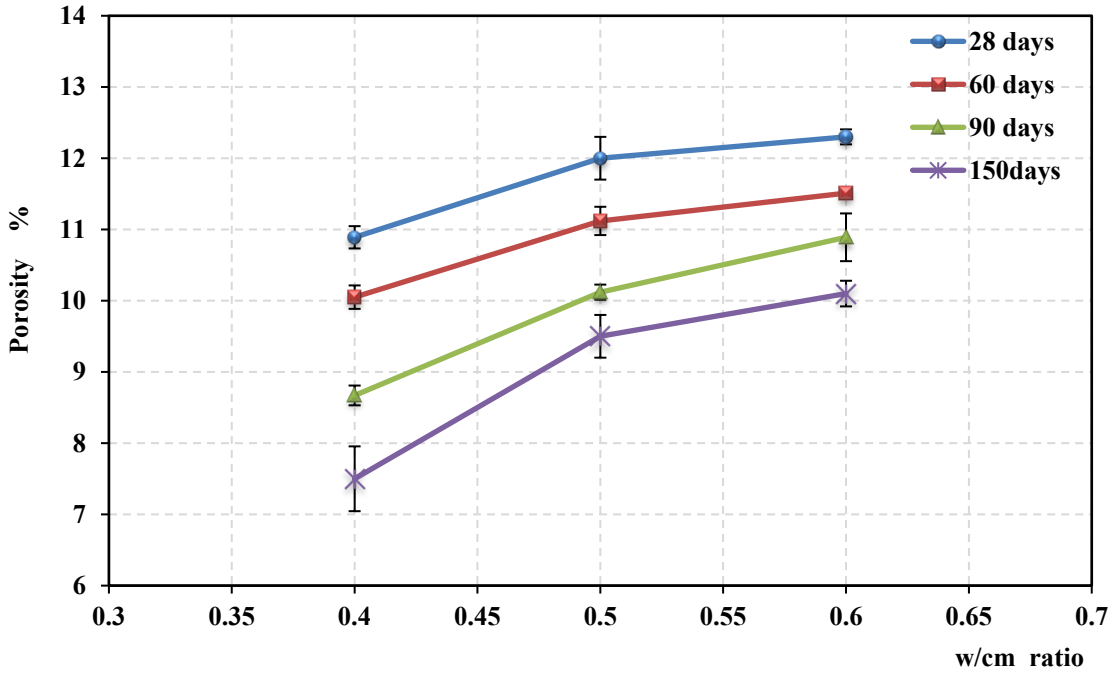

Figure 4.3: Effect of w/cm ratio on the porosity of concrete

Table 4.1: The change in porosity and water absorption with respect to mix M 0.4

Mixes Designation	w/binder	Change in porosity with respect M 0.4 at				Change in water absorption with respect M 0.4 at			
		28 days	60 days	90 days	150 days	28 days	60 days	90 days	150 days
M 0.5	0.5	10.1	11.0	16.1	26.7	16.0	15.6	17.5	26.5
M 0.6	0.6	12.8	15.0	25.3	34.7	14.0	20.0	27.5	38.2
M 0.5 +PFA	0.5	13.8	0.1	1.1	4.0	16.0	4.4	2.5	5.9
M 0.5 + GGBS	0.5	6.4	0.9	11.5	21.3	8.0	4.4	12.5	23.5

On the other hand, the impact of cement replaced by the SCMs, GGBS and PFA is presented in Figure 4.2. The results showed that the replacement of cement by GGBS and PFA has a higher impact on decreasing the porosity with the progression of age than in the mix M 0.5. The mix M 0.5+PFA is found to have the smallest porosity and water absorption compared with Mixes M 0.5 and M 0.5+GGBS.

For the reduction of the porosity in concrete incorporating GGBS and PFA, it is essentially that SCMs are in a finely divided state as it is only then that silica in these materials can combine with calcium hydroxide (produced by the hydrating Portland cement) in the presence of water to form stable calcium silicates which have cementitious properties which may fill the microstructure of concrete (Roy and Indorn, 1982; Meusel and Rose, 1983; Neville, 2011).

Finally, the porosity is an important factor affecting the penetration of chloride (d_{cl^-}) and diffusivity of carbonic ions (CO_3^{2-}) in concrete. Thus, the results of porosity will be used to justify the results of chloride penetration, carbonation depth and corrosion rate and in the modelling of diffusion of the Cl^- and CO_3^{2-} in concrete with different exposure conditions according to the study area (Iraq and UK) to predict the effect of climate parameters, chloride concentration and carbonation depth in concrete structures.

4.3.2 Compressive and Splitting Tensile Strength of Concrete

The results of 28, 60, 90 and 150 days compressive, splitting and flexural tensile strength for the mixes with various w/cm ratios and supplementary cementitious materials are listed in Table 4.2. The results demonstrate that the strength, compressive, splitting and flexural of concrete significantly increase with a decrease in the w/cm ratio and the strength, compressive and splitting of concrete mixes with SCMs was less than M 0.5 at different curing age as shown Figures 4.4 and 4.5. The results indicate that all specimens exhibited a continuous gain in compressive and splitting tensile strength as hydration progresses with age as shown in Figures 4.4 and 4.5.

This increase in compressive and splitting strength with age is due to the continuation of the hydration process, which generates new hydration products to increase the binding materials within the concrete structure and an enhancement of micro-pore structure as shown in Figure 4.2.

The data indicates that the 0.4 w/cm ratio provided the highest strength for these mixes, beyond this value (w/cm= 0.4), the compressive and splitting strength decrease with increasing w/cm ratio at different ages of the test.

Table 4.2: Mechanical properties of mixes used in the study*

Mixes Designation	$\frac{w}{cm}$	Age day	Compressive strength MPa	Splitting strength MPa	Flexural strength MPa
M 0.4	0.4	28	51.5	3.3	-
		60	53.2	3.5	3.8
		90	57.8	3.7	-
		150	60.5	3.8	-
M 0.5	0.5	28	40.1	2.9	-
		60	48.1	3	3.6
		90	50.9	3.4	-
		150	53	3.6	-
M 0.6	0.6	28	36.3	2.5	-
		60	39.7	2.6	3.4
		90	43.3	2.8	-
		150	45.6	3	-
M 0.5 + 0.35 PFA	0.5	28	24.5	2.6	-
		60	31.6	2.8	4.4
		90	35.5	2.9	-
		150	38.3	3.2	-
M 0.5+0.3 GGBS	0.5	28	39.6	2.8	-
		60	47.2	3.0	3.6
		90	48.2	3.1	-
		150	51.2	3.3	-

*These results are average of three samples.

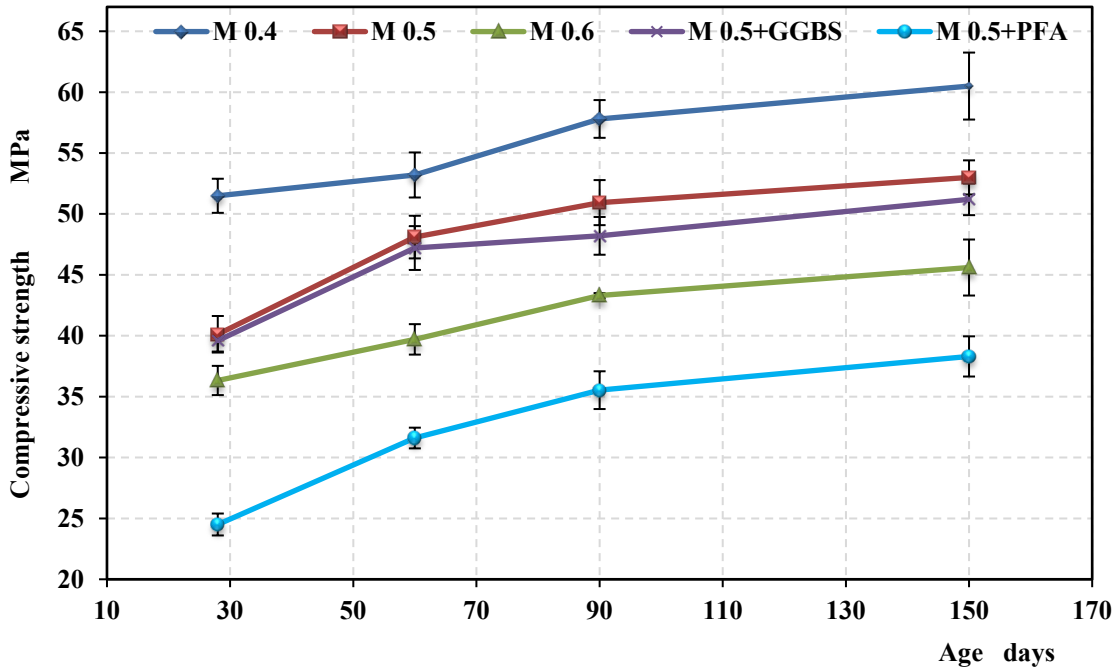

Figure 4.4: The compressive strength of concrete mixes

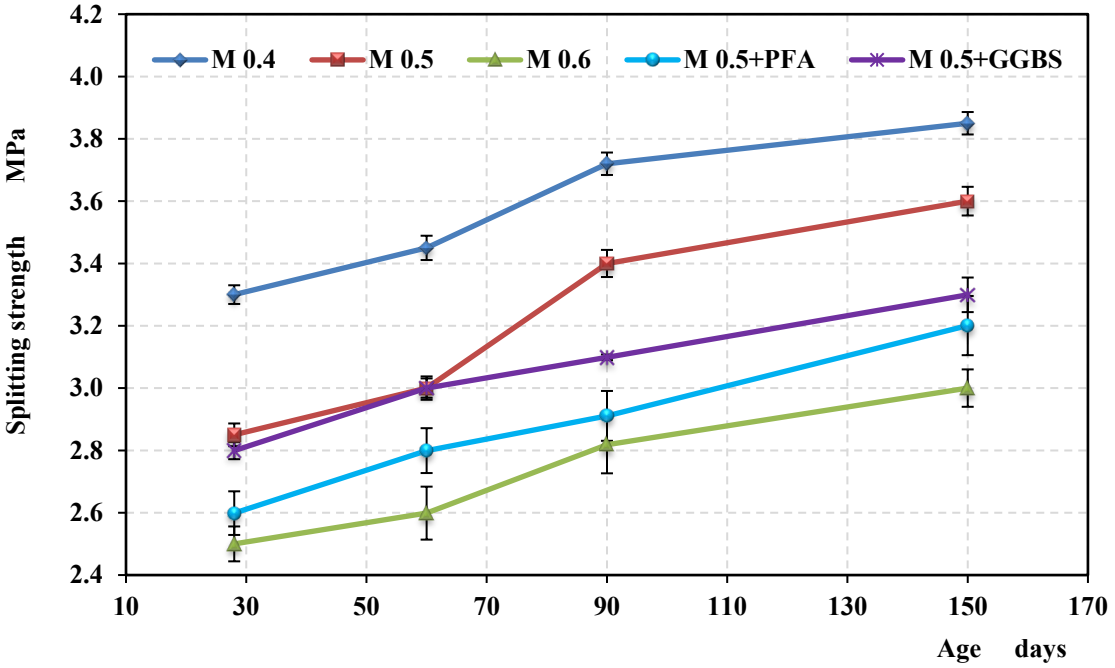

Figure 4.5: Splitting Tensile strength of concrete mixes

On the other hand, the influence of incorporating supplementary cementing replacement material such as GGBS and PFA on the compressive and splitting strength of concrete is also illustrated in Table 4.2 and Figures 4.4-4.5. The results indicate that 35% PFA and 30% GGBS cement replacement decreased the compressive and splitting strength when compared with the strength of OPC concrete (M 0.5) at different age. The

strength was slightly less in M 0.5+GGBS cement replacement compared with M 0.5 as shown in Figures 4.4 and 4.5.

It has been seen that there was a decrease in strength when the w/cm ratio exceeded the value of 0.4; this decrease is attributed to excess water. The excess water will form voids within concrete causing a reduction in the density of concrete. Whereas, the strength increases with an increase in density and reduction of porosity as shown in Table 4.2 and A.1(Appendix A) (Neville and Brooks, 1987). It has also been noticed that the presence of GGBS and PFA in the mixes leads to lower compressive and tensile strength. In these mixes, PFA and GGBS are used as a partial substitution for cement and the gain of hydration of these materials is less than the growth of cement in the short term. On the other hand, the progress of strength of these materials in the long term depends on their activity (fineness and chemical composition etc.) (Ramezanianpour and Malhotra, 1995). In SCMs, the progression of strength due to hydration, can be measured by the activity index (strength of 50% replacement /strength of 0% replacement). The activity index of GGBS was 65% and 90% at 7 and 28 days respectively as shown in Table 3.7.

The effect of the porosity of concrete on compressive strength at the different curing ages is presented in Figure 4.6; it shows the porosity of concrete decreased with the progression of age. The compressive strength of the concrete also increases with progression in curing time and decrease the porosity. Also, this relationship was the exponential relationship between porosity and compressive strength of concrete for each of the single blends of cement type regardless of the water-cement ratio and curing age. These relationships within the same cement type for mixes used for concrete showed a strong correlation (correlation coefficient, R^2 were ≥ 0.90) (Lian *et al*., 2011). That conferred more confidence for the clarification of compressive strength gained with dropping the porosity of concrete (Song, 2014).

Finally, the compressive and tensile strength of concrete is very strongly affected by concrete porosity; reduction in porosity can increase the strength significantly. This change in porosity of concrete can be induced by increasing the solid particle gains in concrete mass (hydration products) due to the progress in curing period (Neville, 2011).

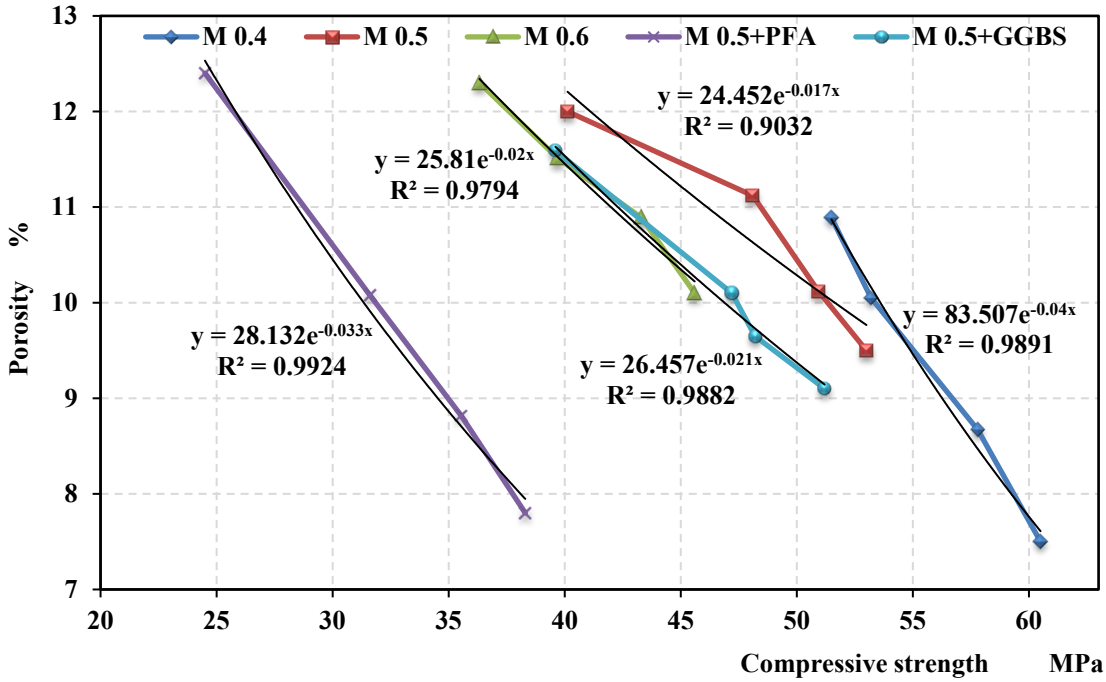

Figure 4.6: Relationship between porosity and the compressive strength

In addition, relationships between compressive strength and the splitting tensile strength of concrete are found and plotted in Figure 4.7. The Results showed there is strongly relationship between compressive and splitting tensile strength of concrete, as the compressive strength increases, the splitting tensile strength also increases; the relationships are proposed as can be seen in Equation 4.1.

$$f_{sp} = 2.7453\, ln(f_{cu}) - 7.4645 \qquad (4.1)$$

where:

f_{sp} is the splitting strength in MPa and f_{cu} is the compressive strength in MPa.

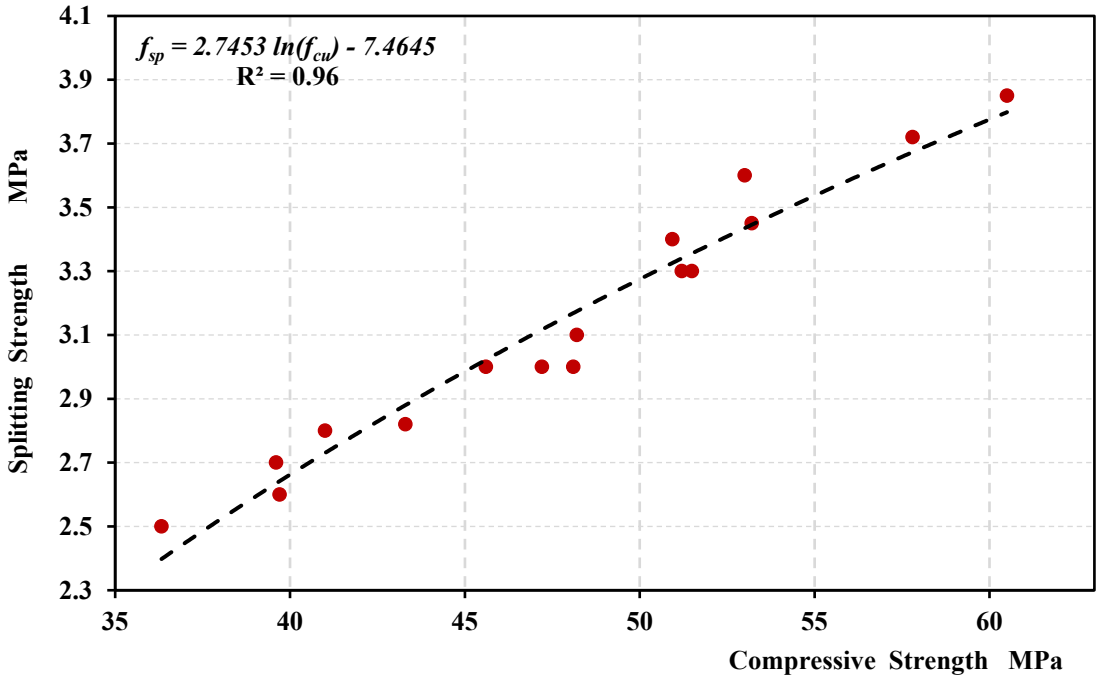

Figure 4.7: Relationship between the compressive strength and splitting tensile strength

4.3.3 Gas Permeability in Concrete

A Gas permeability test was used to assess the micro- pore structure of concrete and crack width by measuring permeability or continuous pores in concrete samples. The values of gas permeability coefficient known as the Darcy's factor, K_i for the concrete samples at age of 90 days are presented in Figure 4.8 and Table A.2 (Appendix A). The results indicate the gas permeability coefficient increased with an increase w/cm ratio and crack width in un-cracked and cracked concrete samples.

On the other hand, no significant change in gas permeability was observed for different crack width on K_i values as shown in Figure 4.8. However, the gas permeability coefficient in mix M 0.5+ GGBS for a different crack width increased slightly. While, the K_i in mix M 0.5 + PFA for a crack width of 0.1mm increased significantly and beyond crack width 0.1mm the increase was slightly with an increase crack width as shown in Figure 4.8.

This increase of K_i values for concrete causes the increase of the volume of connective voids in the micro- pore structure of concrete or the continuous porosity of concrete (RILEM TC-116-PCD: 1999) due to an increase in the w/cm ratio (as mentioned in section 4.3.1)

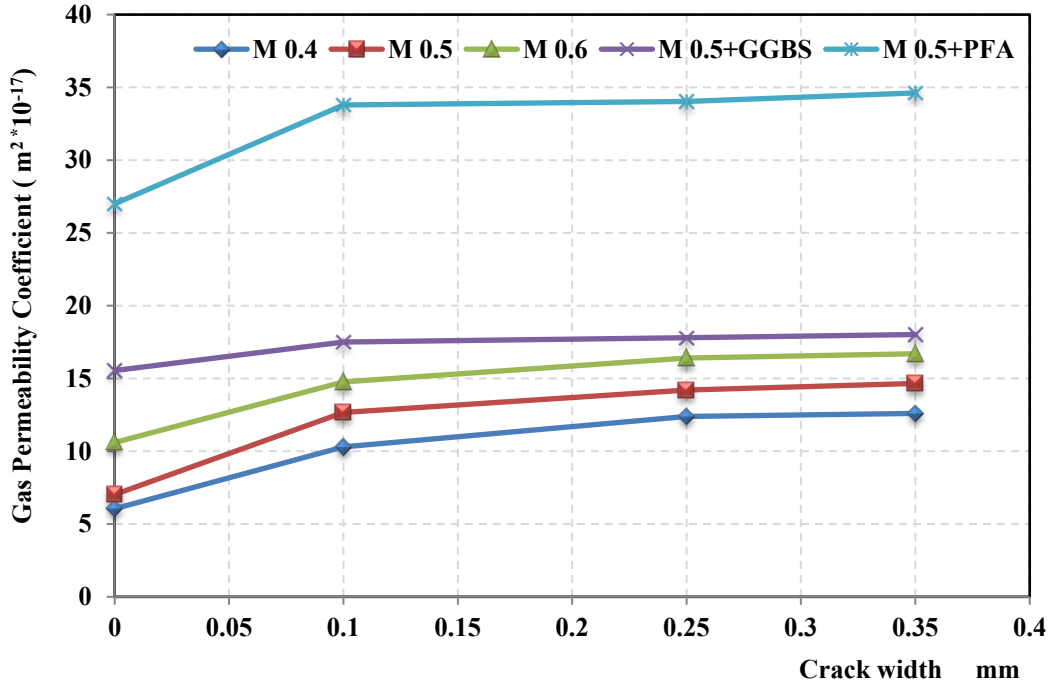

Figure 4.8: Gas permeability coefficient, K_i

4.3.4 Chloride Permeability and Diffusion Migration Coefficient

The chloride migration coefficient, D_{nssm} and chloride penetration in concrete by using method described in NT Build 492: 1999 for all mixes were experimentally measured at ages 28 and 150 days, the results of these tests are summarized in Figures 4.9 and 4.10 and in Table A.3 (Appendix A). Results presented in graphs indicate the reduction in D_{nssm} and chloride penetration with the progress of curing age.

The D_{nssm} and chloride penetration for the mix with w/cm ratio 0.4, is lowest for mixes without SCMs and the mix has highest compressive strength in both ages of testing. The mixes have a w/cm ratio up to (M 0.4), the chloride penetration increases in concrete as shown in Figure 4.11. Hence, the D_{nssm} value and chloride penetration depth in concrete also increases.

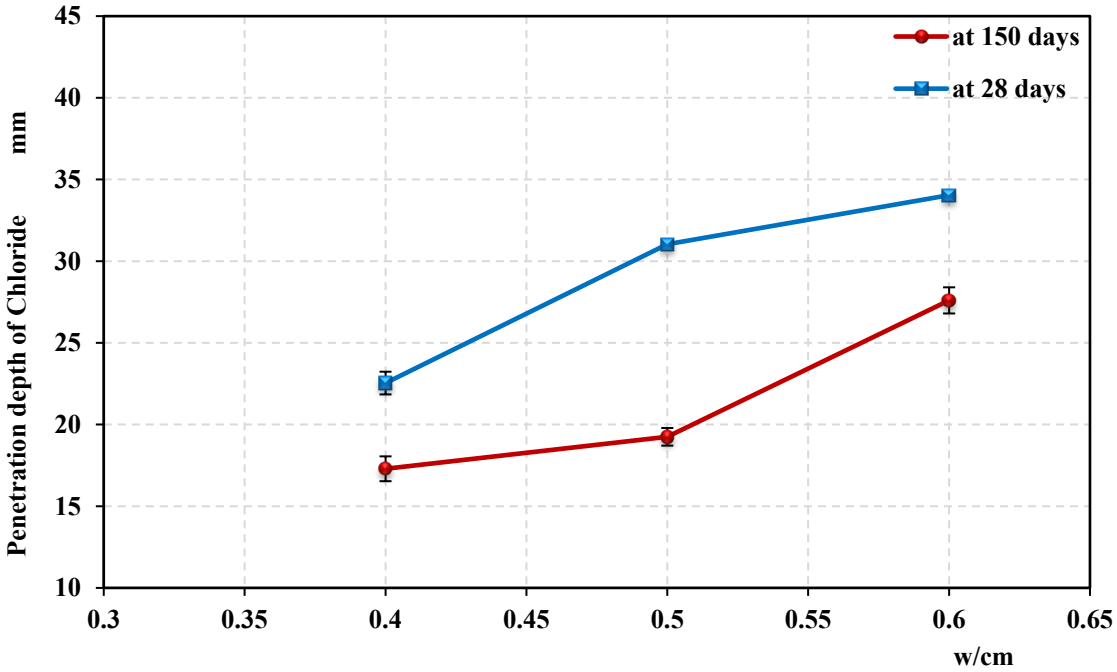

Figure 4.9: Effect of water-cement ratio on chloride penetration (for OPC only mixes)

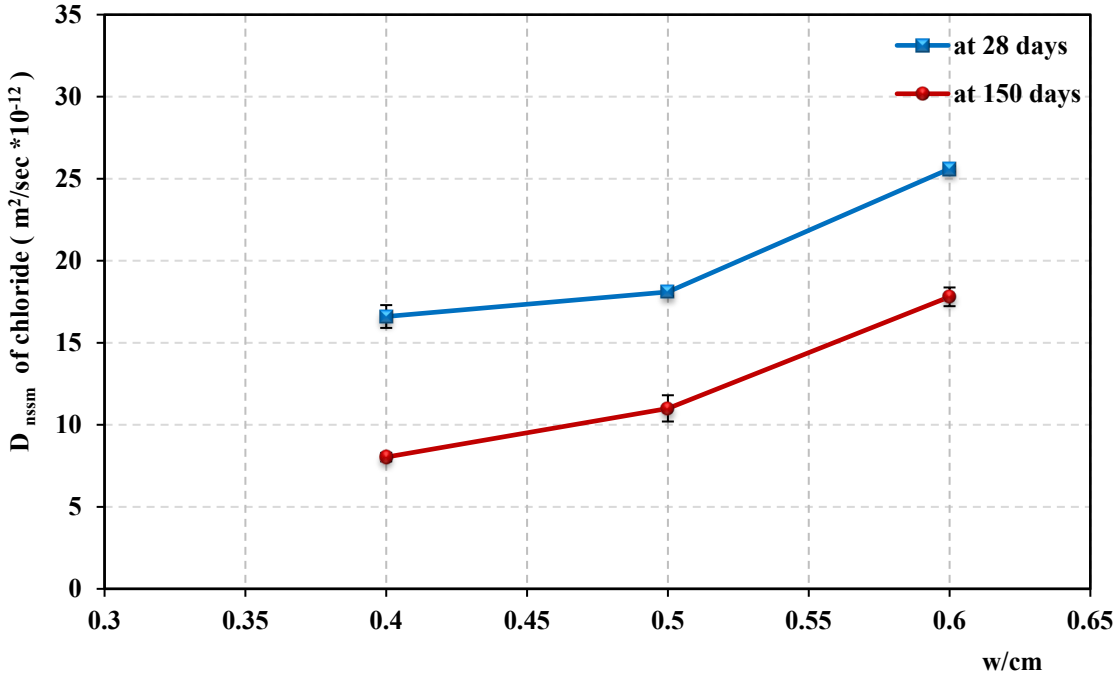

Figure 4.10: Effect of water- cement ratio on chloride migration coefficient D_{nssm} (for OPC only mixes)

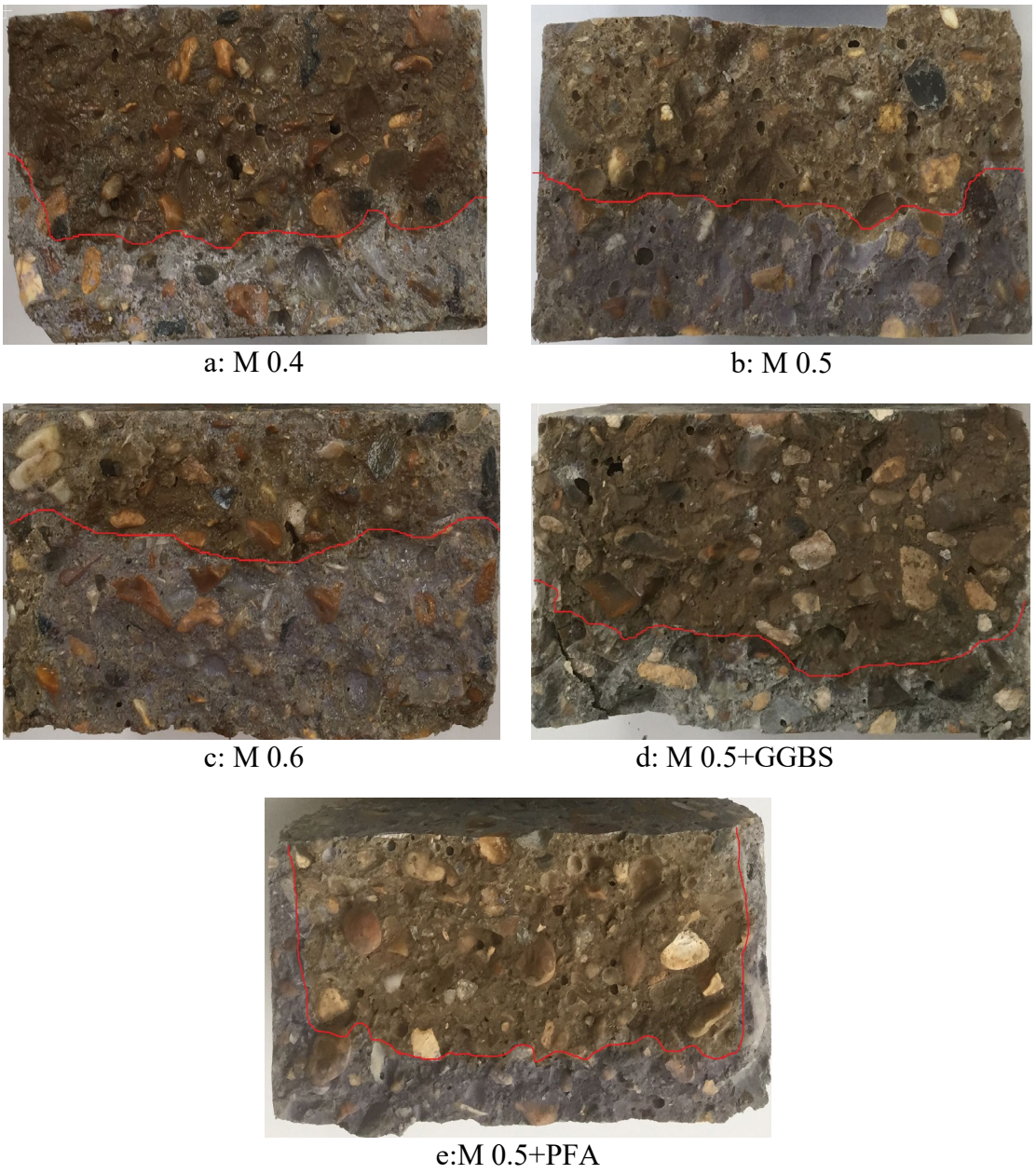

a: M 0.4 b: M 0.5

c: M 0.6 d: M 0.5+GGBS

e:M 0.5+PFA

Figure 4.11: Chloride penetration due to chloride migration test.

The D_{nssm} value increased significantly with increased w/cm ratio in mixes for both ages due to higher the volume of connective pores in the concrete mass and an increase in the permeability of the concrete. Therefore, the results of the migration chloride coefficient D_{nssm} increases with increasing the porosity of concrete as shown in Figure 4.12.

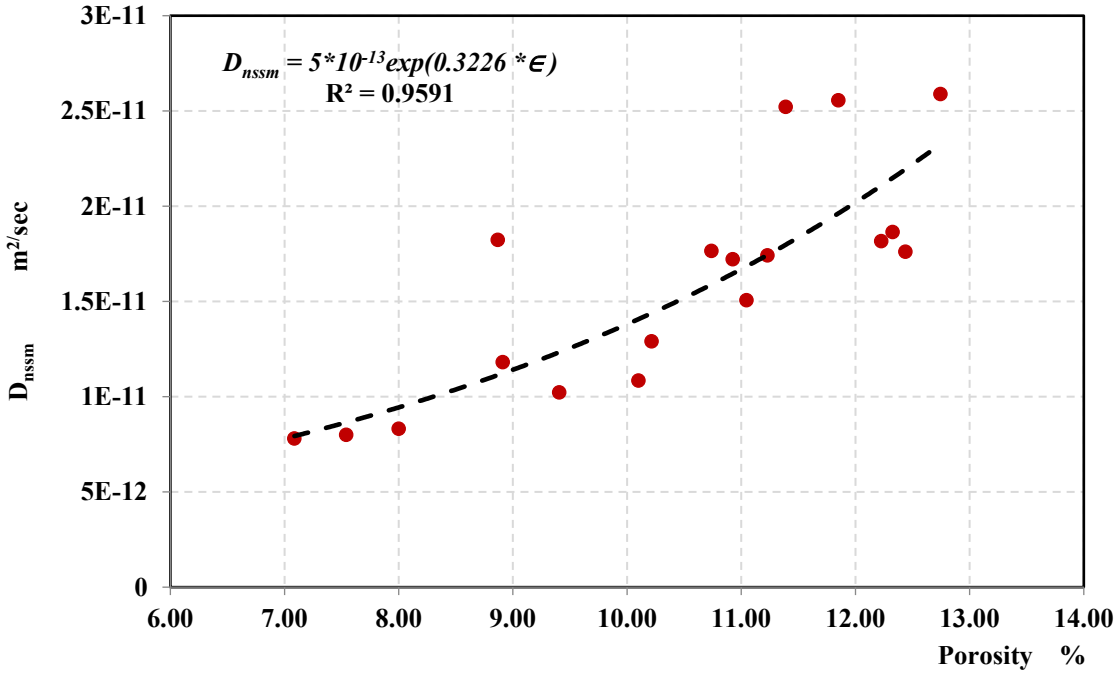

Figure 4.12: Relationship between the porosity (∈) of concrete and chloride diffusion coefficient (D_{nssm})

The reduction in D_{nssm} and chloride penetration at age 150 days and respectively the D_{nssm} at age 28 days results from a decrease in the volume of connective pores in cement paste and an increase in the solid particle gains in concrete mass (hydration products) due to the progress in the curing period (Neville, 2011). This progress will densify the matrix of the interfacial transition zones ITZ between cement paste and both types of aggregate (Mehta and Monteiro, 2006).

The percentages of increase in chloride penetration depth for mixes having a w/cm ratio 0.5 and 0.6 were 37% and 51%, and 11% and 59% at 28 and 150 days respectively compared to the corresponding mixture which had w/cm ratio 0.4. Also, the percentages of increase in chloride migration coefficient for mixes having w/cm ratio 0.5 and 0.6 were 36% and 122%, and 9% and 54% at 28 and 150 days respectively compared to the corresponding mix which had w/cm ratio, 0.4.

The D_{nssm} and chloride penetration depth for concrete incorporating GGBS and PFA at ages 28 and 150 days are plotted in Figures 4.13 and 4.14.This results show the reduction in D_{nssm} and chloride penetration when OPC is replaced by SCMs, PFA and GGBS at the two ages. The percentage of decrease in chloride penetration depth for mixes having GGBS and PFA were (28% and 23%) and (22% and 19%) at 28 and 150 days

respectively compared to the corresponding mixture which does not have SCMs as shown in Figure 4.13. The percentages of decrease in D_{nssm} for mixes which have GGBS and PFA were 45% and 36%, and 35% and 33% at 28 and 150 days respectively compared to the corresponding mixture which does not have SCMs as shown in Figure 4.14.

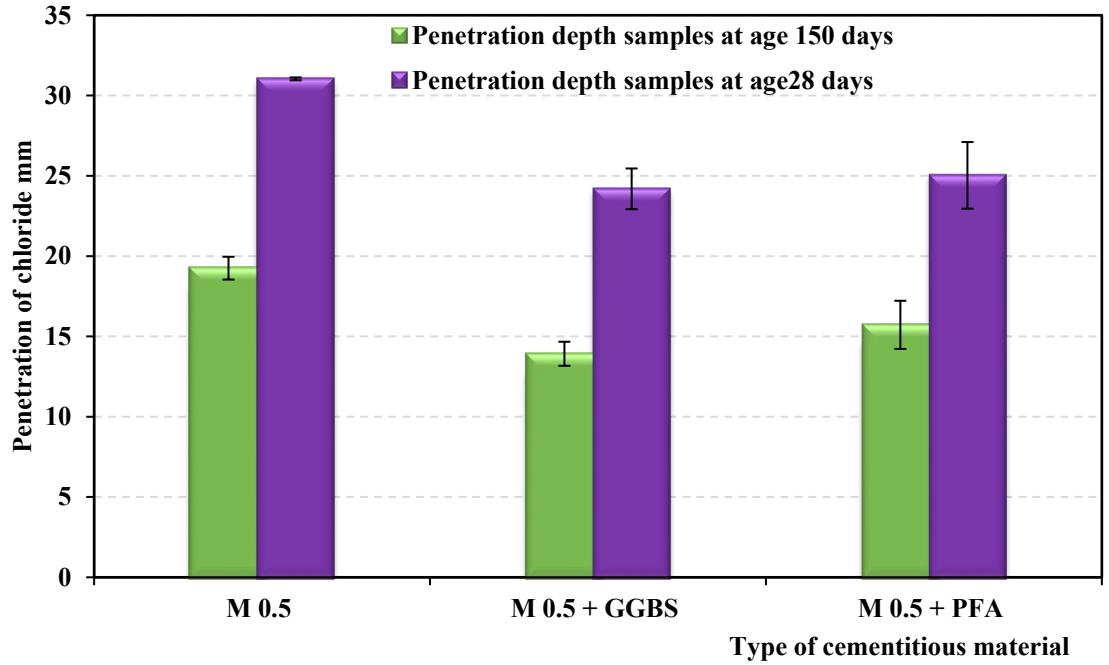

Figure 4.13: Effect of type of SCMs on chloride penetration due to migration test

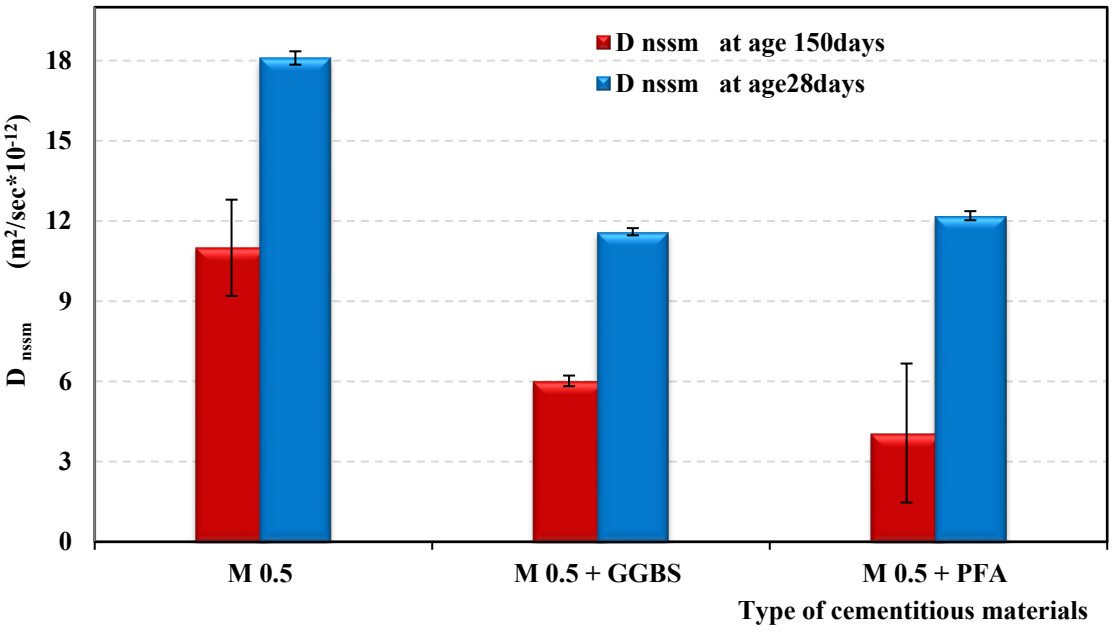

Figure 4.14: Effect of type of SCMs on chloride diffusion coefficient (D_{nssm})

The main reason for this reduction in D_{nssm} and chloride penetration is the supplementary cementitious materials (SCMs), such as PFA, slag, silica fume, and metakaolin and other natural pozzolans, which have a significant impact on the ability of concrete to resist the penetration of chloride ions. This benefit is largely ascribed to the refined pore structure that results from the appropriate use of SCMs which, in turn, results in reduced permeability and ionic diffusivity (Thomas *et al*., 2012; Srinivasan and Gibb, 2018).

The results also indicate that the chloride migration coefficients in various mixes of concrete were reduced with an increased curing period. This reduction in both is due to the improvement of the micro-pore structure of concrete by increasing solid particle gains in concrete mass due to hydration of cementitious materials with time. The percentages of decrease of D_{nssm} for mixes between 28 days and 150 days were (52%, 39%, 30%, 48% and 67%) for mixes M 0.4, M 0.5, M 0.6, M 0.5+GGBS and M 0.5+PFA respectively.

The reduction in diffusion coefficient of chloride with progresses of exposure age is called the ageing factor. Takewaka and Mastumoto (1988) proposed a formula to compute the ageing factor between the two values of the diffusivity of chloride coefficient $D_c(t)$ at two ages as Equation 4.2:

$$m = ln \frac{\left\{\frac{D_C(t)}{D_C(t_{ex})}\right\}}{\left\{\frac{t_{ex}}{t}\right\}} \qquad (4.2)$$

where:

t_{ex} is initial exposure time (28 days), t is specific time (150 days), $D_c(t_{ex})$ is the diffusion coefficient at t_{ex}, m is the ageing factor (diffusivity reduction factor).

Table A.3 (Appendix A) is presented with the ageing factors for all mixes used; they ranged from 0.21 to 0.42 for mixes without additive materials, and 0.43 and 0.65 were for mixes with GGBS and PFA respectively. The ageing factor is likely to be between 0.2 and 0.8 (CEB-FIP, 2010; ACI Committee 365, 2008; Wang *et al*., 2016).

The microstructure of concrete, the permeability of concrete, development of strength of concrete and type of cementitious material used in concrete, such as cement,

fly ash and GGBS have an important impact on the chloride diffusion coefficient (Vu and Stewart, 2000).

The compressive strength and splitting strength of concrete have been significantly associated with the quantity, volume, type and distribution of pores in the concrete mass, which probably gives information about the overall quality of the concrete. It is essential to assess the relationship between the grade of concrete strength and chloride ingress resistance of concrete. Therefore, chloride ingress properties in the concrete or D_{nssm} have been closely correlated with the compressive strength and splitting strength of concrete. The results of D_{nssm} and strength test indicates towards the strong relationship between chloride ingress resistance of concrete and compressive and splitting strength. Non-linear regression analysis was employed, and correlation coefficients were found, $R^2 > 0.94$ as shown in Figures 4.15 and 4.16. Hence, the compressive and splitting strength of concrete can be appropriately used to estimate the chloride penetration resistance of the same type of cement mixtures of concrete.

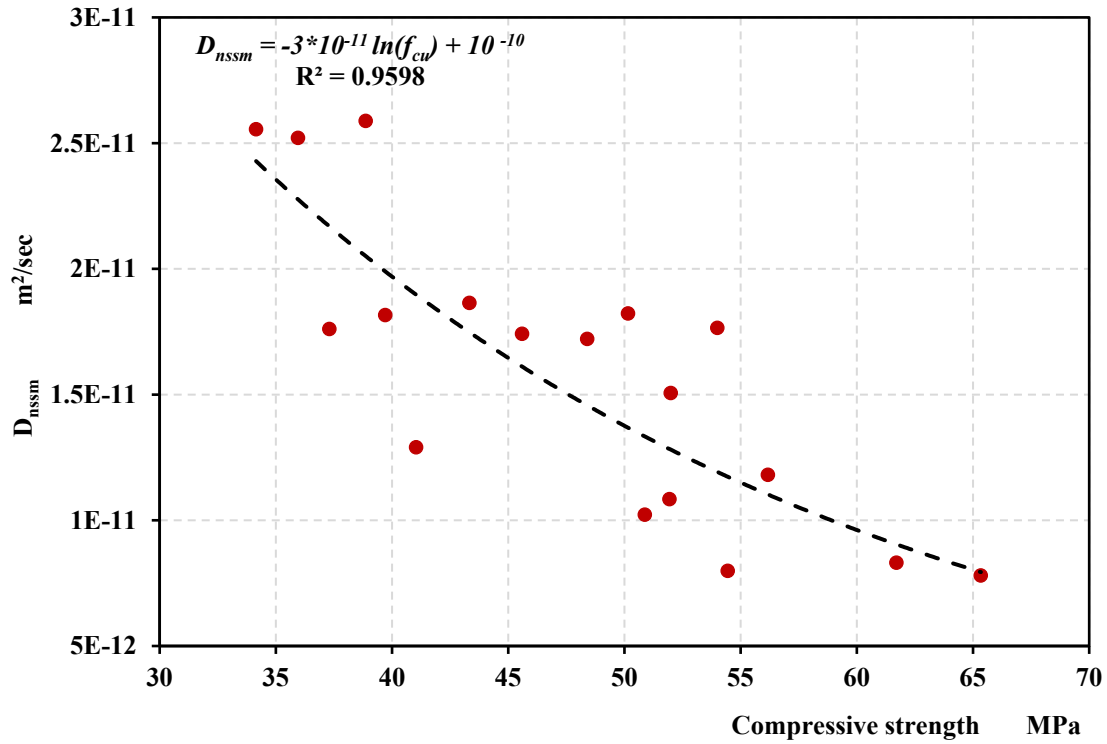

Figure 4.15: Relationship between compressive strength and chloride diffusion coefficient (D_{nssm})

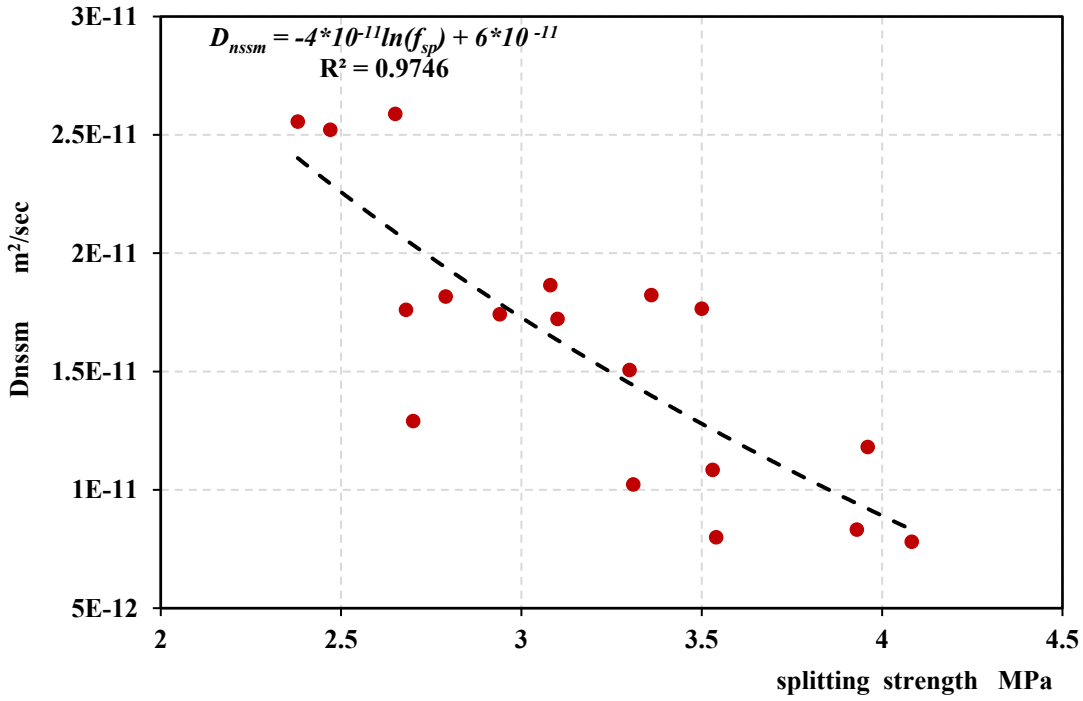

Figure 4.16: Relationship between splitting tensile strength and chloride diffusion coefficient (D_{nssm})

4.4 Summary

In this study, three of the water-cement ratios (0.4, 0.5 and 0.6) and the remaining two have the same w/cm ratio (0.5) but OPC was partially replaced by supplementary cementitious materials, SCMs (GGBS and PFA). The effect of w/cm ratio and the effect of partially replacement of OPC with PFA and GGBS on the porosity, water absorption, gas permeablitiy and chloride penetration were examined experimentaly. The results showed that:

- The increase of water - cenment ratio and use GGBS are significant factors on the flowing ability of fresh concrete (workability), consistency and uniformity of mixes without segregation and bleeding.
- The microstructure of concrete (porosity or connective pores) mainly affects by w/cm ratio, type of cementitious materials, the degree of hydration of cementitious materials and curing period. The porosity or permeation properties is an indicator of the microstructure in the concrete mass.
- The results of the porosity measurements might suggest a lower percentage of water absorption for specimen mix M 0.4 for 150 days due to their more developed pore structure commensurate with a higher degree of hydration.
- The movement or transportation of gases (gas permeability), liquids (water absorption and porosity), and ions (migration of chloride coefficient) through concrete are important because of their interactions with concrete constituents or the pores in concrete mass.
- Diffusion migration of chloride ions is the process by which matter is transported from one part of a system to another due to applied voltage to accelerate the penetration of chloride in concrete samples. This process of transport of chloride ions depends on the pore structure of the concrete mass. Thus:
  - The chloride migration coefficient D_{nssm} increased significantly with increasing w/cm ratio of mixes at different curing ages.
  - The chloride migration coefficient D_{nssm} of concrete with SCMs (GGBS and PFA) decreased significantly at different curing ages.
  - The chloride ingress properties in the concrete or D_{nssm} have been closely correlated with the porosity, compressive strength and splitting strength of concrete.

CHAPTER V: CARBONATION IN CONCRETE

5.1 Introduction

In this chapter, the results of carbonation are presented and discussed with the main focus on three aspects; the impact of climate change parameters (temperature, relative humidity and carbon dioxide concentration) on the depth of carbonation (DoC).

The following concrete mixes were studied. Three of them were cement based mixes with three different water/cement ratios (0.4, 0.5 and 0.6) and the other two had the same water/cement ratio (0.5) but SCMs , PFA and GGBS was replaced by Portland cement in the mix in order to get the variety of properties and microstructure of concrete.

The assessment of carbonation depth in the reinforced concrete samples was carried out using different methods, phenolphthalein indicator, X-ray diffraction analysis (XRD) and apparent pH and consumed OH^-. Mostly standard test methods have been used to measure the DoC in concrete.

5.2 Depth of Carbonation in Concrete

Carbonation is known as a neutralizing process, a chemical reaction of $Ca(OH)_2$ and calcium- silicate- hydrate (C-S-H) with CO_2 to form $CaCO_3$ and water. And the depth of carbonation (DoC) is a measure of diffusivity of carbon dioxide in concrete and reduction in alkalinity of pore water solution in concrete. There are several methods used to investigate the DoC, all methods depend on a chemical basis as follows;

5.2.1 Depth of Carbonation by Phenolphthalein indicator

The traditional method to determine the DoC is using a spray of the phenolphthalein pH indicator onto the surface of a freshly split concrete prism. The conditioned prisms were taken out of the carbonation incubator after 8 weeks of exposure and tested as designated by Al-Amoudi *et al*. (1991). For the uncracked sample, the average DoC, X_p

of the colourless phenolphthalein region was measured from three points, perpendicular to the two edges of the split face, both immediately after spraying the indicator and also 24 hours later. While, in the case of the cracked sample, the DoC, X_p of the colourless phenolphthalein region was measured from the top points of the crack tip, perpendicular to the two edges of the face exposed to CO_2 environment. The average depth of the colourless region due to using a spray of the phenolphthalein or DoC, X_p for the mixes used in the study are presented in Figures 5.1 and 5.6 and listed in Tables A.4-A.6 (Appendix A).

The results of the depth of carbonation, DoC were classified according to the affected parameters. Internal factors are related to the concrete composition, w/cm ratio, crack width and replacing of OPC by SCMs (GGBS and PFA), whilst external environment factors included the concentration of CO_2, temperature and relative humidity.

a: Internal Factors Influencing the Depth of Carbonation

The influence of internal factors on the DoC by using phenolphthalein indicator was examined and the results illustrated as follows:

(i): Effect of w/cm Ratio on DoC

In this study, the results indicate the DoC was a function of w/cm ratio and increased significantly with the increase in w/cm ratio of concrete mixes as shown in Figures 5.1 and 5.2. The percentage increase in carbonation depth for the mix with w/cm 0.5 (M 0.5) and the mix with w/cm ratio 0.6 (M 0.6) in comparison to mix w/cm 0.4 (M 0.4) are listed in Table 5.1. The amount of increase percentage in DoC of uncracked samples (M 0.5 and M 0.6) higher than this percentage in cracked samples as shown in Table 5.1.

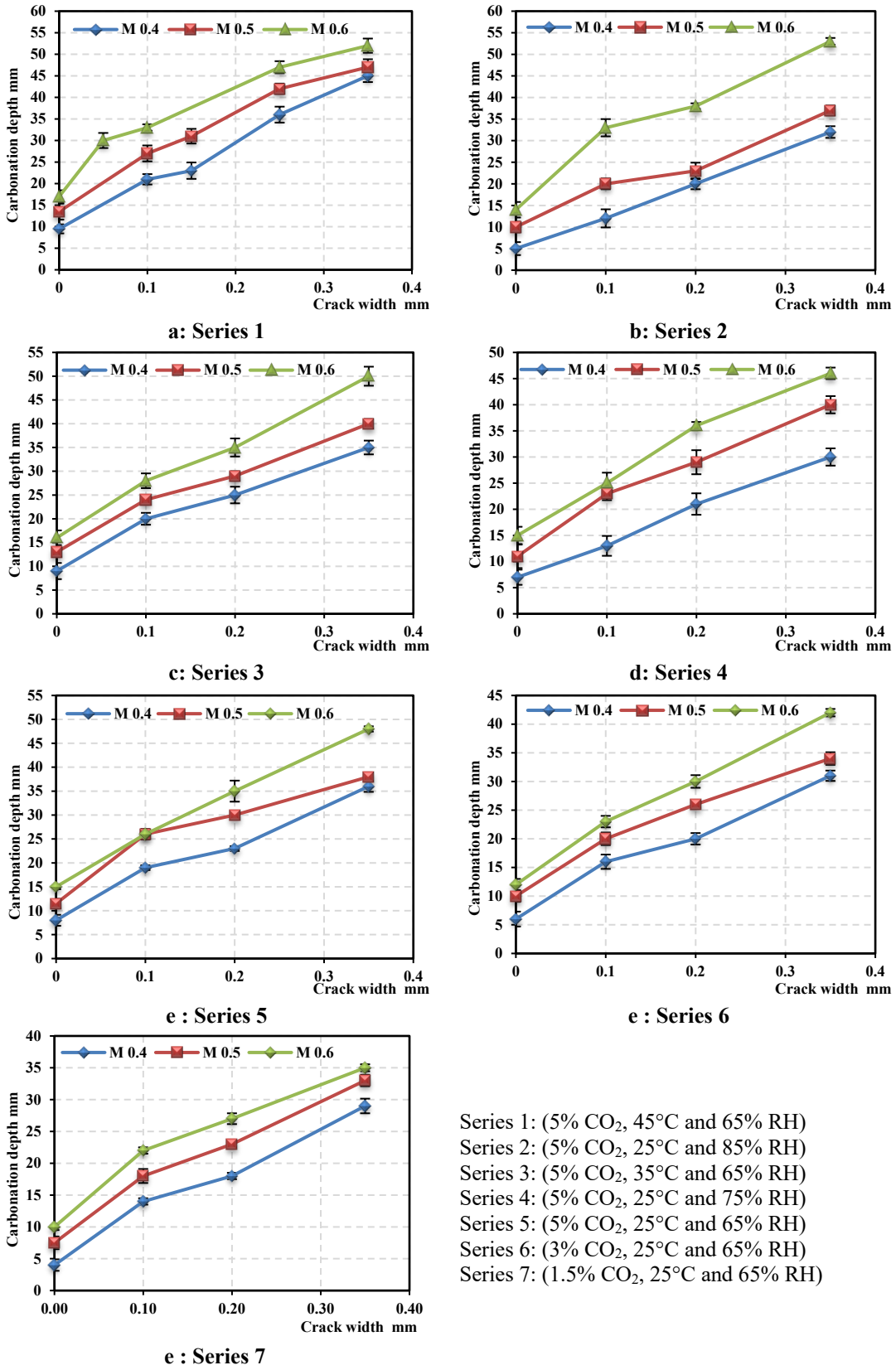

Series 1: (5% CO_2, 45°C and 65% RH)
Series 2: (5% CO_2, 25°C and 85% RH)
Series 3: (5% CO_2, 35°C and 65% RH)
Series 4: (5% CO_2, 25°C and 75% RH)
Series 5: (5% CO_2, 25°C and 65% RH)
Series 6: (3% CO_2, 25°C and 65% RH)
Series 7: (1.5% CO_2, 25°C and 65% RH)

Figure 5. 1: Effect of w/cm and crack width on the depth of carbonation (DoC) in different environmental exposure conditions

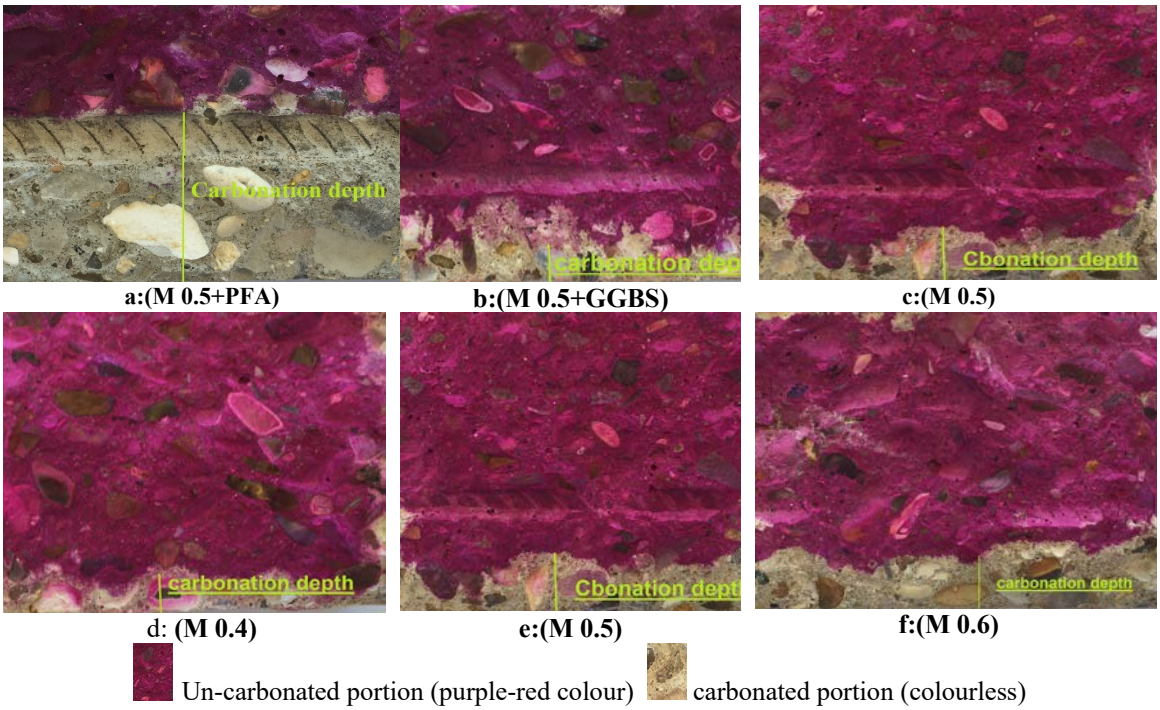

Figure 5.2 Carbonation depth of mixes used in the study (Series1)

Table 5.1: Increase percentage in DoC due to change in w/cm ratio

Case	Sample	Increase percentage in DoC in samples (%)						
		Series 1	Series 2	Series 3	Series 4	Series 5	Series 6	Series 7
M 0.5 / M 0.4	Uncracked	42	100	44	57	44	67	88
	0.05-0.15 mm	29	67	20	77	37	25	29
	0.15-0.25 mm	35	15	16	38	30	30	28
	0.25-0. 35 mm	17	16	14	33	6	10	65
M 0.6 / M 0.4	Uncracked	79	150	78	114	88	100	150
	0.05-0.15 mm	43	67	40	92	37	44	57
	0.15-0.25 mm	43	55	40	71	52	50	50
	0.25-0. 35 mm	31	22	43	53	33	35	75

The effect of compressive strength (which is a function of w/cm ratio) on the carbonation depth is depicted in Figure 5.3-a. The increase in DoC for the uncracked concrete samples with the decrease in compressive strength is due to the increase in the volume of permeable voids that assist CO_2 penetration. Where, Roy *et al*.(1999) reported

that the rate of carbonation is inversely proportional to the strength for concrete without SCMs Furthermore, a key factor controlling carbonation rate is the diffusivity of the hardened cement paste, which is a function of the pore system of the hardened cement paste during the period when the diffusion of CO_2 takes place (Neville, 2011) (see Figure 5.3-b).

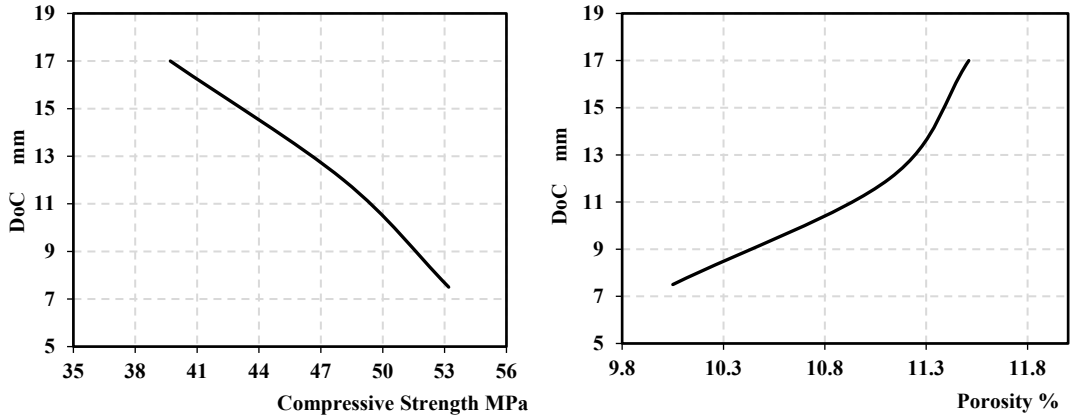

a: Effect of Compressive strength on DoC **b: Effect of porosity on DoC**

Figure 5.3: Effect of compressive strength and porosity on DoC for sample exposed to an accelerated carbon dioxide environment

Figure 5.3 showed the porosity and compressive strength of concrete have a significant impact on the depth of carbonation, DoC. Therefore, it was found that as the compressive strength of the concrete increases (due to decrease w/cm ratio and porosity decreases) there is a corresponding decrease in the DoC. The influence of compressive strength of concrete (f_{cu}) and porosity ($\in$) on DoC has been statistically considered as shown in Equation 5.1

$$DoC = 0.021232 * \in^{3.198} exp(-0.0284 f_{cu}) \qquad (5.1)$$

where:

DoC is Depth of Carbonation (mm), f_{cu} is compressive strength (MPa) and $\in$ is the porosity (%).

It showed that the DoC increases with an increase in w/cm ratio due to the increase in porosity (see Figure 4.3-b) and a decrease in compressive strength (see Figure 4.3-a). This approach appears to be very rational since the DoC, porosity and compressive strength are significantly controlled by the micro-pore structure of concrete (Chi *et al.* 2002). The increase of DoC for un-cracked concrete samples with an increase of w/cm ratio is a result of the increase in porosity and number of connective voids in concrete

mass that help the CO_2 penetrates (the concrete), and consequently enable carbonation to occur.

(ii) Effect of Crack Width on DoC

The results illustrate that the DoC was also a function of crack widths and the DoC increases from the exposed surface considerably with the increase in crack width at the given cross-section of concrete samples as shown in Figures 5.1 and 5.6. Carbonation rates in the vicinity of the crack openings are considerably higher due to relatively faster penetration of the CO_3^{2-} ion into the crack followed by orthogonal outward diffusion into the un-cracked concrete parts surrounding the crack and reaction with Ca^{2+} to form $CaCO_3$ (colourless region due to carbonation as shown in Figure 5.4). Therefore, the DoC measured in the cracked samples is always deeper than the DoC obtained at uncracked samples for all mixes, and this significant increase in DoC for cracked samples with respect to the control concrete samples is shown in Figure 5.1 and in Table B.2 (Appendix B).

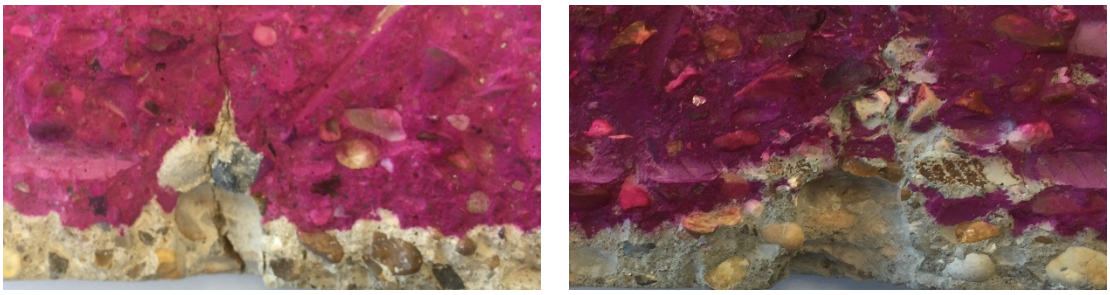

a:M 0.6-cracked 0.2 mm-Series 3 b: Mo.5+PFA-cracked 0.2 mm -Series 3

Figure 5.4: Effect of crack width on the diffusion of CO_2 and reduction in pH level in concrete

Other important observations from the results are; Firstly, the carbonation depth within un-cracked areas of cracked concrete samples (away from the discrete cracks) is considerably less than the carbonation depth in un-cracked control samples; Figure 5.2-a (un-cracked sample) has a mean DoC of 26 mm versus Figure 5.4-b (cracked sample) has a mean DoC of 18 mm. This has not been reported in previous literature and the reasons for this are being investigated in detail.

Secondly, the crack width and depth affect the transport mechanism of CO_3^{2-} ions into the crack opening. On the other hand, connective pores due to an increase w/cm ratio (porosity) in concrete may provide additional penetration of CO_3^{2-} ions in the crack wall.

Hence, an increase in colourless region area (carbonation area) perpendicular to the crack walls can also be observed in Figure 5.4 (a and b) and Table 5.1.

Finally, the increase of DoC for concrete mixes with an increase in the w/cm ratio and crack width is a result of an increase in the crack openings, the porosity of concrete, and volume of permeable voids which help CO_2 to penetrate and react with water to form carbonate acid. The latter reacts with $Ca(OH)_2$ (aq) to bring about the carbonation. The strong evidence and correlation of the influence of permeable voids (measured by gas permeability) (RILEM TC 116-PCD: 1999) on the depth of carbonation, DoC is illustrated in Figure 5.5.

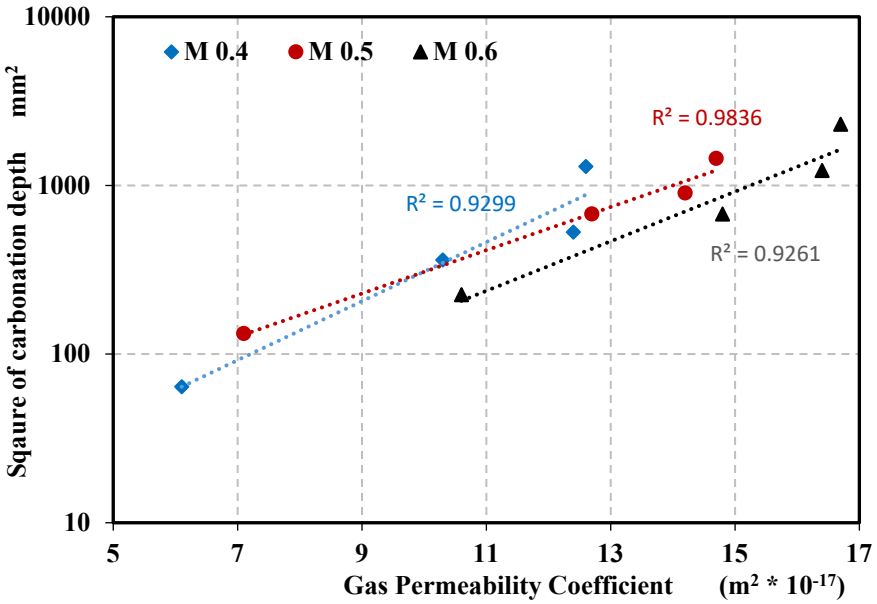

Figure 5.5: DoC as a function of concrete gas permeability

(iii): Effect of Supplementary Cementitious Materials (SCMs) on DoC

The results also illustrated the mixes incorporating the supplementary cementitious material such as GGBS and PFA have a higher DoC than DoC of mixes without these materials, hence the DoC in M 0.5+PFA showed the highest reduction in alkalinity by consumption of $Ca(OH)_2$ and formation of calcium carbonate for all series. This can be linked to the reduction of $Ca(OH)_2$ that is consumed by the SCMs to produce C-H-S gel and $CaCO_3$ (Roy and Indorn, 1982) as shown in Equation 2.1. The impact of replacing OPC by GGBS and PFA with different crack widths for all exposure environmental conditions investigated in this study is presented in Figures 5.6.

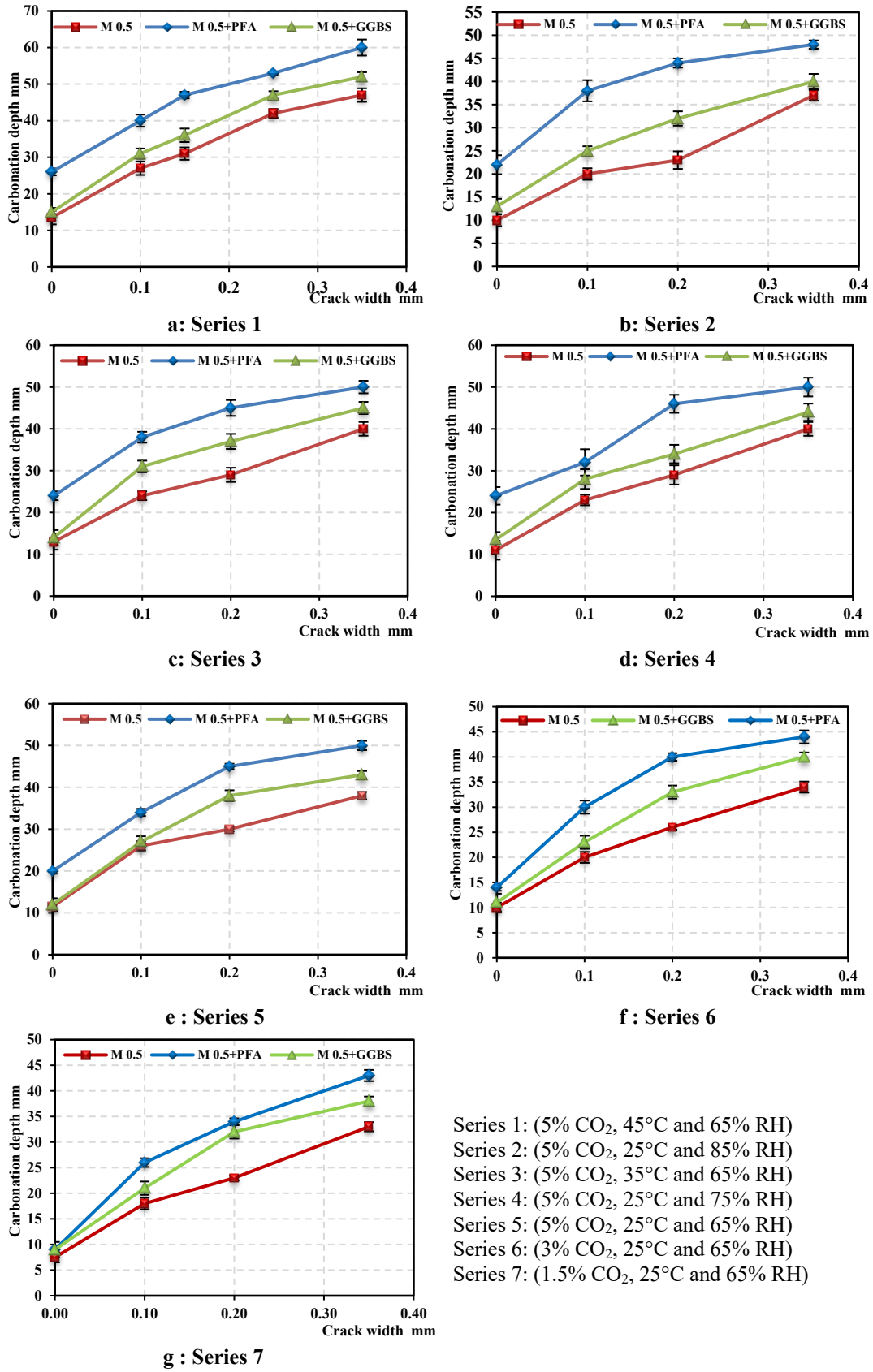

Series 1: (5% CO_2, 45°C and 65% RH)
Series 2: (5% CO_2, 25°C and 85% RH)
Series 3: (5% CO_2, 35°C and 65% RH)
Series 4: (5% CO_2, 25°C and 75% RH)
Series 5: (5% CO_2, 25°C and 65% RH)
Series 6: (3% CO_2, 25°C and 65% RH)
Series 7: (1.5% CO_2, 25°C and 65% RH)

Figure 5.6: Effect of SCMs (GGBS and PFA) and crack width on the depth of carbonation (DoC) in different environmental exposure conditions

The increase in DoCs for M 0.5+PFA and M 0.5+GGBs for all series are shown in Figure 5.6. For example, the increased percentages of DoCs for M 0.5+PFA-Series1 were 174%, 90%, 104% and 47% for samples, which have a crack width (0, 0.1, 0.2 and 0.3), respectively where the mix has the same w/cm ratio, M 0.5. Whilst the changes in carbonation depth for M 0.5+GGBS compared with mix M 0.5 were (58%, 48%, 57% and 31%) for samples which have crack widths of (0, 0.1,0.2 and 0.3) respectively. It seems obvious that the mixes M 0.5+GGBS and M 0.5+PFA were less resistant to carbonation than the control mix M 0.5.

The phenolphthalein solution that was used to determine the DoC is the measurement of the pH or alkalinity indicator of concrete, and $Ca(OH)_2$ is the main source of the alkalinity in pore water solution. The mixes incorporating the SCMs, PFA are likely to have a lower quantity of $Ca(OH)_2$ due to the fact that there is a lesser quantity of Portland cement available to form $Ca(OH)_2$ in the blended cements as well as the pozzolanic reactions in blended cements converting calcium hydroxide to produce secondary C-S-H in the first days of hydration (Roy and Indorn, 1982; Maso, 1996). In carbonation of concrete, another amount of $Ca(OH)_2$ and C-S-H have been converted due to reaction with CO_2(He, 2010). For two reasons, the DoC for mixes GGBS and PFA was relatively higher than mix M 0.5. More detail for effect of SCMs on DoC will show in XRD analysis and pH test section.

b: External Factors Influencing the Depth of Carbonation

The influence of external factors on the DoC by using phenolphthalein indicator was examined and the results illustrated as follows:

(i): Effect of Temperature on DoC

The effect of the temperature on the DoC for mixes used in the study for CO_2 5% and RH 65% for 8 weeks, are presented in Figure 5.7. The samples were exposed to three different temperatures, 25ºC, 35ºC, and 45ºC. Samples exposed to these conditions showed that the (DoC) increases relatively with the temperature. Also, it was noted that when the samples were exposed to accelerated CO_2 condition at 45°C, the higher the w/cm ratio in the samples' mix design, the less resistance of carbonation was found as shown in Figure 5.8 (a, b and c).

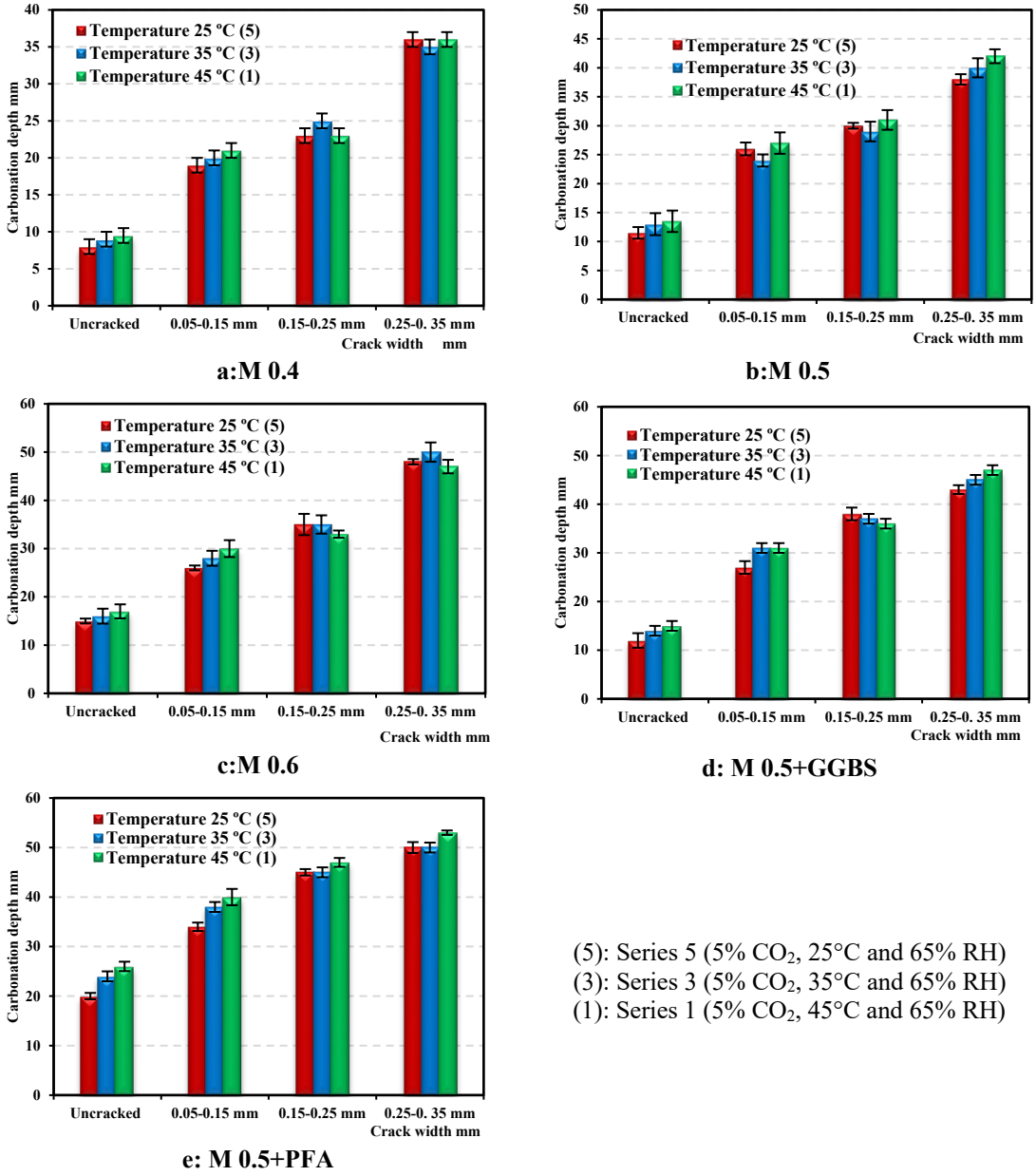

(5): Series 5 (5% CO_2, 25°C and 65% RH)
(3): Series 3 (5% CO_2, 35°C and 65% RH)
(1): Series 1 (5% CO_2, 45°C and 65% RH)

Figure 5.7: Effect of temperature on carbonation depth for different crack width in the concrete sample exposed to RH = 65% and CO_2= 5% for 8 weeks period

a:M 0.6, 25 °C T b:M 0.6, 35 °C T c:M 0.6, 45 °C T

Figure 5.8: Effect of temperature on DoC for M 0.6-uncracked, CO_2 5% and RH 65%

Exposing at elevated temperatures altered the mineral composition of cement products due to carbonation and increased its depth in samples, but the performances of some of the cracked samples were not consistent with the results of the un-cracked

samples as shown in Figure 5.7.The results also show that the DoC in concrete increases with increasing w/cm ratio with different temperatures and crack width, the percentage increases in DoC for samples (sound and cracked) with respect to the control concrete samples are presented in Tables B.1and B.2 (Appendix B) and ranged approximately (1.13-1.19) times for the DoC with temperature 45ºC with respect to the DoC with temperature 25ºC.

The reason for these results is that the spread of CO_2 molecules in the pore solution of concrete accelerates when the environment temperature increases the activate transport of CO_2. The effect of accelerating CO_2 molecules' condition with an increase in temperature encourages the diffusion of carbonate ions into concrete, due to amplified molecular activity and the chemical reaction rate between carbonate ion CO_3^{2-} and Ca^{2+} in the pore water of concrete and increasingly forms $CaCO_3$ (Yoon *et al*., 2007; Talukdar *et al.,* 2012). Also, Carbonation is a phenomenon driven by transport: a temperature increase is favourable for carbonation since it raises the diffusivity of CO_2 through the carbonated layer towards the $CaCO_3$ precipitation zone. In the same way, calcium ionic diffusion from the sound core to the precipitation zone is also enhanced. Transport can be described using the classical Arrhenius activation law with an activation energy of about 15–20 kJ/mol for CO_2 gas diffusion and 44 kJ/mol for calcium diffusion (Hernández *et al*., 1997; Fuhrmann *et al*., 1989)

(ii): Effect of Relative Humidity on DoC

The samples have been exposed to three targets of relative humidity, 65 %, 75% and 85% with accelerated CO_2 environment 5% and temperature 25°C. The DoCs of all cases with different cracks width over the 8 weeks period are illustrated in Figures 5.9 and 5.10. The overall trend in these figures is that of decreasing DoC with increasing RH. However, the DoC does not appear to change at a constant rate over the range of RH investigated. For almost all of the samples with different cracks width and w/cm, the maximum carbonation depth occurred at 65% target RH. On the other hand, there are two cases unlike the general trend due to other factors, such as crack width, which might have influenced the DoC at this RH values such as crack width. In addition, the results indicated the (DoC) in concrete increases with an increase w/cm ratio with different RH and crack width. The increases in (DoC) for samples (sound and cracked) with respect to the control concrete samples are presented in Figure 5.10.

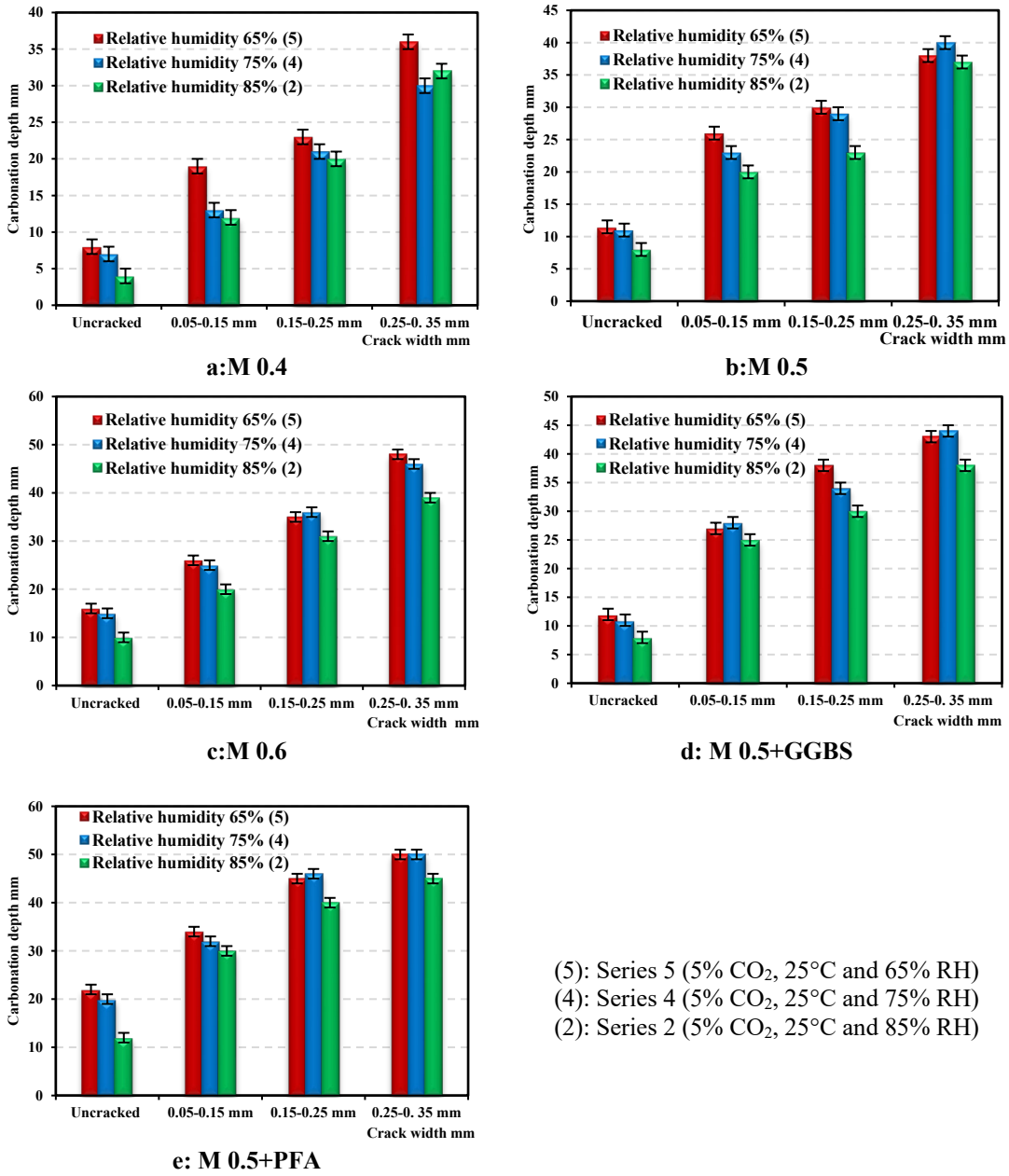

(5): Series 5 (5% CO_2, 25°C and 65% RH)
(4): Series 4 (5% CO_2, 25°C and 75% RH)
(2): Series 2 (5% CO_2, 25°C and 85% RH)

Figure 5.9: Effect of relative humidity on carbonation depth for different crack width in the concrete sample exposed to T =25°C and CO_2=5% for 8 weeks period.

The results show the RH affects the DoC, the effect is not the same for all the mixes investigated. The effect of w/cm ratio on DoC is the highest at 65% RH and is the least at 85% RH as shown in Figure 5.10. This can be attributed to the fact that the pores are free of moisture at low RH, i.e. the impact of open porosity is gotten at the low RH. Overall the tendency of declining DoC with increasing RH within this range is like that which could be expected. However, what the results show is that there is a wide range of variability depending on the mix proportions and the quality of the concrete (Roy *et al*., 1999; Russell *et al*., 2001).

a:M 0.6, 65% RH **b:M 0.6, 75% RH** **c:M 0.6, 85% RH**

Figure 5.10: Effect of RH on DoC for M 0.6 – Uncracked, CO_2 5% and T =25°C for 8 weeks

On the other hand, there is a combined effect of temperature and relative humidity on carbonation depth, especially in a hot-humidity zone. Water retention is also affected by temperature: for a given RH, a temperature increase reduces the water retained at equilibrium (Drouet *et al.*, 2015). Because the water content impacts both CO_2 diffusion and the chemical reactions, it is impossible to predict the influence of water retention modifications induced by temperature on carbonation. Moreover, temperature also impacts water transport; drying is faster when the temperature is increased (Wong *et al*., 2001). From this perspective, the interaction between carbonation and water transport appears to be essential and even more important than at an ambient temperature.

(iii): Effect of CO_2 Concentration on DoC

The depths of carbonation were measured at the age of 8 weeks as shown in Figure 5.11. It can be seen that the carbonation depth increases with an increase of CO_2 concentration. The influence of an increased CO_2 concentration with the w/cm ratio and crack width have a considerable impact on DoC. Concrete specimens of M 0.6 and M 0.5 illustrated higher DoC than those of M 0.4 with different crack width as shown in Figures 5.11 and 5.12. The rate of carbonation increases with an increase in CO_2 concentration, especially for concrete specimens with higher w/cm ratios, the transport taking place through the pore system in hardened cement paste (Ngala and Page, 1997). GGBS and PFA replacement results are a slightly higher DoC. However, the pozzolanic reaction and filling effect is beneficial in minimizing the pore size and volumes.

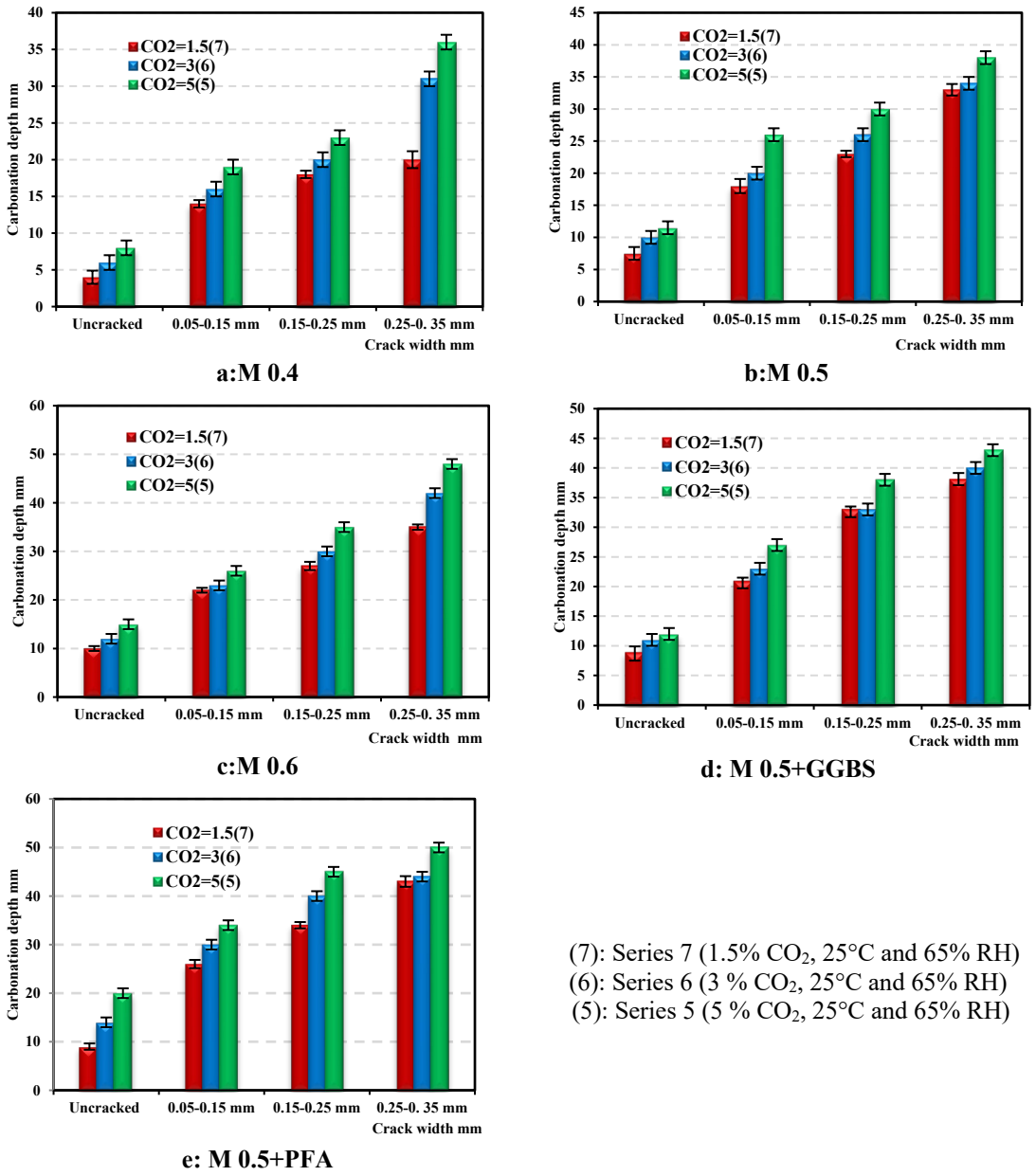

(7): Series 7 (1.5% CO_2, 25°C and 65% RH)
(6): Series 6 (3 % CO_2, 25°C and 65% RH)
(5): Series 5 (5 % CO_2, 25°C and 65% RH)

Figure 5.11: Effect of CO_2 concentration on carbonation depth for different crack widths in the concrete sample exposed to RH =65% and relative humidity =65% for 8 weeks period

Castellote *et al*. (2009) reported that the carbonation phenomena in the concrete samples have been caused in a progressive polymerisation of C-S-H that have caused the production of a Ca-modified silica gel and calcium carbonate. And the carbonation of C-S-H and Ca $(OH)_2$ changes simultaneously and the polymerisation of the C-S-H after carbonation increases with the increase in CO_2 concentration.

The results indicate that a linear correlation between the DoC and the increase in the CO_2 concentration as shown in Figure 5.13. These results are compatible with the

observation that was achieved by Chi *et al*. (2002). Finally, the changes in the mineralogy of cement products due to accelerated carbonation is the same in high concentration CO_2 environments up to 10 %. Beyond that, the results of carbonation in a microstructure do not correspond to those of natural carbonation at an ambient concentration of CO_2 (0.03%) (Castellote *et al*., 2009).

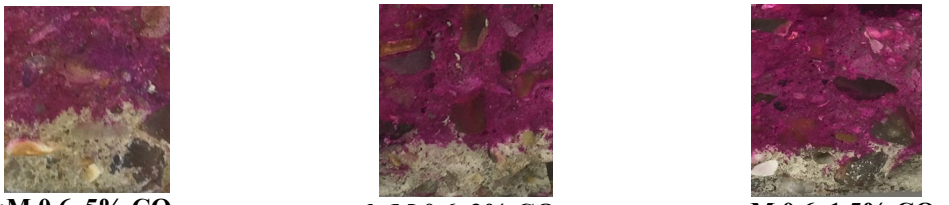

a:M 0.6, 5% CO_2 b:M 0.6, 3% CO_2 c:M 0.6, 1.5% CO_2

Figure 5.12: Effect of CO_2 concentration on DoC for M 0.6 – Uncracked, RH 65% and T =25°C for 8 weeks

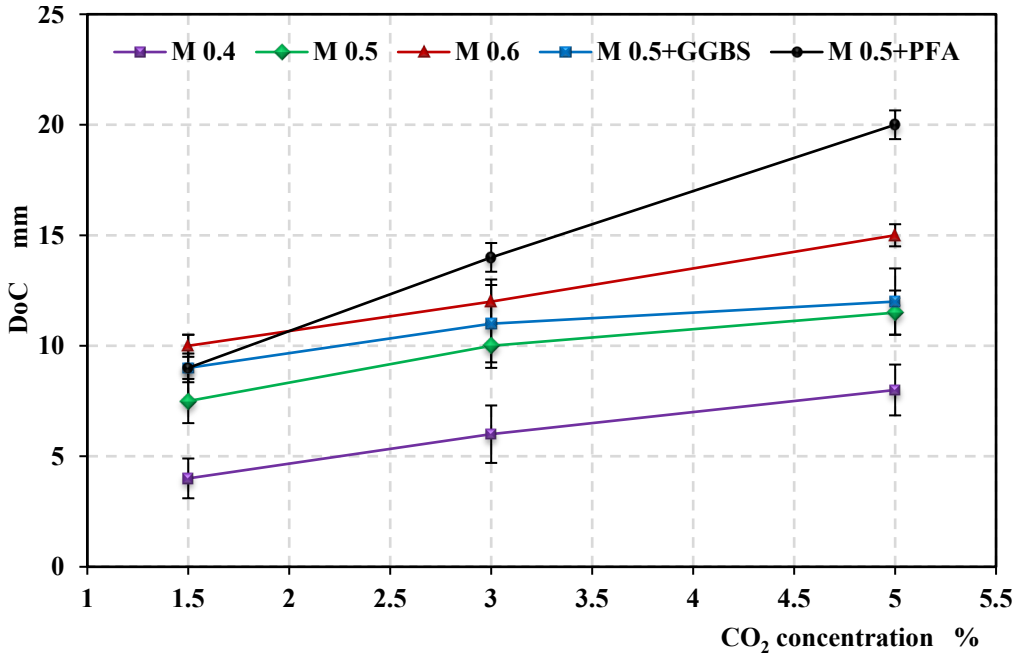

Figure 5.13: Effect of CO_2 concentration on DoC in different concrete mixes

Finally, Loo *et al*. (1994); Yoon *et al.* (2007); Kwon *et al*. (2011) demonstrated the DoC varies linearly with the square root of exposure time, which can be called the square-root-t-law. Therefore, from the statistical analysis of results with an accelerated CO_2 condition and normal CO_2 concentration (350 ppm), a linear equation is formulated to relate the depth of carbonation tested in natural environments ($DoC_{n,t}$) with the accelerated carbonation depth (DoC_a) and different properties of concrete (w/cm ratio) defined in this study, as follows:

$$DoC_{n,t} = A_a \, DoC_a \sqrt{t} \qquad (5.2)$$

$$A_a = 0.15 \frac{C_{co_2}^{0.0034}}{RH} {}^{w}/_{cm} \quad (5.3)$$

where:

$DoC_{n,t,}$ and DoC_a are the depth of carbonation in (mm) in the normal environment and accelerated condition respectively, A_a is the slope of the relationship, (C_{CO2}) is the concentration of CO_2 in ppm, t: time in a week and w/cm is the water-cementitious material ratio in (%).

5.2.2 Depth of Carbonation by X-Ray Diffraction Analysis

As mentioned previously, the carbonation processes in concrete sample change the mineralogical of the $Ca(OH)_2$ and C-S-H to form the $CaCO_3$. In order to identify the impact of CO_2 diffusivity on the change in mineralogical composition, X-ray diffraction analysis (XRD) was employed. Due to carbonation, some changes in relative intensities of crystalline phases (peaks) with the depth of carbonated concrete have been detected. The change in peak intensity would be attributed either to a change in the degree of crystallization of the specified phase and/or a change in its quantity (Maroliya, 2012). The noticeable change in mineralogical composition due to carbonation might have an impact on the physical and chemical properties of carbonated concrete (Dyer, 2014). The relative intensity or main peaks of $Ca(OH)_2$ are noticed at angles of diffraction (2θ) 18.1° and 34.1° (International Center for Diffraction Data, ICDD) (Blanton *et al*., 1995) at depth of 40 mm as shown in Figure 5.14-c.

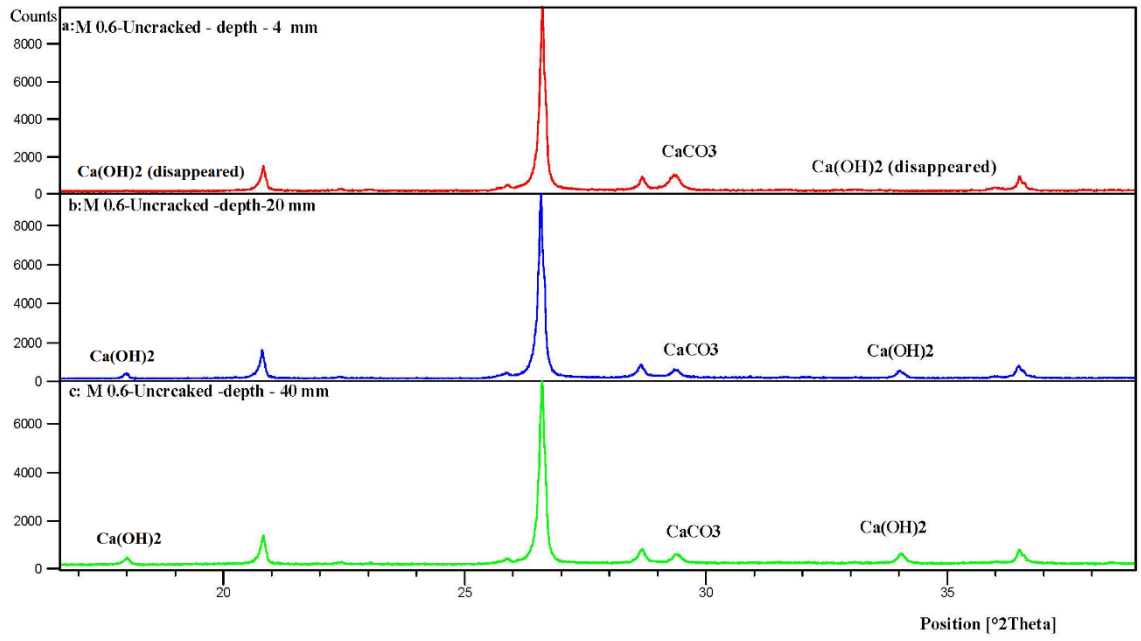

Figure 5.14: Carbonation process was investigated by XRD and identified the $Ca(OH)_2$ and $CaCO_3$ with depth(a:4mm,b:20mm and 40mm) and carbonation degree

It reduces or disappears as the degree of carbonation increases in the samples (at depth 4 mm) (Figure5.13-a). On the other hand, the intensity of $CaCO_3$ phase for the main peak can be detected at angle of diffraction (2θ) 29.39°, which increases in the samples with the increase in carbonation degree (toward the surface) (max. intensity of peak is at depth 4 mm) (Figure 5.13-a) and reduces gradually when decreasing the carbonation degree (toward the depth, 20 mm and 40 mm) as shown in Figure 5.14-b and 5.13-c.

The conditioned concrete powder samples at the crack location with eight different depths from the surface exposed to different CO_2 concentration, relative humidities, and temperatures were tested. The X-ray analysis results indicate four main crystalline structures in the concrete powder sample: quartz, feldspar, $Ca(OH)_2$ and $CaCO_3$. Among these, quartz and feldspar come from aggregates and are basically the same in all samples. However, the contents of $Ca(OH)_2$ and $CaCO_3$ varies with the degree of carbonation of the sample. The changes in the amount of $CaCO_3$ and $Ca(OH)_2$ can be observed through the changes in the peaks obtained from the XRD analysis (Chang and Chen, 2006). Graphs show the relative intensity of X-Ray Diffraction at various concrete depths for different mixes used in this study (for both cracked and un-cracked samples), which are shown in Figure 5.15.

These graphs present the distributions of $Ca(OH)_2$ and $CaCO_3$ in concrete specimens with different w/cm ratios and SCMs, which had undergone accelerated carbonation for 8 weeks. At 8 weeks of accelerated carbonation, the surface has been fully carbonated; all $Ca(OH)_2$ at the surface of the specimens is found to be completely converted into $CaCO_3$. Notably, the $CaCO_3$ content decreases in the powder samples are taken from the surface to the interior of the concrete sample, while the $Ca(OH)_2$ content increases because carbonation is more intensive at the surface than in the interior, such that more $Ca(OH)_2$ has already been converted into $CaCO_3$ at the surface. With the depth of concrete sample, the carbonation degree decreases and the $Ca(OH)_2$ content increases as the $CaCO_3$ content diminishes as shown obviously in Tables A.16-A.30 (Appendix A). If the transition point where the relative intensity distribution of $Ca(OH)_2$ and $CaCO_3$ approximately approaches the horizontal, it is taken as the depth of carbonation front (X_f) as shown in Figure 5.15.

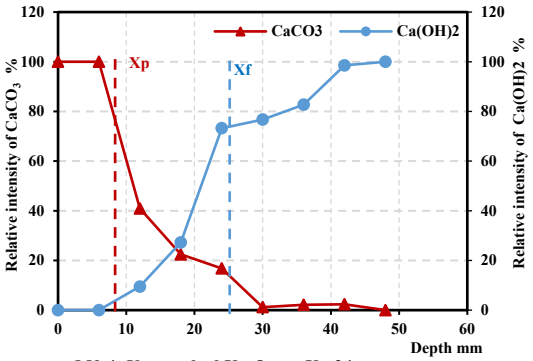

a:M0.4- Un-cracked,X_p=8mm ,X_f=24mm

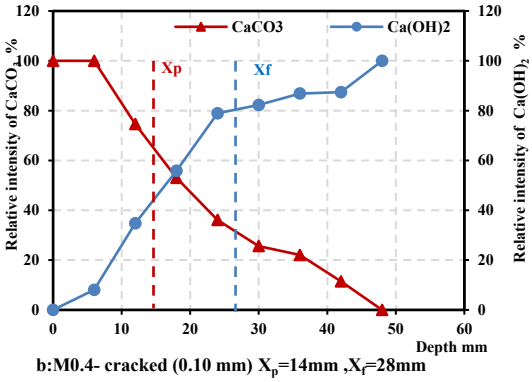

b:M0.4- cracked (0.10 mm) X_p=14mm ,X_f=28mm

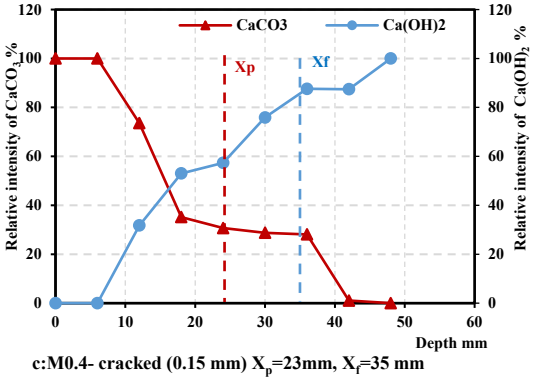

c:M0.4- cracked (0.15 mm) X_p=23mm, X_f=35 mm

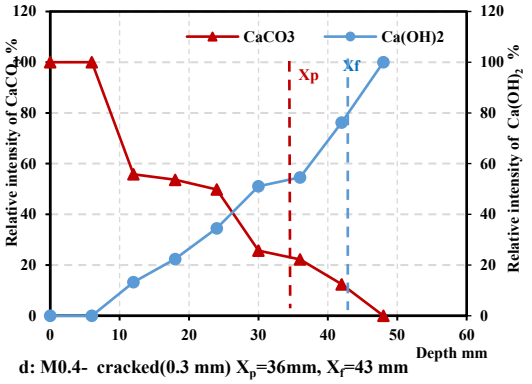

d: M0.4- cracked(0.3 mm) X_p=36mm, X_f=43 mm

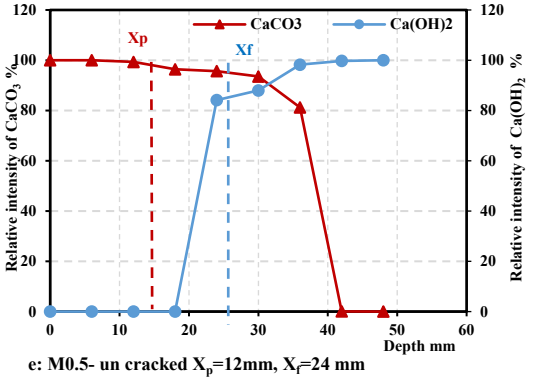

e: M0.5- un cracked X_p=12mm, X_f=24 mm

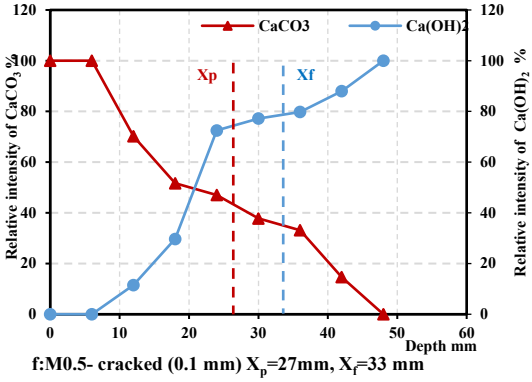

f:M0.5- cracked (0.1 mm) X_p=27mm, X_f=33 mm

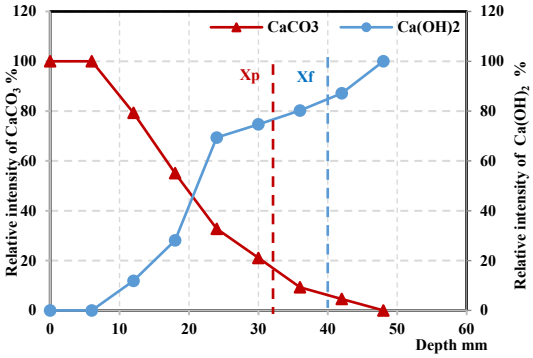

g: M0.5- cracked (0.15 mm) Xp=31mm, X_f=40 mm

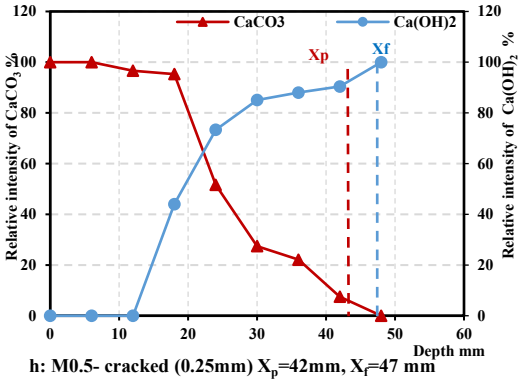

h: M0.5- cracked (0.25mm) X_p=42mm, X_f=47 mm

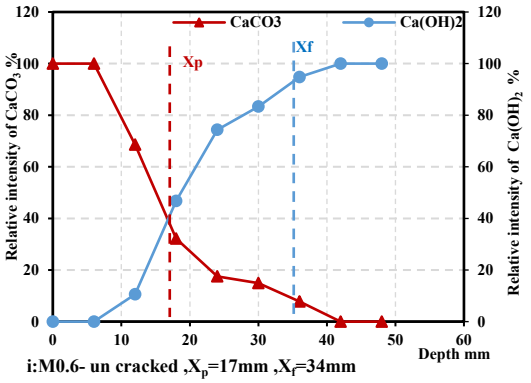

i:M0.6- un cracked ,X_p=17mm ,X_f=34mm

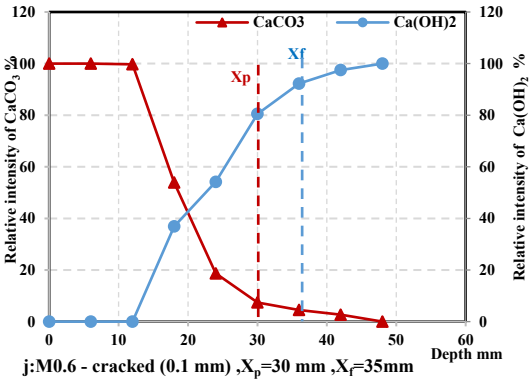

j:M0.6 - cracked (0.1 mm) ,X_p=30 mm ,X_f=35mm

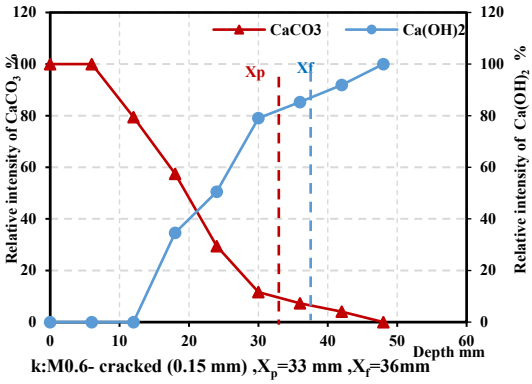

k:M0.6- cracked (0.15 mm) ,X_p=33 mm ,X_f=36mm

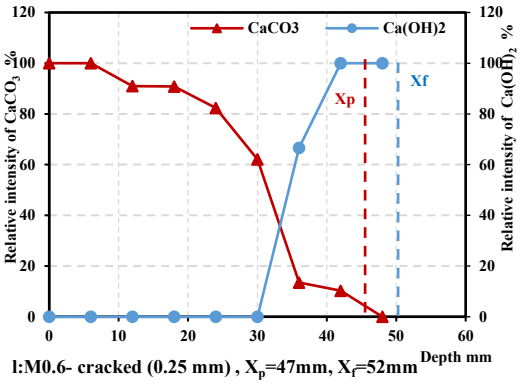

l:M0.6- cracked (0.25 mm) , X_p=47mm, X_f=52mm

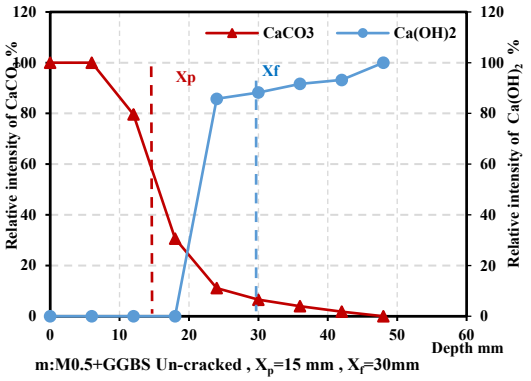

m:M0.5+GGBS Un-cracked , X_p=15 mm , X_f=30mm

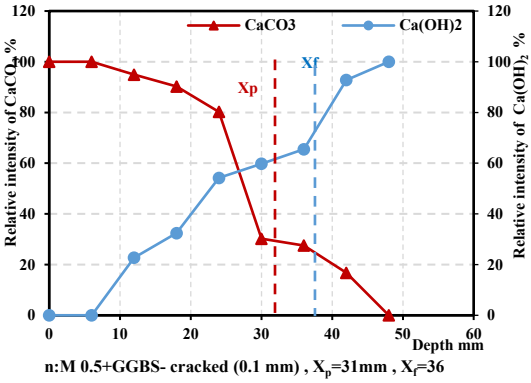

n:M 0.5+GGBS- cracked (0.1 mm) , X_p=31mm , X_f=36

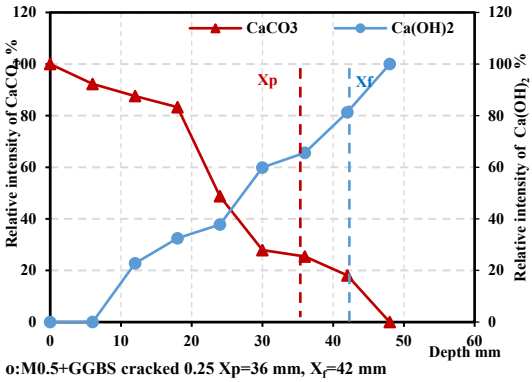

o:M0.5+GGBS cracked 0.25 Xp=36 mm, X_f=42 mm

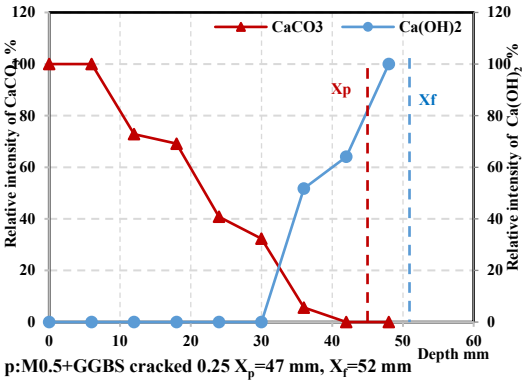

p:M0.5+GGBS cracked 0.25 X_p=47 mm, X_f=52 mm

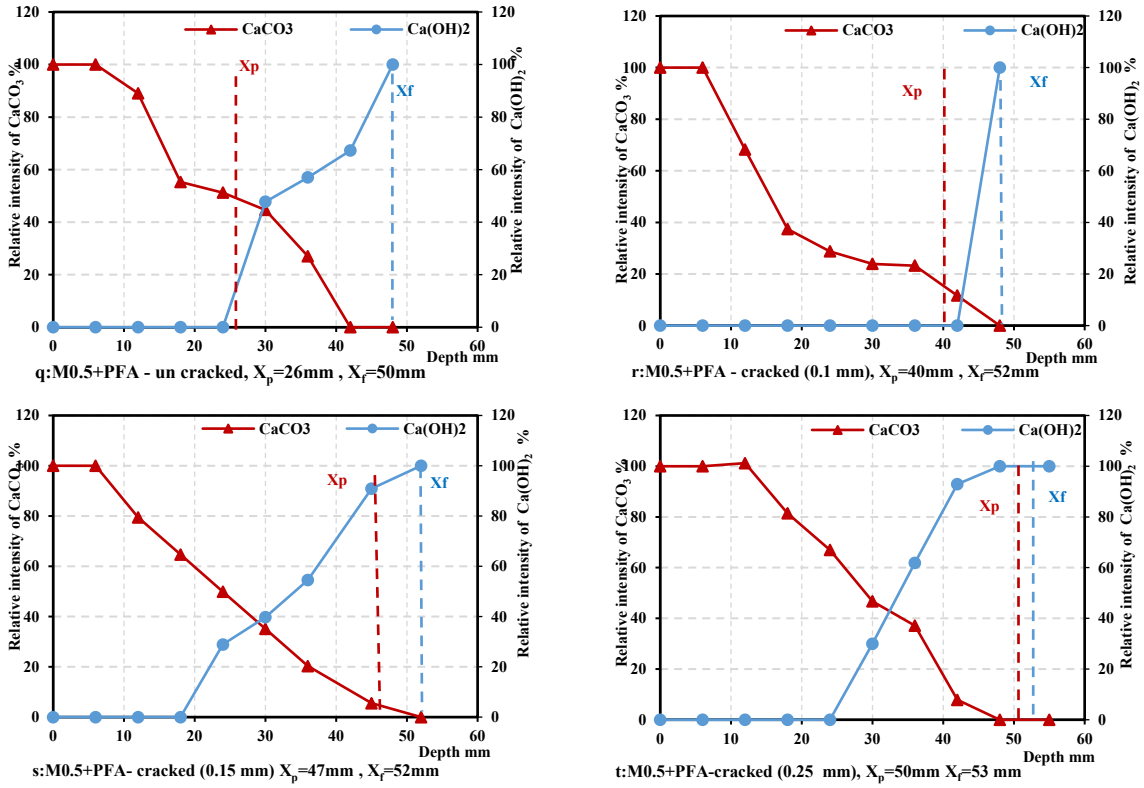

Figure 5.15: Relative intensity of XRD analysis for $CaCO_3$ and $Ca(OH)_2$ in the concrete samples (un-cracked and cracked 0.25-0.35 mm) with exposure to CO_2 for 8 weeks

XRD investigation made it possible to gain a better understanding of the mineral-structural changes induced due to exposure to CO_2 environment. On the other hand, this analysis (XRD) is useful to investigate the influence of porosity, crack width and SCMs on carbonation by providing evidence of impact on these parameters by determining relative intensities of $Ca(OH)_2$ consumed and $CaCO_3$ formed with a depth of concrete samples. The XRD investigation showed the variation in relative intensities of $Ca(OH)_2$ and $CaCO_3$ depending on properties of concrete (w/cm ratio or porosity), as shown in Figure 5.14 (a and e). The influence of diffusivity of CO_2 in cracked concrete samples was the main reason for decrease the relative intensity of $Ca(OH)_2$ and increase the relative intensity of $CaCO_3$ at great depth, as shown in Figure 5.15.

For the effect of replacement of SCMs, the results of XRD analysis for GGBS and PFA samples confirm the effect of these materials on DoC which is achieved by the phenolphthalein indicator. The results of XRD showed the mixes incorporating supplementary cementitious materials, SCMs (GGBS and PFA) have less $Ca(OH)_2$ than the OPC mixes at a different depth. Thus, relative intensities of $Ca(OH)_2$ remains low at a deep depth, while the concentration of $CaCO_3$ remains high at that depth. This is likely

to be owing to the fact that there is a lower quantity of OPC available to form $Ca(OH)_2$ in the blended cement with GGBS and PFA as well as the pozzolanic reactions in blended cement converting $Ca(OH)_2$ to form secondary C-S-H (Neville, 2011).

Accordingly, the depth of carbonation, DoC is represented in the literature using two distinct parameters, X_p and X_f. The depth of carbonation, X_p relates to the depth where concrete depth is considered fully carbonated and the pH of pore water in the concrete is about 9 (Neville, 2011) and it can be measured by using a phenolphthalein pH indicator. While, the depth of carbonation front, X_f relates to the depth beyond which concrete is still unaffected by the carbonation. At this depth, the pH of pore water of concrete maintains an original pH of concrete, which is around 13. The zone between X_p and X_f can be considered partially carbonated with pH value varying between 9 and 13.

X_p has been obtained from Figure 5.1 and Tables A.4. to A.6(Appendix A), using a phenolphthalein indicator whereas X_f can be taken as the point on the graphs of the relative Intensity X-Ray Diffraction curve where the curve for $Ca(OH)_2$ approaches horizontal (i.e. no further change in $Ca(OH)_2$ beyond this depth is expected). The X_p and X_f depths for both cracked and un-cracked concrete samples are presented in Figure 5.14 and Table 5.2 for Series 1 and Table A.22 (Appendix A) for other series used in this study. The relative intensity peaks for XRD analysis of $Ca(OH)_2$ and $CaCO_3$ with different depths in concrete is presented in Table A.7 to A.21(Appendix A) for all series used in the study.

In most of the series of un-cracked concrete samples, the carbonation front depth, X_f is approximate twice time of the depth of fully carbonation, X_p, which confirms the results of Chang and Chen (2006). In cracked concrete, crack width can be the main channel for CO_2 intrusion so that DoC is reported to increase with crack width. The above relationship does not hold true and the difference between X_p and X_f is considerably smaller than in the case of un-cracked concrete, which agrees with the results of Park (2008) for un-cracked concrete samples.

The diffusivity of CO_2 and reaction with $Ca(OH)_2$ and C-S-H is the main factor in finding the carbonation degree and determine three distinct regions of fully carbonated, partly carbonated and noncarbonated zones in carbonated concrete. The front of carbonation is the starting point of carbonation of concrete and consumption of $Ca(OH)_2$. In the cracked sample, the diffusivity of CO_2 is faster using the pathway of the crack to

reach the deep point in the concrete sample. Finally, the results from the XRD investigation also helps in identifying areas of fully carbonated and un-carbonated concrete in greater detail including the partially carbonated zones (Chang and Chen, 2006).

Table 5.2: Carbonation front (X_f) by XRD analysis, and fully carbonation depth (X_p)

Sample	Carbonation depth and front (mm) for crack width							
	Uncracked		0.05-0.15mm		0.15-0.25 mm		0.25-0.35 mm	
	X_p	X_f	X_p	X_f	X_p	X_f	X_p	X_f
M 0.4	9.5	32	21	28	23	35	36	43
M 0.5	13.5	25	27	33	31	40	42	47
M 0.6	17	34	30	35	33	36	47	52
M 0.5+GGBS	15	30	31	38	36	42	47	52
M 0.5+PFA	26	50	40	52	47	52	50	53

5.2.3 Depth of Carbonation by pH and Consumed OH^- Method

The formation of $CaCO_3$ and $CaMg(CO_3)_2$ in concrete sample and consumption of $Ca(OH)_2$ and C-S-H, are significantly influenced by the pH of pore water in concrete, where pH can reduce to 9 in the full carbonated samples as shown in Equation 2.1. The results of measured apparent pH of the concrete powder samples are presented in Figure 16 (a, b, c, d and e) for Series 1 and Table A.23 to A.37 (Appendix A) for other series in the study.

The results clearly depict the reduction in apparent pH value near the exposed surface for all samples but rise to over 12 at a depth of about 50mm. This can be used as (a control sample) to establish the consummation of $[OH^-]$ and the carbonation front. It is also worth noting that for the cracked samples, the apparent pH value converges with the value of uncracked samples at a depth of about 50mm, which relates to the depth of cracks within the samples. The results also illustrate the effect of supplementary cementitious materials, SCMs on pH level in the pores water solution of concrete, where the replacing OPC by these material leads to a reduction in the pH values due to consuming the $Ca(OH)_2$ at hydration to produce the secondary C-S-H (Maso, 1996; Neville, 2011) and carbonation because of the formation of $CaCO_3$(Dyer, 2014).

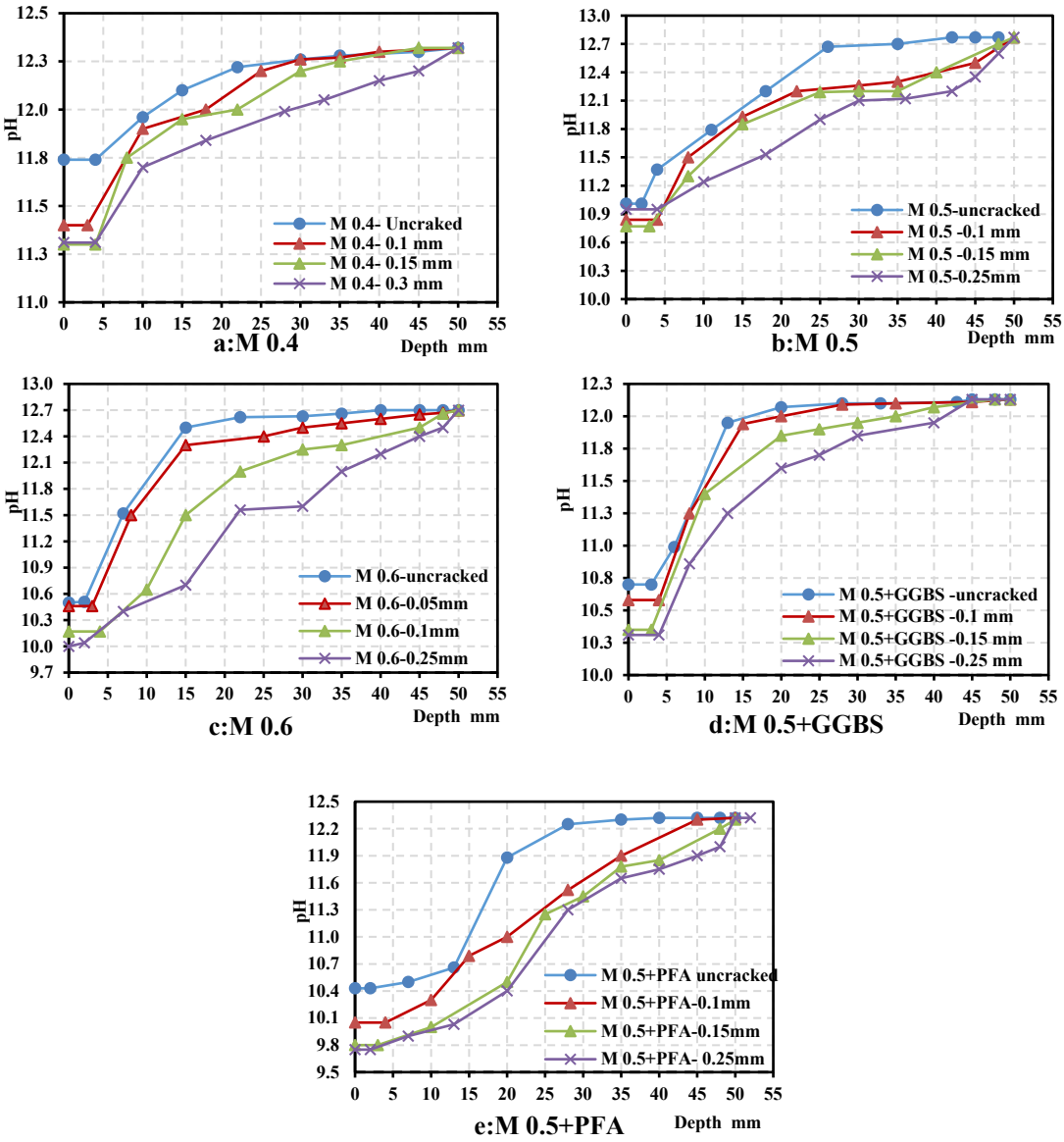

Figure 5.16: Effect of carbonation on the pH level of concrete samples exposed to the accelerated environment (CO_2=5%, T=45 ºC and RH =65% (Series 1)) for 8 weeks

The main reason for the reduction in the pH is due to the reaction of the CO_3^{-2} and consumption is the major contribution of alkalinity in concrete, $Ca(OH)_2$ and C-S-H, and formation of $CaCO_3$ (Neville, 2011; Dyer, 2014). The consumed OH^- values (mol/kg) due to the carbonation process for all samples are illustrated in Figure 5.17 for Series 1. Where, X_p is the boundary between the full carbonated and partially carbonated zone, and X_f is the boundary between partially carbonated and non-carbonated zones (that indicates the carbonation front). At the carbonation front, X_f, the OH^- is at the verge of reacting with CO_3^{-2} dissolved in pore water solution to form $CaCO_3$.

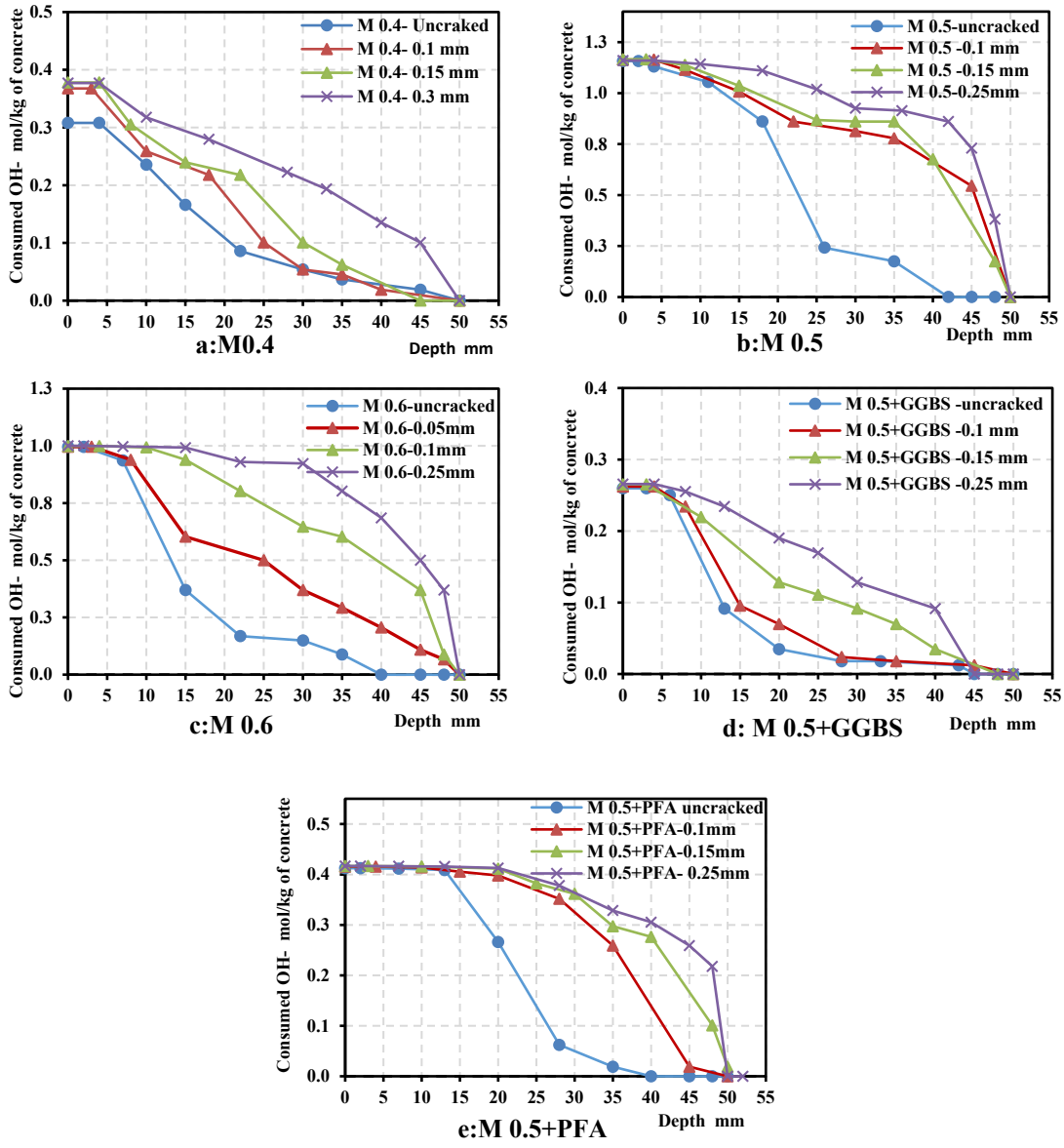

Figure 5.17: The profile of consumed OH^- for the concrete sample exposed to the accelerated environment (CO_2=5%, T=45 ºC and RH =65% (Series 1)) for 8 weeks

The depth of X_p and X_f are summarized in Tables 5.3 for Series1 and Table A.38 (Appendix A) for other series in the study. The results of consumed OH^- shows a significant influence of w/cm ratio, crack width and supplementary cementitious materials on the consumption of OH^- and reduce the alkalinity level in concrete. The increase in w/cm ratio leads to an increase of consumption of OH^- and increased depth of carbonation front.

Table 5.3: Carbonation front by apparent pH and consumed OH^-, and carbonation depth for conditioned samples of Series 1

Sample	DoC (X_p) ; Carbonation front (X_f) (mm) for crack width							
	Uncracked		0.05-0.15mm		0.15-0.25 mm		0.25-0.35 mm	
	X_p	X_{f1}	X_p	X_{f1}	X_p	X_{f1}	X_p	X_{f1}
M 0.4	9.5	35	21	40	23	45	36	50
M 0.5	13.5	42	27	48	31	50	42	50
M 0.6	17	45	30	50	33	50	47	50
M 0.5+GGBS	15	35	31	40	36	45	47	45
M 0.5+PFA	26	40	40	48	47	50	50	50

The carbonation might have an impact on the mineralogical composition and this change leads to modification in the physical and chemical properties of carbonated concrete (Chang and Chen, 2006). The results also indicate the carbonation front measured in the cracked specimen is always deeper than the carbonation front obtained in un-cracked specimens for all mixes. The reduction in pH level (and increase in the consumed OH^-) with an increase in w/cm ratios and replacement of SCMs can be attributed to increased porosity and a decrease in the compressive strength (as previously discussed in relation to data presented in Figure 5.3). Hence, the reduction in apparent pH (and increase in the consumption of OH^-) in samples with PFA and GGBS are higher than OPC based concrete samples. The mixes containing SCMs, PFA and GGBS have less calcium hydroxide than the Portland cement mixes. This is likely to be due to the fact that there is a lower quantity of Portland cement available to form calcium hydroxide in the blended cement as well as the pozzolanic reactions in blended cement converting calcium hydroxide to form secondary C-S-H (Roy and Indorn, 1982; Maso, 1996). The consequence of the lesser quantity of calcium hydroxide in the mixes containing SCMs is that they carbonate more readily as demonstrated in the pH profiles and carbonation depths (McPolin *et al*., 2007).

The carbonation of hydration products of cementitious materials can mainly be regarded as the reaction between the CO_2 and the $Ca(OH)_2$ and C-S-H. Based on reaction kinetics, it is believed that when the CO_2 concentration is relatively low, the reaction of CO_2 with $Ca(OH)_2$ takes place much more easily. Therefore, we can take the front of CO_2 ingress as the location where the $Ca(OH)_2$ content (or the content of OH^-) starts to

decrease (Wang *et al*., 2016). It should be noted that carbonation takes place in pore solution, but the amount of OH^- detected by this pH test method involves all [OH^-] both in pore solution and in crystallized Ca $(OH)_2$ form. However, the reaction of CO_2 and [OH^-] must be taking place in the pore solution. There is an equilibrium between [OH^-] concentration in pore solution and crystallized solid $Ca(OH)_2$ (Wang *et al*., 2016).

Consequently, the apparent pH and consumed OH^- investigation made it possible to gain a better understanding of the influence of mineralogical-structural changes induced due to exposure to a CO_2 environment and carbonation. Results from the apparent pH and consumed OH^- technique also assisted in identifying areas of fully carbonated and un-carbonated concrete in greater detail including the partially carbonated zones.

Finally, the reduction in alkalinity level of concrete surrounding the rebars was observed in cracked concrete since the crack opening initially helps to transport the CO_2 deeper inside the exposed surface at the crack locations from where the CO_2 diffuses inside the cracked surface orthogonal to the surface of cracks as can be seen in Figure 5.18. On the other hand,the carbonation leads to induce depassivation of steel embedded in concrete (Van den Heede and De Belie, 2018).

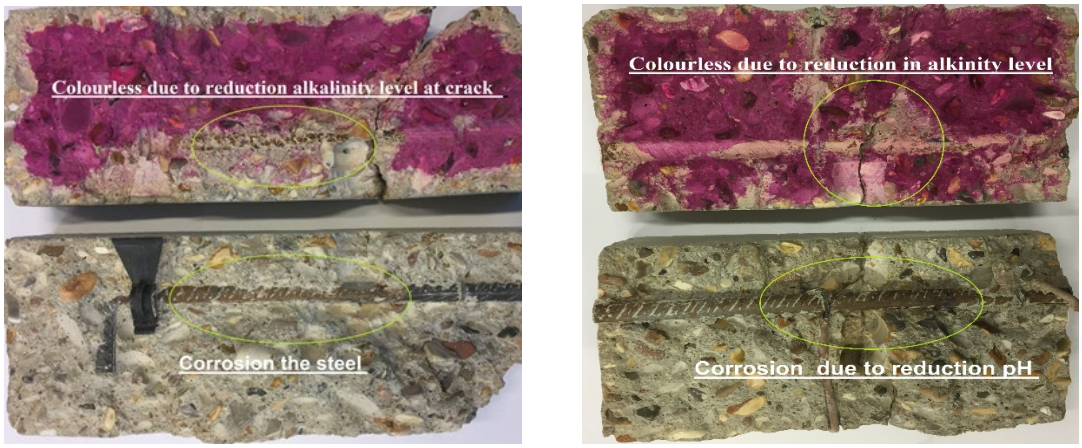

a:(M 0.5+PFA with crack width 0.25 mm) Cl^- =0.29% by mass of cement

b: (M 0.4 with crack width 0.25 mm) Cl^- =0.26% by mass of cement

Figure 5.18: Effect of the crack on carbonation depth

5.3 Summary

This study has considered the influence of the exposure environment and properties of concrete on the DoC in concrete structures. The effect of three levels of CO_2, RH, temperatures and w/cm ratio on DoC have been investigated. Carbonation depth was determined using an accelerated environment test programme by using a phenolphthalein

indicator, XRD analysis and apparent pH of powdered concrete. The main conclusions that can be drawn from the results are as follows; -

- Carbonation depth is controlled by the concentration of carbon dioxide at exposure environmental condition by diffusion acting as a driving force in concrete.
- The crack width significantly increases the DoC and reduces the alkalinity of concrete by consuming the OH^- ions and reduces the pH level for all mixes used in the study for the different levels of CO_2, RH, and temperature.
- Carbonation rates in the vicinity of the cracks are considerably higher due to relatively faster penetration of a CO_2 into the crack followed by orthogonal outward diffusion into the un-cracked concrete surrounding the crack.
- XRD investigation made it possible to gain a better understanding of the mineral- structural changes induced due to exposure to CO_2 environment.
- The SCMs have a vital role on DoC, whereby the replacement of OPC by SCMs such as PFA and GGBS has a significant increase in the carbonation and reduction in pH level and consumed alkalinity compounds in concrete.
- The carbonation depths, X_p and front X_f, are affected by the material behaviours such as permeation properties (permeability and gas permeability), and compressive strength due to the impact of diffusivity of CO_2.
- For samples exposed to an accelerated CO_2 environment, an increase in RH led to a reduction in the DoC.
- The increment in the temperature increased the DoC due to relatively fast penetration of CO_2 into the concrete and an increase in the reaction rate with cement products.
- The results indicate a linear correlation between the DoC and the increase in the CO_2 concentration.
- Results from the apparent pH and consumed OH^- technique helps in identifying areas of fully carbonated and un-carbonated concrete in greater detail including the partially carbonated zones.
- Identification of the three zones of carbonation in concrete may help in applying concepts that pertain to composite materials in the analysis of the mechanical behaviours of carbonated concrete structures. However, concerning reinforcement corrosion, the pH value using a phenolphthalein indicator is a good indication for corrosion initiation.

CHAPTER VI: CHLORIDE PENETRATION AND CORROSION RATE

6.1 Introduction

In this chapter, the experimental results of chloride penetration and corrosion rate are presented. The results and the discussion focus mainly on two aspects; the impact of the properties of concrete (w/cm ratios and crack widths) and climate parameters (temperature, relative humidity, and carbon dioxide concentration) on the chloride penetration and corrosion rate for reinforced concrete samples. Five mixes were examined in this section of study and standard test and investigation methods were used to measure the chloride concentration and corrosion rate in reinforced concrete samples.

6.2 Chloride Penetration

Three series of concrete prisms have been investigated by changing the temperature during exposure to chloride environment, Series 1 with 40 °C, Series 2 with 30°C and Series 3 with 20 °C. These specimens were exposed to three sequences, wetting, drying and aeration for 15 weeks. The duration of exposure is shown in Figure 3.14 (Chapter 3). The specimens were split longitudinally, and the freshly fractured first face was sprayed with a 0.1 M solution of $AgNO_3$ to determine the chloride penetration depth (d_{cl^-}) (Yuan *et al*., 2008; He *et al*., 2012). The second face was drilled with different depths to collect the concrete powder to experimentally determine chloride concentration (total and free chloride). Two forms of chlorides ions can be found in concrete powder, free chloride ions (dissolved chloride) and bound chloride ions are chemically constrained with hydrated cement compounds, C_2S, C_3S, and C_3A (Katwan, 1988). The chloride diffusion coefficient and the properties of concrete are the major factors affecting chloride concentration in concrete. The results of the chloride penetrations (total and free chloride) and the amount of bound chloride (as elaborated previously in chapter 3) are listed in Tables 6.1 through to 6.15 and are discussed in the following sections.

Table 6.1: The total, free and bound chloride with different depths for mix samples M 0.4 were exposed to chloride spraying for 15 weeks at 20 °C (Series 3)

Sample	Chloride Concentration by mass of cementitious materials (%) for samples											
	Un-cracked			Crack width 0.05-0.15 mm			Crack width 0.15-0.25 mm			Crack width 0.25-0.35 mm		
Depth mm	Total Cl^-	Free Cl^-	Bound Cl^-	Total Cl^-	Free Cl^-	Bound Cl^-	Total Cl^-	Free Cl^-	Bound Cl^-	Total Cl^-	Free Cl^-	Bound Cl^-
0 - 6	1.73	1.69	0.04	1.84	1.00	0.84	2.13	1.96	0.17	1.23	1.11	0.12
6 -12	1.54	1.20	0.34	1.39	1.02	0.37	1.54	1.26	0.28	1.29	1.19	0.10
12 - 18	0.94	0.87	0.07	1.24	0.98	0.26	1.24	1.16	0.08	1.15	1.07	0.08
18 - 24	0.64	0.55	0.09	0.82	0.75	0.07	0.94	0.85	0.09	1.16	1.02	0.14
24 - 30	0.35	0.09	0.26	0.35	0.34	0.01	0.79	0.69	0.10	0.92	0.58	0.34
30 - 36	0.20	0.03	0.17	0.20	0.17	0.03	0.35	0.32	0.03	0.52	0.47	0.05
36 - 42	0.20	0.04	0.16	0.20	0.16	0.04	0.35	0.30	0.05	0.37	0.32	0.05
Penetration depth of chloride measured by $AgNO_3$ (mm)	23			24			42			42		

Table 6.2: The total, free and bound chloride with different depths for mix M 0.5 were exposed to chloride spraying for 15 weeks at 20 °C (Series 3)

Sample	Chloride Concentration by mass of cementitious materials (%) for samples											
	Un-cracked			Crack width 0.05-0.15 mm			Crack width 0.15-0.25 mm			Crack width 0.25-0.35 mm		
Depth mm	Total Cl^-	Free Cl^-	Bound Cl^-	Total Cl^-	Free Cl^-	Bound Cl^-	Total Cl^-	Free Cl^-	Bound Cl^-	Total Cl^-	Free Cl^-	Bound Cl^-
0 - 6	2.67	2.58	0.09	2.85	2.68	0.18	2.11	2.01	0.10	2.48	2.36	0.11
6 -12	1.93	1.84	0.09	2.48	2.43	0.05	2.30	1.94	0.36	2.48	2.33	0.15
12 - 18	1.55	1.19	0.36	1.93	1.84	0.09	2.11	1.36	0.75	2.48	2.10	0.38
18 - 24	0.80	0.76	0.04	1.18	1.06	0.11	1.74	1.64	0.10	2.30	2.16	0.14
24 - 30	0.44	0.25	0.19	0.80	0.75	0.05	0.99	0.99	0.00	1.18	1.13	0.05
30 - 36	0.25	0.21	0.04	0.44	0.39	0.05	0.61	0.54	0.08	0.80	0.71	0.09
36 - 42	0.25	0.15	0.10	0.44	0.33	0.11	0.44	0.38	0.06	0.61	0.50	0.11
Penetration depth of chloride measured by $AgNO_3$ (mm)	28			56			60			58		

Table 6.3: The total, free and bound chloride with different depths for mix M 0.6 were exposed to chloride spraying for 15 weeks at 20 °C (Series 3)

Sample	Chloride Concentration by mass of cementitious materials (%) for samples											
	Un-cracked			Crack width 0.05-0.15 mm			Crack width 0.15-0.25 mm			Crack width 0.25-0.35 mm		
Depth mm	Total Cl^-	Free Cl^-	Bound Cl^-	Total Cl^-	Free Cl^-	Bound Cl^-	Total Cl^-	Free Cl^-	Bound Cl^-	Total Cl^-	Free Cl^-	Bound Cl^-
0 - 6	2.48	2.36	0.12	2.26	2.13	0.13	3.78	2.96	0.82	3.12	2.70	0.43
6 -12	2.70	2.21	0.48	2.90	2.58	0.32	2.90	2.13	0.78	2.90	2.05	0.85
12 - 18	2.04	1.55	0.48	2.26	2.13	0.13	2.26	1.50	0.76	2.70	1.63	1.07
18 - 24	1.38	1.26	0.12	1.82	1.69	0.13	2.04	1.70	0.34	2.26	1.36	0.89
24 - 30	1.16	0.87	0.29	1.60	1.51	0.09	1.82	1.73	0.09	2.04	1.61	0.43
30 - 36	0.51	0.44	0.07	1.38	1.23	0.15	1.60	1.44	0.16	1.82	1.35	0.47
36 - 42	0.51	0.40	0.12	0.94	0.84	0.10	1.16	1.09	0.07	1.38	1.29	0.09
Penetration depth of chloride measured by $AgNO_3$ (mm)	35			60			60			60		

Table 6.4: The total, free and bound chloride with different depths for mix M 0.5 + GGBS were exposed to chloride spraying for 15 weeks at 20 °C (Series 3)

Sample	Chloride Concentration by mass of cementitious materials (%) for samples											
	Un-cracked			Crack width 0.05-0.15 mm			Crack width 0.15-0.25 mm			Crack width 0.25-0.35 mm		
Depth mm	Total Cl^-	Free Cl^-	Bound Cl^-	Total Cl^-	Free Cl^-	Bound Cl^-	Total Cl^-	Free Cl^-	Bound Cl^-	Total Cl^-	Free Cl^-	Bound Cl^-
0 - 6	2.67	2.34	0.33	2.11	2.01	0.10	1.93	0.85	1.08	2.30	1.74	0.56
6 -12	2.85	1.34	1.51	2.11	1.96	0.15	2.30	0.86	1.44	2.11	1.21	0.90
12 - 18	1.36	0.76	0.60	1.36	1.28	0.09	1.36	0.59	0.78	1.74	1.19	0.55
18 - 24	0.80	0.40	0.40	1.18	0.48	0.70	1.18	1.05	0.13	1.36	0.99	0.38
24 - 30	0.61	0.15	0.46	0.80	0.59	0.21	0.99	0.16	0.83	1.18	0.61	0.56
30 - 36	0.44	0.09	0.35	0.61	0.43	0.19	0.80	0.19	0.61	0.99	0.46	0.53
36 - 42	0.44	0.13	0.31	0.61	0.34	0.28	0.61	0.15	0.46	0.61	0.41	0.20
Penetration depth of chloride measured by $AgNO_3$ (mm)	17			37			41			56		

Table 6.5: The total, free and bound chloride with different depths for mix M 0.5 + PFA were exposed to chloride spraying for 15 weeks at 20 °C (Series 3)

Sample	Chloride Concentration by mass of cementitious materials (%) for samples											
	Un-cracked			Crack width 0.05-0.15 mm			Crack width 0.15-0.25 mm			Crack width 0.25-0.35 mm		
Depth mm	Total Cl^-	Free Cl^-	Bound Cl^-	Total Cl^-	Free Cl^-	Bound Cl^-	Total Cl^-	Free Cl^-	Bound Cl^-	Total Cl^-	Free Cl^-	Bound Cl^-
0 - 6	1.36	1.33	0.04	1.74	1.11	0.63	1.55	1.19	0.36	1.74	1.46	0.28
6 -12	1.74	1.09	0.65	1.74	1.26	0.48	1.74	1.34	0.40	1.93	1.88	0.05
12 - 18	1.55	0.84	0.71	1.55	1.14	0.41	1.63	1.01	0.61	1.74	1.41	0.33
18 - 24	0.80	0.36	0.44	1.18	0.81	0.36	1.36	0.71	0.65	1.55	1.45	0.10
24 - 30	0.44	0.10	0.34	0.61	0.28	0.34	0.80	0.56	0.24	0.99	0.41	0.58
30 - 36	0.44	0.05	0.39	0.44	0.23	0.21	0.61	0.18	0.44	0.61	0.25	0.36
36 - 42	0.44	0.04	0.40	0.44	0.18	0.26	0.44	0.18	0.26	0.44	0.28	0.16
Penetration depth of chloride measured by $AgNO_3$ (mm)	13.5			42			52			54		

Table 6.6: The total, free and bound chloride with different depths for mix M 0.4 were exposed to chloride spraying for 15 weeks at 30 °C (Series 2)

Sample	Chloride Concentration by mass of cementitious materials (%) for samples											
	Un-cracked			Crack width 0.05-0.15 mm			Crack width 0.15-0.25 mm			Crack width 0.25-0.35 mm		
Depth mm	Total Cl^-	Free Cl^-	Bound Cl^-	Total Cl^-	Free Cl^-	Bound Cl^-	Total Cl^-	Free Cl^-	Bound Cl^-	Total Cl^-	Free Cl^-	Bound Cl^-
0 - 6	2.13	2.01	0.13	4.07	3.14	0.93	5.41	4.81	0.59	6.30	5.93	0.37
6 -12	1.84	1.66	0.18	3.18	2.94	0.24	3.32	3.26	0.06	4.36	3.76	0.61
12 - 18	1.36	0.80	0.55	2.13	1.49	0.64	2.58	2.49	0.08	3.70	2.57	1.12
18 - 24	0.94	0.43	0.51	1.88	1.34	0.34	2.23	2.11	0.11	3.13	3.01	0.11
24 - 30	0.64	0.43	0.22	1.49	1.17	0.32	1.69	1.35	0.33	2.58	2.09	0.49
30 - 36	0.38	0.33	0.04	0.94	0.92	0.02	1.49	1.30	0.19	2.18	2.01	0.17
36 - 42	0.30	0.27	0.03	0.49	0.40	0.09	1.29	1.09	0.20	1.24	1.19	0.05
Penetration depth of chloride measured by $AgNO_3$ (mm)	18.5			35			44			54		

Table 6.7: The total, free and bound chloride with different depths for mix M 0.5 were exposed to chloride spraying for 15 weeks at 30 °C (Series 2)

Sample	Chloride Concentration by mass of cementitious materials (%) for samples											
	Un-cracked			Crack width 0.05-0.15 mm			Crack width 0.15-0.25 mm			Crack width 0.25-0.35 mm		
Depth mm	Total Cl^-	Free Cl^-	Bound Cl^-	Total Cl^-	Free Cl^-	Bound Cl^-	Total Cl^-	Free Cl^-	Bound Cl^-	Total Cl^-	Free Cl^-	Bound Cl^-
0 - 6	4.16	3.92	0.24	4.53	4.26	0.27	4.53	4.25	0.28	4.91	3.87	1.03
6 -12	3.29	3.16	0.13	3.60	3.13	0.47	3.97	3.78	0.20	4.04	2.97	1.07
12 - 18	2.07	1.94	0.14	2.48	2.17	0.31	3.23	2.75	0.47	3.42	1.95	1.47
18 - 24	1.74	1.34	0.40	2.11	1.50	0.61	2.48	1.91	0.57	2.76	1.28	1.49
24 - 30	1.37	1.12	0.25	1.74	1.31	0.43	1.98	1.59	0.39	2.11	1.17	0.94
30 - 36	0.81	0.37	0.44	1.37	0.64	0.73	1.43	0.79	0.64	1.55	0.62	0.94
36 - 42	0.62	0.09	0.53	0.62	0.47	0.15	1.00	0.33	0.66	1.18	0.35	0.83
Penetration depth of chloride measured by $AgNO_3$ (mm)	27			37.5			47			57		

Table 6.8: The total, free and bound chloride with different depths for mix M 0.6 were exposed to chloride spraying for 15 weeks at 30 °C (Series 2)

Sample	Chloride Concentration by mass of cementitious materials (%) for samples											
	Un-cracked			Crack width 0.05-0.15 mm			Crack width 0.15-0.25 mm			Crack width 0.25-0.35 mm		
Depth mm	Total Cl^-	Free Cl^-	Bound Cl^-	Total Cl^-	Free Cl^-	Bound Cl^-	Total Cl^-	Free Cl^-	Bound Cl^-	Total Cl^-	Free Cl^-	Bound Cl^-
0 - 6	4.22	4.14	0.08	4.66	4.17	0.48	5.62	4.67	0.95	6.10	5.52	0.58
6 -12	3.19	2.46	0.73	4.22	3.77	0.45	5.22	3.22	1.99	5.76	5.32	0.44
12 - 18	2.43	1.57	0.86	2.91	2.59	0.32	4.00	3.36	0.65	5.01	4.45	0.56
18 - 24	2.04	1.47	0.56	2.58	1.89	0.69	3.13	2.33	0.80	3.80	3.35	0.45
24 - 30	1.60	1.03	0.58	2.04	0.73	1.30	2.25	1.60	0.66	3.04	2.75	0.29
30 - 36	0.95	0.45	0.49	1.60	0.73	0.87	1.60	1.00	0.60	2.50	1.73	0.77
36 - 42	0.72	0.38	0.34	1.17	0.72	0.45	1.38	0.90	0.48	1.63	1.35	0.28
Penetration depth of chloride measured by $AgNO_3$ (mm)	37			38			44			58		

Table 6.9: The total, free and bound chloride with different depths for mix M 0.5 + GGBS were exposed to chloride spraying for 15 weeks at 30 °C (Series 2)

Sample	Chloride Concentration by mass of cementitious materials (%) for samples											
	Un-cracked			Crack width 0.05-0.15 mm			Crack width 0.15-0.25 mm			Crack width 0.25-0.35 mm		
Depth mm	Total Cl^-	Free Cl^-	Bound Cl^-	Total Cl^-	Free Cl^-	Bound Cl^-	Total Cl^-	Free Cl^-	Bound Cl^-	Total Cl^-	Free Cl^-	Bound Cl^-
0 - 6	5.65	4.37	1.28	6.02	5.18	0.84	6.21	6.20	0.01	5.71	5.35	0.37
6 -12	3.41	2.45	0.96	3.60	3.26	0.34	3.79	2.55	1.24	4.16	2.32	1.84
12 - 18	1.55	1.24	0.31	1.74	1.68	0.06	1.89	0.93	0.96	2.30	0.95	1.35
18 - 24	1.00	0.21	0.79	1.18	1.07	0.11	1.18	0.47	0.71	1.74	0.35	1.39
24 - 30	0.81	0.18	0.63	1.00	0.70	0.29	1.00	0.36	0.64	1.37	0.17	1.20
30 - 36	0.62	0.20	0.42	1.00	0.13	0.87	0.81	0.25	0.56	1.00	0.23	0.77
36 - 42	0.44	0.16	0.28	0.81	0.26	0.54	0.62	0.19	0.43	0.81	0.18	0.63
Penetration depth of chloride measured by $AgNO_3$ (mm)	14.5			47			48			50		

Table 6.10: The total, free and bound chloride with different depths for mix M 0.5 + PFA were exposed to chloride spraying for 15 weeks at 30 °C (Series 2)

Sample	Chloride Concentration by mass of cementitious materials (%) for samples											
	Un-cracked			Crack width 0.05-0.15 mm			Crack width 0.15-0.25 mm			Crack width 0.25-0.35 mm		
Depth mm	Total Cl^-	Free Cl^-	Bound Cl^-	Total Cl^-	Free Cl^-	Bound Cl^-	Total Cl^-	Free Cl^-	Bound Cl^-	Total Cl^-	Free Cl^-	Bound Cl^-
0 - 6	3.60	3.39	0.21	3.72	3.64	0.08	3.79	3.67	0.11	4.50	4.37	0.14
6 -12	3.23	2.26	0.97	3.60	3.03	0.57	3.60	3.11	0.49	4.03	3.79	0.25
12 - 18	1.70	0.86	0.83	1.74	1.42	0.32	1.80	0.96	0.84	3.23	3.12	0.11
18 - 24	1.00	0.26	0.74	1.00	0.28	0.72	1.27	0.25	1.02	2.11	1.86	0.25
24 - 30	0.81	0.24	0.57	0.81	0.38	0.43	1.08	0.30	0.79	1.61	1.54	0.07
30 - 36	0.81	0.26	0.55	0.74	0.35	0.40	0.90	0.18	0.72	1.46	1.34	0.13
36 - 42	0.62	0.17	0.45	0.65	0.20	0.45	0.71	0.25	0.46	0.90	0.80	0.11
Penetration depth of chloride measured by $AgNO_3$ (mm)	14.5			43			59			60		

Table 6.11: The total, free and bound chloride with different depths for mix M 0.4 were exposed to chloride spraying for 15 weeks at 40 °C (Series 1)

Sample	Chloride Concentration by mass of cementitious materials (%) for samples											
	Un-cracked			Crack width 0.05-0.15 mm			Crack width 0.15-0.25 mm			Crack width 0.25-0.35 mm		
Depth mm	Total Cl^-	Free Cl^-	Bound Cl^-	Total Cl^-	Free Cl^-	Bound Cl^-	Total Cl^-	Free Cl^-	Bound Cl^-	Total Cl^-	Free Cl^-	Bound Cl^-
0 - 6	4.07	3.33	0.74	3.62	2.85	0.77	4.17	3.77	0.4	3.57	2.78	0.79
6 -12	3.47	1.7	1.77	3.11	2.41	0.7	4.02	3.35	0.67	3.35	2.61	0.74
12 - 18	1.88	0.81	1.07	2.13	1.97	0.16	3.57	2.93	0.64	2.92	2.18	0.74
18 - 24	1.64	0.47	1.17	1.98	1.23	0.75	3.18	2.62	0.56	2.53	1.65	0.88
24 - 30	1.14	0.24	0.9	1.39	1.07	0.32	2.43	1.93	0.5	1.69	0.87	0.82
30 - 36	0.99	0.24	0.75	0.94	0.85	0.09	2.08	1.17	0.91	1.04	0.33	0.71
36 - 42	0.75	0.15	0.6	0.49	0.2	0.29	1.54	1.07	0.47	0.94	0.24	0.7
Penetration depth of chloride measured by $AgNO_3$ (mm)	28			55			60			75		

Table 6.12: The total, free and bound chloride with different depths for mix M 0.5 were exposed to chloride spraying for 15 weeks at 40 °C (Series 1)

Sample	Chloride Concentration by mass of cementitious materials (%) for samples											
	Un-cracked			Crack width 0.05-0.15 mm			Crack width 0.15-0.25 mm			Crack width 0.25-0.35 mm		
Depth mm	Total Cl^-	Free Cl^-	Bound Cl^-	Total Cl^-	Free Cl^-	Bound Cl^-	Total Cl^-	Free Cl^-	Bound Cl^-	Total Cl^-	Free Cl^-	Bound Cl^-
0 - 6	3.41	3.2	0.21	4.84	3.95	0.89	5.28	4.31	0.97	4.96	4.71	0.25
6 -12	3.97	3.4	0.57	4.91	4.38	0.53	4.72	3.08	1.64	4.96	4.45	0.51
12 - 18	3.23	3.14	0.09	3.63	2.97	0.66	4.41	2.62	1.79	3.91	3.40	0.51
18 - 24	2.61	2.44	0.17	2.73	1.3	1.43	4.03	2.15	1.88	3.66	2.62	1.04
24 - 30	1.74	1.64	0.1	1.87	0.97	0.9	3.41	1.75	1.66	3.29	2.36	0.93
30 - 36	1.18	0.94	0.24	1.55	0.65	0.9	2.36	0.86	1.50	2.34	1.57	0.77
36 - 42	0.96	0.7	0.26	1.3	0.62	0.68	0.93	0.07	0.86	1.04	0.52	0.52
Penetration depth of chloride measured by $AgNO_3$ (mm)	40			60			65			75		

Table 6.13: The total, free and bound chloride with different depths for mix M 0.6 were exposed to chloride spraying for 15 weeks at 40 °C (Series 1)

Sample	Chloride Concentration by mass of cementitious materials (%) for samples											
	Un-cracked			Crack width 0.05-0.15 mm			Crack width 0.15-0.25 mm			Crack width 0.25-0.35 mm		
Depth mm	Total Cl^-	Free Cl^-	Bound Cl^-	Total Cl^-	Free Cl^-	Bound Cl^-	Total Cl^-	Free Cl^-	Bound Cl^-	Total Cl^-	Free Cl^-	Bound Cl^-
0 - 6	3.71	3.37	0.34	6.65	5.68	0.97	6.04	5.22	0.82	6.21	5.01	1.20
6 -12	2.91	2.63	0.28	5.01	3.74	1.27	4.51	4.36	0.15	5.01	3.18	1.83
12 - 18	2.79	1.75	1.04	2.83	1.37	1.46	3.37	3.02	0.35	4.24	2.31	1.93
18 - 24	2.09	1.55	0.54	2.18	1.59	0.59	2.79	2.12	0.67	3.78	1.75	2.03
24 - 30	1.53	1.25	0.28	1.77	1.21	0.56	2.29	2.10	0.19	2.98	1.43	1.55
30 - 36	0.94	0.75	0.19	1.60	1.18	0.42	2.21	1.88	0.33	2.18	1.38	0.80
36 - 42	0.75	0.30	0.45	0.94	0.64	0.30	1.63	1.07	0.56	1.53	0.95	0.58
Penetration depth of chloride measured by $AgNO_3$ (mm)	41			73			73			75		

Table 6.14: The total, free and bound chloride with different depths for mix M 0.5 + GGBS were exposed to chloride spraying for 15 weeks at 40 °C (Series 1)

Sample	Chloride Concentration by mass of cementitious materials (%) for samples											
	Un-cracked			Crack width 0.05-0.15 mm			Crack width 0.15-0.25 mm			Crack width 0.25-0.35 mm		
Depth mm	Total Cl^-	Free Cl^-	Bound Cl^-	Total Cl^-	Free Cl^-	Bound Cl^-	Total Cl^-	Free Cl^-	Bound Cl^-	Total Cl^-	Free Cl^-	Bound Cl^-
0 - 6	4.83	4.45	0.38	5.28	4.97	0.31	7.01	6.02	0.99	7.08	6.07	1.01
6 -12	4.68	4.19	0.49	4.72	4.45	0.27	6.29	5.50	0.79	6.92	5.76	1.16
12 - 18	4.47	4.14	0.33	4.35	4.20	0.15	5.79	4.49	1.30	5.93	4.45	1.48
18 - 24	3.65	3.14	0.51	3.19	2.39	0.80	4.93	3.82	1.11	5.60	4.19	1.41
24 - 30	1.88	0.85	1.03	2.07	1.94	0.13	4.35	3.61	0.74	4.99	3.93	1.06
30 - 36	0.99	0.23	0.76	1.85	1.68	0.17	2.82	1.64	1.18	4.00	3.40	0.60
36 - 42	0.85	0.36	0.49	1.20	1.05	0.15	1.80	1.19	0.61	2.77	1.22	1.55
Penetration depth of chloride measured by $AgNO_3$ (mm)	25			60			60			75		

Table 6.15: The total, free and bound chloride with different depths for mix M 0.5 + PFA were exposed to chloride spraying for 15 weeks at 40 °C (Series 1)

Sample	Chloride Concentration by mass of cementitious materials (%) for samples											
	Un-cracked			Crack width 0.05-0.15 mm			Crack width 0.15-0.25 mm			Crack width 0.25-0.35 mm		
Depth mm	Total Cl^-	Free Cl^-	Bound Cl^-	Total Cl^-	Free Cl^-	Bound Cl^-	Total Cl^-	Free Cl^-	Bound Cl^-	Total Cl^-	Free Cl^-	Bound Cl^-
0 - 6	2.96	2.22	0.74	3.72	1.78	1.94	3.41	2.93	0.48	4.50	4.19	0.31
6 -12	3.17	2.40	0.77	3.87	1.98	1.89	3.52	2.77	0.75	4.04	2.75	1.29
12 - 18	2.05	0.91	1.14	2.51	0.79	1.72	3.03	2.24	0.79	3.19	2.09	1.10
18 - 24	1.64	0.31	1.33	1.86	0.50	1.36	2.59	1.42	1.17	2.51	1.57	0.94
24 - 30	1.32	0.08	1.24	1.63	0.79	0.84	1.82	0.97	0.85	2.01	1.05	0.96
30 - 36	1.05	0.12	0.93	1.40	0.67	0.73	1.28	0.39	0.89	1.37	0.55	0.82
36 - 42	0.54	0.08	0.46	1.00	0.50	0.50	1.12	0.20	0.92	1.24	0.40	0.84
Penetration depth of chloride measured by $AgNO_3$ (mm)	26			50			52			75		

6.2.1 Chloride Penetration in Concrete

The accelerated method was used to simulate the exposure environment conditions namely; chloride concentration and the temperature to quicken the chloride ingress in concrete specimens. The silver nitrate ($AgNO_3$) colorimetric method was employed to measure penetration depths of the chloride front (d_{cl^-}) and chloride concentration at the color change boundary (C_d) for all specimens of concrete mixes. The results from all the series are presented in Tables 6.1 to 6.15 and Figure 6.2 showing effects due to changes in temperature, crack width and type of cementitious materials. The colorimetric method is color change boundary(C_d) due to the chemical reaction between Cl^- and OH^- ion in concrete samples (in the pores solution of hydrated cementitious materials in concrete) with Ag^+ (from $AgNO_3$ solution) (Yuan *et al.*, 2008; He *et al.*, 2012) as shown in Equations 6.1- 6. 2 and Figure 6.1.

$$Ag^+ + Cl^- = AgCl \downarrow \qquad (6.1)$$

$$Ag^+ + OH^- = AgOH = Ag_2O \downarrow \qquad (6.2)$$

The results of these reaction are precipitation of AgCl (silvery-white and solubility product is 1.8 $*10^{-10}$ at 25 °C) and Ag_2O (brown solubility product is 2.6 $*10^{-8}$ at 25 °C) (Yuan *et al*., 2008; He *et al*., 2011)

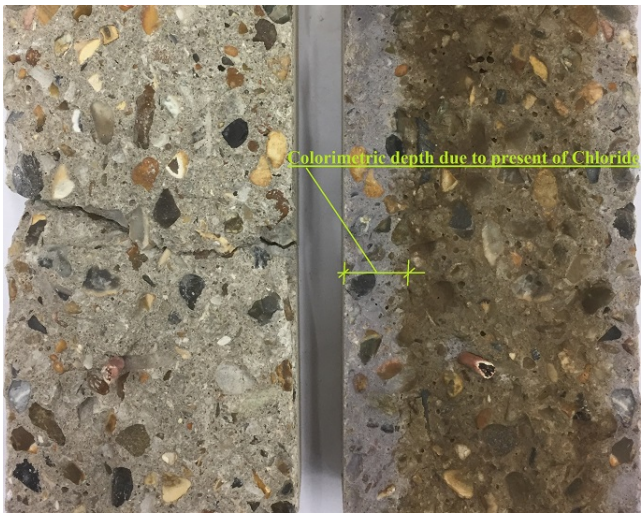

Figure 6.1: Silver nitrate colorimetric method to determine chloride penetration depth (d_{cl^-}) for (M 0.4- un-cracked -Series 1(30 °C))

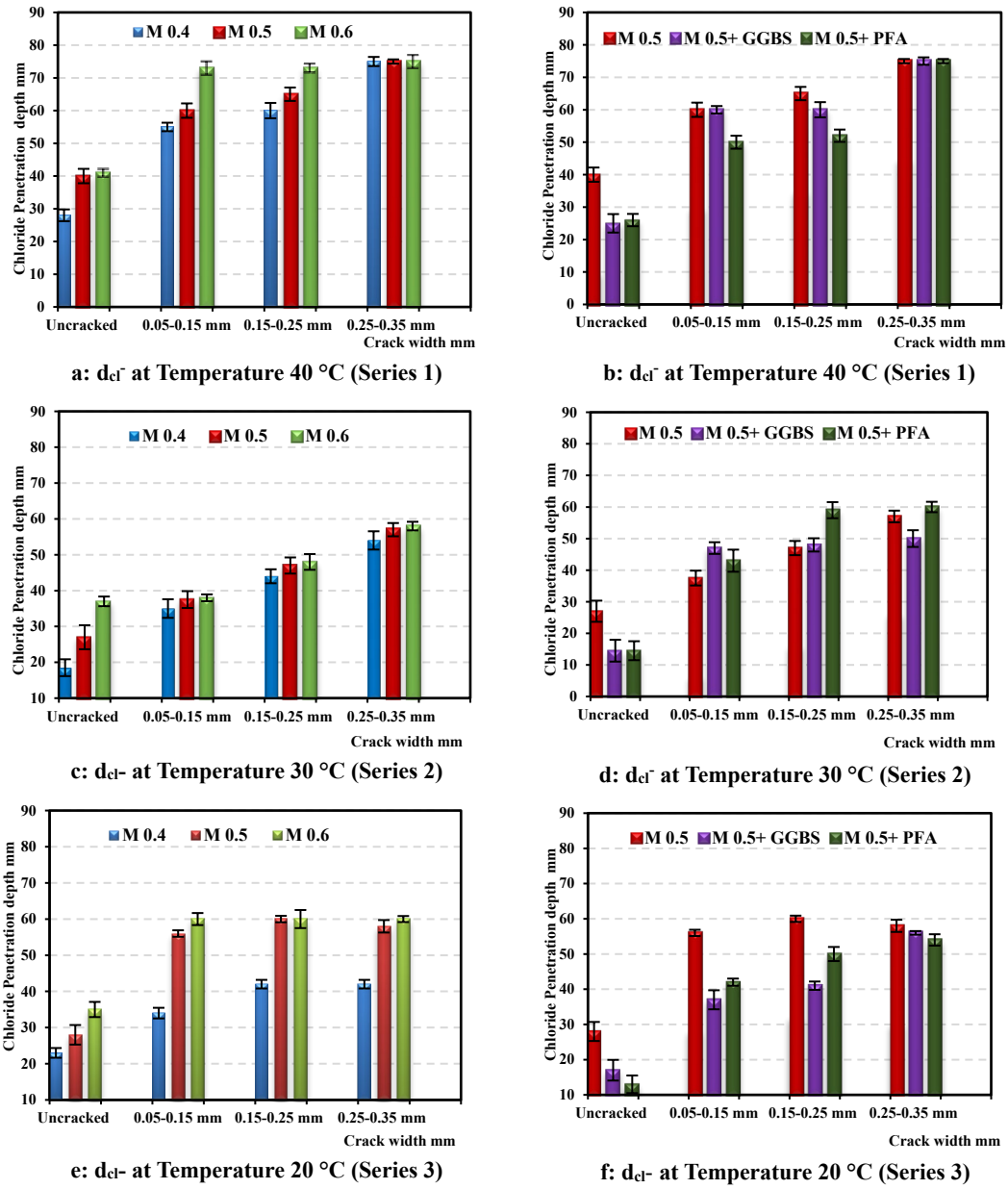

a: d_{cl}^- at Temperature 40 °C (Series 1)

b: d_{cl}^- at Temperature 40 °C (Series 1)

c: d_{cl}^- at Temperature 30 °C (Series 2)

d: d_{cl}^- at Temperature 30 °C (Series 2)

e: d_{cl}^- at Temperature 20 °C (Series 3)

f: d_{cl}^- at Temperature 20 °C (Series 3)

Figure 6.2: Effect of w/cm and crack width on chloride penetration depth (d_{cl}^-)

The results of three series indicated three main characteristics:

(i): The Effect of w/cm Ratio on Chloride Penetration (d_{cl}^-)

The results exhibited deeper chloride penetration of the front depth with an increasing w/cm ratio from 0.4 to 0.5 and 0.6 for all exposure temperatures (see Figure 6.3), with different values of differences in d_{cl}^- due to the effect of temperature and crack width. In addition, the precipitation of AgCl and Ag_2O was formed due to the reactions of the different color of mixes as shown in Figure 6.3. In addition, the results show the increase of w/cm ratio has a significant impact on the penetration of chloride in a cracked

sample by increasing color change boundary around the crack (width, depth) with an increase w/cm ratio as shown in Figures 6.4.

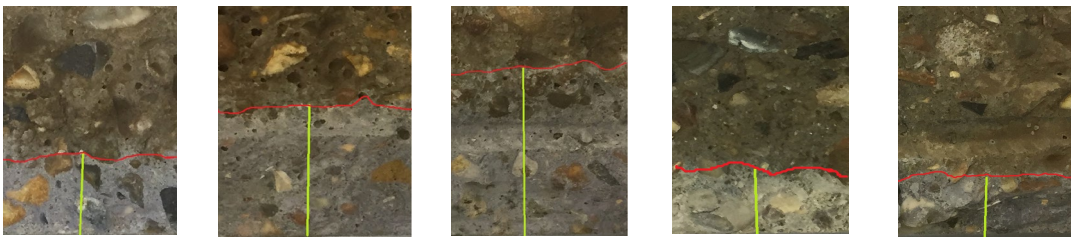

a:M 0.4 b: M 0.5 c: M 0.6 d: M 0.5+GGBS e: M 0.5+ PFA

Figure 6.3: Effect the w/cm ratio and type of cement of d_{cl}^- for un-cracked sample exposed to chloride sparing at temperature 30 °C (Series 2)

The increased percentages in d_{cl}^- due to increasing w/cm ratio are shown in Figure 6.2 and the highest increase of percentages in d_{cl}^- was in un-cracked samples and this percentage decreased sharply with increasing crack width. While, in cracked specimens, the influence of crack width on chloride penetration is higher than the effect w/cm ratio, particularly in samples from Series1 and 2, 40 °C and 30 °C respectively. However, the performance in samples from Series 3, 20 °C was slightly different.

On the other hand, the results indicated the tested powder from the interface layer or chloride front, d_{cl}^- for un-cracked samples had chloride concentrations varying from 0.44% to 1.88 % by weight of cementitious as illustrated in Table 6.16.

The $AgNO_3$-based colorimetric methods can potentially measure two variables, chloride penetration depth (d_{cl}^-) and chloride concentration at the color change boundary (C_d). In this study, the smaller volume of $AgNO_3$ solution with 0.1 mole/l was used to determine the lower color change boundary, has the brightest color of the boundary of chloride penetration depth(d_{cl}^-) (He *et al*., 2012). The boundaries of colored areas due to the spraying of $AgNO_3$ solution are because the precipitate formed on the surface of concrete may be a mixture of silver oxide and silver chloride. It means the increase of the boundaries of colored areas shows the increased penetration of chloride ions in concrete as well as hydroxide ions as shown in Equation 6.1- 6.2.

Table 6.16: Depth of chloride front by $AgNO_3$ test (d_{cl}^-) and total Cl^- concentration at the interface layer

Sample	Series 1 Temperature 40 °C		Series 2 Temperature 30 °C		Series 3 Temperature 20 °C	
	d_{cl}^- (mm)	Total Cl^- (%)	d_{cl}^- (mm)	Total Cl^- (%)	d_{cl}^- (mm)	Total Cl^- (%)
M 0.4	28	1.14	18.5	0.94	23	0.64
M 0.5	40	0.96	27	1.37	28	0.44
M 0.6	41	0.75	37	0.72	35	0.51
M0.5+GGBS	25	1.88	14.5	1.55	17	1.36
M0.5+PFA	26	1.32	14.5	1.7	13.5	1.55

* Total Cl^- [% by mass of cementitious materials]

Chloride penetration depth, d_{cl}^- increased with the increase of w/cm. The transport mechanisms of fluid in concrete mainly depend on the volume of internal voids or connective porosity in the structure of concrete (Basheer *et al*., 2001). These voids increase by increasing the w/cm ratio (see Figure 4.2). Therefore, the chloride transport in concrete and d_{cl}- increases with the increase of w/cm ratio due to the volume of voids in the concrete structure.

(ii): The Effect of Crack Width on Chloride Penetration (d_{cl}^-)

The results are presented in Table 6.1- 6.15 and Figures 6.2 (a-e), showed that the chloride penetration depth (d_{cl}^-) and the color change boundary (C_d) were a function of crack widths for the all mixes used. The results illustrate that the chloride penetration depth increases significantly with the increase in crack width for all exposure temperatures and w/cm ratios as shown in Figure 6.4 (for Series 1). This figure also shows that the changes in the color change boundary near the cracks are significantly deeper.

In addition, the increase of crack width leads to raising the color change boundaries in the concrete tested. Diffusivity of chloride in the vicinity of the cracks is considerably higher due to the relatively faster penetration of Cl^- ions into the crack followed by orthogonal outward diffusion into the un-cracked concrete surrounding the crack.

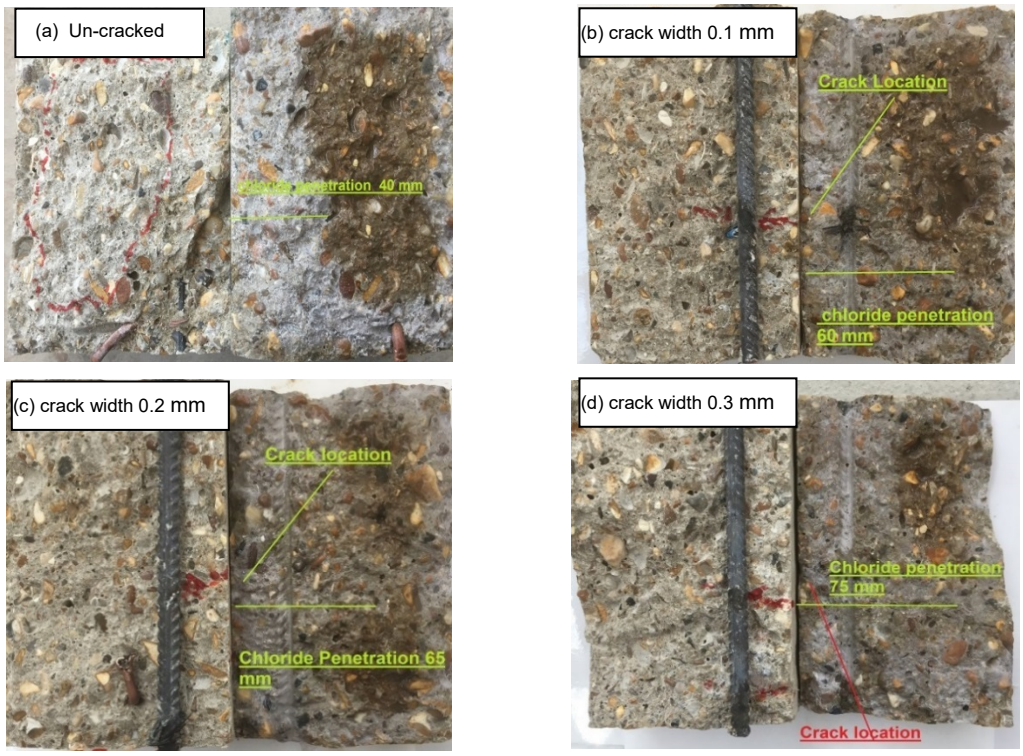

Figure 6.4: Effect of the crack width on chloride penetration -M 0.5 Samples (Series1with 40℃)

The speed of chloride ions penetration depends on pore-microstructure and especially the porosity of the concrete. Finally, the increase in the amount of chloride solution in a cracked location in concrete leads to an increase in the chloride penetration depth (Audenaert *et al*., 2009; Shao-feng *et al*., 2011) as illustrated in Figure 6.5.

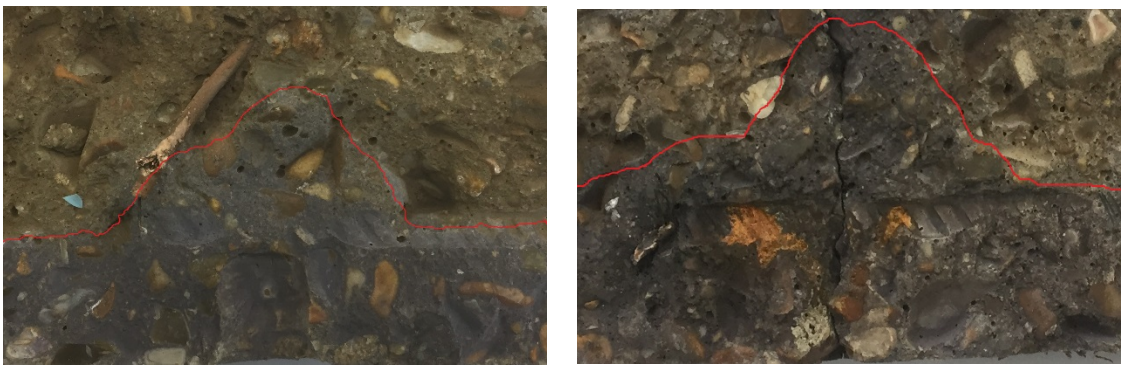

M 0.4-crack width 0.1 mm M 0.5-crack width 0.1 mm

Figure 6.5: The Effect of w/cm ratio on the penetration of chloride in the cracked sample (Series 3 with 20 °C)

(iii): The Effect of SCMs on Chloride Penetration (d_{cl}^-)

The results also showed that the partial replacement of OPC with SCMs, GGBS, and PFA leads to less chloride penetration in concrete; generally, the d_{cl}^- of these samples (with GGBS and PFA) is less than the d_{cl}^- of control mixes as shown in Table 6.1-6.15. The results of SCMs mixes have an effect similar to that of crack widths on d_{cl}^- to control mixes (M 0.5). In addition, the experimental results found that the use of GGBS and PFA mix in concrete can change the precipitation color formed by the reaction of Ag NO_3 with hydrated cement products in concrete samples as exhibited in Figure 6.6.

a: M 0.5 b: M0.5+GGBS c: M0.5+PFA

Figure 6.6: The Effect of the replacing of (GGBS and PFA) on precipitation color due to using $AgNO_3$ to investigate the d_{cl}^-

The samples incorporating SCMs, GGBS and PFA decreased color change boundaries (C_d) and chloride penetration depth (d_{cl}^-). The mineral additives are a principal factor to consider in decreasing the permeability of concrete (Teng *et al.*, 2013; Wang *et al.*, 2016). These SCMs have a significant impact on the ability of concrete to resist the penetration of chloride ions. This benefit is largely credited to the refined pore structure that results from the appropriate use of SCMs which, in turn, results in reduced permeability and ionic diffusivity. However, SCMs also alter the composition and, hence, the chloride binding capacity of the hydrated phases (Thomas *et al*., 2012; Ukpata *et al*., 2018).

Finally, the precipitation color formed due to using the $AgNO_3$-based colorimetric method with a concentration of 0.1 M $AgNO_3$ produced assorted colors as shown in Figures 6.4 and 6. 6. The variation in precipitation color is due to the amount and the differences in cementitious materials between the mixes. Where, the color formed as a

result of this reaction depends on the type of precipitation produced, AgCl and Ag_2O, due to the concentration of Cl^- and OH^- ions in concrete (Yuan *et al*., 2008; He *et al*., 2011; He *et al*., 2012). This is the main reason for the change in precipitation color in mixes incorporating SCMs such as GGBS and PFA.

(iv): The Effect of Temperature on Chloride Penetration (d_{cl}^-)

The environment exposure condition has an impact on chloride penetration in concrete structures, hence the different temperature exposures of chloride spraying have been investigated in this study. The influence of environmental temperature on chloride penetration depth, d_{Cl}- is summarized in Tables 6.1- 6.15 and Figure 6.7 for different w/cm ratios and crack widths. These results indicated the increase in temperature has a considerable impact on depths of the chloride front (d_{cl}^-) and chloride concentration at the color change boundary (C_d) for all specimens of concrete mixes. Generally, the increase in the chloride environment temperature increased the penetrability of chloride in concrete by increasing the activity of chloride diffusion in the concrete sample as shown in Figure 6.8. Where, the activation energy for chloride diffusing in concrete can magnify with an increase in the temperature according to Arrhenius's Law (Yokozeki *et al*., 2003). On the other hand, some cases were different with common performance due to the influence of other parameters that lead to a change in the results in these cases and the chloride ingress into the concrete matrix is dominated by a complex interaction between physical and chemical processes (Bastidas-Arteaga *et al.,* 2010).

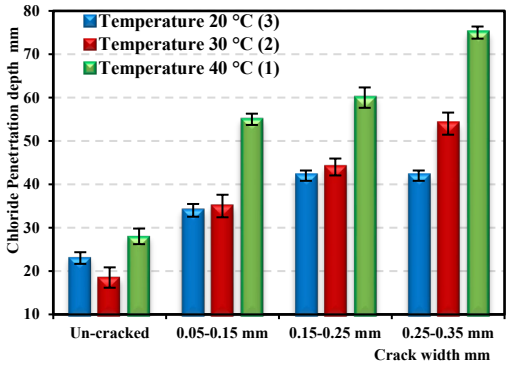

Figure 5.1- a:M 0.4

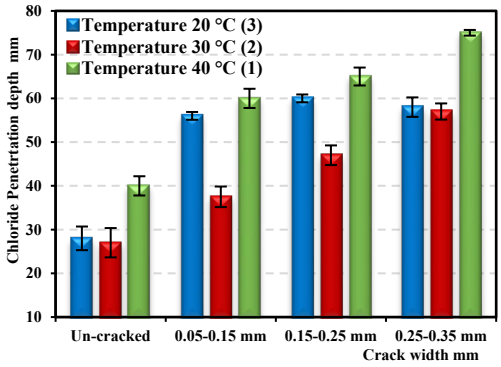

Figure 5.1- b:M 0.5

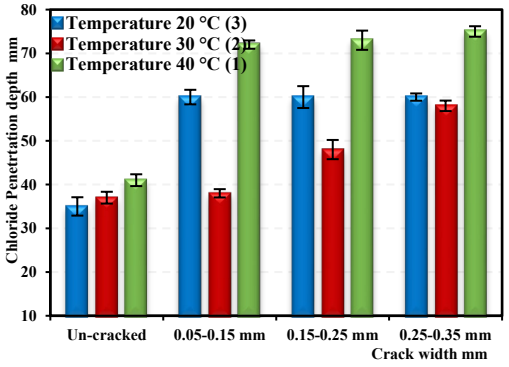

Figure 5.1-c:M 0.6

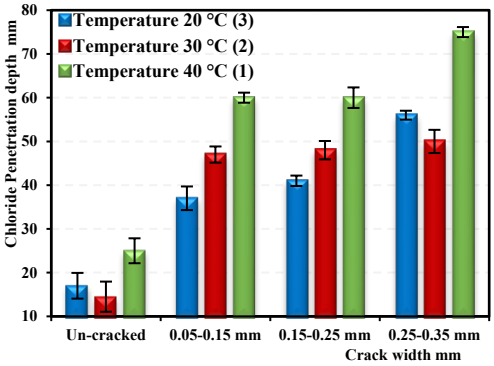

Figure 5.1-d: M 0.5+GGBS

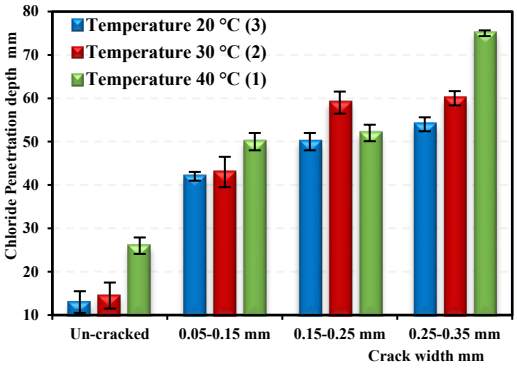

Figure 5.1-e: M 0.5+PFA

(1) Series 1 with a temperature of 40 °C
(2) Series 2 with a temperature of 30 °C
(3) Series 3 with a temperature of 20 °C

Figure 6.7: The Effect of temperature on chloride penetration depth (d_{cl}^{-}) for different crack widths in the concrete prism exposed to chloride spraying for a 15 weeks period

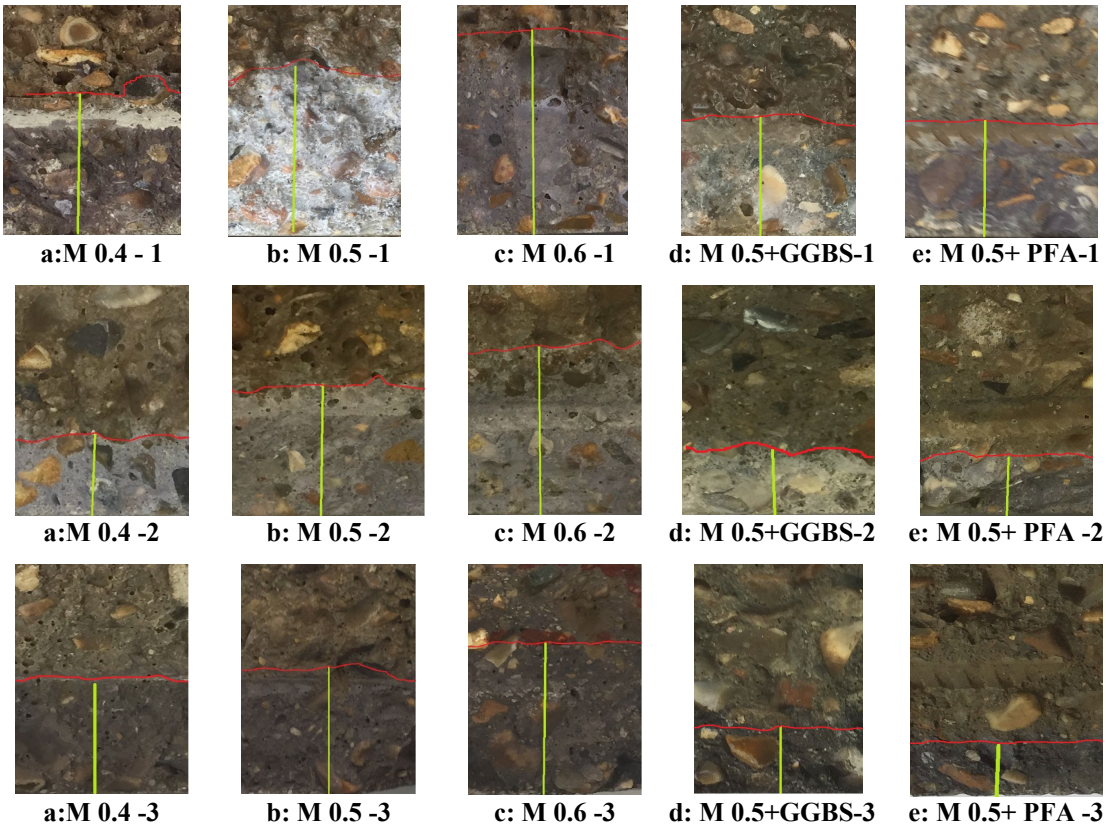

Figure 6.8: Effect of w/cm ratio and type of cement of d_{cl}^- for the uncracked sample exposed to different chloride sparing temperature (20 °C (3), 30 °C(2) and 40 °C(1))

6.2.2 Total Chloride Concentration Profile

The total chloride concentrations for all mixes were experimentally found according to BS EN 14629: 2007 using the chloride titration method. In this study, three series of exposure temperatures were investigated, 20, 30 and 40 °C; they are reported in Tables 6.1 to 6.15 and separately presented in Figures 6.9 to 6.11, illustrating the changes in the acid-soluble chloride content with depth of concrete sample due to exposure to an accelerated chloride environmental conditions.

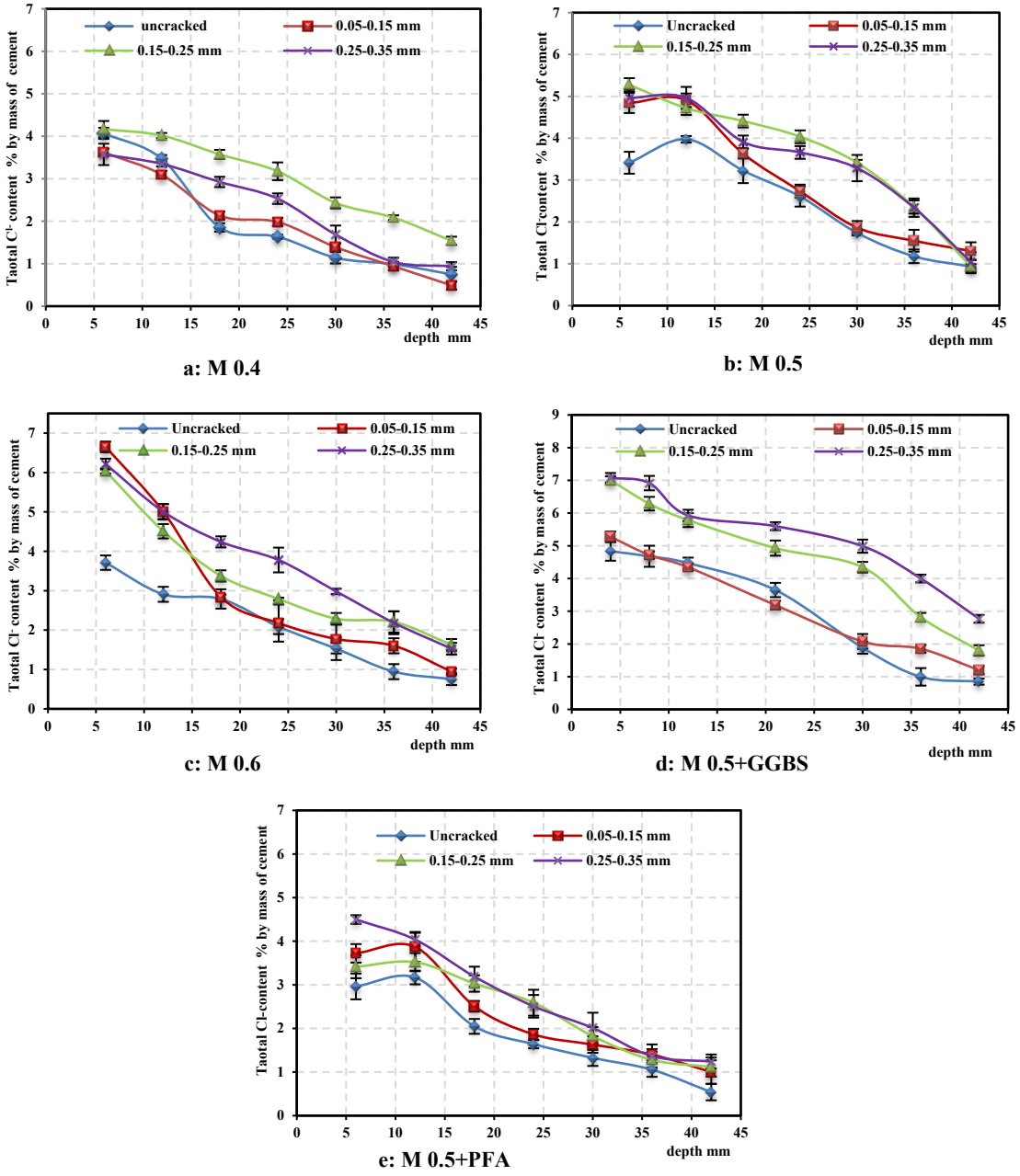

Figure 6.9: Total chloride concentration profile of mixes exposed to chloride spraying at 40 ºC for 15 weeks (Series 1)

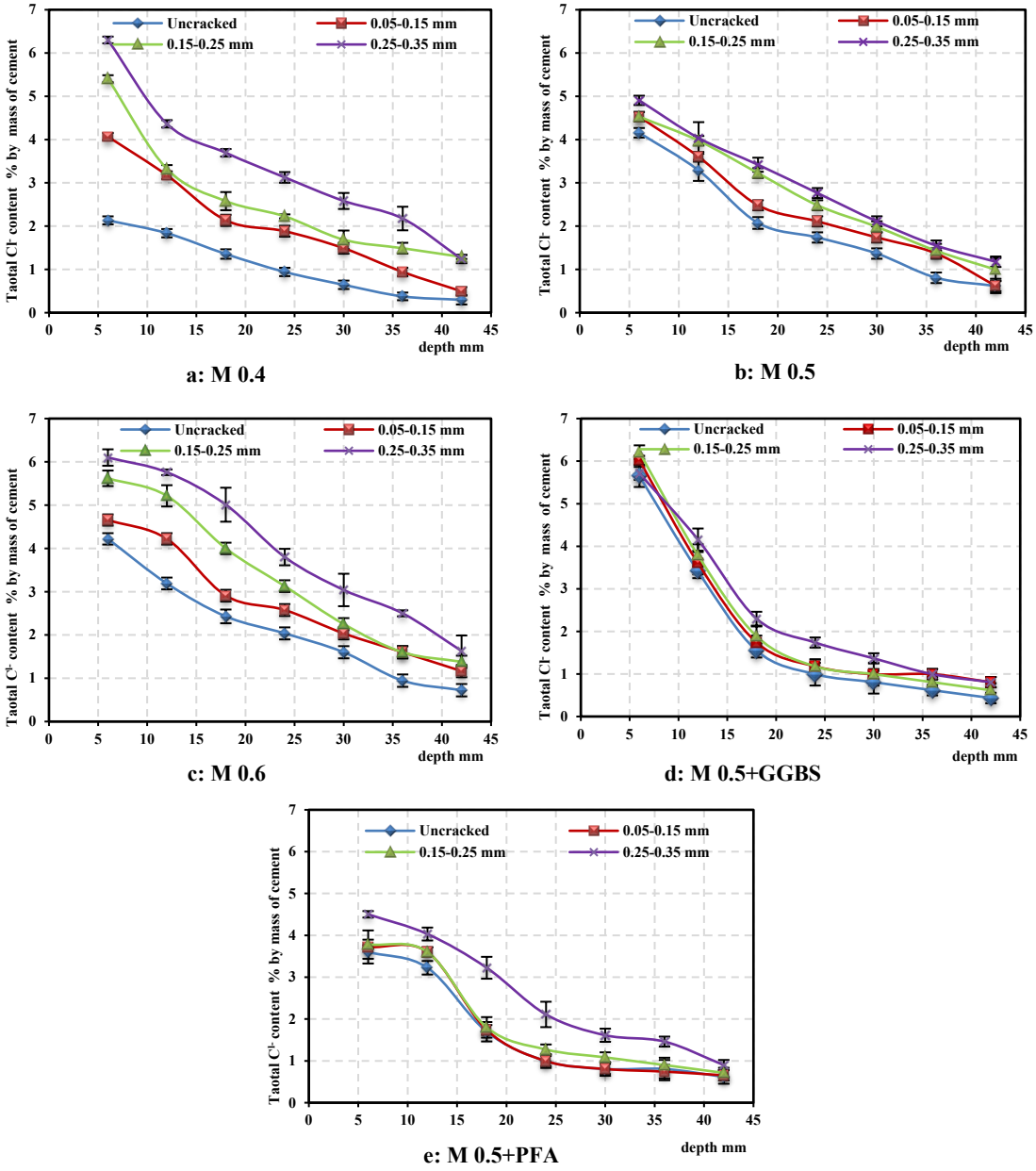

Figure 6.10: Total chloride concentration profile of mixes exposed to chloride spraying at 30 ºC for 15 weeks (Series 2)

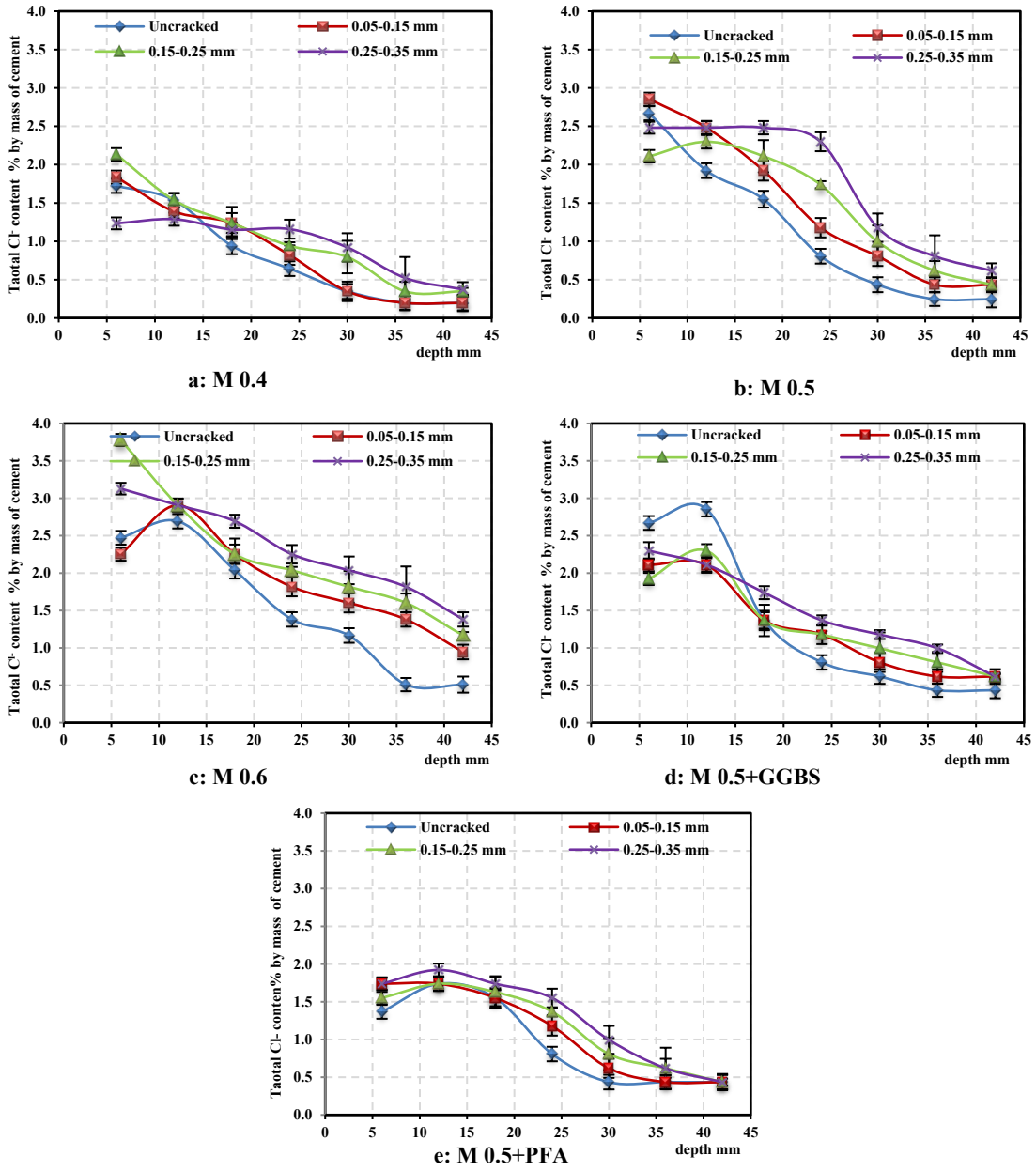

Figure 6.11: Total chloride concentration profile of mixes exposed to chloride spraying at 20 ºC for 15 weeks (Series 3)

The chloride content profile or concentration with the depth and non-linear regression of Fick's Second Law were employed to find the apparent diffusion coefficient, D_a and surface chloride concentration, C_s by the least square difference between the experimental data of chloride concentration and the non-linear best fitting of Equation 2.34 according to BS EN 12390-11: 2015 and ASTM C1556-11a: 2016 as shown in Figure 3.16. The chloride concentration profile can offer insight to evaluate the chloride resistance of concrete. The apparent chloride diffusion, D_a and surface chloride concentration, C_s are presented in Tables 6.17-6.19 and Figures 6.12. The results show

the total concentration profile influenced significantly by w/cm ratio, crack width and supplementary cementitious materials, will be discussed using the D_a and C_s results as following.

Table 6.17: Summarary of apparent diffusion coefficient (D_a)and surface chloride concentration(C_s) at 40 °C (Series1)

Sample	Un-cracked		0.05-0.15 mm		0.15-0.25 mm		0.25-0.35 mm	
	D_a*	C_s**	D_a*	C_s**	D_a*	C_s**	D_a*	C_s**
M 0.4	22	4.18	22	4.60	30	5.86	30	5.44
M 0.5	22	5.00	22	5.50	30	6.80	32	7.07
M 0.6	23	5.21	25	6.13	30	6.75	30	7.36
M 0.5+ GGBS	25	6.02	26	6.28	30	7.07	30	7.33
M 0.5+ PFA	23	4.45	26	4.97	30	5.24	30	6.02

*Apparent diffusion coefficient (D_a) in $*10^{-12}$ m^2/sec.
** Surface chloride concentration (C_s) in % by mass of cementitious materials.

Table 6.18: Summary of apparent diffusion coefficient (D_a)and surface chloride concentration(C_s) at 30 °C (Series2)

Sample	Un-cracked		0.05-0.15 mm		0.15-0.25 mm		0.25-0.35 mm	
	D_a*	C_s**	D_a*	C_s**	D_a*	C_s**	D_a*	C_s**
M 0.4	18	3.35	20	4.39	28	5.02	30	5.86
M 0.5	20	4.71	22	5.24	28	6.02	30	6.28
M 0.6	22	4.91	23	5.83	28	6.44	30	7.24
M 0.5+ GGBS	22	5.24	22	5.76	24	5.24	28	6.28
M 0.5+ PFA	20	4.19	23	4.71	25	4.97	30	5.50

Table 6.19: Summary of apparent diffusion coefficient (D_a)and surface chloride concentration(C_s) at 20 °C (Series 3)

Sample	Un-cracked		0.05-0.15 mm		0.15-0.25 mm		0.25-0.35 mm	
	D_a*	C_s**	D_a*	C_s**	D_a*	C_s**	D_a*	C_s**
M 0.4	14	2.72	14	2.93	17	3.14	17	3.35
M 0.5	15	3.66	16	3.93	20	4.19	22	4.45
M 0.6	20	4.29	20	4.91	22	5.21	24	5.21
M 0.5+ GGBS	16	3.14	18	3.40	20	3.66	24	4.19
M 0.5+ PFA	12	2.88	14	3.40	15	3.51	16	3.93

(i): The Effect of w/cm Ratio on Chloride Concentration

The graphs in Figures 6.9 to 6.11 (a, b and c) show that the chloride penetrates progressively further into the concrete by increasing the w/cm ratio with respect to mix M 0.4, to M0.5 and M 0.6 for all exposure temperature. The first layers of concrete, in particular, were a higher concentration and beyond that the concentration decreases with depth. This performance of the concentration profile is based on external exposure conditions and resistance of concrete to the penetrability of chlorides such as permeability and cracking. In Figure 6.12 and Tables 6.17-6.19, for un-cracked and almost cracked samples, the apparent chloride diffusion coefficient, D_a and chloride surface concentration C_s increased significantly with increasing w/cm ratio at all exposure temperatures of the chloride spray. It is generally accepted that the influence of an increased w/cm ratio decreases chloride resistance of concrete. In this study, whether an increased w/cm ratio behaves the rising trend on D_a value and C_s for all tested samples. To obtain more insight into the effect of lowering the w/cm ratio on minimising chloride ingress in concrete, non-steady state diffusion coefficient values were considered in the analysis.

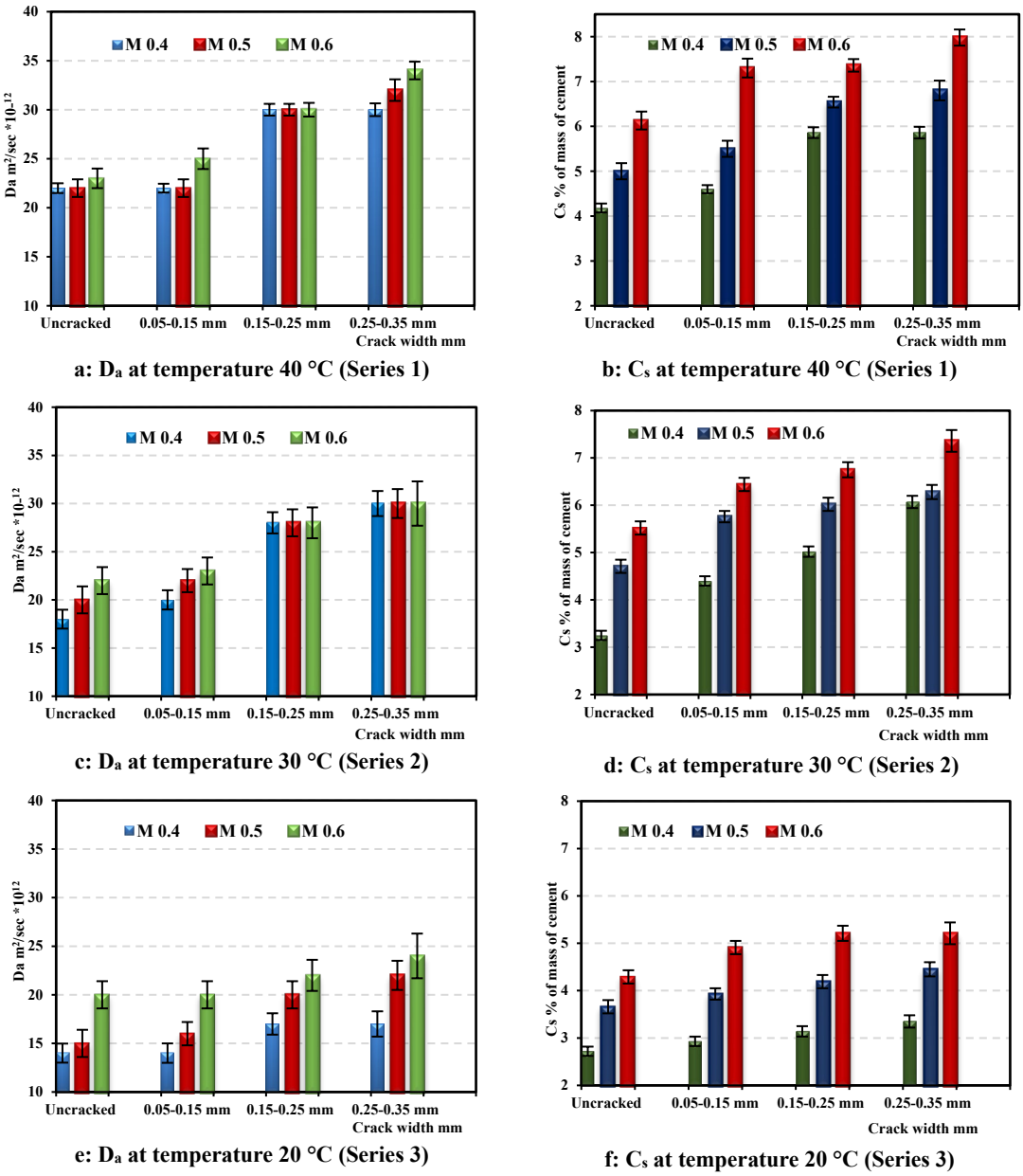

a: D_a at temperature 40 °C (Series 1)

b: C_s at temperature 40 °C (Series 1)

c: D_a at temperature 30 °C (Series 2)

d: C_s at temperature 30 °C (Series 2)

e: D_a at temperature 20 °C (Series 3)

f: C_s at temperature 20 °C (Series 3)

Figure 6.12: The effect of w/cm (M 0.4, M0.5 and M0.6) and crack width on D_a and C_s for a concrete prism with different crack width and temperature exposure

From the chloride concentration profiles, Figures (6.9 to 6.11) generally illustrate a maximum chloride level of several millimeters into the concrete, which would be typical of the distribution of the chlorides in an intermittent wetting /drying exposure of chloride solution (Polder and Peelen, 2002). During aeration and wetting of samples as shown in Figure 3.14, the chloride solution penetrates a layer of concrete whilst during the drying phase the evaporation front moves inwards from the surface. Therefore, as evaporation occurs, some chloride ions transfer outwards (McPolin *et al.*, 2005).

The method of determination of apparent chloride diffusion, D_a is built on surface chloride content, C_s and vice versa. It is a standard method and it is used to measure the resistivity of concrete against the penetration of chloride. On the other hand, the D_a and C_s can be used in a database, to use in the modelling of chloride penetration in different exposure conditions according to the study area (Iraq and UK) to predict the change in concentration in concrete structures due to climate change.

There is an agreement between researchers on the w/cm ratio of the mix and on the degree of hydration of cement that will significantly influence the capillary porosity of the cement paste. And the degree of hydration depends on the type of cement, (in this study, it was the same type). Thus, the increase of w/cm increases the capillary pores, at water/cement ratios higher than about 0.38, the volume of the gel is not sufficient to fill all the space available to it, which means that there will be some volume of capillary pores left and these volumes of pores will remain even after the process of hydration has been completed (Neville, 2011) . According to calculation details of cement hydration by Neville (2011), the products of cement hydration in w/cm ratio (0.5) may leave more capillary pores and they will increase with an increase in w/cm ratio, such as 0.6 due to the increase of water quantity relative to cement. Finally, the changes in the w/cm ratio considerably affect the microstructure of the concrete by a reduction in gel/space ratio and microstructure of the concrete due to a decrease in the amount of cement and an increase in water, these capillary pores or permeable voids form well paths, transporting chloride deeper into the concrete (Song *et al*., 2008).

(ii): The Effect of Crack Width on Chloride Concentration

The crack width, W_c considerably influences the ability of chloride ions to penetrate along a crack by increasing the chloride concentration with depth for all mixes as shown in Figures 6.9-6.11. The crack width and depth affect the mechanism of penetration of chloride ions into the opening of the crack and the penetration of chloride changes accordingly. In this study, structural cracks were used ($W_c > 0.1$ mm). Therefore, the mechanism of chloride penetration is variable. The results indicated that a crack width of less than 0.15 mm gave the highest combined effect of crack and permeability of concrete in chloride penetration and the diffusion process of chloride along the crack path appears to be a limiting factor controlling the diffusion process perpendicular to the crack wall for all mixes. The crack width, $W_c \geq 0.15$ mm, appears to have provided an additional

surface area (along the crack walls) for the transport of chloride ions into the concrete. Hence, an increase in chloride penetration perpendicular to the crack walls can also be observed (see Figure 6.13), which is similar to the chloride penetration profile from the surface of an uncracked concrete

a **b**

Figure 6.13: Chloride penetration through the crack, (a) longitudinal section in the crack, (b)

According to the chloride concentration profile, the D_a and C_s for all sample with different (w/cm ratio, exposure temperature and using SCMs) increased with increasing the crack width as shown in Figures 6.12 and Tables 6.17-6.19. The impact of crack width on D_a and C_s is presented in the percentage change as shown in Table 6.20.

In sound concrete, the transport of chloride into concrete can occur due to a combination of the concentration gradient, the pressure gradient and capillary sorption causing the flow of chloride through permeable pores by combined transport methods such as diffusion, permeation and capillary sorption (Basheer *et al*., 2001) . However, in cracked concrete samples, the new factor of transport properties in concrete are represented through the permeability of concrete, which is likely to be significantly affected by the formation of cracks. The presence of cracks in concrete may influence the transport of chloride ions in concrete; they have a significant impact on diffusion and permeation of chloride ion in concrete through permeable pores. Where, the chloride diffusion coefficient in concrete may be increased according to crack width due to a change of mechanism of chloride transport (Kwon *et al*., 2009; Shao-feng *et al*., 2011). In other words, for the sake of simplicity, the flux of chloride ions is not obtained by integrating the flow contributions of numerous pores, but by two macroscopic factors (volume and averaged crack width) which reveal the apparent chloride diffusivity (Ishida *et al*., 2014). Furthermore, the chloride concentration and penetration depth may change

in the same crack width due to the natural formation of cracks in the sample (width, depth, and tortuosity) or because of the method of measuring the diffusion coefficient of chloride. Finally, the increase in the total chloride concentration with an increasing crack width is the result of increased open exposure area to chloride solution as well as penetration through the voids or the porosity in concrete (Park *et al*., 2012). Figure 6.12 shows the influence of the crack on chloride penetration throughout the crack path.

Table 6.20: Percentage Changes in (D_a)and (C_s) for all mixes due to the crack width

Series	Sample	Change percentage in D_a and C_s for different crack width %					
		0.05-0.15 mm		0.15-0.25 mm		0.25-0.35 mm	
		D_a	C_s	D_a	C_s	D_a	C_s
Series 1 40 °C	M 0.4	0.0	10.0	36.4	40.2	36.4	30.1
	M 0.5	0.0	10.0	36.4	36.0	45.5	41.4
	M 0.6	8.7	17.7	30.4	29.6	30.4	41.3
	M 0.5+GGBS	4.0	4.3	20.0	17.4	20.0	21.8
	M 0.5 +PFA	13.0	11.7	30.4	17.8	30.4	35.3
Series 2 30 °C	M 0.4	11.1	31.0	55.6	49.9	66.7	74.9
	M 0.5	10.0	11.3	40.0	27.8	50.0	33.3
	M 0.6	4.5	18.7	27.3	31.2	36.4	47.5
	M 0.5+GGBS	0.0	9.9	9.1	0.0	27.3	19.8
	M 0.5 +PFA	15.0	12.4	25.0	18.6	50.0	31.3
Series 3 20 °C	M 0.4	0.0	7.7	21.4	15.4	21.4	23.2
	M 0.5	6.7	7.4	33.3	14.5	46.7	21.6
	M 0.6	0.0	14.5	10.0	21.4	20.0	21.4
	M 0.5+GGBS	12.5	8.3	25.0	16.6	50.0	33.4
	M 0.5 +PFA	16.7	18.1	25.0	21.9	33.3	36.5

(iii): The Effect of SCMs on Chloride Concentration

The results of mixes incorporating SCMs, M 0.5+GGBS, and M 0.5+PFA, showed the total concentration of chloride at a depth between 0-24 mm remains high, and the

reduction of concentration with depth at this zone was minor, while, the decrease of chloride content in the zone beyond the first one reduced sharply. In addition, the results from samples of M 0.5+PFA showed the total chloride concentration was less than the concentration of chloride in mix M 0.5 for all series. In addition, Figure 6.14 illustrates the apparent chloride diffusion coefficient D_a and chloride surface concentration, C_s changed slightly with replacing OPC with SCMs, GGBS, and PFA, at all the exposure temperatures of chloride spraying. In almost all of the results of samples incorporating PFA, the results of D_a and C_s were less than D_a and C_s of the same w/cm ratio, M 0.5.

In general, the replacement of OPC by GGBS in concrete (M 0.5+GGBS and M 0.5+PFA) may refine pore networks and improve chloride binding capacities (see section 6.2.3) and subsequently decrease chloride transport through concrete compared to that of M 0.5 concretes (Yuan *et al*., 2009; Thomas *et al*., 2012; Zeng *et al*., 2012; Salaiai and Hameed, 2017). Where, the pore structure of SCMs can be defined by, pore size distribution, pore specific surface area, total porosity as well as some characteristic pore sizes. The pore structure is the result of the observed hydration processes of cement and SCMs. Both chemical reaction kinetics and physical packing of hydrates account for the pore structure. The hydration kinetics is quantified by cement hydration degree and the formed gel/space ratio due to the consumption of the $Ca(OH)_2$ by a mineral additive and the production of additional gel. Among the pore structure characteristics, the total porosity and specific surface area are found to correlate linearly with the cement hydration degree (Neville, 2011; Zeng *et al*., 2012).

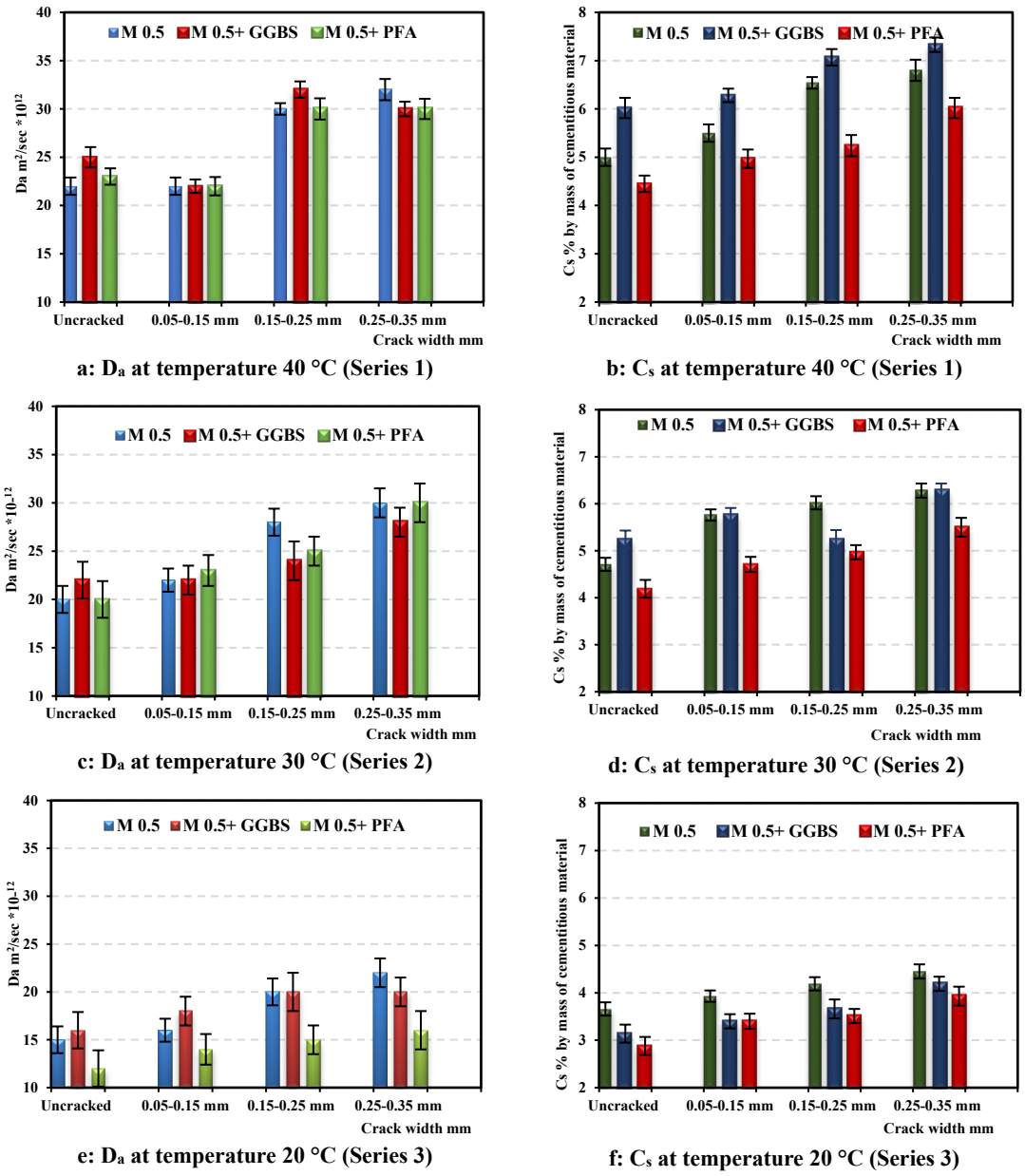

Figure 6.14: Effect of supplementary cementing materials (GGBS and PFA) on D_a and C_s for a concrete prism with different crack width and temperature exposure

(iv): The Effect of Temperature on Chloride Concentration

The significant factor influencing the concentration of chloride in concrete is the temperature of environmental exposure. Because the activation energy or ion conductivity of chloride diffusing in media can be amplified by increasing the temperature or the ion conductivity is temperature dependent, which is considered by Arrhenius's Law (Yokozeki *et al.*, 2003). The chloride diffusion coefficient D_a and surface concentration, C_s values of concrete mixes are the main methods investigating the influence of the exposure temperature on chloride concentration. The influence of

environmental temperature on chloride diffusion coefficient, D_a and surface concentration, C_s is presented Figures 6.15-6.16 for different w/cm ratio, crack width and supplementary cementitious materials. The experimental results indicated that D_a and C_s are increased by increasing the temperature of chloride exposure.

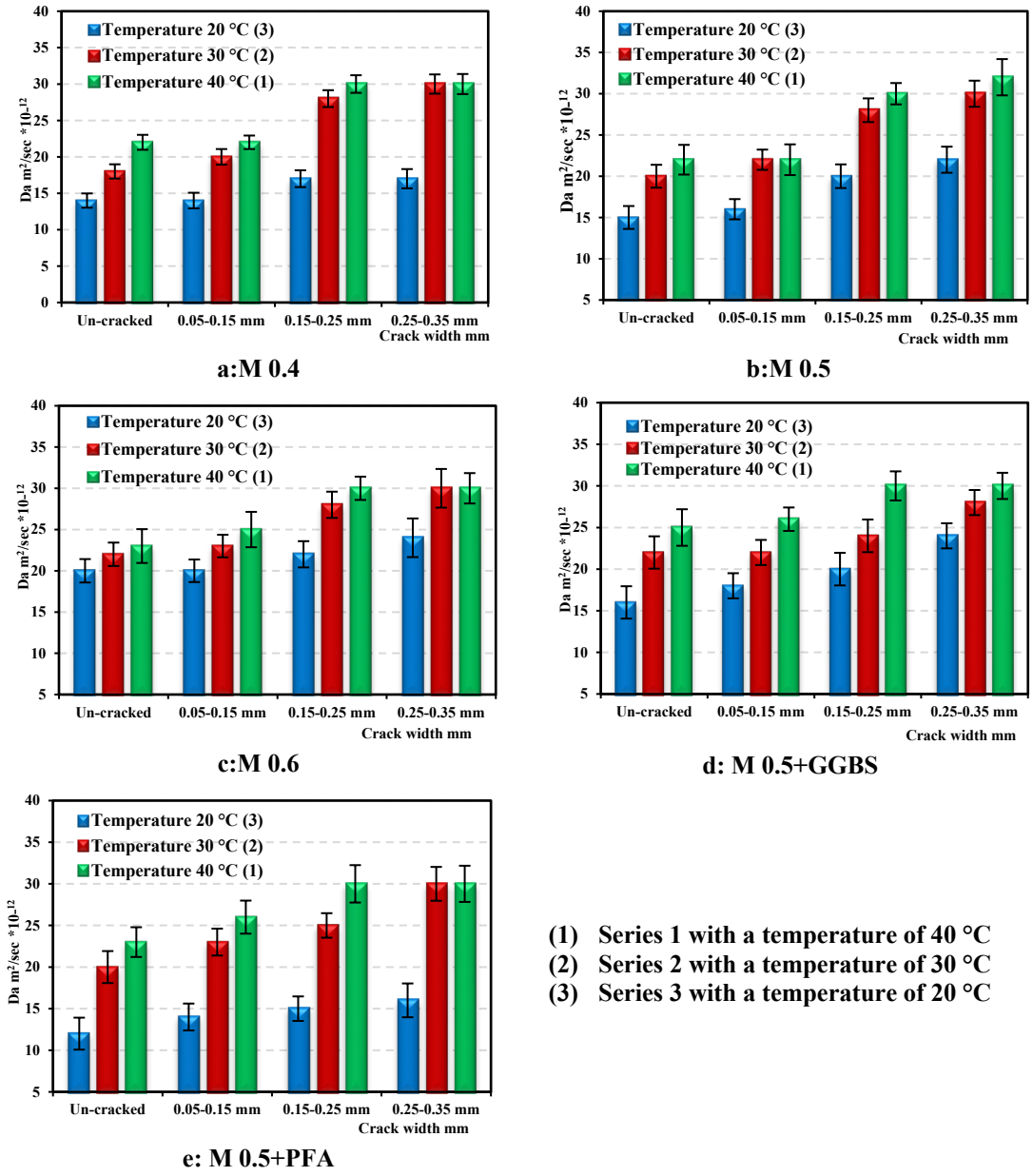

(1) Series 1 with a temperature of 40 °C
(2) Series 2 with a temperature of 30 °C
(3) Series 3 with a temperature of 20 °C

Figure 6.15: The Effect of temperature on apparent chloride diffusion coefficient (D_a) for different crack width in the concrete prism exposed to chloride spraying

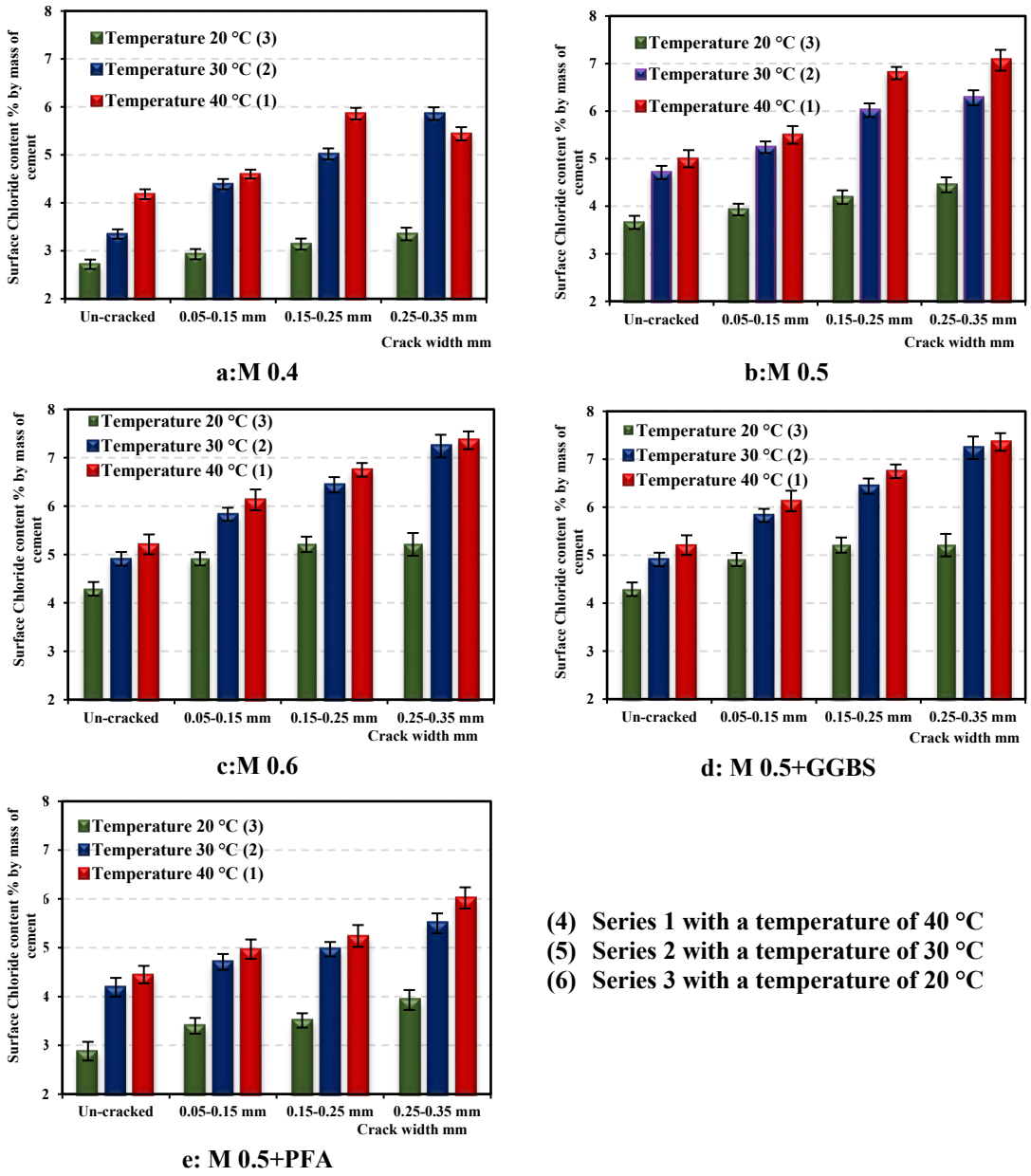

(4) Series 1 with a temperature of 40 °C
(5) Series 2 with a temperature of 30 °C
(6) Series 3 with a temperature of 20 °C

Figure 6.16: The Effect of temperature on surface chloride concentration (C_s) for different crack width in the concrete prism exposed to chloride spraying

Finally, the main factors strongly affecting the chloride ingress phenomenon are the weather conditions (temperature and humidity) in the surrounding environment, the chloride binding and the concrete aging (Saetta *et al*., 1993; Martın-Pérez, *et al*., 2001). On the other hand, this condition may account for the time-variant nature of humidity and temperature significantly influencing the time to corrosion initiation due to an increase in chloride concentration and activity of corrosion (Bastidas-Arteaga *et al*., 2011).

6.2.3 The Chloride Binding Capacity of Concrete

There are two forms of chloride in the concrete which is exposed to chloride solution conditions. The first form, the bound chloride, is chemically bound by the reaction of the chloride ions with the hydrates of cement compounds and physically bound by absorbing the ion on the surface of C-S-H. The impact of the binding of chloride in concrete is to decrease the quantity of mobile ions. The second form, is commonly named a free chloride, can permeate through concrete and corrode the steel bar at a specific concentration.

The results of the powder X-ray diffraction analysis show the part of chloride that penetrates concrete exposed to environmental chloride, has been bound by hydrated cement compounds and formed ($3CaO - Al_2O_3 - CaCl_2 - 10H_2O$), it is called Friedel's salt. The semi-quantitative analysis of XRD of Friedel's salt is identified as the peak position (2 Theta) for all mixes between 11.18° to11.26° in the solid phase. (Talero *et al*., 2011) reported the main peak of this component within the range of 11.16–11.34°. Figure 6.17 shows this identification of the formation of Friedel's salt in the concrete sample exposed to accelerated chloride environment.

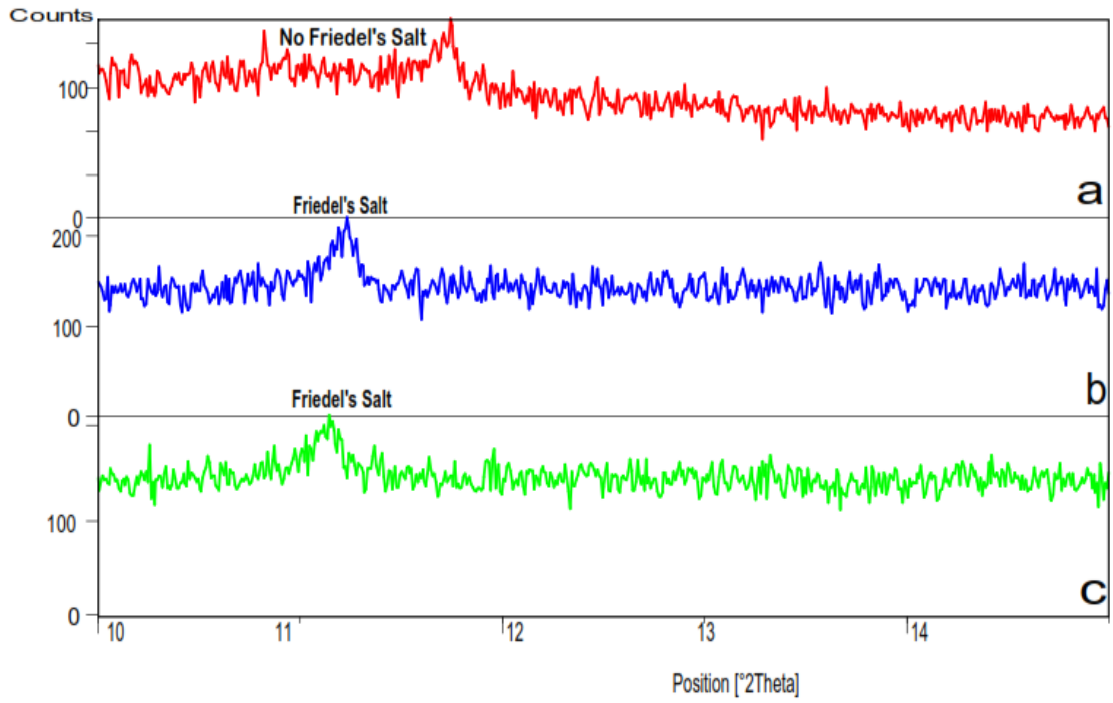

Figure 6.17: Friedel's salt was found by XRD analysis, (a) sample of M 0.4 was not exposed to a chloride environment, (b and c) samples exposed to chloride with crack width 0.05 mm and 0.2 mm respectively

The total, free and bound chlorides are presented in Tables 6.1 to 6.15 for all concrete mixes, there is a relationship between total and free chlorides which is shown in the typical graph as illustrated in Figure 6.18 and Equation 6.3. While, Equation 6.4 represents the relationship between free and bound chloride.

$$Cl_t = a_1 \, ln\,(Cl_f) + b_1 \tag{6.3}$$

$$Cl_b = \frac{(\propto_l * Cl_f)}{(1+\beta_l \, Cl_f)} \tag{6.4}$$

where:

Cl_t , Cl_f and Cl_b are total, free and bound chloride respectively in % by mass of the cementitious materials, a_1 and b_1 are constants, and $\propto_l$ and β_l are Langmuir Isotherm constants (Thomas *et al*., 2012).

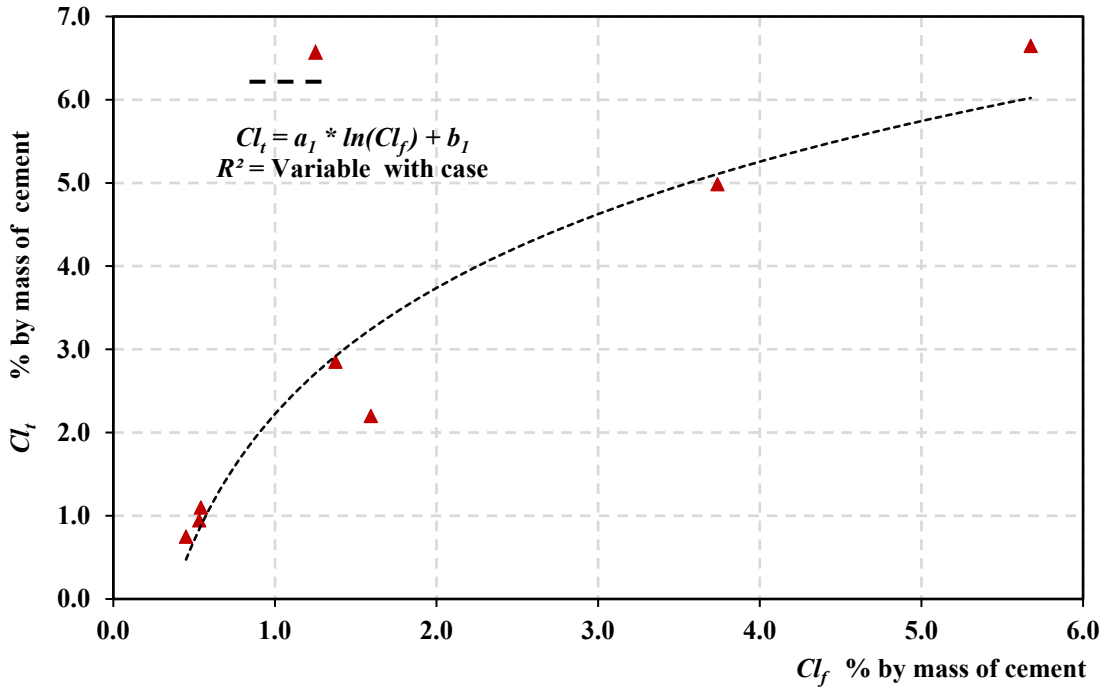

Figure 6.18: Typical graph of the relationship between total and free chloride for mixes exposed to chloride spraying

The following constants (a_1, b_1, $\propto_l$ and β_l) for all mixes used in the study are listed in Tables 6.21 to 6.23. These relationships are an important guide to Cl_t, Cl_f, and Cl_b, they can be used in the modelling of chloride penetration because as mentioned previously every form of chloride has an impact on the durability of concrete structures.

Table 6.21: Coefficients equations that connect between Cl_t , Cl_f and Cl_b according to Equations 6.3 and 6.4 for Series 1(40 ºC)

Mixes Designation	Sample with a crack width	Coefficient equation between Cl_t& Cl_f			Langmuir Isotherm coefficient for Cl_f & Cl_b	
		a_1	b_1	R^2	$\propto_l$	β_l
M 0.4	Un-cracked	0.26	1.01	0.96	27.31	25.47
	0.05-0.15 mm	0.58	1.3	0.93	2.40	1.25
	0.15-0.25 mm	0.47	1.02	0.95	1.50	2.00
	0.25-0.35 mm	0.25	0.83	0.95	1.75	1.60
M 0.5	Un-cracked	0.40	0.85	0.95	0.43	1.27
	0.05-0.15 mm	0.37	0.98	0.99	3.54	4.25
	0.15-0.25 mm	0.22	0.97	0.95	11.84	7.09
	0.25-0.35 mm	0.34	0.94	0.96	1.40	1.80
M 0.6	Un-cracked	0.27	0.73	0.95	1.17	1.6
	0.05-0.15 mm	0.36	1.03	0.98	2.93	2.31
	0.15-0.25 mm	0.53	0.89	0.95	0.72	0.83
	0.25-0.35 mm	0.42	0.92	0.95	3.97	3.32
M 0.5 +GGBS	Un-cracked	0.26	0.90	0.96	1.75	2.75
	0.05-0.15 mm	0.51	0.96	0.96	0.12	0.34
	0.15-0.25 mm	0.57	1.17	0.96	2.00	1.50
	0.25-0.35 mm	0.5	1.24	0.98	2.50	1.50
M 0.5 +PFA	Un-cracked	0.16	0.83	0.95	24.01	14.83
	0.05-0.15 mm	0.24	0.88	0.93	5.92	4.58
	0.15-0.25 mm	0.2	0.76	0.97	12.5	12.5
	0.25-0.35 mm	0.28	0.89	0.94	9.10	9.50

Table 6.22: Coefficients equations that connect between Cl_t , Cl_f and Cl_b according to Equations 6.3 and 6.4 for Series 2 (30 °C)

Mixes Designation	Sample with a crack width	Coefficient equation between Cl_t & Cl_f			Langmuir Isotherm coefficient for Cl_f & Cl_b	
		a_1	b_1	R^2	$\propto_l$	β_l
M 0.4	Un-cracked	0.21	0.66	0.97	0.30	1.20
	0.05-0.15 mm	0.37	0.91	0.81	0.40	1.00
	0.15-0.25 mm	0.60	1.04	0.90	0.30	1.25
	0.25-0.35 mm	0.75	1.15	0.94	0.25	0.90
M 0.5	Un-cracked	0.16	0.65	0.74	0.35	1.00
	0.05-0.15 mm	0.31	0.83	0.92	0.40	1.20
	0.15-0.25 mm	0.26	0.80	0.88	0.35	1.10
	0.25-0.35 mm	0.30	0.95	0.94	1.00	1.00
M 0.6	Un-cracked	0.23	0.72	0.95	0.60	1.00
	0.05-0.15 mm	0.25	0.78	0.89	0.45	1.20
	0.15-0.25 mm	0.42	0.99	0.92	0.55	0.80
	0.25-0.35 mm	0.49	0.98	0.96	0.20	1.10
M 0.5 +GGBS	Un-cracked	0.24	0.90	0.84	0.60	1.20
	0.05-0.15 mm	0.23	0.80	0.65	0.40	1.20
	0.15-0.25 mm	0.30	1.01	0.94	0.95	1.50
	0.25-0.35 mm	0.25	1.01	0.95	1.80	1.50
M 0.5 +PFA	Un-cracked	0.19	0.75	0.97	1.00	1.50
	0.05-0.15 mm	0.21	0.74	0.91	0.65	1.25
	0.15-0.25 mm	0.19	0.76	0.95	0.65	1.25
	0.25-0.35 mm	0.42	0.88	0.95	0.10	0.70

Table 6.23: Coefficients equations that connect between Cl_t , Cl_f and Cl_b according to Equations 6.3 and 6.4 for Series 3 (20 ºC)

Mixes Designation	Sample with a crack width	Coefficient equation between Cl_t& Cl_f			Langmuir Isotherm coefficient for Cl_f & Cl_b	
		a_1	b_1	R^2	$\propto_l$	β_l
M 0.4	Un-cracked	0.08	0.40	0.84	0.20	0.20
	0.05-0.15 mm	0.17	0.53	0.82	0.15	0.20
	0.15-0.25 mm	0.21	0.56	0.93	0.15	0.15
	0.25-0.35 mm	0.16	0.47	0.96	0.90	0.10
M 0.5	Un-cracked	0.15	0.51	0.91	0.90	0.10
	0.05-0.15 mm	0.21	0.57	0.93	0.95	0.10
	0.15-0.25 mm	0.21	0.57	0.90	0.85	0.20
	0.25-0.35 mm	0.25	0.61	0.96	0.90	0.10
M 0.6	Un-cracked	0.20	0.51	0.95	0.85	0.15
	0.05-0.15 mm	0.27	0.54	0.94	0.95	0.10
	0.15-0.25 mm	0.43	0.72	0.91	0.85	0.25
	0.25-0.35 mm	0.34	0.67	0.76	0.70	0.10
M 0.5 +GGBS	Un-cracked	0.15	0.59	0.86	0.50	0.10
	0.05-0.15 mm	0.16	0.50	0.89	0.85	0.05
	0.15-0.25 mm	0.10	0.49	0.60	0.45	0.15
	0.25-0.35 mm	0.20	0.62	0.91	0.65	0.10
M 0.5 +PFA	Un-cracked	0.07	0.37	0.87	0.55	0.05
	0.05-0.15 mm	0.13	0.47	0.96	0.70	0.10
	0.15-0.25 mm	0.11	0.45	0.90	0.65	0.10
	0.25-0.35 mm	0.13	0.46	0.96	0.90	0.10

For Series 1, Equation 6.5 was based on non-linear regression of the results of total chloride and free chloride which are reported in Tables 6.1- 6.15. The curve fitting of Equation 6.5 and the results of free and bound chloride were employed to obtain

Equation 6.6. These Equations with their constants can be used in modelling and simulation of chloride penetration for concrete mixes used in the current study:

$$Cl_t = 0.36\, ln(Cl_f) + 0.96 \qquad 0.93 \leq R^2 \leq 0.99 \qquad (6.5)$$

$$Cl_b = \frac{(5.84 * Cl_f)}{(1+5.01\, Cl_f)} \qquad (6.6)$$

The diffusion of chloride procedure via concrete exposed to a chloride solution clearly involved the binding of chloride impact the duration of the test period. The bound chloride increases with increasing the free chloride in pore solution voids in concrete structures (Song, 2014). The results of the chloride binding capacity of the samples incorporating the supplementary cementitious materials, GGBS and PFA increased compared with M 0.5. The main reason for the chloride binding capacity in these is the high alumina content in GGBS and PFA, resulting in the formation of more Friedel's salt (Mohammed and Hamada, 2003; Yuan *et al.*, 2009; Ukpata *et al.*, 2018) as shown in Figure 6.15. Where, the alumina content in GGBS and PFA was 13.2% and 23% respectively, while the alumina content in OPC is 4.3% as shown in Tables 3.7, 3.9 and 3.11.

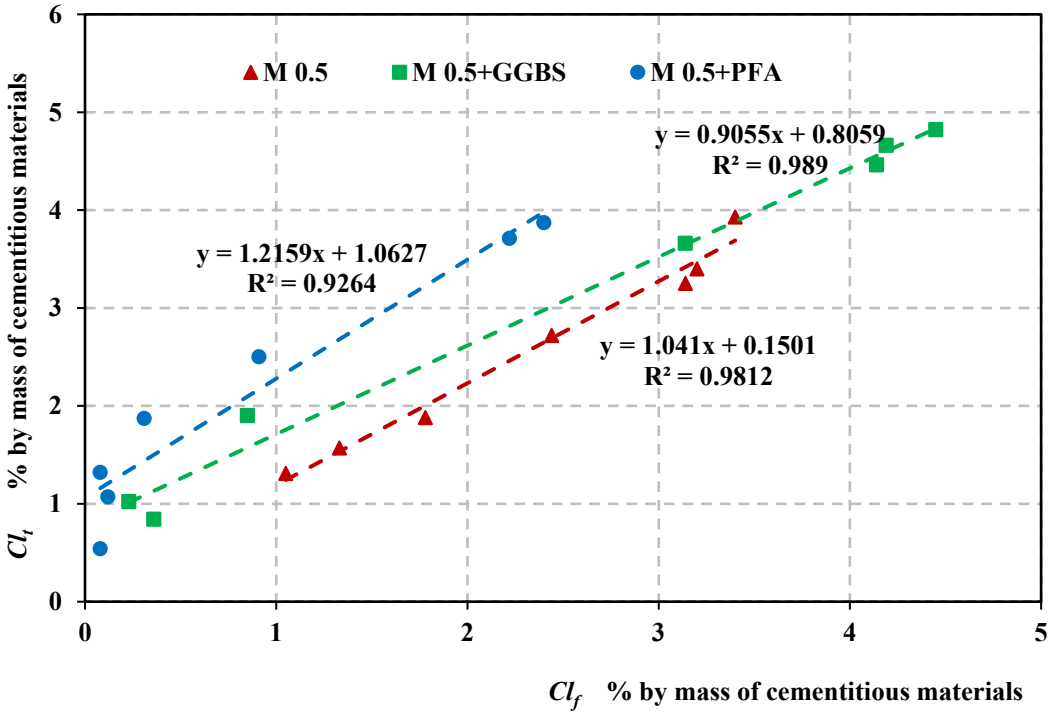

Figure 6.19: Effect of the supplementary cementitious materials (GGBS and PFA) on bound chloride

6.3 The Effect of Carbonation on Chloride Penetration

One series of concrete prisms has been used to investigate the effect of exposure to a CO_2 environment (carbonation) on chloride concentration and penetration by exposing this series to an accelerated CO_2 environment of 5%, 65% relative humidity and temperature of 25°C for 5 weeks. These specimens were exposed to three sequences, chloride spraying solution environment with 5% NaCl (chloride fog) then they were exposed to a CO_2 environment (for carbonated samples) beyond that the samples were backed to chloride fog. The specimens were split longitudinally and the chloride penetration depth, d_{cl^-} was measured using silver nitrate ($AgNO_3$) colorimetric method, and chloride concentration, total and free by titration of chloride. The results of these examinations are listed in Tables 6.24 through to 6.28.

6.3.1 The Effect of Carbonation on Chloride Penetration in Concrete

The results exhibit higher chloride penetration for samples exposed to a CO_2 environment for all the w/cm ratios and crack widths when compared with specimens from Series 3 (un-carbonated) as presented in Figure 6.20. Key observations from these results are:

The impact of carbonation on chloride penetration was obvious in un-cracked samples M 0.4 and M 0.5, M 0.5+GGBS and M 0.5+PFA. While, in the concrete samples M 0.6, the effect of w/cm (or porosity) was higher than the impact of carbonation on chloride penetration depth, d_{cl^-}. The influence of carbonation on d_{cl^-} can be summarized as percentage increment for different w/cm ratios and crack widths as illustrated in Table 6.29.

The results also depict an increase in chloride penetration with the increase in w/cm ratio for different sets of concrete samples (i.e. with carbonation), particularly for the un-cracked samples. This can be explained by the fact that the w/cm ratio affects the volume of internal voids or porosity in the concrete that in turn affect the chloride ions transport mechanisms in concrete, i.e. diffusion, permeation, sorption and permeability (Basheer *et al*., 2001).

Table 6.24: The total, free and bound chloride with different depths for mix samples M 0.4 were exposed to chloride spraying for 15 weeks at 20 °C and 5 weeks CO_2 Environment condition

Sample	Chloride Concentration by mass of cementitious materials (%) for samples											
	Un-cracked			Crack width 0.05-0.15 mm			Crack width 0.15-0.25 mm			Crack width 0.25-0.35 mm		
Depth mm	Total Cl^-	Free Cl^-	Bound Cl^-	Total Cl^-	Free Cl^-	Bound Cl^-	Total Cl^-	Free Cl^-	Bound Cl^-	Total Cl^-	Free Cl^-	Bound Cl^-
0 - 6	0.94	0.89	0.05	1.44	1.38	0.06	1.44	1.22	0.22	1.29	1.18	0.11
6 -12	1.54	1.05	0.49	1.59	0.85	0.74	1.59	1.31	0.28	1.66	1.16	0.50
12 - 18	1.09	0.65	0.44	1.14	0.58	0.56	1.21	0.99	0.22	1.29	0.75	0.54
18 - 24	0.79	0.31	0.48	1.07	0.53	0.54	1.07	0.91	0.16	1.21	0.94	0.27
24 - 30	0.49	0.23	0.26	0.54	0.36	0.18	0.54	0.51	0.03	1.14	0.28	0.86
30 - 36	0.35	0.04	0.31	0.40	0.18	0.22	0.40	0.39	0.01	0.62	0.21	0.41
36 - 42	0.20	0.03	0.17	0.25	0.13	0.12	0.25	0.24	0.01	0.47	0.09	0.38
Penetration depth of chloride measuring by $AgNO_3$ (mm)	33			51			62			70		

Table 6.25: The total, free and bound chloride with different depths for mix samples M 0.5 were exposed to chloride spraying for 15 weeks at 20 °C and 5 weeks CO_2 Environment condition

Sample	Chloride Concentration by mass of cementitious materials (%) for samples											
	Un-cracked			Crack width 0.05-0.15 mm			Crack width 0.15-0.25 mm			Crack width 0.25-0.35 mm		
Depth mm	Total Cl^-	Free Cl^-	Bound Cl^-	Total Cl^-	Free Cl^-	Bound Cl^-	Total Cl^-	Free Cl^-	Bound Cl^-	Total Cl^-	Free Cl^-	Bound Cl^-
0 - 6	1.18	1.11	0.06	1.93	1.79	0.14	3.04	1.10	1.94	3.04	1.44	1.60
6 -12	1.55	1.29	0.26	1.74	1.61	0.13	2.85	1.48	1.38	2.85	1.79	1.06
12 - 18	1.36	1.24	0.13	1.74	1.59	0.15	2.67	1.69	0.98	2.67	1.25	1.41
18 - 24	0.99	0.83	0.16	1.55	1.46	0.09	1.93	1.74	0.19	2.48	1.39	1.09
24 - 30	0.80	0.45	0.35	0.99	0.96	0.03	1.36	1.16	0.20	2.30	2.16	0.14
30 - 36	0.44	0.43	0.01	0.80	0.78	0.03	1.18	0.69	0.49	1.36	1.13	0.24
36 - 42	0.44	0.39	0.05	0.61	0.50	0.11	0.61	0.60	0.01	1.18	1.06	0.11
Penetration depth of chloride measuring by $AgNO_3$ (mm)	37			58			60			60		

Table 6.26: The total, free and bound chloride with different depths for mix samples M 0.6 were exposed to chloride spraying for 15 weeks at 20 °C and 5 weeks CO_2 Environment condition

Sample	Chloride Concentration by mass of cementitious materials (%) for samples											
	Un-cracked			Crack width 0.05-0.15 mm			Crack width 0.15-0.25 mm			Crack width 0.25-0.35 mm		
Depth mm	Total Cl^-	Free Cl^-	Bound Cl^-	Total Cl^-	Free Cl^-	Bound Cl^-	Total Cl^-	Free Cl^-	Bound Cl^-	Total Cl^-	Free Cl^-	Bound Cl^-
0 - 6	2.90	2.11	0.79	2.48	1.99	0.48	2.48	1.32	1.16	2.90	1.83	1.07
6 -12	2.48	1.76	0.72	2.36	1.95	0.41	2.36	0.25	2.11	3.12	1.25	1.88
12 - 18	2.04	1.47	0.57	2.04	1.73	0.31	2.26	1.45	0.81	2.90	2.17	0.73
18 - 24	1.82	1.70	0.12	2.04	1.63	0.41	2.16	1.14	1.01	2.70	2.32	0.38
24 - 30	1.60	1.29	0.31	2.04	1.47	0.57	2.04	2.02	0.01	2.04	1.63	0.41
30 - 36	1.38	1.20	0.18	1.60	1.14	0.45	1.82	0.97	0.85	1.82	1.55	0.26
36 - 42	2.90	2.11	0.79	2.48	1.99	0.48	2.48	1.32	1.16	2.90	1.83	1.07
Penetration depth of chloride measuring by $AgNO_3$ (mm)	35			60			60			60		

Table 6.27: The total, free and bound chloride with different depths for mix samples M 0.5 + GGBS were exposed to chloride spraying for 15 weeks at 20 °C and 5 weeks CO_2 Environment condition

Sample	Chloride Concentration by mass of cementitious materials (%) for samples											
	Un-cracked			Crack width 0.05-0.15 mm			Crack width 0.15-0.25 mm			Crack width 0.25-0.35 mm		
Depth mm	Total Cl^-	Free Cl^-	Bound Cl^-	Total Cl^-	Free Cl^-	Bound Cl^-	Total Cl^-	Free Cl^-	Bound Cl^-	Total Cl^-	Free Cl^-	Bound Cl^-
0 - 6	1.34	1.14	0.20	1.24	1.19	0.05	1.61	0.98	0.64	1.61	1.39	0.23
6 -12	1.15	0.95	0.20	1.34	1.28	0.06	1.43	1.16	0.26	1.51	1.23	0.29
12 - 18	0.86	0.80	0.06	0.96	0.85	0.11	1.15	1.05	0.10	1.34	0.78	0.56
18 - 24	0.59	0.58	0.01	0.86	0.78	0.09	0.96	0.89	0.08	1.15	0.61	0.54
24 - 30	0.50	0.39	0.11	0.50	0.43	0.08	0.68	0.43	0.25	0.96	0.43	0.54
30 - 36	0.44	0.35	0.09	0.44	0.30	0.14	0.44	0.38	0.06	0.86	0.24	0.63
36 - 42	0.44	0.25	0.19	0.44	0.43	0.01	0.44	0.25	0.19	0.68	0.30	0.38
Penetration depth of chloride measuring by $AgNO_3$ (mm)	23			38			48			63		

Table 6.28: The total, free and bound chloride with different depths for mix samples M 0.5+PFA were exposed to chloride spraying for 15 weeks at 20 °C and 5 weeks CO_2 Environment condition

Sample	Chloride Concentration by mass of cementitious materials (%) for samples											
	Un-cracked			Crack width 0.05-0.15 mm			Crack width 0.15-0.25 mm			Crack width 0.25-0.35 mm		
Depth mm	Total Cl^-	Free Cl^-	Bound Cl^-	Total Cl^-	Free Cl^-	Bound Cl^-	Total Cl^-	Free Cl^-	Bound Cl^-	Total Cl^-	Free Cl^-	Bound Cl^-
0 - 6	1.55	1.38	0.18	2.11	1.99	0.13	1.74	1.01	0.73	2.30	1.35	0.95
6 -12	1.74	1.05	0.69	1.93	1.91	0.01	1.93	0.75	1.18	2.11	0.73	1.39
12 - 18	0.99	0.91	0.08	1.55	1.33	0.23	1.74	0.79	0.95	2.01	1.14	0.88
18 - 24	0.80	0.76	0.04	1.36	1.14	0.23	1.55	1.41	0.14	1.55	0.91	0.64
24 - 30	0.61	0.11	0.50	0.99	0.85	0.14	1.18	0.39	0.79	1.18	0.65	0.53
30 - 36	0.44	0.06	0.38	0.61	0.38	0.24	0.61	0.51	0.10	0.80	0.41	0.39
36 - 42	0.44	0.08	0.36	0.44	0.19	0.25	0.44	0.25	0.19	0.61	0.59	0.03
Penetration depth of chloride measuring by $AgNO_3$ (mm)	19			49			60			62		

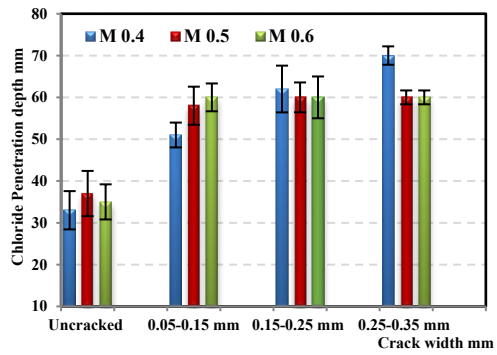

a:d_{cl}- for carbonated

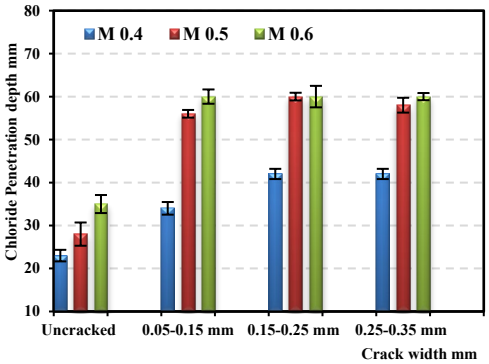

b: d_{cl}- for Un-carbonated- Series 3

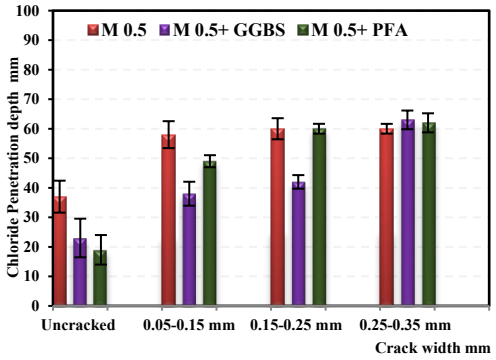

c: d_{cl}- for carbonated

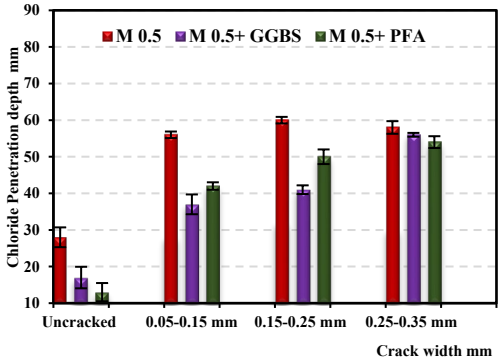

d: d_{cl}- for Un-**Carbonated sample – Series 3**

Figure 6.20: Effect of w/cm ratio and supplementary cementitious materials on chloride penetration(d_{cl}^-) for un-carbonated and carbonated samples

Table 6.29: Increased percentage in chloride penetration depth for the carbonated sample with respect to un-carbonated for different w/cm ratio and type of SCMs

Sample	Increase percentage in d_{cl}^- for crack width (%)			
	Un-cracked	0.05 -0.15 mm	0.15-0.25 mm	0.25-0.35 mm
M 0.4	43	50	48	67
M 0.5	32	4	0	3
M 0.6	0	0	0	0
M 0.5+GGBS	35	3	2	13
M 0.5+PFA	46	17	20	15

On the other hand, the chloride penetration depth increases with the crack widths for all mixes until a threshold crack width is reached, which is estimated from Figure 6.20 to be around 0.15 mm. The crack width and depth affect the transport

mechanism of chloride ions into the crack opening, since wider cracks may allow the chloride solution to penetrate into the cracks (Audenaert *et al*., 2009).

The $AgNO_3$ solution spray reacts with chloride ions to form a mixture of silver oxide and silver chloride that precipitates on the concrete surface and changes color forming a boundary corresponding to the chloride penetration depth within the concrete specimen. It means the increase of the boundaries of colored areas is due to the increase of penetration of chloride ions into concrete due to the influence of carbonation and w/cm ratio as shown in Figure 6.21.

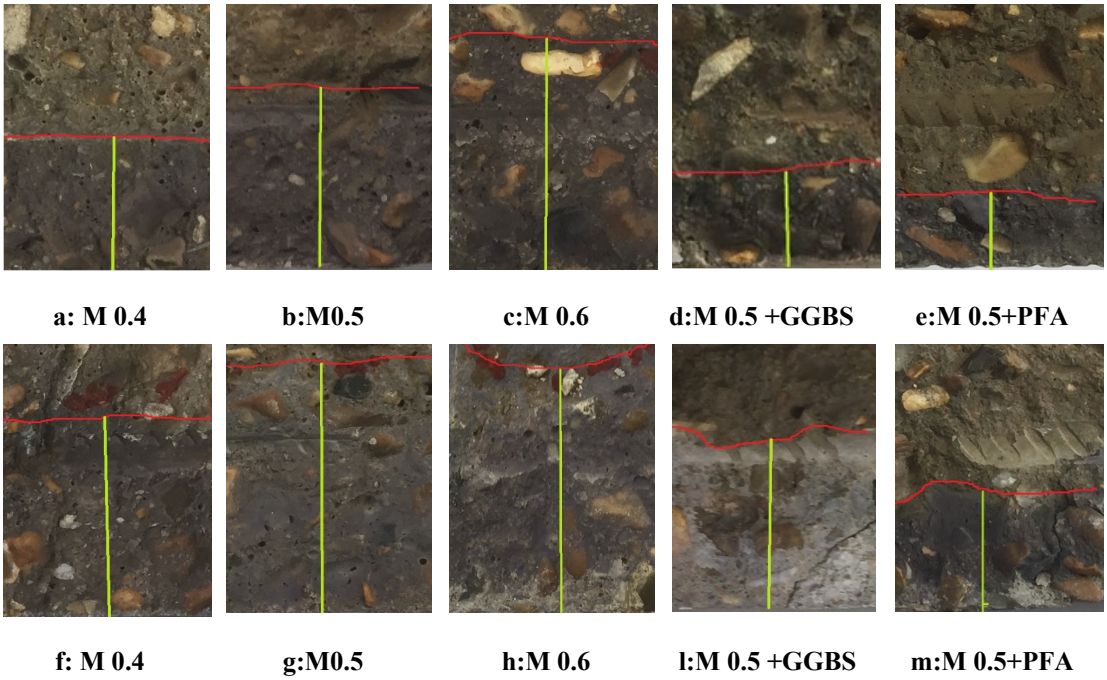

Figure 6.21: The effect of carbonation and w/cm ratio on d_{cl}^- for un-cracked samples (a, b, c d, and e) and carbonated samples (f,g,h,l, and m)

The main reason for the increase in the penetration of chloride due to carbonation is due to the mineral changes in concrete. This can be attributed to the fact that the carbonation reduces the pH of the pore water in concrete as a result of consumption of the main contributor to alkalinity in concrete, $Ca(OH)_2$ and forming calcium carbonate (Dyer, 2014; Vanoutrive *et al*., 2019). The carbonation products are a significant factor in the liberation of bound chlorides (calcium chloroaluminate) in cement mortar in concrete samples (Wan *et al*., 2013).

6.3.2 The Effect of Carbonation on Chloride Concentration Profile

The total chloride concentrations for all mixes were experimentally examined according to BS EN 14629: 2007 using the chloride titration method for samples exposed to a cycle of chloride -CO_2 -chloride environment. In this study, two series of exposure type have been investigated, carbonated and un-carbonated; they are plotted separately in Figure 6.22, illustrating the changes of acid-soluble chloride content with depth within the accelerated process for all concrete mixes, both carbonated and un-carbonated.

The results from mixes M 0.4, M 0.5 and M 0.6 showed there is a slight change in chloride concentration with carbonated samples and the difference in chloride concentration (at internal layers) in carbonated samples were higher than in un-carbonated. According to this variation in chloride concentration, the D_a and C_s values for the carbonated sample were higher than the values in the un-carbonated sample for sound and cracked samples as shown in Table 6.30 and Figure 6.23. The influence of CO_2 environment exposure on chloride diffusion coefficient and surface concentration are presented in Figure 6.23.

Table 6.30: Summary of Apparent diffusion coefficient (D_a)and surface chloride concentration(C_s) at 20 °C (carbonated)

Sample	Un-cracked		0.05-0.15 mm		0.15-0.25 mm		0.25-0.35 mm	
	D_a*	C_s**	D_a*	C_s**	D_a*	C_s**	D_a*	C_s**
M 0.4	14	2.72	14	2.93	17	3.35	18	3.35
M 0.5	15	3.93	18	4.08	22	4.71	28	4.97
M 0.6	22	4.6	24	5.21	24	5.21	25	5.83
M 0.5+ GGBS	12	2.62	14	2.88	14	3.14	16	3.93
M 0.5+ PFA	10	3.14	14	3.93	16	4.19	18	4.45

* D_a in (m^2/sec)

** C_s in % by mass of cementitious materials

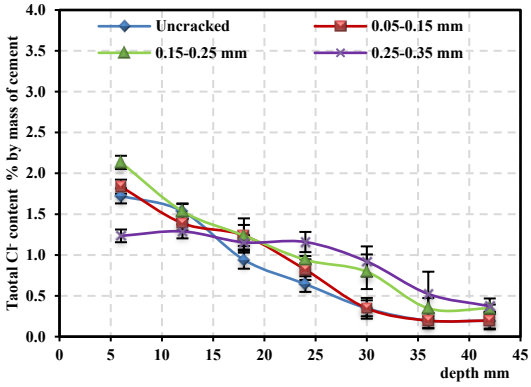

a: M 0.4-un-carbonated

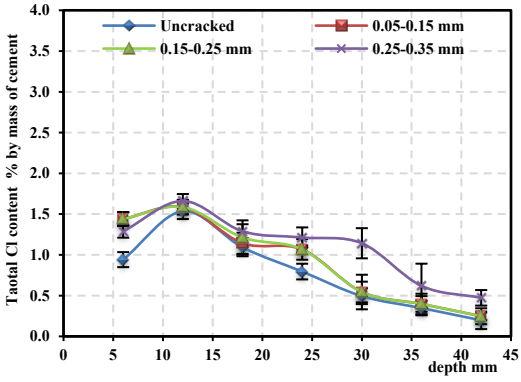

a-1: M 0.4 –carbonated

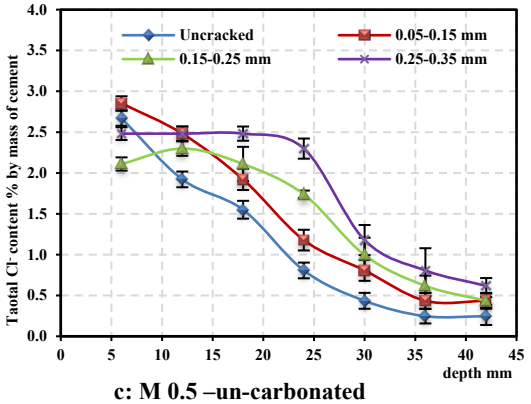

c: M 0.5 –un-carbonated

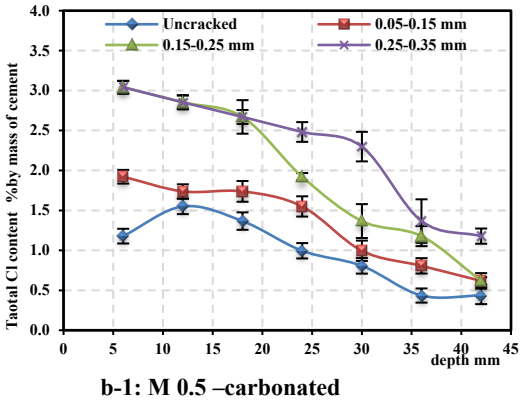

b-1: M 0.5 –carbonated

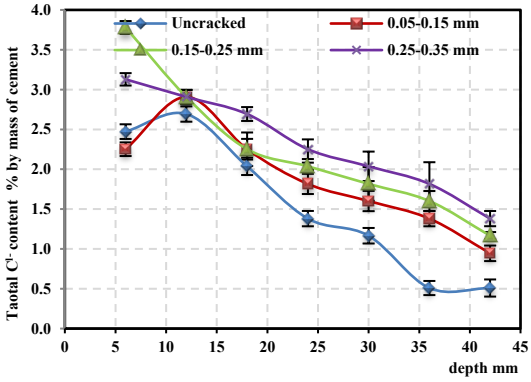

c: M 0.6 –un-carbonated

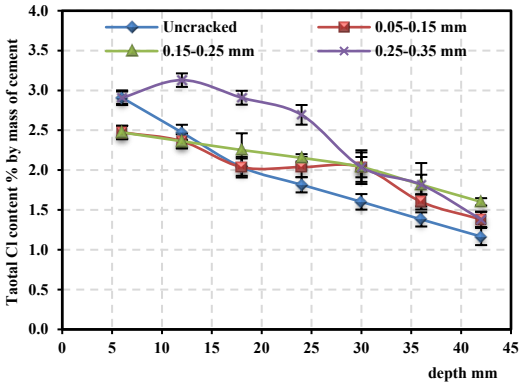

c-1: M 0.6 –carbonated

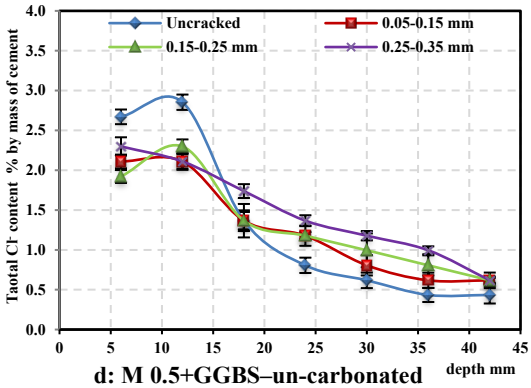

d: M 0.5+GGBS–un-carbonated

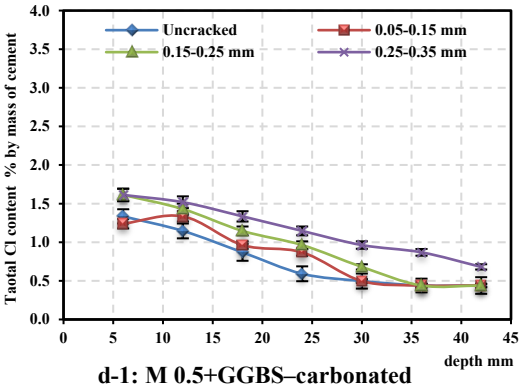

d-1: M 0.5+GGBS–carbonated

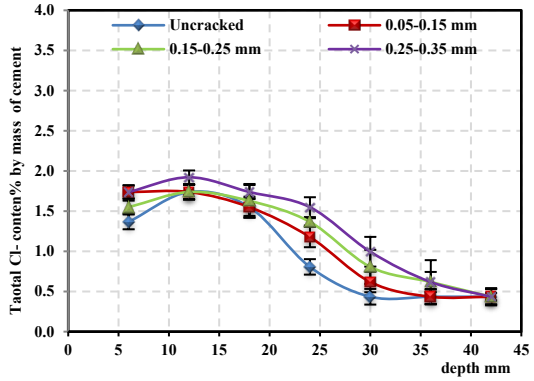

e: M 0.5+PFA–un-carbonated

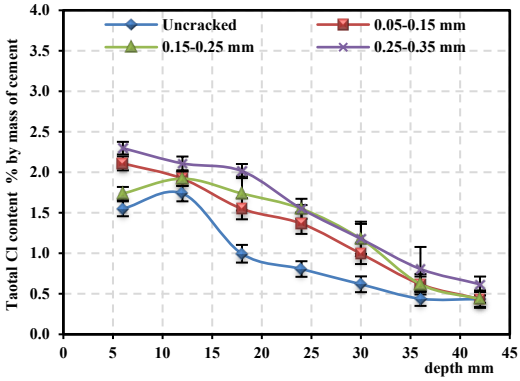

e-1: M 0.5+PFA- carbonated

Figure 6.22: Total chloride concentration profile of mixes exposed to chloride-CO_2 - chloride

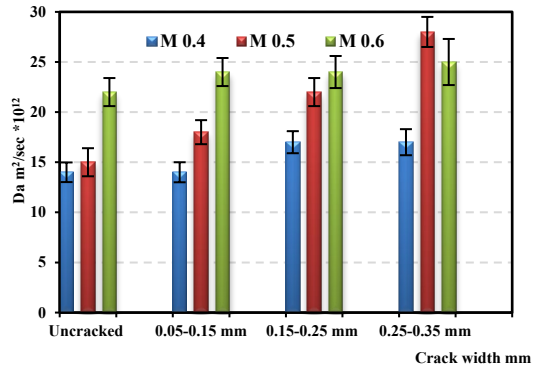

a-1: D_a carbonated

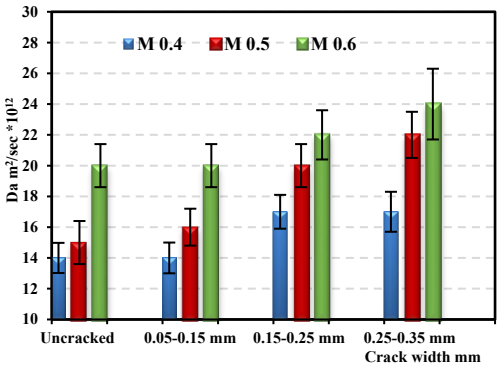

a: D_a un-carbonated -Series 3

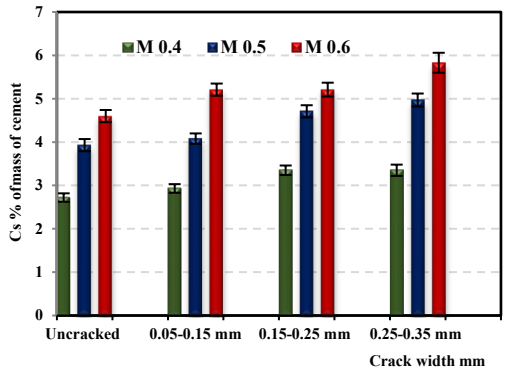

b-1: C_s carbonated

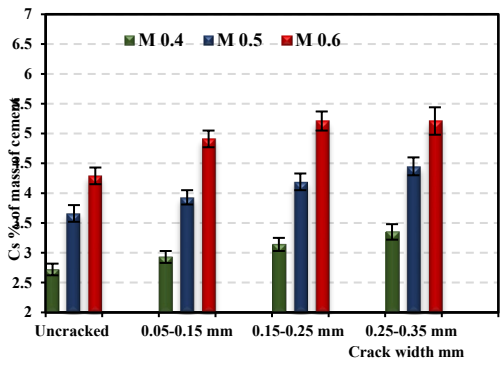

b: C_s un-carbonated-Series 3

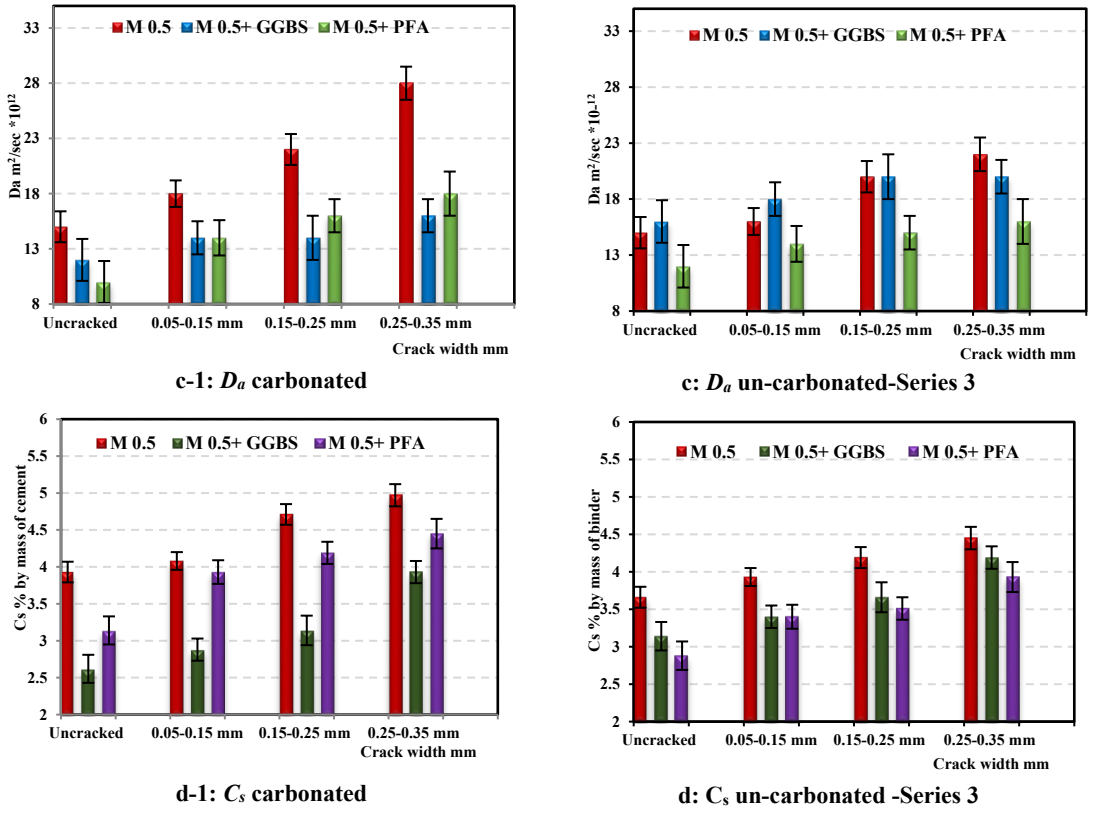

Figure 6.23: Effect of carbonation on D_a and C_s for concrete mixes used

Furthermore, the performance of the mixes containing SCMs was complicated and varied with mix M 0.5 regarding the influence of carbonation on the chloride concentration. However, the depth of carbonation of M 0.5+GGBS was higher than M 0.5 due to carbon dioxide ingress and the formation of carbonation as shown in Figure 6.24, the chloride concentration (chloride diffusion and surface concentration) was less than with un-carbonated samples (Figure 6.23). The main reason for this reduction is due to a decrease in the porosity and closing of continues pores due to carbonation and later hydration of GGBS that leads to a decrease in the penetration of chloride in concrete (Dyer, 2014).

Carbonation leads to an observed change in chloride concentration (Figures 6.22-6.23). For all mixes, the contents of chloride in the concrete samples (M 0.4, M 0.5 and M0.6) exposed to accelerated carbonation are higher than those subjected to the natural atmosphere. Due to the carbonation, a decrease of the total porosity of hardened cement products and the content of dissolved water that enters pores during saturation is one of the reasons for the increase of chloride content in the concrete sample after carbonation. Nevertheless, in the carbonated state some compounds become unstable and

then the bound chloride is freed back into the pore solution. On the other hand, carbonation is a significant factor in reducing the pH and working to liberate the bound chlorides in cement and encourage the increase of chloride penetration in the concrete samples which leads to an increase in the chloride concentration (Wan *et al*., 2013).

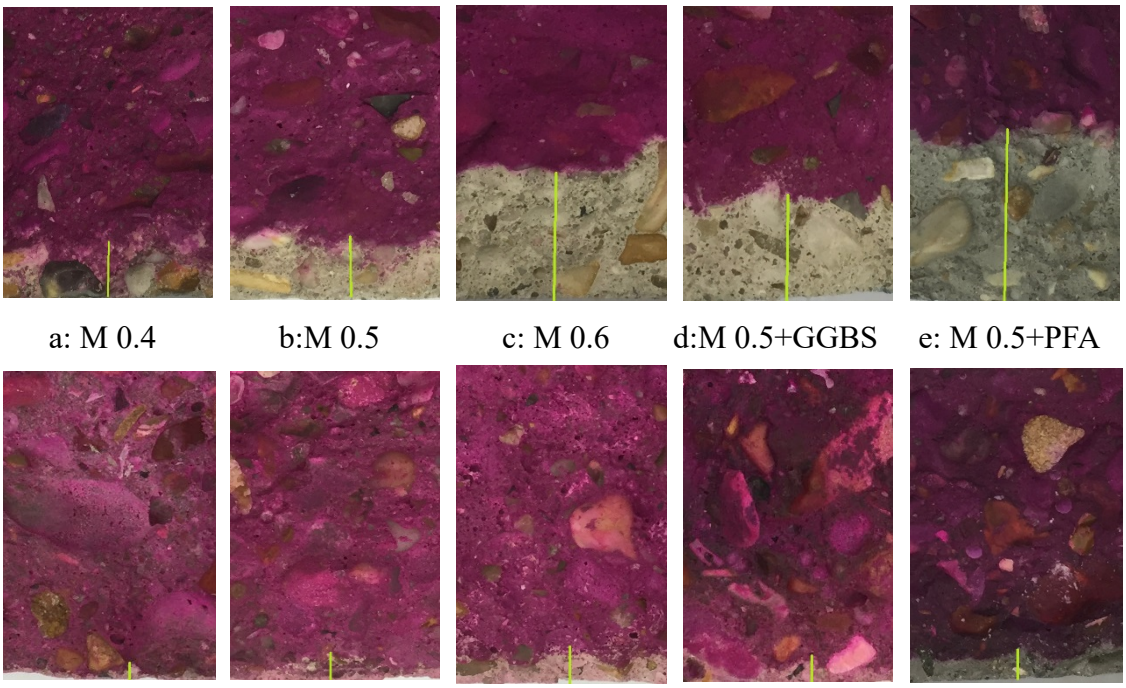

a: M 0.4 b:M 0.5 c: M 0.6 d:M 0.5+GGBS e: M 0.5+PFA

f: M 0.4 g: M 0.5 h: M 0.6 l:M 0.5+GGBS m: M 0.5+PFA

Figure 6.24: DoC in the concrete sample exposed to (5% CO_2, 65% RH and 25 °C) for the carbonated sample (a, b, c, d, and e) and un-carbonated samples (f, g, h, l, and m) (Yellow line represent the depth of carbonation)

6.4 Corrosion Tests Results

Reinforced concrete prisms were moist cured and dried in a laboratory environment before being exposed to cyclic wetting with a chloride solution spray, air purge and drying period as described in chapter three. The exposure of reinforced concrete prisms to the chloride environment-induced an electrochemical reaction between the reinforcement and its environment. This reaction can be measured using common techniques such as half-cell potential and linear polarization resistance, LPR, in order to determine the state of corrosion of the reinforcement.

6.4.1 Half-Cell Potential Results

Electrical potential for corrosion of reinforced concrete samples was measured using the standard half-cell technique defined in ASTM C876: 2015. Potential of the bars was determined with respect to a saturated calomel electrode (SCE), immersed in the 5% NaCl solution as shown in Figure 3.29. Half-cell potentials results for reinforced concrete prisms at different age of exposure, are illustrated in Figures 6.25-6.27.

The results showed that the potentials of steel reinforcement were influenced by: (i): Progress in the age as the electrode potential of steel increased with the progress of the exposure age to chloride solution. In the discussion of results, the ASTM C 876: 2015 criteria (for a saturated calomel electrode-SCE) was considered, which are described in Table 3.14 and it is useful for the interpretation of these results (Bouteiller *et al*., 2012). The results showed the most samples had potential exceeded (in the negative) the passive condition of the above criteria after 20 days of exposure because potentials were more positive than -126 mV SCE. The potential of electrode dropped than -126 mV (intermediate corrosion risk). Consequently, the results showed the specimens were increased the potential more negative than -276 mV SCE, E_{corr}. (there is a greater than 90% probability that corrosion is occurring).A sharp potential decrease was observed after week 60 at least (for example Series 2 and 3 in samples (M 0.5, M 0.6 and M 0.5+ PFA), E_{corr} decrease happened after 70 days, for Series 1, the samples (M 0.5, M 0.6 and M 0.5+GGBS), the E_{corr} drop occurred after 60 days). On the other hand, half-cell potential values for samples M 0.4 (all series) remained in more positive than -126 mV SCE, there is a greater than 90% probability that no corrosion is occurring.

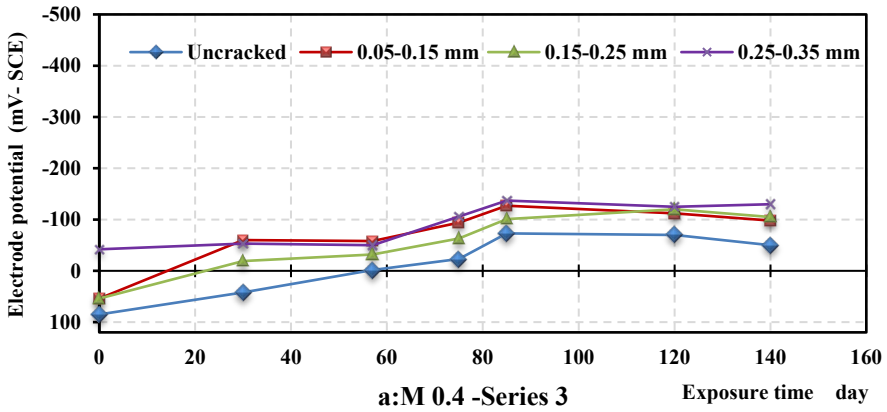

a:M 0.4 -Series 3

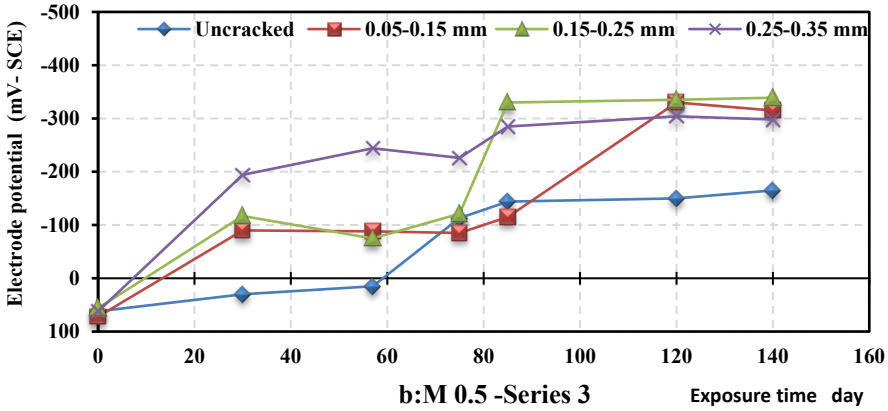

b:M 0.5 -Series 3

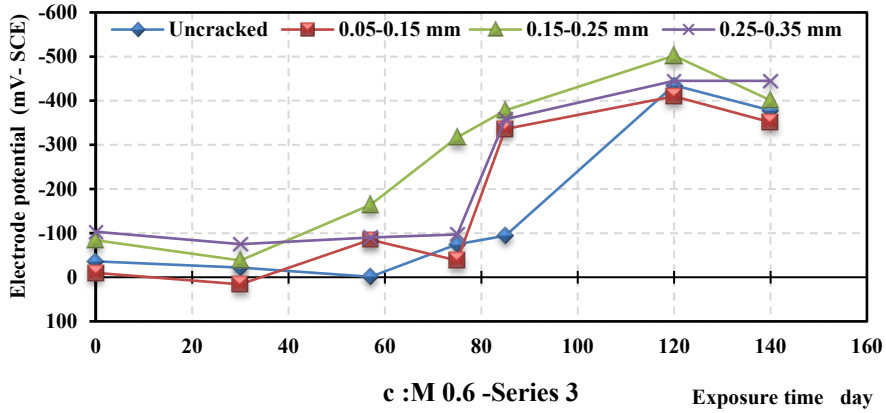

c :M 0.6 -Series 3

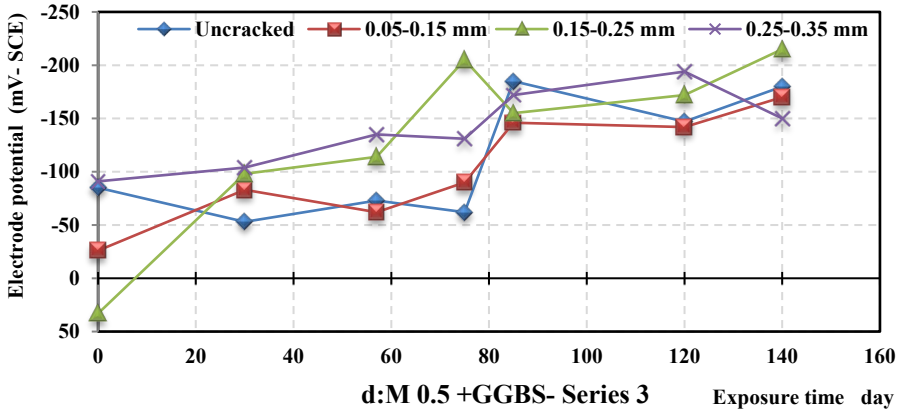

d:M 0.5 +GGBS- Series 3

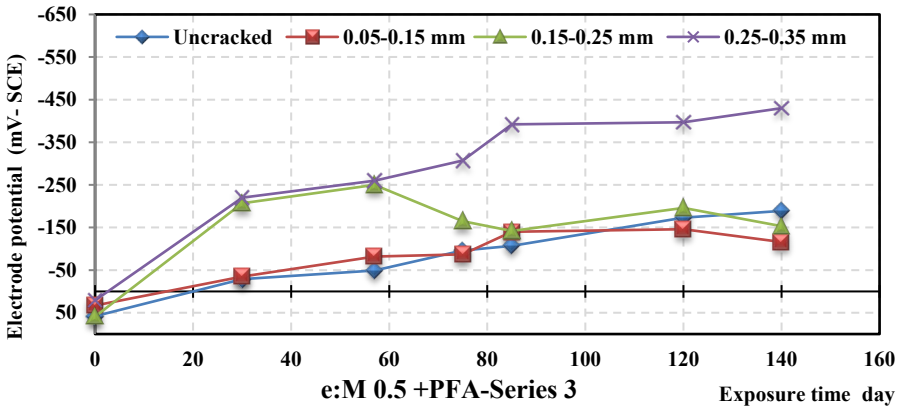

Figure 6.25: Effect of crack width on half-cell potential in reinforced concrete prism at temperature 20 °C (Series 3-uncarbonated)

(ii) w/cm ratio of concrete as half-cell potential generally increased by increasing the w/cm of concrete around the steel reinforcement. The results also exhibited the increase in w/cm ratio of reinforced concrete accelerating the potential drop in reinforcement and leading to an increase of the probability of corrosion. As mentioned previously, the potential values almost samples of mix M 0.4 (w/cm= 0.4) remained in the range of uncertain corrosion due to chlorides concentration did not reach the sufficient concentration to induce the corrosion in the rebar as shown in Tables 6.1, 6.6 and 6.11. Conversely, for steel bar in the more porous concrete specimens (M 0.6-un-cracked) a significant decrease in the potential drop was noticed with time. After the many wetting-drying cycles, the potential values of the specimens more positive than -126 mV were in the range of uncertain corrosion. A drastic potential drop was observed after week 10 for specimen's series 3 and after week 8 for specimen's Series 1 more negative than -276 mV, E_{corr}, leading to values that belonged to the 90% confidence interval for corrosion and that were attributed to the penetration of chlorides at the rebar level (in accordance with the chloride determinations at Table 6.1-6.15). Table 6.31 is listed all the cases have E_{corr} more negative than -276 and the time of arrival this potential drop.

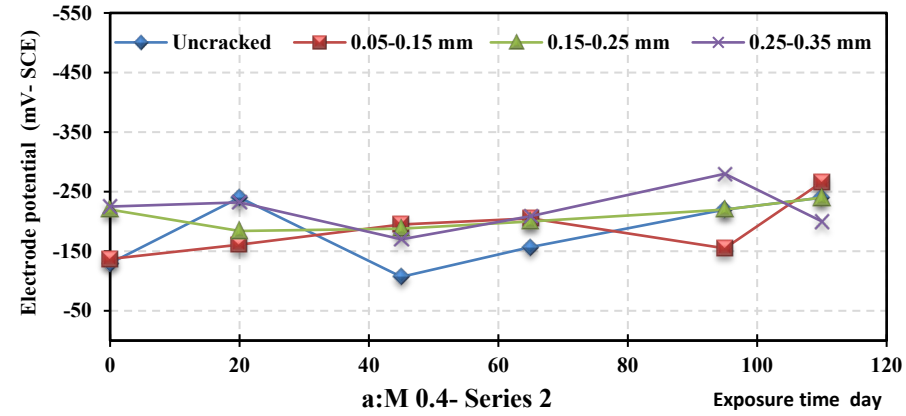

a:M 0.4- Series 2

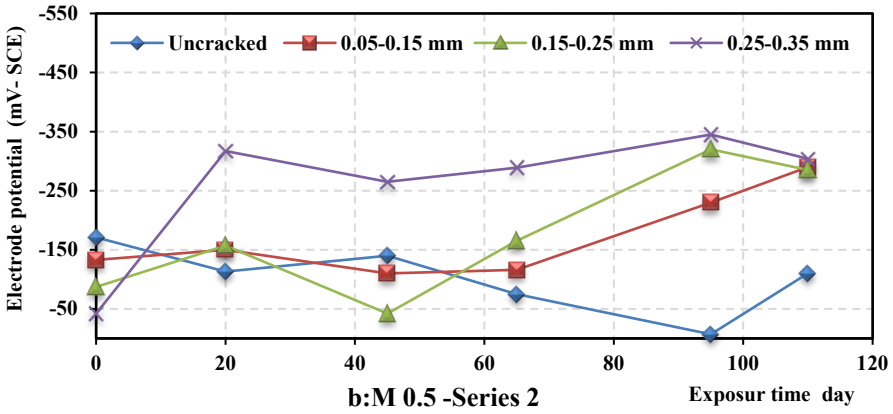

b:M 0.5 -Series 2

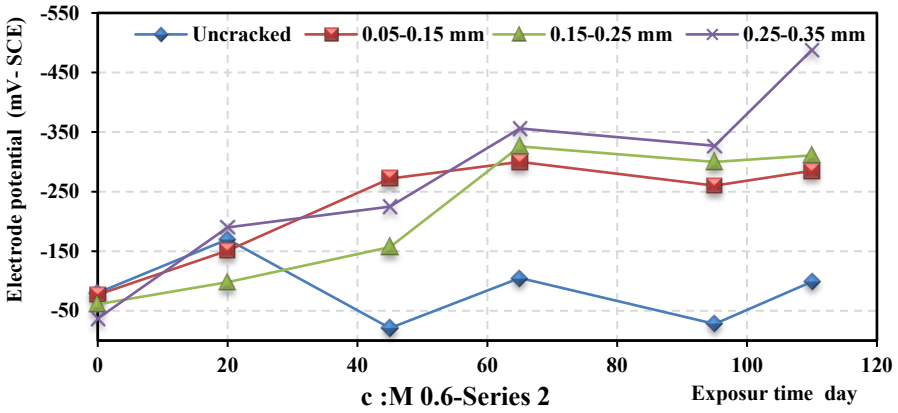

c :M 0.6-Series 2

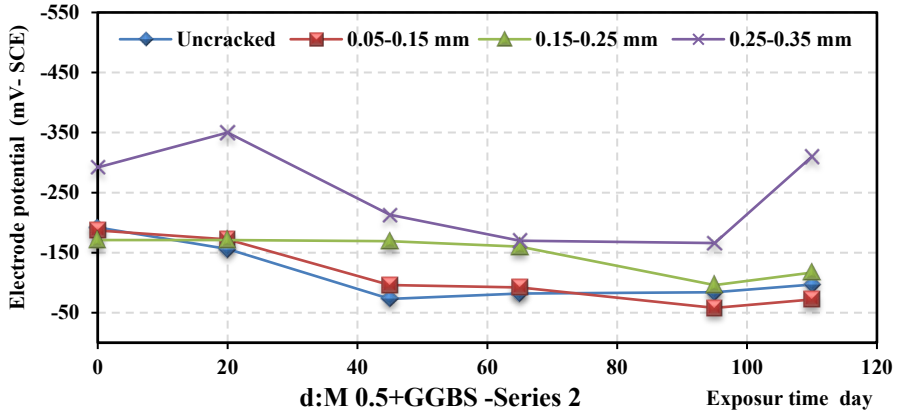

d:M 0.5+GGBS -Series 2

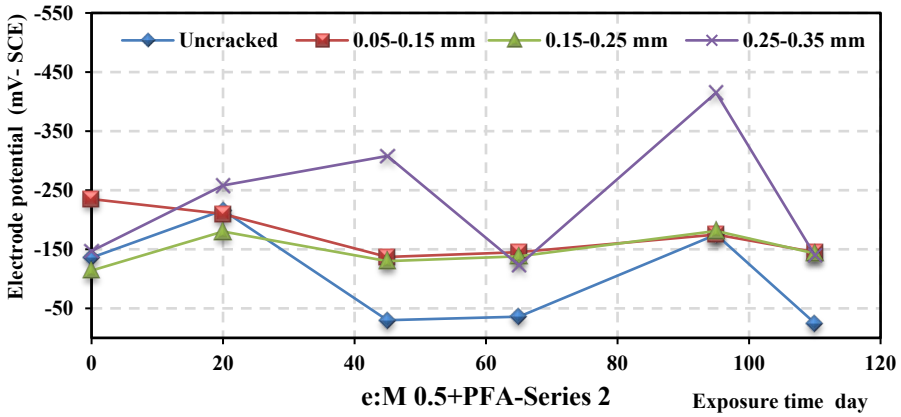

Figure 6.26: Effect of crack width on half-cell potential in reinforced concrete prism at temperature 30 °C (Series 2)

(iii) Crack width, easing the transport of salts throughout the crack accelerated the increase of half-cell potential of steel. The results also demonstrated the presence of crack has a strong impact on the potential drop of rebar and accelerated the transition from passive to active corrosion stage. Where, the crack opening can transport the chloride solution and oxygen and reach reinforcement faster. The results showed that the potential drop values of almost samples remained in the range of uncertain corrosion at the many of wetting-drying cycle. Then, sharp potential drop was seen after week 9 for specimens (M 0.5 and M 0.6) series 3, at week 3-7 for (M 0.5 and M 0.6) series 2, at week 8 for specimens (M 0.5 and M 0.6) series 1 for all cracked samples with different crack width, more negative than-276 mV, E_{corr}. Table 6.31 listed all the cases have E_{corr} more negative than -276 and the time of arrival this potential drop. The effect of crack opening on the potential drop was combined with other parameters such as the temperature of exposure and w/cm ratio and type of cementitious materials because the trend of the effect of crack was variable with different cases as shown in Table 6.31.

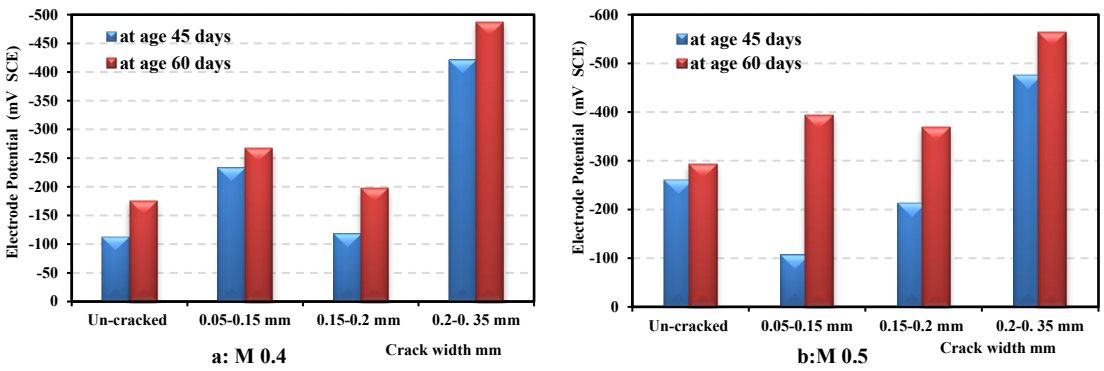

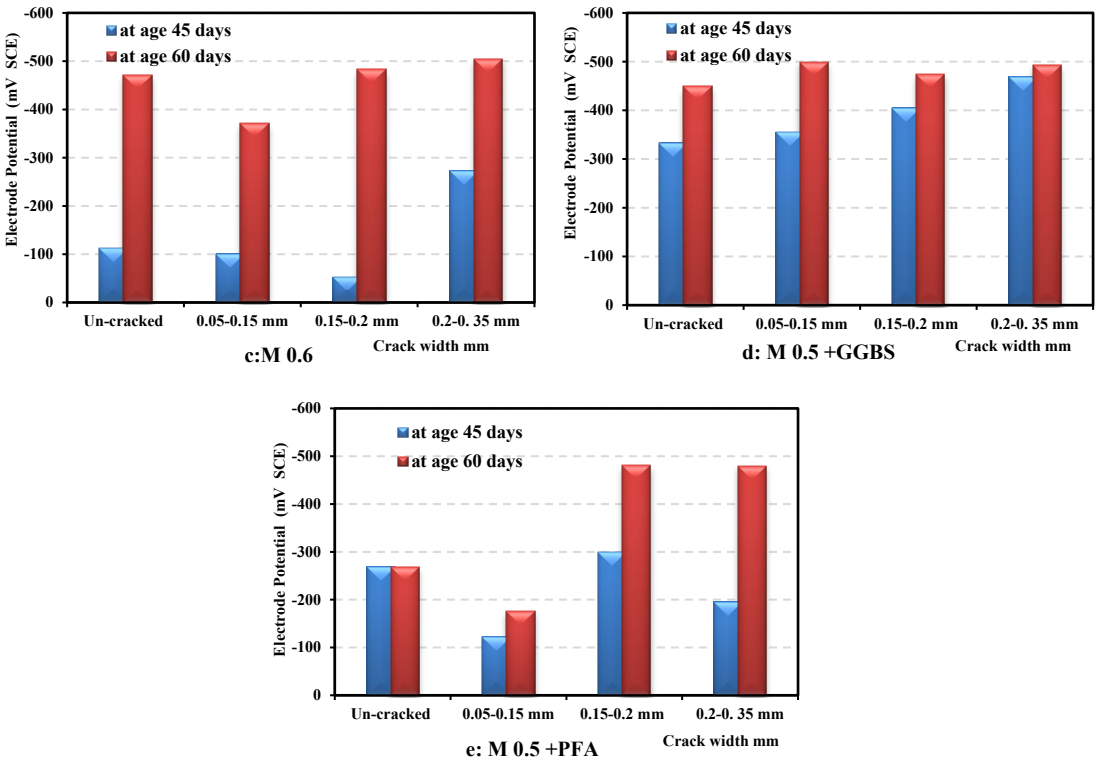

Figure 6.27: Effect of crack width on half-cell potential in Reinforced concrete prism exposed to temperature 40 °C

(iv) Finally, SCMs, PFA, improved the microstructures of concrete leads to keep on steel reinforcement by decreasing the degradation in electrode potential of steel. The influence of SCMs on the measurement of the potential drop in reinforced concrete samples is presented in Table 6.31. Where, the samples having PFA, M 0.5+PFA for series 2 and 3 (sound and cracked) continued in the range of uncertain corrosion at all the wetting-drying cycles. While, specimens M 0.5+PFA –for Series 1, crack width more than 0.15 mm and 0.25 mm have a potential drop more negative than -276 mV and the age of arrivals of this stage at 45 days and 60 days respectively as shown in Figure 6.27- e. The potential value of samples of M 0.5+PFA have the crack width of (0.25-0.35mm) in Series 2 and 3 decreased and became in the high probability of corrosion at 80 days and 85 days respectively. On the other hand, the specimens incorporating GGBS, M 0.5+ GGBS, in Series 2 and 3 (sound and cracked) maintained on the potential of a half-cell in uncertain corrosion stage, (≥-276). While, the group of specimens in series 1 (temperature 40 °C), the potentials value decreased at 45 days and they were in the stage of the high probability of corrosion occurred as shown in Figure 6.28- a.

Table 6.31: Summary of half – cell potential more negative than -276 mV and the age

Series	Sample	Un-cracked		0.05-0.15 mm		0.15-0.25 mm		0.25-0.35 mm	
		E_{corr} ≤-276	Age* day	E_{corr} ≤-276	Age* day	E_{corr} ≤-276	Age* day	E_{corr} ≤-276	Age* day
Series 1	M 0.4	-	-	-	-	-	-	Y	45
	M 0.5	Y	60	Y	60	Y	60	Y	45
	M 0.6	Y	60	Y	60	Y	60	Y	45
	M 0.5+ GGBS	Y	45	Y	45	Y	45	Y	45
	M 0.5+ PFA	-	-	-	-	Y	45	Y	60
Series 2	M 0.4	-	-	-	-	-	-	-	-
	M 0.5	-	-	Y	110	Y	95	Y	95
	M 0.6	-	-	Y	65	Y	65	Y	65
	M 0.5+ GGBS	-	-	-	-	-	-	-	-
	M 0.5+ PFA	-	-	-	-	-	-	Y	80
Series 3	M 0.4	-	-	-	-	-	-	-	-
	M 0.5	-	-	Y	120	Y	85	Y	85
	M 0.6	Y	110	Y	85	Y	75	Y	80
	M 0.5+ GGBS	-	-	-	-	-	-	-	-
	M 0.5+ PFA	-	-	-	-	-	-	Y	85

E_{corr}: Half-cell potential is more negative than -276 mV, high probability that corrosion is occurring.
* Age: Time of arrival half-cell potential-SCE is ≤ -276 mV.
Y: Yes, E_{corr} ≤ -276 mV.

Half-cell potential technique is the most common method used for predicting the risk of reinforcement corrosion. The drop of half-cell potential is often inconclusive to detect the change from passive to active corrosion state because the reading itself is highly affected by the moisture of the sample, the sample oxygen content, the type of cement (Portland or others), the deterioration type due to carbonation or chlorides attack, all of them can be influenced the results and therefore lead to erroneous judgment (Bouteiller *et al*., 2012).

a: M 0.5+PFA with crack width 0.25mm, E_{corr} = - 482 mV

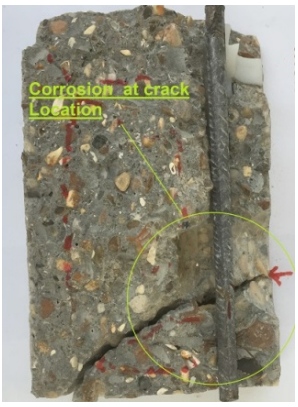

b:M 0.5+GGBS with crack width 0.15 mm E_{corr}= - 475 mV

Figure 6.28: Corrosion state for M 0.5+GGBS and M 0.5+PFA – Series1

In the experimental results, as such factors were almost constant, E_{corr} was compared versus total or free chloride content at the steel rebar level for these samples (see Tables 6.1- 6.15). Considering a drastic decrease of half-cell potential leading to values more negative than -276 mV (SCE) (Song and Saraswathy, 2007), it was possible to assess the transition from passive to active corrosion in M0.5 and M0.6 specimens by a chloride concentration higher than 1% for total chloride or higher than 0.3% (Tuutti, 1982; Bouteiller *et al*., 2012) for free chloride as shown in Tables 6.1- 6.15 and Table 6.16. However, for more discussion about these results will be explained in the next section to understand accurate these results compared with LPR results and determine active corrosion in these specimens.

6.4.2 Linear Polarization Resistance Results

The linear polarization resistance is the electrical resistivity of the protected passive film PPF at the surface of the reinforcement steel bar. In general, it is determined graphically from the slope of the current density (μA/cm^2) - potential (mV) curves. The smaller slope, the easier for the charge to transfer across the metal/electrolyte interface, and therefore the corrosion current density is bigger and, consequently, the corrosion reaction rate is quicker (Mancio *et al*., 2005).

Polarization resistance, *Rp* for steel in concrete mixes determined by linear polarization resistance, LPR (Ohm cm^2) reading were measured at different age of exposure to chloride environment with different temperatures (Series). The corrosion current density (i_{corr}) (μA/cm^2) is found by using the Stern-Geary Equation (i_{corr} =B/Rp) for reinforcement concrete sample (Katwan, 1988). *B* is constant, it is commonly

considered equal to 26 mV for active corrosion and 52 mV for the passive state (Andrade and González, 1978). In the present study, since the attention is brought to the transition state from passive to active corrosion state, the *B* constant was fixed to 26 mV in all cases (Bouteiller *et al*., 2012). Considering the RILEM (TC 154-EMC) (Andrade and Alonso, 2004) and (Andrade *et al*., 1990) recommendations, there are four corrosion levels expressed according to the corrosion current densities i_{corr} as shown in Table 6.32, are useful for the interpretation of these results. In the discussion section of corrosion rate will be considered the third level of corrosion class, that i_{corr} greater than 0.5 $\mu A/cm^2$, moderate to high corrosion, it will be symbolized, M as shown in Table 6.32.

Table 6.32: Corrosion current vs. condition of the rebar (Andrade *et al*., 1990)

Corrosion current density (i_{corr})	The condition of the rebar
$i_{corr} < 0.1\ \mu A/cm^2$	Passive condition
i_{corr} 0.1 - 0.5 $\mu A/cm^2$	Low to moderate corrosion
i_{corr} 0.5 - 1.0 $\mu A/cm^2$	Moderate to high corrosion
$i_{corr} > 1.0\ \mu A/cm^2$	High corrosion rate

The evolution corrosion current densities for all concrete specimens exposed to chloride ingress were given in Figures 6.29-6.31, and these results of i_{corr} were affected by: (i) Progress in the age, the i_{corr} values increased with progressing the exposure age to chloride solution. The corrosion evolution increased with time for different exposure temperature. The progress of corrosion current density for specimens varied according to the other parameters, w/cm ratio, crack width and type of cementitious materials. The results showed the many of samples had corrosion current density exceeded the passive condition of the above recommendation after 20 days of exposure to chloride environment because of corrosion current density, i_{corr}, were lower than 0.1 $\mu A/cm^2$. After that age of exposure, i_{corr} increased higher than 0.1 $\mu A/cm^2$ (Low to moderate corrosion). Consequently, the results showed the specimens were increased the i_{corr} of more than 0.5 $\mu A/cm^2$, (moderate to high corrosion). A sharp i_{corr} increase was observed after week 60 at least (for example Series 2 and 3 in samples (M 0.5 and M 0.6), i_{corr} increased after 70 days, for series 1, the samples (M 0.5, M 0.6, M 0.5+GGBS and M 0.5+PFA), the i_{corr} increased sharply after 60 days). However, i_{corr} values for the rebar in samples, M 0.4-un-cracked (all series) remained passive state (less 0.1 $\mu A/cm^2$) during the overall period of chloride exposure (see Table 6.33).

(ii) w/cm ratio of concrete, i_{corr} generally would be increased with increased the w/cm of concrete covering the steel reinforcement. The results also showed the increase in w/cm ratio of reinforced concrete increase the i_{corr} in steel rebar significantly and the probability of active condition corrosion increases. The corrosion rate values for almost samples of M 0.4 (w/cm = 0.4) remained in the range of passive condition corrosion; this showed that chlorides did not reach with adequate concentration to initiate passive layer of steel reinforcement rebar and occurred the active corrosion (see Tables 6.1, 6.7 and 6.11) as shown in Figure 6.32-b. Conversely, for rebar in the more porous concrete specimens (M 0.6-un-cracked) a significant increase of i_{corr} was observed with time. After the few days cycles, the i_{corr} values of these specimens were higher than 0.5 µA/cm^2 and became in the active corrosion range. The i_{corr} increased drastically after week 10 for specimen's Series 3 and after week 8 for specimen's Series 1 more than 0.5 µA/cm^2, leading to values that belonged to the high confidence interval for corrosion and that were attributed to the penetration of chlorides at the rebar level (in accordance with the chloride determinations at Table 6.1-6.15) as shown in Figure 6.32-a. All the cases have i_{corr} more than 0.5 µA/cm^2 and the time of arrival this corrosion rate is listed in Table 6.33.

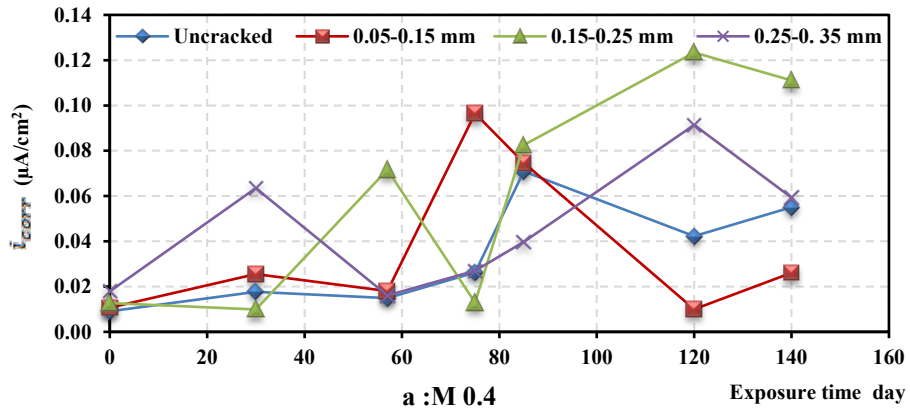

a :M 0.4

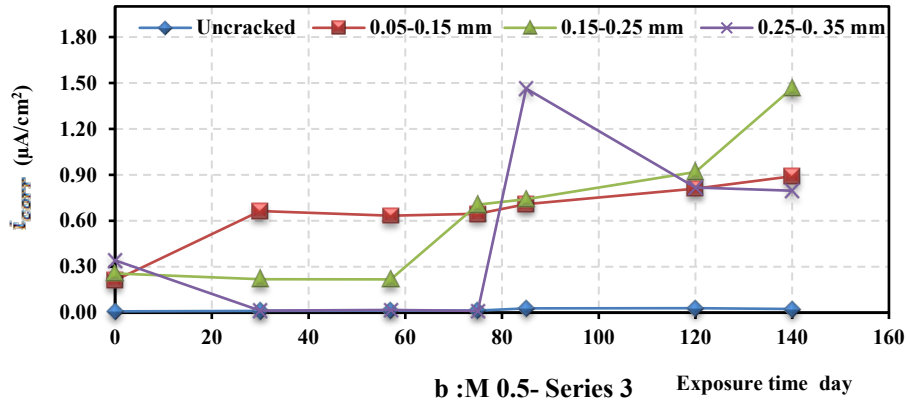

b :M 0.5- Series 3

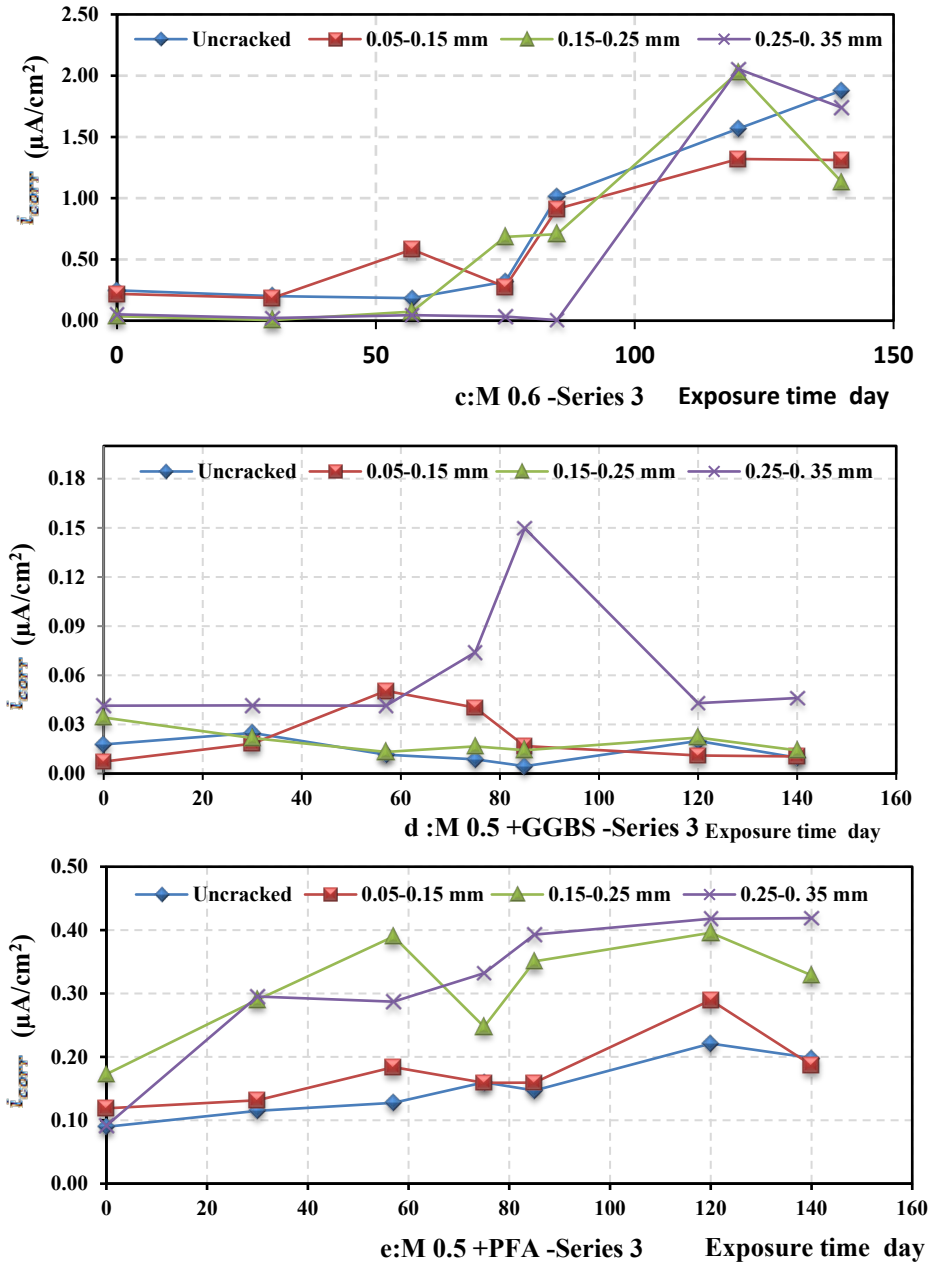

Figure 6.29: Effect of crack width on Corrosion current density of reinforced concrete prism at temperature 20 °C (Series 3- Un-carbonated)

(iii) Crack width, the transport of salts and oxygen throughout the crack was faster and i_{corr} increased considerably. The results also demonstrated the presence of crack has a significant impact on the corrosion of steel rebar and transfers from passive to active corrosion stage in a shorter time. The i_{corr} for the cracked specimens are higher than those of the un-cracked specimens due to the crack opening can transport the chloride solution and oxygen to steel reinforcement quickly. The corrosion rates for the most cracked specimens have exceeded the 0.1 µA/cm^2, which is conventionally suggested to level the evolution from passive to active corrosion as shown in Table 6.33.

Firstly, the results showed that the i_{corr} values of almost cracked samples remained in the range of passive corrosion at the few of the wetting-drying cycle. Then, i_{corr} was progressively seen after week 10 for specimens (M 0.5 and M 0.6) Series 3, at week 5-7 for (M 0.5 and M 0.6) Series 2, at week 8 for specimens (M 0.5 and M 0.6) Series 1 for all cracked samples with different crack width, more than 0.5 µA/cm^2. Figure 6.32-a shows the visual examination of the steel surface and the evolution of corrosion. The presence of cracks affects i_{corr} and corrosion process, both initiation and propagation. This effect was combined with other parameters such as the temperature of exposure and w/cm ratio and type of cementitious materials because the trend of the effect of crack varies with the other cases as shown in Table 6.33.

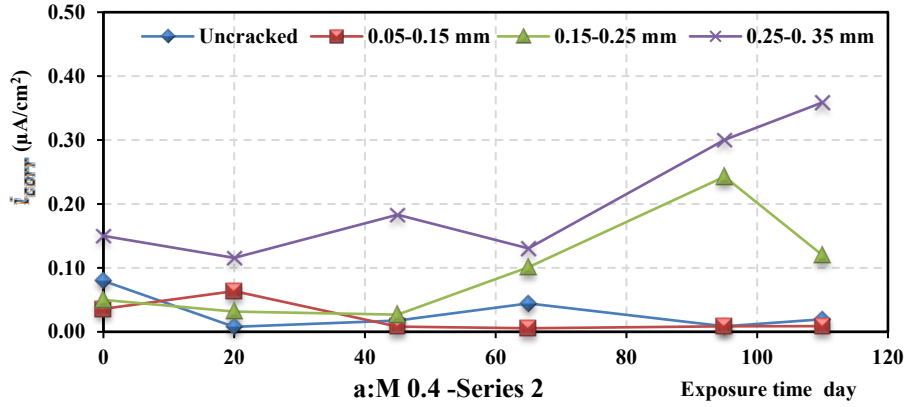

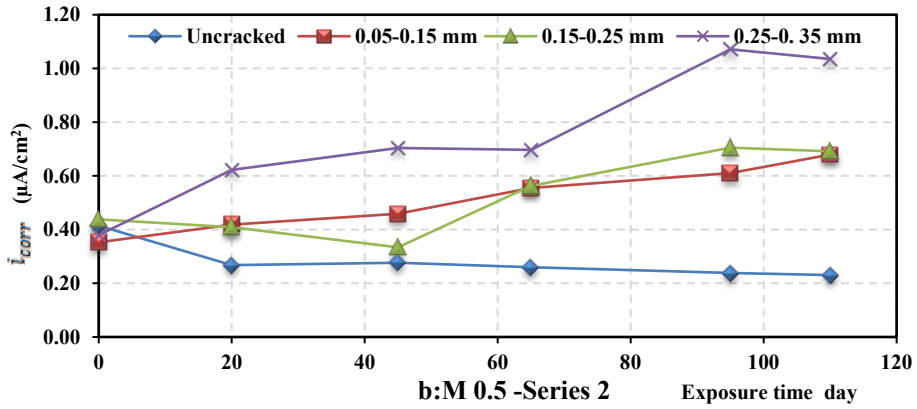

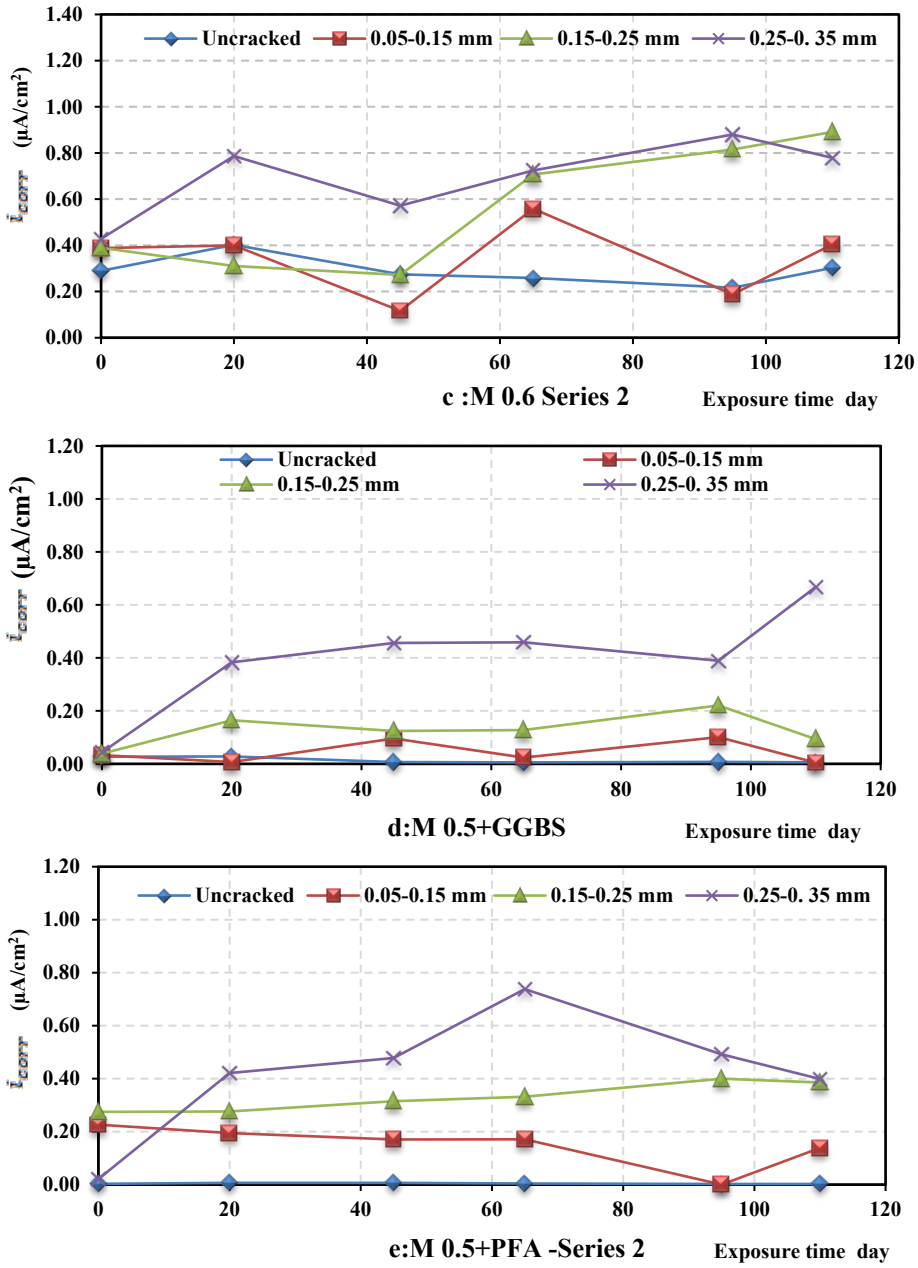

Figure 6.30: Effect of crack width on corrosion current density of reinforced concrete prism at temperature 30 °C (Series 2)

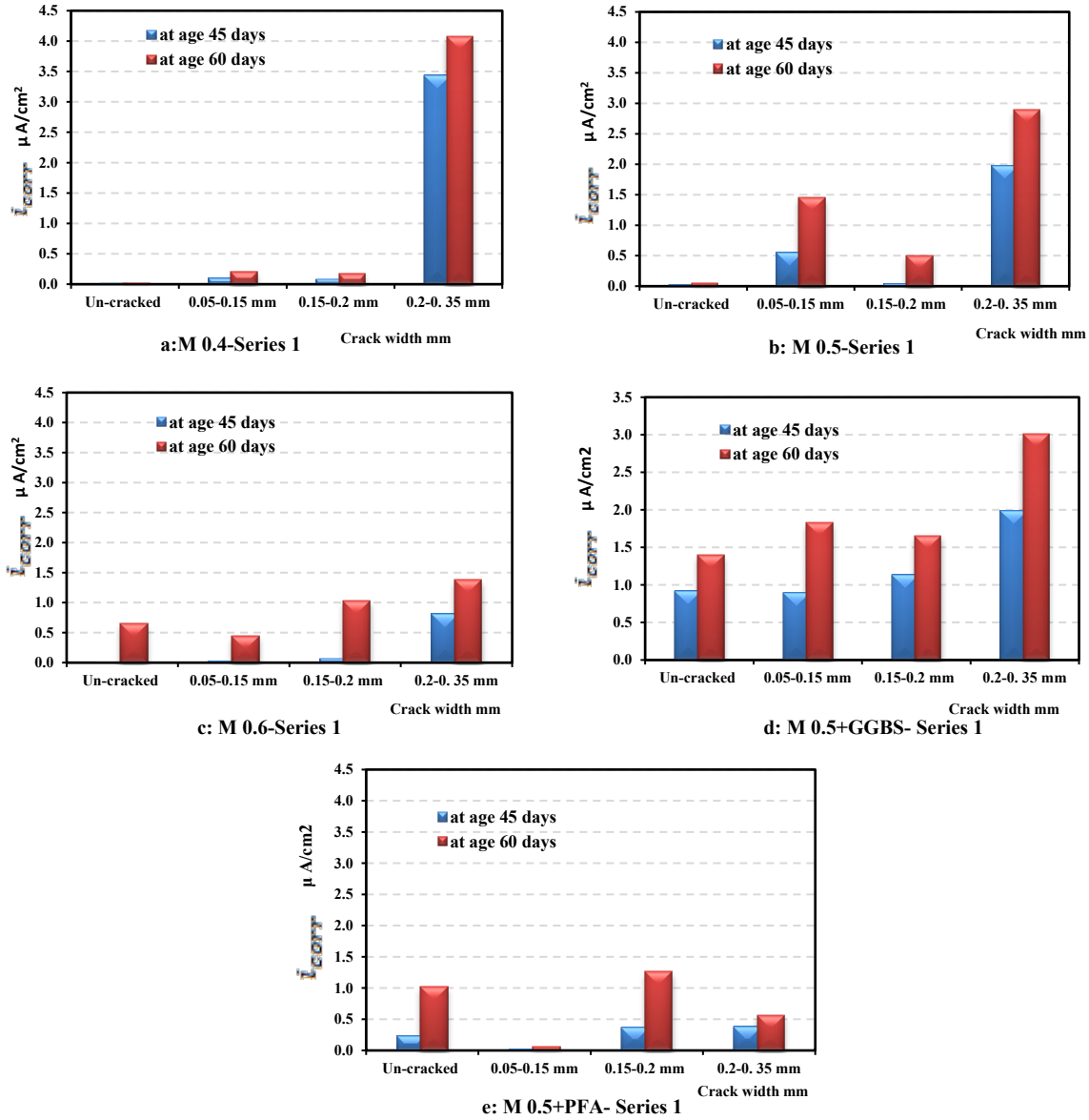

Figure 6.31: Effect of crack width on corrosion current density of reinforced concrete prism exposed to temperature 40 °C

(iv): SCMs, PFA and GGBS have a significant resistance to diffuse chloride solution, the use of SCMs leads to enhancing the micro-structures of concrete and decrease the progress i_{corr} of steel reinforcement with age. Table 6.33 showed the influence of SCMs on i_{corr} values. Where, the samples having PFA, M 0.5+PFA for Series 2 and 3 (sound and cracked) were in the passive corrosion at the all of the wetting-drying cycle's periods. While, specimens M 0.5+PFA -for Series 1, crack width more than 0.25 mm have i_{corr} more than 0.5 µA/cm^2 and the age of arrivals of this stage at 60 days, the visual examination of steel surface was obvious in Figure 6.32-d. The i_{corr} values for samples M 0.5+PFA with crack width (0.25-0.35mm) in Series 2 increased and became in the high probability of corrosion at 85 days. However, the specimens incorporating GGBS, M 0.5+

GGBS, in series 2 and 3 (sound and cracked) remained in passive -low corrosion stage, (≤ 0.5 μA/cm^2) overall period of chloride exposure (15 weeks). While, the group of specimens in Series 1 (temperature 40 °C), the current corrosion densities values increased at 45 days and they were in the stage of the moderate-high probability of corrosion occurred as shown in Figure 6.32- e.

Table 6.33: Summary of i_{corr} higher than 0.5 μA/cm^2 and the age of arrival this level

Series	Sample	Un-cracked		0.05-0.15 mm		0.15-0.25 mm		0.25-0.35 mm	
		$i_{corr} \geq$ 0.5	Age* day	$i_{corr} \geq$ 0.5	Age* day	$i_{corr} \geq$ 0.5	Age* day	$i_{corr} \geq$ 0.5	Age* day
	M 0.4	-	-	-	-	-	-	M	45
	M 0.5	-	-	M	45	M	60	M	45
Series 1	M 0.6	M	60	M	60	M	45	M	45
	M 0.5+ GGBS	M	45	M	45	M	45	M	45
	M 0.5+ PFA	M	60	-	-	M	60	M	60
	M 0.4	-	-	-	-	-	-	-	-
	M 0.5	-	-	M	60	M	60	M	40
Series 2	M 0.6	-	-	M	65	M	60	M	30
	M 0.5+ GGBS	-	-	-	-	-	-	M	110
	M 0.5+ PFA	-	-	-	-	-	-	M	80
	M 0.4	-	-	-	-	-	-	-	-
	M 0.5	-	-	M	30	M	75	M	85
Series 3	M 0.6	M	85	M	85	M	75	M	85
	M 0.5+ GGBS	-	-	-	-	-	-	-	-
	M 0.5+ PFA	-	-	-	-	-	-	-	-

Corrosion current (i_{corr}) higher than 0.5 μ A/cm^2, the corrosion is occurring with range moderate to high.
*Age: Time of arrival i_{corr} higher than 0.5 μ A/cm^2.
M: Moderate to high corrosion rate.

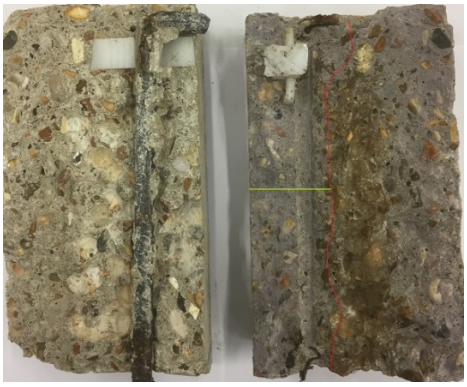

a: M 0.6-un-cracked -Series 2

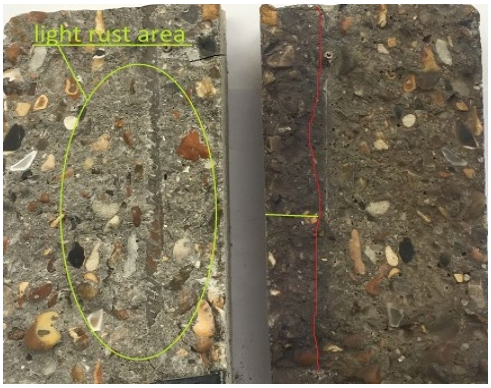

b: M 0.4 un-cracked -Series 2

c: M 0.6 with crack width 0.3mm -Series 1

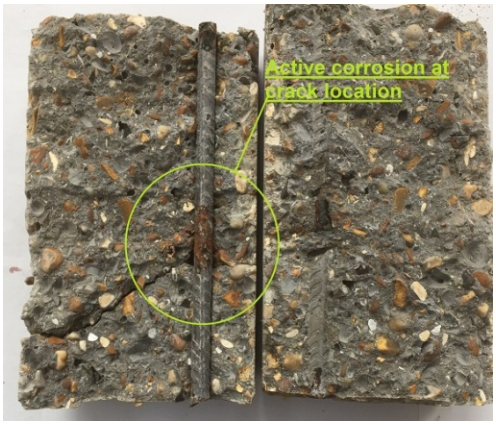

d: M 0.5+PFA with crack width 0.35mm-Series 1

e: M 0.5+GGBS with crack width 0.15mm -Series1

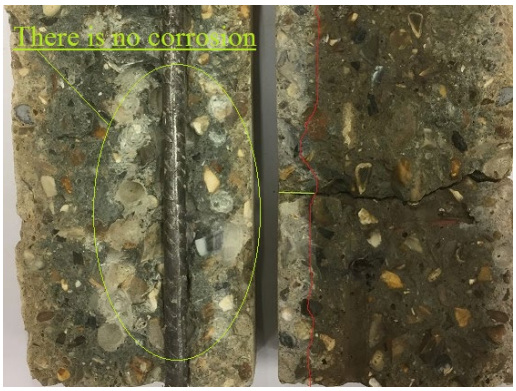

f: M 0.5+GGBS- Un-cracked Series 2

Figure 6.32: The condition of the steel bars and the surrounding concrete

The visual investigation of rebar surface of split concrete samples observed some points, Figure 6.32 shows the examination of the steel reinforcement (specimen used to find the chloride concentration) after 15 weeks of wetting-drying cycles to different temperatures of chloride spray. The quality and quantity of rust color depended mainly on properties of concrete (w/cm ratio), crack width and cementitious materials type. The rust color appeared between red-brown to black. Magnetite, Fe_3O_4, has a grey-black appearance and hematite, Fe_2O_3, is red-brown. Approximately, the results of E_{corr} and i_{corr}

were matched with the visual investigation of the rebar surface. For example, E_{corr} and $í_{corr}$ of M 0.5+PFA- 0.3mm- Series 1were 480 mV and 3μA/cm^2 respectively and identified there is corrosion occurred in the sample and the visual investigation of rebar surface showed the rusted surface had spread out on the steel rebar at the cracked location as shown in Figure 6.32-d. Whereas, for the M 0.5+GGBS- un-cracked concretes as shown in Figure 6.32-f, the steel rebar embedded in Series 2, no sign of corrosion was seen after 15 weeks and E_{corr} and $í_{corr}$ of these samples did not indicate to the presence of corrosion as well.

The LPR is the electrical resistivity of the steel rebar and protected passive film PPF at the surface of the steel bar. The chloride ions in concrete penetrate progressively with time by the microstructure and permeability properties of concrete and the chloride and carbon dioxide ion play a vital role in penetrating and initiating corrosion of steel in concrete (Silva, 2013). The corrosion is an electrochemical or chemical interaction between steel and its environment (Revie and Uhlig, 2008). The chloride ion produces corrosion in three stages. The depassivation occurs when chloride ions dissolved in the pore water of concrete. This change in environment condition provides a change in LPR value and these values increase with time due to an increase of chloride concentration with time. When this concertation approaches specific level, threshold value. (Angst *et al*., 2009) pointed out the chloride threshold value may be ranged between 0.04 % and 8.34% by weight of cement. At threshold value, chloride ions penetrate and break down the depassivation of steel in concrete as the pH of pore water of concrete falls lower than 11(Neville, 2011). The initiation of corrosion and absorption of the chlorides maybe continue due to the penetration of chloride with time during the wetting-drying cycle. The last stage of corrosion, the hydroxyl ions work with chlorides to interact with ferrous ions to appearance the corrosion products at chloride concentration exceeds 0.6 of hydroxyl ions concentration (Broomfield, 2007). All these chemical reactions in the rebar surface and concrete can be increased and changed the electrical resistivity with time. Hence, the LPR tendency to decrease and the corrosion rate will gradually increase with the progress of the time.

As showed previously in chloride concentration (see section 6.2), in un-cracked concrete, the transport of chloride ions into concrete can happen by different methods (diffusion, permeation and capillary sorption) (Basheer *et al*., 2001) and the transport properties of concrete are mainly depended on the porosity of concrete and formation of

crack. The w/cm ratio and type of cementitious materials can mainly affect the porosity, preamble voids and the path of transport for chloride into concrete (Song *et al*., 2008). Where, the chloride penetration resistance of concrete decreases with increasing w/cm ratios. That leads to an increase in the electrochemical reaction, initiation and propagation of corrosion because of corrosion performance of rebars embedded in concrete seems to be mainly dependent on w/cm ratio and cementitious materials type (Bouteiller *et al*., 2012). Regarding OPC concretes specimens, corrosion onset for M 0.6 specimens has higher porosity as observed in section 4.3.1, was highlighted from a potential drop, E_{corr} (Figures 6.25 and 6.27-c) together with an increase of corrosion rate (Figures 6.29 and 6.31-c) after few weeks depending on exposure temperature. Whilst, the less porous M 0.4 specimens did not corrode significantly during the 15 weeks of chloride wetting-drying cycling as half-cell potential values remained in the uncertain corrosion range (Figures 6.25 and 6.27-a) and as corrosion currents were lower than 0. 1 $\mu A/cm^2$ (Figures 6.29 and 6.31- a). Moreover, from visual examination of the steel rebars after 16 weeks, M 0.6 specimen showed corroded surface as shown in Figure 6.32-a while in M 0.4 specimen only a light rust area was seen in Figure 6.32-b. Finally, the increase w/cm ratio achieves the decrease in the concrete quality by increasing the porosity and water absorption as well as a decrease in the strength, and at final, the decreasing concrete quality gives increases in the corrosion rate (Otieno *et al*., 2008).

On the other hand, the presence of cracks in concrete may negatively influence the significant parameters of transport of chloride ion in reinforced concrete and hence the chloride ingress rate, thereby influencing reinforcement corrosion process (Jacobsen *et al*., 1996). The cracks perform as preferential channels for the diffusivity of several types of potentially aggressive agents such as chloride ions, Cl^-, and carbonic ions, CO_3^{2-}. They have a significant impact on diffusion and permeation of these species in concrete. Many studies (Francois and Arliguie, 1991; Jang *et al*., 2011; Van den Heede *et al.*, 2014) concluded that chloride ions penetrate rapidly through cracks and accelerate chloride-induced corrosion due to an increase of concrete penetrability. Regarding the crack width, the time required to initiate corrosion is shorter for one with the wider crack (Berke *et al*., 2014). In general, the corrosion rate increases with increasing crack widths but is sensitive to concrete quality (permeation properties) (Otieno *et al*., 2008; Quero and Garcia, 2010). This is the general idea of the effect the crack on corrosion rate. However, the crack width has a different performance of corrosion rate. In small crack width, the corrosion products

due to the first corrosion process affects the penetration of chloride by filling the end of crack opening and sometimes the supplementary cementitious materials may be self-healing of the crack by new hydration products later (Ismail *et al*., 2008; Van den Heede *et al*., 2014).

The durability properties in term corrosion and chloride penetration of the concrete incorporating supplementary cementitious materials improved significantly by reducing the corrosion rate and potential drop due to decrease chloride penetration and increase in chloride binding capacity as shown in Figure 6.19. The enhancement in the microstructure of the concrete due to decrease the permeable voids and capillary pores is the main reason of the reduction of chloride conductivity and improvement of chloride penetration resistance (Ramezanianpour and Malhotra, 1995; Otieno *et al*., 2014; Zang and Zhao, 2018). Some results of E_{corr} and corrosion rate in normal condition (without effect of temperature) may affect by high content of component such as manganese and sulfur species like S^{-2} (Jarrah *et al*., 1995), but actually, visual examination of steel, the rebars did not refer to any sign of corrosions after 15 weeks as shown in Figure 6.32-f. Therefore, from these results, Bouteiller *et al*. (2012) concluded that rebar corrosion in concretes based on GGBS cement should not be characterised using ASTM 876: 2015 standard and RILEM recommendations (Andrade and Alonso, 2004).

6.5 The Effect of Carbonation on Corrosion Rate

One series of concrete prisms was used to investigate the effect on carbonation on corrosion rate by exposing this series to an accelerated environment of carbon dioxide with 5% CO_2, 65% relative humidity and 25 °C for 5 weeks. These specimens have been exposed to three sequences, chloride spraying solution environment with 5% NaCl then they were exposed to CO_2 environment (for carbonated samples) beyond that the samples were backed to chloride spraying solution. The half-cell potential, $E_{corr,}$ and linear polarization resistance, LPR were measured to determine the state of corrosion of reinforcement as follow:

6.5.1 Effect of Carbonation on Half-Cell Potential (E_{corr})

The half-cell potential (electrode potential, E_{corr}) measured at various intervals during the exposure of samples to chloride fog, with the aim to detect the transition from passive to active corrosion condition, is presented in Figure 6.33. ASTM C876: 2015 provides a useful interpretation of these results. Key observations from these results are: (i) : Figures 6.33 (a-1, b-1, c-1, d-1, and e-1) present the results of carbonated samples for the five mixes used in this study. The exposure of samples to the CO_2 environment has a considerable impact on the electrode potential of steel reinforcement. A step-change in potential drop can be seen at around 80 days in all carbonated samples (during the period of CO_2 exposure), whereas the potential values for samples M 0.4 remained more positive than -126 mV SCE (> 90% probability of no corrosion) for the control samples.

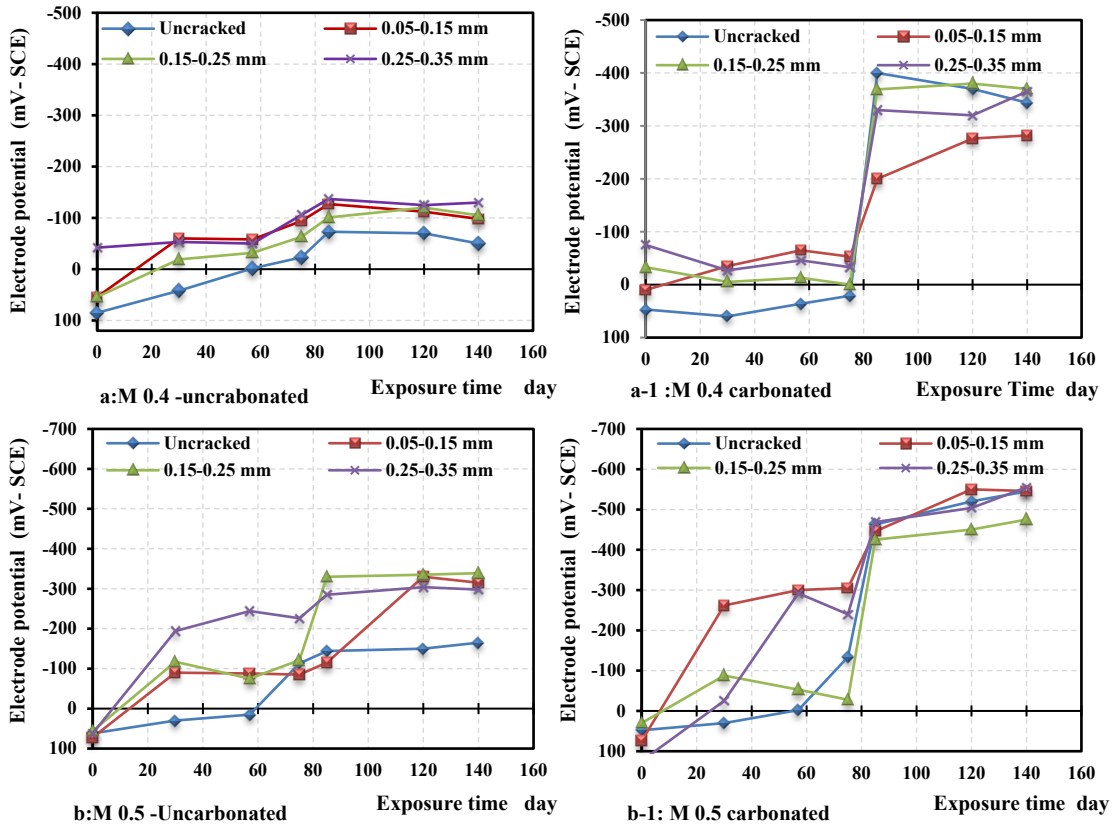

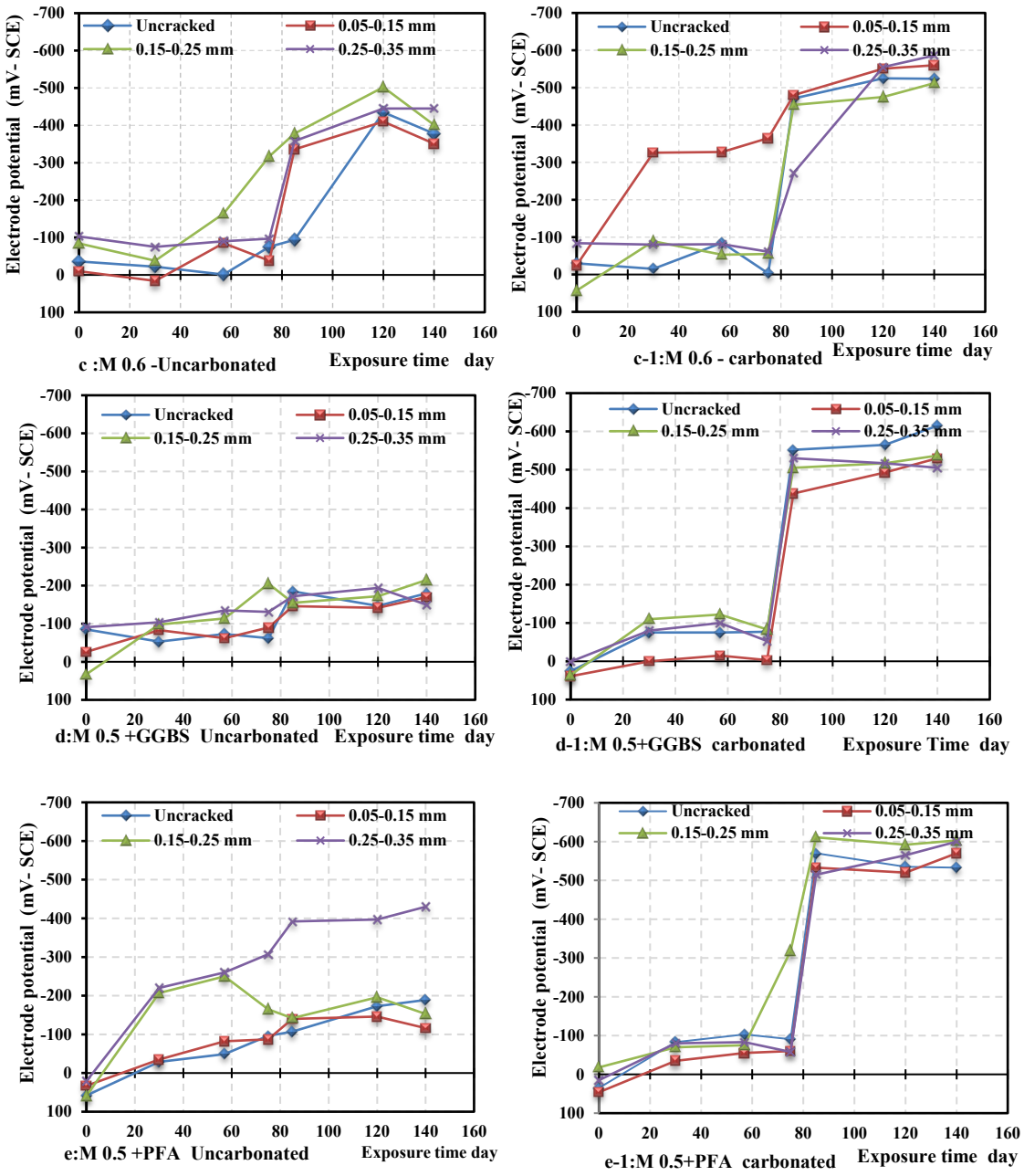

Figure 6.33: Effect of carbonation on half-cell potential of reinforced concrete samples

The results showed the E_{corr} are more negative than -276 mV SCE, (there is a greater than 90% probability that corrosion is occurring), the severe drop occurred at 70 days for both series (un-carbonated and carbonated) in samples (M 0.5 and M 0.6). On the other hand, half-cell potential values for samples M 0.4, M 0.5+GGBS and M 0.5+PFA (before carbonated) remained in more positive than -126 mV SCE, there is a greater than 90% probability that no corrosion is occurring. This suggests that the corrosion conditions have been altered (from passive to active corrosion state) for this concrete mix due to the presence of carbonation. Table 6.34 details which samples had exceeded the threshold

value of more negative than -276mV (>90% probability of active corrosion), and their respective exposure duration when the threshold was reached. The main reason for a step change and considerable values in E_{corr} is due to exposure to the cycle of chloride spraying condition with CO_2 environment that leads to a reduction the pH level in the concrete surrounding steel reinforcement bar.

(ii) : The negative values of half-cell potential generally increased with the increase in w/cm of concrete (i.e. between M 0.4, M 0.5, and M 0.6 concrete mixes) for both controlled and carbonated specimen as shown in Table 6.34.

(iii) : The cracks within the samples increase the transport of chloride, accelerating the transition of corrosion from passive to an active state. This can be seen from Figure 6.33 where the electrode potential value generally increased with the increase in crack width. Hence, the probability of corrosion is proportional to the crack width. For carbonated samples, the impact of crack opening on the potential drop was not clear since samples changed from passive to active corrosion condition during the CO_2 exposure phase.

The drop of half-cell potential is often inconclusive to detect the change from passive to active corrosion state because the reading itself is highly affected by the reduction of pH due to carbonation. Considering a drastic decrease of half-cell potential leading to values more negative than −276 mV (SCE) (Song and Saraswathy, 2007), it was possible to assess the transition from passive to active corrosion in M 0.5 and M 0.6 specimens by a chloride concentration higher than 1% for total chloride or free chloride higher than 0.3% (Tuutti, 1982; Bouteiller *et al*., 2012) as shown in Figure 6.22. However, for more discussion about these results will be explained in the next section to understand accurate these results compared with LPR results and determine active corrosion in these specimens.

Table 6.34: Summary of half - cell potential less than -276 mV and the age

Series	Sample	Un-cracked		0.05-0.15 mm		0.15-0.25 mm		0.25-0.35 mm	
		E_{corr} ≤-276	Age* day	E_{corr} ≤-276	Age* day	E_{corr} ≤-276	Age* day	E_{corr} ≤-276	Age* day
Series 3- carbonated	M 0.4	Y	85	Y	85	Y	85	Y	85
	M 0.5	Y	85	Y	85	Y	85	Y	85
	M 0.6	Y	85	Y	30	Y	85	Y	75
	M 0.5+ GGBS	Y	85	Y	85	Y	85	Y	85
	M 0.5+ PFA	Y	85	Y	85	Y	85	Y	85

E_{corr}: Half-cell potential is more negative than -276 mV, high probability that corrosion is occurring.
* Age: Time of arrival half-cell potential-SCE is ≤ -276 mV.
Y: Yes, E_{corr} ≤ -276 mV.

6.5.2 The Effect of Carbonation on Linear Polarization Resistance (LPR)

Polarization resistance (Rp) for steel in concrete mixes determined by linear polarization resistance, LPR technique were measured at different age of exposure to chloride environment with different environment condition (chloride- CO_2- chloride) to the corrosion current density, i_{corr}.

The evolution corrosion current densities for all concrete specimens exposed to chloride ingress and CO_2 condition were presented in Figure 6.34, and these results of the corrosion current density, i_{corr} of steel reinforcement were affected significantly by the carbonation state and reduce pH for all samples.

According to recommendations of the RILEM (TC 154-EMC)(2000); Bouteiller, *et al*. (2012) ; Andrade and Alonso (2004), corrosion current densities, i_{corr} may be used to determine corrosion levels. In the discussion section of corrosion rate will be considered the third level of corrosion class, that the corrosion current density, i_{corr} greater than 0.5 $\mu A/cm^2$, moderate to high corrosion, it will be symbolized, M as shown in Table 6.35.

For effect of the exposure age, the corrosion evolution is increasing with time for different exposure condition and the progress in corrosion current density for specimens were different according to the other conditions such as exposure condition, w/cm ratio and crack width. The results showed the most samples had corrosion current density

exceeded the passive condition of the above recommendation after 20 days of exposure to chloride environment because of corrosion current density, i_{corr}, were lower than 0.1 μ A /cm^2. After that time, i_{corr} increased than 0.1 μ A/cm^2 (Low to moderate corrosion**)**. Consequently, the results showed the i_{corr} increased more than 0.5 μ A /cm^2, (moderate to high corrosion), that happened drastically after 60 days for cracked samples of (M 0.5, M 0.6, M 0.5+GGBS and M 0.5+PFA). While, for the all samples in this Series 3 (carbonated sample), the corrosion current density, i_{corr} increased sharply again after 80 days in the samples as shown in Figure 6.34, beyond they exposed to CO_2 environment condition. On the other hand, the i_{corr} values for the rebar in samples, M 0.4 remained passive (less 0.1 μ A /cm^2) during the period of chloride exposure till they were exposed to CO_2 condition.

The results also showed the increase in w/cm ratio of reinforced concrete increased the corrosion current density, i_{corr} of reinforcement to reach the active corrosion range. The corrosion rate values for almost samples M 0.4 (w/cm = 0.4) remained in the range of passive condition corrosion; this showed that chlorides was not reached with adequate concentration to initiate passive layer of steel reinforcement rebar beyond they were exposed to CO_2 condition the pH has been dropped due to carbonation (Figure 6.24) and that leads to the corrosion current density, i_{corr} of steel reinforcement progressed and the corrosion occurred as shown in Figure. 6.35-c.

Conversely, for rebar in the more porous concrete specimens (M 0.5 and M 0.6) a significant increase of i_{corr} was observed with time. After the few wetting-drying cycles, these values of the specimens (higher than 0.5 μA/cm^2) were in the range of corrosion. A sharp i_{corr} increase was noticed after week 10 for specimen's series (3- carbonated), leading to values that belonged to the high confidence interval for corrosion and that were attributed to the penetration of chlorides at the rebar level (in accordance with the chloride determinations at as shown in Figures 6.22(b-1 and c-1). Moreover, from visual examination of the steel rebars after 16 weeks, M 0.6 (carbonated and uncarbonated) specimen showed corroded surface, while in M 0.4 specimen only a black rust area was shown in Figures 6.35. Table 6.35 is listed all the cases have i_{corr} more than 0.5 μA/cm^2 and the time of arrival this corrosion rate.

As showed previously in chloride concentration section (6.3), the factors affecting chloride concentration were carbonation, w/cm and crack width. Therefore, these factors have a significant role in progress in corrosion by increasing the chloride concentration.

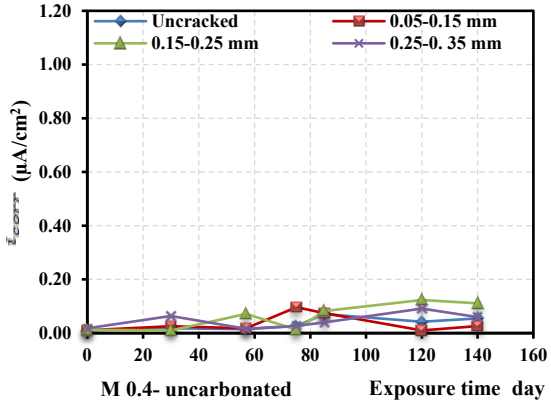

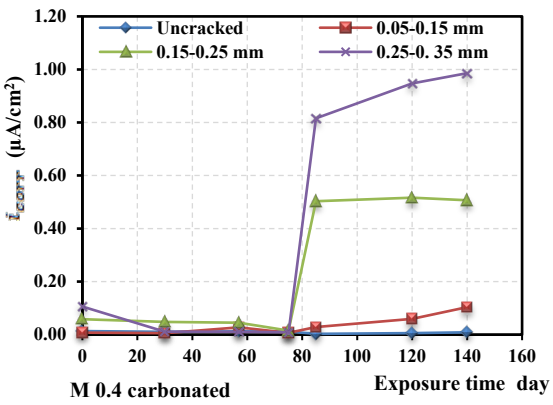

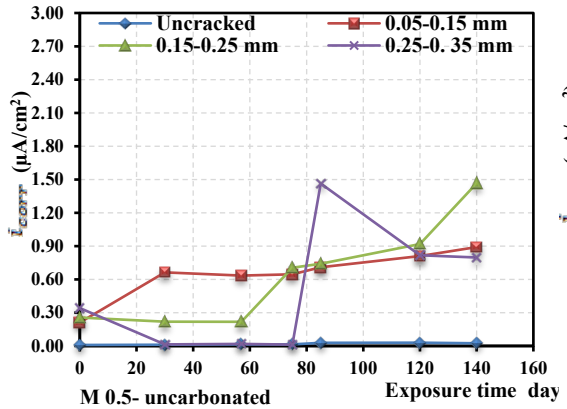

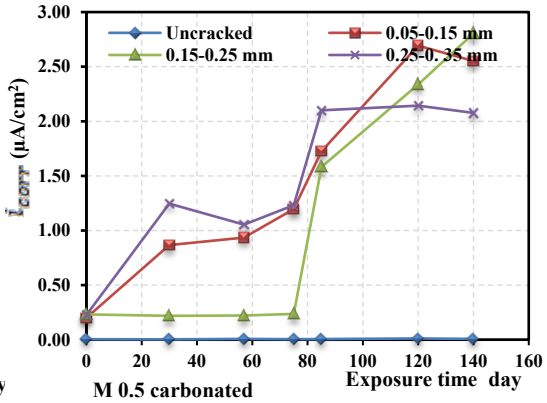

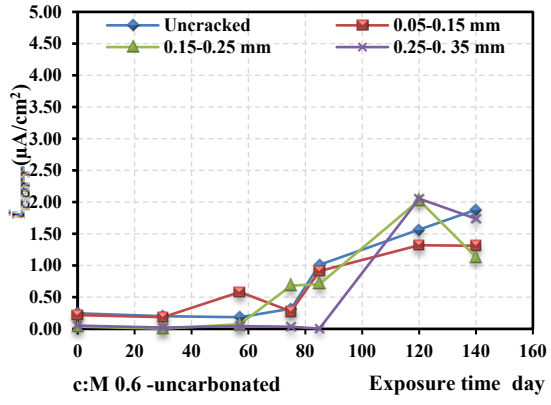

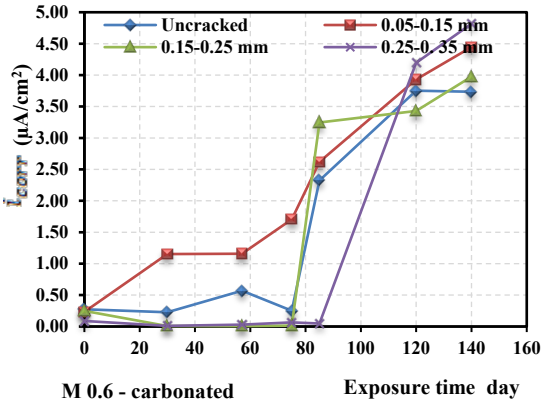

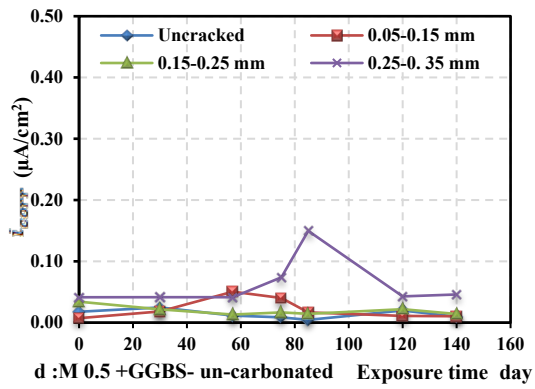

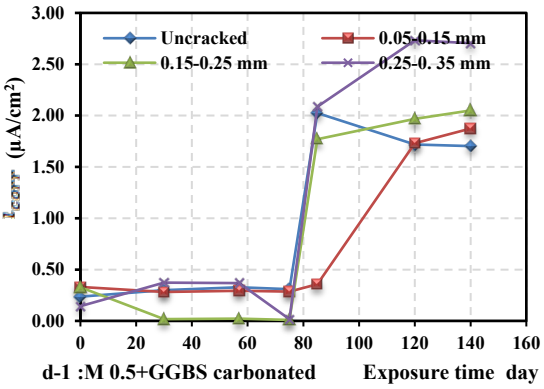

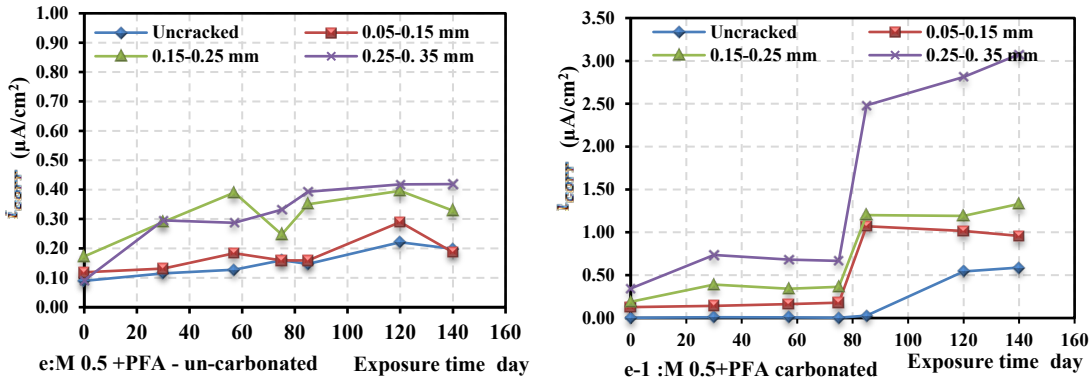

Figure 6.34: Effect of w/cm and carbonation on corrosion current density of reinforced concrete prism

In carbonated samples, the presence of a small chloride in carbonated concrete accelerates the corrosion rate due to reducing the water solution pH of concrete pores that leads to change the environment of microstructures of concrete (Neville, 2011; Wan *et al*., 20.13). Additionally, reinforced concrete structures are more vulnerable to corrosion by the combined impact of chloride and carbonation than those with only one of the two sources (Broomfield, 2007). The carbonation in concrete structures is the onset of chemical and physical processes toward the deterioration of concrete structures and appropriate environment to activate the chloride role in the initiation stage of the reinforcement in concrete structures.

Table 6.35: Summary of i_{corr} higher than 0.5 µA/cm^2 and the age of arrival this level

Series	Sample	Un-cracked		0.05-0.15 mm		0.15-0.25 mm		0.25-0.35 mm	
		$i_{corr} \geq 0.5$	Age* day	$i_{corr} \geq 0.5$	Age* day	$i_{corr} \geq 0.5$	Age* day	$i_{corr} \geq 0.5$	Age* day
Series 3 carbona - ted	M 0.4	-	-	-	-	-	-	M	85
	M 0.5	-	-	M	30	M	85	M	30
	M 0.6	M	85	M	30	M	85	M	85
	M 0.5+ GGBS	M	85	M	85	M	85	M	85
	M 0.5+ PFA	M	120	M	30	M	85	M	85

Corrosion current (i_{corr}) higher than 0.5 µ A/cm^2, the corrosion is occurring with range moderate to high.
*Age: Time of arrival i_{corr} higher than 0.5 µ A/cm^2.
M: Moderate to high corrosion rate.

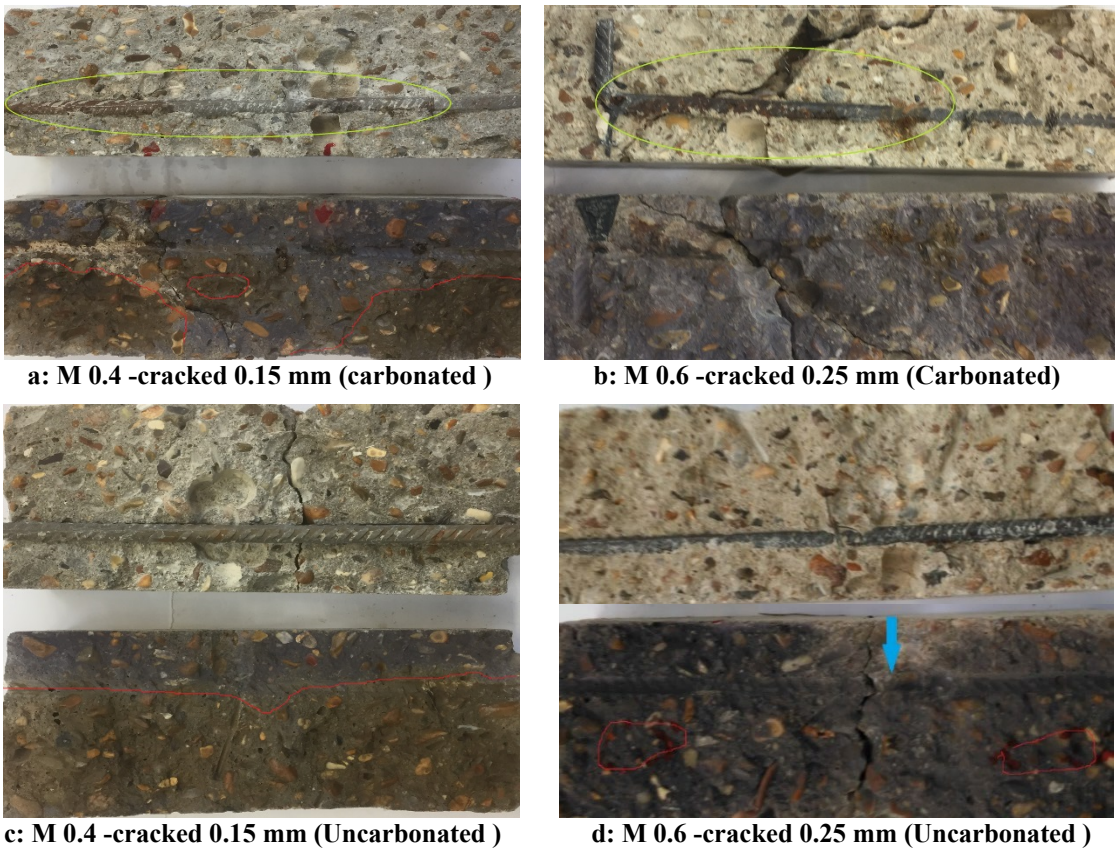

a: M 0.4 -cracked 0.15 mm (carbonated) b: M 0.6 -cracked 0.25 mm (Carbonated)

c: M 0.4 -cracked 0.15 mm (Uncarbonated) d: M 0.6 -cracked 0.25 mm (Uncarbonated)

Figure 6.35: Effect the carbonation on corrosion rate (a and b) carbonated, (c and d) uncarbonated

Finally, environmental deterioration is induced by the conditions of the surrounding environment (e.g., temperature, humidity, carbonation, chloride ingress,). The main effect of the combined action of operational and environmental demands on reinforced concrete structures is a loss of resistance due to corrosion. The reinforced concrete structures are susceptible to corrosion when they are placed in atmospheres with high concentrations of chloride ions or carbon dioxide (Bastidas-Arteaga *et al*., 2010).

6.6 Summary

In this chapter of the study, the impact of exposure environmental condition, temperature, properties of concrete and crack width on the chloride penetration and corrosion rate in reinforced concrete prisms were examined. The effect of three levels of temperatures, crack width and w/cm ratio and carbonated specimens on chloride penetration and corrosion rate were investigated. The main conclusions of this section of the study can be drawn as follows:

- Chloride penetration, d_{cl}^- and C_{cl}- are affected by the concrete properties such as permeation properties (permeability and gas permeability) and strength of concrete.
- The chloride penetration depth is affected by the crack width. For a crack width of 0.15 mm or less, the effect increases by increasing crack width. For grater crack width of 0.15 mm, the behavior of diffusion of chloride is the same as exposed surface.
- The penetration of chloride in the concrete structures increases with increasing w/cm for OPC cement concrete. Whereas, the concrete mixes with SCMs, PFA, and GGBS have significant resistance to chloride penetration.
- The apparent chloride diffusion coefficient, D_a and surface concentration of chloride, C_s increases when increasing the w/cm ratio due to the greater permeation properties (porosity and permeability).
- These results of the study indicate that the increase in temperature has a significant impact on depths of the chloride front (d_{cl}^-) and chloride concentration at the color change boundary (C_d) and diffusion chloride coefficient.
- The chloride penetration depth and chloride concentration in carbonated concrete specimens (exposed to CO_2 condition) were deeper and higher than in control specimens (un-carbonated) for all w/cm ratios and crack width.
- The electrode half-cell potential and corrosion rate are affected by the material behaviors such as porosity due to an increased Cl^- concentration in concrete.
- The carbonation accelerated the combined effect of CO_2 and Cl^- induced corrosion by increasing free chloride concentration and reducing the pH level in concrete.
- The increase in temperature has a considerable impact on electrode half-cell potential, $E_{corr,}$ and corrosion rate, i_{corr} due to an increased chloride concentration and diffusion chloride coefficient, D_a for all specimens of concrete mixes.
- The cracks in concrete samples accelerated chloride-induced corrosion by increasing concrete penetrability of chloride and increasing its concentration.

- The use of LPR measurements in the monitoring of corrosion status for cracked concrete was found to be well-matched with half-cell potential measurements.
- In carbonated samples, measuring the DoC by using a phenolphthalein indicator and pH investigation made it possible to better understand the impact of carbonation induced due to exposure to CO_2 on chloride penetration and corrosion rate.
- In carbonated samples and those exposed to chloride environment, the electrode half-cell potential, E_{corr} and corrosion rate, i_{corr} are affected by the material properties such as porosity due to the impact of diffusivity of CO_2 and Cl^-.
- The SCMs, such as GGBS and PFA have two contradictory performances with regard to the corrosion. The chloride penetration in concrete incorporating these materials was lower than d_{Cl^-} in M0.5 cement concrete, while the DoC in M0.5+GGBS and M 0.5+PFA was higher than DoC in M 0.5 concrete mix. Therefore, the decrease in the effect of the Cl^- environment, and an increase in the effect of a CO_2 environment should be considered in corrosion rate.

CHAPTER VII: MODELLING AND SIMULATION OF CHLORIDE PENETRATION AND DEPTH OF CARBONATION

7.1 Introduction

This chapter focuses on the modelling of the impact of climate change on the durability of concrete infrastructures, in particular, chloride penetration and carbonation depth in concrete structures.

The goals of the project presented in this chapter are to model the chloride penetration and depth of carbonation in concrete structures. The numerical modelling is validated and compared with experimental data presented in previous chapters, in particular, chloride concentration and carbonation depth. In this numerical investigation, climate change, atmospheric temperature, relative humidity and carbon dioxide concentrations of IPCC-2014 scenarios have been considered in modelling for chloride concentration profile and carbonation depth.

7.2 Chloride Penetration Model for Concrete Structures

The two mechanisms for chloride transport in cementitious materials under usual conditions are (i) diffusion, i.e., the transportation of chloride ions within the pore solution caused by their concentration gradient; and (ii) convection, i.e., the transportation of chloride ions together with the pore solution within the concrete caused by the moisture/humidity gradient (Basheer, 2001; Martin-Perez *et al.,* 2001). These methods are a diffusive- convective–phenomenon. One-dimensional ingress of chloride ions into partially saturated concrete due to both diffusion and convection can be described using the following partial differential Equation (Ishida *et al.*, 2014; Val and Trapper, 2008):

$$\frac{\partial C_{Cl}}{\partial t} = -\frac{\partial}{\partial x}\left[D_{eff}\frac{\partial C_{Cl}}{\partial x} + u_D C_{Cl}\right] + R_{Cl} \qquad (7.1)$$

where:

C_{Cl} is the total concentration of chloride ions (kg of Cl^- per m^3 of concrete) , D_{eff} is the effective chloride diffusion coefficient (m^2/s), u_D is the Darcy Law coefficient which describes the humidity diffusion or so-called velocity vector of ions due to the bulk movement of pore solution phase (m/s), R_{Cl}: bound chloride due to the reaction of chloride with cement compounds, and t denotes time (s).

The computational domain and the initial and the boundary condition of Equation 7.1 are the following:

$$C_{Cl}(x,t) \qquad 0 \le x \le d \quad and \quad 0 \le t \le \infty \tag{7.2}$$

$$C_{Cl}(x,0) = C_i \qquad \text{for} \quad t = 0 \tag{7.3}$$

$$C_{Cl}(0,t) = C_s \qquad for \quad t > 0 \tag{7.4}$$

$$\frac{d}{dx} C_{Cl}(L,t) = 0 \qquad zero - flux\ boundary \tag{7.5}$$

where:

C_s is surface chloride concentration; d is the total depth of sample and C_i is the initial value which sometimes is assumed to be zero

The flowchart for the development model accounting for the chloride penetration of the concrete structure is illustrated in Figure 7.1.

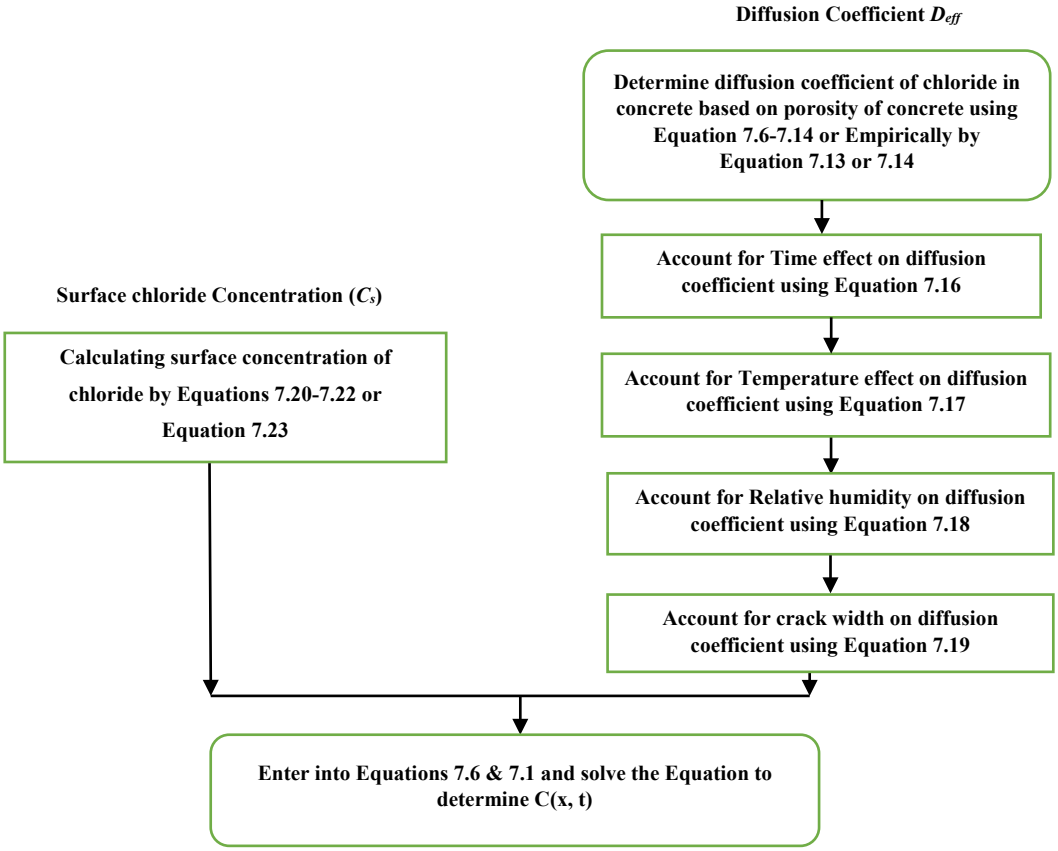

Figure 7.1:Flowchart for the determination of chloride profile

7.2.1 Diffusion Coefficient of Chloride

The transportation of chloride ions is mainly affected by the density of concrete, ρ, the porosity of media ($\in$), tortuosity of pores (Ω) and degree of saturation of porous media (S) as shown in Equation 7.6 (Ishida *et al*., 2014).

$$D_{eff} = \frac{\in S}{\Omega\, \rho} D_a \qquad (7.6)$$

where:

D_a is the apparent chloride diffusion coefficient.

Only capillary and gel pores, which can act as transport paths for chloride ions, or locations for chemical reactions, are considered. The porosity in cement paste is the sum of the volume of the capillary pores and the gel pores to total volume of cement paste, while in concrete the porosity,$\in$ is the sum of the porosity of the cementitious paste pores, aggregate pores and voids in an intermediate transition zone, ITZ zones between cement paste and aggregate.

Diffusion paths of chloride ions in concrete are constrained because micro-structure of concrete in terms of pore structure is often tortuous compared with diffusion paths ions in free water and directions of paths of diffusion are not parallel to the concentration gradient. Tortuosity (Ω) is presented to account for this complex micro pore structure of concrete. Tortuosity is a reduction factor in terms of chloride permeation rate due to the complexity of the micro-pore structure of concrete mass as shown in Figure 7.2 and the tortuosity is a function of porosity in cement paste as shown in Equation 7.7 (Ishida *et al*., 2014).

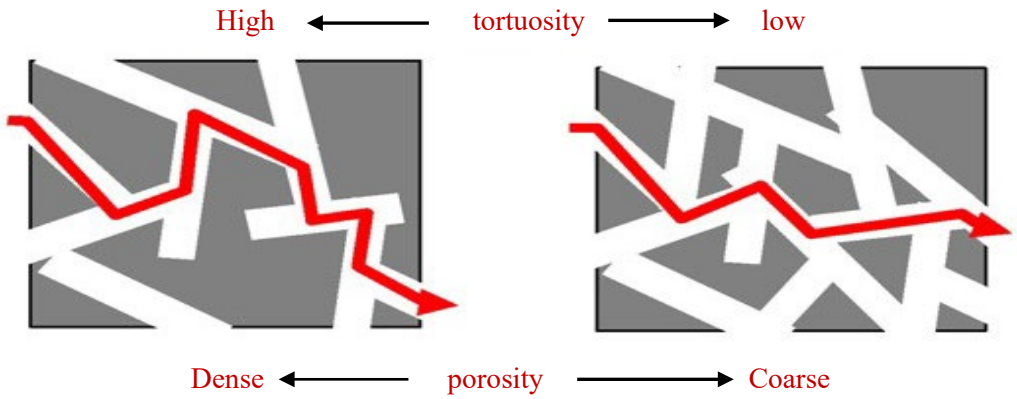

Figure 7.2:Schematic of micro-pore structure of concrete and tortuosity (Ω) (Ishida *et al*., 2014)

$$\Omega = -1.5\, tanh\left(8.0\left(\emptyset_{paste} - 0.25\right)\right) + 2.5 \qquad (7.7)$$

where:

$\emptyset_{paste}$ is the porosity of capillary and gel pores in cement paste (m^3/m^3).

Figure 7.3 illustrates the influence of tortuosity on the chloride concentration profile for two cases (Ω = 1.9 for porosity equal to 0.3 and Ω = 3.0 for porosity equal to 0.2 %). The value of the degree of saturation of porous media (S) changes according to the moisture in the pore structures. The value of (S) is between 0 to 1. It is difficult to account for measure the tortuosity and degree of saturation because it is necessary to measure the path direction of pores and the volume of water. In this study, Ω and S will be taken as 3 and 1 respectively.

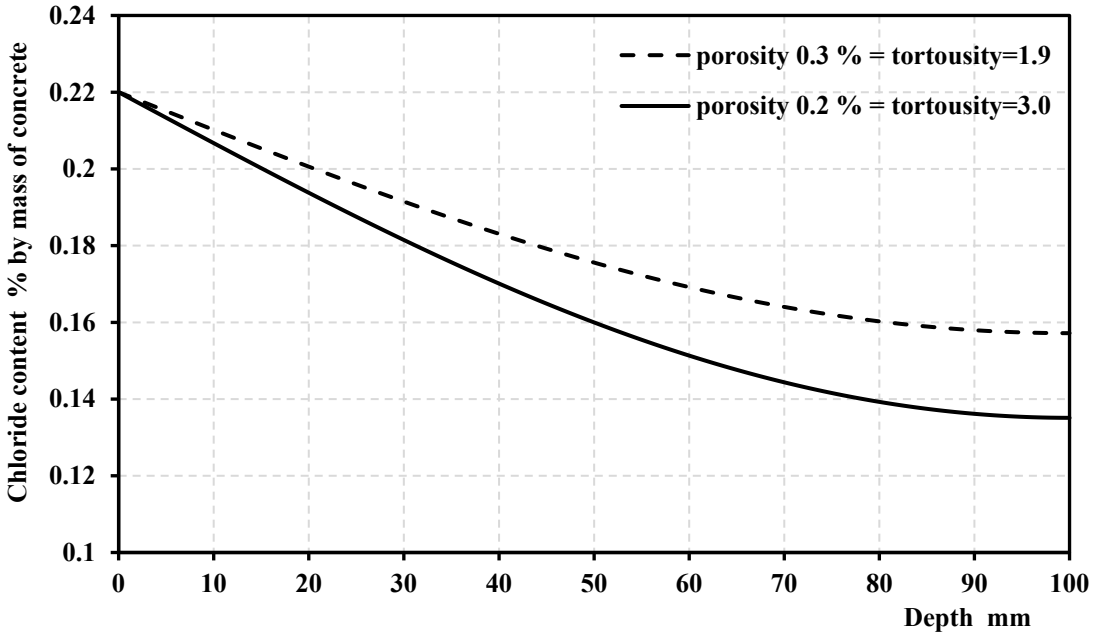

Figure 7.3 Effect of tortuosity factor on the concentration of chloride profile for C_s= 0.22% by mass of concrete.

There are two approaches to an estimate of the diffusion coefficient of chloride: (i): Scientific modelling of D_a: This type of modelling is based on a scientific activity or basic knowledge about the phenomenon under study and seeks (Manson *et al*., 2003). In this study, modelling of D_a describes the different chemical and physical processes that are involved during the ingress of chloride. In this model, the transport and mass balance equation considering the interaction between the ions in the pore solution and the

cementitious matrix is considered. Basically, the diffusion coefficient of chloride in pore solution (free space) (D_{Cl}) is expressed according to Einstein's theory of relativity (Ishida *et al.*, 2014), when the concentration of chloride ions is around 3% NaCl (by mass) by:

$$D_{Cl} = RT\frac{\lambda_{ion}}{Z_{Cl}^2 F^2} \quad (7.8)$$

where:

R is the gas constant (8.314 J/ mol K), T: temperature (K), Z_{Cl} is the electric charge of the chloride ion (=−1C), F is Faraday's constant (9.65×10^4 C/mol), λ_{ion} is ion conductivity ($S.m^2/mol$).

Concerning the molar conductivity of an ion, λ_{ion}, may be affected by temperature dependency, the influence of temperature in λ_{ion} is considered according to the Arrhenius's Law (Yokozeki *et al*., 2003) as shown:

$$\lambda_{ion} = \lambda_{(25)} exp\left[-\frac{E_a}{R}\left(\frac{1}{T}-\frac{1}{298}\right)\right] \quad (7.9)$$

where:

$\lambda_{(25)}$ is Ion conductivity at 25°C, $\lambda_{25}=7.63\times10^{-3}$ ($S.m^2/mol$), E_a is the activation energy for free pore fluid (17.6×10^3 (J/mol)). The D_{Cl} at 25 °C is 2.0310^{-9} m^2/sec. The activity of chloride ion in penetration or diffusion coefficient can be increased by 12% if the temperature is increased to 30 °C.

Essentially, the size and connectivity of the pore structures are considered the main path of diffusion of fluid in concrete and this system of pores mainly depends on the water/cementitious materials (w/cm) ratio (Neville, 2011; Shi *et al*., 2014). When the porosity and w/cm ratio are lower, the pore system and path of transportation of chloride ions may be tight, which gives a lower transport rate of fluid and a lower active diffusivity. In order to find the diffusion coefficient of chloride in concrete, the term ($D_{a,ref}$) needs to consider the pore volume percentage in cement paste (V_v), based on the quantity of water remaining and not used in the hydration process as estimated by Papadikas and Tsimas (2002), and the fraction of aggregate in concrete factor (f_{agg}) as assumed by Shi *et al*. (2014).

$$D_{a,ref} = D_{Cl}\, V_v\, f_{agg} \quad (7.10)$$

$$V_V = \left(\frac{\frac{w-0.267(C+P)}{\rho_W}}{\frac{C}{\rho_C}+\frac{P}{\rho_P}+\frac{W}{\rho_W}}\right)^3 \quad (7.11)$$

$$f_{agg} = \frac{1-V_a}{1+V_a} \quad (7.12)$$

where:

C is the cement content (kg), w is the water content (kg), ρ_C is the absolute density of cement (3150 kg/m^3), ρ_w is the density of water (1000 kg/m^3), ρ_P is the absolute density of supplementary cementing materials(1800-2800 kg/m^3), V_a is aggregate weight to concrete weight ratio and P is the amount of supplementary cementing materials(kg).

(ii): Empirical modelling of coefficient of chloride, D_a: which generally utilize experimental data to predict chloride ingress in concrete. The time dependency of D_a and some of the other parameters have been considered to propose the empirical models of D_a. It was found that the most critical factor influencing apparent diffusion of concrete is the porosity of concrete. The w/cm ratio has a significant impact on the porosity of the concrete. Therefore, the correlation between apparent diffusion coefficient D_a and effective porosity or w/cm can be used to model the depth of chloride penetration due to exposure to wet-dry cycles of chloride solution. The experimental results of this study showed the temperature of exposure chloride spraying considerably affected the penetrability of chloride in concrete samples. Finally, D_a can be considered as a function of a concrete type, w/cm ratio and exposure condition e.g. temperature RH and the duration of exposure and age of concrete.

The Life -365 (ACI 365.1 R: 2014) proposed the model of diffusion chloride coefficient at 28 days with a temperature of 20°C with the w/cm ratio for concrete without supplementary cementitious materials, SCMs as shown in Equation 7.13.

$$D_{a(28)} = 10^{\left(-12.06+2.4\frac{w}{c}\right)} \quad (7.13)$$

From the experimental data obtained through this study (Tables 6.17 to 6.19), the influence of w/cm and temperature (T) on apparent diffusion coefficient, D_a (as shown in Equation 7.14 and Figure 7.4) has been calculated by linear regression analysis using the statistical programme, Statistics. The main data from Series 1, 2 and 3 was used in this analysis to find the w/cm and temperature influence. The correlation coefficient (R) was

0.9384 and all correlations were statistically significant at the P= 0.0017 level (see section C-1-a (Appendix C)).

$$D_a = \left(1.3889 + 18.3333\ \frac{w}{c} + 0.3\ T\right) 10^{-12} \qquad (7.14)$$

where:

The apparent diffusion coefficient, D_a in m^2/s at 15 weeks of exposure duration and the temperature, T is in (°C)

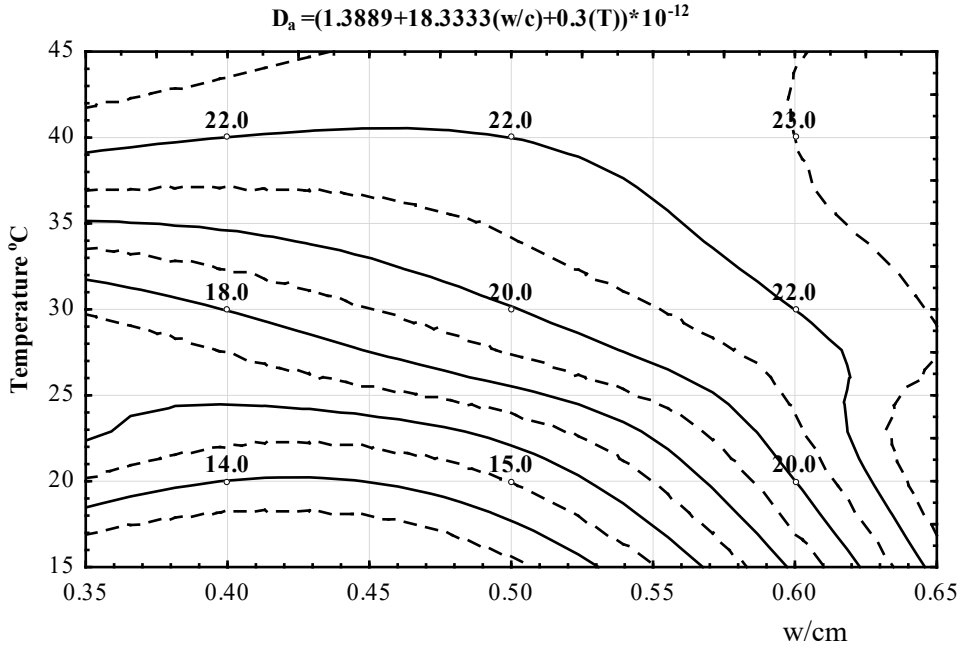

Figure 7.4: Effect of w/cm ratio and temperature on apparent diffusion coefficient (D_a = *10^{-12} m^2/sec)

In addition to the period of duration exposure and the age of the concrete, D_a is thought to be a function of concrete type, w/cm ratio and exposure condition e.g. temperature and relative humidity, etc. Vu and Stewart (2000); Val and Trapper (2008) considered the effect of temperature, T, pore relative humidity on D_a, but they were not considered the influence of crack and properties of concrete on the D_{CO2}. On the other hand, Sheo-Feng *et al.* (2011) reported the crack width, W_c on diffusion chloride coefficient based on an artificial crack without taking into consideration the type of concrete. Because the main objective of this study is to investigate the effect of climate change on the durability of concrete. The study should focus on the effects of global climate change, change in CO_2 concentrations, temperature, relative humidity and crack width as well as the properties of concrete (different types of concrete). For the simulation

of D_a, these parameters, *T, RH,* W_c and properties of concrete will be taken into consideration (Equation 7.15) and predicted chloride concentration with depth and time to determine the initiation of corrosion time due to chloride penetration.

$$D_a = D_{a,ref} f_{C1}(t) f_{C2}(T) f_{C3}(RH)\, f_{C4}(W_c) \qquad (7.15)$$

where:

$D_{a,ref}$ is the value of D_a at reference condition (i.e. at the reference temperature, time and relative humidity) and it can be obtained by either Equation 7.10 or 7.13, $f_{c1}(t), f_{c2}(T), f_{c3}(RH)\ and\ f_{c4}(W_c)$ are functions of time, temperature, relative humidity and crack width, respectively. Analytical explanation of these factions will be given in the following section.

Bamforth *et al*. (1997) reported the D_a decreased rapidly in the first five years, beyond that it may be a constant value, Takewaka and Mastumoto (1988) proposed the dependency of this coefficient $D_a(t)$ on the exposure period t , using empirical formula which designates the reduction of diffusion coefficient with time according to the materials (e.g. mix proportions) and the environment (e.g. temperature and humidity). The following equation has frequently been suggested in the literature:

$$f_{c1}(t) = \left\{\frac{t_{ex}}{t}\right\}^m, t>t_{ex}\ ,\ 0 \le m \le 1 \qquad (7.16)$$

where:

t_{ex} is initial exposure time, t is a specific time and m is the ageing factor (diffusivity reduction factor), depending on the development of strength of the concrete, w/cm ratio and type of cementitious materials used in mortar /concrete such as cement, silica fume, fly ash and GGBS and environmental conditions (Broomfield, 2007). In experimental results, the ageing factor values were 0.21-0.65 according to w/cm ratio as shown in Table A.3(Appendix A). CEB-FIP (2010); ACI Committee 365(2018); Wang *et al*. (2016) reported the ageing factor is likely to be between 0.2 and 0.8. On the other hand, the ACI Committee 365(2018) reported the relationship shown in Equation 7.13 is assumed to be only valid up to 25 years, beyond which $D(t)$ stays constant at the D_a (25 years) value and the diffusion coefficient stops continually decreasing with time.

The impact of temperature on all chemical reactions is based on the Arrhenius Equation. The diffusivity of chloride ions in concrete is one of the chemical reactions.

The diffusivity of Cl^- can be broken down into two sequences, the CO_2 spreads in concrete and dissolves into the pore water coating the pore walls and some of the amount of chloride may react with dissolved hydrated products of cement which form Friedel's salt. Val and Trapper (2008); Thomas *et al*. (2012) have proposed Equation 7.17 to simulate the temperature dependence of the diffusion coefficient of chloride in concrete.

$$f_{c2}(T) = exp[\frac{U_c}{R}(\frac{1}{T_{ref}} - \frac{1}{T})] \quad (7.17)$$

where:

U_C is the diffusion activation energy. The activation energy for chloride diffusing in concrete has been experimentally determined by Page *et al*. (1981),depending on its water-cementitious materials ratio (w/cm) and are 41.8±4.0 (kJ/mol) for w/cm = 0.4, 44.6±4.3 (kJ/mol) for w/cm = 0.5, and 32.0±2.4 (kJ/mol) for w/cm = 0.6. R is the gas constant (8.314 J/mole. K), T_{ref} is a reference temperature (298 K) and T is the temperature of interest (K).

Relative humidity or moisture content is one important factor influencing the chloride concentration in concrete, to consider. Where pore water transports the chloride ions and oxygen to the concrete-steel interface surface. In other words, moisture content controls the availability of chloride and oxygen at the steel surface (Markeset and Myrdal, 2008). Val and Trapper (2008) have proposed the function of relative humidity related to chloride penetration in terms of diffusion of chloride coefficient, as given in Equation 7.18.

$$f_{c3}(h) = \left[1 + \frac{(1-h)^4}{(1-h_c)^4}\right]^{-1} \quad (7.18)$$

where:

$f_{c3}(h)$ is a function of relative humidity, h is the humidity percentage, h_c is the critical humidity level at which the diffusion coefficient drops halfway between its maximum and minimum value (hc=0.75) (Val and Trapper, 2008).

Angst *et al.* (2009) also reported that the amount of water in the concrete pores influences the distribution between bound and free chloride and therefore determines the free chloride concentration in pore liquid. On the other hand, the optimum relative humidity to achieve movement of chloride in concrete ranges between 90 and 95 (Shi *et al*., 2014).

Finally, the presence of cracks and permeable pores in concrete has a significant impact on diffusion and permeation of chloride ions in concrete (Sheo -Feng *et al*., 2011). The type and width of the crack influence the permeability of chloride in concrete. Results of previous studies have shown that the crack opening significantly influences the ability of chloride ions to diffuse along a crack. On the other hand, no chloride diffusion occurs in cracks with an opening of critical value (threshold value) or less (Ismail *et al*., 2004). At crack openings greater than the threshold value, chloride diffusion along the crack path depends on mortar age (Ismail *et al*., 2008). The chloride ions mainly penetrate the sides of the crack-like external layer of the sample.

From the experimental data obtained through this research (Tables 6.17to 6.19), the influence of crack width (W_c) on the apparent diffusion coefficient, D_a (as shown in Equation 7.19 and Figure 7.5) has been calculated by non-linear regression analysis using the statistical programme, Statistics. The main data from Series 1,2 and 3 were used in this analysis to find the crack factor influence, $f_{c4(Wc)}$. The correlation coefficient (R) was 0.956 and all correlations were statistically significant at the P= 0.000 level (see section C.1-b in Appendix C).

$$f_{c4(W_c)} = 0.934W_c^{\,2} + 0.974W_c + 1 \qquad (7.19)$$

where:

$f_{c4(Wc)}$ is Proportion of diffusion coefficient in the cracked sample ($D_{a(cracked)}$) to diffusion coefficient in the un-cracked sample ($D_{a(un\text{-}cracked)}$); W_c is the crack width in mm.

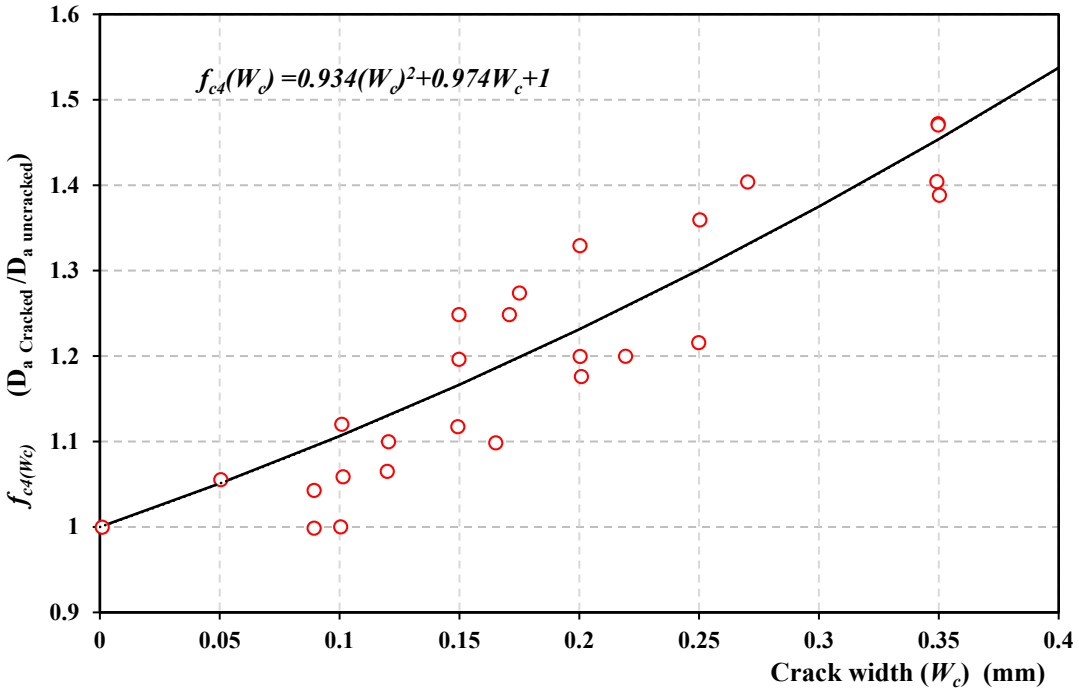

Figure 7.5: Effect of crack width on the chloride diffusion coefficient

7.2.2 The Surface Concentration of Chloride

The surface concentration of chloride ions on the first layer of the sample can be obtained according to environmental conditions. In addition to the time and age of exposure, surface concentration of chloride, C_s is thought to be a function of concrete properties, w/cm ratio (Chalee *et al*., 2009), exposure environment e.g. marine and de-icing state (Song *et al*., 2008; ACI Committee 365: 2018) and exposure condition e.g. temperature and relative humidity, etc.

Firstly, for concrete structures exposed to the de-icing environment, Kassir and Ghosn (2002) proposed a surface chloride concentration model based on field investigations by testing 15 bridges' decks exposed to deicing salt in the snow belt region for 15 years as shown in Figure 7.6.

$$C_s = C_o(1 - e^{-\alpha t}) \qquad (7.20)$$

where:

C_o is maximum value of chloride (5.343 kg/m^3), α is age factor and equal to 0.25 (year $^{-1}$), and t is the time measured in years.

A ramp-type surface chloride concentration was applied by Phurkhao and Kassir (2005) for surface chloride on bridge decks which is mainly derived from de-icing salt and t_o as shown in Figure 7.6 and Equations 7.21 to7.22.

$$C_s(t) = \frac{C_o}{t_o}\, t \qquad 0 \le t \le t_o \qquad (7.21)$$

$$C_s(t) = C_o \qquad t \ge t_o \qquad (7.22)$$

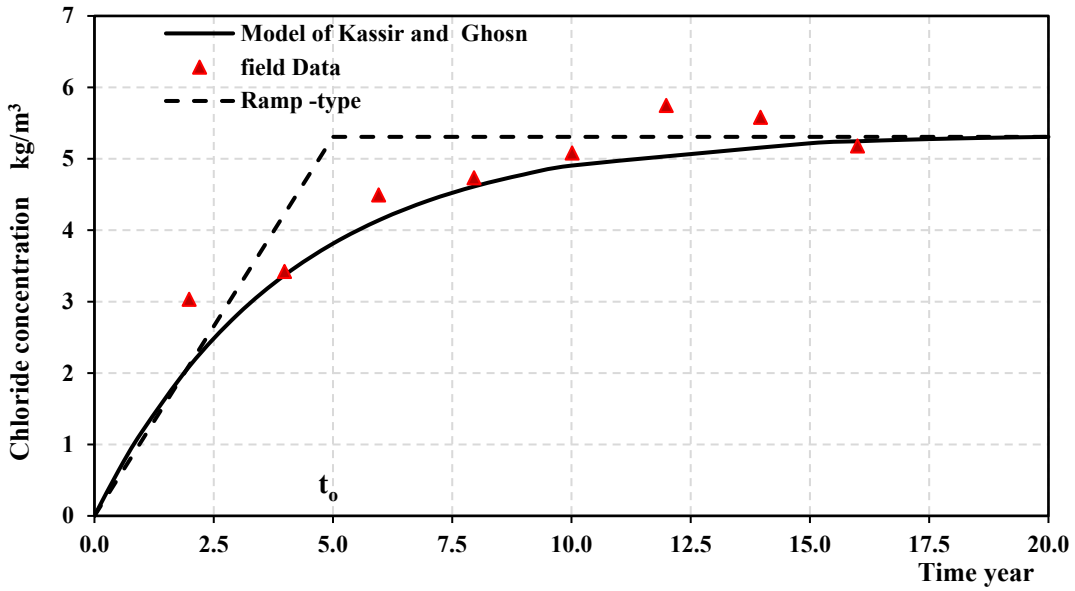

Figure 7.6: Exponential representation of the C_s data Phurkhao and Kassir (2005)

Secondly, for concrete structures exposed to the marine environment, Song *et al*. (2008) proposed a model to predict the surface chloride concentration considering the time-dependence, the initial build-up of chlorides on the surface of concrete and the type of exposure (e.g. tidal/splash, submerged zone, and aerated zone). These models cannot be used to predict the chloride concentration of concrete structures exposed to a marine environment for both very short and long term. The chloride content at an early stage of exposure in a chloride environment is invalidated. The following model empirically derived from published data on C_s is proposed to consider the initial build-up of chlorides as shown in Equation 7.23 (Song *et al*., 2008).

$$C_s(t) = C_{si} + \beta\, ln(t) \qquad (7.23)$$

where:

$C_s(t)$is surface chloride concentration at time t (% /m^3); C_{si} is surface chloride at the standard time (1 year or 28 days) (%/m^3) and β is a constant value.

The values of C_{si} and β are based on the environmental condition, e.g. 3.0431% by mass of cement and 0.685 respectively.

7.3 Numerical Analysis of Chloride, $CO_{2(aq)}$ and $Ca(OH)_{2(aq)}$ Penetration in Concrete Structures

7.3.1 Introduction

The finite element methods have become a commonly used method to solve a group of applications in engineering fields. The finite element method, FEM is based on the separation of structures into a finite elements number linked by nodes (Cook, 2007). The uses of the FEM method has improved significantly as personal computers have become more readily accessible. Many scientific engineering finite elements modelling packages have been produced such as ADINA, ABAQUS, ANSYS, COMSOL, etc. In the present study, a non-linear finite element technique (NLFET) was used to determine chloride ions concentration profile and the depth of carbonation by finding the diffusivity of $CO_{2(aq)}$ and $Ca(OH)_{2(aq)}$ in concrete using the commercially existing FEM package COMSOL Multiphysics version 5 (COMSOL, 2015). In the first case, this software was used to simulate the chloride concentration profile in concrete. In the second case, the software was used to simulate the diffusivity of $CO_{2(aq)}$ and $Ca(OH)_{2(aq)}$ in concrete. In both cases, Transport of Diluted Species in Porous Media Method (tds) was used.

7.3.2 Theory of the Transport of Species (Cl^-, $CO_{2(aq)}$ and $Ca(OH)_{2(aq)}$)

The transportation of diluted species interface offers a predefined exhibiting environment for studying the evolution of chemical species transported by diffusion and convection. The interface assumes that all species are dilute; which means that their concentration is small compared to a solvent fluid or solid. As a rule of thumb, a mixture containing several species can be considered diluted when the concentration of the solvent is more than 90 mole %. Due to the dilution, mixture properties such as density and viscosity can be assumed to correspond to those of the solvent. Fick's law governs the diffusion of the solutes dilute mixtures or solutions (Yoon *et al*., 2007; Dyer, 2014). The transportation of diluted species interface supports the simulation of chemical species transport by convection and diffusion in one dimensional (1D), two dimensions (2D), three dimensions (3D) as well as for axisymmetric models:

a. Mass Balance Equation

b. Convective Term Formulation

c. Solving a Diffusion Equation Only

a: Mass Balance Equation

The default node attributed to the Transport of Diluted Species Interface assumes chemical species transport through diffusion and convection and it implements the mass balance equation (Bastidas-Arteaga *et al.*, 2010; Val and Trapper, 2008; Ishida *et al*., 2014):

$$\frac{\partial c}{\partial t} + u\nabla_c = \nabla(D_s\nabla_c) + R_c \qquad (7.24)$$

where:

c is the concentration of the species (mole/m^3 or % by mass of cement), ∇_c is $\frac{\partial c}{\partial x}$, D_s is the diffusion coefficient of species (m^2/s), R_c is a reaction rate expression for the species (mole/(m^3·s)) and u is the velocity vector (m/s).

The first term on the left-hand side of Equation 7.24 corresponds to the accumulation (or indeed consumption) of the species. The second term accounts for the convective transport due to a velocity field u. This field can be expressed analytically or can be obtained from coupling this physics interface to one that describes fluid flow

(momentum balance). To include convection in the mass balance equation, an expression that includes the spatial and time variables, or else the velocity vector component variable names from a fluid flow interface can be entered into the appropriate field. The velocity fields from existing fluid flow interfaces are available directly as predefined fields. On the right-hand side of the mass balance equation (Equation 7.24), the first term describes the diffusion transport. A field for the diffusion coefficient is available in the interface and an equation that relates to another variable, such as temperature, can be entered there. The node has a matrix that is used to describe the diffusion coefficient if it is vectorized or is a tensor. An isotropic diffusion can, therefore, be simulated here. Finally, the second terms on the right-hand side of Equation 7.24 represent a source or sink term (consumption, see Equations 7.48 and 7.49), typically due to a chemical reaction. In order for the chemical reaction to be specified, another node must be added to the Transport of Diluted Species interface- the Reaction node, which has a field to specify a reaction equation using the variable names of all participating species.

b. Convective Term Formulation

The default node attributed to The Transport of Diluted Species Interface assumes chemical species transport through diffusion and convection and implements the mass balance equation in Equation 6.24. There are two ways to present a mass balance where chemical species transport occurs through diffusion and convection. These are the non-conservative and the conservative formulations of the convective term:

$$non-conservative: \quad \frac{\partial c}{\partial t} + u\nabla c = \nabla(D_c \nabla c) + R_c \tag{7.25}$$

$$\text{conservative:} \quad \frac{\partial c}{\partial t} + \nabla(cu) = \nabla(D_c \nabla c) + R_c \tag{7.26}$$

Each formulation is treated slightly different by the solver algorithms. In these equations D_s (SI unit: m^2/s) is the diffusion coefficient of species, R_c (SI unit: $mol/(m^3 \cdot s)$) is a production or consumption rate expression, and u (SI unit: m/s) is the solvent velocity field. The diffusion process can be anisotropic, in which case D_s is a tensor. If the conservative formulation is expanded using the chain rule, then one of the terms from the convection part, $c\nabla \cdot u$, would equal zero for an incompressible fluid and would result in the non-conservative formulation above. This is, in fact, the default formulation in this interface and ensures that nonphysical source terms cannot come from the solution of a flow field.

c. Solving a Diffusion Equation Only

Remove the convection term from Equation 7.25 and Equation 7.26 by clearing the Convection check box in the Transport Mechanisms section for The Transport of Diluted Species interface. The equation then becomes:

$$\frac{\partial c}{\partial t} = \nabla(D\nabla c) + R \qquad (7.27)$$

7.3.3 Model Geometry and Meshing using Programme

The geometry of the full specimen was characterised by a two-dimensional full specimen (100*100*500 mm). The mesh settings determine the resolution of the finite element mesh used to discretize the model. The finite element technique is the method to divide the model into small elements of geometrically simple shapes. This was achieved by defining boundary conditions. Figure 7.7 demonstrates the simple schematic of the mesh model geometry of concrete samples (with and without a crack) which were modelled as collected together to simulate this model. The concrete was modelled with a 3-node free triangle element available in the programme's element library. This element type has concentrated integration stiffness (Ngo and Scordelis, 1967). This element can be also used for nonlinear analysis counting that of integration. The maximum and minimum element size of the mesh, and the curvature factor was 1.3 mm, 0.004 mm and 0.6 respectively.

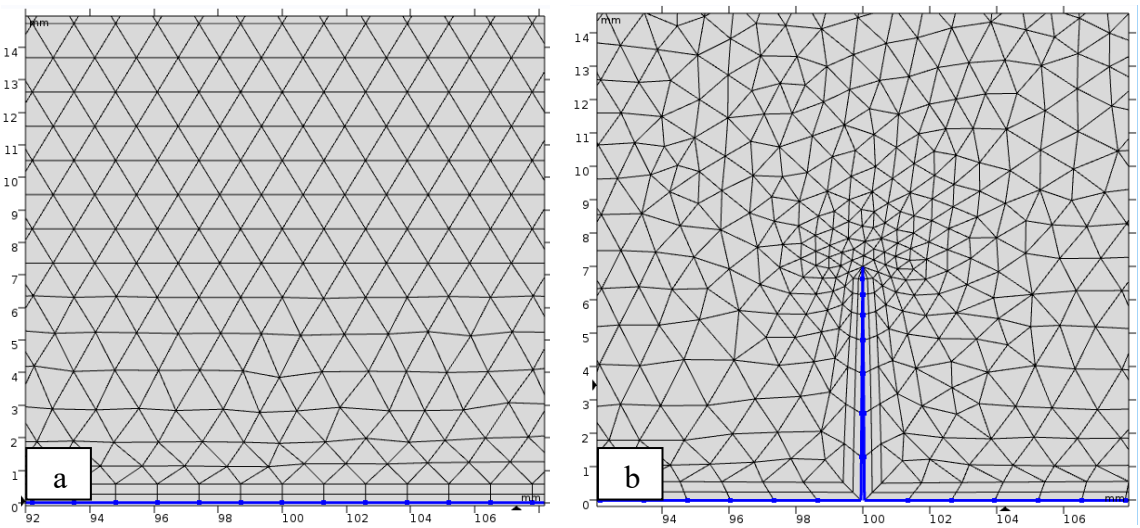

Figure 7.7: Geometry of meshing, a: Un-cracked sample, b: Cracked sample

7.3.4 Frame Work of Numerical Analysis of Species Diffusion

In this section, the numerical results of the diffusivity of chloride ions (Cl^-), aqueous of carbon dioxide ($CO_{2(aq)}$) and Aqueous of calcium hydroxide($Ca(OH)_{2(aq)}$) in different concrete specimens were plotted. All the samples were modelled with the FE package COMSOL Multiphysics. Where the diffusivity of Cl^-, $CO_{2\ (aq)}$ and $Ca(OH)_{2(aq)}$ have been modelled.

Numerical analysis of diffusivity is based on properties of concrete samples; some properties were obtained from Chapter 4 such as density, porosity, and compressive strength. While, the other parameters were computed from the proposed model in the first section of the current chapter such as the chloride diffusion coefficient in section 7.2 and carbon dioxide diffusion coefficient in section 7.6, whilst the modulus of elasticity, Poisson's ratio were based on the proposed equations by AL-Ameeri *et al*.(2013) and thermal conductivity, T_C depended on relationships of ACI 122R(2002). The steps using numerical analysis is shown in Figure 7.8. Some of the samples were uncracked and the others were cracked. The crack depth (d_{crack}) was found by using ultrasonic pulse velocity and summarised many of the samples as shown in Figure C-3(Appendix C). These results are dependent on the geometry of shape in the simulation. All the properties of concrete that were used in simulation and numerical analysis are summarised in Table 7.1.

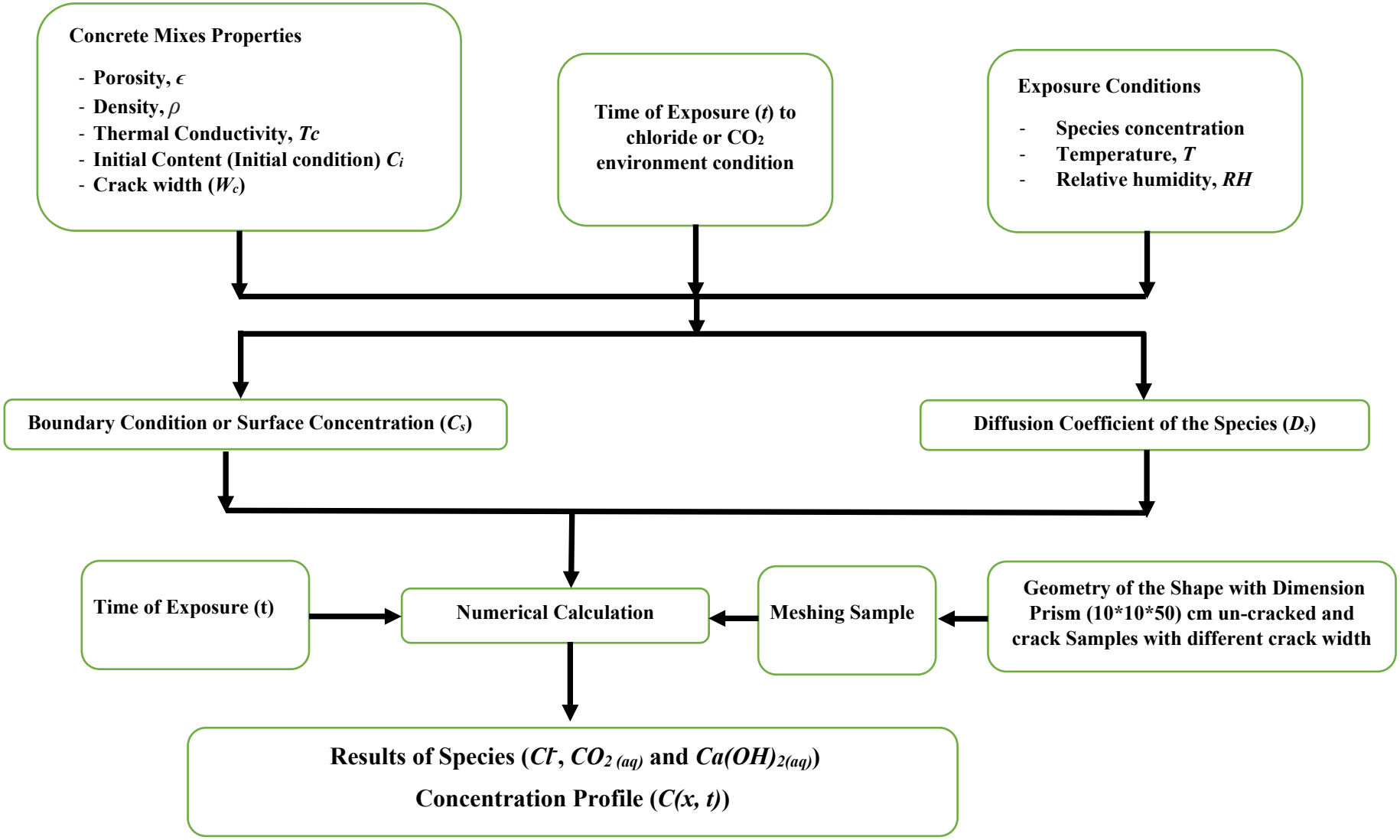

Figure 7.8: Flowchart of numerical analysis using the FEA programme

Table 7.1: The properties of concrete used in numerical analysis

Mix	Density, Wet 100% ρ kg/m^3	Density, Wet 50% kg/m^3	Density, Dry kg/m^3	Porosity ϵ %	Comp. Strength MPa	Modulus of Elasticity E_C (Gpa)*	Poisson's ratio** μ	T_C*** (W/m. K)
M 0.4	2301	2257	2214	9	57.8	43.5	0.17	1.15
M 0.5	2249	2198	2148	10	50.93	40.5	0.18	1.06
M 0.6	2237	2182	2128	11	43.3	36.5	0.20	1.03
M 0.5 + 0.3 GGPS	2254	2205	2157	10	35.53	31.8	0.22	1.07
M 0.5 + 0.35 PFA	2261	2217	2173	9	48.2	39.1	0.19	1.09

*M.O.E is the modulus of elasticity was computed by Equation 7.28-a and 7.28-b (AL-Ameeri *et al*., 2013) or (ACI 318:2014) respectively:

$$M.O.E = 24.16 * ln(fcu) - 55.691 \quad (7.1\text{-a})$$

$$M.O.E = 57000 * (fcu)^{0.5} \quad (7.2\text{-b})$$

** Poisson's was calculated according to AL-Ameeri and AL-Rawi (2009).

*** T_C is the thermal conductivity was determined by Equation 7.29 (ACI 122R: 2002), it is in (W/m. K).

$$T_c = 0.072\, e^{0.00125\rho_d} \quad (7.29)$$

where: ρ_d denotes the oven- dry density in kg/m^3.

7.4 Verification of Numerical Analysis of Chloride Concentration in Concrete Samples

The verification of the chloride transport model was done by comparing two types of experimental results for two cases, un-cracked and cracked:

a: Experimental Results of This Study

In the experimental programme, 180 concrete prisms (10*10*500 cm) were tested. These were un-cracked and cracked respectively. For the un-cracked and cracked specimens, different w/cm ratios were tested, while for the cracked ones, different crack width and depth were examined. These specimens were exposed to chloride spraying with 5% NaCl on one surface for about 115 days to simulate the penetration of chloride in a one-dimensional flow, as presented in Figure 7.9. The profile of total chloride content was measured by the titration technique and the results of the cases are presented in Table 6.1-6.15.

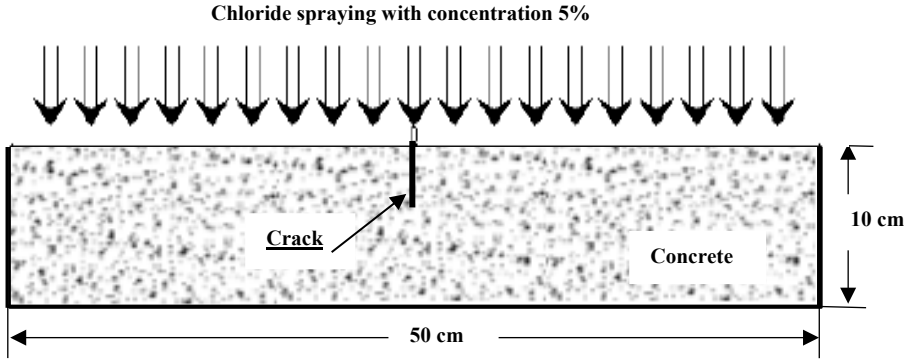

Figure 7.9: Schematic of sample exposed to chloride spraying condition

In this research, a finite element programme was used to solve Equation 7.1, which governs the time-dependent mass transfer of chloride and convection flow. The programme is validated by comparing its results with available experimental data collected in the experimental programme. The use of FEA is based on the computed properties of concrete and the mixture. For any arbitrary initial state (in this case, initial chloride content was 0.26-0.5 % by mass of cement according to the mix proportion) and boundary conditions or membrane (in this case, surface chloride concentration), the vapour pressure in pores (u_D), relative humidity (RH), and moisture distribution or degree of saturation (S) are mathematically simulated according to a moisture transport model (convection) that considers both vapor and liquid phases of mass transport (diffusion). The moisture distribution, RH, and micro-pore structure characteristics, in turn, control the Cl^- diffusion and rate of various chemical reactions under arbitrary environmental

conditions (e.g temperature) (Ishida *et al*., 2014). In this section of the study, the chloride transportation in uncracked and cracked concrete will be simulated as shown in Figure 7.9. The diffusion chloride coefficients (D_a) for the sample are computed according to Equations 7.1-7.19 and presented in Tables 7.2. While, surface chloride concentrations (C_s) are used for experimental data as shown in Tables 6.17-6.18. In this study, un-cracked and three crack width levels were simulated. The width and depth of crack were based on Figure C-3 using crack width 0.05-0.15mm, 0.15-0.25mm and 0.25-0.35 mm with crack depth 20, 30 and 35 mm respectively. To simplify the analysis, a numerical analysis was used by (FEM) to compute the chloride concentrations profile, *C (x, t)* as shown in Figure 7.10. Where, simulation figures of chloride concentration profile show the influence of the crack in an increase of penetration and concentration of chloride with an increase in the crack width and depth.

Table 7.2: $D_{a,\,ref}$ value with fraction aggregate, pore volume ratio, temperature, relative humidity, and crack width

Sample	V_a	f_{agg}	V_v	$D_{a,ref}$ at 40 °C $m^2/sec * 10^{-12}$			
				Un-cracked	**0.05-0.15 mm**	**0.15-0.25 mm**	**0.25-0.35 mm**
M 0.4	0.695	0.180	0.185	21	22	26	29
M 0.5	0.738	0.151	0.320	19.6	23.6	26.5	29.3
M 0.6	0.759	0.137	0.353	23.3	26.6	30	33.4
M 0.5 + 0.35 PFA	0.738	0.151	0.353	22.3	25.2	28.4	31.6
M 0.5 + 0.30 GGBS	0.738	0.151	0.364	24.5	27.6	31.1	32.9

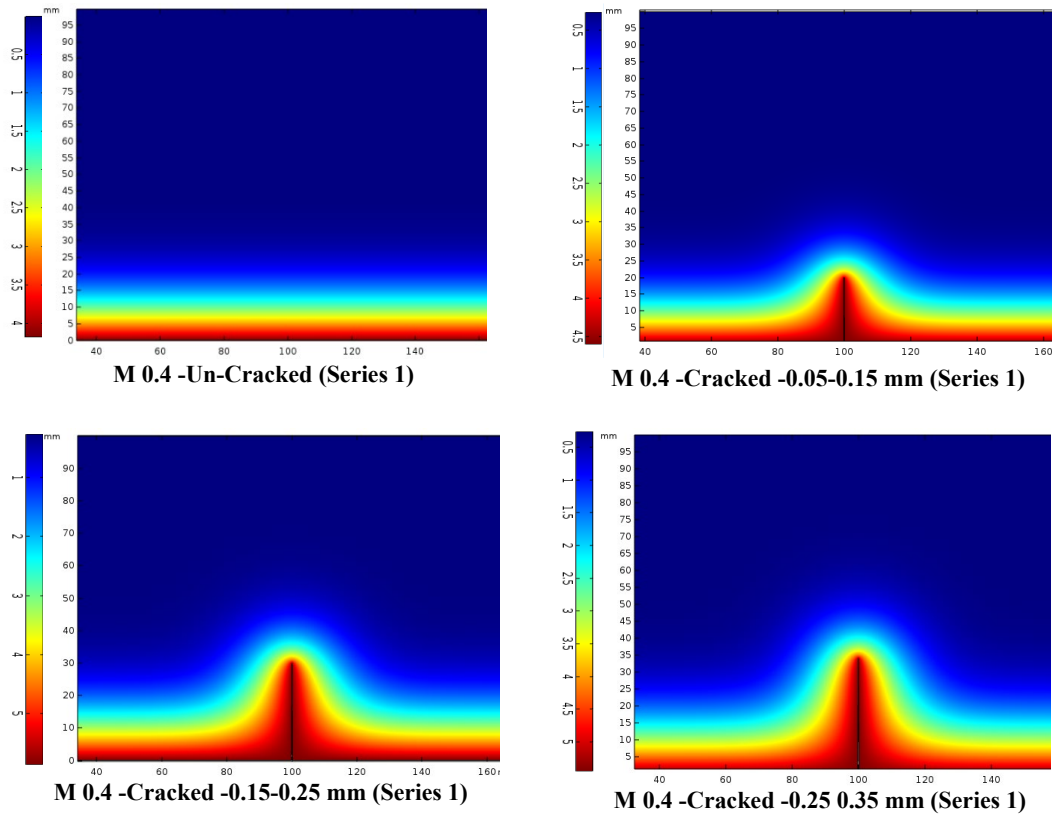

Figure 7.10: Chloride concentration distribution in the samples with and without a crack due to exposure to chloride environment at 40 ºC for 115 days

The computational results of chloride concentration by solving the partial differential equation shown in Equation 7.1 compared with experimental results for Series 1 (at temperature 40 ºC) (cracked and Uncracked) are presented in Figure 7.11 according to Ning and Li (2015). A qualitative difference in trend is seen in the square of this correlation coefficient, R^2 between the model predicted and the experimental results as shown in Figure 7.11 and in Table 7.3. The analytical results from using a model based on diffusion-convection illustrated the shape of the distribution of chloride concentration obtained from the analysis and experimental data were well-matched. Where, in the analytical results, the surface concentration was relatively high, with a trend of a sharp reduction in chloride concentration with depth. On the other hand, the experimental results using the titration method in the test showed the actual measured value of chloride concentration at the first point of depth was a curve that is convex downwards. This kind of anomaly between both results has been reported in the past research as well (Ishida *et al*., 2014).

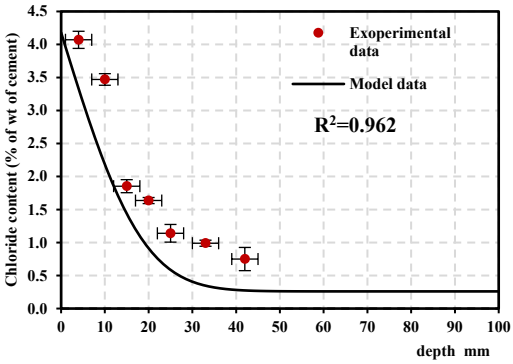

a: M 0.4 Un-Cracked (Series 1)

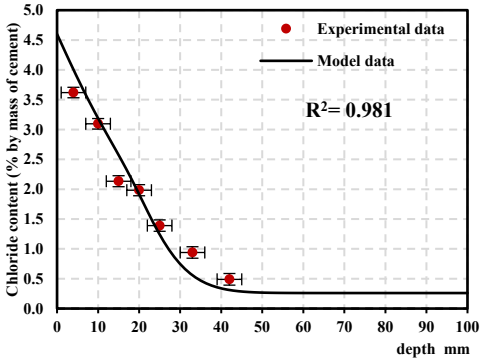

b:M 0.4 Cracked -0.05-0.15 mm (Series 1)

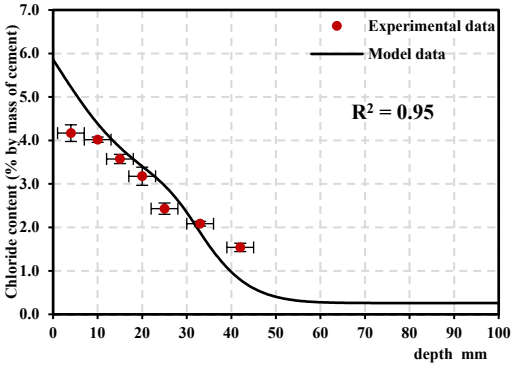

c:M 0.4 Cracked -0.15-0.25 mm (Series 1)

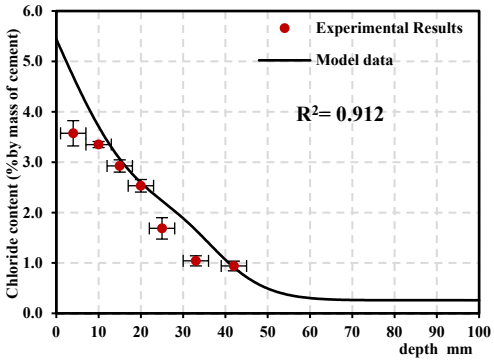

d:M 0.4 Cracked -0.25-0.35 mm (Series 1)

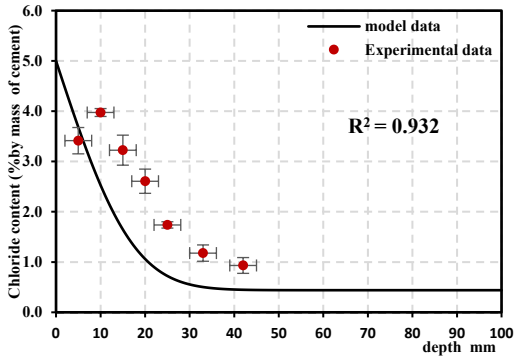

e:M 0.5 Un-Cracked (Series 1)

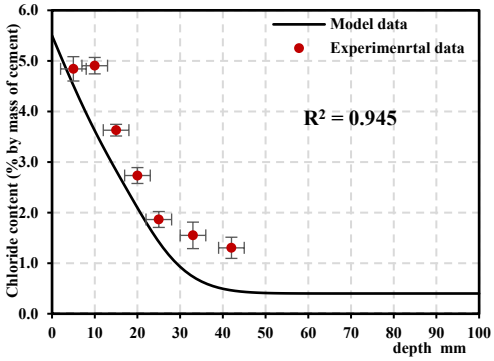

f:M 0.5 Cracked -0.05-0.15 mm (Series 1)

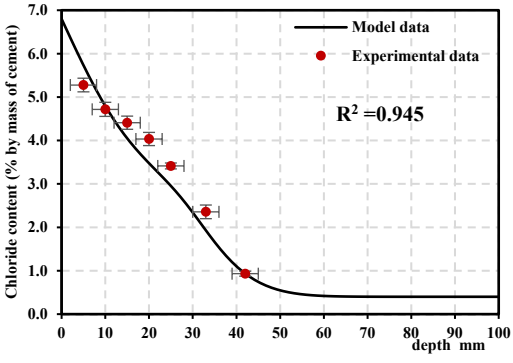

g:M 0.5 Cracked -0.15-0.25 mm (Series 1)

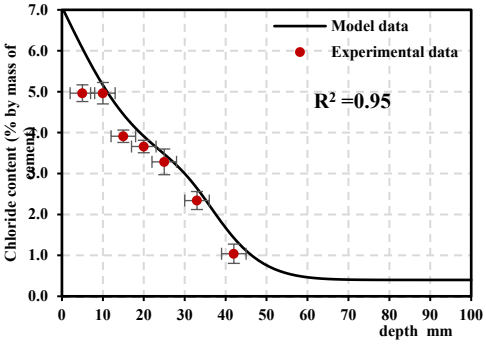

h:M 0.5 Cracked -0.25 0.35 mm (Series 1)

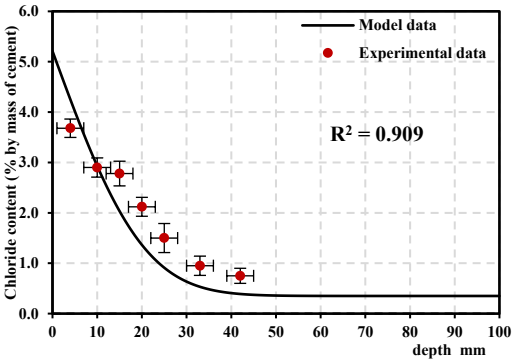

i:M 0.6 Un-Cracked (Series 1)

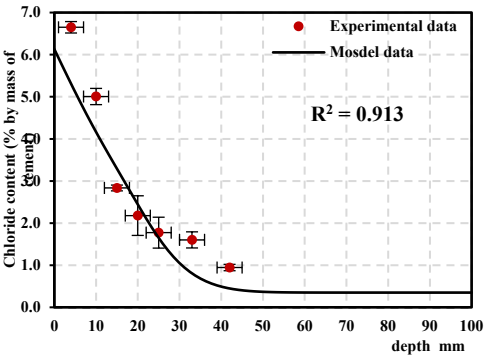

j:M 0.6 Cracked -0.05-0.15 mm (Series 1)

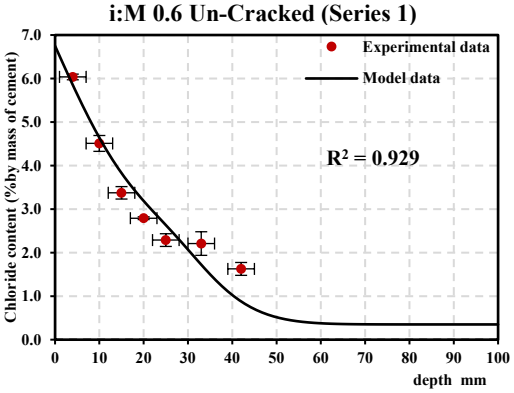

k:M 0.6 Cracked -0.15-0.25 mm (Series 1)

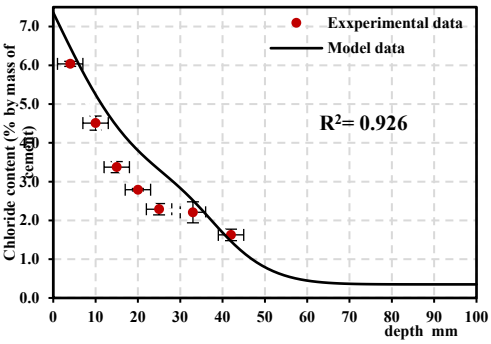

l:M 0.6 Cracked -0.25-0.35 mm (Series 1)

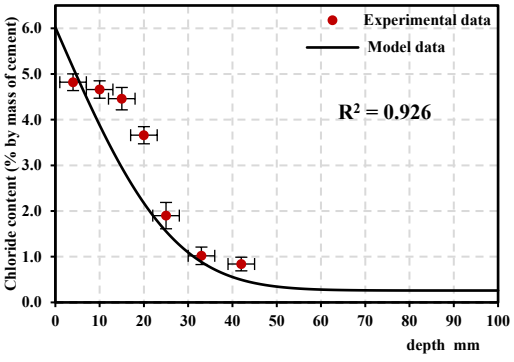

m:M GGBS Un-Cracked (Series 1)

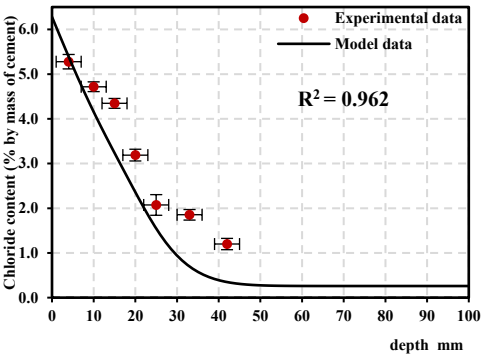

n:M GGBS Cracked -0.05-0.15 mm (Series 1)

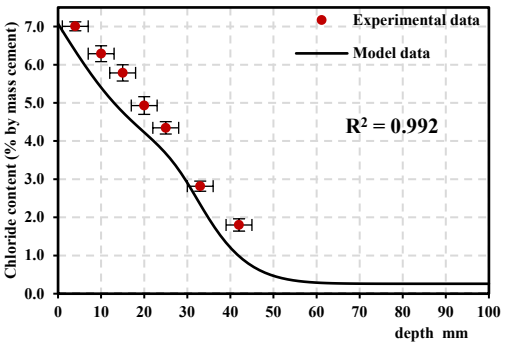

o:M GGBS Cracked -0.15-0.25 mm (Series 1)

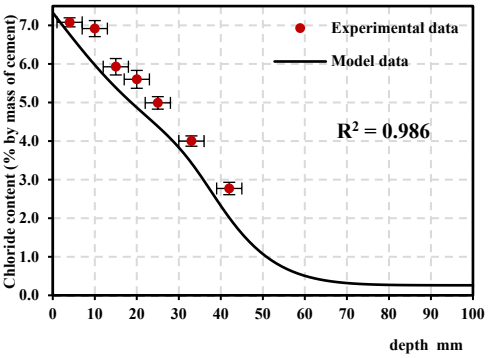

p:M GGBS Cracked -0.25-0.35 mm (Series 1)

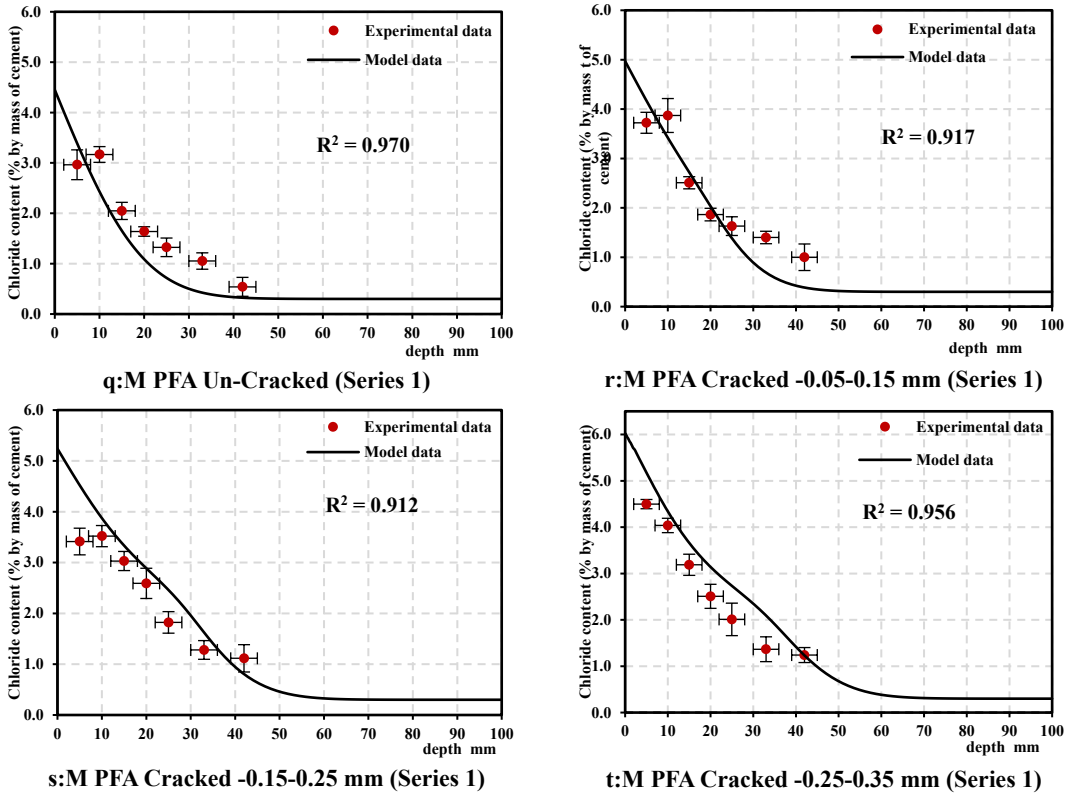

Figure 7.11: Chloride concentration, numerical vs experimental results for Series 1(40 ºC)

Table 7.3: Correlation coefficient, R^2 of model predicted chloride concentration and the experiment results for Series 2(30 º C) and Series 3(20 º C)

Sample	Un-cracked		0.05-0.15 mm		0.15-0.25 mm		0.25-0.35 mm	
	Series 2	Series 3	Series 2	Series 3	Series 2	Series 3	Series 2	Series 3
M 0.4	0.947	0.915	0.986	0.984	0.881	0.984	0.973	0.846
M 0.5	0.983	0.931	0.978	0.948	0.989	0.941	0.985	0.850
M 0.6	0.989	0.96	0.977	0.976	0.965	0.974	0.964	0961
M 0.5+ GGBS	0.936	0.888	0.9	0.932	0.877	0.907	0.934	0.982
M 0.5+ PFA	0.948	0.916	0.897	0.918	0.916	0.898	0.980	0.892

It can be seen from Figure 7.11, the analytical data of model matched well with the experimental results l in about 54 of the 60 figures (the R^2 values of the most of these graphs were more than 0.90). The fit is less favourable in these cases; however, the trends are still correct even here. Overall this model (in Equation 7.15) can be used to forecast

the chloride concentration profile in concrete with different scenarios of chloride exposure (e.g. marine and de-icing salts).

b: Experimental Results from the Literature Studies

The experimental results were presented in chapter six and used for the comparison with the numerical data, resulting from the accelerated chloride penetration. The surface chloride concentration, C_s and diffusion coefficient of chloride, D_a were significantly higher than those cited in those studied for the actual field investigation of the concrete structure exposed to de-icing salt which is often spread on highways and structures in the winter (Anderson, 1997).

The transport and distribution of chloride ions in concrete structures is a function of the environmental condition, mainly the concentration and duration of the solution in contact with the concrete surface (Nilson *et al*., 1996). The concrete structures that are exposed to de-icing salts have boundary condition that varies with time, in wintertime parts of the concrete structure are exposed to a saturated salt solution that diluted as the ice and snow melts. This exposure may be repeated frequently, sometimes once a day. Rainwater works to move the chloride inward and outward due to moisture flow in concrete and ion diffusion (Nilsson *et al*., 1997).

On the other hand, this model can be used to predict the chloride concentration profile for the marine structures, or the samples submerge in NaCl more than 3%. The studies reported the concentration of NaCl in seawater is lower than 3%. By using the chloride transport model described in the previous sections, transport simulation was carried out.

(i): For verification, a concrete specimen (25×25×10 cm) was cast with ordinary Portland cement, OPC,30% PFA and 50% GGBS. The water-to-cementitious materials ratio (w/cm) and aggregate to binder (A/cm) were 50% and 5 respectively (McPolin *et al*., 2005). After 28 days of curing, the specimens were immersed in 0.55 M NaCl solution for 48 weeks, and the profile of total chloride content was measured using the potentiometer technique. Numerical results in comparison with the respective experimental results from McPolin *et al.* (2005) are presented in Table 7.4 and Figure 7.12 (b to d).

Table 7.4: D_a and C_s value with fraction aggregate and pores volume ratio and T=20 ºC and RH=40% computing according to mixes in (McPolin *et al.*, 2005)

Sample	w/cm	V_a	F_{agg}	V_v	D_a m^2/sec *10^{-12}	C_s % mass of cement
OPC 100%	0.5	0.77	0.13	0.29	14.8	3.6
OPC +30 PFA	0.5	0.77	0.13	0.28	16.2	4.5
OPC +30 GGBS	0.5	0.77	0.13	0.28	16.3	4.5

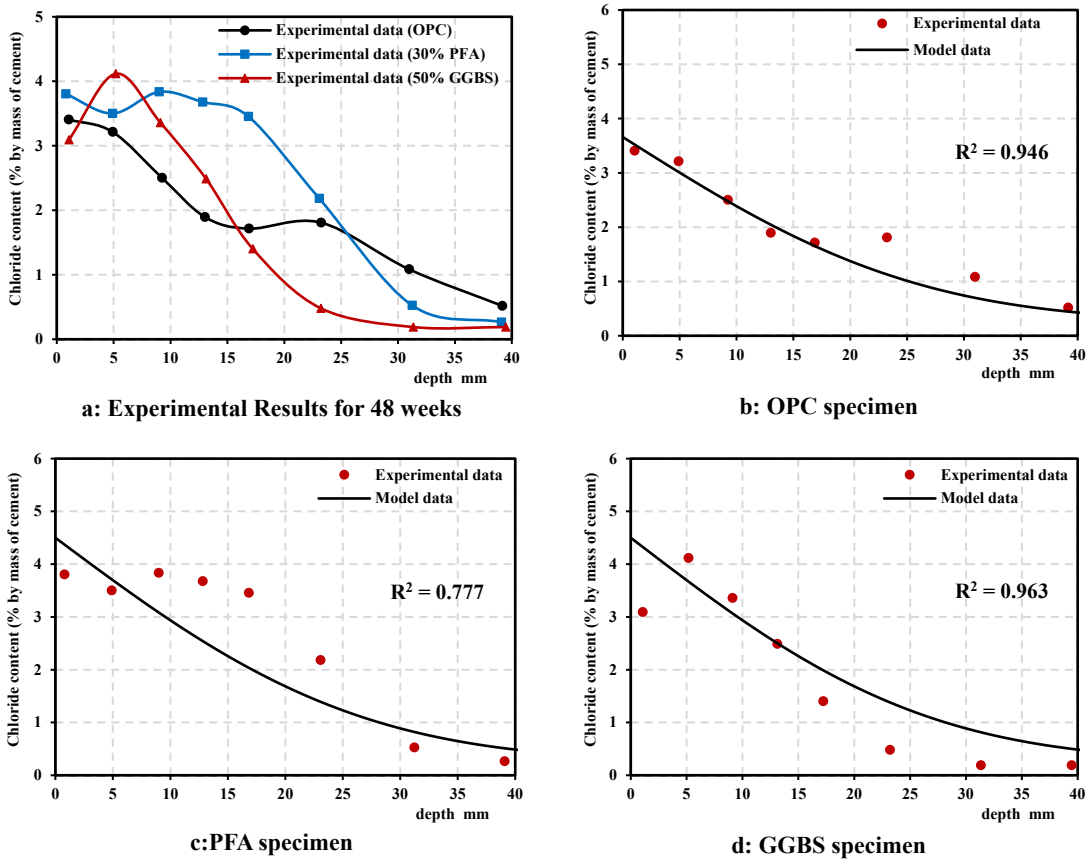

Figure 7.12: Chloride concentration, numerical vs experimental results for McPolin et al. (2005) for samples exposed to (0.55 M NaCl and 20 ºC for 48 weeks)

There is a qualitative difference in trend between the experimental and model-predicted results as shown in R^2 values in Figure 7.12. The analytical data from the employed model illustrated that the shape of the distribution of chloride concentration for both was compatible for specimens (OPC and 50 GGBS). Whereas, in the sample containing 30 PFA, there was a relatively high qualitative difference between the

experimental and simulation results. Because these types of materials tend to prevent deep chloride penetration, the concentration of chloride becomes high in the first layers of concrete and beyond that, the concentration decreases sharply. On the other hand, the simulation of this performance may be difficult. These kinds of anomalies between both results have also been reported in past research (Ishida *et al*., 2014). (ii) A beam-shaped concrete specimen (15×18×100 cm) cast with ordinary Portland cement. The water-to-cementitious materials ratio (w/cm) and aggregate to concrete ratio were 43% and 60% respectively (Shao-Feng *et al*., 2011). After 28 days of curing, the specimens were immersed in 5% NaCl solution for 30 weeks, and the profile of total chloride content was measured by the potentiometer technique for un-cracked and cracked specimens. The numerical analysis of these cases compared with experimental results are presented in Figure 7.13 (a and b).

(ii) A field investigation was carried out at port wharves which had been operated for 8 years. Two groups of cores have been taken from the concrete deck slab (loading platform) which is located over the sea, un-cracked and cracked with a crack width of 0.2 mm (Kwon *et al*., 2009). Some assumptions have been made in order to compute and simulate these cases. Figures 7.13 (c and d) show a two-dimensional profile of chloride concentration ascertained by numerical analysis and comparison with the experiment and model data of the chloride profile in the uncracked and cracked concrete specimens.

The numerical results for the previous two cases (as shown in Figure 7.13) match up well with the experimental data, which offers independent verification of the proposed model to predict the chloride profile in un-cracked and cracked concrete according to R^2 value (Ning and Li, 2015).

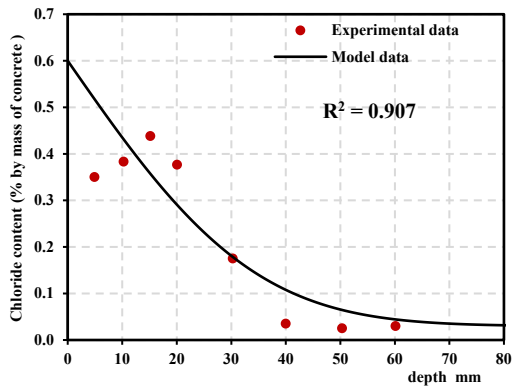

a: Un-cracked specimen

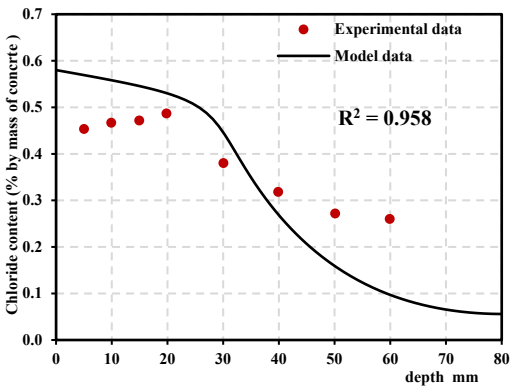

b: Cracked specimen (crack width 0.25 mm)

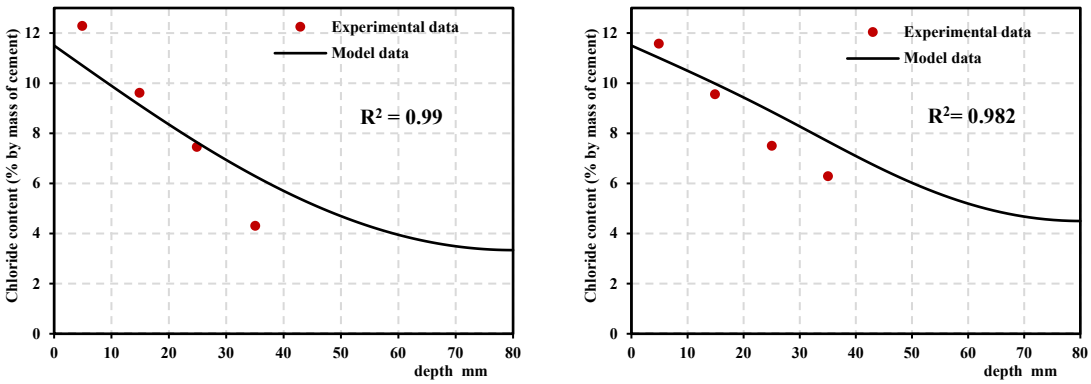

c: Un-cracked specimen d: Cracked specimen (crack width 0.2 mm)

Figure 7.13: Chloride concentration, numerical vs experimental results for (a and b for Shao-Feng *et al*. (2011) and (c and d for Kwon *et al*. (2009)

7.5 Numerical Prediction of Chloride Concentration in Concrete Structure due to Climate Change

The surface chloride concentration of the environment is the main driving force for chloride penetration in concrete structures. The model selects the rate of chloride build-up and the maximum surface concentration based on the type of exposure (and structure) and the geographic location or the severity of exposure of concrete structures to environment chlorides (ACI 365- 2018). There are two main categories of exposure environments, can be classified into two levels of chloride concentration due to the concentration of chloride solution and number repeated cycle exposed to the following:

a: Structures Exposed to De-icing Salt

The first categories are the structures exposed to de-icing salts e.g. bridge decks and parking structures. The exposure of the concrete sample to an accelerated environment condition is quite different from the exposure of the sample to deicing salt. Where, in the accelerated method, the concentration of chloride solution and the number of repeated exposure cycles is much higher than the exposure of the concrete to deicing salt. Therefore, the surface chloride content can be higher because of C_s or the boundary condition is approximately linear in increase with the increase of the concentration of solution up to 15% (Singhal *et al*., 1992). In the case of de-icing salt, it summarises the main scenario of surface chloride concentration in concrete structures with time because de-icing salt can be used in forecasting the chloride concentration in concrete structures as follows:

(i): Life-365 (2018) also assumes that initially, the C_s increases linearly with increasing time of exposure but remains almost constant after a period of time. The model determines the maximum surface chloride concentration reach the maximum C_s and the time taken to reach that maximum, depending on the type of structure (e.g. bridge deck), its geographic location and exposure based on field data. For example, the urban bridge assumes a maximum C_s between 0.68-0.85 (wt. % mass of concrete) depending on the usage of de-icing salt and the wash-off that happens on bridges exposed to rain and the rate of build-up varies by geographical location from 0.015 – 0.08 (% /year).

(ii) Phurkhao and Kassir (2005) proposed a ramp-type surface chloride concentration applied for surface chloride of bridge decks as shown in Equations 6.17 - 6.18 and Figure 6.6.

(iii): Weyers (1998) assumed the surface chloride concentration of bridge decks as a constant value which ranges from 0 to 2.4, 2.4 to 4.7, 4.7 to 5.9 and 5.9 to 8.9 kg/m³ (0 to 0.1, 0.1 to 0.2, 0.2 to 0.25 and 0.25 to 0.38 by mass of concrete) depending on environment (low, moderate, high and severe corrosion environments). He stated that as a bridge deck is subjected to a continually changing chloride exposure, the surface chloride concentration is not constant but time-dependent. This increase is relatively fast and reaches a quasi-constant concentration in about 5 years. It is therefore practical and reasonable to assume a constant surface chloride concentration.

In this case, de-icing salt exposure, the hypothetical sample of the concrete structure in London city was employed to predict the chloride concentration profile due to this exposure environment condition (temperature, relative humidity, and climate change scenario). According to the proposed methodology of chloride concentration as shown in Figure 7.8, the calculation and assumption will be used as follows:

Example 7.1

1- Concrete properties
   - w/cm ratio = 0.5, density =2400 kg/m^3, porosity = 0.12%.
   - V_a =0.738, V_v = 0.32 and the fraction of aggregate factor, f_{agg}= 0.151.
   - initial content of chloride, C_i = 0.
2- Exposure condition
   - Chloride spraying amount = 1 kg/m^2.

- Temperature as shown in Figure 7.14 -a.
- Relative humidity as shown in Figure 7.14 -b.
- Climate change in Temperature will reach 4.2 ºC RH decrease by about 9%in 2080 (UKCP', 2010).

3- Time of exposure: (25 and 50 years)

4- Boundary condition or surface concentration (C_s) will use two approaches:
   - use the limitation of Life 365-2018 for urban structures where the C_s increases linearly between 0-8 years by 0 - 0.68 % by mass of concrete and is constant beyond 8 years at 0.68 % by mass of concrete as shown in Figure 2.15.
   - use the limitation of Phurkhao and Kassir (2005) for structures the C_s increases linearly between 0-5 year for 0 – 0.223 % by mass of concrete and be constant beyond 5 years at 0.223 % by mass of concrete as shown in Figure 7.6.

5- The diffusion coefficient of chloride (D_a): compute and calibrated by age, and crack width factor by Equations 7.15 to 7.19 (first assumption) and account temperature and relative humidity effect according to climate change with UKCP'09(2010) models (scenarios) by Equations 7.15 to 7.19 (second assumption).

6- The shape of sample: deck slab which is 250 mm thick, one uncracked and another cracked with crack width 0.15 mm and depth 20 mm.

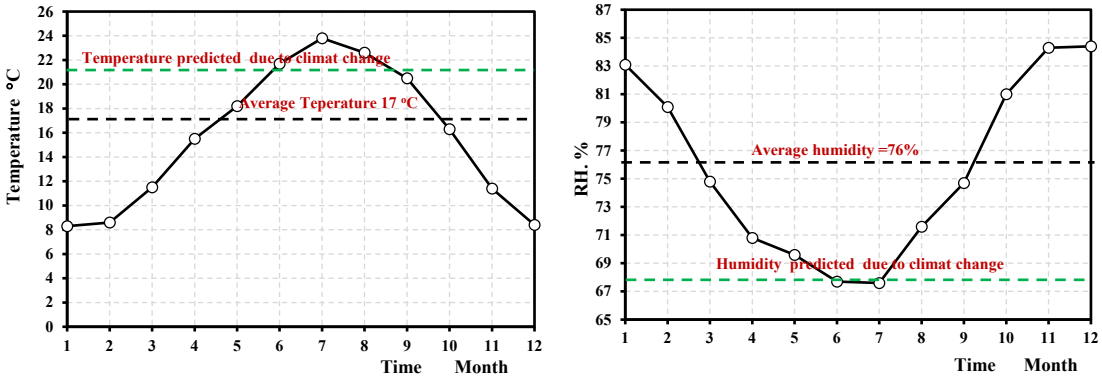

a: average max. temperature b: average RH

Figure 7.14: The annual maximum temperature and relative humidity of London (average of period 2004-2014)

According to the assumptions in example 7.1, the properties and type of exposure condition, the diffusion coefficient, D_a, and the effect of the time, temperature, humidity,

and cracked factors are presented in Table 7.5. The C_s is used according to two assumptions, Life 365:2018 and Phurkhao and Kassir (2005). The Life 365: 2018 assumes the maximum C_s =0.68 (% by mass of concrete) at 7.5 years. Whereas, Phurkhao and Kassir (2005) proposed the maximum C_s is 0.223 (% by mass of concrete) at 5 years. Both assumptions determine the C_s as being a constant beyond the maximum time as shown in Figure 7.6 and 2.15. The C_s values for both cases are listed in Table 7.5.

Chloride profiles after 25 and 50 years of exposure for two cases (cracked with cracked width 0.15 mm and un-cracked) without the impact of climate change (in temperature and relative humidity) would be as shown in Figures 7.15 to 7.18. On the other hand, temperature and humidity factor at 25 and 50 years old due to climate change were considered in the chloride concentration profile and these factors affecting the diffusion coefficient were 1.1 and 1.25 respectively.

Table 7.5: The Time, temperature, relative humidity and crack width dependent of D_a

Sample	D_a and at age and Temperature $m^2/sec *10^{-12}$, % (mass of concrete)							
	25 years old Without the effect of T and RH		25 years With the effect of T and RH		50 years old Without the effect of T and RH		50 years With the effect of T and RH	
	D_a	C_s	D_a	C_s	D_a	C_s	D_a	C_s
w/cm = 0.5 – un-cracked for (Life 365: 2018)	14	0.68	15.3	0.68	14	0.68	17.5	0.68
w/cm= 0.5 – un-cracked for Phurkhao and Kassir (2005)	14	0.22	15.3	0.22	14	0.22	17.5	0.22
w/cm= 0.5 –cracked 0.15mm mm for (Life 365: 2018)	17	0.68	18.6	0.68	17	0.68	21.3	0.68
w/cm= 0.5 –cracked 0.15mm for Phurkhao and Kassir (2005)	17	0.22	18.6	0.22	17	0.22	21.3	0.22

In Figures 7.15-7.18, the predicted results for the chloride concentration profile in the concrete bridge deck exposed to the de-icing salts environmental conditions under the influence of climate change (change in temperature) according to UKCP'09(2010) scenarios for two approaches and cases (cracked with cracked width 0.15 mm and Un-cracked) are presented.

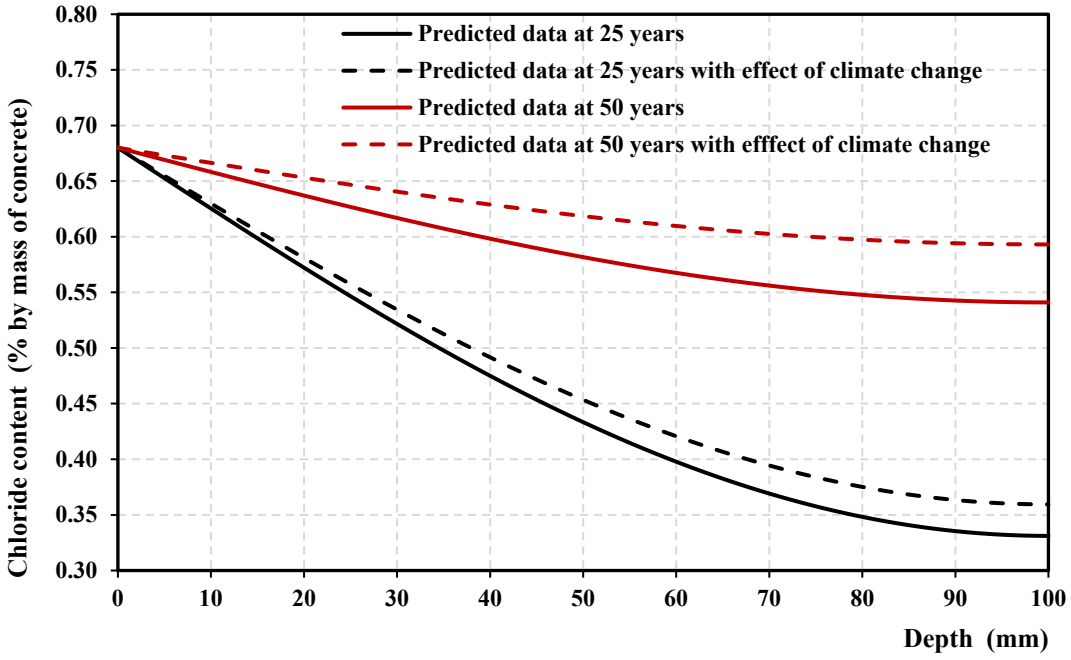

Figure 7.15: Model prediction of chloride concentration at un-cracked bridge deck in the city of London due to de-icing salt according to Life -365: 2018

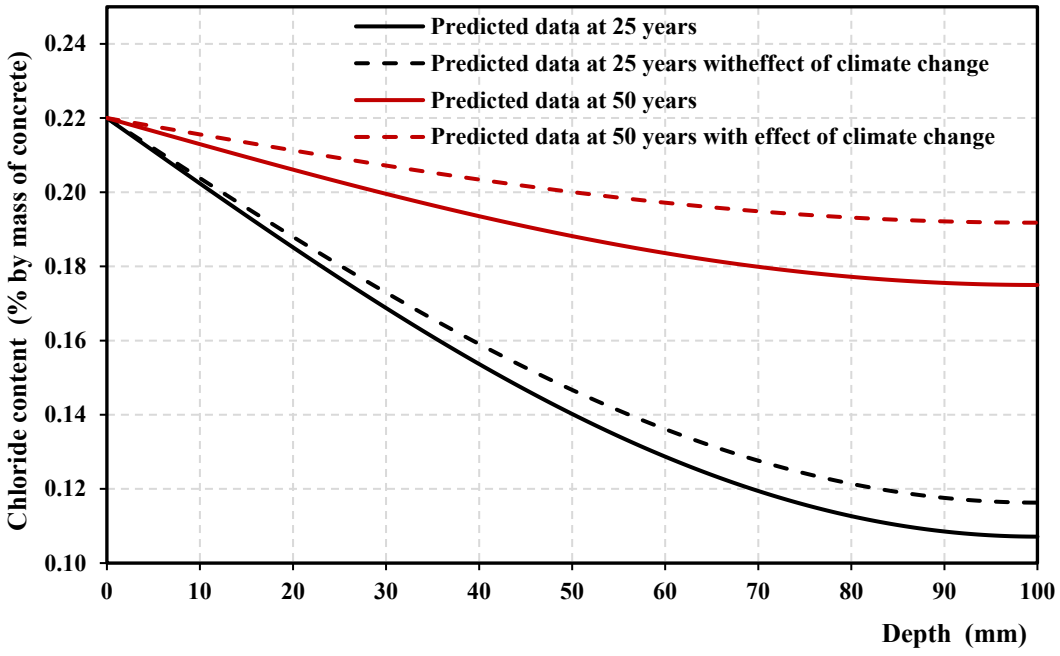

Figure 7.16: Model prediction of chloride concentration at un-cracked bridge deck in the city of London due to de-icing salt according to assumption Phurkhao and Kassir (2005)

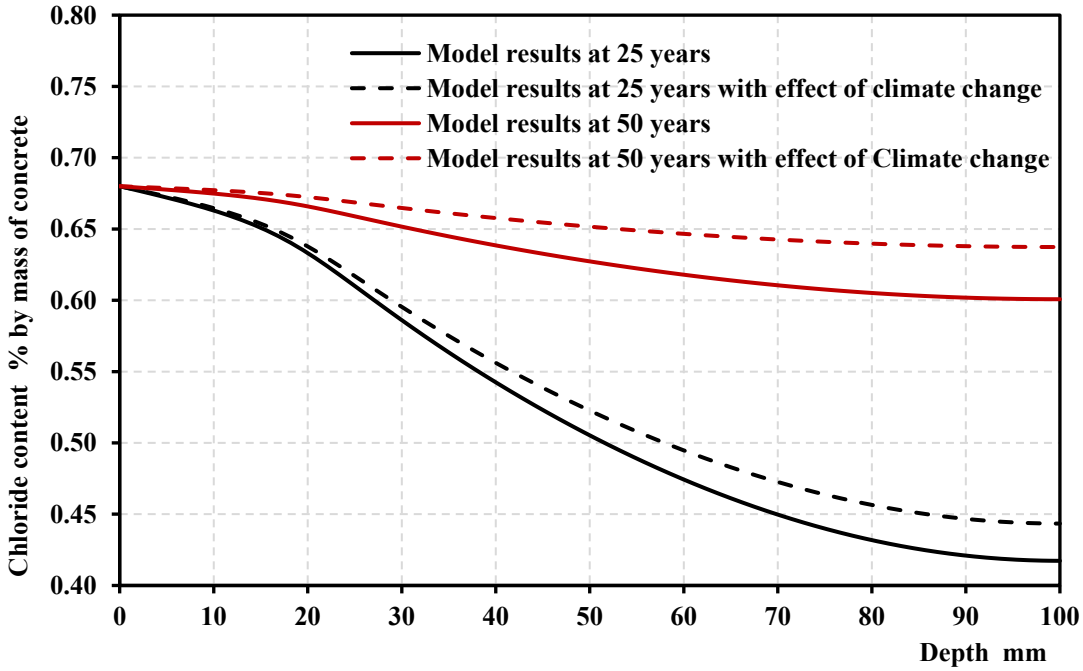

Figure 7.17: Model prediction of chloride concentration at cracked bridge deck (0.15 mm depth 20 mm) in the city of London due to de-icing salt according to Life 365: 2018

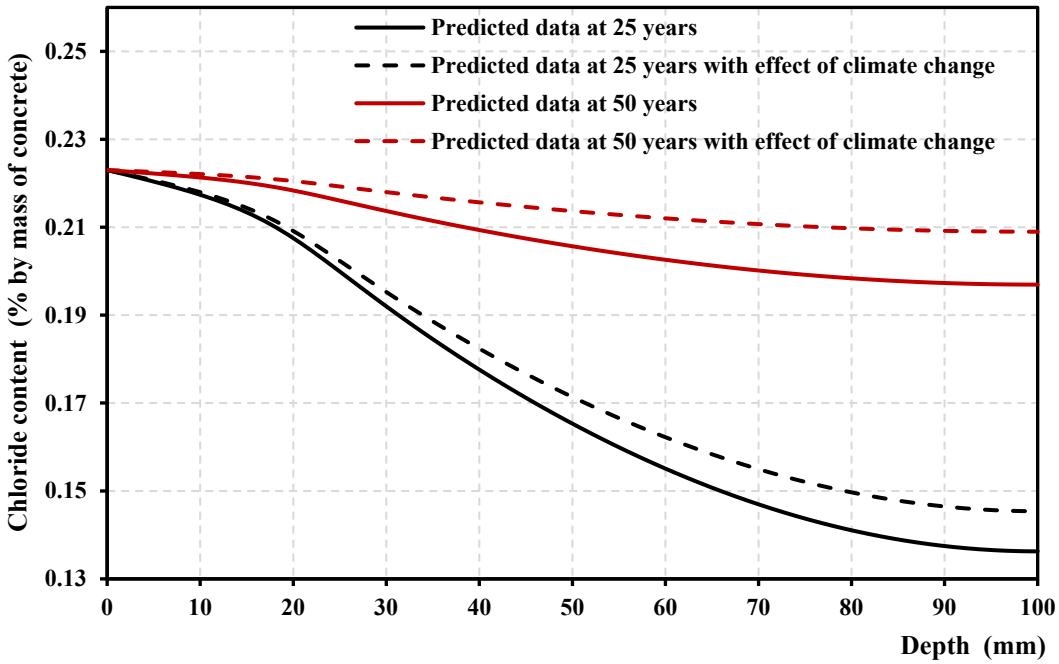

Figure 7.18: Model prediction of chloride concentration at cracked bridge deck (0.15 mm depth 20 mm) in the city of London due to de-icing salt according to assumption Phurkhao and Kassir (2005)

According to these results, the chloride concentration for both exposure ages of simulation (25 and 50 years) increases by increasing the temperature and decreasing relative humidity due to climate change as the UKCP'09(2010) scenarios. The percentage increase of chloride concentration at depth 50 mm (minimum requirement of concrete cover) according to BS 8100: 1997 and BS 8500-1: 2015 is 4.6 % and 5.8 for exposure age, 25 and 50 years respectively (uncracked concrete bridge deck) for two approaches to C_s concentration. While, the percentage for the cracked concrete deck (0.15 mm and depth 20 mm) for both approaches is 3.5% and 3.8% for exposure age, 25 and 50 years respectively.

The results of the simulation for different surface chloride concentration and status of concrete (with and without a crack) as shown in Figures 7.15 to 7.18 illustrated the concentration of chloride content are affected significantly by a change in temperature and humidity due to climate change for both durations of exposure and status of the concrete surface, cracked and uncracked.

In both cases, of cracked and un-cracked bridge deck concrete, the trend of predicted depths of chloride penetration by both approaches are relatively close in layers of concrete less than 20 mm deep. Beyond that depth, the influence of a change in temperature and humidity on chloride concentration increases with increasing depth of concrete for the two durations of exposure, 25 and 50 years. The percentage increase of chloride concentration at 50 years was higher than the percentage at 25 years due to an increase in chloride diffusion and an increase in temperature with the duration of exposure (Val and Trapper, 2008; Thomas *et al*., 2012).

b: Structures Exposed to a Marine Environment

The second category includes all the concrete structures which are exposed to a marine environment or which are located in coastal regions e.g. marine splash zone (defined as being in the tidal range or within 1 m of the high tide level), and Marine spray zone (defined as being more than 1 m above the high-tide level but occasionally exposed to saltwater spray). For example, Life-365 (2018) also assumes that initially, the C_s increases linearly with increasing time of exposure but remains almost constant after a period. The maximum C_s and the time taken to reach that maximum depends on the type of structure location (e.g. Marine splash zone, and Marine spray zone). The maximum C_s

for a marine splash zone and marine spray zone are 0. 8 and 1 (wt. % of concrete) respectively. On the other hand, Song *et al*. (2008) proposed a relationship between C_s and the time (time-dependent) as shown in Equation 6.24. Where, $C_S(t)$ denotes surface chloride concentration at time t (% by mass of cement); C_0 is surface chloride at the standard time (1 year) according to the mix design used in this for w/cm ratio 0.4, the C_0 = 0.72 % by mass of cement and α is a constant value = 0.162 and this equation will become as shown in Equation 7.30:

$$C_s(t) = 0.72 + 0.162\, ln(t) \qquad (7.31)$$

A marine exposure environment, the hypothetical sample of the concrete structure in the city of Basra at the south of Iraq is presented. Many of the concrete structures in this city are exposed to a marine environment such as port wharves. The average concentration of chloride ion in water in this part of the Arab Gulf is 2% (3.2 % NaCl) (Iraqi Environment Ministry). This case will be employed to predict the chloride concentration profile due to marine exposure conditions.

According to the methodology proposed from the chloride profile in Figure 7.9, the calculation and assumption will be used depending on Example 7.2 as follows:

Example 7.2

1- Concrete properties
   - w/cm ratio = 0.4, density =2400 kg/m^3, porosity = 0.10%.
   - V_a =0.695, V_v= 0.185 and the fraction of aggregate factor, f_{agg}= 0.18.
   - initial content of chloride, C_i = 0.
2- Exposure condition
   - Chloride concentration in marine environment = 3.2 %.
   - Temperature as shown in Figure 7.19 -a.
   - Relative humidity as shown in Figure 7.19 -b.
   - Climate change in Temperature will reach 4 ºC in 2100 (IPCC - 2014).
3- Time of exposure: (25 and 50 years)
4- Boundary condition or surface concentration (C_s):
   - Uses the limitation of Life 365-2018 for urban structures the C_s increases linearly between 0-10 years by 0 - 1 % by mass of concrete and is constant beyond 10 years at 1 % by mass of concrete as shown in Figure 2.15.

- Uses the proposed Equation by Song *et al*. (2008) for structures where the C_s is time-dependent as shown in Equation 7.24.

5- The diffusion coefficient of chloride (D_a): compute according to Equations 7.3 to 7.7 and calibrated by age, temperature, and relative humidity and crack width factor in Equations 7.10 -7.14.

6- The shape of the sample: deck slab is the port, 250 mm thick, one uncracked and another cracked with a crack width of 0.15 mm and a depth of 20 mm.

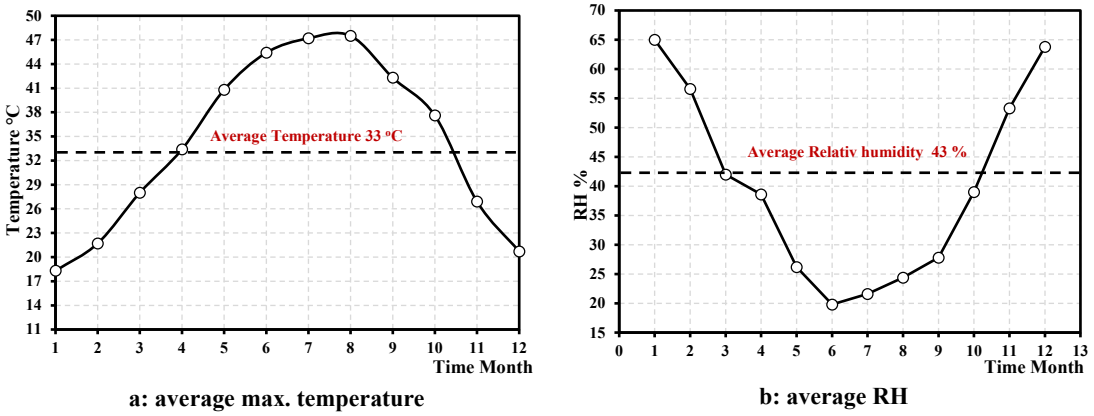

a: average max. temperature b: average RH

Figure 7.19: The annual maximum temperature and relative humidity of Basra (average of period 2004-2014)

According to the assumptions in Example 7.2, the properties and type of exposure conditions, the diffusion coefficient (D_a) after accounting for the impact of time, temperature, humidity, and cracked parameters are presented in Table 7.6. The surface chloride concentration, C_s is used according to two assumptions, Life 365(2018) and Song *et al*. (2008). The trend of both assumptions is different. Life 365(2018) assumes C_s increases with the time for 10 years with a rate of 0.1(% mass of concrete) per year, then it is to be constant at 1(% mass of concrete). While Song *et al*. (2008) assume the C_s increases with time as shown in Equation 7.30. Both assumptions for both cases (cracked and un-cracked) are listed in Table 7.6.

In Figures 7.20-7.23, the predicted results for chloride concentration profile in the concrete bridge deck exposed to the marine environmental conditions under the influence of climate change (change in temperature) according to IPCC (2014) scenarios for two approaches and cases (cracked with cracked width 0.15 mm and un-cracked) are presented. According to these results, the chloride concentration for both exposure ages of simulation (25 and 50 years) increases by increasing the temperature due to climate

change as the IPCC (2014) scenarios. The percentages increase of chloride concentration at depth 50 mm (minimum requirement of concrete cover) according to BS 8100: 1997 and BS 8500-1: 2015 are 3.5 % and 3.6 for exposure age, 25 and 50 years respectively (uncracked concrete bridge deck) for two approaches to C_s concentration. While, the percentages increase for the cracked concrete deck (0.15 mm and depth 20 mm) for both approaches is 3% and 2% for exposure age, 25 and 50 years respectively.

Table 7.6: D_a is dependent on the time, temperature, relative humidity and crack width

Sample	D_a and C_s $m^2/sec *10^{-12}$, % (mass of concrete)							
	25 years old Without the effect of T and RH		25 years With the effect of T and RH		50 years old Without the effect of T and RH		50 years With the effect of T and RH	
	D_a	C_s	D_a	C_s	D_a	C_s	D_a	C_s
w/cm = 0.4 – Un-cracked for (Life 365: 2018)	16.9	1.0	18.3	1.0	16.9	1.0	19.9	1.0
w/cm= 0.4 – Un-cracked for Song *et al*. (2005)	16.9	1.2	18.3	1.2	16.9	1.3	19.9	1.3
w/cm= 0.4 –cracked 0.15mm mm for (Life 365: 2018)	20.5	1.0	22.3	1.0	20.5	1.0	24.1	1.0
w/cm= 0.4 –cracked 0.15mm for Song *et al*. (2005)	17.0	1.2	18.6	1.2	17.0	1.3	21.3	1.3

The marine environment has a more significant impact on concrete structures than de-icing salt due to the higher concentration of chloride solution and the number of repeated exposure cycles on the concrete structures, which leads to increasing the surface chloride concentration, C_s as well as diffusion coefficient, D_a. Hence, all assumptions regarding chloride penetration suggest the C_s in marine exposure is higher than de-icing salt exposure. For Example, the Life 365(2018) proposes the C_s in marine condition at 10 years is 1 % (mass of concrete), while C_s in de-icing salt for urban highway bridges is 0.68 % (mass of concrete).

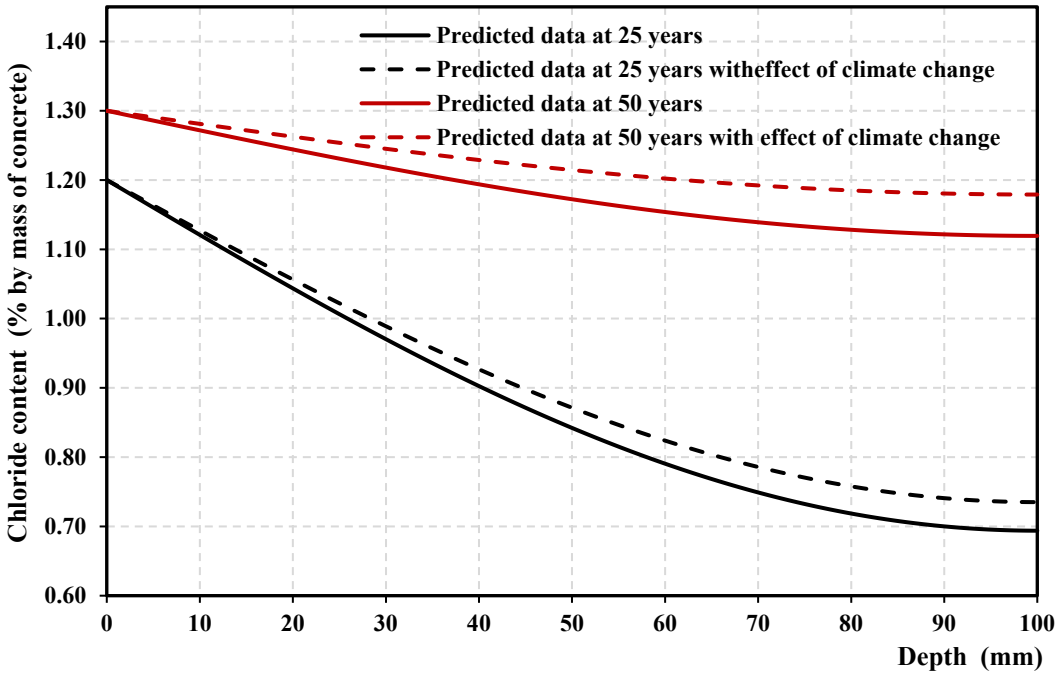

Figure 7.20: Model prediction of chloride concentration at the un-cracked deck in the city of Basra due to the exposure to marine conditions according to the assumption of Life 365 (2018)

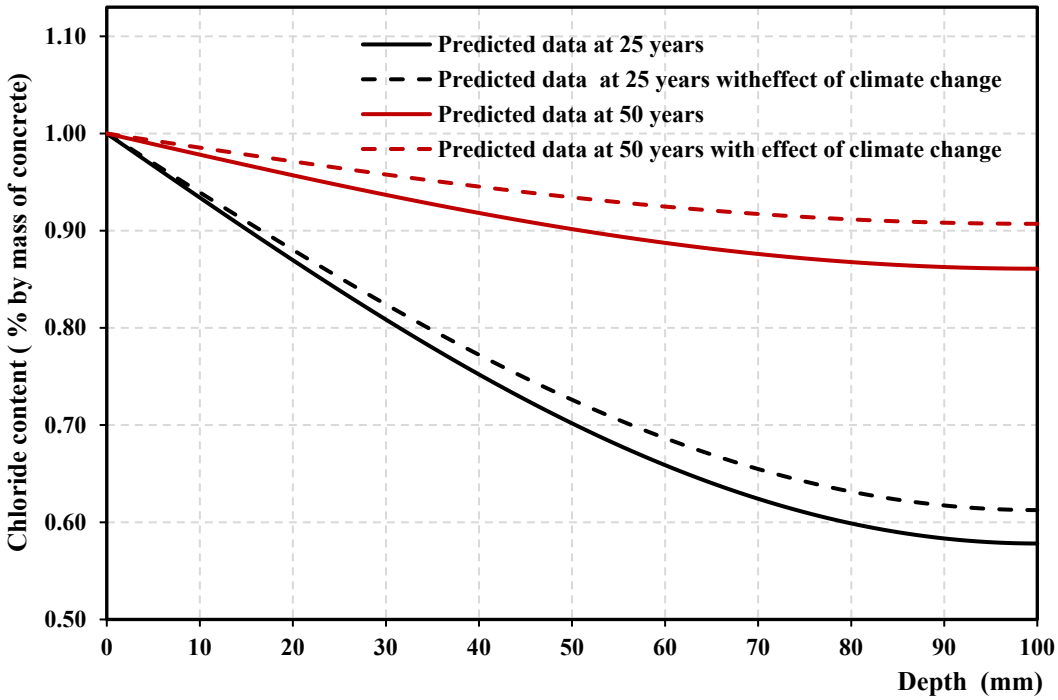

Figure 7.21: Model prediction of chloride concentration at the un-cracked deck (0.15 mm depth 20 mm) in the city of Basra due to exposure to marine conditions according to the assumption of Song *et al*. (2008)

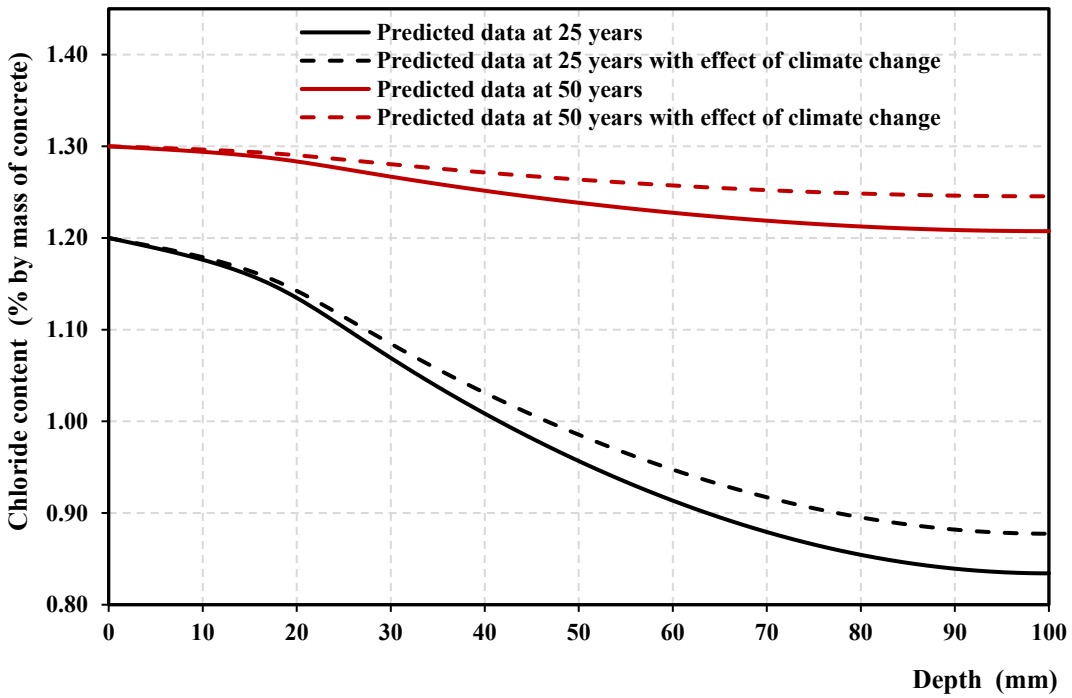

Figure 7.22: Model prediction of chloride concentration at the cracked deck (0.15 mm depth 20 mm) in the city of Basra due to the exposure to marine conditions according to the assumption of Life 365 (2018)

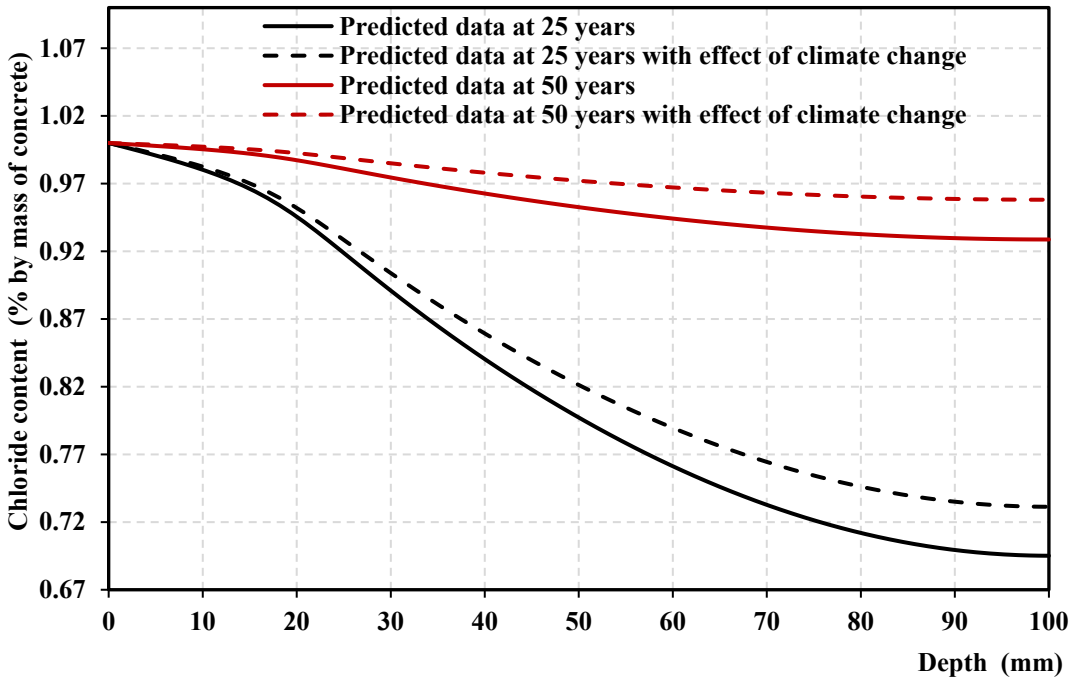

Figure 7.23: Model prediction of chloride concentration at the cracked deck in the city of Basra due to the exposure to marine conditions according to the assumption of Song *et al*. (2008)

The results of simulations for different surface chloride concentrations approach and status illustrated the concentration of chloride content are affected significantly by a change in temperature and humidity due to climate change, duration of exposure and status of the concrete surface (cracked or uncracked).

In both cases, of cracked and un-cracked concrete deck, the trend of predicted depths of chloride penetration by both approaches are relatively close with layers of concrete less than 20 mm deep. Beyond that depth, the influence of a change in temperature and humidity on chloride concentration increases with increasing depth of concrete for two durations of exposure, 25 and 50 years. The percentage increase of chloride concentration at 50 years was higher than that percentage at 25 years due to an increase in chloride diffusion and an increase in temperature with duration of exposure (Val and Trapper 2008; Thomas *et al*., 2012; Srinivasan and Gibb, 2018).

7.6 Carbonation Depth Models for Concrete Structures

Carbon dioxide (CO_2) significantly impacts the durability of concrete structures, particularly in carbonation and chloride penetration, and its concentration varies with time due to the increase in greenhouse gas emission (GHG) worldwide. As mentioned previously, the Inter-governmental panel on climate change (IPCC) has a new scenario projection, IPCC (2014), in terms of emission of GHG, CO_2, and temperature. RCP 8.5 is the worst exception scenario of IPCC (2014); it forecasts that carbon dioxide concentration may exceed 1000 ppm and the mean increase of temperature may range between 2.8 to 5.75°C. These projected scenarios of IPCC (2014) were depended upon and employed in the modelling of carbonation depth.

7.6.1 Engineering Model Simulating the Carbonation Depth for Concrete Structures

As mentioned in chapter 2, most of the models that have been proposed to simulate the carbonation depth are based on the diffusion of either the first or the second of Fick's law. In this study, Fick's Second Law is used because this diffusion of the atmospheric CO_2 is a non-steady state or variable with time due to a changing concentration gradient with time (IPCC- 2014).

The atmospheric CO_2 dissolves and reacts with water in the pores of concrete creating carbonate acid, H_2CO_3 and the soluble $Ca(OH)_2$ in pores of concrete can uptake H_2CO_3 to appreciate $CaCO_3$ as shown in Equations 7.31 and 7.32. These reactions make to be CO_2 concentration (C_{CO2}) in concrete is changeable with a depth of concrete and time.

$$CO_{2(gas)} + H_2O = H_2CO_3 \quad (7.32)$$

$$H_2CO_3 + Ca(OH)_2 = Ca_2CO_3 + 2H_2O \quad (7.33)$$

This modelling is a chemical - empirical model based on Fick's Second Law to predict carbonation depth, where $CO_{2(aq)}$ concentration changes with location and time factor, ∂x and ∂t respectively due to the uptake of $Ca(OH)_{2(aq)}$. This reaction mainly depends on the diffusion of carbon dioxide coefficient, D_{CO_2}, as shown in Equation 7.33 (Lagerblad, 2005).

$$\frac{\partial}{\partial t}(C_{CO_{2(aq)}}) = D_{CO_2}\frac{\partial^2}{\partial x^2}(C_{CO_2}) \quad (7.34)$$

CEB-FIP (2013) and Dyer (2014) proposed the modifications of Equation 7.33 in Equations 7.34-7.36 could predict the depth of carbonation (DoC) in concrete; this Equation is a function of diffusivity and concentration of carbon dioxide in concrete (Yoon *et al*., 2007, Kwon *et al.*, 2014).

$$DoC = \sqrt{\frac{2D_{CO_2}(C_{CO_2}/100)t}{a}} \quad (7.35)$$

$$DoC(t) = K_1\sqrt{t} \quad (7.36)$$

$$K_1 = \sqrt{\frac{2D_{CO_2}(C_{CO_2}/100)}{a}} \quad (7.37)$$

where:

D_{CO2} is the CO_2 diffusion coefficient, C_{CO2} is atmospheric CO_2 concentration %, a is the amount of CO_2 uptake to complete carbonation as computed by Equation 7.37, K_1 is carbonation rate ($mm/\sqrt{y}$) and it is the slope of the curve of the relationship between $x(t)$and $\sqrt{t}$ (Russell *et al*., 2001; Lagerblad, 2005).

$$a = 0.75 * C * CaO * \propto_H \frac{M_{CO_2}}{M_{CaO}} \quad (7.38)$$

where:

This modification assumes 75% of CaO can carbonate, C is the unit content of cement (kg per m^3 of concrete), CaO is the percentage content of CaO by mass (calcium oxide, 0.65), $\propto_H$ is the hydration rate (0.85), and M_{CO_2} and M_{CaO} are the molar weight of CO_2= 44 and CaO= 56 respectively (Lagerblad, 2005; Yoon *et al.*, 2007).

Carbonation rate (K_1) has been computed as in Equation 7.38.

$$K_1 = \sqrt{\frac{2D_{CO_2}(C_{CO_2}/100)}{0.326\,C}} \tag{7.39}$$

Papadikas and Tsimas (2002) proposed carbonation rate, K_1, involving the weight of total cementitious materials (cement + supplementary cement materials) to be more comprehensive for cementitious materials by:

$$K_1 = \sqrt{\frac{2D_{CO_2}(C_{CO_2}/100)}{0.218\,(C+kP)}} \tag{7.40}$$

where:

k is an efficiency factor for resisting against carbonation (0.5 to 0.7) Papadikas and Tsimas (2002) and P = amount of SCMs such as GGBS and PFA.

7.6.2 Diffusion Coefficient of Carbon Dioxide (D_{CO2})

Essentially, the size and connectivity of the pore in the structure of concrete is the main path of diffusion of CO_2 in concrete. This porous media mainly depends on the water/cementitious materials (w/cm) ratio and the degree of hydration of cement (Neville, 2011).

Papadikas *et al*. (1991); Papadikas and Tsimas. (2002) proposed an empirical equation to calculate the effective diffusivity of CO_2 in concrete (D_{CO_2}) based on its porosity by:

$$D_{CO_2,ref} = 6.1 * 10^{-6}\left(\frac{(w-0.267(C+kP))/1000}{\frac{C+kP}{\rho_C}+\frac{w}{\rho_w}}\right)^3 \tag{7.41}$$

where:

C is the cement content (kg), w is the water content (kg), ρ_C is the absolute density of cement (3050 - 3150 kg/m^3), ρw is the density of water (1000 kg/m^3).

The absolute density of supplementary cementing materials is not equal to the absolute density of cement, for example, the absolute density of fly ash ranges between 1900-2800 kg/m^3, while, absolute density of cement is about 3150 kg/m^3 and it may be less than 3150 kg/m^3 if the cement contains limestone or any additive material that has density lower than the density of cement. In this study, this equation needs to convert according to these properties of the material in order to find porosity of concrete correctly, as shown in Equation 7.41.

$$D_{CO_2,ref} = 6.1 * 10^{-6} \left(\frac{\frac{w-0.267(C+kP)}{\rho_w}}{\frac{C}{\rho_C}+\frac{kP}{\rho_P}+\frac{W}{\rho_w}} \right)^3 \qquad (7.42)$$

where:

ρ_P is the absolute density of supplementary cementing materials.

The calculations are based on Fick's Second Law and considered the different variables. The rate of carbonation is used to find out when carbonation reaches the reinforcement steel. This is basically the same type of calculation that is needed to calculate CO_2 uptake over time. The basis of the attempt is to find a value for concrete in a defined climatic condition and then add environmental factors to obtain the DoC after a certain time. The diffusion coefficient of carbon dioxide in concrete (D_{CO2}) is adjusted by different variables which consider microstructures, climatic condition, temperature and relative humidity and cracks. Talukdar *et al.* (2012) considered the effect of temperature, *T*, pore relative humidity, *RH* on D_{CO2}, but they did not consider the influence of crack and properties of concrete on the D_{CO2}. On the other hand, Kwon and Na (2011) takes into account the effect of crack width, W_c on the D_{CO2}, based on field investigation without consideration to the type of concrete. Because the main objective of this study is to investigate the effect of climate change on the durability of concrete structures. The study should focus on the effects of global climate change, change in CO_2 concentrations, temperature, relative humidity and crack width as well as the properties of concrete (different types of concrete). Therefore, these parameters, *T, RH, W* and properties of concrete will be considered in this study to account for the D_{CO2} as shown in Equation 7.42 and in predicting the DoC and the initiation of corrosion time, t_i due to carbonation.

$$D_{CO2} = D_{CO_{2},ref} f_{C1}(T) f_{C2}(RH) f_{C3}(W_c) \quad (7.43)$$

where:

$D_{CO2,ref}$ is the value of D_{CO2} at the reference condition (i.e. at the reference temperature, time and relative humidity) and it can be obtained by Equation 7.41, $f_{c1}(T), f_{c2}(RH), f_{c3}(W_c)$ are a function of temperature, relative humidity and crack width respectively. Analytical explanation of these factions will be given in the following section.

a. Relative Humidity Dependence on D_{CO2}

Consideration of humidity impact on the diffusivity of carbon dioxide as proposed by Papadikas and Tsimas (2002) based on the experimental test to measure the D_{CO2} with different relative humidity directly as shown:

$$f_{c2}(RH) = (1 - RH)^{2.2} \quad (7.44)$$

where:

$f_{c2}(RH)$ is the effective factor of diffusivity of CO_2 in concrete due to relative humidity, RH is the ambient relative humidity expressed as a fraction not less than 50%.

b. Temperature Dependence on D_{CO2}

The diffusivity of CO_2 can be broken down into two sequences, the CO_2 spreads in concrete and dissolves into the pore water coating the pore walls and reacting with dissolved $Ca(OH)_{2(aq)}$ to form $CaCO_3(s)$ which precipitates out of the solution (Dyer, 2014). Yoon *et al*. (2007); Talukdar *et al*. (2012) have employed the Arrhenius Equation (Equation 7.44) to account for the temperature dependence on the diffusion coefficient of CO_2 in concrete.

$$f_{c1}(T) = exp[\frac{U_c}{R}(\frac{1}{T_{ref}} - \frac{1}{T})] \quad (7.45)$$

where:

U_C is the diffusion activation energy, the activation energy for CO_2 diffusing in concrete has been experimentally determined at 39,000 J/mole K, R is the gas constant (8.314 J/mole. K), T_{ref} is a reference temperature (298 K) and T is the temperature of interest (K).

Nevertheless, the experimental data of the present study investigated the effect of temperature on DoC as shown in Table A.5 (Appendix A) and Table B.1(Appendix B).

This data on the effect of temperature on this study and He (2010) showed an effect much lower than the results from using the Arrhenius Equation. Where, increased percentage in DoC due to the influence of temperature ranged from 3% to 23 % for different types of concrete and temperature (see Table A.5 (Appendix A)). Table 7.7 and Figure 7.24 show temperature dependence factor, f_{c1}(T) values of using Arrhenius Equation and data obtained from the analysis of experimental data.

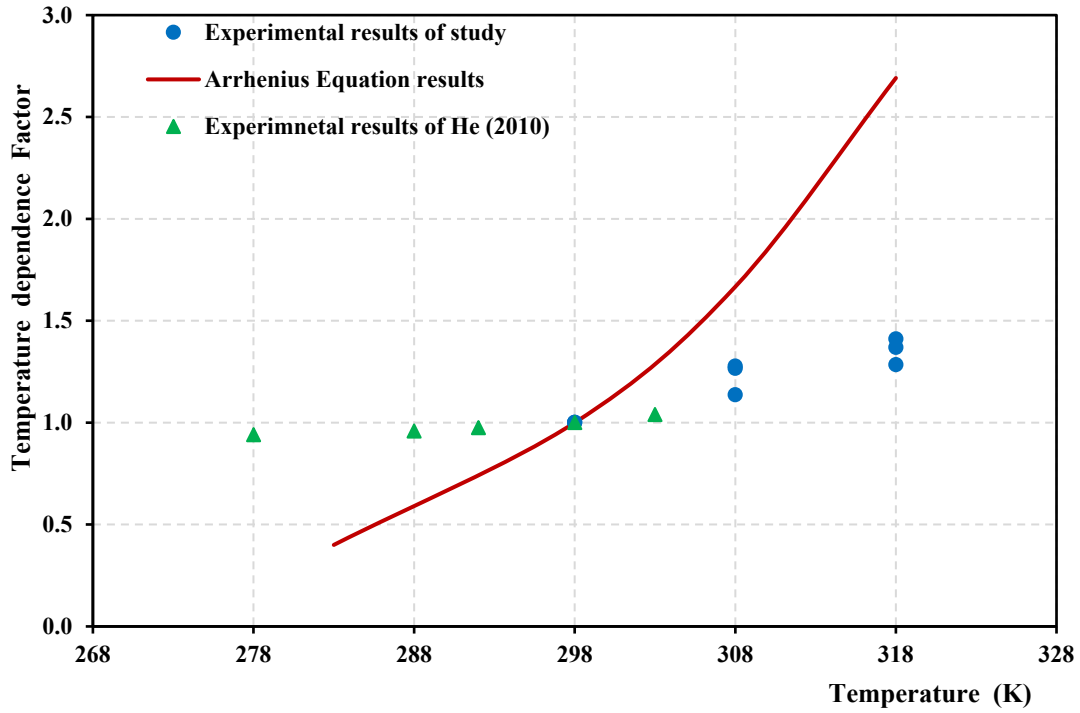

Figure 7.24: Temperature dependence factor for using Arrhenius Equation vs experimental data

Table 7.7: $f_{c1}(T)$ values of applying Arrhenius Equation and values obtained by analysing of experimental data

Temperature K	f_{c1}(T) obtained by applying Arrhenius Equation	f_{c1}(T) proposed by analysing experimental data
298	1.00	1.00
308	1.67	1.17
318	2.69	1.38

From the experimental data obtained through this study, the influence of temperature (T) on the diffusion coefficient of CO_2 (D_{CO2}) to find $f_{c1(T)}$ (as shown in Table

A-5 (Appendix A) and B-1(Appendix B)) has been calculated by doing non-linear regression analysis using the statistical programme, Statistics as shown in Equation 7.45. The main data for the series exposed to temperatures 25, 35 °C and 45 °C was used in this analysis to find the temperature influence on $f_{c1(T)}$. The correlation coefficient (R) was 0.87 and all correlations were statistically significant at the P= 0.000 level confidence 95% (alpha 0.005) (see section C.1-c in Appendix C).

$$f_{c1}(T) = exp[(b)\ \frac{U_c}{R}(\frac{1}{T_{ref}} - \frac{1}{T})] \quad (7.46)$$

where: *b* is the adjustment factor (0.322).

c. Crack Dependence on D_{CO2}

The cracks in concrete have a significant impact on the penetrability of carbon dioxide. As a result, the carbonation may be faster in cracked concrete compared with un-cracked concrete (Song *et al.*, 2006). Kwon and Na (2011); Smilauer *et al*. (2013) suggested a model predict the depth of carbonation (DoC) in cracked concrete for field investigation with crack widths of 0.1 mm and 0.2 mm by:

$$DoC = \left(2.816\sqrt{W_c} + 1\right)K\sqrt{t} \quad (7.47)$$

where:

W_c = crack width, K is the carbonation rate in the uncracked sample.

In order to achieve crack factor $f_{c3(W)}$ for wide range of crack width W_c (0.05 to 0.35 mm), the influence of crack width on the diffusion coefficient of CO_2 (D_{CO2}) was based on the experimental data and calculated by non-linear regression analysis (least squares) using the statistical programme ,Statistics as shown in Equation 7.47 and Figure 7.25. The input data was $f_{c3(W)}$, and crack width for the cracked and non-incorporating SCMs specimens for the series exposed to 1.5-5 % CO_2 conditions (as shown in Table B.2(Appendix B)). The correlation coefficient (R) was 0. 85 and all correlations were statistically significant at the P= 0.000 level and level confidence 95% (alpha 0.05) and the predicted and observed values are presented in Figure 7.26.

$$f_{c3(W_c)} = (11.4\sqrt{W_c} + 1) \quad (7.48)$$

where:

W_c is the crack width in mm and $f_{c3(W)}$ is the proportion of the diffusion coefficient of carbonation in the cracked sample ($D_{CO2(cracked)}$) to the diffusion coefficient of carbonation in the un-cracked sample ($D_{CO2(un\text{-}cracked)}$).

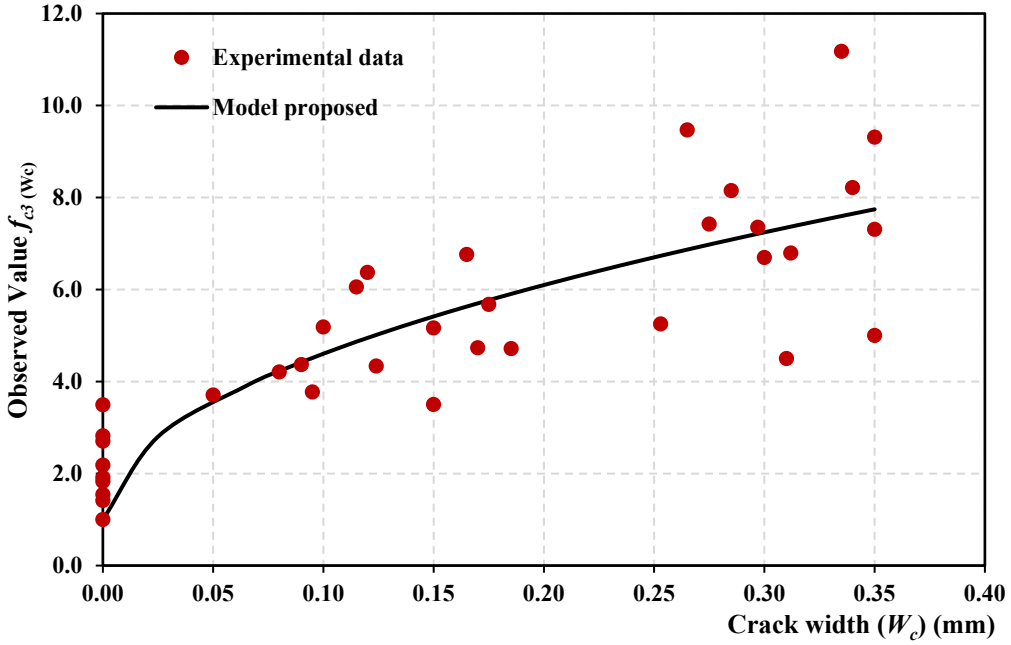

Figure 7.25: Effect of crack width on carbonation rate

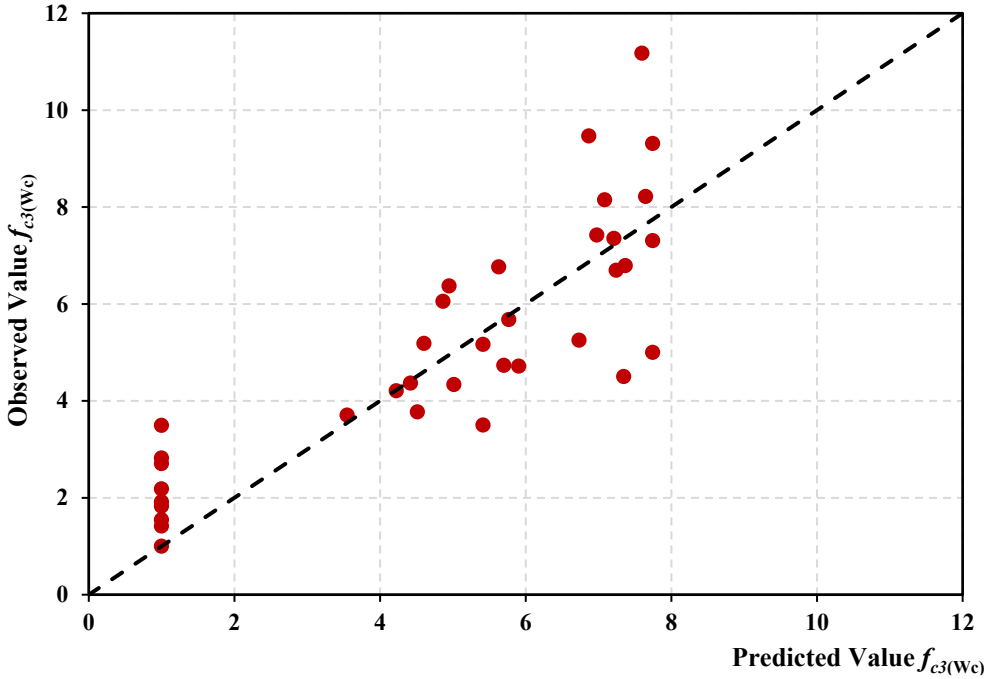

Figure 7.26: Observed and predicted values of the model proposed of cracked factor ($f_{c3(Wc)}$)

7.6.3 Verification of the Modelling of Carbonation Rate Evolution

In an experimental programme, 420 concrete prisms, 10*10*500 cm were tested. These were un-cracked and cracked samples respectively. For the un-cracked and cracked specimens, different w/cementitious materials ratios were tested, while for the cracked ones, different crack width and depth were examined. These specimens were exposed to a CO_2 environment with 5-1.5% (depending on series) for about 8 weeks at one surface to simulate the penetration of CO_2 in one- dimensional flow as presented in Figure 7.27. The DoC was measured using the phenolphthalein method and the results of all cases are presented in Figure 5.1 and in Tables A.4 -A.6 (Appendix A).

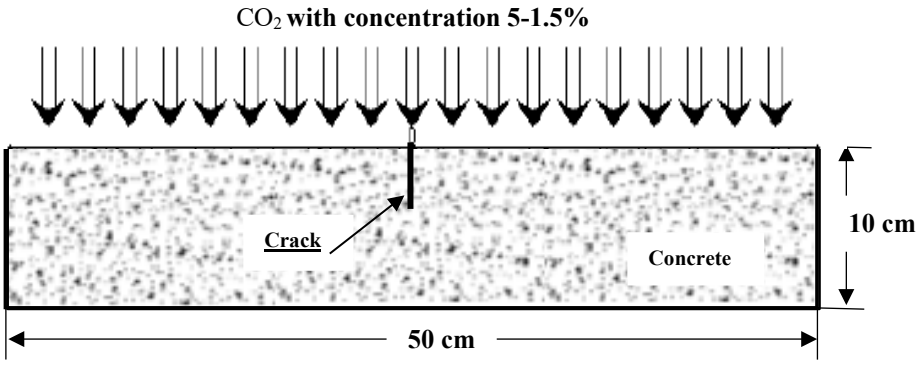

Figure 7.27: Schematic of sample exposed to CO_2 condition

In this study, an engineering model was used to predict the carbonation rate or depth, which governs the chemical reaction (uptake) of CO_2 by $Ca(OH)_2$ and C-S-H. The model was validated by experimental data obtained from the experimental programme and literature studies. The modelling was based on the variation of the diffusion coefficient of CO_2 due to change in properties of concrete, relative humidity (RH), temperature and CO_2 concentration. Those variables mathematically simulated the uptake of the CO_2. The moisture distribution, RH, and micro-pore structure characteristics, in turn, control the CO_2 diffusion of various chemical reactions under arbitrary environmental conditions (e.g temperature). In this part of the study, the CO_2 transportation in un-cracked and cracked concrete to find DoC will be simulated as shown in Figure 7.28.

The diffusion carbon dioxide coefficients, D_{CO2} for the sample are computed according to Equations 7.42-7.47 and presented in Tables B.3(Appendix B).

The influence of properties of concrete, the crack width, RH, CO_2 concentration and temperature were considered in the model in Equations 7.33 to 7.47 and verified by experimental results in this study as shown in Figures 7.28 (a-h). A qualitative difference in trend is seen in the square of this correlation coefficient, R^2 between the model predicted and the experiment results as shown in these Figures. The results for (M 0.5, M 0.6 and M 0.5+PFA) through use of engineering modelling showed the shape of the progress of the carbonation rate obtained with crack width from the analysis and experimental data was well-matched. On the other hand, in some cases (M 0.4 and M 0.5+ GGBS), the analytical results of carbonation rate with crack width were relatively high. The experimental results using the phenolphthalein method in the test showed the actual measured value of carbonation depth at the first point of the depth of the concrete which has a pH ≤ 9.

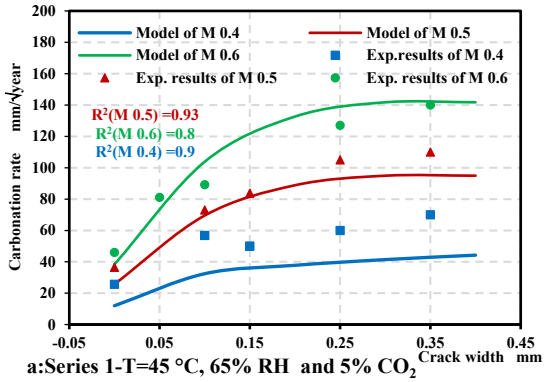

a:Series 1-T=45 °C, 65% RH and 5% CO_2

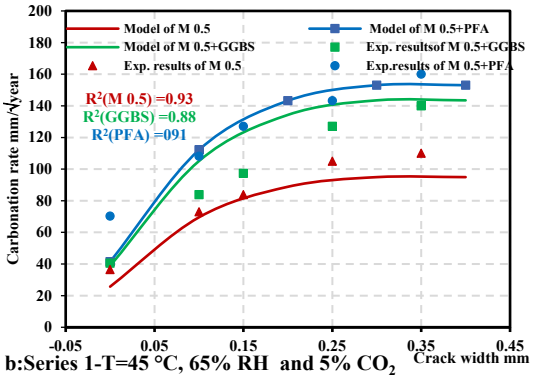

b:Series 1-T=45 °C, 65% RH and 5% CO_2

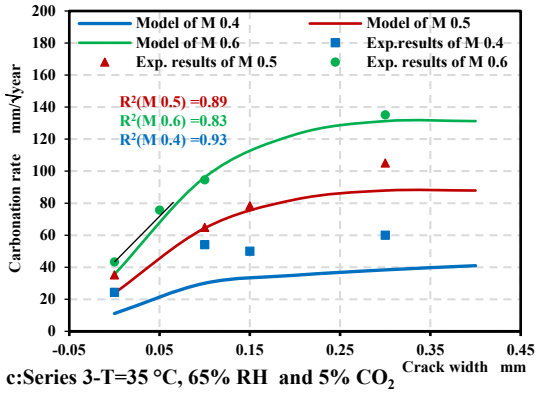

c:Series 3-T=35 °C, 65% RH and 5% CO_2

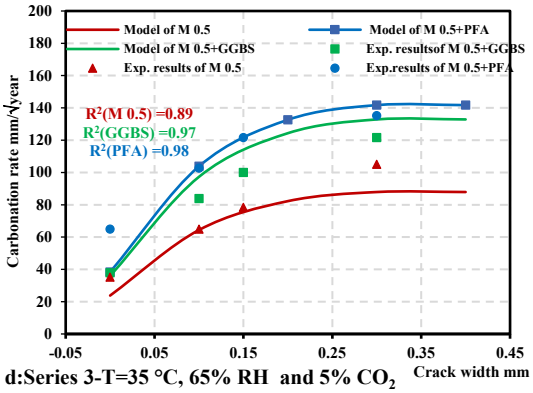

d:Series 3-T=35 °C, 65% RH and 5% CO_2

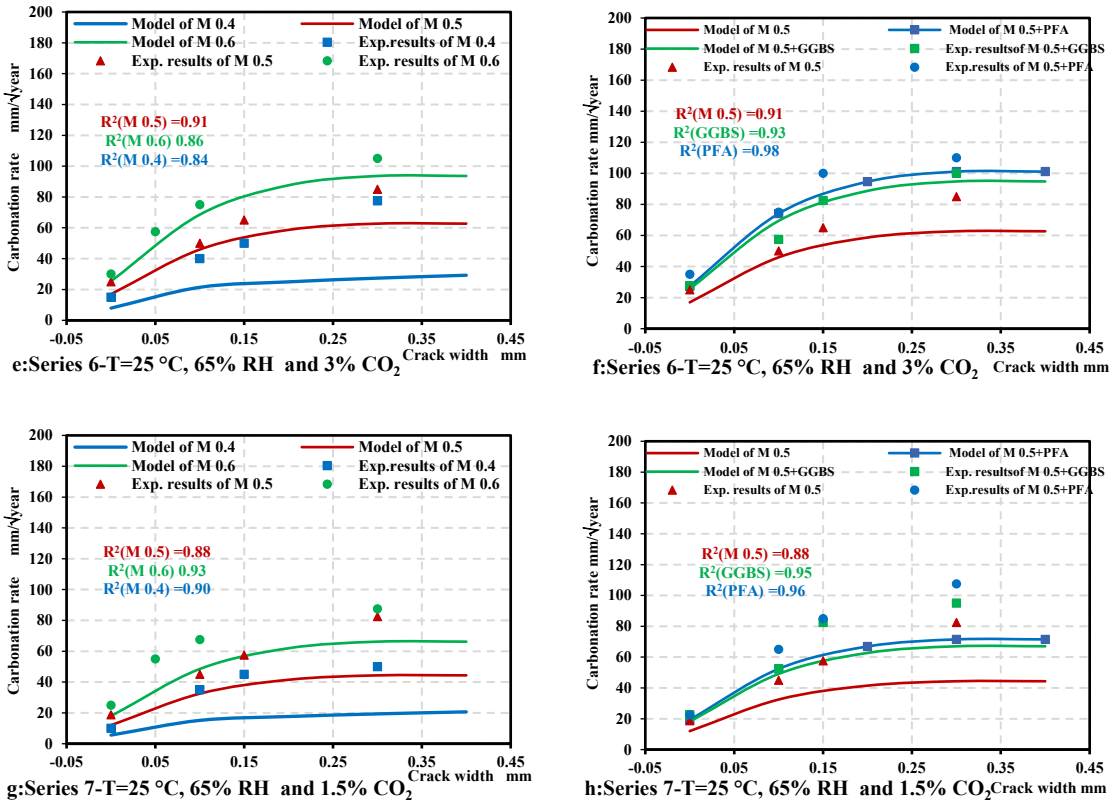

Figure 7.28: Comparison of model predictions vs experimental results for the different scenarios of exposure condition and different crack width

It can be seen from Figure 7.28, the predicted data resulting from modelling matches well with the experimental data in about 21 of the 24 curves (the R^2 values of most of these graphs were more than 0.85). The fit is less favourable in these cases; however, the trends are still correct even here. Overall this model can be used to forecast the carbonation rate or depth for different crack widths in concrete and different scenarios of exposure conditions (e.g. CO_2, temperature and relative humidity).

Secondly, for verification with studies from literature, firstly three concrete cube specimens (10×10×10 cm) were cast, with OPC. The w/cm ratio and aggregate to cementitious materials (A/cm) were 50% and 4.3 respectively (Talukdar *et al.*, 2012). After 28 days of curing, the specimens were exposed to 6% CO_2, 65% RH and 30 °C for 8 weeks. The computational results showed $f_{c2(RH)}$ = 0.099, $f_{c1(T)}$ =1.1 and D_{CO2} =1.5*10^{-8} m^2/sec, and the calculation of this case compared with experimental results are presented in Figure 7.29-a. Secondly, three cube concrete specimens (10×10×10 cm) were cast, with ordinary Portland cement. The w/cm was 48% (Chi *et al.*, 2002). After 28 days of curing, the specimens were exposed to 5% CO_2, 55% RH and

30°C for 8 weeks. The computational results showed $f_{c2(RH)}$ = 0.133, $f_{c1(T)}$ =1.1 and D_{CO2} =1.6*10^{-8} m^2/sec, and the calculation of this case compared with experimental results are presented in Figure 7.29-b. The carbonation depth was measured using the phenolphthalein technique for both cases.

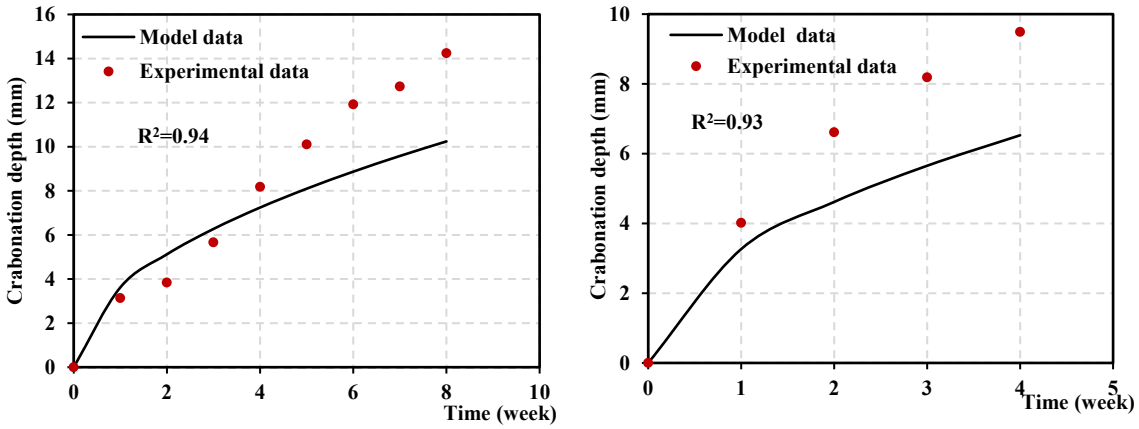

a: Talukdar *et al.* (2012) **b: Chi *et al.* (2002)**

Figure 7.29: Model simulation vs experimental carbonation depth for (a) Talukdar *et al.* (2012) and (b) Chi *et al.* (2002)

From Figure 7.29, there is a qualitative difference in trend between the experimental results and those predicted by the model as shown in R^2 values. The analytical data obtained by employing the model illustrated that the shape of the progress of carbonation depth for this case was quite well matched. The difference between the analytical results and experimental data is due to the model assuming that calcium compounds can react about 0.75 %, while the experimental results are based on the change in the colour of carbonated concrete which has a pH ≤ 9 due to use the phenolphthalein alkalinity indicator. This method of investigating carbonation only determines the full carbonated zone (Chi *et al.*, 2002).

7.6.4 Prediction of DoC in Concrete Structure due to Climate Change using Engineering Model

The carbon dioxide concentration increases highly with time according to the scenarios of IPCC (2014). It is necessary to determine this concentration in order to predict the rate of carbonation in concrete structures; in addition, the effect of this change on temperature and relative humidity should be considered in the calculation of carbonation rate. The influence of change in CO_2, temperature, relative humidity and properties of concrete (crack width) is taken into account in the carbonation rate. The change in carbonation rate with a $\pm$15% change in each of the above parameters is presented in Figure 7.30.

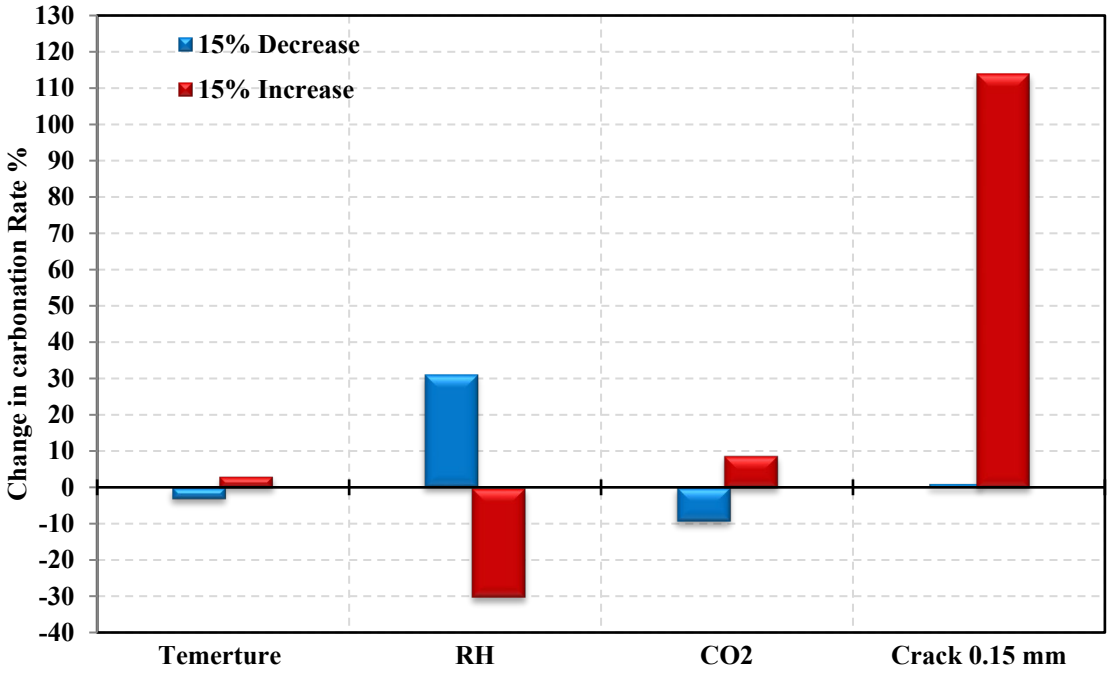

Figure 7.30: Effect of $\pm$15% change in temperature (25$\pm$15%), relative humidity (65$\pm$15%), CO_2 concentration (1000 $\pm$15%) and crack (0.15 mm) on carbonation rate

It can be noted that the effect of the crack on the carbonation rate is the highest in case that there is a 15% increment in temperature while, change in temperature appears to have a minimum effect on carbonation rate. Also, the presence of moisture in connective porosity has a significant role in the penetration of carbon dioxide and the reaction process of carbonation. The propagation of carbonation rate slows down when the concrete pores are fully water-saturated (RH > 85%) due to the diffusion of CO_2 and reactions of carbonate ion with hydrated cement products which hardly react (Kropp and Hilsdorf, 2005). In lower moisture content (below 50%) or dry concrete, the carbon

dioxide can penetrate deeply but there is insufficient moisture for the carbonation reaction to take place. Thus, carbonation rate reduces at a lower water content owing to the inadequate water in the pores (Tarun and Rakesh, 2010; Lagerblad, 2005). Thirdly, the increase in CO_2 concentration has a significant impact on the carbonation rate, because the increment in CO_2 increases the penetration and quantity CO_2 (aq) in concrete which leads to an increase in the DoC. There is a linear correlation between the CO_2 concentration in the environment and DoC (Chi *et al*., 2002). Fourthly, the results showed that the carbonation rate is relatively increased at temperatures higher than the ambient temperature. The effect of temperature is difficult to estimate because different contradictory mechanisms are at work. The temperature modifies the solubility of the reactants: the higher the temperature, the lower the calcium solubility and CO_2 contents in solution (Ishida *et al*., 2014).

The IPCC (2014), (AR5-RCP 8.5) predicted that the change in carbon dioxide over the 21st century will be up to 1000 ppm and that will lead to an increase in the temperature range of between 2.8 and 5.75°C. The increase in carbon dioxide and temperature for the worst scenarios of IPCC -2014 forecasts, RPC 8.5 and RCP 6.0 over the 21st -22nd century are shown in Figure 7.31. The influence of climate change, atmospheric temperature, and carbon dioxide concentrations of IPCC (2014) was established in this study in order to predict the change in carbonation depth.

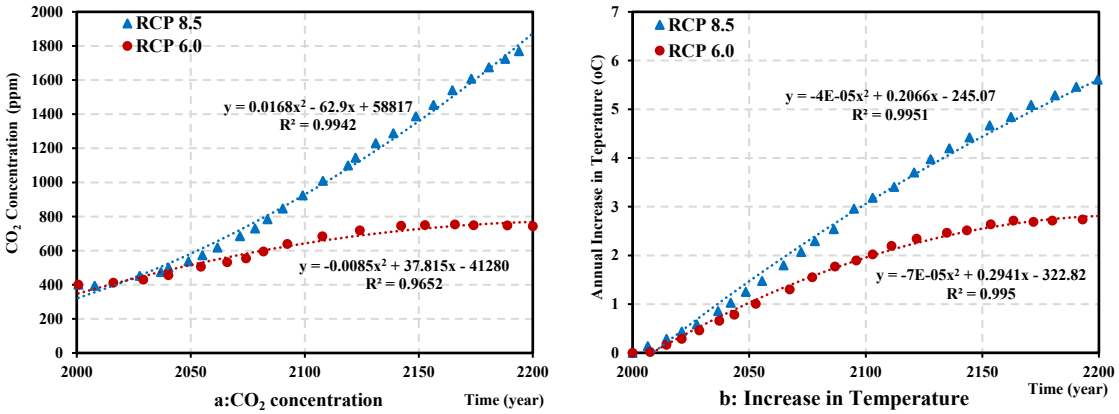

Figure 7.31: Prediction of atmospheric CO_2 concentration and increase in temperature over the period 2000-2200 for the worst scenarios, RCP 8.5 and RCP 6.0 in (IPCC , 2014- AR5)

The atmospheric carbon dioxide concentration, temperature, and humidity of the exposure environment are the main driving forces for carbon dioxide penetration in concrete structures (Yoon *et al.,* 2007, Talukdar *et al*., 2012b). The modelling of the rate of carbonation considered the surface exposure condition, CO_2, RH and T and properties

of the concrete structure. There are two main cases of exposure environment, which can be investigated looking at two levels of CO_2 concentration according to the two worst scenarios, RCP 8.5 and RCP 6.0 as follows.

a: Structures Exposed to Carbonation in London-UK

In this case, the hypothetical samples of the concrete structure in the city of London were employed to predict the carbonation depth due to this exposure environment condition (CO_2, temperature, relative humidity, and climate change scenario RCP 8.5 and RCP 6.0). According to the methodology proposed for carbonation rate in the previous section, the following calculations and assumptions will be used:

1- Concrete properties
   - w/cm ratio = 0.4, 0.5 and 0.6, cement content 513,410 and 350 kg/m^3 respectively.
   - $V_v = 6.1*10^{-3}$, $22.5*10^{-3}$ and $42.6*10^{-3}$ for w/cm 0.4, 0.5 and 0.6 respectively.
2- Exposure condition
   - CO_2 concentration = 400 ppm at year 2000.
   - Temperature is shown in Figure 7.14 (a) and $f_{c1(T)} = 0.869$ to 0.886 (variable over time due to climate change).
   - Relative humidity as shown in Figure 7.14 –b and $f_{c2(RH)}$= 0.043 to 0.065 (variable with time due to climate change).
   - Climate change: The changes in CO_2 and temperature are shown in Figure 7.31(a, b) respectively and RH decreases by about 9% in 2080(UKCP'09 (2010). The average values CO_2, temperature and relative humidity were calculated over the time period are not peak values at time t to account for CO_2 concentration, $f_{c1(T)}$ and $f_{c2(RH)}$.
3- Time of exposure: (100 years)
4- Boundary condition or surface concentration CO_2 is shown in Figure 7.31(a).
5- The diffusion coefficient of chloride (D_{CO2}): accounts for and calibrated by properties of mixes used, RH, T and crack width factor using Equations 7.42 to 7.47 (control case) and account for climate change (change in CO_2 concentration, temperature and relative humidity) according to UKCP'09 (2010) and IPCC (2014) models (scenarios) (second case).
6- The shape of the sample: Girder or column, one uncracked and another cracked with a crack width of 0.05- 0.4 mm.

According to these assumptions, the properties of concrete, crack width and type of exposure condition, the diffusion coefficient (D_{CO2}) beyond considering the impact of the change in CO_2 concentration, temperature, and humidity due to RCP 8.5 and RCP 6.0 are presented in Table 7.8.

Table 7.8: Temperature, relative humidity and crack width dependent on D_{CO2}

Sample & Case		CO_2 ppm	D_{CO2} for samples with crack width $m^2/sec *10^{-8}$			
			Un-cracked	0.05-0.15 mm	0.15-0.25 mm	0.25-0.35 mm
M 0.4	Without effect of CC	400	0.14	0.64	0.85	1.01
	With effect of CC	1000	0.21	0.99	1.3	1.56
M 0.5	Without effect of CC	400	0.51	2.36	3.12	3.71
	With effect of CC	1000	0.79	3.63	4.81	5.71
M 0.6	Without effect of CC	400	0.97	4.49	5.94	7.06
	With effect of CC	1000	1.50	6.91	9.16	10.88

*CC: climate change due to change in temperature and humidity.

Carbonation depths due to exposure conditions over a period of up to 100 years for two scenarios of IPCC-2014, for M 0.4, M 0.5 and M 0.6 (un-cracked samples), with and without the impact of climate change (change in CO_2, temperature and relative humidity) were shown in Figures 7.32 (a, b and c). On the other hand, change in climate change parameters for different crack widths was considered in the carbonation rate as shown in Figure 7.33.

The predicted results of carbonation depth in concrete members exposed to a CO_2 environment condition due to the influence of climate change parameters for IPCC (2014) on (RCP 8.5 and RCP 6.0 scenarios) increased when considering the increase in CO_2, temperature and reduction in humidity for both exposure condition scenario as shown in Figures 7.32. When comparing depth of carbonation for un-cracked samples at 100 years for all w/cm ratios, the DoC is 65% and 47% higher for RCP 8.5 and RCP 6.0 scenarios respectively, compared with the case when the effect of changing CO_2 concentration, temperature and RH are ignored. While, the percentages in DoC for the cracked concrete member (different crack width and w/cm ratio) is 46 % due to the exposure condition scenario, RCP 8.5.

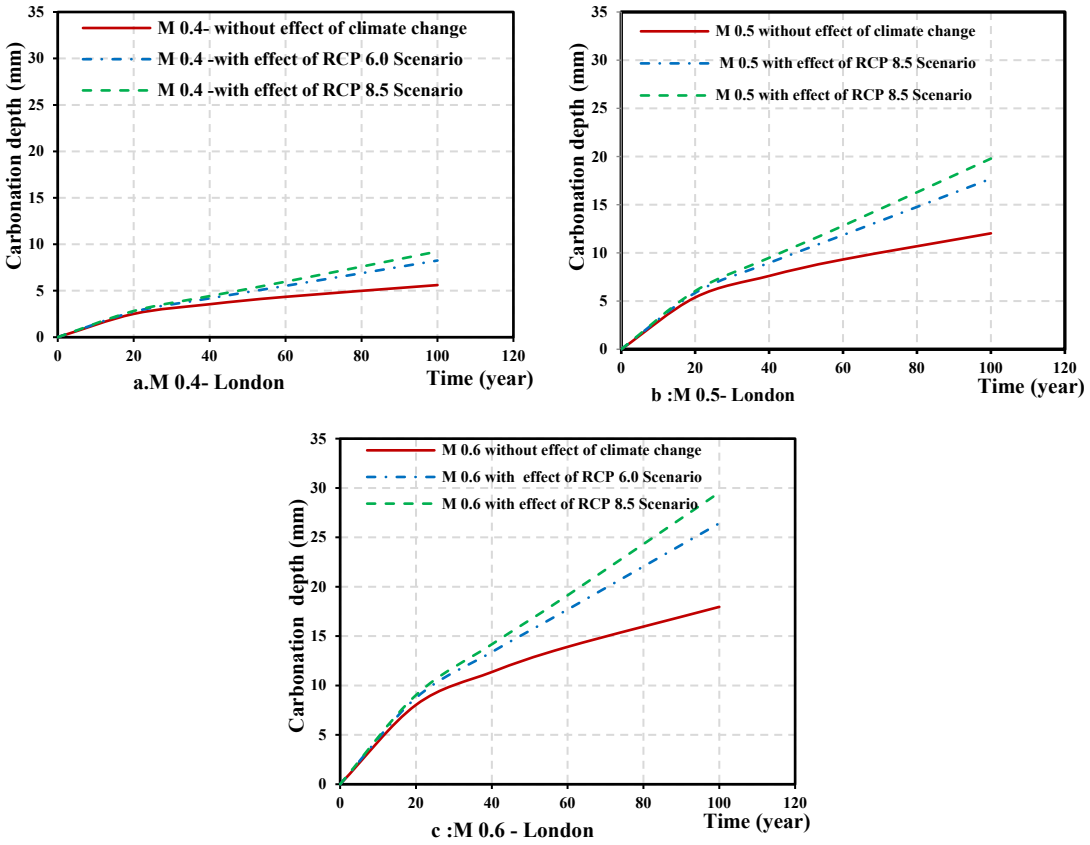

Figure 7.32: Effect of climate change scenarios on the prediction of the carbonation depth for a un-cracked member in the city of London

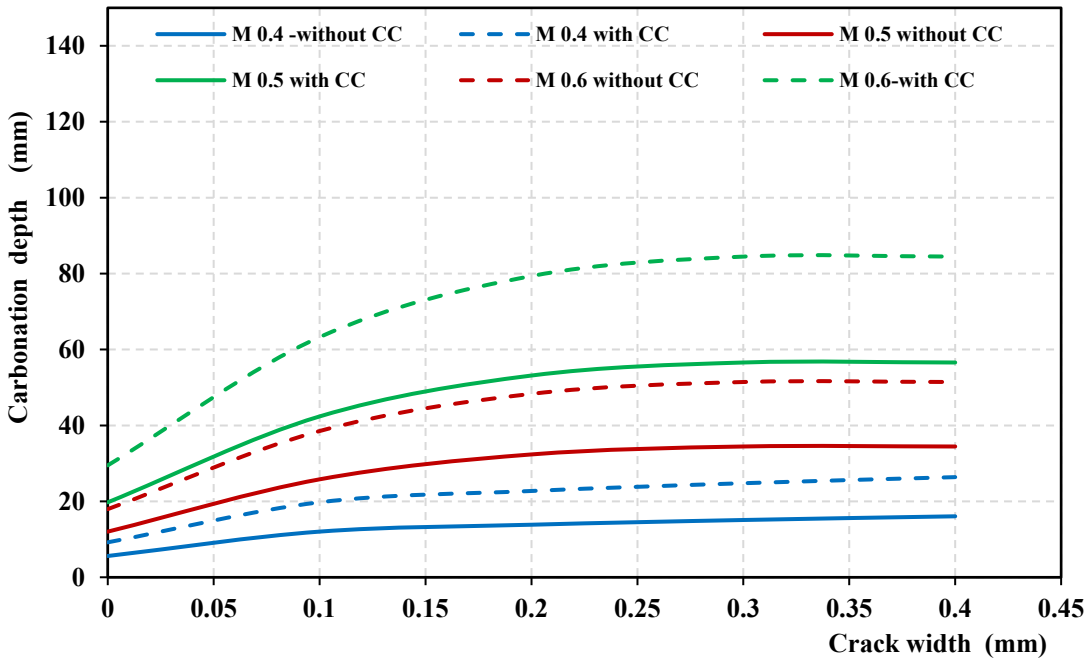

Figure 7.33: Effect of crack width and climate change for (RCP 8.5) on the carbonation depth of structures in the city of London

b: Structures Exposed to Carbonation in Basra-Iraq

In this case, the hypothetical samples from the concrete structures in the city of Basra were employed to predict the DoC due to the following exposure to environmental conditions such as (CO_2, temperature, relative humidity, and climate change scenario RCP 8.5 and RCP 6.0). According to the proposed methodology of the carbonation rate in the previous section, the calculation and assumption will be as follows:

1- Concrete properties
   - w/cm ratio = 0.4, 0.5 and 0.6, cement content 513, 410 and 350 kg/m^3 respectively.
   - $V_v = 6.1*10^{-3}$, $22.5*10^{-3}$ and $42.6*10^{-3}$ for w/cm 0.4, 0.5 and 0.6 respectively.
2- Exposure conditions
   - CO_2 concentration = 500 ppm at year 2000.
   - Temperature is shown in Figure 7.19 (a), and $f_{c1(T)}$ =1.14 to 1.18 (variable over time due to climate change).
   - Relative humidity as shown in Figure 7.19 –b, and $f_{c2(RH)}$= 0.271.
   - Climate change: The change in CO_2 and temperature are shown in Figure 7.31(a, b) respectively (IPCC-2014). The average values CO_2 and temperature were calculated over the time period are not peak values at time t to account for CO_2 concentration, $f_{c1(T)}$ and $f_{c2(RH)}$.
3- Time of exposure: (100 years)
4- Boundary condition or surface concentration CO_2 is shown in Figure 7.31(a).
5- The diffusion coefficient of chloride (D_{CO2}): accounting for and calibrated by properties of mixes used, RH, T and crack width factor using Equations 7.42 to 7.47 (control case) and consider the change in CO_2 concentration, temperature and relative humidity due to climate change according to IPCC (2014) models (scenarios) (second case).
6- The shape of the sample: Girder or column, one un-cracked and another cracked with a crack width of 0.05- 0.4 mm.

According to the assumptions, the properties of concrete, crack width and type of exposure condition, the diffusion coefficient (D_{CO2}) beyond considering the impact of the change in CO_2 concentration, temperature and humidity due to RCP 8.5 and RCP 6.0 are presented in Table 7.9.

Table 7.9: Temperature, relative humidity and crack width dependent on D_{CO2}

Sample & Case		CO_2 ppm	D_{CO2} for samples with crack width $m^2/sec *10^{-8}$			
			Un-cracked	0.05-0.15 mm	0.15-0.25 mm	0.25-0.35 mm
M 0.4	Without effect of CC	500	0.92	4.24	5.62	6.68
	With effect of CC	1000	0.99	4.54	6.02	7.15
M 0.5	Without effect of CC	500	3.39	15.61	20.67	24.56
	With effect of CC	1000	3.63	16.71	22.12	26.28
M 0.6	Without effect of CC	500	6.45	29.71	39.34	46.74
	With effect of CC	1000	6.90	31.79	42.10	50.02

*CC: climate change due to change in temperature and humidity.

Carbonation depths due to exposure conditions over a period of up to 100 years for two scenarios of IPCC-2014, for M 0.4, M 0.5 and M 0.6 (un-cracked samples), with and without the impact of climate change (change in CO_2, temperature and relative humidity) were shown in Figures 7.34 (a, b and c). On the other hand, change in climate change parameters for different crack widths was considered in the carbonation rate as shown in Figure 7.35.

The predicted results of carbonation depth in concrete members exposed to CO_2 environment conditions due to the influence of climate change parameters for IPCC (2014) models (RCP 8.5 and RCP 6.0 scenarios) increased when considering the increase in CO_2, temperature and the reduction in humidity for both exposure condition scenarios as shown in Figure 7.34. The percentage increase in DoC for uncracked members at 100 years of exposure time, with changing CO_2 concentration, temperature and relative humidity is about 25% and 13% for RCP 8.5 and RCP 6.0 scenarios respectively at 100 years of exposure time for all w/cm ratios. While, the percentage in DoC for the cracked concrete member (different crack width and w/cm ratio) is 27% due to the exposure condition scenario, RCP 8.5.

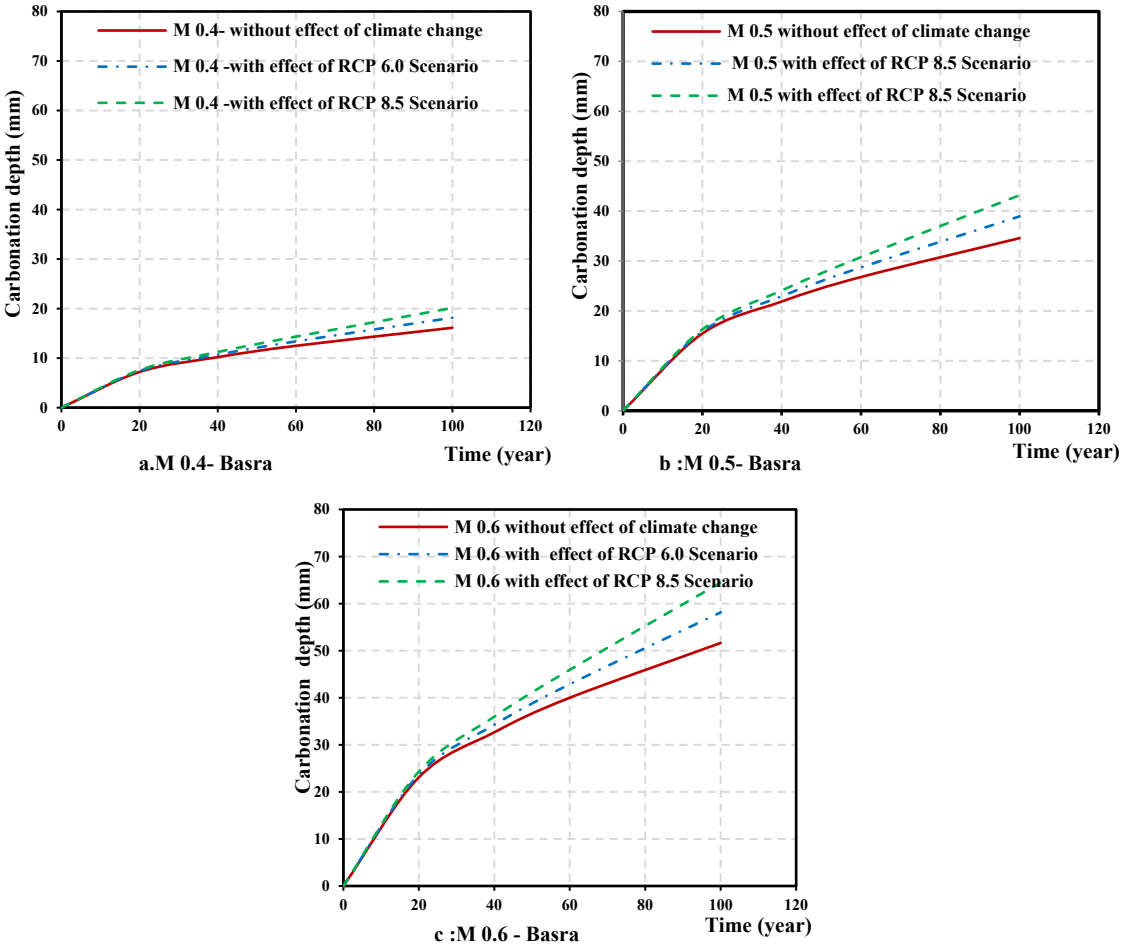

Figure 7.34: Effect of climate change scenarios on the prediction of the carbonation depth for a un-cracked member in the city of Basra

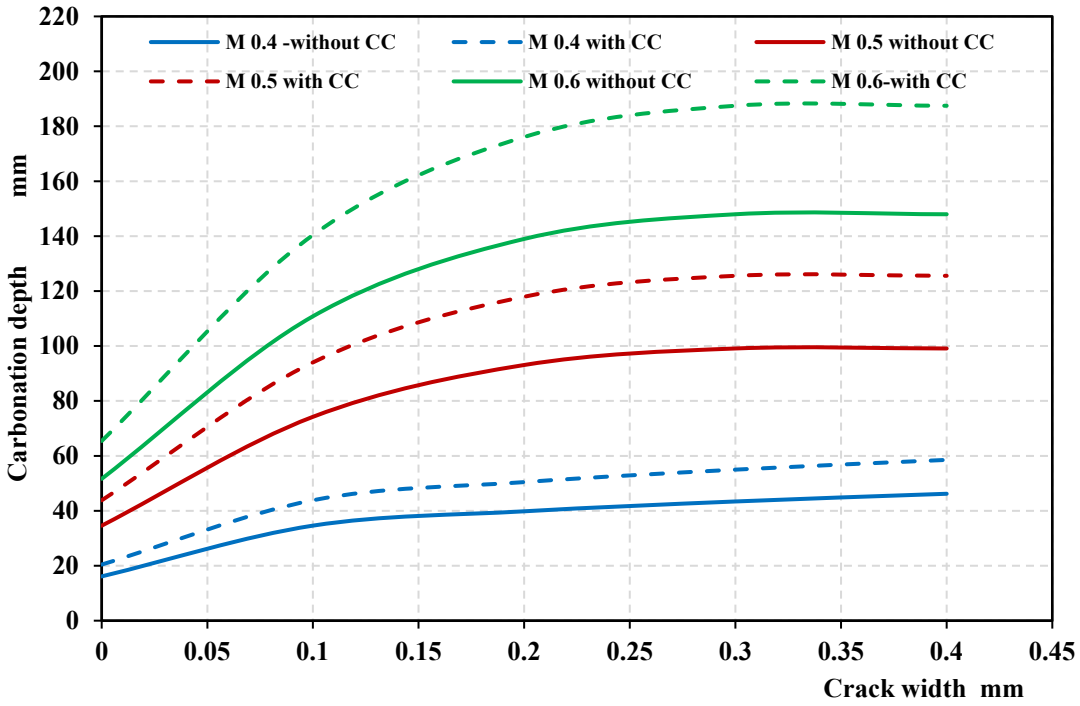

Figure 7.35: Effect of crack width and climate change for (RCP 8.5) on the carbonation depth of structures in the city of Basra

c: Prediction of Corrosion Initiation Time due to Carbonation in Concrete Structures and Climate Change

It is noticed that for both cities, London and Basra, over 100 years with different concrete properties used in the construction of the structures, there is an obvious impact of climate change on carbonation depths. However, it is also important to consider what the actual effects of climate change will be on the service life of a structure. As mentioned previously as shown in Figure 2.7, it is observed that corrosion may occur when the distance between the carbonation depth and the reinforcement bar surface is less than 1-5 mm (Yoon *et al*., 2007). However, probabilistic analyses for assessing durability design specifications tend to ignore this effect (CEB-FIP, 2013). Hence, the time to corrosion initiation, t_i occurs when carbonation depth is equal to the depth of the concrete cover. The times to initiation, t_i due to carbonation induced corrosion for each of the mixes (assuming a concrete cover of 25 mm) for two cases of structures in London and Basra are listed in Table 7.10. The results from Basra (moderate humidity, and higher temperatures) were more prone to corrosion than a cooler, wetter city such as London.

Table 7.10: Time to corrosion initiation due to carbonation – constructed in Year 2000.

Mix designation	Scenario	London City structures		Basra City structures	
		Time to initiation (year)*	Ultimate carbonation Depth (mm) **	Time to initiation (year)*	Ultimate carbonation Depth (mm) **
M 0.4	Control condition	> 100	6	> 100	16
	RCP 8.5	> 100	9	> 100	20
	RCP 6.0	> 100	8	> 100	18
M 0.5	Control condition	> 100	12	50	34
	RCP 8.5	> 100	20	41	43
	RCP 6.0	> 100	17	44	39
M 0.6	Control condition	> 100	17	25	51
	RCP 8.5	82	29	20	64
	RCP 6.0	92	26	22	58

*Time of initiation of corrosion is the time at the DoC= 25 mm.

** Ultimate carbonation Depth is at Year 2100.

7.6.5 Numerical Model Simulating the Depth of Carbonation for Concrete Structures

This method of finding carbonation depth relies upon a numerical model involving the simultaneous solution of equations for the diffusivity of $CO_{2(aq)}$ and the reaction of $Ca(OH)_{2(aq)}$ in concrete specimens (Park, 2008) as shown in Figure 7.36 by:

$$\frac{\partial}{\partial t}[CO_{2(aq)}] = D_{CO_2}\frac{\partial^2}{\partial x^2}[CO_{2(aq)}] - \frac{k_c}{2}[CO_{2(aq)}][Ca(OH)_{2(aq)}] \quad (7.49)$$

$$\frac{\partial}{\partial t}[Ca(OH)_{2(aq)}] = D_{Ca(OH)_2}\frac{\partial^2}{\partial x^2}[Ca(OH)_{2(aq)}] - \frac{k_c}{2}[CO_{2(aq)}][Ca(OH)_{2(aq)}] \quad (7.50)$$

where:

$CO_{2(aq)}$, $Ca(OH)_{2(aq)}$ are Aqueous concentration of CO_2 *and* $Ca(OH)_2$ respectively, *kc is* the rate constant of reaction *x* is the depth of concrete and time *t.*

The numerical analysis of ($CO_{2(aq)}$ and $[Ca(OH)_{2(aq)}$) diffusivity is based on properties of concrete samples and external conditions; some properties were obtained from chapter four such as density, porosity and compressive strength. Other properties were calculated in the section (7.6.1) such as the carbon dioxide diffusion coefficient, whilst the modulus of elasticity, Poisson's ratio was based on the proposed equations by AL-Ameeri *et al*. (2013) and thermal conductivity, *Tc* depends on the relationships of ACI 122R(2002). The steps of using the simulation are summarized in Figures 7.8 and 7.37. All the properties of concrete which were used in simulation and numerical analysis are summarized in Table 7.1.

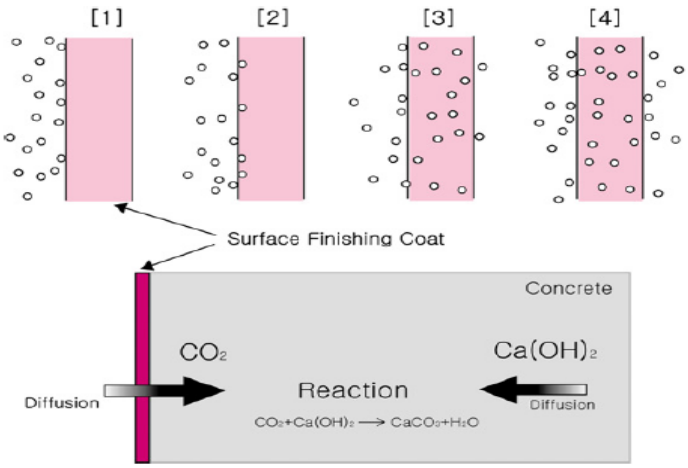

Figure 7.36: Diffusion of carbon dioxide and concrete carbonation (Park, 2008)

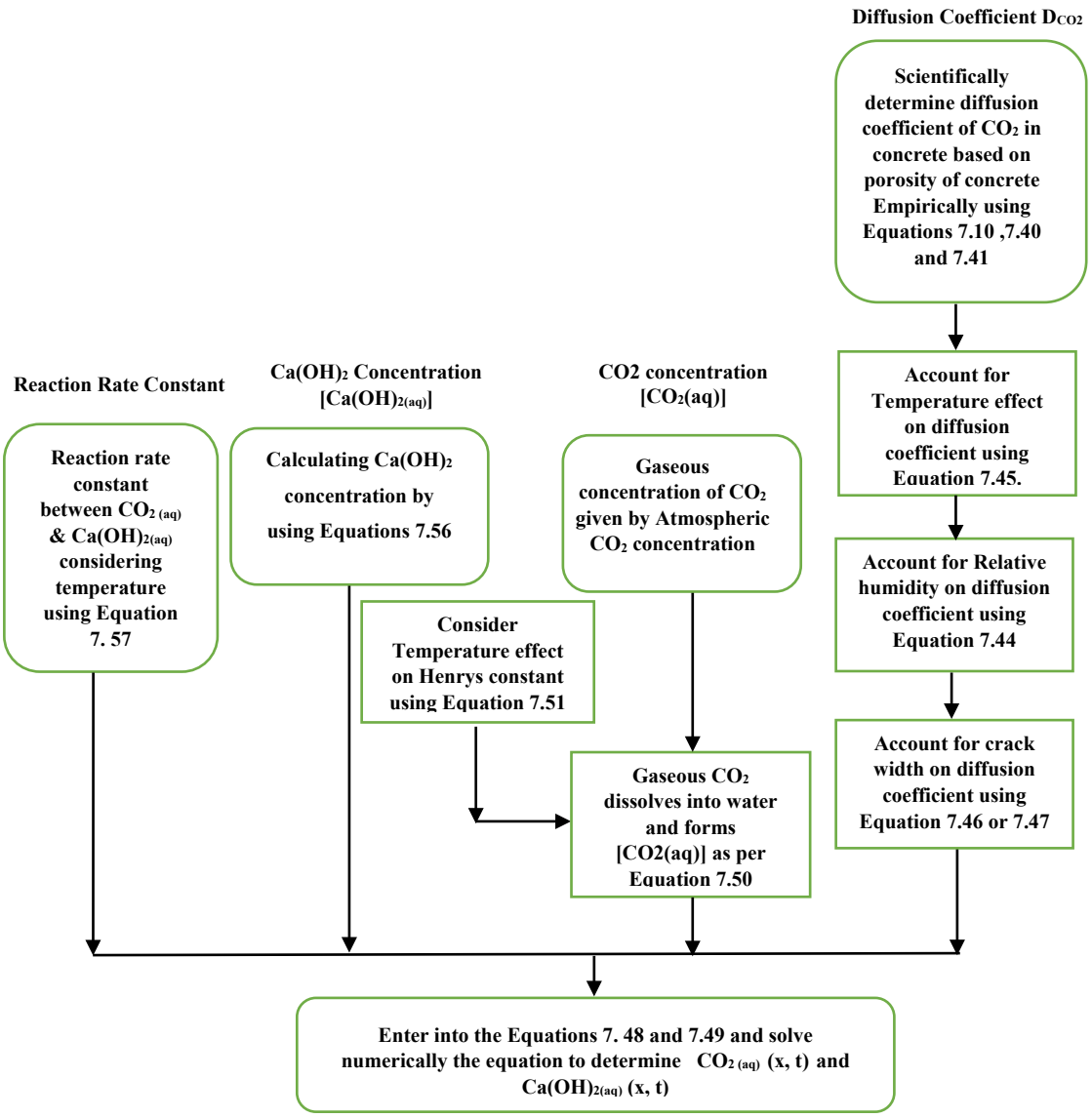

Figure 7.37: Flowchart for the determination of concentration of $CO_{2\,(aq)}$ and $Ca(OH)_{2(aq)}$

Firstly, the gaseous diffusion of CO_2 is important in the carbonation of concrete and the diffusion coefficient of carbon dioxide has been described in section 7.6.1. Upon reaching a given point in the concrete sample, the gaseous CO_2 dissolves into water and forms dissolved aqueous $CO_{2\,(aq)}$ at that location at concentration governed by Henry's Law (Yoon *et al.*, 2007).

$$[CO_{2(aq)}] = HRTCO_{2(g)} \tag{7.51}$$

where:

$CO_{2(g)}$ is a concentration of CO_2 as gas in an environment condition, H is the Henry's constant (mole/m^3 atm), R is the gas constant and T is the temperature (K).

Henry's constant is temperature-dependent as shown in Equation 7.51 (Fogg and Sangster, 2003):

$$H(T) = H_{ref}\, exp\left[\Delta\left(\frac{1}{T_{ref}} - \frac{1}{T}\right)\right] \quad (7.52)$$

where:

H_{ref} is the reference Henry's constant (34.2 mol/m^{3}atm) and Δ is an enthalpy constant (2400 K).

For example, the [$CO_{2(aq)}$] was calculated and used as 1.14 M at 30 °C and 6 % $CO_{2(g)}$.

Secondly, the dissolved aqueous $Ca(OH)_{2(aq)}$ concentration in the solution of concrete depends on the degree of hydration, cement content and cement compounds, C_3S and C_2S (Park, 2008). The total amount of Ca $(OH)_2$ in the solid phase of cementation composite is calculated from the chemical composition of the hydration of cement compounds, C_3S, and C_2S as shown in Equations (Neville, 2011; Ishida *et al*., 2014):

$$2C_3S + 6H \rightarrow C_3S_2H_3 + 3CH \quad (7.53)$$

$$2C_2S + 4H \rightarrow C_3S_2H_3 + CH \quad (7.54)$$

where:

C_3S is Tricalcium silicate and its molar weight (228 g/mole), C_2S is Dicalcium silicate and its molar weight (172 g/mol) and CH is calcium hydroxide and its molar weight (74 g/mole).

Then;

$$C_{CH} = \frac{M_{CH}}{2*M_{C_2S}} * C_{C_2S} + \frac{3M_{CH}}{2*M_{C_3S}} * C_{C_3S} \quad (7.55)$$

where:

C_{CH} is $Ca(OH)_2$ content, M_{CH}, M_{C_2S} and M_{C_3S} are molecular weight of $Ca(OH)_2$, C_2S and C_3S respectively, C_{C_2S} and C_{C_3S} are C_2S and C_3S percentage by weight of cement respectively.

So, the concentration of $Ca(OH)_2$ can be determined by cement content and degree of cement hydration by:

$$[Ca(OH)_2] = \frac{C_{CH}*C*\propto}{M_{CH}} \quad (7.56)$$

where:

$[Ca(OH)_2]$ is $Ca(OH)_2$ concentration in mole/m^3 , M_{CH} is molecular weight of $Ca(OH)_2$(74 g/mole), C is the weight of cement in m^3 and $\propto$ is hydration degree.

In the cement used in this study, the C_2S and C_3S percentages were 15.36% and 55% by weight of cement respectively and assuming the hydration of cement was 90%, then [$Ca(OH)_2$] by :

$$[Ca(OH)_2] = 3.685\ C \qquad (7.57)$$

For example, [$Ca(OH)_2$] was calculated for cement content mix 380 kg in m^3 was 1400 mol/m^3 (1.4 M).

The diffusion coefficient of $Ca(OH)_2$ was taken as $1*10^{-12}$ m^2/s in analysis of diffusivity of calcium hydroxide (Papadikas *et al*., 1991), where Park (2008) confirmed that the diffusion coefficient of $Ca(OH)_2$ may be kept at $1*10^{-12}$ m^2/s and the rate of reaction may be upped a thousand fold with a slight change in depth of carbonation.

Thirdly, it is also significant to find the rate of reaction between $CO_{2(aq)}$ with $Ca(OH)_{2(aq)}$ to form $CaCO_3$, as this is also temperature-dependent. Khunthongkeaw and Tangtermsirikul (2005) proposed a second-order relationship with a rate constant of reaction:

$$k_C = A\ e^{\frac{-U}{RT}} \qquad (7.58)$$

where:

k_c is the reaction rate constant for the reaction between $CO_{2(aq)}$ with $Ca(OH)_{2(aq)}$ at the temperature of interest (m^3/mol/s), U is the reaction activation energy (40,000 J/mol K) and A is the pre-exponential factor (1390 m^3/mol/s).

The domain, the initial and the boundary condition of Equation 7.58 to 7.65 are:

$$CO_{2(g)}(x,t) \quad 0 \le x \le L \ and \ 0 \le t \le \infty \qquad (7.59)$$

$$CO_{2(g)}(x,0) = 0 \quad for\ x > 0 \qquad (7.60)$$

$$CO_{2(g)}(0,t) = CO_{2(g)}(atm) \quad for\ t > 0 \qquad (7.61)$$

$$\frac{d}{dx} CO_{2(g)}(L,t) = 0 \quad zero - flux\ boundary \qquad (7.62)$$

$$Ca(OH)_{2(g)}(x,t) \quad 0 \le x \le L \ and \ 0 \le t \le \infty \qquad (7.63)$$

$$Ca(OH)_{2(g)}(x,0) = Ca(OH)_{2(aq)i} \quad for\ x > 0 \qquad (7.64)$$

$$\frac{d}{dx}Ca(OH)_{2(aq)}(0,t) = 0 \quad zero - flux\ boundary \qquad (7.65)$$

$$\frac{d}{dx}Ca(OH)_{2(aq)}(L,t) = 0 \quad zero - flux\ boundary \qquad (7.66)$$

where:

L is the thickness of the concrete sample

For concrete, the thermal diffusivity is much greater than the mass diffusivity. Therefore, the temperature of the concrete is assumed to be uniform at any time so that there is no need to also solve the energy equation or to account for the heat of the reaction (Talukdar *et al*., 2012a). A flowchart to demonstrate how Equation 7.48 and 7.49 are formulated is shown in Figures 7.8 and 7.37. To simplify the analysis, a numerical analysis was used to solve these equations simultaneously, and determine the concentrations of $CO_{2\,(aq)}$ and $Ca(OH)_{2(aq)}$ at a given location and time within the concrete specimen due to exposure to CO_2 environment as shown in Figure 7.38. The simulation of the concentration of $CO_{2\,(aq)}$ and $Ca(OH)_{2(aq)}$ profile is presented in Figures 7.39 and 7.40 respectively for example in the case of Talukdar *et al.* (2012a).

The results illustrate the concentration of $CO_{2(aq)}$ reduces with depth due to the decrease of $CO_{2(aq)}$ diffusivity into the concrete depth. Whilst, the concentration $Ca(OH)_{2(aq)}$ raises with depth due to a decrease of consumption of $Ca(OH)_{2(aq)}$ into the concrete depth owing to reduced formation of calcium carbonate.

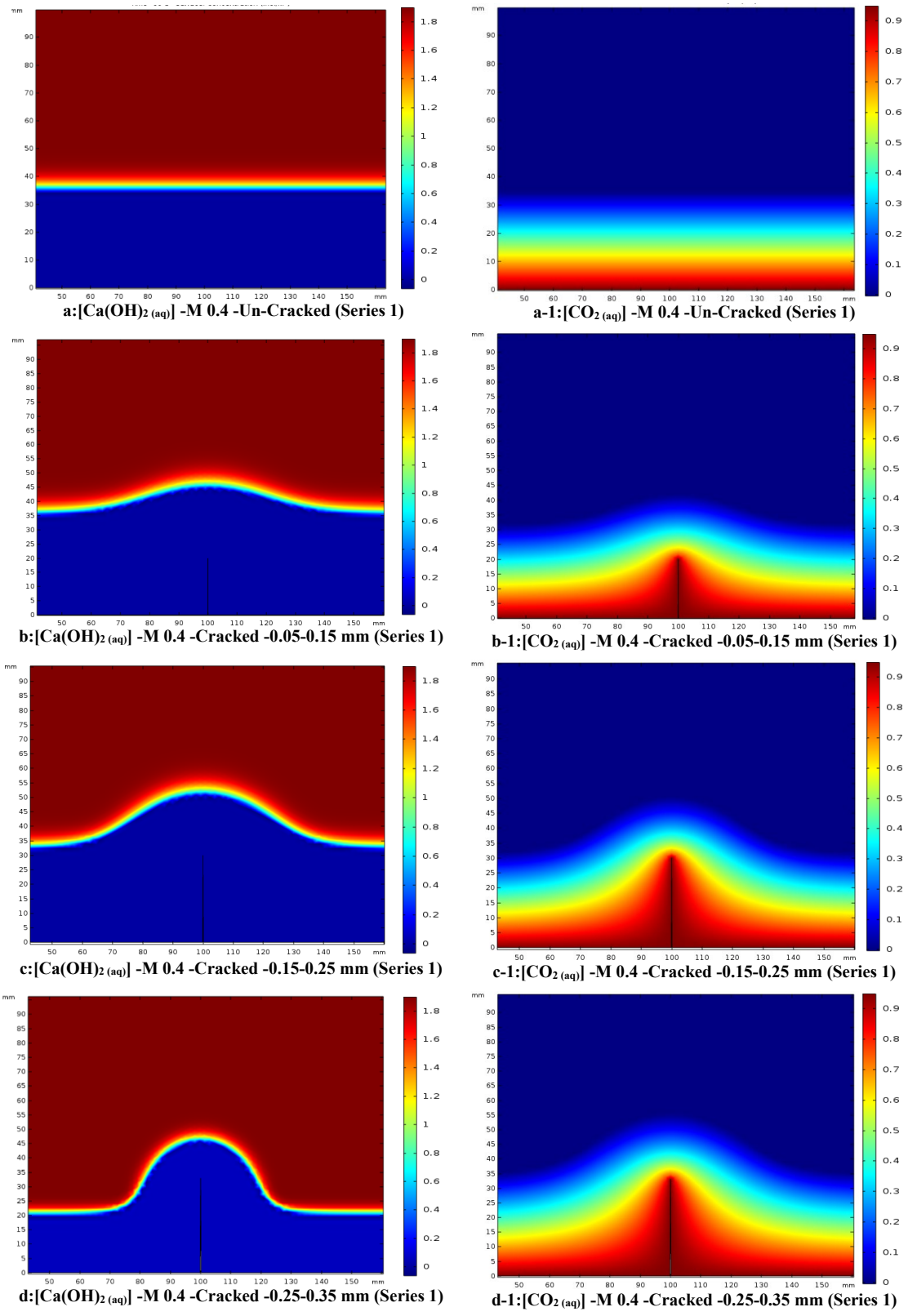

Figure 7.38:[$CO_{2\,(aq)}$] and [$Ca(OH)_{2\,(aq)}$] concentration distribution in the samples with and without a crack due to exposure to 5% CO_2 environment at 45 ºC and 65% RH for 8 weeks

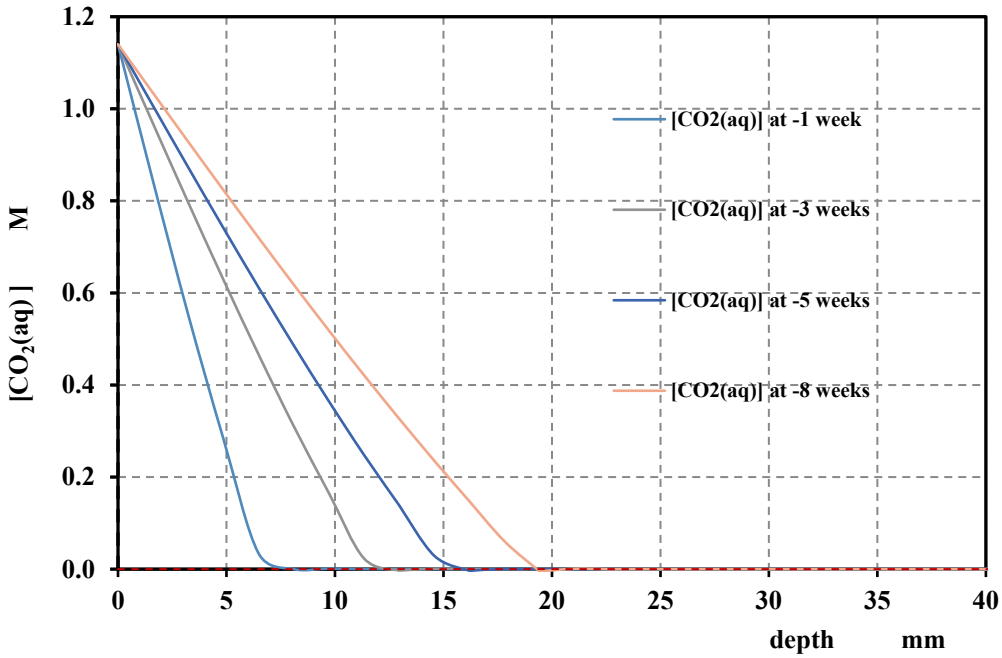

Figure7.39: $CO_{2(aq)}$ concentration profile in concrete sample for 6% $CO_{2\,(g)}$,experimental case of Talukdar *et al.* (2012a)

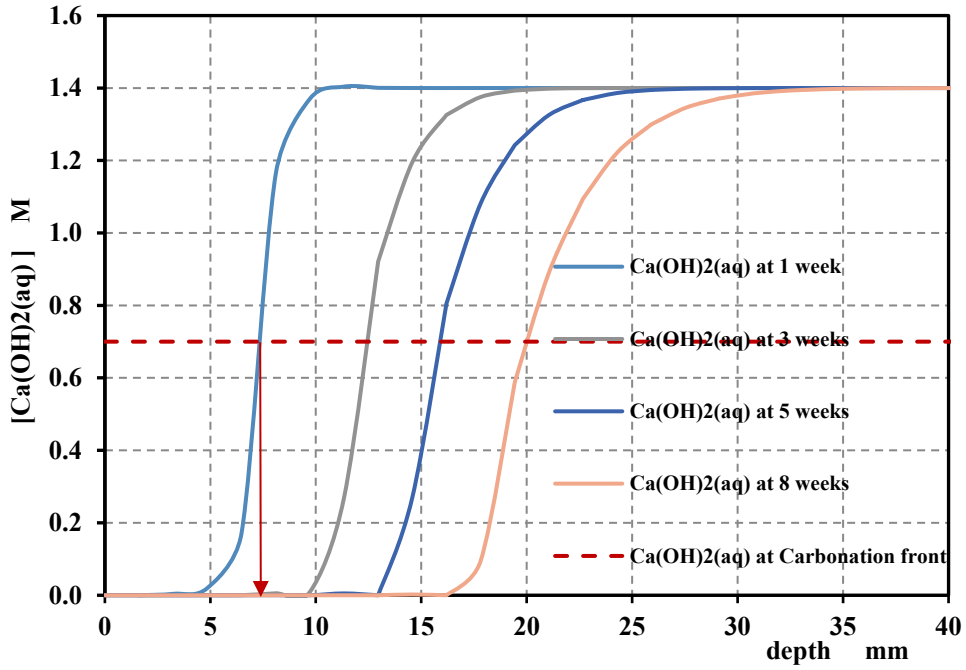

Figure7.40: $Ca(OH)_{2(aq)}$ concentration profile in concrete sample for 380 kg cement content ,experimental case of Talukdar *et al.*(2012a)

Finally, the depth of carbonation, DoC can be determined using two assumptions:

- Park (2008) found the pH of concrete drops to 9 at 50% consumption of $Ca(OH)_2$ in the concrete mixes. Therefore, Park (2008) assumed the location of the carbonation front, X_f by modelling to find the location where 50% of the $Ca(OH)_2$ is consumed. Then, the depth of carbonation, DoC is half of the carbonation front depth, X_f (Chang and Chen, 2006).

- Ehrlich *et al*. (2015) reported, in an aqueous solution containing $10^{-4.16}$ M $Ca(OH)_2$, $CaCO_3$ will precipitate and form if the concentration of CO2(aq) exceeds $10^{-4.16}$. This is because the product of the concentration of two ions of ($CO_{2(aq)}$ and $Ca(OH)_{2(aq)}$) could exceed the solubility constant (K_{sol}) for $CaCO_3$, $10^{-8.32}$. Therefore, the minimum concentration of CO_2(aq) to form the $CaCO_3$ (carbonation components) should be more equal or more than $10^{-4.16}$ ($6.92*10^{-5}$ M). Then, the carbonation depth may be at this point of concentration $10^{-4.16}$ M $CO_{2(aq)}$; beyond this depth, the concentration of $CO_{2(aq)}$ is less and $CaCO_3$ will not precipitate.

According to the two assumptions, the depth of carbonation, DoC for experimental cases are simulated and presented in the next section.

7.6.6 Verification of Numerical Modelling of Carbonation Depth

In this section, numerical model was used to predict the carbonation rate or depth, which governs the chemical reaction of $CO_{2(aq)}$ with cementitious compounds, $Ca(OH)_{2(aq)}$ and C-S-$H_{(aq)}$. The model is validated by comparing its results with available experimental results of this study and other studies in the literature. A model based on the variation of the diffusion coefficient of $CO_{2\ (aq)}$ and $Ca(OH)_{2(aq)}$ due to changes in the properties of concrete, relative humidity (RH), temperature and CO_2 concentration is used. Those variables are numerically simulated according to a $CO_{2\ (aq)}$ transport model and consumption of $Ca(OH)_{2\ (aq)}$ which considers mass transport (diffusion). The moisture distribution, RH, and micro-pore structure characteristics, in turn, control the CO_2 and $Ca(OH)_2$ diffusion and rate of various chemical reactions under arbitrary environmental conditions (e.g. temperature). In this section of the study, the $CO_{2\ (aq)}$ and $Ca(OH)_{2(aq)}$ transportation and reaction in uncracked and cracked concrete are presented in Figure 7.27 and used in the simulation. The diffusion carbon dioxide coefficients (D_{CO2}) for the sample are computed according to Equations 7.41-7.47 and presented in

Tables B.3. Predicted data of DoC in comparison with the respective experimental results scenarios are presented in Figure 7.41(a-f)

The influence of properties of concrete, the crack width, RH, CO_2 concentration and temperature were considered in the numerical modelling in Equations 7.48 to 7.49 and verified by experimental data in this study as shown in Figures 7.41(a-f). The predicted data of carbonation depth in cracked samples showed that by increasing the crack width and depth an increase of penetration and reaction of $CO_{2\ (aq)}$ with $Ca(OH)_2$ to precipitate $CaCO_3$. A qualitative difference in trend is seen in the square of this correlation coefficient, R^2 between the predicted modelling data and the experiment results as shown in the same figure.

The progress of carbonation depth obtained from predicted data for (M 0.4, M 0.5 and M 0.6) samples by using numerical modelling was well-matched with experimental data for un-cracked and cracked samples.

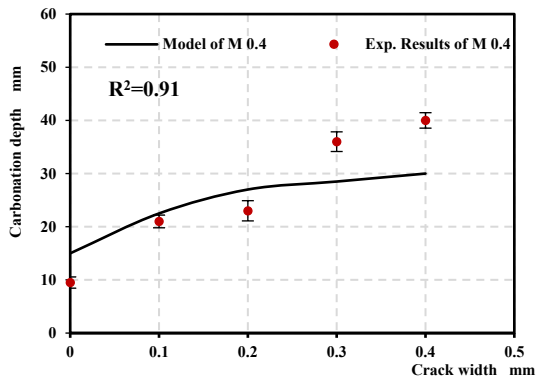

a:M 0.4 - (Series 1- 45 °C, 65% RH and 5 CO_2)

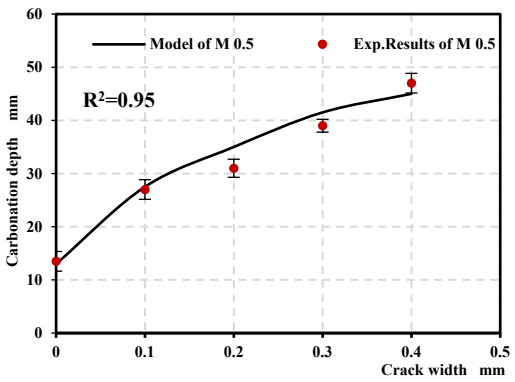

b:M 0.5 - (Series 1- 45 °C, 65% RH and 5 CO_2)

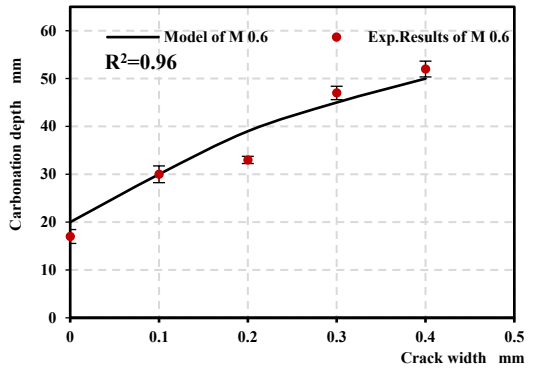

c:M 0.6 - (Series 1- 45 °C, 65% RH and 5 CO_2)

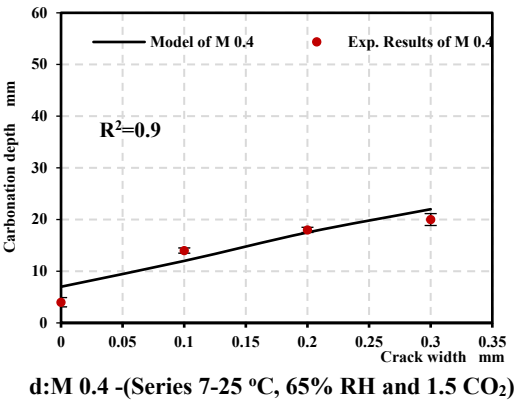

d:M 0.4 -(Series 7-25 °C, 65% RH and 1.5 CO_2)

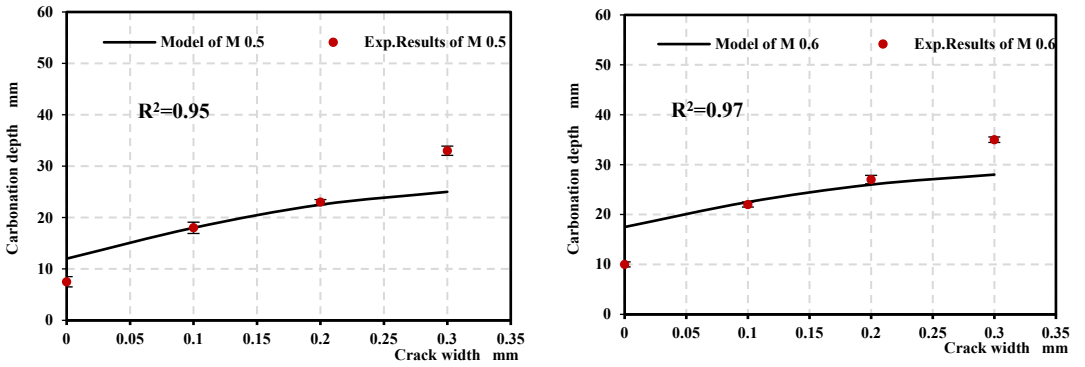

e:M 0.5 - (Series 7-25 °C, 65% RH and 1.5 CO_2) f:M 0.6 - (Series 7-25 oC, 65% RH and 1.5 CO2)

Figure 7.41: Carbonation depth- Numerical vs experimental results for Series 1(45°C, 65%RH and 5%CO_2) and Series 7 (25°C, 65%RH and 1.5% CO_2)

On the other hand, two studies, Talukdar *et al*. (2012) and Chi *et al.* (2002) have been employed in the verification of the engineering model (section 7.6.1.1) which will be used to verify the numerical modelling. The predicted data and experimental results for both cases are presented in Figures 7.42.

It can be seen from these figures; the modelling data matches with the experimental results well (regression factor, R^2 =0.94). Overall this model can be used to predict carbonation depths in future climate change scenarios.

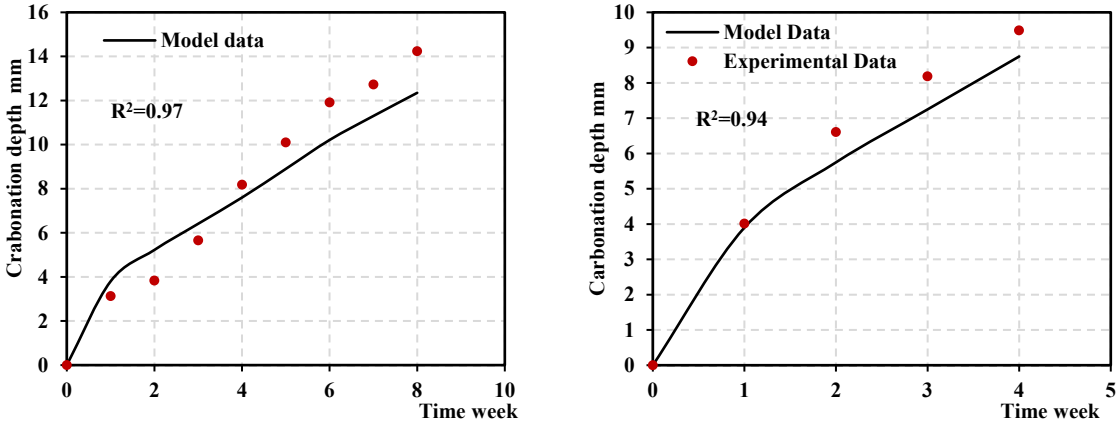

a: Talukdar *et al.* (2012) b: Chi *et al.*(2002)

Figure 7.42: Carbonation depth- Numerical vs experimental results for (a)Talukdar *et al*. (2012a) and (b) Chi *et al*. (2002)

7.6.7 Prediction of Depth of Carbonation in Concrete Structures due to Climate Change by Numerical Modelling

As mentioned previously in section 7.6.4, there are changes in climate, CO_2, T, and RH, over the (21^{st}) century as shown in Figure 7.31. These influences in atmospheric temperature and carbon dioxide concentrations of IPCC(2014) will be established in this study to forecast the change in carbonation depth numerically.

The city of London was selected, and carbonation progression depth for a hypothetical concrete samples, having w/cm ratios, 0.4, 0.5 and 0.6 and properties of these mixes as shown in section 7.6.1.2, were modelled. Based on the Assessment Report –Working Group III in Emission Scenarios (IPCC, 2014- AR5,WGIII), three emission scenarios were considered, the worst-case scenario (RCP 8.5), case scenario (RCP 6.0), and the control scenario (CO_2 levels held constant at initial levels of 400 ppm). Corresponding to the forecast of mean global temperature increases are obtained using data reported in the (IPCC, 2014- AR5) as shown in Figure 7.31. Based on this data, using the method originally described in the previous section, the assumption and calculation will be used as shown in section 7.6.4 and Table B.3(Appendix B). A simplified climate model was developed which allowed for the development of equations for emissions, temperature, and humidity over the next 100 years for the city of London. The numerical modelling developed a carbonation model to predict the DoC, considering for the first time, time-varying concentrations of CO_2, temperature, and humidity. Essentially, this numerical modelling simultaneously solves equations for the diffusion and reaction of $CO_{2(aq)}$ and $Ca(OH)_{2(aq)}$ in concrete based on Fick's Second Law. This model was used to determine the carbonation in the case of no climate change effects (CO_2, T, and RH) and the other cases with the effect of change in (CO_2, T, and RH) due to climate change. The concrete members, having different w/cm ratios (un-cracked samples) and environmental conditions were considered to forecast the DoC up to 100 years of results due to exposure conditions for the three scenarios. Assuming the building goes into service in the year 2000, the carbonation depths for each mix for the three scenarios are presented in Figure 7.43 (a-c). On the other hand, changes in climate change parameters for different crack widths were considered for the carbonation rate as shown in Figure 7.44.

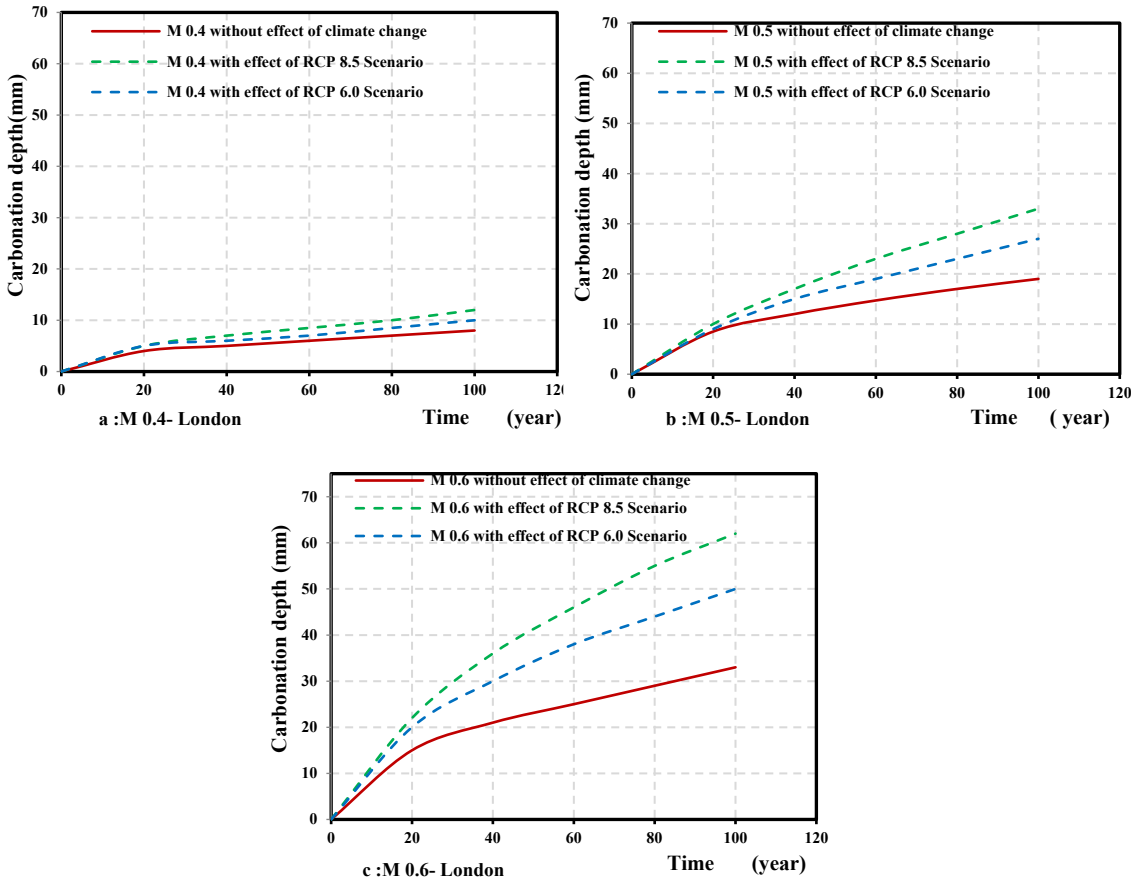

Figure 7.43: Effect of climate change scenarios on the prediction of carbonation depth for a un-cracked member in the city of London

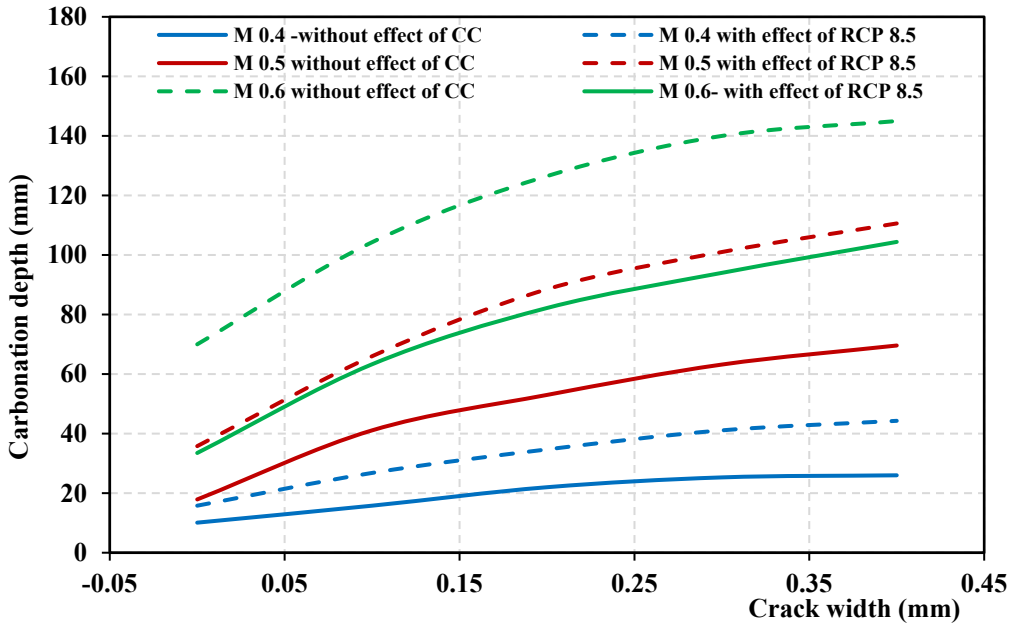

Figure 7.44: Effect of crack width and climate change for (RCP 8.5) on the carbonation depth of structures in the city of London in the Year 2100

From these figures, some of the observations are made.

(i): The analytical results of carbonation depth in concrete members exposed to CO_2 environment condition due to the influence of climate change parameters for IPCC (2014) models (RCP 8.5 and RCP 6.0 scenarios) increased with the increase in CO_2, temperature and reduction humidity for both exposure condition scenarios. The percentage increase in the ultimate carbonation depths comparing the control condition for the three scenarios is listed in Table 7.11. While, the percentages increase in carbonation depth for the cracked concrete members (different crack widths and w/cm ratios) due to exposure condition scenario, RCP 8.5 was 63%,69% and 63% for M 0.4, M 0.5 and M 0.6 respectively.

Table 7.11: Effect of climate change scenarios RCP 8.5 and RCP 6.0 on carbonation progress in concrete members in the city of London

Mix designation	Scenario	Percentage increase in the ultimate carbonation depth (mm) at				
		2020	2040	2060	2080	2100
M 0.4	RCP 8.5	25	40	42	43	50
	RCP 6.0	25	20	17	21	25
M 0.5	RCP 8.5	18	42	56	65	74
	RCP 6.0	25	29	25	35	42
M 0.6	RCP 8.5	47	71	84	90	88
	RCP 6.0	33	43	52	52	52

(ii): Carbonation progress due to the change in CO_2 and temperature is higher due to the increase of porosity of concrete (properties of concrete dependent). Carbonation progress for Mix M 0.6 with w/cm ratio 0.6 for both scenarios was higher than carbonation depths for mixes M 0.4 and M 0.5.

(iii): It is seen that climate change does not begin to seriously affect the rate of carbonation until about 30 years into the future (in these simulations, the year 2030). It is only after 30 years that we start to see the carbonation depth curves for the RCP 8.5 and RCP 6.0 scenarios begin to seriously divert from the control curves for all mixes.

Finally, it is noticed that over 100 years, for these cases, there is an obvious impact of climate change on carbonation depths. However, it is also important to consider what the actual effects of climate change will be on the service life of a structure. As mentioned previously as shown in Figure 2.7. it is observed that corrosion may occur when the distance between the carbonation depth and the reinforcement bar surface is less than 1-5 mm (Yoon *et al*., 2007). However, probabilistic analyses for assessing durability design specifications tend to ignore this effect (CEB-FIP, 2013). Hence, the time to corrosion initiation, t_i occurs when the carbonation depth is equal to the depth of concrete cover. The times to initiation, t_i due to carbonation induced corrosion for each of the mixes (assuming the concrete cover is 25 mm) for two cases of structures in London are listed in Table 7.12.

Table 7.12: Time to corrosion initiation due to carbonation – constructed in the Year 2000

Mix designation	Scenario	Time to initiation (year)*	Ultimate carbonation Depth (mm)**
M 0.4	Control condition	> 100	8
	RCP 8.5	> 100	13
	RCP 6.0	> 100	10
M 0.5	Control condition	> 100	18
	RCP 8.5	60	33
	RCP 6.0	100	28
M 0.6	Control condition	60	34
	RCP 8.5	21	62
	RCP 6.0	24	50

*Time to initiation of corrosion is the time at the DoC= 25 mm.
** Ultimate carbonation Depth is at Year 2100.

The main factors affecting an increase in the carbonation depth or rate is the increase of carbon dioxide concentration as well as the increase in temperature and decrease in the relative humidity. The IPCC (2014), (AR5-RCP 8.5) have forecasted the change in carbon dioxide over the (21^{st}) century will reach up to double concentration by 2100 compared with 2000 that lead to an increase in the average temperature of 4.2°C as shown in Figure 7.31. As mentioned previously, the atmospheric carbon dioxide concentration, temperature, and humidity of the exposure environment are the main

driving force for carbon dioxide penetration in concrete structures (Yoon *et al*., 2007, Talukdar *et al*., 2012b). The model of the rate of carbonation is based on surface exposure conditions, CO_2, RH and T and properties of concrete structure (Lagerblad, 2005).

Finally, considering that the structures in these cases would likely be subjected to deterioration by means other than carbonation during the same time, the reduction in initiation time caused by climate change factors would be one of many factors affecting the service life. Secondly, it is noted that there is a minimal reduction in propagation time (the difference between the time to initiation and time to failure) between the control cases, and the climate change cases, for each respective mix. Therefore, in the short term, it is reasonable to conclude that climate change will not significantly affect the durability of our concrete infrastructure. However, it was noted earlier that the effects of climate change, in fact, become significant after approximately 30 years.

7.7 Summary

The modelling and simulation of the impact of climate change parameters on the durability of concrete structures, in particular, chloride penetration and carbonation depth are presented in this chapter. The modelling of the chloride penetration and carbonation depth have been developed and proposed to consider the main factors of study, such as the properties of concrete and climate parameters. The modelling has been validated by experimental results. Climate change, atmospheric temperature, and carbon dioxide concentrations of IPCC (2014) scenarios were considered in chloride concentration and carbonation depth.

- A model for the prediction of the chloride profile (concentration with the depth of concrete) based on mechanisms of chloride transport methods in cementitious materials, the diffusion, and the convection or advective in concrete exposed to a salt solution under de-icing and marine conditions has been developed.
- In the modelling of chloride, the diffusion chloride coefficient, $D_{a,ref}$ considered internal affected factors such as the porosity, tortuosity of voids in concrete (Ω) and the fraction of aggregate in concrete.
- In the modelling of chloride concentration, the diffusion chloride coefficient, D_a was considered the effect of crack and external affected factors such as the temperature, relative humidity.

- The modelling of chloride profile was based on Fick's Second Law of Diffusion (as shown below) and solved numerically to find the concentration of chloride with depth and the time $C_{Cl}(x, t)$. The numerical modelling has been validated by experimental results from this study and other studies for two cases of concrete, both uncracked and cracked concrete samples. The results of the model proposed were generally a good fit and well-matched with the distribution of chloride concentration profiles obtained from concretes exposed to chloride conditions in these studies. Therefore, this modelling can be used to predict chloride concentration with the depths in the control condition and in future climate change scenarios. Two approaches of prediction of surface concentration C_s were used in both environmental conditions, de-icing and marine to investigate the impact of climate change on of chloride concentration profile in the long term of 50 years.
- The influence of climate change (increase in temperature, and reduction of the relative humidity) has a significant impact on the chloride concentration profile as follows:

- For the de-icing environment condition (London case), the percentage increase in chloride concentration at a depth of 50 mm (minimum requirement of concrete cover) was 5.8 % and 3.8% for uncracked and cracked concrete decks respectively at an exposure age of 50 years for two approaches of C_s concentration.
- For marine environment conditions (Basra case), the percentage increase in chloride concentration at a depth of 50 mm were 3.6 % and 3% for uncracked and cracked concrete decks respectively at an exposure age of 50 years for two approaches of C_s concentration.
- The impact of the crack on chloride concentration was observable for both environment conditions (de-icing and marine), duration of exposure and in both cases (the control case and the case including a climate change effect). The path of crack opening helps chloride to penetrate quickly and increases the chloride concentration into the un-cracked concrete surrounding the crack

- Climate change will affect the progression of chloride concentration and induce corrosion in our concrete structures due to approaching the threshold of chloride concentration induced corrosion. The chloride concentration in deeper depths will be much higher in the long term and harsher exposure conditions such as the worst-case scenario of RCP 8.5.

- The two modelling approaches were proposed in this study to predict the carbonation depth, one is based on uptake of the carbon dioxide by cementitious materials using a solution of Fick's Second Law of Diffusion (engineering modelling). The second approach is based on mechanisms of the $CO_{2(aq)}$ diffusion and $Ca(OH)_{2(aq)}$ reaction mechanisms in cementitious materials, in concrete exposed to carbon dioxide environment conditions.
- In both models of carbonation depth, the diffusion chloride coefficient, D_{CO2} considered internally affected factors such as the porosity and tortuosity of voids in concrete (Ω).
- In the modelling of carbonation, the diffusion of carbon dioxide coefficient, D_{CO2} considered the effect of crack and externally affected factors such as temperature and relative humidity.
- An integrated carbonation model was developed to predict the depth of carbonation in non-pozzolanic, uncracked and cracked concrete specimens, considering properties of concrete, concentrations of CO_2, temperature and humidity. The numerical model was verified by experimental results from this study and other studies for two cases of concrete, uncracked and cracked concrete samples.
- The influence of climate change due to the increase in CO_2 and temperature and reduction in the relative humidity has a considerable impact on the depth of carbonation. For example, the results from the city of Basra (moderate humidity, and higher temperatures) were more prone to corrosion than a cooler, wetter city such as London. And this impact is much higher with an increase in the w/cm ratio due to an increase in the porosity and diffusivity of CO_2 in concrete structures.
- Climate change will affect the progression of carbonation and induce corrosion in our concrete structures. Ultimate carbonation depths will be much higher in the long term and in harsher exposure conditions such as the worst-case scenario of RCP 8.5.
- Although in the near future, climate change will have an unnoticeable effect on the durability of concrete structures constructed in the Year 2000, the real effects of climate change will become evident after approximately 30 years. Therefore, structures being constructed in 2020–2030 may have to consider degradation due to climate change when they are being designed.

CHAPTER VIII: CONCLUSIONS AND RECOMMENDATIONS

8.1 General

The overall aims of this study were to identify and investigate the potential impact of global climate change on infrastructure and durability with special emphasis on existing reinforced concrete structures in the UK and Iraq. This investigation is based on establishing a methodology that effectively utilises the experimental data obtained through the experimental programme and develops integrated models accounting for the significant factors of climate change and micro-pore structures of concrete in the assessment and health monitoring of the existing concrete structures. The study focused on the phenomena governing deterioration in concrete structures, carbonation, chloride penetration and corrosion rate. The following conclusions can be drawn from this study.

8.2 Conclusions from the Experimental Investigation

An experimental investigation into the effect of w/cm ratio, CO_2 concentration, temperature and relative humidity on the carbonation depth, the chloride penetration and the corrosion rate, has been conducted. Based on these experimental results, the main conclusions that can be drawn are as follows:

8.2.1 Properties of Concrete Mixes Used in the Study

Five mix designs were examined in this study. Three of the mixes were cement-based mixes with w/cm ratios of 0.4, 0.5 and 0.6 respectively, and the remaining two had the w/cm ratio of 0.5 but some of the quantity of the cement was replaced with supplementary cementitious materials (SCM) such as PFA and GGBS in order to create a variety of properties and microstructures of concretes.

The properties of fresh and hardened concrete such as slump, compressive and tensile strengths, water absorption, gas permeability and chloride permeability were tested for the mixes. These properties are very important and for that reason, the effect of different water/cementitious materials ratios on these properties has been investigated to use in assessment and discussion of the carbonation, chloride concentration and corrosion rate results. These are important in the modelling and simulation part as well. The main conclusions that can be drawn from the results are as follows; -

- The microstructure of concrete is mainly affected by the w/cm ratio, the type of cementitious materials, the degree of hydration of cementitious materials and the curing period. The porosity or permeation properties can be used as an indicator of the micro-pore structure in the concrete mass.
- The reduction in porosity for mixes with a lower w/cm ratio can be attributed to a relatively well-developed gain and pore structure commensurate with a higher degree of hydration. This corroborates well with the increase in curing age.
- The porosity or permeation properties of the concrete decrease by decreasing the w/cm ratio and increasing the curing period due to an increase in the degree of hydration. The addition of SCMs also reduces the porosity of mixes when compared to its cement-based counterpart due to the consumption of $Ca(OH)_2$ and production of additional C-S-H.
- Water absorption is related not only to the pores structure of concrete but also to the moisture condition of the concrete pores.
- The movement or transportation of gases (gas permeability), liquids (water absorption and porosity), and ions (migration of chloride coefficient) through concrete are important because of their interactions with concrete constituents or pore water, and thus it can alter the integrity of concrete, directly and indirectly, leading to the deterioration of structures due to chloride and carbon dioxide penetration in concrete structures (Explained in the next sections).
- Diffusion migration of chloride ions is the process by which matter is transported from one part of a system to another due to applied power which accelerates the penetration of chloride in concrete samples. This process of transportation of chloride ions depends on the micro-pore structure of concrete. Thus: -
  - The chloride migration coefficient D_{nssm} decreases significantly by decreasing the w/cm ratio of mixes and increasing the curing period of concrete.

- The chloride migration coefficient D_{nssm} of concrete with SCMs (GGBS and PFA) decreases considerably at different curing ages due to the resistance of these materials to chloride penetration.
- The chloride ingress properties in the concrete or D_{nssm} strongly correlate with the porosity, compressive strength and splitting strength of concrete.

8.2.2 Depth of Carbonation (DoC)

The influence of both the exposure environment and the properties of concrete was investigated the DoC in concrete structures. Three levels of CO_2, RH, temperatures and the w/cm ratio have been used for this investigation. The effect of cracks caused by loading on the carbonation depth was also considered in addition to the above-mentioned conditions. Carbonation depth was determined using an accelerated environment test programme using a phenolphthalein indicator, XRD analysis, and apparent pH and consumed OH^-. The depth of carbonation, X_p was determined by the phenolphthalein indicator, while the carbonation front, X_f was measured by XRD analysis, and apparent pH and consumed OH^- technique. Furthermore, the effect of replacing OPC by SCMs, PFA and GGBS on the DoC in un-cracked and cracked concrete was also investigated. The main conclusions that can be drawn from the results are that the process of carbonation is controlled by the diffusion of carbon dioxide through the already carbonated surface zone towards the reaction front.

- Carbonation rate is controlled by the concentration of carbon dioxide at exposure environmental conditions by diffusion acting as a driving force in concrete.
- The carbonation rate of concrete has been closely correlated with the connective porosity and compressive strength of concrete.
- The crack width significantly increases the DoC and reduces the alkalinity of concrete by consuming the OH^- ions and reducing the pH level for all mixes used in the study, across different levels of CO_2, RH, and temperature.
- Carbonation rates in the vicinity of the cracks are considerably higher due to relatively faster penetration of CO_2 into the crack followed by orthogonal outward diffusion into the un-cracked concrete surrounding the crack.
- The most important parameter for the carbonation rate of concrete exposed to CO_2 conditions, is the moisture concentration of the concrete in service: pores saturated

with water are impermeable for the gaseous CO_2, and therefore the diffusion coefficient for carbon dioxide is a function of the water content of the concrete.

- XRD investigation made it possible to gain a better understanding of the mineral-structure changes induced due to exposure to a CO_2 environment. Results from the XRD investigation also helps in identifying areas of fully carbonated and un-carbonated concrete in greater detail including the partially carbonated zones.
- The SCMs have a vital role in DoC, whereby the replacement of OPC by SCMs such as PFA and GGBS shows a significant increase in the penetration of carbonation and reduction in pH level. This is due to consumption of alkalinity compounds in concrete and the micro-pore structure is therefore redistributed and becomes coarser.
- The carbonation depths, X_p and front X_f, are affected by the material properties such as permeation properties (water and gas permeability), and compressive strength due to the impact of diffusivity of CO_2.
- For samples exposed to an accelerated CO_2 environment, the relative humidity has a significant impact on the DoC. The maximum carbonation depth occurred at 65% target RH beyond that value, the increase in RH led to a reduction in the DoC due to a decrease in the CO_2 diffusion into concrete samples.
- The increment in the temperature increases the DoC due to the relatively fast penetration of CO_2 into the concrete and an increase in the reaction rate with cement products, which led to the formation of the carbonation compound, $CaCO_3$.
- The results associated with DoC indicate a linear correlation between the DoC and the increase in the CO_2 concentration due to the carbonation of C-S-H and Ca $(OH)_2$ changing simultaneously and the polymerisation of the C-S-H after carbonation increases with the increase in CO_2 concentration.
- Results from the apparent pH and consumed OH^- technique help in identifying areas of fully carbonated and un-carbonated concrete in greater detail including the partially carbonated zones.
- Identification of three zones of carbonation in concrete may help in applying concepts that pertain to composite materials in the analysis of the mechanical behaviours of carbonated concrete structures. However, concerning reinforcement corrosion, measuring the pH value using a phenolphthalein indicator is a good indication for corrosion initiation.

8.2.3 Chloride Penetration

In this part of the study, the impact of the exposure environment such as temperature, and the properties of the concrete crack width on the chloride penetration in concrete structures, was also examined. The effects of three levels each of temperature, crack width and w/cm ratio and one series of carbonated specimens on chloride penetration were investigated. Chloride penetration was investigated using an accelerated environment test programme using wet-dry aeration cycle. The chloride front, d_{Cl^-} and chloride profile within the concrete depth, C_{Cl^-} were determined by $AgNO_3$ spraying and titration with 0.1M $AgNO_3$ respectively. Additionally, the influence of replacing OPC by SCMs, PFA and GGBS on the chloride penetration in un-cracked and cracked concrete was also investigated. The main conclusions of this section are as follows:

- Chloride penetration, d_{Cl^-} and C_{Cl^-} are affected by the material properties such as permeation properties (water and gas permeability) and strength of concrete.
- Chloride penetration in the vicinity of the cracks is considerably higher due to the relatively faster penetration of Cl^- into the crack followed by orthogonal outward diffusion into the un-cracked concrete surrounding the crack.
- The crack width significantly increases the chloride penetration depth for all mixes used. The increasing percentage of chloride penetration depth for cracked samples relative to the un-cracked concrete samples, is influenced by crack width and w/cm ratio.
- The penetration of chloride in the concrete structure increases with increasing w/cm for OPC concrete. Whereas, the OPC concrete mixes with SCMs , PFA and GGBS have significant resistance to chloride penetration due to the refinement of the concrete pore structure and an increased chloride binding capacity, respectively. Therefore, the concentration of chloride in the first layers of the concrete sample was relatively higher compared with the same w/cm ratio (M 0.5).
- The apparent chloride diffusion coefficient, D_a and surface concentration of chloride, C_s increased when increasing the w/cm ratio due to the greater the permeation properties (porosity and permeability) of concrete. On the other hand, D_a and C_s increase when increasing the crack width due to greater transport of chloride solution throughout the cracks. The crack factor, $f_{c4(W_c)}$ ($D_{a\ cracked}$ / $D_{a\ un\text{-}cracked}$) was experimentally considered as shown in Equation (7.19).

$$f_{c4(W_c)} = 0.934{W_c}^2 + 0.974W_c + 1$$

- The increase in temperature has a considerable impact on depths of the chloride front (d_{cl}^-) and chloride concentration by increasing the colour change boundary (C_d) for all concrete specimens tested. Generally, an increase in the chloride environment temperature increased the penetrability of chloride in concrete due to an increase in the activity of chloride diffusion in the concrete sample. On the other hand, some cases were different with common performance due to the influence of other parameters leading to a change in the results of these cases and the chloride ingress into the concrete matrix is dominated by a complex interaction between physical and chemical processes. The relationship of D_a with temperature was considered by experimental results as shown in Equation (7.14):

$$D_a = \left(1.3889 + 18.3333\ \frac{w}{c} + 0.3\ T\right) 10^{-12}$$

- The permeation properties of OPC concrete have a significant influence on the surface chloride concentration C_s of concrete which is exposed to chloride environmental conditions.
- The chloride penetration significantly increases within the concrete samples exposed to the CO_2 environment for most mixes used in the study. The impact of carbonation on chloride penetration was obvious in un-cracked samples M 0.4 and M0.5, M 0.5+GGBS and M 0.5+PFA. While, in the concrete samples M 0.6, the effect of w/cm and porosity was higher than the effect of carbonation on chloride penetration depth, d_{Cl}-.
- The capacity for immobilization of chloride depends on the type of cementitious materials and quantity of additions used. Therefore, additional information data on the cement composition and materials used for concrete production is necessary.
- The silver nitrate colorimetric method is used to measure the chloride penetration depth, the precipitate formed on the surface of concrete may be a mixture of silver oxide and silver chloride. In the carbonated samples, the amount of silver chloride formed increases linearly as the (OH^-/Cl^-) decreases.

8.2.4 Corrosion rate

In this part of the study, exposure to environmental conditions such as temperature and the properties of concrete crack width were considered in the corrosion of reinforced

concrete prisms. The influence of three levels of temperatures, crack width and w/cm ratios and one series of carbonated specimens on corrosion was investigated. Corrosion was tested using an accelerated environment test programme using a wet-dry-aeration cycle, and the electrical potential for corrosion was measured using half-cell potential, E_{corr}. While, the corrosion rate or corrosion current density, i_{corr} was found by using the Stern-Geary Equation (i_{corr} =B/Rp) and tested by linear polarization resistance, LPR for the reinforced concrete samples. The influence of partially replacing OPC cement with SCMs, PFA and GGBS on the E_{corr} and i_{corr} in un-cracked and cracked concrete was also considered. The main conclusions from the corrosion results are as follows:

- The electrode half -cell potential and corrosion rate are affected by the material behaviours such as porosity, compressive strength due to an increased concentration of Cl^- in concrete.
- The carbonation accelerated the combined effect of CO_2 and Cl^- induced corrosion by increasing free chloride concentration and reducing the pH level in concrete.
- The increase in temperature has a considerable impact on electrode half -cell potential, E_{corr} and corrosion rate, i_{corr} due to an increased chloride concentration and diffusion chloride coefficient, D_a for all specimens of concrete mixes. Generally, the increase of the corrosion environment temperature increases with the increasing activity of chloride diffusion in the concrete sample. Finally, the increase in temperature resulted in reduced initiation and propagation time of corrosion and affected the service life of reinforced concrete structures
- The half-cell corrosion potential and linear polarization resistance in the reinforcement steel bar is significantly higher in carbonated samples when exposed to a chloride environment and progressively increases with the exposure time to chloride conditions.
- The cracks in concrete samples accelerated chloride-induced corrosion by increasing penetrability of chloride and increasing its concentration. In general, the corrosion rate increases with increasing crack width but sometimes is sensitive to concrete quality at small crack widths.
- The use of LPR measurements in the monitoring of corrosion status in cracked concrete was found to be well-matched with half-cell potential measurements.

- In carbonated samples, measuring the DoC by using a phenolphthalein indicator and pH investigation made it possible to better understand the impact of carbonation induced due to exposure to CO_2 on chloride penetration and corrosion rate.
- In carbonated samples and those exposed to chloride environment, the electrode half - cell potential, E_{corr} and corrosion rate, i_{corr} are affected by the material properties such as porosity, compressive strength due to the impact of diffusivity of CO_2 and Cl^-.
- The SCMs, namely GGBS and PFA have two contradictory performances with regard to corrosion. The chloride penetration in concrete incorporating these materials was lower than d_{cl^-} in M0.5 cement concrete, while the DoC in M0.5+GGBS and M 0.5+PFA was higher than DoC in M 0.5 concrete. Therefore, the decrease in the effect of the Cl^- environment, and an increase in the effect of a CO_2 environment should be considered in corrosion rate.
- The results of the study have shown that for concrete specimens exposed to carbonation and chlorides, cracks influence the corrosion rate, therefore, these factors should be considered in service life prediction models.

8.3 Conclusions from the Theoretical and Modelling Results

This part focuses on the modelling and simulation of the impact of climate change parameters on the durability of concrete structures, in particular, chloride penetration and carbonation depth. The analytical and numerical modelling of the chloride penetration and carbonation depth have been developed and proposed to consider the main factors of study, properties of concrete and climate parameters. The models have been validated through the experimental results. Finally, climate change, atmospheric temperature, and carbon dioxide concentrations of IPCC- 2014 scenarios were considered in chloride concentration and carbonation depth.

- A model for the prediction of the chloride profile (concentration with the depth of concrete) based on mechanisms of chloride transport methods in cementitious materials, the diffusion, and the convection or advective in concrete exposed to a salt solution under de-icing and marine conditions, has been developed.
- The diffusion chloride coefficient, $D_{a,ref}$ considered to be affected by internal factors such as the porosity, tortuosity of voids in concrete (Ω) and the fraction of aggregate in concrete as shown in Equation (7.10):

$$D_{a,ref} = D_{Cl}\, V_v\, f_{agg}$$

- In the modelling of chloride concentration, the diffusion chloride coefficient, D_a considered the effect of crack and external factors affected such as the temperature, relative humidity as shown in Equation (7.15):

$$D_a = D_{a,ref} f_{C1}(t) f_{C2}(T) f_{C3}(RH)\, f_{C4}(W_c)$$

- An approach considering the influence of crack width on the diffusion chloride coefficient, D_a was proposed in this study based on the experimental programme to compute the D_a and it was used to predict the depth of chloride concentration as illustrated in Equation (7.19):

$$f_{c4(W_C)} = 0.934{W_c}^2 + 0.974W_c + 1$$

- The modelling of the chloride profile was based on Fick's Second Law of Diffusion (as shown below) and solved with a numerical technique by using the non-linear finite elements technique, NLFET to find the concentration of chloride with depth and time C_{Cl} (x, t) as illustrated in Equation (7.1).

$$\frac{\partial C_{Cl}}{\partial t} = -\frac{\partial}{\partial x}\left[D_{eff}\frac{\partial C_{Cl}}{\partial x} + uC_{Cl}\right] + R_{Cl}$$

This model and its numerical solution have been verified and validated by experimental results from this study and other studies for two cases of concrete, un-cracked and cracked concrete samples. The analytical results of a numerical modelling solution of the model proposed were generally a good fit and well-matched with the distribution of chloride concentration profiles obtained from concretes exposed to chloride conditions in these studies. Therefore, this modelling can be used to predict chloride concentration at the depths in the control condition and in future climate change scenarios.

- In modelling data of chloride concentration, it has been shown that the chloride concentration may correlate to the permeability of concrete.
- Two approaches of surface concentration, C_s were used in both environmental conditions, de-icing and marine, to investigate the impact of climate change on the chloride concentration profile in the long term of 50 years.
- Two approaches to the prediction of climate change were employed to use in the forecasting of chloride concentration profiles and carbonation depths. In the case of

the UK (London) and the case of Iraq (Basra), the UKCP'09 and IPCC-2014 have been used respectively.

- The influence of climate change (increase in temperature, and reduction of the relative humidity) has a significant impact on the chloride concentration profile as follows:
  - For the de-icing environment condition (London case), the percentage increase in chloride concentration at a depth of 50 mm (minimum requirement of concrete cover) was 5.8 % and 3.8% for un-cracked and cracked concrete deck respectively at an exposure age of 50 years for the two approaches of C_s.
  - For marine environment conditions (Basra case), the percentage increase in chloride concentration at a depth of 50 mm were 3.6 % and 3% for un-cracked and cracked concrete decks respectively at an exposure age of 50 years for the two approaches of C_s.
  - The impact of the crack on chloride concentration was observable for both environment conditions (de-icing and marine), duration of exposure and in both cases (the control case and the case including a climate change effect). The path of the crack opening helps chloride to penetrate quickly and increases the chloride concentration into the un-cracked concrete surrounding the crack
- Climate change can affect the progression of chloride concentration and induce corrosion in our concrete infrastructure by approaching the threshold of chloride concentration induced corrosion. The chloride concentration in deeper depths will be much higher in the long term and in harsher exposure conditions such as the worst-case scenario of RCP 8.5.
- The modelling approaches were proposed in this study to predict the carbonation depth. One is based on the uptake carbon dioxide by cementitious materials using a solution of Fick's Second Law of Diffusion (Engineering modelling). The second approach is based on mechanisms of the $CO_{2(aq)}$ diffusion and $Ca(OH)_{2(aq)}$ reaction mechanisms in cementitious materials, in concrete exposed to carbon dioxide environment conditions.
- In both models of carbonation depth, the diffusion carbon coefficient, D_{CO2} considered internally affected factors such as the porosity and tortuosity of voids in concrete (Ω).
- In the modelling of carbonation, the diffusion of carbon dioxide coefficient, D_{CO2} considered the effect of cracks and externally affected factors such as the temperature and relative humidity as shown in Equation (7.42):

$$D_{CO2} = D_{CO2,ref} f_{C1}(T) f_{C2}(RH) f_{C3}(W_c)$$

- The approach of the influence of crack width on the diffusion carbon dioxide coefficient, D_{CO2} was proposed in this study based on the experimental programme to compute the D_{CO2} and used to predict the depth of carbonation as illustrated in Equation (7.47):

$$f_{c3(W_c)} = (11.4\sqrt{W_c} + 1)$$

- The dissolved aqueous $Ca(OH)_{2(aq)}$ concentration in the solution of concrete (without SCMs) depends on the degree of hydration, cement content and cement compounds, C_3S and C_2S. The total amount of $Ca(OH)_2$ in the solid phase of cementation composite is calculated from the chemical composition of the hydration of cement compounds, C_3S, and C_2S as shown in Equation (7.54):

$$C_{CH} = \frac{M_{CH}}{2*M_{C_2S}} * C_{C_2S} + \frac{3M_{CH}}{2*M_{C_3S}} * C_{C_3S}$$

So, the concentration of $Ca(OH)_2$ can be determined by cement content and degree of cement hydration as shown in Equation (7.55):

$$[Ca(OH)_2] = \frac{C_{CH}*Q*\propto}{M_{CH}}$$

In the cement is used in this study, the C_2S and C_3S percentages were 15.36% and 55% by weight of cement respectively and assuming the hydration of cement was 90%, then $[Ca(OH)_2]$ as shown in Equation (7.56):

$$[Ca(OH)_2] = 3.685\ Q$$

An integrated carbonation model has been developed to predict the depth of carbonation in non-pozzolanic, un-cracked and cracked concrete specimens, considering properties of concrete, concentrations of CO_2, temperature and humidity. This modelling of carbonation was based on Fick's Second Law of Diffusion for the diffusivity of $CO_{2(aq)}$ and consumption of $Ca(OH)_{2(aq)}$ in concrete specimens (as shown below) and solved with numerical technique by non-linear finite elements technique (NLFET) to find the concentration of $CO_{2(aq)}$ and $Ca(OH)_{2(aq)}$ with depth and time, $C_{CO2}(x, t)$ and $C_{Ca(OH)2}(x, t)$ as shown in Equations 7.48 and 7.49 respectively:

$$\frac{\partial}{\partial t}[CO_{2(aq)}] = D_{CO_2}\frac{\partial^2}{\partial x^2}[CO_{2(aq)}] - \frac{k_c}{2}[CO_{2(aq)}][Ca(OH)_{2(aq)}]$$

$$\frac{\partial}{\partial t}[Ca(OH)_{2(aq)}] = D_{Ca(OH)_2}\frac{\partial^2}{\partial x^2}[Ca(OH)_{2(aq)}] - \frac{k_c}{2}[CO_{2(aq)}][Ca(OH)_{2(aq)}]$$

Two assumptions are made, the first depending on the consumption of $Ca(OH)_{2(aq)}$ and the second based on $C_{CO2}(x, t)$ to form $CaCO_3$. This modelling and its numerical solution have been verified and validated by experimental results from this study and other studies for two cases of concrete, un-cracked and cracked concrete samples. The analytical results of a numerical modelling solution (based on diffusion-convection) were generally a good fit and well-matched with the carbonation depth or rate obtained from concretes exposed to CO_2 conditions in these studies. Therefore, the purpose is to use this model to predict the potential impact of future global climate change scenarios on carbonation depth or the rate in reinforced concrete structures.

- The influence of climate change due to the increase in CO_2 and temperature and reduction in the relative humidity has a considerable impact on the depth of carbonation. For example, the results from Basra (moderate humidity, and higher temperatures) were more prone to corrosion than a cooler, wetter city such as London. This impact is much higher with an increase in the w/cm ratio due to an increase in the porosity and diffusivity of CO_2 in concrete structures.
- Climate change will affect the progression of carbonation and induce corrosion in our concrete infrastructure. Ultimate carbonation depths will be much higher in the long term and in harsher exposure conditions such as the worst-case scenario of RCP8.5.
- Although in the near future, climate change will have an unnoticeable effect on the durability of concrete structures constructed in the Year 2000, the real effects of climate change will become evident after approximately 30 years. Therefore, structures being constructed in 2020–2030 may have to consider degradation due to climate change when they are being designed.

8.4 Recommendations

In addition to the results and conclusions obtained from the present work, future investigation and recommendations could be continued along the following lines:

- The use of SCMs in concrete structures is important to reduce CO_2 emission. Thus, it is necessary to do a comprehensive study using these materials in carbonation depth and chloride penetration in concrete structures using the data to verify the integrated modelling of carbonation depth and chloride penetration.
- The effect of carbonation on chloride penetration and the corrosion rate is significant. Therefore, a generic framework for both, carbonation and chloride penetration and

performance prediction should be developed to find a wide range of data sources and build a database and model of the combined effect on the durability of concrete structures.

- The present study shows the significance and the need for alternative corrosion protection methods in reinforced concrete structures exposed to chloride and wet/dry environments. It is important to investigate the effectiveness of these protection methods in such an environment and provide guidelines on which of these methods are the most reliable and cost-effective depending on the environmental conditions of the concrete.
- In order to accurately identify the effects of chlorides on reinforced concrete structures, preparation of integrated field studies must include investigation of chloride performance at a later age and investigate the effects of ageing as time progresses, using them as inputs to improve upon service life modelling.
- The use of inhibitors is a commonly used method for the protection of steel from corrosion. Thus, a study is recommended to investigate the effectiveness of these inhibitors on carbonation in concrete.

REFERENCES

AASHTO T 277 (2015). "Standard Method of Test for Electrical Indication of Concrete's Ability to Resist Chloride Ion Penetration".

Ahlström, J. (2014). "Corrosion of steel in concrete at various moisture and chloride levels."

AL-Ameeri, A. and R. AL-Rawi (2009). " A Study on Properties of Iraqi Steel slag as a Fine Aggregate in Concrete ". *Journal of Building Technology*, Saudi Arabia 13/2009.

Al-Ameeri, A., K. AL-Hussain and M. Essa (2013). "Predicting a Mathematical Models of Some Mechanical Properties of Concrete from Non-Destructive Testing." Civil and Environmental Research 3: 78-97.

Al-Amoudi, O. S. B. and M. Maslehuddin (1991). "Carbonation and corrosion of rebars in salt contaminated OPC/PFA concretes." Cement and concrete research 21(1): 38-50.

Al-Khayat, H., M. Haque and N. Fattuhi (2002). "Concrete carbonation in arid climate." Materials and Structures 35(7): 421.

Al-Samaraai, M.and Z. Raouf. (1999). "Non –destructive testing". Shariqia University.

Al-Tayyib, A.-H. J. and S. Khan (1988). "Corrosion rate measurements of reinforcing steel in concrete by electrochemical techniques". Materials Journal 85(3): 172-177.

American Code Institute, ACI 318 (2014). "Building Code Requirements for Structural Concrete".

American Code Institute, ACI 365.1 R (2014). "Service-Life Prediction—State-of-the-Art Report".

American Code Institute, ACI Committee 122 R. (2002). "Guide to thermal properties of concrete and masonry systems".

American Concrete Institute, (2008), ACI Committee 201.2R,08. " Guide to Durable Concrete". Farmington Hills, Mich.: ACI.

American Concrete Institute, (2008), ACI Committee 222R,01. "Protection of Metals in Concrete Against Corrosion". Farmington Hills, Mich.: ACI.

American Concrete Institute, (2008). ACI Committee 365 Part 5. "Service-life prediction: state of the art report". Manual of concrete practice. Farmington Hills, Mich.ACI.

American Society for Testing and Materials, ASTM C 1152(2012) "Acid-Soluble Chloride in Mortar and Concrete".

American Society for Testing and Materials, ASTM C 597(2016). "Standard Test Method for Pulse Velocity through Concrete".

American Society for Testing and Materials, ASTM C 876(2015). "Half-Cell Potentials of Uncoated Reinforcing Steel in Concrete".

American Society for Testing and Materials, ASTM C114(2015). "Chemical Analysis of Hydraulic Cement".

American Society for Testing and Materials, ASTM C1202 (2012). "Electrical Indication of Concrete's Ability to Resist Chloride Ion Penetration".

American Society for Testing and Materials, ASTM C192 (2016). "Standard Practice for Making and Curing Concrete Test Specimens in the Laboratory".

American Society for Testing and Materials, ASTM C642:2013, "Density, Absorption, and Voids in Hardened Concrete".

American Society for Testing and Materials, ASTM, C 1556 – 11a (2016) "Determining the Apparent Chloride Diffusion Coefficient of Cementitious Mixtures by Bulk diffusion".

Amey, S. L., D. A. Johnson, M. A. Miltenberger and H. Farzam (1998). "Predicting the service life of concrete marine structures: an environmental methodology." Structural Journal 95(2): 205-214.

Andersen, A. (1997). "Investigation of chloride penetration into bridge columns exposed to de-icing salt. " HETEK-report No. 82, Danish Road Directorate: 37.

Andrade, C. (1993). "Calculation of chloride diffusion coefficients in concrete from ionic migration measurements." Cement and concrete research 23(3): 724-742.

Andrade, C. and C. Alonso (2004). "Test methods for on-site corrosion rate measurement of steel reinforcement in concrete by means of the polarization resistance method. " Materials and Structures 37(9), 623-643.

Andrade, C. and J. González (1978). "Quantitative measurements of corrosion rate of reinforcing steels embedded in concrete using polarization resistance measurements. " Materials and Corrosion 29(8), 515-519.

Andrade, C., C. Alonso, S. Feliu and J. Gonzalez (1997). "Advances in the on-site electrochemical measurement of reinforcement corrosion and their use in predicting residual life." Corrosion & materials 22(4): 8-12.

Andrade, C., M. C. Alonso and J. A. Gonzalez (1990). "An initial effort to use the corrosion rate measurements for estimating rebar durability".Corrosion rates of steel in concrete, ASTM International.

Angst, U., B. Elsener, C. K. Larsen and Ø. Vennesland (2009). "Critical chloride content in reinforced concrete—a review". Cement and concrete research 39(12): 1122-1138.

Angst, U., Ø. Vennesland and R. Myrdal (2009). "Diffusion potentials as source of error in electrochemical measurements in concrete." Materials and Structures 42(3): 365-375.

Ann, K., J. Ahn and J. Ryou (2009). "The importance of chloride content at the concrete surface in assessing the time to corrosion of steel in concrete structures". Construction and Building Materials 23(1): 239-245.

Archuleta Jr, L., P. Tikalsky and R. Carrasquillo (1986). "Production of concrete containing fly ash for structural application". Internal Report Number 364-1.

Atiş, C. D. (2004). "Carbonation-porosity-strength model for fly ash concrete". Journal of Materials in Civil Engineering 16(1): 91-94.

Audenaert, K., G. De Schutter and L. Marsavina (2009). "Influence of cracks and crack width on penetration depth of chlorides in concrete". European journal of environmental and civil engineering 13(5), 561-572.

Babaei, K. (1985). "Evaluation of half-cell corrosion detection test for concrete bridge decks". Washington state department of transportation in cooperation with the United States department of transportation federal highway administration, Final report November 86.

Bamforth, P., W. F. Price and M. Emerson (1997). "International Review of Chloride Ingress Into Structural Concrete". A Trl Report (Trl 359), Thomas Telford.

Bandy, R. (1980). "The simultaneous determination of tafel constants and corrosion rate—a new method". Corrosion Science 20(8-9): 1017-1028.

Basheer, L., J. Kropp and D. J. Cleland (2001). "Assessment of the durability of concrete from its permeation properties: a review ". Construction and building materials 15(2-3), 93-103.

Bastidas-Arteaga, E., A. Chateauneuf, M. Sánchez-Silva, P. Bressolette and F. Schoefs (2010). "Influence of weather and global warming in chloride ingress into concrete: A stochastic approach".Structural Safety 32(4): 238-249.

Bastidas-Arteaga, E., A. Chateauneuf, M. Sánchez-Silva, P. Bressolette and F. Schoefs (2011). "A comprehensive probabilistic model of chloride ingress in unsaturated concrete". Engineering Structures 33(3): 720-730.

Bastidas-Arteaga, E., A. Chateauneuf, M. Sánchez-Silva, P. Bressolette and F. Schoefs (2010). "Influence of weather and global warming in chloride ingress into concrete: A stochastic approach". Structural Safety 32(4): 238-249.

Berke, N., 2006.Corrosion of Reinforcing steel. In Lamond,J. and Pieltert,J. (2006). "Significance of Tests and Properties of Concrete and Concrete-Making Materials". STP 169D, New York: West Conshohocken .

Berke, N., A. Bentur and S. Diamond (2014). "Steel corrosion in concrete: fundamentals and civil engineering practice". CRC Press.

Bernstein, L., P. Bosch, O. Canziani, Z. Chen, R. Christ, O. Davidson, W. Hare, S. Huq, D. Karoly and V. Kattsov (2008). Climate change 2007: Synthesis report: An assessment of the intergovernmental panel on climate change, IPCC-2007.

Bertolini, L., B. Elsener, P. Pedeferri, E. Redaelli and R. B. Polder (2013). "Corrosion of steel in concrete: prevention, diagnosis, repair ". John Wiley & Sons.

Bertolini, L., M. Carsana and P. Pedeferri (2013). "Corrosion behaviour of steel in concrete in the presence of stray current". Corrosion science 49(3): 1056-1068.

Bilcik, J. and I. Holly (2013). "Effect of reinforcement corrosion on bond behaviour". Procedia Engineering 65: 248-253.

Blanton, T., T. Huang, H. Toraya, C. Hubbard, S. Robie, D. Louer, H. Göbel, G. Will, R. Gilles and T. Raftery (1995). "JCPDS—International Centre for Diffraction Data round robin study of silver behenate. A possible low-angle X-ray diffraction calibration standard". Powder Diffraction 10(2): 91-95.

Bouteiller, V., C. Cremona, V. Baroghel-Bouny and A. Maloula (2012). "Corrosion initiation of reinforced concretes based on Portland or GGBS cements: Chloride contents and electrochemical characterizations versus time". Cement and Concrete Research 42(11): 1456-1467.

British Committee for Standardization, BS 4449:2005+A3(2016). "Steel for the reinforcement of concrete. Weldable reinforcing steel. Bar, coil and decoiled product". British Standard Institution.

British Committee for Standardization, BS 8100 (1997). "Code of practice for design and construction". British Standards Institution.

British Committee for Standardization, BS 812-118(1988). "Testing aggregates — Part 118 Methods for determination of sulphate content". British Standard Institution.

British Committee for Standardization, BS 8500-1 (2015). "Method of specifying and guidance for the specifier ". British Standards Institution.

British Committee for Standardization, BS 8500-1 (2015). "Method of specifying and guidance for the specifier ". British Standards Institution.

British Committee for Standardization, BS.882 (1983). "Aggregate from natural sources for concrete". British Standard Institution.

British Committee for Standardization, BS8100 (1997). "Code of practice for design and construction". British Standards Institution.

British Committee for Standardization, BS8500-1 (2015). "Method of specifying and guidance for the specifier ". British Standards Institution.

Broomfield, J. P. (2003). "Corrosion of steel in concrete: understanding, investigation and repair ". CRC Press.

Broomfield, J. P. (2007). "Corrosion of steel in concrete: understanding, investigation and repair ". Taylor &Francis.

Brown, M.C. (1999). "Assessment of commercial corrosion inhibiting admixtures for reinforced concrete". (Doctoral dissertation, Virginia Tech).

Browne, R. (1982). "Durability of Building Materials". Elsevier Scientific Publishing.

Castel, A., R. Francois and G. Arliguie (1999). "Effect of loading on carbonation penetration in reinforced concrete elements". Cement and Concrete Research 29(4): 561-565.

Castellote, M. and C. Andrade (2006). "Round-Robin test on methods for determining chloride transport parameters in concrete". Materials and Structures 39(10): 955.

Castellote, M., C. Andrade and C. Alonso (2001). "Measurement of the steady and non-steady-state chloride diffusion coefficients in a migration test by means of monitoring the conductivity in the anolyte chamber. Comparison with natural diffusion tests". Cement and Concrete Research 31(10): 1411-1420.

Castellote, M., L. Fernandez, C. Andrade and C. Alonso (2009). "Chemical changes and phase analysis of OPC pastes carbonated at different CO_2 concentrations". Materials and Structures 42(4): 515-525.

Chalee, W., C. Jaturapitakkul and P. Chindaprasirt (2009). "Predicting the chloride penetration of fly ash concrete in seawater". Marine structures 22(3): 341-353.

Chandler, K. A. (1985). Marine and offshore corrosion, Elsevier.

Chang, C.-F. and J.-W. Chen (2006). "The experimental investigation of concrete carbonation depth". Cement and Concrete Research 36(9): 1760-1767.

Chen, D. and S. Mahadevan (2008). "Chloride-induced reinforcement corrosion and concrete cracking simulation". Cement and Concrete Composites 30(3): 227-238.

Chi, J. M., R. Huang and C. Yang (2002). "Effects of carbonation on mechanical properties and durability of concrete using accelerated testing method". Journal of marine science and technology 10(1): 14-20.

Collepardi, M., A. Marcialis and R. Turriziani (1972). "Penetration of chloride ions into cement pastes and concretes". Journal of the American Ceramic Society 55(10): 534-535.

Cook, R. D. (2007). "Concepts and applications of finite element analysis". John Wiley & Sons.

Crank, J. (1979). "The mathematics of diffusion ". Oxford university press.

Czarnecki, L. and P. Woyciechowski (2013). "Prediction of the reinforced concrete structure durability under the risk of carbonation and chloride aggression". Bulletin of the Polish Academy of Sciences: Technical Sciences 61(1): 173-181.

Drouet, E., Poyet, S., Le Bescop, P., Torrenti, J.M. and Bourbon, X., (2019). "Carbonation of hardened cement pastes: Influence of temperature". *Cement and Concrete Research*, 115:445-459.

Drouet, E., S. Poyet and J.-M. Torrenti (2015). "Temperature influence on water transport in hardened cement pastes". Cement and Concrete Research 76: 37-50.

DuraCrete (2000). "Statistical Quantification of the Variables in the Limit State Functions".BRITE EURAM, Probabilistic Performance based Durability Design of Concrete Structures,Document BE95-1347/R9.

Dyer, T. (2014). "Concrete durability". Crc Press.

Ehlen, M. A., M. D. Thomas and E. C. Bentz (2009). "Life-365 service life prediction modelTM version 2.0". Concrete international 31(05): 41-46.

Ehrlich, H. L., D. K. Newman and A. Kappler (2015). "Ehrlich's geomicrobiology ". CRC press.

Elbusaefi, A. A. (2014). "The effect of steel bar corrosion on the bond strength of concrete manufactured with cement replacement materials ". PhD. Thesis. Cardiff University.

El-Reedy, M. A. (2017). "Steel-reinforced concrete structures: assessment and repair of corrosion ". CRC press.

European Committee for Standardization, BS EN 12350 part 2(2009). "Testing fresh concrete. Slump test". British Standard Institution.

European Committee for Standardization, BS EN 12390 part- 2(2009). "Testing hardened concrete. Making and curing specimens for strength tests". British Standard Institution.

European Committee for Standardization, BS EN 12390, Part 11(2015) ." Testing hardened concrete: Determination of the chloride resistance of concrete, unidirectional diffusion". British Standard Institution

European Committee for Standardization, BS EN 12390, part 3(2000). "Testing hardened Concrete. Compressive strength of test specimens". British Standard Institution.

European Committee for Standardization, BS EN 12390, part 5(2009). "Testing hardened Concrete. Flexural strength of test specimens". British Standard Institution.

European Committee for Standardization, BS EN 12390, part 6(2000). "Testing hardened Concrete. Tensile splitting strength of test specimens". British Standard Institution.

European Committee for Standardization, BS EN 12390, part 7(2000). "Testing hardened Concrete. Density of hardened concrete". British Standard Institution.

European Committee for Standardization, BS EN 12504 part 4(2004). "Determination of ultrasonic pulse velocity". British Standard Institution.

European Committee for Standardization, BS EN 14629(2007). "Products and systems for the protection and repair of concrete structures —Test methods —Determination of chloride content in hardened concrete". British Standard Institution

European Committee for Standardization, BS EN 15167-part 1(2006). "Ground granulated blast furnace slag for use in concrete, mortar and grout: Definitions, specifications and conformity criteria". British Standard Institution.

European Committee for Standardization, BS EN 1744-1(2009). "Tests for chemical properties of aggregates: Part 1: Chemical analysis".

European Committee for Standardization, BS EN 197-part 1(2011). "Cement: Composition, specifications and conformity criteria for common cements". British Standard Institution.

European Committee for Standardization, BS EN 450-part 1(2012). "Fly ash for concrete: Definition, specifications and conformity criteria". British Standard Institution.

European Committee for Standardization, BS EN 933-1(1997). " Tests for geometrical properties of aggregates. Determination of particle size distribution. Sieving method". British Standard Institution.

European Committee for Standardization, BS EN ISO 10523:2012. "Water quality — Determination of pH". British Standard Institution.

European Committee for Standardization, CEN/TS 12390-10(2007). "Testing hardened concrete: Determination of the carbonation resistance of concrete at atmospheric levels of carbon dioxide". British Standard Institution.

European Standard EN 13295 (2004)." Products and systems for the protection and repair of concrete structures — Test methods — Determination of resistance to carbonation". British Standard Institution.

Feitler, H. (1971). "The scale meter: a new method for determining the critical pH of scaling". Materials Protection and Performance 11(1).

Fifer Bizjak, K., A. Dawson, I. Hoff, L. Makkonen, J. S. Ylhäisi and A. Carrera (2015). "The impact of climate change on the European road network". Proceedings of the ICE-Transport 167(5): 281-295.

Fogg, P. G., J. Sangster, Y.-N. Lee, S. Schwartz and P. Warneck (2003). "Chemicals in the atmosphere: solubility, sources and reactivity ". Wiley Chichester.

Fontana, M. G. (2005). "Corrosion engineering".Tata McGraw-Hill Education.

Francois, R. and G. Arliguie (1991) ". Reinforced concrete: correlation between cracking and corrosion". Special Publication 126, 1221-1238.

Frederiksen, J. M., L. Mejlbro and L.-O. Nilsson (2009). "Fick's 2nd law-Complete solutions for chloride ingress into concrete–with focus on time dependent diffusivity and boundary condition" .Report TVBM 3146.

Fuhrmann, M., R. Pietrzak, J. Heiser, E.-M. Franz and P. Colombo (1989). "The effects of temperature on the leaching behavior of cement waste forms-the cement/sodium sulfate system". MRS Online Proceedings Library Archive 176.

Gjorv, O. E. (1975). "Control of steel corrosion in concrete sea structures". Special Publication 49: 1-10.

Global Carbonation Atlas (2014). "Carbonation Emission". [Online] available at: *http://www.globalcarbonatlas.org/?q=en/emissions*.

Grace Construction Products (2006). "Understanding AASHTO T277 and ASTM C1202 Rapid chloride permeability test". Technical Bulletin TB-0100. Cambridge, USA: W.R. Grace and Co.

Grantham, M. (2003). "Diagnosis, inspection, testing and repair of reinforced concrete structures". Advanced Concrete Technology 2: 1-54.

Grassl, P., H. S. Wong and N. R. Buenfeld (2010). "Influence of aggregate size and volume fraction on shrinkage induced micro-cracking of concrete and mortar". Cement and concrete research 40(1): 85-93.

Haque, M. and H. Al-Khaiat (1997). "Carbonation of concrete structures in hot dry coastal regions." Cement and Concrete Composites 19(2): 123-129.

Hartt, W. H. (2009). "Effect of concrete crack width on corrosion of embedded reinforcement ". Research Report, Florida: Morada Court Boca Raton.

Hausmann, D. (1967). "Steel corrosion in concrete--How does it occur?" Materials protection.

He, F., C. Shi, Q. Yuan, C. Chen and K. Zheng (2012). "AgNO3-based colorimetric methods for measurement of chloride penetration in concrete". Construction and Building Materials 26(1): 1-8.

He, F., C. Shi, Q. Yuan, X. An and B. Tong (2011). "Calculation of chloride concentration at color change boundary of AgNO3 colorimetric measurement". Cement and Concrete Research 41(11): 1095-1103.

Hernández, M. S., A. Guerrero, S. Goñi and M. P. Lorenzo (1997). "Effect of the temperature on the leaching performance of the cement-based immobilization systems: sulfate and chloride behavior". Cement and concrete research 27(4): 515-524.

Hobbs, D. (1974). "Influence of aggregate restraint on the shrinkage of concrete ". Journal Proceedings.

Hoffman, P. and R. Weyers (1994). "Predicting critical chloride levels in concrete bridge decks". Structural safety and reliability: Proceedings of ICOSSAR 93: 957-959.

Hoffman, P. C. and R. E. Weyers (1996). "Probabilistic durability analysis of reinforced concrete bridge decks". Probabilistic Mechanics & Structural Reliability, ASCE.

Huang, N., J. Chang and M. Liang (2012). "Effect of plastering on the carbonation of a 35-year-old reinforced concrete building". Construction and Building Materials 29: 206-214.

Huet, B., L'hostis, V. L., Santarini, G., Feron, G. and Idrissi, H. (2007). "Steel corrosion in concrete: Deterministic modelling of cathodic reaction as a function of water saturation degree". Corrosion Science, Vol. 49, 1918-1932.

Hussain, S., A. Al-Musallam and A. Al-Gahtani (1995). "Factors affecting threshold chloride for reinforcement corrosion in concrete". Cement and Concrete Research 25(7): 1543-1555.

International Federation for Structural Concrete, CEB-FIP (2013). "Model Code for Concrete Structures 2010". Wilhelm Ernst & Sohn, Verlag für Architektur und technische Wissenschaften GmbH & Co. KG, Rotherstraße 21, 10245 Berlin, Germany.

Ishida, T., T. Kishi and K. Maekawa (2014). " Multi-scale modeling of structural concrete ". Crc Press.

Ismail, M., A. Toumi, R. Francois and R. Gagné (2004). "Effect of crack opening on the local diffusion of chloride in inert materials". Cement and Concrete Research 34(4): 711-716.

Ismail, M., A. Toumi, R. François, et al. (2008). "Effect of crack opening on the local diffusion of chloride in cracked mortar samples ". Cement and concrete research 38(8-9), 1106-1111.

Jacobsen, S., J. Marchand and B. Gerard (1998). "Concrete crack: I. durability and self-healing-a review, concrete under severe conditions". E&FN Spon, Tromso.

Jacobsen, S., J. Marchand and L. Boisvert (1996). " Effect of cracking and healing on chloride transport in OPC concrete ". Cement and Concrete Research 26(6), 869-881.

Jang, S. Y., B. S. Kim and B. H. Oh (2011). "Effect of crack width on chloride diffusion coefficients of concrete by steady-state migration tests". Cement and Concrete Research 41(1), 9-19.

Jarrah, N. R., O. S. B. Al-Amoudi, M. Maslehuddin, et al. (1995). "Electrochemical behaviour of steel in plain and blended cement concretes in sulphate and/or chloride environments". Construction and Building Materials 9(2), 97-103.

Kamaitis, Z. (2008). "Modelling of corrosion protection for reinforced concrete structures with surface coatings". Journal of Civil Engineering and Management 14(4): 241-249.

Kassir, M. K. and M. Ghosn (2002). "Chloride-induced corrosion of reinforced concrete bridge decks". Cement and Concrete Research 32(1): 139-143.

Katwan, M. (1988). "Corrosion fatigue of reinforced concrete". PhD, Thesis. University of Glasgow.

Khunthongkeaw, J. and S. Tangtermsirikul (2005). "Model for simulating carbonation of fly ash concrete". Journal of materials in civil engineering 17(5): 570-578.

Kim, Y. Y., J. M. Kim, J.-W. Bang and S.-J. Kwon (2014). "Effect of cover depth, w/c ratio, and crack width on half-cell potential in cracked concrete exposed to salt sprayed condition". Construction and Building Materials 54: 636-645.

Kwon, S. J., U. J. Na, S. S. Park and S. H. Jung (2009). "Service life prediction of concrete wharves with early-aged crack: Probabilistic approach for chloride diffusion". Structural Safety 31(1): 75-83.

Kwon, S.-J. and U.-J. Na (2011). "Prediction of durability for RC columns with crack and joint under carbonation based on probabilistic approach". International Journal of Concrete Structures and Materials 5(1): 11-18.

Kwon, S.-J., B. J. Lee and Y. Y. Kim (2014). "Concrete mix design for service life of RC structures under carbonation using genetic algorithm". Advances in Materials Science and Engineering 2014.

Lagerblad, B. (2005). "Carbon dioxide uptake during concrete life cycle–state of the art". Swedish Cement and Concrete Research Institute CBI, Stockholm.

Lamond, J. F. and J. H. Pielert (2006). "Significance of tests and properties of concrete and concrete-making materials ". Astm West Conshohocken, PA.

Lea, F. M. (1971). "Some Special Cements and Cement Properties". The Chemistry of Cement and Concrete, Chemical Publishing Company, NY, U.S.A., Chapter 17, 544-547.

Letcher, T. M. (2015). "Climate change: observed impacts on planet Earth". Elsevier.

Li, L., A. A. Sagüés and N. Poor (1999). "In situ leaching investigation of pH and nitrite concentration in concrete pore solution". Cement and Concrete Research 29(3): 315-321.

Li, L., A. A. Sagüés and N. Poor (1999). "In situ leaching investigation of pH and nitrite concentration in concrete pore solution". Cement and Concrete Research 29(3): 315-321.

Lian, C., Y. Zhuge and S. Beecham (2011). "The relationship between porosity and strength for porous concrete". Construction and Building Materials 25(11), 4294-4298.

Life-365^{TM} Consortium II. LIFE-365 (2018). " Service life prediction model, computer program for predicting the service life and life-cycle costs of reinforced concrete exposed to chlorides ". Version 2.2.3, 2018.

Lin, G., Y. Liu and Z. Xiang (2010). "Numerical modeling for predicting service life of reinforced concrete structures exposed to chloride environments". Cement and concrete composites 32(8): 571-579.

Lindvall,A.(1998). "Duracrete –Probabilistic performance-based durability design of concrete structures". 2nd International PhD Symposium in Civil Engineering, Budapest.

Liu, T. and R. Weyers (1998). "Modeling the dynamic corrosion process in chloride contaminated concrete structures". Cement and Concrete Research 28(3): 365-379.

Loo, Y., M. Chin, C. Tam and K. Ong (1994). "A carbonation prediction model for accelerated carbonation testing of concrete". Magazine of Concrete Research 46(168): 191-200.

Luping, T. and J. Gulikers (2007). "On the mathematics of time-dependent apparent chloride diffusion coefficient in concrete". Cement and concrete research 37(4): 589-595.

Luping, T. and L.-O. Nilsson (1993). "Rapid determination of the chloride diffusivity in concrete by applying an electric field". Materials Journal 89(1): 49-53.

Mancio, M., C. Carlos Jr, J. Zhang, J. T. Harvey, P. J. Monteiro and A. Ali (2005). "Laboratory Evaluation of Corrosion Resistance of Steel Dowels in Concrete Pavement ".

Marchand, J. and E. Samson (2009). "Predicting the service-life of concrete structures–Limitations of simplified models". Cement and concrete composites 31(8): 515-521.

Markeset, G. and R. Myrdal (2008). "Modelling of reinforcement corrosion in concrete-State of the art". COIN Project report no7, SINTEF Building and Infrastructure: 1891-1978.

Maroliya, M. (2012). "A qualitative study of reactive powder concrete using X-ray diffraction technique". Journal of Engineering IOSR Journal of Engineering (2): 12-16.

Marriaga, L. and Claisse, P. 2009. "Determination of the concrete chloride diffusion coefficient based on an electrochemical test and an optimization model". Materials Chemistry and Physics.117; pp. 536-543.

Marsavina, L., K. Audenaert, G. De Schutter, N. Faur and D. Marsavina (2009). "Experimental and numerical determination of the chloride penetration in cracked concrete". Construction and Building Materials 23(1): 264-274.

Martın-Pérez, B., S. Pantazopoulou and M. Thomas (2001). "Numerical solution of mass transport equations in concrete structures". Computers & Structures 79(13): 1251-1264.

Maruya, T., K. Hsu, H. Takeda and S. Tangtermsirikul (2003). "Numerical modeling of steel corrosion in concrete structures due to chloride ion, oxygen and water movement". Journal of Advanced Concrete Technology 1(2): 147-160.

Maruya, T., Y. Matsuoka and S. Tangtermsirikul (1998). "Modeling of chloride ion movement at the surface layer of hardened concrete". Doboku Gakkai Ronbunshu 1998(585): 79-95.

Maso, J. (1996). "Interfacial transition zone in concrete". RILEM State-of-the-art Report (E&FN Spon, London).

Mason, R. L., R. F. Gunst and J. L. Hess (2003). "Statistical design and analysis of experiments: with applications to engineering and science ". John Wiley & Sons.

Matsushita, F., Y. Aono and S. Shibata (2000). "Carbonation degree of autoclaved aerated concrete". Cement and Concrete Research 30(11): 1741-1745.

McPolin, D., P. Basheer, A. Long, K. Grattan and T. Sun (2005). "Obtaining progressive chloride profiles in cementitious materials". Construction and Building Materials 19(9): 666-673.

McPolin, D., P. Basheer, A. Long, K. Grattan and T. Sun (2007). "New test method to obtain pH profiles due to carbonation of concretes containing supplementary cementitious materials". Journal of Materials in Civil Engineering 19(11): 936-946.

Mehta, P. K. and P. J. Monteiro (2006). "Microstructure and properties of hardened concrete ". McGraw-Hill New York.

Mejlbro, L. (1996). "The complete solution of Fick's second law of diffusion with time-dependent diffusion coefficient and surface concentration". Durability of concrete in saline environment: 127-158.

Meusel, J. and J. Rose (1983). "Production of granulated blast furnace slag at sparrows point, and the workability and strength potential of concrete incorporating the slag ". Special Publication 79, 867-890.

Mohammed, T. and H. Hamada (2003). "Relationship between free chloride and total chloride contents in concrete ". Cement and Concrete Research 33(9), 1487-1490.

Montes, P., T. W. Bremner and D. H. Lister (2004). "Influence of calcium nitrite inhibitor and crack width on corrosion of steel in high performance concrete subjected to a simulated marine environment". Cement and Concrete Composites 26(3): 243-253.

Morcous, G. and Z. Lounis (2005). "Prediction of onset of corrosion in concrete bridge decks using neural networks and case-based reasoning". Computer-Aided Civil and Infrastructure Engineering 20(2): 108-117.

Neville, A. M. (2011). "Properties of Concrete ". 4th edition. London Pearson Education Limited.

Neville, A. M. and J. J. Brooks (1987). "Concrete technology". 2nd edition, London Pearson Education.

Ngala, V. and C. Page (1997). "Effects of carbonation on pore structure and diffusional properties of hydrated cement pastes". Cement and Concrete Research 27(7): 995-1007.

Ngo, D. and A. C. Scordelis (1967). "Finite element analysis of reinforced concrete beams". Journal Proceedings, 64(3): 152-163.

Nilsson, L., E. Poulsen, P. Sandberg, H. Sørensen and O. Klinghoffer (1996). "HETEK, Chloride penetration into concrete, state-of-the-art, transport processes, corrosion initiation, test methods and prediction models". Denmark, ISSN/ISBN: 0909-4288.

Nilsson, L., E. Poulsen, P. Sandberg, H. Sørensen and O. Klinghoffer (1996). "HETEK, Chloride penetration into concrete, State-of-the-Art, Transport processes, corrosion initiation, test methods and prediction models". Denmark, ISSN/ISBN: 0909-4288.

Nilsson, L., P. Sandberg, E. Poulsen, L. Tang, A. Andersen and J. Frederiksen (1997). "A system for estimation of chloride ingress into concrete, theoretical background". HETEK, Danish Road Directorate, Report.

Ning, C. and B. Li (2015). "Probabilistic approach for estimating plastic hinge length of reinforced concrete columns". Journal of Structural Engineering 142(3), 04015164.

Nordic Council minister NT Build 492 (1999). " Chloride migration coefficient from non-steady-state migration experiments".

Nordic Council minister, NT Build 208 (1996). "Concrete hardened: chloride content by Volhard titration ".

Otieno, M., H. Beushausen and M. Alexander (2014). "Effect of chemical composition of slag on chloride penetration resistance of concrete". Cement and Concrete Composites 46, 56-64.

Otieno, M., M. Alexander and H. Beushausen (2009). "Corrosion propagation in cracked and uncracked concrete". Concrete Repair, Rehabilitation and Retrofitting II: 2nd International Conference on Concrete Repair, Rehabilitation and Retrofitting, ICCRRR-2, 24-26 November 2008, Cape Town, South Africa, CRC Press.

Pachauri, R. and L. Meyer (2014). "Climate change 2014: Synthesis report. fifth assessment report of the intergovernmental panel on climate change". Tech. Rep.

Pachauri, R. K., M. R. Allen, V. R. Barros, J. Broome, W. Cramer, R. Christ, J. A. Church, L. Clarke, Q. Dahe and P. Dasgupta (2014). Climate change 2014: synthesis report. Contribution of Working Groups I, II and III to the fifth assessment report of the Intergovernmental Panel on Climate Change, IPCC-2014.

Pack, S.-W., M.-S. Jung, H.-W. Song, S.-H. Kim and K. Y. Ann (2010). "Prediction of time dependent chloride transport in concrete structures exposed to a marine environment". Cement and Concrete Research 40(2): 302-312.

Page, C., N. Short and A. El Tarras (1981). "Diffusion of chloride ions in hardened cement pastes". Cement and concrete research 11(3): 395-406.

Papadakis, T. (2002). "Effect of supplementary cementing materials on concrete resistance against carbonation and chloride ingress". Cement and concrete research 30(2): 291-299.

Papadakis, V. G., C. G. Vayenas and M. N. Fardis (1991). "Fundamental modeling and experimental investigation of concrete carbonation". Materials Journal 88(4): 363-373.

Papadakis, V. G., C. G. Vayenas and M. N. Fardis (1991). "Physical and chemical characteristics affecting the durability of concrete". Materials Journal 88(2): 186-196.

Park, D. (2008). "Carbonation of concrete in relation to CO_2 permeability and degradation of coatings". Construction and building Materials 22(11): 2260-2268.

Park, S.-S., S.-J. Kwon and S. H. Jung (2012). "Analysis technique for chloride penetration in cracked concrete using equivalent diffusion and permeation". Construction and Building Materials 29: 183-192.

Petcherdchoo, A. (2013). "Time dependent models of apparent diffusion coefficient and surface chloride for chloride transport in fly ash concrete". Construction and Building Materials 38: 497-507.

Phurkhao, P. and M. Kassir (2005). "Note on chloride-induced corrosion of reinforced concrete bridge decks". Journal of engineering mechanics 131(1): 97-99.

Polder, R. B. and W. H. Peelen (2002). "Characterisation of chloride transport and reinforcement corrosion in concrete under cyclic wetting and drying by electrical resistivity". Cement and Concrete Composites 24(5), 427-435.

Poulsen, E. and L. Mejlbro (2006). "Diffusion of chloride in concrete: theory and application ". CRC Press.

Quero, V. G. J., P. Montes-Garcia and T. Bremner (2010). " Influence of concrete cracking on the corrosion of steel reinforcement". 6th International Conference on Concrete under Severe Conditions-Environment and Loading, " CONSEC'10.

Ramezanianpour, A. and V. Malhotra (1995). "Effect of curing on the compressive strength, resistance to chloride-ion penetration and porosity of concretes incorporating slag, fly ash or silica fume". Cement and concrete composites 17(2), 125-133.

Revie, R. W. (2008). "Corrosion and corrosion control: an introduction to corrosion science and engineering". John Wiley & Sons.

RILEM TC 116-PCD (1999). "Measurement of the gas permeability of concrete - Cembureau Method ". Materials and Structures/Matériaux et Constructions, Vol. 32, April 1999, 174-179.

RILEM TC 178-TMC (2003). " testing and modelling chloride penetration in concrete, Analysis of total chloride content in concrete". Institute of Construction Sciences "Eduardo Torroja" (CSIC).

RILEM, T. "116-PCD (1999). " Recommendations: A Preconditioning of concrete test specimens for the measurement of gas permeability and capillary absorption of water". Mater Struct 32: 174-176.

Roy, D. and G. Indorn (1982). "Hydration, structure, and properties of blast furnace slag cements, mortars, and concrete". Journal Proceedings. 79(6): 444-457.

Roy, S., K. Poh and D. Northwood (1999). "Durability of concrete—accelerated carbonation and weathering studies". Building and environment 34(5): 597-606.

Russell, D., P. M. Basheer, G. B. Rankin and A. E. Long (2001). "Effect of relative humidity and air permeability on prediction of the rate of carbonation of concrete". Proceedings of the Institution of Civil Engineers-Structures and Buildings 146(3): 319-326.

Saetta, A. V., R. V. Scotta and R. V. Vitaliani (1993). "Analysis of chloride diffusion into partially saturated concrete". Materials Journal 90(5): 441-451.

Salaiai, K. and R. Hameed (2017). " Effects of supplementary cementitious materials on durability –experimental study ". Proceedings of the 1st International ICT Conference on cement and concrete technology, Muscat, November 2017(Military Technological College), 226-248.

Saleem, M., M. Shameem, S. Hussain and M. Maslehuddin (1996). "Effect of moisture, chloride and sulphate contamination on the electrical resistivity of Portland cement concrete". Construction and Building Materials 10(3): 209-214.

Santhanam, M., M. D. Cohen and J. Olek (2002). "Modeling the effects of solution temperature and concentration during sulfate attack on cement mortars". Cement and Concrete Research 32(4): 585-592.

Schießl, P. and M. Raupach (1997). "Laboratory studies and calculations on the influence of crack width on chloride-induced corrosion of steel in concrete". Materials Journal 94(1): 56-61.

Shao-feng, Z., L. Chun-hua and L. Rong-gui (2011). "Experimental determination of chloride penetration in cracked concrete beams". Procedia Engineering 24: 380-384.

Shetty, M. (2005). "Concrete technology." S. chand & company LTD: 420-453.

Shi, X., N. Xie, K. Fortune and J. Gong (2012). "Durability of steel reinforced concrete in chloride environments: An overview". Construction and Building Materials 30: 125-138.

Silva, N. (2013). "Chloride induced corrosion of reinforcement steel in concrete-Threshold values and ion distributions at the concrete-steel interface". Chalmers University of Technology.

Singhal, D., R. Agrawal and B. Nautiyal (1992). "Chloride resistance of SFRC. Fiber reinforced cement and concrete". Proceeding of the fourth international symposium held by RILEM, July 20-23 1992, University of Sheffield.

Smilauer, V., L. Jendele and J. Cervenka (2013). "Prediction of Carbonation and Chloride Ingress in Cracked Concrete Structures". BHV Topping and P. Iványi, Editors. Proceedings of the Fourteenth International Conference on Civil, Structural and Environmental Engineering Computing.

Song, H.-W. and V. Saraswathy (2007). "Corrosion monitoring of reinforced concrete structures-A". Int. J. Electrochem. Sci 2: 1-28.

Song, H.-W., C.-H. Lee and K. Y. Ann (2008). "Factors influencing chloride transport in concrete structures exposed to marine environments". Cement and Concrete Composites 30(2): 113-121.

Song, H.-W., C.-H. Lee and K. Y. Ann (2008). "Factors influencing chloride transport in concrete structures exposed to marine environments". Cement and Concrete Composites 30(2), 113-121.

Song, H.-W., S.-J. Kwon, K.-J. Byun and C.-K. Park (2006). "Predicting carbonation in early-aged cracked concrete". Cement and Concrete Research 36(5): 979-989.

Song, H.-W., S.-W. Pack, C.-H. Lee and S.-J. Kwon (2006). "Service life prediction of concrete structures under marine environment considering coupled deterioration". Restoration of buildings and monuments= Bauinstandsetzen und Baudenkmalpflege 12(4): 265-284.

Song, Z. (2014). "Enhancing the service life of concrete exposed to chloride attack". PhD Thesis. University of Dundee.

Sosdean, C., D. Gubencu, G. De Schutter and L. Marsavina (2014). "Experimental determination of chloride penetration in concrete with real cracks. Fracture at all Scales". Springer: 195-208.

Srinivasan,s. and I. Gibb(2018). "Climate resilient concrete structures in marine environment of Bangladesh". Proceedings of a Sixth International Conference on the Durability of Concrete Structures, Leeds, July 2018(University of Leeds) 321-336.

Stanish, K. and M. Thomas (2003). "The use of bulk diffusion tests to establish time-dependent concrete chloride diffusion coefficients". Cement and Concrete Research 33(1): 55-62.

Stern, M. and A. L. Geary (1957). "Electrochemical polarization I. A theoretical analysis of the shape of polarization curves". Journal of the electrochemical society 104(1): 56-63.

Stern, M. and E. Weisert (1959). " Experimental observations on the relation between polarization resistance and corrosion rate". Proc. Am. Soc. Test. Mater.

Stewart, M. G. and D. V. Rosowsky (1998). "Time-dependent reliability of deteriorating reinforced concrete bridge decks". Structural safety 20(1): 91-109.

Stewart, M. G., X. Wang and M. N. Nguyen (2011). "Climate change impact and risks of concrete infrastructure deterioration". Engineering Structures 33(4): 1326-1337.

Stewart, M. G., X. Wang and M. N. Nguyen (2012). "Climate change adaptation for corrosion control of concrete infrastructure". Structural Safety 35: 29-39.

Sulapha, P., S. Wong, T. Wee and S. Swaddiwudhipong (2003). "Carbonation of concrete containing mineral admixtures". Journal of materials in civil engineering 15(2): 134-143.

Suryavanshi, A. and R. N. Swamy (1996). "Stability of Friedel's salt in carbonated concrete structural elements". Cement and Concrete Research 26(5): 729-741.

Takewaka, K. and S. Mastumoto (1988). "Quality and cover thickness of concrete based on the estimation of chloride penetration in marine environments". Special Publication 109: 381-400.

Talero, R., L. Trusilewicz, A. Delgado, et al. (2011). "Comparative and semi-quantitative XRD analysis of Friedel's salt originating from pozzolan and Portland cement". Construction and building materials 25(5), 2370-2380.

Talukdar, S. and N. Banthia (2013). "Carbonation in concrete infrastructure in the context of global climate change: development of a service lifespan model". Construction and Building Materials 40: 775-782.

Talukdar, S., N. Banthia and J. Grace (2012-a). "Carbonation in concrete infrastructure in the context of global climate change–Part 1: Experimental results and model development". Cement and Concrete Composites 34(8): 924-930.

Talukdar, S., N. Banthia, J. Grace and S. Cohen (2012-b). "Carbonation in concrete infrastructure in the context of global climate change: Part 2–Canadian urban simulations". Cement and Concrete Composites 34(8): 931-935.

Tang, L. (1997). " Chloride penetration profiles and diffusivity in concrete under different exposure conditions". Chalmers University of Technology.

Tang, L. and H. Sørensen (2001). "Precision of the Nordic test methods for measuring the chloride diffusion/migration coefficients of concrete". Materials and Structures 34(8): 479.

Tarun, R. and K. Rakesh (2010). "Global warming and cement-based materials ". UWM Center for By-Products Utilization.

Tawfiq, O.H. (1993). "Effect of Exposure conditions and ,ix ingredients on durability of reinforced concrete in saline environments". M.Sc. Thesis, University of Technology.

Teng, S., T. Y. D. Lim and B. S. Divsholi (2013). "Durability and mechanical properties of high strength concrete incorporating ultra-fine ground granulated blast-furnace slag ". Construction and Building Materials 40, 875-881.

Teychenné, D.C, E Franklin, R.E. and H. C. Erntroy (1988), "Design of normal concrete mixes. Second edition". Building Research Establishment. Garston, Watford.

Thiery, M., G. Villain, P. Dangla and G. Platret (2007). "Investigation of the carbonation front shape on cementitious materials: effects of the chemical kinetics". Cement and concrete research 37(7): 1047-1058.

Thomas, M., R. Hooton, A. Scott, et al. (2012). "The effect of supplementary cementitious materials on chloride binding in hardened cement paste". Cement and Concrete Research 42(1), 1-7.

Tikalsky, P. (2005). "Monte carlo simulation of chloride diffusion in concrete exposed to de-icing salts. Concrete for Transportation Infrastructure". Proceedings of the International Conference held at the University of Dundee, Scotland, UK on 5–7 July 2005, Thomas Telford Publishing.

Trejo, D., C. Halmen and K. Reinschmidt (2008). "Corrosion performance tests for reinforcing steel in concrete ". technical report, Texas Transportation Institute.

Tuutti, K. (1982). " Corrosion of steel in concrete". Stockholm, Swedish Cement and Concrete Research Institute.

Uji, K., Y. Matsuoka and T. Maruya (1990). "Formulation of an equation for surface chloride content of concrete due to permeation of chloride". Elsevier Applied Science: 258-267.

UKCP09,(2010). " UK Climate Projections science report: Climate change projections". ". [Online] available at: http://ukclimateprojections.defra.gov.uk.pdf.

Ukpata, J., Basheer,P and L. Black (2018). "Influence of exposure environments on the durability of slag blended cements ". Proceedings of a Sixth International Conference on the Durability of Concrete Structures, Leeds, July 2018(University of Leeds) 345-352.

Val, D. V. and P. A. Trapper (2008). "Probabilistic evaluation of initiation time of chloride-induced corrosion". Reliability Engineering & System Safety 93(3): 364-372.

Valdez, B., M. Schorr, M. Quintero, R. García and N. Rosas (2010). "Effect of climate change on durability of engineering materials in hydraulic infrastructure: an overview". Corrosion Engineering, Science and Technology 45(1): 34-41.

Vallini, D. and J. M. Aldred (2003). "Durability assessment of concrete specimens in the tidal and splash zones in Fremantle port. Coasts & Ports 2003 Australasian Conference ". Proceedings of the 16th Australasian Coastal and Ocean Engineering Conference, the 9th Australasian Port and Harbour Conference and the Annual New Zealand Coastal Society Conference, Institution of Engineers, Australia.

Van den Heede, P. and N. De Belie (2018). "Estimated Service Life of Carbonation Exposed (Cracked) Concrete with Pozzolans or Self-healing Agents ". Proceedings of a Sixth International Conference on the Durability of Concrete Structures, Leeds, July 2018(University of Leeds) 46-52.

Van den Heede, P., M. Maes and N. De Belie (2014). "Influence of active crack width control on the chloride penetration resistance and global warming potential of slabs made with fly ash+ silica fume concrete". Construction and Building Materials 67, 74-80.

Vanoutrive,H., Cizer, Ö., Minne, P. and E. Gruyaert (2019). " Carbonation of cement paste with supplementary cementitious materials including the effect on chloride ingress and frost salt scaling". Proceedings of the International Conference on

sustainable materials, systems and structures (SMSS2019) PhD symposium, Rovinj, Croatia, March 2019(Rilem Publications S.A.R.L.), 1-2.

Vennesland, Ø., M.-Á. Climent and C. Andrade (2013). "Recommendation of RILEM TC 178-TMC: Testing and modelling chloride penetration in concrete".

Venu, K., K. Balakrishnan and K. Rajagopalan (1965). "A potentiokinetic polarization study of the behaviour of steel in NaOH-NaCl system". Corrosion Science 5(1): 59-69.

Vu, K. A. T. and M. G. Stewart (2000). "Structural reliability of concrete bridges including improved chloride-induced corrosion models". Structural safety 22(4): 313-333.

Wan, X.-m., F. H. Wittmann, T.-j. Zhao and H. Fan (2013). "Chloride content and pH value in the pore solution of concrete under carbonation". Journal of Zhejiang University SCIENCE A 14(1): 71-78.

Wang, J., P. M. Basheer, S. V. Nanukuttan, A. E. Long and Y. Bai (2016). "Influence of service loading and the resulting micro-cracks on chloride resistance of concrete". Construction and Building Materials 108: 56-66.

Wang, X., M. Nguyen, M. Stewart, M. Syme and A. Leitch (2010). "Analysis of climate change impacts on the deterioration of concrete infrastructure–synthesis Report". Part 3: Case Studies of Concrete Deterioration and Adaptation. Published by CSIRO, Canberra. ISBN978 0 643(10364): 1.

Wang, Y., Basheer, M., Nanukuttan, S.and Bai, Y.2016. "Progress of Carbonation in Chloride Contaminated Concretes". 5th International Conference on Durability of Concrete Structures Jun 30–Jul 1, 2016. Shenzhen University, Shenzhen, Guangdong Province, P.R.China, 317-327.

Weyers, R. E. (1998). "Service life model for concrete structures in chloride laden environments". Materials Journal 95(4): 445-453.

Wong, S., T. Wee, S. Swaddiwudhipong and S. Lee (2001). "Study of water movement in concrete". Magazine of Concrete Research 53(3): 205-220.

Yokozeki, K., K. Watanabe, D. Hayashi, N. Sakata and N. Otsuki (2003). "Modeling of ion diffusion coefficients in concrete considering with hydration and temperature effects". Doboku Gakkai Ronbunshu 2003(725): 131-142.

Yoon, I.-S., O. Çopuroğlu and K.-B. Park (2007). "Effect of global climatic change on carbonation progress of concrete". Atmospheric environment 41(34): 7274-7285.

Yu, C.-W. and J. W. Bull (2006). "Durability of materials and structures in building and civil engineering". Whittles Publishing, Dunbeath, Scotland

Yuan, Q., C. Shi, F. He, et al. (2008). "Effect of hydroxyl ions on chloride penetration depth measurement using the colorimetric method". Cement and concrete research 38(10), 1177-1180.

Yuan, Q., C. Shi, G. De Schutter, et al. (2009). "Chloride binding of cement-based materials subjected to external chloride environment–a review". Construction and Building Materials 23(1), 1-13.

Yuan, Q., C. Shi, G. De Schutter, K. Audenaert and D. Deng (2009). "Chloride binding of cement-based materials subjected to external chloride environment–a review". Construction and Building Materials 23(1): 1-13.

Yuan, Y. and J. Jiang (2011). "Prediction of temperature response in concrete in a natural climate environment". Construction and Building Materials 25(8): 3159-3167.

Zeng, Q., K. Li, T. Fen-Chong, et al. (2012). "Pore structure characterization of cement pastes blended with high-volume fly-ash ". Cement and Concrete Research 42(1), 194-204.

Zhang, X. and Y. Zhao (2018). " Investigation on the influence of concrete pores on steel corrosion process ". Proceedings of a Sixth International Conference on the Durability of Concrete Structures, Leeds, July 2018(University of Leeds) 395-401.

Zhao, Y. and H. Lin (2018). "The Bond Behaviour between Concrete and Corroded Reinforcement: State of the Art". Proceedings of a Sixth International Conference on the Durability of Concrete Structures, Leeds, July 2018(University of Leeds) 63-73.

Zibara, H. (2001). "Binding of external chlorides by cement pastes ". National Library of Canada Bibliothèque nationale du Canada.

Živica, V. (2002). "Significance and influence of the ambient temperature as a rate factor of steel reinforcement corrosion". Bulletin of Materials Science 25(5): 375-379.

Zuquan, J., Wel, S., Yunsheng, Z., Jinyang, J. and L. Jianzhong (2007). "Interaction between sulfate and chloride solution attack of concretes with and without fly ash". Cement and Concrete Research, Vol.37, 1223-1232.

PUBLICATION

1- **AL-Ameeri, A., Rafiq, M., Tsioulou, O**. Influence of Cracks on the Carbonation Resistance of Concrete Structure. *Sixth International Conference on Durability of Concrete Structures* (*ICDCS 2018*), 18-20 July 2018, Leeds - UK. [online] available at: (https://www.researchgate.net/publication/326535118).

2- **AL-Ameeri, A., Rafiq, M., Tsioulou, O**. Influence of Exposure Environments on the Carbonation Resistance of Concrete Structures. *International Conference on Sustainable Materials, Systems and Structures* (*SMSS 2019*). *Durability, Monitoring and Repair of Structures*, 20-22 March 2019 – Rovinj - Croatia. available at: (http://grad.hr/rilem.smss/)

3- **AL-Ameeri, A., Rafiq, M., Tsioulou, O**. Effect of Cracks on Alkalinity Level of Concrete Structure Exposed to CO2 Environment Conditions. *Euro Coal Ash 2019*,10-12 June 2019-Dundee - Scotland. [online] available at: (https://www.dropbox.com/sh/h1rb765mkou4mqs/AAC1XHCk6TC-8l8S5sYuSjsWa?dl=0&preview=EuroCoalAsh2019Proceedings.pdf)

4- **AL-Ameeri, A., Rafiq, M., Tsioulou, O**. Influence of Carbonation on the Resistance of Concrete Structures to Chloride Penetration and Corrosion. *Concrete Solutions 2019*,7th international conference of repair, 30 Sept to 2 Oct 2019, Technical University of Cluj-Napoca-Romania. [online] available at: (https://doi.org/10.1051/matecconf/201928908001)

Appendix A

A-1 Concrete Mixing Stages

- The half weight of coarse aggregate and fine aggregate were mixed for 1 minute.
- Adding the whole amount of cement into the mixer for 1 minute.
- Adding the second half weight of coarse aggregate and adding water gradually to the drum of the mixer and mixing for 1.5 minutes.
- Stopping the mixer and accumulating the materials in the centre of it, finally, the mixer is turned on for 1.5 minutes.

The total duration of mixing was about 5 minutes.

Table A.1: Fresh and microstructure properties of mixes used in the study

Mixes Designation	$\frac{w}{binder}$	Slump mm	Age day	Density kg/m^3	Porosity %	Water absorption %
M 0.4	0.4	110	28	2467	10.9	5.0
			60	2445	10.01	4.6
			90	2425	8.7	3.9
			150	2430	7.5	3.8
M 0.5	0.5	130	28	2444	12	5.7
			60	2416	11.1	5.2
			90	2390	10.1	4.7
			150	2380	9.5	4.5
M 0.6	0.6	140	28	2398	12.3	5.7
			60	2389	11.5	5.4
			90	2388	10.9	5.1
			150	2380	10.1	4.75
	0.5	140	28	2444	12.4	5.8

Mixes Designation	w / binder	Slump mm	Age day	Density kg/m^3	Porosity %	Water absorption %
M 0.5 + 0.35 PFA	0.5	120	60	2383	10.1	4.7
			90	2383	8.8	4.1
			150	2347	7.8	3.8
M 0.5+0.3 GGBS			28	2435	11.6	5.4
			60	2397	10.0	4.6
			90	2387.5	9.7	4.5
			150	2380	9.1	4.3

Table A.2: Effect of crack width and types of mixes on gas permeability*

Crack width mm	Gas permeability coefficient, K, *10^{-17}, m^2				
	M 0.4	M 0.5	M 0.6	M 0.5 + GGBS	M 0.5+ PFA
Uncracked	6.10	7.10	10.60	15. 60	27.00
0.05- 0.15	10.30	12.70	14.80	17.50	33.80
0.15 - 0.25	12.40	14.20	16.40	17.80	34.10
0.25- 0.35	12.60	14.70	16.70	18.10	34.60

*These results are average of three samples.

Table A.3: Result of chloride permeability test by NT Build 492-1999 *

Mix	$\frac{w}{binder}$	Penetration of chloride (mm) at		D_{nssm} (m^2/sec *10^{-12}) at		Ageing factor (m)
		28 days	150 days	28 days	150 days	
M 0.4	0.4	22.50	17.30	16.60	8.03	0.42
M 0.5	0.5	31.00	19.25	18.10	11.10	0.30
M 0.6	0.6	34.00	27.60	25.60	17.80	0.21
M 0.5 + GGBS	0.5	24.20	13.92	11.60	6.02	0.43
M 0.5 + PFA	0.5	25.00	14.74	12.20	4.07	0.65

*These results are average of three samples.

Table A.4: Effect of CO_2 concentration on DoC for Scenario a

Sample	$\frac{w}{binder}$	Crack width mm	Carbonation depth (mm) for Temperature 25 ºC, Relative humidity 65% and		
			CO_2=1.5% (7)	CO_2=3% (6)	CO_2=5% (5)
M 0.4	0.4	0	4	6	8
		0.05-0.15	14	16	19
		0.15-0.25	18	20	23
		0.25-0. 35	20	31	36
M 0.5	0.5	0	7.5	10	11.5
		0.05-0.15	18	20	26
		0.15-0.25	23	26	30
		0.25-0. 35	33	34	38
M 0.6	0.6	0	10	12	15
		0.05-0.15	22	23	26
		0.15-0.25	27	30	35
		0.25-0. 35	35	42	48
M 0.5+ 0.3GGBS	0.5	0	9	11	12
		0.05-0.15	21	23	27
		0.15-0.25	33	33	38
		0.25-0. 35	38	40	43
M 0.5+ 0.35 PFA	0.5	0	9	14	20
		0.05-0.15	26	30	34
		0.15-0.25	34	40	45
		0.25-0. 35	43	44	50

Table A.5: Effect of Temperature on DoC for Scenario b

Sample	$\frac{w}{binder}$	Crack width mm	Carbonation depth (mm) for , Relative humidity 65% CO_2=5% and Temperature 25 ºC (5)	Temperature 35 ºC (3)	Temperature 45 ºC (1)
M 0.4	0.4	0	8	9	9.5
		0.05-0.15	19	20	21
		0.15-0.25	23	25	23
		0.25-0. 35	36	35	36
M 0.5	0.5	0	11.5	13	13.5
		0.05-0.15	26	24	27
		0.15-0.25	30	29	31
		0.25-0. 35	38	40	42
M 0.6	0.6	0	15	16	17
		0.05-0.15	26	28	30
		0.15-0.25	35	35	33
		0.25-0. 35	48	50	47
M 0.5+ 0.3GGBS	0.5	0	12	14	15
		0.05-0.15	27	31	31
		0.15-0.25	38	37	36
		0.25-0. 35	43	45	47
M 0.5+ 0.35 PFA	0.5	0	20	24	26
		0.05-0.15	34	38	40
		0.15-0.25	45	45	47
		0.25-0. 35	50	50	53

Table A.6: Effect Relative humidity on DoC for *Scenario c*

Sample	$\frac{w}{binder}$	Crack width mm	Carbonation depth (mm) for Temperature 25 ºC, CO_2=5% and		
			Relative humidity 65% (5)	Relative humidity 75% (4)	Relative humidity 85% (2)
M 0.4	0.4	0	8	7	5
		0.05-0.15	19	13	12
		0.15-0.25	23	21	20
		0.25-0. 35	36	30	32
M 0.5	0.5	0	11.5	11	10
		0.05-0.15	26	23	20
		0.15-0.25	30	29	23
		0.25-0. 35	38	40	37
M 0.6	0.6	0	15	15	14
		0.05-0.15	26	25	33
		0.15-0.25	35	36	38
		0.25-0. 35	48	46	50
M 0.5+ 0.3GGBS	0.5	0	12	11	10
		0.05-0.15	27	28	25
		0.15-0.25	38	34	32
		0.25-0. 35	43	44	40
M 0.5+ 0.35 PFA	0.5	0	20	24	22
		0.05-0.15	34	32	33
		0.15-0.25	45	46	44
		0.25-0. 35	50	50	48

Table A.7: Effect of CO_2 on XRD peak of $CaCO_3$ and $Ca(OH)_2$ with different depths for Scenario a of (M 0.4) due to exposure to CO_2 environmental conditions for 8 weeks

Environmental conditions	Relative intensity of XRD (%) at Temperature 25 ºC, Relative humidity 65% and																							
	CO_2 1.5% (7)								CO_2 3% (6)								CO_2 5% (5)							
Crack width	**Un-cracked**		**0.05-0.15 mm**		**0.15-0.25 mm**		**0.25-0.35 mm**		**Un-cracked**		**0.05-0.15 mm**		**0.15-0.25 mm**		**0.25-0.35 mm**		**Un-cracked**		**0.05-0.15 mm**		**0.15-0.25 mm**		**0.25-0.35 mm**	
Depth mm	**$Ca(OH)_2$**	**$CaCO_3$**	**$Ca(OH)_2$**	**$CaCO_3$**	**$Ca(OH)_2$**	**$CaCO_3$**	**$Ca(OH)_2$**	**$CaCO_3$**	**$Ca(OH)_2$**	**$CaCO_3$**	**$Ca(OH)_2$**	**$CaCO_3$**	**$Ca(OH)_2$**	**$CaCO_3$**	**$Ca(OH)_2$**	**$CaCO_3$**	**$Ca(OH)_2$**	**$CaCO_3$**	**$Ca(OH)_2$**	**$CaCO_3$**	**$Ca(OH)_2$**	**$CaCO_3$**	**$Ca(OH)_2$**	**$CaCO_3$**
0	0	100	0	100	0	100	0	100	0	100	0	100	0	100	0	100	0	100	0	100	0	100	0	100
4 - 6	0	100	0	100	0	100	0	100	0	100	0	100	0	100	0	100	0	100	0	100	0	100	0	100
6 -12	20	75	44	65	23	52	3	58	0	64	11	86	4	100	14	58	0	94	12	72	0	100	0	61
12 - 18	64	42	74	54	40	51	14	41	27	50	21	72	10	43	22	25	32	83	17	48	8	94	36	35
18 - 24	66	28	90	49	44	33	48	32	48	27	24	53	30	40	41	24	56	46	29	47	23	56	36	12
24 - 30	83	26	93	48	78	30	77	26	94	26	64	29	63	27	76	15	66	29	63	38	51	56	49	3
30 - 36	92	7	96	42	84	5	78	18	94	14	75	16	77	17	77	6	74	15	85	36	84	47	82	2
36 - 42	100	0	100	0	100	0	100	0	100	0	100	0	100	17	100	0	91	4	100	0	100	44	100	0
42 - 48	100	0	100	0	100	0	100	0	100	0	100	0	100	0	100	0	100	0	100	0	100	0	100	0

Table A.8: Effect of CO_2 on XRD peak of $CaCO_3$ and $Ca(OH)_2$ with different depths for Scenario a of (M 0.5) due to exposure to CO_2 environmental conditions for 8 weeks

Environmental conditions	Relative intensity of XRD (%) at Temperature 25 ºC, Relative humidity 65% and																							
	CO_2 1.5% (7)								CO_2 3% (6)								CO_2 5% (7)							
Crack width	**Un-cracked**		**0.05-0.15 mm**		**0.15-0.25 mm**		**0.25-0.35 mm**		**Un-cracked**		**0.05-0.15 mm**		**0.15-0.25 mm**		**0.25-0.35 mm**		**Un-cracked**		**0.05-0.15 mm**		**0.15-0.25 mm**		**0.25-0.35 mm**	
Depth mm	**$Ca(OH)_2$**	**$CaCO_3$**	**$Ca(OH)_2$**	**$CaCO_3$**	**$Ca(OH)_2$**	**$CaCO_3$**	**$Ca(OH)_2$**	**$CaCO_3$**	**$Ca(OH)_2$**	**$CaCO_3$**	**$Ca(OH)_2$**	**$CaCO_3$**	**$Ca(OH)_2$**	**$CaCO_3$**	**$Ca(OH)_2$**	**$CaCO_3$**	**$Ca(OH)_2$**	**$CaCO_3$**	**$Ca(OH)_2$**	**$CaCO_3$**	**$Ca(OH)_2$**	**$CaCO_3$**	**$Ca(OH)_2$**	**$CaCO_3$**
0	0	100	0	100	0	100	0	100	0	100	0	100	0	100	0	100	0	100	0	100	0	100	0	100
4 - 6	0	100	0	100	0	100	0	100	0	100	0	100	0	100	0	100	0	100	0	100	0	100	0	100
6 -12	64	35	0	88	0	71	37	27	3	75	0	92	0	65	0	73	44	93	0	34	0	51	0	87
12 - 18	78	20	31	86	43	22	45	23	46	59	24	76	15	60	19	54	45	76	11	28	9	50	14	73
18 - 24	83	16	44	52	45	17	59	21	47	54	37	75	20	27	32	51	69	20	30	27	22	34	27	53
24 - 30	84	15	73	39	85	16	83	20	84	40	79	38	53	24	75	39	93	10	61	23	31	2	63	48
30 - 36	93	6	81	35	92	14	99	16	95	21	99	22	92	24	83	7	96	8	86	13	68	1	66	33
36 - 42	100	0	100	0	100	0	100	0	100	0	100	0	100	0	100	0	100	0	100	0	100	0	100	0
42 - 48	100	0	100	0	100	0	100	0	100	0	100	0	100	0	100	0	100	0	100	0	100	0	100	0

Table A.9: Effect of CO_2 on XRD analysis for $CaCO_3$ and $Ca(OH)_2$ with different depths for Scenario a of (M 0.6) due to exposure to CO_2 environmental conditions for 8 weeks

Environmental conditions	Relative intensity of XRD (%) at Temperature 25 ºC, Relative humidity 65% and CO_2=5%																							
	CO_2 1.5% (7)								CO_2 3% (6)								CO_2 5% (7)							
Crack width	**Un-cracked**		**0.05-0.15 mm**		**0.15-0.25 mm**		**0.25-0.35 mm**		**Un-cracked**		**0.05-0.15 mm**		**0.15-0.25 mm**		**0.25-0.35 mm**		**Un-cracked**		**0.05-0.15 mm**		**0.15-0.25 mm**		**0.25-0.35 mm**	
Depth mm	**$Ca(OH)_2$**	**$CaCO_3$**	**$Ca(OH)_2$**	**$CaCO_3$**	**$Ca(OH)_2$**	**$CaCO_3$**	**$Ca(OH)_2$**	**$CaCO_3$**	**$Ca(OH)_2$**	**$CaCO_3$**	**$Ca(OH)_2$**	**$CaCO_3$**	**$Ca(OH)_2$**	**$CaCO_3$**	**$Ca(OH)_2$**	**$CaCO_3$**	**$Ca(OH)_2$**	**$CaCO_3$**	**$Ca(OH)_2$**	**$CaCO_3$**	**$Ca(OH)_2$**	**$CaCO_3$**	**$Ca(OH)_2$**	**$CaCO_3$**
0	0	100	0	100	0	100	0	100	0	100	0	100	0	100	0	100	0	100	0	100	0	100	0	100
4 - 6	0	100	0	100	0	100	0	100	0	100	0	100	0	100	0	100	0	100	0	100	0	100	0	100
6 -12	0	65	0	74	0	80	0	91	8	54	0	47	0	37	0	28	0	90	26	90	0	37	0	80
12 - 18	49	22	0	40	39	45	0	87	51	32	6	36	0	33	0	18	28	58	29	86	19	35	0	74
18 - 24	72	16	52	39	40	40	0	62	56	29	21	27	10	16	22	14	40	40	43	79	27	18	0	61
24 - 30	97	13	91	31	90	40	95	55	86	1	63	26	74	14	90	10	53	23	44	21	78	15	32	37
30 - 36	99	11	92	6	96	37	98	31	98	1	93	10	89	1	92	8	81	11	76	5	78	13	84	30
36 - 42	100	0	100	0	100	0	100	0	100	0	100	0	100	0	100	0	100	0	100	0	100	0	85	28
42 - 48	100	0	100	0	100	0	100	0	100	0	100	0	100	0	100	0	100	0	100	0	100	0	100	0

Table A.10: Effect of CO_2 on XRD analysis for $CaCO_3$ and $Ca(OH)_2$ with different depths for Scenario a of (M 0.5+ GGBS) due to exposure to CO_2 environmental conditions for 8 weeks

Environmental conditions	Relative intensity of XRD (%) at Temperature 25 ºC, Relative humidity 65% and																							
	CO_2 1.5% (7)								CO_2 3% (6)								CO_2 5% (5)							
Crack width	**Un-cracked**		**0.05-0.15 mm**		**0.15-0.25 mm**		**0.25-0.35 mm**		**Un-cracked**		**0.05-0.15 mm**		**0.15-0.25 mm**		**0.25-0.35 mm**		**Un-cracked**		**0.05-0.15 mm**		**0.15-0.25 mm**		**0.25-0.35 mm**	
Depth mm	**$Ca(OH)_2$**	**$CaCO_3$**	**$Ca(OH)_2$**	**$CaCO_3$**	**$Ca(OH)_2$**	**$CaCO_3$**	**$Ca(OH)_2$**	**$CaCO_3$**	**$Ca(OH)_2$**	**$CaCO_3$**	**$Ca(OH)_2$**	**$CaCO_3$**	**$Ca(OH)_2$**	**$CaCO_3$**	**$Ca(OH)_2$**	**$CaCO_3$**	**$Ca(OH)_2$**	**$CaCO_3$**	**$Ca(OH)_2$**	**$CaCO_3$**	**$Ca(OH)_2$**	**$CaCO_3$**	**$Ca(OH)_2$**	**$CaCO_3$**
0	0	100	0	100	0	100	0	100	0	100	0	100	0	100	0	100	0	100	0	100	0	100	0	100
4 - 6	0	100	0	100	0	100	0	100	0	100	0	100	0	100	0	100	0	100	0	100	0	100	0	100
6 -12	0	60	0	82	0	76	0	95	0	62	0	41	0	87	0	59	0	71	0	82	16	93	18	88
12 - 18	0	25	0	54	0	59	0	65	20	48	26	41	18	86	20	31	14	52	23	78	23	69	15	74
18 - 24	27	6	58	29	36	56	0	50	49	10	46	35	22	76	35	27	45	45	25	39	26	57	39	46
24 - 30	47	4	82	28	49	49	74	35	69	3	85	23	83	76	83	25	67	43	59	13	97	44	52	42
30 - 36	53	0	95	20	65	26	81	31	83	2	92	4	99	6	92	4	71	37	91	6	99	12	80	37
36 - 42	100	0	100	0	100	0	100	0	100	0	100	0	100	0	100	0	100	0	100	0	100	0	100	0
42 - 48	100	0	100	0	100	0	100	0	100	0	100	0	100	0	100	0	100	0	100	0	100	0	100	0

Table A.11: Effect of CO_2 on XRD analysis for $CaCO_3$ and $Ca(OH)_2$ with different depths for Scenario a of (M 0.5+ PFA) due to exposure to CO_2 environmental conditions for 8 weeks

Environmental conditions	Relative intensity of XRD (%) at Temperature 25 ºC, Relative humidity 65% and																							
	CO_2 1.5% (7)								CO_2 3% (6)								CO_2 1% (7)							
Crack width	**Un-cracked**		**0.05-0.15 mm**		**0.15-0.25 mm**		**0.25-0.35 mm**		**Un-cracked**		**0.05-0.15 mm**		**0.15-0.25 mm**		**0.25-0.35 mm**		**Un-cracked**		**0.05-0.15 mm**		**0.15-0.25 mm**		**0.25-0.35 mm**	
Depth mm	**$Ca(OH)_2$**	**$CaCO_3$**	**$Ca(OH)_2$**	**$CaCO_3$**	**$Ca(OH)_2$**	**$CaCO_3$**	**$Ca(OH)_2$**	**$CaCO_3$**	**$Ca(OH)_2$**	**$CaCO_3$**	**$Ca(OH)_2$**	**$CaCO_3$**	**$Ca(OH)_2$**	**$CaCO_3$**	**$Ca(OH)_2$**	**$CaCO_3$**	**$Ca(OH)_2$**	**$CaCO_3$**	**$Ca(OH)_2$**	**$CaCO_3$**	**$Ca(OH)_2$**	**$CaCO_3$**	**$Ca(OH)_2$**	**$CaCO_3$**
0	0	100	0	100	0	100	0	100	0	100	0	100	0	100	0	100	0	100	0	100	0	100	0	100
4 - 6	0	100	0	100	0	100	0	100	0	100	0	100	0	100	0	83	0	100	0	100	0	100	0	100
6 -12	0	41	0	78	0	70	0	98	0	46	0	52	0	86	0	83	0	99	0	62	0	49	0	97
12 - 18	0	34	0	78	0	56	0	77	0	13	0	49	0	67	39	81	0	51	0	52	28	28	0	88
18 - 24	56	29	0	11	0	32	0	74	46	9	0	46	51	64	41	54	63	40	23	25	65	28	0	85
24 - 30	71	15	63	5	0	18	0	57	55	8	44	4	54	5	50	39	65	30	65	10	94	21	56	73
30 - 36	89	10	75	2	89	17	0	54	89	6	54	3	78	3	81	37	73	8	91	8	100	0	91	12
36 - 42	100	0	100	0	100	0	100	0	100	0	100	0	100	0	100	0	100	0	100	0	100	0	100	0
42 - 48	100	0	100	0	100	0	100	0	100	0	100	0	100	0	100	0	100	0	100	0	100	0	100	0

Table A.12: Effect of temperature on XRD peak of $CaCO_3$ and $Ca(OH)_2$ with different depths for Scenario b of (M 0.4) due to exposure to CO_2 environmental conditions for 8 weeks

Environmental conditions	Relative intensity of XRD (%) at Relative humidity 65%, CO_2 5% and																							
	Temperature 25 ºC (5)								Temperature 35 ºC (3)								Temperature 45 ºC (1)							
Crack width	**Un-cracked**		**0.05-0.15 mm**		**0.15-0.25 mm**		**0.25-0.35 mm**		**Un-cracked**		**0.05-0.15 mm**		**0.15-0.25 mm**		**0.25-0.35 mm**		**Un-cracked**		**0.05-0.15 mm**		**0.15-0.25 mm**		**0.25-0.35 mm**	
Depth mm	**$Ca(OH)_2$**	**$CaCO_3$**	**$Ca(OH)_2$**	**$CaCO_3$**	**$Ca(OH)_2$**	**$CaCO_3$**	**$Ca(OH)_2$**	**$CaCO_3$**	**$Ca(OH)_2$**	**$CaCO_3$**	**$Ca(OH)_2$**	**$CaCO_3$**	**$Ca(OH)_2$**	**$CaCO_3$**	**$Ca(OH)_2$**	**$CaCO_3$**	**$Ca(OH)_2$**	**$CaCO_3$**	**$Ca(OH)_2$**	**$CaCO_3$**	**$Ca(OH)_2$**	**$CaCO_3$**	**$Ca(OH)_2$**	**$CaCO_3$**
0	0	100	0	100	0	100	0	100	0	100	0	100	0	100	0	100	0	100	0	100	0	100	0	100
4 - 6	0	100	0	100	0	100	0	100	0	100	0	100	0	100	0	100	0	100	0	100	0	100	0	100
6 -12	0	94	12	72	0	100	0	61	23	89	28	63	4	62	1	94	9	41	35	75	32	74	13	56
12 - 18	32	83	17	48	8	94	36	35	30	73	32	59	21	52	2	89	27	22	56	53	53	35	22	54
18 - 24	56	46	29	47	23	56	36	12	43	46	36	55	30	41	43	86	73	17	79	36	57	31	34	50
24 - 30	66	29	63	38	51	56	49	3	50	17	44	53	82	26	46	77	77	1	82	26	76	29	51	26
30 - 36	74	15	85	36	84	47	82	2	57	10	83	51	82	25	71	72	83	2	87	22	88	28	55	22
36 - 42	91	4	100	0	100	44	100	0	95	6	95	7	95	3	82	13	99	2	87	11	87	1	76	12
42 - 48	100	0	100	0	100	0	100	0	100	0	100	0	100	0	100	0	100	0	100	0	100	0	100	0

Table A.13: Effect of temperature on XRD peak of $CaCO_3$ and $Ca(OH)_2$ with different depths for Scenario b of (M 0.5) due to exposure to CO_2 environmental conditions for 8 weeks

Environmental conditions	Relative intensity of XRD (%) at Relative humidity 65%, CO_2 5% and																							
	Temperature 25 ºC (5)								Temperature 35 ºC (3)								Temperature 45 ºC (1)							
Crack width	**Un-cracked**		**0.05-0.15 mm**		**0.15-0.25 mm**		**0.25-0.35 mm**		**Un-cracked**		**0.05-0.15 mm**		**0.15-0.25 mm**		**0.25-0.35 mm**		**Un-cracked**		**0.05-0.15 mm**		**0.15-0.25 mm**		**0.25-0.35 mm**	
Depth mm	**$Ca(OH)_2$**	**$CaCO_3$**	**$Ca(OH)_2$**	**$CaCO_3$**	**$Ca(OH)_2$**	**$CaCO_3$**	**$Ca(OH)_2$**	**$CaCO_3$**	**$Ca(OH)_2$**	**$CaCO_3$**	**$Ca(OH)_2$**	**$CaCO_3$**	**$Ca(OH)_2$**	**$CaCO_3$**	**$Ca(OH)_2$**	**$CaCO_3$**	**$Ca(OH)_2$**	**$CaCO_3$**	**$Ca(OH)_2$**	**$CaCO_3$**	**$Ca(OH)_2$**	**$CaCO_3$**	**$Ca(OH)_2$**	**$CaCO_3$**
0	0	100	0	100	0	100	0	100	0	100	0	100	0	100	0	100	0	100	0	100	0	100	0	100
4 - 6	0	100	0	100	0	100	0	100	0	100	0	100	0	100	0	100	0	100	0	100	0	100	0	100
6 -12	44	93	0	34	0	51	0	87	14	89	9	80	4	96	0	99	0	99	12	70	12	79	0	97
12 - 18	45	76	11	28	9	50	14	73	25	49	15	57	9	84	0	73	0	96	30	52	28	55	44	95
18 - 24	69	20	30	27	22	34	27	53	74	43	47	47	12	42	0	68	84	96	73	47	69	33	73	52
24 - 30	93	10	61	23	31	2	63	48	85	31	88	12	49	28	18	58	88	94	77	38	75	21	85	27
30 - 36	96	8	86	13	68	1	66	33	98	15	96	11	76	21	69	55	98	81	80	33	80	9	88	22
36 - 42	100	0	100	0	100	0	100	0	99	8	92	8	99	6	86	20	100	0	88	15	87	5	90	7
42 - 48	100	0	100	0	100	0	100	0	100	0	100	0	100	0	100	0	100	0	100	0	100	0	100	0

Table A.14: Effect of temperature on XRD analysis for $CaCO_3$ and $Ca(OH)_2$ with different depths for Scenario b of (M 0.6) due to exposure to CO_2 environmental conditions for 8 weeks

Environmental conditions	Relative intensity of XRD (%) at Relative humidity 65%, CO_2 5% and																							
	Temperature 25 ºC (5)								Temperature 35 ºC (3)								Temperature 45 ºC (1)							
Crack width	**Un-cracked**		**0.05-0.15 mm**		**0.15-0.25 mm**		**0.25-0.35 mm**		**Un-cracked**		**0.05-0.15 mm**		**0.15-0.25 mm**		**0.25-0.35 mm**		**Un-cracked**		**0.05-0.15 mm**		**0.15-0.25 mm**		**0.25-0.35 mm**	
Depth mm	**$Ca(OH)_2$**	**$CaCO_3$**	**$Ca(OH)_2$**	**$CaCO_3$**	**$Ca(OH)_2$**	**$CaCO_3$**	**$Ca(OH)_2$**	**$CaCO_3$**	**$Ca(OH)_2$**	**$CaCO_3$**	**$Ca(OH)_2$**	**$CaCO_3$**	**$Ca(OH)_2$**	**$CaCO_3$**	**$Ca(OH)_2$**	**$CaCO_3$**	**$Ca(OH)_2$**	**$CaCO_3$**	**$Ca(OH)_2$**	**$CaCO_3$**	**$Ca(OH)_2$**	**$CaCO_3$**	**$Ca(OH)_2$**	**$CaCO_3$**
0	0	100	0	100	0	100	0	100	0	100	0	100	0	100	0	100	0	100	0	100	0	100	0	100
4 - 6	0	100	0	100	0	100	0	100	0	100	0	100	0	100	0	100	0	100	0	100	0	100	0	100
6 -12	0	90	26	90	0	37	0	80	0	79	0	92	0	89	0	95	11	69	0	100	0	79	0	91
12 - 18	28	58	29	86	19	35	0	74	0	68	27	69	0	88	0	90	47	32	37	54	35	58	0	91
18 - 24	40	40	43	79	27	18	0	61	86	10	45	65	0	73	0	81	74	18	54	19	51	29	0	82
24 - 30	53	23	44	21	78	15	32	37	91	8	63	57	46	66	78	59	83	15	80	7	79	12	0	62
30 - 36	81	11	76	5	78	13	84	30	92	1	94	33	91	30	78	53	95	8	92	5	85	7	67	13
36 - 42	100	0	100	0	100	0	85	28	98	1	96	4	97	5	98	4	100	0	98	3	92	4	100	10
42 - 48	100	0	100	0	100	0	100	0	100	0	100	0	100	0	100	0	100	0	100	0	100	0	100	0

Table A.15: Effect of temperature on XRD analysis for $CaCO_3$ and $Ca(OH)_2$ with different depths for Scenario b of (M 0.5+ GGBS) due to exposure to CO_2 environmental conditions for 8 weeks

Environmental conditions	Relative intensity of XRD (%) at Relative humidity 65%, CO_2 5% and																							
	Temperature 25 ºC (5)								Temperature 35 ºC (3)								Temperature 45 ºC (1)							
Crack width	**Un-cracked**		**0.05-0.15 mm**		**0.15-0.25 mm**		**0.25-0.35 mm**		**Un-cracked**		**0.05-0.15 mm**		**0.15-0.25 mm**		**0.25-0.35 mm**		**Un-cracked**		**0.05-0.15 mm**		**0.15-0.25 mm**		**0.25-0.35 mm**	
Depth mm	**$Ca(OH)_2$**	**$CaCO_3$**	**$Ca(OH)_2$**	**$CaCO_3$**	**$Ca(OH)_2$**	**$CaCO_3$**	**$Ca(OH)_2$**	**$CaCO_3$**	**$Ca(OH)_2$**	**$CaCO_3$**	**$Ca(OH)_2$**	**$CaCO_3$**	**$Ca(OH)_2$**	**$CaCO_3$**	**$Ca(OH)_2$**	**$CaCO_3$**	**$Ca(OH)_2$**	**$CaCO_3$**	**$Ca(OH)_2$**	**$CaCO_3$**	**$Ca(OH)_2$**	**$CaCO_3$**	**$Ca(OH)_2$**	**$CaCO_3$**
0	0	100	0	100	0	100	0	100	0	100	0	100	0	100	0	100	0	100	0	100	0	100	0	100
4 - 6	0	100	0	100	0	100	0	100	0	100	0	100	0	100	0	100	0	100	0	100	0	100	0	100
6 -12	0	71	0	82	16	93	18	88	0	95	0	84	0	97	0	72	0	80	23	95	23	88	0	73
12 - 18	14	52	23	78	23	69	15	74	24	92	19	53	31	77	12	61	0	31	32	90	32	83	0	69
18 - 24	45	45	25	39	26	57	39	46	41	27	44	42	35	65	27	59	86	11	54	80	38	49	0	41
24 - 30	67	43	59	13	97	44	52	42	66	14	60	22	54	40	51	41	88	7	60	30	60	28	0	32
30 - 36	71	37	91	6	99	12	80	37	86	12	74	13	67	29	64	28	92	4	65	28	66	25	52	6
36 - 42	100	0	100	0	100	0	100	0	96	3	89	8	83	21	73	18	93	2	93	17	81	18	64	0
42 - 48	100	0	100	0	100	0	100	0	100	0	100	0	100	0	100	0	100	0	100	0	100	0	100	0

Table A.16: Effect of temperature on XRD analysis for $CaCO_3$ and $Ca(OH)_2$ with different depths for Scenario b of (M 0.5+ PFA) due to exposure to CO_2 environmental conditions for 8 weeks

Environmental conditions	Relative intensity of XRD (%) at Relative humidity 65%, CO_2 5% and																							
	Temperature 25 ºC (5)								Temperature 35 ºC (3)								Temperature 45 ºC (1)							
Crack width	**Un-cracked**		**0.05-0.15 mm**		**0.15-0.25 mm**		**0.25-0.35 mm**		**Un-cracked**		**0.05-0.15 mm**		**0.15-0.25 mm**		**0.25-0.35 mm**		**Un-cracked**		**0.05-0.15 mm**		**0.15-0.25 mm**		**0.25-0.35 mm**	
Depth mm	**$Ca(OH)_2$**	**$CaCO_3$**	**$Ca(OH)_2$**	**$CaCO_3$**	**$Ca(OH)_2$**	**$CaCO_3$**	**$Ca(OH)_2$**	**$CaCO_3$**	**$Ca(OH)_2$**	**$CaCO_3$**	**$Ca(OH)_2$**	**$CaCO_3$**	**$Ca(OH)_2$**	**$CaCO_3$**	**$Ca(OH)_2$**	**$CaCO_3$**	**$Ca(OH)_2$**	**$CaCO_3$**	**$Ca(OH)_2$**	**$CaCO_3$**	**$Ca(OH)_2$**	**$CaCO_3$**	**$Ca(OH)_2$**	**$CaCO_3$**
0	0	100	0	100	0	100	0	100	0	100	0	100	0	100	0	100	0	100	0	100	0	100	0	100
4 - 6	0	100	0	100	0	100	0	100	0	100	0	100	0	100	0	100	0	100	0	100	0	100	0	100
6 -12	0	99	0	62	0	49	0	97	0	88	0	84	0	87	0	99	0	89	0	68	0	79	0	100
12 - 18	0	51	0	52	28	28	0	88	0	75	0	83	0	84	0	99	0	55	0	37	0	65	0	81
18 - 24	63	40	23	25	65	28	0	85	29	64	33	82	0	72	0	98	0	51	0	29	29	50	0	67
24 - 30	65	30	65	10	94	21	56	73	58	17	83	59	31	64	34	95	48	45	0	24	40	35	30	47
30 - 36	73	8	91	8	100	0	91	12	63	13	84	51	63	19	47	59	57	27	0	23	55	20	62	37
36 - 42	100	0	100	0	100	0	100	0	78	1	86	6	94	3	75	20	67	0	0	12	91	6	93	8
42 - 48	100	0	100	0	100	0	100	0	100	0	100	0	100	0	100	0	100	0	100	0	100	0	100	0

Table A.17: Effect of Relative humidity on XRD analysis for $CaCO_3$ and $Ca(OH)_2$ with different depths for Scenario c of (M 0.4) due to exposure to CO_2 environmental conditions for 8 weeks

Environmental conditions	Relative intensity of XRD (%) at Temperature 25 ºC, CO_2 5% and																							
	Relative humidity 65% (5)								Relative humidity 75% (4)								Relative humidity 85% (2)							
Crack width	**Un-cracked**		**0.05-0.15 mm**		**0.15-0.25 mm**		**0.25-0.35 mm**		**Un-cracked**		**0.05-0.15 mm**		**0.15-0.25 mm**		**0.25-0.35 mm**		**Un-cracked**		**0.05-0.15 mm**		**0.15-0.25 mm**		**0.25-0.35 mm**	
Depth mm	**$Ca(OH)_2$**	**$CaCO_3$**	**$Ca(OH)_2$**	**$CaCO_3$**	**$Ca(OH)_2$**	**$CaCO_3$**	**$Ca(OH)_2$**	**$CaCO_3$**	**$Ca(OH)_2$**	**$CaCO_3$**	**$Ca(OH)_2$**	**$CaCO_3$**	**$Ca(OH)_2$**	**$CaCO_3$**	**$Ca(OH)_2$**	**$CaCO_3$**	**$Ca(OH)_2$**	**$CaCO_3$**	**$Ca(OH)_2$**	**$CaCO_3$**	**$Ca(OH)_2$**	**$CaCO_3$**	**$Ca(OH)_2$**	**$CaCO_3$**
0	0	100	0	100	0	100	0	100	0	100	0	100	0	100	0	100	0	100	0	100	0	100	0	100
4 - 6	0	100	0	100	0	100	0	100	0	100	0	100	0	100	0	100	0	100	0	100	0	100	0	90
6 -12	0	94	12	72	0	100	0	61	51	65	0	89	5	100	0	60	49	88	36	86	18	43	22	90
12 - 18	32	83	17	48	8	94	36	35	57	65	29	69	40	88	44	42	58	50	60	72	38	41	37	89
18 - 24	56	46	29	47	23	56	36	12	68	49	42	55	62	79	48	41	63	36	86	57	45	40	48	87
24 - 30	66	29	63	38	51	56	49	3	73	37	79	33	81	21	71	29	75	29	88	47	58	27	59	74
30 - 36	74	15	85	36	84	47	82	2	89	35	96	3	85	19	76	16	80	8	93	26	59	20	60	39
36 - 42	91	4	100	0	100	44	100	0	100	0	100	0	100	18	100	0	90	2	97	13	82	14	91	14
42 - 48	100	0	100	0	100	0	100	0	100	0	100	0	100	0	100	0	100	0	100	0	95	6	100	0

Table A.18: Effect of Relative humidity on XRD analysis for $CaCO_3$ and $Ca(OH)_2$ with different depths for Scenario c of (M 0.5) due to exposure to CO_2 environmental conditions for 8 weeks

Environmental conditions	Relative intensity of XRD (%) at Temperature 25 ºC, CO_2 5% and																							
	Relative humidity 65% (5)								Relative humidity 75% (4)								Relative humidity 85% (2)							
Crack width	**Un-cracked**		**0.05-0.15 mm**		**0.15-0.25 mm**		**0.25-0.35 mm**		**Un-cracked**		**0.05-0.15 mm**		**0.15-0.25 mm**		**0.25-0.35 mm**		**Un-cracked**		**0.05-0.15 mm**		**0.15-0.25 mm**		**0.25-0.35 mm**	
Depth mm	**$Ca(OH)_2$**	**$CaCO_3$**	**$Ca(OH)_2$**	**$CaCO_3$**	**$Ca(OH)_2$**	**$CaCO_3$**	**$Ca(OH)_2$**	**$CaCO_3$**	**$Ca(OH)_2$**	**$CaCO_3$**	**$Ca(OH)_2$**	**$CaCO_3$**	**$Ca(OH)_2$**	**$CaCO_3$**	**$Ca(OH)_2$**	**$CaCO_3$**	**$Ca(OH)_2$**	**$CaCO_3$**	**$Ca(OH)_2$**	**$CaCO_3$**	**$Ca(OH)_2$**	**$CaCO_3$**	**$Ca(OH)_2$**	**$CaCO_3$**
0	0	100	0	100	0	100	0	100	0	100	0	100	0	100	0	100	0	100	0	100	0	100	0	100
4 - 6	0	100	0	100	0	100	0	100	0	100	0	100	0	100	0	100	0	100	0	100	0	100	0	100
6 -12	44	93	0	34	0	51	0	87	0	72	0	70	0	68	0	88	29	62	24	90	16	80	13	93
12 - 18	45	76	11	28	9	50	14	73	22	53	0	54	44	45	0	49	74	39	39	78	39	43	18	65
18 - 24	69	20	30	27	22	34	27	53	55	36	15	52	48	42	0	39	74	18	53	70	44	31	26	54
24 - 30	93	10	61	23	31	2	63	48	97	29	40	40	63	39	32	29	78	13	69	55	45	27	60	53
30 - 36	96	8	86	13	68	1	66	33	97	22	64	11	95	36	90	11	81	11	75	44	55	7	71	39
36 - 42	100	0	100	0	100	0	100	0	100	0	100	0	100	0	100	0	91	3	85	15	95	2	90	39
42 - 48	100	0	100	0	100	0	100	0	100	0	100	0	100	0	100	0	100	0	100	0	100	0	100	0

Table A.19: Effect of Relative humidity on XRD analysis for $CaCO_3$ and $Ca(OH)_2$ with different depths for Scenario c of (M 0.6) due to exposure to CO_2 environmental conditions for 8 weeks

Environmental conditions	Relative intensity of XRD (%) at Temperature 25 ºC, CO_2 5% and																							
	Relative humidity 65% (5)								Relative humidity 75% (4)								Relative humidity 85% (2)							
Crack width	**Un-cracked**		**0.05-0.15 mm**		**0.15-0.25 mm**		**0.25-0.35 mm**		**Un-cracked**		**0.05-0.15 mm**		**0.15-0.25 mm**		**0.25-0.35 mm**		**Un-cracked**		**0.05-0.15 mm**		**0.15-0.25 mm**		**0.25-0.35 mm**	
Depth mm	**$Ca(OH)_2$**	**$CaCO_3$**	**$Ca(OH)_2$**	**$CaCO_3$**	**$Ca(OH)_2$**	**$CaCO_3$**	**$Ca(OH)_2$**	**$CaCO_3$**	**$Ca(OH)_2$**	**$CaCO_3$**	**$Ca(OH)_2$**	**$CaCO_3$**	**$Ca(OH)_2$**	**$CaCO_3$**	**$Ca(OH)_2$**	**$CaCO_3$**	**$Ca(OH)_2$**	**$CaCO_3$**	**$Ca(OH)_2$**	**$CaCO_3$**	**$Ca(OH)_2$**	**$CaCO_3$**	**$Ca(OH)_2$**	**$CaCO_3$**
0	0	100	0	100	0	100	0	100	0	100	0	100	0	100	0	100	0	100	0	100	0	100	0	100
4 - 6	0	100	0	100	0	100	0	100	0	100	0	100	0	100	0	100	0	100	0	100	0	100	0	100
6 -12	0	90	26	90	0	37	0	80	0	62	0	96	0	59	0	98	21	53	28	62	7	79	0	89
12 - 18	28	58	29	86	19	35	0	74	0	52	0	88	0	57	0	93	59	50	52	47	8	53	28	67
18 - 24	40	40	43	79	27	18	0	61	43	24	0	84	0	48	0	89	65	15	81	43	41	50	42	63
24 - 30	53	23	44	21	78	15	32	37	74	24	63	16	72	43	22	88	76	9	83	39	47	35	66	53
30 - 36	81	11	76	5	78	13	84	30	90	6	93	4	94	37	37	82	87	9	89	22	49	9	86	46
36 - 42	100	0	100	0	100	0	85	28	100	0	100	0	100	0	100	0	95	5	93	3	95	6	92	4
42 - 48	100	0	100	0	100	0	100	0	100	0	100	0	100	0	100	0	100	0	100	0	100	0	100	0

Table A.20: Effect of Relative humidity on XRD analysis for $CaCO_3$ and $Ca(OH)_2$ with different depths for Scenario c of (M 0.5+ GGBS) due to exposure to CO_2 environmental conditions for 8 weeks

Environmental conditions	Relative intensity of XRD (%) at , Temperature 25 ºC, CO_2 5% and																							
	Relative humidity 65% (5)								Relative humidity 75% (4)								Relative humidity 85% (2)							
Crack width	**Un-cracked**		**0.05-0.15 mm**		**0.15-0.25 mm**		**0.25-0.35 mm**		**Un-cracked**		**0.05-0.15 mm**		**0.15-0.25 mm**		**0.25-0.35 mm**		**Un-cracked**		**0.05-0.15 mm**		**0.15-0.25 mm**		**0.25-0.35 mm**	
Depth mm	**$Ca(OH)_2$**	**$CaCO_3$**	**$Ca(OH)_2$**	**$CaCO_3$**	**$Ca(OH)_2$**	**$CaCO_3$**	**$Ca(OH)_2$**	**$CaCO_3$**	**$Ca(OH)_2$**	**$CaCO_3$**	**$Ca(OH)_2$**	**$CaCO_3$**	**$Ca(OH)_2$**	**$CaCO_3$**	**$Ca(OH)_2$**	**$CaCO_3$**	**$Ca(OH)_2$**	**$CaCO_3$**	**$Ca(OH)_2$**	**$CaCO_3$**	**$Ca(OH)_2$**	**$CaCO_3$**	**$Ca(OH)_2$**	**$CaCO_3$**
0	0	100	0	100	0	100	0	100	0	100	0	100	0	100	0	100	0	100	0	100	0	100	0	100
4 - 6	0	100	0	100	0	100	0	100	0	100	0	100	0	100	0	100	0	100	0	100	0	100	0	100
6 -12	0	71	0	82	16	93	18	88	0	37	0	95	0	68	0	88	18	55	0	63	13	57	29	70
12 - 18	14	52	23	78	23	69	15	74	19	34	0	61	0	42	37	79	61	35	27	57	45	46	42	67
18 - 24	45	45	25	39	26	57	39	46	41	23	40	40	22	30	48	75	63	30	62	52	51	42	46	59
24 - 30	67	43	59	13	97	44	52	42	55	10	79	3	59	18	69	64	69	20	70	42	52	37	60	56
30 - 36	71	37	91	6	99	12	80	37	100	5	95	1	82	15	94	35	75	10	82	28	53	25	63	21
36 - 42	100	0	100	0	100	0	100	0	100	0	100	0	100	0	100	0	76	9	91	8	95	22	68	7
42 - 48	100	0	100	0	100	0	100	0	100	0	100	0	100	0	100	0	77	4	100	0	100	0	91	1

Table A.21: Effect of Relative humidity on XRD analysis for $CaCO_3$ and $Ca(OH)_2$ with different depths for Scenario c of (M 0.5+ PFA) due to exposure to CO_2 environmental conditions for 8 weeks

Environmental conditions	Relative intensity of XRD (%) at Temperature 25 ºC, CO_2 5% and																							
	Relative humidity 65% (5)								Relative humidity 75% (4)								Relative humidity 85% (2)							
Crack width	**Un-cracked**		**0.05-0.15 mm**		**0.15-0.25 mm**		**0.25-0.35 mm**		**Un-cracked**		**0.05-0.15 mm**		**0.15-0.25 mm**		**0.25-0.35 mm**		**Un-cracked**		**0.05-0.15 mm**		**0.15-0.25 mm**		**0.25-0.35 mm**	
Depth mm	**$Ca(OH)_2$**	**$CaCO_3$**	**$Ca(OH)_2$**	**$CaCO_3$**	**$Ca(OH)_2$**	**$CaCO_3$**	**$Ca(OH)_2$**	**$CaCO_3$**	**$Ca(OH)_2$**	**$CaCO_3$**	**$Ca(OH)_2$**	**$CaCO_3$**	**$Ca(OH)_2$**	**$CaCO_3$**	**$Ca(OH)_2$**	**$CaCO_3$**	**$Ca(OH)_2$**	**$CaCO_3$**	**$Ca(OH)_2$**	**$CaCO_3$**	**$Ca(OH)_2$**	**$CaCO_3$**	**$Ca(OH)_2$**	**$CaCO_3$**
0	0	100	0	100	0	100	0	100	0	100	0	100	0	100	0	100	0	100	0	100	0	100	0	100
4 - 6	0	100	0	100	0	100	0	100	0	100	0	100	0	100	0	100	0	100	0	100	0	100	0	100
6 -12	0	99	0	62	0	49	0	97	0	78	0	74	0	93	0	93	0	69	0	80	0	58	0	47
12 - 18	0	51	0	52	28	28	0	88	0	76	0	65	0	72	0	58	0	36	30	63	0	29	36	35
18 - 24	63	40	23	25	65	28	0	85	0	67	0	52	0	58	0	48	67	9	53	29	18	25	40	18
24 - 30	65	30	65	10	94	21	56	73	42	41	29	32	0	45	0	33	67	8	68	26	32	15	46	15
30 - 36	73	8	91	8	100	0	91	12	98	6	75	30	78	11	81	31	78	4	77	18	42	14	61	12
36 - 42	100	0	100	0	100	0	100	0	100	0	100	0	100	0	100	0	95	4	93	3	90	8	86	4
42 - 48	100	0	100	0	100	0	100	0	100	0	100	0	100	0	100	0	100	0	100	0	100	0	100	0

Table A. 22: Carbonation front (X_f) by XRD analysis and depth of carbonation (X_p)

Series	Sample	Carbonation depth and front (mm) for crack width							
		Uncracked		0.05-0.15mm		0.15-0.25 mm		0.25-0.35 mm	
		X_p	X_f	X_p	X_f	X_p	X_f	X_p	X_f
Series 1	M 0.4	9.5	32	21	28	23	35	36	43
	M 0.5	13	25	27	33	31	40	42	47
	M 0.6	17	34	30	35	33	36	47	52
	M 0.5+GGBS	15	30	31	38	36	42	47	52
	M 0.5+PFA	26	50	40	52	47	52	50	53
Series 2	M 0.4	5	12	12	24	20	30	32	37
	M 0.5	10	20	23	30	23	30	37	43
	M 0.6	14	28	33	40	38	48	52	58
	M 0.5+GGBS	13	26	25	30	32	42	40	48
	M 0.5+PFA	22	44	38	44	44	50	48	53
Series 3	M 0.4	7.5	15	20	25	25	30	35	40
	M 0.5	12	24	24	30	27	42	40	45
	M 0.6	16	32	35	40	42	47	57	60
	M 0.5+GGBS	14	30	31	38	37	48	45	50
	M 0.5+PFA	24	48	43	48	51	56	54	60
Series 4	M 0.4	7	14	13	26	21	30	30	40
	M 0.5	11	22	23	30	29	34	40	48
	M 0.6	15	30	25	40	36	42	46	55
	M 0.5+GGBS	14	28	28	38	34	42	44	48

Series	Sample	Carbonation depth and front (mm) for crack width							
		Uncracked		0.05-0.15mm		0.15-0.25 mm		0.25-0.35 mm	
		X_p	X_f	X_p	X_f	X_p	X_f	X_p	X_f
	M 0.5+PFA	24	48	40	45	46	52	50	55
Series 5	M 0.4	8	18	19	30	23	30	36	43
	M 0.5	11.5	23	26	30	30	40	38	43
	M 0.6	15	30	26	32	35	42	48	52
	M 0.5+GGBS	12	30	27	40	38	45	43	50
	M 0.5+PFA	20	42	34	42	45	50	50	55
Series 6	M 0.4	6	12	16	24	20	30	31	41
	M 0.5	10	20	20	30	26	36	34	40
	M 0.6	12	30	23	33	30	38	42	48
	M 0.5+GGBS	11	22	23	30	33	40	40	45
	M 0.5+PFA	14	30	30	40	40	46	44	50
Series 7	M 0.4	4	12	14	22	18	25	29	35
	M 0.5	7.5	15	18	30	23	33	33	40
	M 0.6	10	20	22	32	27	32	35	45
	M 0.5+GGBS	9	22	21	28	32	42	38	45
	M 0.5+PFA	9	20	26	32	34	42	43	50

Table A.23: Effect of CO_2 concentration on pH with different depths for Scenario a of (M 0.4) due to exposure to CO_2 environmental conditions for 8 weeks

Environmental conditions	Apparent pH at Temperature 25 ºC, Relative humidity 65% and											
	CO_2=1.5% (7)				CO_2=3% (6)				CO_2=5% (5)			
Depth mm	Un-cracked	0.05-0.15 mm	0.15-0.25 mm	0.25-0.35 mm	Un-cracked	0.05-0.15 mm	0.15-0.25 mm	0.25-0.35 mm	Un-cracked	0.05-0.15 mm	0.15-0.25 mm	0.25-0.35 mm
0 - 6	12.26	12.02	11.96	11.99	11.49	11.37	11.35	11.45	11.46	11.77	11.57	11.79
6 -12	12.26	12.02	11.96	11.99	11.49	11.37	11.35	11.45	11.46	11.77	11.57	11.79
12 - 18	12.26	12.12	12.03	12.05	11.89	11.76	11.77	11.77	11.69	12.04	11.79	11.99
18 - 24	12.26	12.17	12.03	12.15	12.16	11.71	11.89	11.78	12.18	12.24	12.02	12.21
24 - 30	12.27	12.22	12.23	12.21	12.16	11.91	11.97	11.83	12.32	12.32	12.22	12.26
30 - 36	12.28	12.27	12.28	12.27	12.23	12.23	12.2	12.16	12.44	12.47	12.38	12.3
36 - 42	12.28	12.33	12.31	12.3	12.24	12.21	12.24	12.2	12.46	12.51	12.45	12.43
42 - 48	12.29	12.33	12.31	12.3	12.24	12.25	12.23	12.2	12.49	12.49	12.49	12.47

Table A.24: Effect of CO2 concentration on pH with different depths for **Scenario a** of (M 0.5) due to exposure to CO_2 environmental conditions for 8 weeks

Environmental conditions	Apparent pH at Temperature 25 ºC, Relative humidity 65% and											
	CO_2=1.5% (7)				CO_2=3% (6)				CO_2=5% (5)			
Depth mm	**Un-cracked**	**0.05-0.15 mm**	**0.15-0.25 mm**	**0.25-0.35 mm**	**Un-cracked**	**0.05-0.15 mm**	**0.15-0.25 mm**	**0.25-0.35 mm**	**Un-cracked**	**0.05-0.15 mm**	**0.15-0.25 mm**	**0.25-0.35 mm**
0 - 6	11.73	11.49	11.42	11.71	11.49	11.36	11.30	11.17	11.57	11.37	11.33	11.19
6 -12	11.73	11.49	11.42	11.71	11.49	11.36	11.30	11.17	11.57	11.37	11.33	11.19
12 - 18	12.18	11.93	11.75	12.05	11.78	11.61	11.55	11.48	12.3	11.85	11.61	11.47
18 - 24	12.22	11.97	12.04	12.13	12.13	11.88	11.62	11.59	12.3	11.96	11.89	11.99
24 - 30	12.23	12.08	12.05	12.1	12.14	11.82	11.83	11.76	12.49	12.23	12.23	12.11
30 - 36	12.22	12.17	12.15	12.15	12.25	12.08	12.14	12.07	12.46	12.35	12.23	12.36
36 - 42	12.24	12.22	12.19	12.20	12.26	12.22	12.24	12.21	12.49	12.38	12.35	12.4
42 - 48	12.25	12.28	12.23	12.22	12.25	12.23	12.2	12.25	12.49	12.42	12.45	12.41

Table A.25: Effect of CO2 concentration on pH with different depths for **Scenario a** of (M 0.6) due to exposure to CO_2 environmental conditions for 8 weeks

Environmental conditions	Apparent pH at Temperature 25 ºC, Relative humidity 65% and											
	CO_2=1.5% (7)				CO_2=3% (6)				CO_2=5% (5)			
Depth mm	**Un-cracked**	**0.05-0.15 mm**	**0.15-0.25 mm**	**0.25-0.35 mm**	**Un-cracked**	**0.05-0.15 mm**	**0.15-0.25 mm**	**0.25-0.35 mm**	**Un-cracked**	**0.05-0.15 mm**	**0.15-0.25 mm**	**0.25-0.35 mm**
0 - 6	10.86	10.68	10.95	10.79	10.55	10.33	10.32	10.28	10.85	10.6	10.45	10.12
6 -12	10.86	10.68	10.95	10.79	10.55	10.33	10.32	10.28	10.85	10.6	10.45	10.12
12 - 18	11.19	11.05	11.43	11.29	11.22	10.72	10.63	10.49	11.07	11.1	11.17	10.94
18 - 24	12	11.79	11.88	11.52	11.87	11.52	10.87	11.3	12.12	11.93	11.62	11.54
24 - 30	12.13	12.05	11.91	11.61	12.16	11.93	11.62	11.85	12.32	12.1	11.74	11.88
30 - 36	12.19	12.21	12.2	12.13	12.25	12.24	12.06	12.19	12.4	12.28	11.95	12.11
36 - 42	12.19	12.23	12.2	12.21	12.25	12.26	12.25	12.19	12.45	12.44	12.32	12.28
42 - 48	12.19	12.23	12.2	12.23	12.25	12.26	12.25	12.18	12.45	12.45	12.38	12.31

Table A.26: Effect of CO2 concentration on pH with different depths for **Scenario a** of (M 0.5+GGBS) due to exposure to CO_2 environmental conditions for 8 weeks

Environmental conditions	Apparent pH at Temperature 25 ºC , Relative humidity 65% and											
	CO_2=1.5% (7)				CO_2=3% (6)				CO_2=5% (5)			
Depth mm	**Un-cracked**	**0.05-0.15 mm**	**0.15-0.25 mm**	**0.25-0.35 mm**	**Un-cracked**	**0.05-0.15 mm**	**0.15-0.25 mm**	**0.25-0.35 mm**	**Un-cracked**	**0.05-0.15 mm**	**0.15-0.25 mm**	**0.25-0.35 mm**
0 - 6	10.62	11.24	11.39	11.25	10.69	10.46	10.11	9.85	10.31	10.62	10.63	10.80
6 -12	10.62	11.24	11.39	11.25	10.69	10.46	10.11	9.85	10.31	10.62	10.63	10.80
12 - 18	11.23	11.74	11.82	11.50	11.34	11.46	11.37	11.04	10.91	11.32	11.86	11.84
18 - 24	11.73	11.97	11.96	11.90	11.81	11.86	11.87	11.65	11.88	12.02	12.08	11.98
24 - 30	11.94	12.01	12.06	11.97	12.07	11.93	11.92	11.93	12.21	12.13	12.05	12.14
30 - 36	12.05	12.08	12.04	12.06	12.13	11.95	12.10	12.11	12.3	12.33	12.25	12.24
36 - 42	12.05	12.09	12.11	12.06	12.13	12.10	12.09	12.08	12.39	12.36	12.31	12.31
42 - 48	12.08	12.09	12.15	12.06	12.13	12.14	12.15	12.14	12.36	12.36	12.34	12.33

Table A.27: Effect of CO2 concentration on pH with different depths for **Scenario a** of (M 0.5 +PFA) due to exposure to CO_2 environmental conditions for 8 weeks

Environmental conditions	Apparent pH at Temperature 25 ºC, Relative humidity 65% and											
	CO_2=1.5% (7)				CO_2=3% (6)				CO_2=5% (5)			
Depth mm	**Un-cracked**	**0.05-0.15 mm**	**0.15-0.25 mm**	**0.25-0.35 mm**	**Un-cracked**	**0.05-0.15 mm**	**0.15-0.25 mm**	**0.25-0.35 mm**	**Un-cracked**	**0.05-0.15 mm**	**0.15-0.25 mm**	**0.25-0.35 mm**
0 - 6	11.06	10.67	11.03	10.08	10.16	9.98	9.78	9.81	10.77	10.14	9.72	10.04
6 -12	11.06	10.67	11.03	10.08	10.16	9.98	9.78	9.81	10.77	10.14	9.72	10.04
12 - 18	11.51	11.61	11.74	11.48	9.91	10.61	9.54	9.71	11.2	11.04	10.58	9.68
18 - 24	11.99	11.77	11.81	11.75	11.25	11.43	10.22	10.77	11.37	11.8	11.2	11.45
24 - 30	11.99	11.94	11.96	11.78	11.83	11.67	11.55	11.48	12.13	11.96	11.74	11.68
30 - 36	11.99	11.95	11.96	11.96	12.05	11.89	11.94	11.99	12.16	12.09	11.98	11.98
36 - 42	11.99	12.02	12.03	11.97	12.06	12.05	12.09	12.05	12.16	12.1	12.1	12.14
42 - 48	12.02	12.07	12.03	11.97	12.06	12.04	11.96	11.99	12.16	12.13	12.16	12.14

Table A.28: Effect of Temperature on pH with different depths for **Scenario b** of (M 0.4) due to exposure to CO_2 environmental conditions for 8 weeks

Environmental conditions	Apparent pH at Relative humidity 65% CO_2=5% and											
	Temperature 25 ºC (5)				Temperature 35 ºC (3)				Temperature 45 ºC (1)			
Depth mm	**Un-cracked**	**0.05-0.15 mm**	**0.15-0.25 mm**	**0.25-0.35 mm**	**Un-cracked**	**0.05-0.15 mm**	**0.15-0.25 mm**	**0.25-0.35 mm**	**Un-cracked**	**0.05-0.15 mm**	**0.15-0.25 mm**	**0.25-0.35 mm**
0 - 6	11.46	11.77	11.57	11.79	12.18	11.95	11.87	11.61	11.74	11.4	11.3	11.31
6 -12	11.46	11.77	11.57	11.79	12.26	12.1	11.99	11.95	11.96	11.9	11.75	11.7
12 - 18	11.69	12.04	11.79	11.99	12.3	12.22	12.14	12.01	12.1	12	11.95	11.84
18 - 24	12.18	12.24	12.02	12.21	12.3	12.24	12.14	12.09	12.22	12.2	12	11.99
24 - 30	12.32	12.32	12.22	12.26	12.31	12.32	12.19	12.14	12.26	12.26	12.2	12.05
30 - 36	12.44	12.47	12.38	12.3	12.32	12.33	12.31	12.22	12.28	12.27	12.25	12.15
36 - 42	12.46	12.51	12.45	12.43	12.33	12.33	12.33	12.24	12.3	12.3	12.32	12.2
42 - 48	12.49	12.49	12.49	12.47	12.33	12.33	12.33	12.33	12.32	12.32	12.32	12.32

Table A.29: Effect of Temperature on pH with different depths for **Scenario b** of (M 0.5) due to exposure to CO_2 environmental conditions for 8 weeks

Environmental conditions	Apparent pH at Relative humidity 65% CO_2=5% and											
	Temperature 25 ºC (5)				Temperature 35 ºC (3)				Temperature 45 ºC (1)			
Depth mm	**Un-cracked**	**0.05-0.15 mm**	**0.15-0.25 mm**	**0.25-0.35 mm**	**Un-cracked**	**0.05-0.15 mm**	**0.15-0.25 mm**	**0.25-0.35 mm**	**Un-cracked**	**0.05-0.15 mm**	**0.15-0.25 mm**	**0.25-0.35 mm**
0 - 6	11.57	11.37	11.33	11.19	10.85	11.04	10.59	10.67	11.01	10.84	10.77	10.95
6 -12	11.57	11.37	11.33	11.19	11.9	11.69	11.21	11.09	11.37	11.5	11.3	11.24
12 - 18	12.3	11.85	11.61	11.47	12.28	11.81	11.76	11.24	11.79	11.93	11.85	11.53
18 - 24	12.3	11.96	11.89	11.99	12.28	12.17	11.78	11.75	12.2	12.2	12.19	11.9
24 - 30	12.49	12.23	12.23	12.11	12.29	12.25	12.21	12.21	12.67	12.26	12.2	12.1
30 - 36	12.46	12.35	12.23	12.36	12.33	12.33	12.31	12.27	12.7	12.3	12.2	12.12
36 - 42	12.49	12.38	12.35	12.4	12.33	12.33	12.31	12.27	12.77	12.5	12.4	12.2
42 - 48	12.49	12.42	12.45	12.41	12.33	12.33	12.33	12.29	12.77	12.77	12.7	12.35

Table A.30: Effect of Temperature on pH with different depths for **Scenario b** of (M 0.6) due to exposure to CO_2 environmental conditions for 8 weeks

Environmental conditions	Apparent pH at Relative humidity 65% CO_2=5% and											
	Temperature 25 ºC (5)				Temperature 35 ºC (3)				Temperature 45 ºC (1)			
Depth mm	**Un-cracked**	**0.05-0.15 mm**	**0.15-0.25 mm**	**0.25-0.35 mm**	**Un-cracked**	**0.05-0.15 mm**	**0.15-0.25 mm**	**0.25-0.35 mm**	**Un-cracked**	**0.05-0.15 mm**	**0.15-0.25 mm**	**0.25-0.35 mm**
0 - 6	10.85	10.6	10.45	10.12	9.71	9.71	9.38	9.26	10.5	10.46	10.17	10
6 -12	10.85	10.6	10.45	10.12	9.71	9.71	9.65	9.31	11.52	11.5	10.65	10.4
12 - 18	11.07	11.1	11.17	10.94	11.76	11.65	9.92	9.34	12.5	12.3	11.5	10.7
18 - 24	12.12	11.93	11.62	11.54	12.23	12.04	10.59	9.82	12.62	12.4	12	11.56
24 - 30	12.32	12.1	11.74	11.88	12.29	12.17	12.1	11.91	12.63	12.5	12.25	11.6
30 - 36	12.4	12.28	11.95	12.11	12.3	12.3	12.28	11.98	12.66	12.55	12.3	12
36 - 42	12.45	12.44	12.32	12.28	12.3	12.3	12.3	12.16	12.7	12.6	12.5	12.2
42-48	12.45	12.45	12.38	12.31	12.3	12.3	12.3	12.2	12.7	12.65	12.66	12.4

Table A.31: Effect of Temperature on pH with different depths for **Scenario b** of (M 0.5+GGBS) due to exposure to CO_2 environmental conditions for 8 weeks

Environmental conditions	Apparent pH at Relative humidity 65% CO_2=5% and											
	Temperature 25 ºC (5)				Temperature 35 ºC (3)				Temperature 45 ºC (1)			
Depth mm	**Un-cracked**	**0.05-0.15 mm**	**0.15-0.25 mm**	**0.25-0.35 mm**	**Un-cracked**	**0.05-0.15 mm**	**0.15-0.25 mm**	**0.25-0.35 mm**	**Un-cracked**	**0.05-0.15 mm**	**0.15-0.25 mm**	**0.25-0.35 mm**
0 - 6	10.31	10.62	10.63	10.8	9.67	9.67	9.99	9.8	10.7	10.58	10.35	10.31
6 -12	10.31	10.62	10.63	10.8	10.19	10.87	10.57	10.78	10.99	11.25	11.4	10.86
12 - 18	10.91	11.32	11.86	11.84	11.75	11.67	11.47	11.3	11.95	11.94	11.85	11.25
18 - 24	11.88	12.02	12.08	11.98	12.02	11.91	11.73	11.5	12.07	12	11.9	11.6
24 - 30	12.21	12.13	12.05	12.14	12.1	12	11.8	11.56	12.1	12.09	11.95	11.7
30 - 36	12.3	12.33	12.25	12.24	12.17	12.15	11.9	11.87	12.1	12.1	12	11.85
36 - 42	12.39	12.36	12.31	12.31	12.18	12.17	12.09	12.03	12.11	12.11	12.07	11.95
42-48	12.36	12.36	12.34	12.33	12.18	12.18	12.13	12.1	12.13	12.13	12.13	12.13

Table A.32: Effect of Temperature on pH with different depths for **Scenario b** of (M 0.5+PFA) due to exposure to CO_2 environmental conditions

Environmental conditions	Apparent pH at Relative humidity 65% CO_2=5% and											
	Temperature 25 ºC (5)				Temperature 35 ºC (3)				Temperature 45 ºC (1)			
Depth mm	**Un-cracked**	**0.05-0.15 mm**	**0.15-0.25 mm**	**0.25-0.35 mm**	**Un-cracked**	**0.05-0.15 mm**	**0.15-0.25 mm**	**0.25-0.35 mm**	**Un-cracked**	**0.05-0.15 mm**	**0.15-0.25 mm**	**0.25-0.35 mm**
0 - 6	10.77	10.14	9.72	10.04	9.41	9.21	9.24	9.12	10.43	10.05	9.8	9.75
6 -12	10.77	10.14	9.72	10.04	9.41	9.46	9.37	9.3	10.5	10.3	10	9.9
12 - 18	11.2	11.04	10.58	9.68	9.84	10.31	9.37	9.3	10.66	10.79	10.5	10.03
18 - 24	11.37	11.8	11.2	11.45	11.69	11.44	10.98	9.3	11.88	11	11.25	10.4
24 - 30	12.13	11.96	11.74	11.68	11.83	11.74	11.6	11.55	12.25	11.52	11.45	11.3
30 - 36	12.16	12.09	11.98	11.98	12	11.88	11.8	11.74	12.3	11.9	11.78	11.65
36 - 42	12.16	12.1	12.1	12.14	12.05	11.95	11.9	11.84	12.32	12.3	11.85	11.75
42-48	12.16	12.13	12.16	12.14	12.05	12.05	11.95	11.9	12.32	12.32	12.2	11.9

Table A.33: Effect of Relative humidity on pH with different depths for **Scenario c** of (M 0.4) due to exposure to CO_2 environmental conditions for 8 weeks

Environmental conditions	Apparent pH at Temperature 25 ºC, CO_2=5% and											
	Relative humidity 65% (5)				Relative humidity 75% (4)				Relative humidity 85% (2)			
Depth mm	**Un-cracked**	**0.05-0.15 mm**	**0.15-0.25 mm**	**0.25-0.35 mm**	**Un-cracked**	**0.05-0.15 mm**	**0.15-0.25 mm**	**0.25-0.35 mm**	**Un-cracked**	**0.05-0.15 mm**	**0.15-0.25 mm**	**0.25-0.35 mm**
0 - 6	11.46	11.77	11.57	11.79	11.74	11.5	11.34	11.52	12.15	12.14	11.75	11.46
6 -12	11.46	11.77	11.57	11.79	12.26	11.84	11.66	11.74	12.23	12.22	11.9	11.9
12 - 18	11.69	12.04	11.79	11.99	12.3	12.09	12.06	12.02	12.3	12.25	12.2	12.14
18 - 24	12.18	12.24	12.02	12.21	12.29	12.22	12.16	12.13	12.31	12.28	12.28	12.2
24 - 30	12.32	12.32	12.22	12.26	12.32	12.3	12.23	12.16	12.31	12.29	12.29	12.22
30 - 36	12.44	12.47	12.38	12.3	12.32	12.32	12.26	12.23	12.33	12.3	12.3	12.25
36 - 42	12.46	12.51	12.45	12.43	12.32	12.32	12.27	12.24	12.33	12.31	12.31	12.29
42- 48	12.49	12.49	12.49	12.47	12.32	12.32	12.3	12.28	12.33	12.33	12.33	12.33

Table A.34: Effect of Relative humidity on pH with different depths for **Scenario c** of (M 0.5) due to exposure to CO_2 environmental conditions for 8 weeks

Environmental conditions	Apparent pH at Temperature 25 ºC, CO_2=5% and											
	Relative humidity 65% (5)				Relative humidity 75% (4)				Relative humidity 85% (2)			
Depth mm	**Un-cracked**	**0.05-0.15 mm**	**0.15-0.25 mm**	**0.25-0.35 mm**	**Un-cracked**	**0.05-0.15 mm**	**0.15-0.25 mm**	**0.25-0.35 mm**	**Un-cracked**	**0.05-0.15 mm**	**0.15-0.25 mm**	**0.25-0.35 mm**
0 - 6	11.57	11.37	11.33	11.19	10.05	10.29	10.61	10.31	11.61	11.6	11.62	11.5
6 -12	11.57	11.37	11.33	11.19	10.74	10.93	11.07	10.94	12.18	12.14	12.12	11.83
12 - 18	12.3	11.85	11.61	11.47	11.89	11.3	11.67	11.35	12.32	12.23	12.2	11.86
18 - 24	12.3	11.96	11.89	11.99	12.2	11.74	11.66	11.39	12.33	12.25	12.24	12
24 - 30	12.49	12.23	12.23	12.11	12.2	11.93	11.93	11.84	12.33	12.28	12.23	12.15
30 - 36	12.46	12.35	12.23	12.36	12.29	12.21	12.07	12.22	12.33	12.29	12.26	12.2
36 - 42	12.49	12.38	12.35	12.4	12.3	12.3	12.12	12.23	12.33	12.33	12.27	12.22
42-48	12.49	12.42	12.45	12.41	12.3	12.3	12.2	12.23	12.33	12.33	12.33	12.33

Table A.35: Effect of Relative humidity on pH with different depths for **Scenario c** of (M 0.6) due to exposure to CO_2 environmental conditions for 8 weeks

Environmental conditions	Apparent pH at Temperature 25 ºC , CO_2=5% and											
	Relative humidity 65% (5)				Relative humidity 75% (4)				Relative humidity 85% (2)			
Depth mm	**Un-cracked**	**0.05-0.15 mm**	**0.15-0.25 mm**	**0.25-0.35 mm**	**Un-cracked**	**0.05-0.15 mm**	**0.15-0.25 mm**	**0.25-0.35 mm**	**Un-cracked**	**0.05-0.15 mm**	**0.15-0.25 mm**	**0.25-0.35 mm**
0 - 6	10.85	10.6	10.45	10.12	9.65	9.6	9.85	9.73	11.67	11.66	11.65	11.27
6 -12	10.85	10.6	10.45	10.12	9.65	9.13	9.42	9.32	11.93	11.88	11.81	11.59
12 - 18	11.07	11.1	11.17	10.94	9.65	9.93	9.78	9.4	12.25	12.1	11.95	11.85
18 - 24	12.12	11.93	11.62	11.54	11.77	10.6	10.29	10.23	12.27	12.18	12.13	11.89
24 - 30	12.32	12.1	11.74	11.88	11.98	12.17	12.26	11.68	12.29	12.21	12.17	12.15
30 - 36	12.4	12.28	11.95	12.11	12.22	12.26	12.3	11.63	12.32	12.25	12.22	12.2
36 - 42	12.45	12.44	12.32	12.28	12.22	12.28	12.3	12.2	12.34	12.28	12.24	12.2
42-48	12.45	12.45	12.38	12.31	12.22	12.3	12.3	12.27	12.34	12.3	12.27	12.24

Table A.36: Effect of Relative humidity on pH with different depths for **Scenario c** of (M 0.5+GGBS) due to exposure to CO_2 environmental conditions for 8 weeks

Environmental conditions	Apparent pH at Temperature 25 ºC, CO_2=5% and											
	Relative humidity 65% (5)				Relative humidity 75% (4)				Relative humidity 85% (2)			
Depth mm	**Un-cracked**	**0.05-0.15 mm**	**0.15-0.25 mm**	**0.25-0.35 mm**	**Un-cracked**	**0.05-0.15 mm**	**0.15-0.25 mm**	**0.25-0.35 mm**	**Un-cracked**	**0.05-0.15 mm**	**0.15-0.25 mm**	**0.25-0.35 mm**
0 - 6	10.31	10.62	10.63	10.8	10.29	9.8	9.73	9.65	11.63	11.62	11.61	11.58
6 -12	10.31	10.62	10.63	10.8	11.12	9.99	10	9.9	11.89	11.86	11.84	11.8
12 - 18	10.91	11.32	11.86	11.84	11.72	11.44	11.16	11.07	12	12	11.99	11.95
18 - 24	11.88	12.02	12.08	11.98	11.97	11.9	11.81	11.75	12.09	12.08	12.07	12.02
24 - 30	12.21	12.13	12.05	12.14	12.02	12.02	12	11.97	12.12	12.11	12.1	12.04
30 - 36	12.3	12.33	12.25	12.24	12.16	12.12	12.13	12.1	12.16	12.14	12.13	12.07
36 - 42	12.39	12.36	12.31	12.31	12.23	12.15	12.13	12.14	12.17	12.16	12.14	12.12
42 - 48	12.36	12.36	12.34	12.33	12.23	12.2	12.18	12.16	12.17	12.17	12.17	12.17

Table A.37: Effect of Relative humidity on pH with different depths for **Scenario c** of (M 0.5+ PFA) due to exposure to CO_2 environmental conditions for 8 weeks

Environmental conditions	Apparent pH at Temperature 25 ºC, CO_2=5% and											
	Relative humidity 65% (5)				Relative humidity 75% (4)				Relative humidity 85% (2)			
Depth mm	**Un-cracked**	**0.05-0.15 mm**	**0.15-0.25 mm**	**0.25-0.35 mm**	**Un-cracked**	**0.05-0.15 mm**	**0.15-0.25 mm**	**0.25-0.35 mm**	**Un-cracked**	**0.05-0.15 mm**	**0.15-0.25 mm**	**0.25-0.35 mm**
0 - 6	10.77	10.14	9.72	10.04	9.84	9.24	9.4	9.38	10.5	10.3	10.22	10.2
6 -12	10.77	10.14	9.72	10.04	9.24	9.06	8.97	8.95	10.88	10.75	10.75	10.7
12 - 18	11.2	11.04	10.58	9.68	9.26	9.08	8.89	8.84	11.56	11.54	11.45	11.3
18 - 24	11.37	11.8	11.2	11.45	10.07	10.85	9.36	8.86	11.82	11.8	11.7	11.65
24 - 30	12.13	11.96	11.74	11.68	11.79	11.66	11.39	11.17	12.02	11.93	11.82	11.78
30 - 36	12.16	12.09	11.98	11.98	11.98	11.79	11.84	11.5	12.04	11.95	11.88	11.85
36 - 42	12.16	12.1	12.1	12.14	12.00	12.03	11.92	11.91	12.05	12	11.89	11.85
42 - 48	12.16	12.13	12.16	12.14	12.07	12.04	11.98	11.95	12.05	12.05	11.9	11.9

Table A. 38: Carbonation front (X_{fl}) by pH and consumed OH^- method and depth of carbonation (X_p)

Series	Sample	Carbonation depth and front (mm) for crack width							
		Uncracked		0.05-0.15mm		0.15-0.25 mm		0.25-0.35 mm	
		X_p	X_{fl}	X_p	X_{fl}	X_p	X_{fl}	X_p	X_{fl}
Series 1	M 0.4	9.5	35	21	40	23	45	36	50
	M 0.5	13.5	42	27	48	31	50	42	50
	M 0.6	17	45	30	50	33	50	47	50
	M 0.5+GGBS	15	35	31	40	36	45	47	45
	M 0.5+PFA	26	40	40	48	47	50	50	50
Series 2	M 0.4	5	35	12	42	20	44	32	48
	M 0.5	10	25	23	40	23	45	37	45
	M 0.6	14	40	33	45	38	50	52	50
	M 0.5+GGBS	13	35	25	42	32	45	40	50
	M 0.5+PFA	22	40	38	45	44	50	48	50
Series 3	M 0.4	7.5	30	20	35	25	42	35	48
	M 0.5	13	35	24	35	27	45	40	50
	M 0.6	16	35	35	38	42	45	57	60
	M 0.5+GGBS	14	40	31	45	37	50	45	50
	M 0.5+PFA	24	42	43	48	51	52	54	60
Series 4	M 0.4	7	30	13	35	21	45	30	48
	M 0.5	11	35	23	42	29	42	40	48
	M 0.6	15	35	25	42	36	45	46	50
	M 0.5+GGBS	14	42	28	48	34	48	44	48
	M 0.5+PFA	24	48	40	48	46	48	50	48
Series 5	M 0.4	8	38	19	35	23	42	36	45
	M 0.5	11.5	35	26	45	30	45	38	50
	M 0.6	15	35	26	40	35	45	48	50
	M 0.5+GGBS	12	35	27	38	38	48	43	50
	M 0.5+PFA	20	30	34	40	45	42	50	45

Series	Sample	Carbonation depth and front (mm) for crack width							
		Uncracked		0.05-0.15mm		0.15-0.25 mm		0.25-0.35 mm	
		X_p	X_{fl}	X_p	X_{fl}	X_p	X_{fl}	X_p	X_{fl}
Series 6	M 0.4	6	28	16	30	20	35	31	35
	M 0.5	10	30	20	35	26	40	34	42
	M 0.6	12	30	23	35	30	40	42	40
	M 0.5+GGBS	11	30	23	40	33	42	40	42
	M 0.5+PFA	14	32	30	35	40	40	44	42
Series 7	M 0.4	4	30	14	35	18	42	29	45
	M 0.5	7.5	35	18	40	23	43	33	45
	M 0.6	10	30	22	35	27	40	35	45
	M 0.5+GGBS	9	30	21	32	32	42	38	42
	M 0.5+PFA	9	35	26	35	34	40	43	42

Appendix B

Table B.1: Effect of Temperature on D_{CO2}

w/cm ratio	Crack width (W_c)mm	Temperature C	DoC mm	(A) *	(B) **
0.4	0.00	25	8	1.00	1.00
0.4	0.12	25	19	1.00	1.00
0.4	0.25	25	23	1.00	1.00
0.4	0.34	25	36	1.00	1.00
0.5	0.00	25	11.5	1.00	0.48
0.5	0.12	25	26	1.00	0.53
0.5	0.30	25	30	1.00	0.59
0.5	0.35	25	38	1.00	0.90
0.6	0.00	25	15	1.00	0.28
0.6	0.12	25	26	1.00	0.53
0.6	0.29	25	35	1.00	0.43
0.6	0.34	25	48	1.00	0.56
0.4	0.00	35	9	1.13	1.27
0.4	0.05	35	20	1.05	1.11
0.4	0.17	35	25	1.09	1.18
0.4	0.27	35	35	0.97	0.95
0.5	0.00	35	13	1.13	0.61
0.5	0.08	35	24	0.92	0.59
0.5	0.15	35	29	0.97	0.69
0.5	0.30	35	40	1.05	0.85
0.6	0.00	35	16	1.07	0.36
0.6	0.09	35	28	1.08	0.59

w/cm ratio	Crack width (W_c)mm	Temperature C	DoC mm	(A) *	(B) **
0.6	0.18	35	35	1.00	0.51
0.6	0.28	35	50	1.04	0.53
0.4	0.00	45	9.5	1.19	1.41
0.4	0.10	45	21	1.11	1.22
0.4	0.17	45	23	1.00	1.00
0.4	0.27	45	36	1.00	1.00
0.5	0.00	45	13.5	1.17	0.68
0.5	0.12	45	27	1.04	0.65
0.5	0.30	45	31	1.03	0.59
0.5	0.35	45	42	1.11	0.90
0.6	0.00	45	17	1.13	0.40
0.6	0.12	45	30	1.15	0.65
0.6	0.15	45	33	0.94	0.43
0.6	0.34	45	47	0.98	0.56

*(A) is a ratio of $DOC_{at\ T}$ to DoC at $_{T25}$.

** (B) is the square of the adjusted ratio of $DOC_{at\ T}$ to $DoC_{at\ T25}$ by w/c ratio impact.

Table B.2: Effect of crack width on D_{CO2}

w/c ratio	Crack width (W)mm	CO_2 %	DoC mm	(A) *	(B) **
0.4	0.00	1.5	4	1.00	1.00
0.4	0.15	1.5	14	3.50	12.25
0.4	0.31	1.5	18	4.50	20.25
0.4	0.35	1.5	20	5.00	25.00
0.5	0.00	1.5	7.5	1.00	3.52
0.5	0.05	1.5	18	2.40	9.52
0.5	0.17	1.5	23	3.07	15.35
0.5	0.31	1.5	33	4.40	52.71
0.6	0.00	1.5	10	1.00	6.25
0.6	0.08	1.5	22	2.20	11.95
0.6	0.15	1.5	27	2.70	16.40
0.6	0.30	1.5	35	3.50	37.52
0.4	0.00	3.0	6	1.00	1.00
0.4	0.10	3.0	16	2.67	7.11
0.4	0.19	3.0	20	3.33	11.11
0.4	0.35	3.0	31	5.17	26.69
0.5	0.00	3.0	10	1.00	2.78
0.5	0.09	3.0	20	2.00	6.25
0.5	0.18	3.0	26	2.60	11.42
0.5	0.28	3.0	34	3.40	13.91
0.6	0.00	3.0	12	1.00	4.00
0.6	0.10	3.0	23	1.92	7.59
0.6	0.17	3.0	30	2.50	14.06
0.6	0.27	3.0	42	3.50	22.49
0.4	0.00	5.0	8	1.00	1.00
0.4	0.12	5.0	19	2.38	5.64
0.4	0.25	5.0	23	2.88	8.27

0.4	0.34	5.0	36	4.50	20.25
0.5	0.00	5.0	11.5	1.00	2.07
0.5	0.12	5.0	26	2.26	9.57
0.5	0.30	5.0	30	2.61	11.58
0.5	0.35	5.0	38	3.30	12.17
0.6	0.00	5.0	15	1.00	3.52
0.6	0.12	5.0	26	1.73	5.63
0.6	0.29	5.0	35	2.33	12.61
0.6	0.34	5.0	48	3.20	18.20

*(A) is a ratio of $DOC_{cracked}$ to $DoC_{Uncracked}$.

** (B) is the square of the adjusted ratio of $DOC_{cracked}$ to $DoC_{Uncracked}$ by w/c ratio impact.

Table B.3: D_{CO2} values with pores volume ratio, temperature, relative humidity, and crack width

Sample		C_{CO2} %	$f_{c2(RH)}$	$f_{c1(T)}$	D_{CO2} $m^2/sec *10^{-8}$			
					Un-cracked	0.05-0.15 mm	0.15-0.25 mm	0.25-0.35 mm
Series 1	M 0.4	5	0.099	1.38	0.51	3.73	5.06	6.08
	M 0.5	5	0.099	1.38	1.87	13.71	18.61	22.37
	M 0.6	5	0.099	1.38	3.56	26.08	35.41	42.57
	M 0.5 +0.30 GGBS	5	0.099	1.38	3.63	26.61	36.13	43.44
	M 0.5 + 0.35 PFA	5	0.099	1.38	4.01	29.39	39.91	47.97
Series 3	M 0.4	5	0.099	1.18	0.44	3.20	4.34	5.22
	M 0.5	5	0.099	1.18	1.60	11.75	15.95	19.18
	M 0.6	5	0.099	1.18	3.05	22.36	30.36	36.50
	M 0.5 +0.30 GGBS	5	0.099	1.18	3.12	22.82	30.98	37.24
	M 0.5 + 0.35 PFA	5	0.099	1.18	3.44	25.20	34.21	41.13
Series 6	M 0.4	3	0.099	1	0.37	2.71	3.68	4.42
	M 0.5	3	0.099	1	1.36	9.97	13.53	16.27
	M 0.6	3	0.099	1	2.59	18.97	25.76	30.96
	M 0.5 +0.30 GGBS	3	0.099	1	2.64	19.36	26.28	31.59
	M 0.5 + 0.35 PFA	3	0.099	1	2.92	21.38	29.02	34.89
Series 7	M 0.4	1.5	0.099	1	0.37	2.71	3.68	4.42
	M 0.5	1.5	0.099	1	1.36	9.97	13.53	16.27
	M 0.6	1.5	0.099	1	2.59	18.97	25.76	30.96
	M 0.5 +0.30 GGBS	1.5	0.099	1	2.64	19.36	26.28	31.59
	M 0.5 + 0.35 PFA	1.5	0.099	1	2.92	21.38	29.02	34.89

$f_{c2(RH)}$= 0.099 for 65% RH, $f_{c1(T)}$=2.7, 1.7 and 1 for temperature 45,35 and 25 ^oC respectively

Appendix C

C-1 Model development by the statistical programme

The multiple linear regression analysis was used to build the models. The general purpose of regression analysis is to learn more about the relationship between one or several independent or predictor variables and a dependent or criterion variable. The regression equation or the best-fitting line is determined by minimizing the sum of squares of the residuals between the actual and predicted values of the dependent variables (http://www.statsoft.com).

The various elements of the multiple linear regression equation can be illustrated from the general form of the following equation or any equation according to proposed Equation in the case:

$$Y = a_0 + a_1x_1 + a_2x_2 + \cdots + a_nx_n \qquad \text{(C.1)}$$

where:

Y is the predicted value of the dependent variable.

$x_1, x_2, \ldots, x_n$ are the independent variables (predictors).

a_0 is the intercept coefficient (constant).

$a_1, a_2, \ldots, a_n$ are the partial regression coefficients of the independent variables.

n: the number of independent variables included in the regression equation.

The statistical analysis was done with the aid of computer software STATISTICA version 12-2001.

The standard method or all variables regression method of regression was applied. The following statistical factors are used:

Multiple R: The coefficient of multiple correlations is the positive square root of R-square (the coefficient of multiple determination). This statistical factor is useful in multivariate regression (i.e. multiple independent variables) when it is wanted to describe the relationship between the variables.

R-square: This coefficient of multiple determination measures the reduction in the total variation of the dependent variable due to the (multiple) independent variables.

$$R^2 = 1 - [Residual\ SS/Total\ SS] \qquad \text{(C.2)}$$

Where:

Residual SS: is the error sums of the square.

Total SS: is the total sums of the square.

The R-square value is an indicator of how well the model fits the data, R-square close to 1.0 indicates that it has accounted for almost all of the variability with the variables specified in the model.

Std. Error of estimate: This statistic coefficient measures the dispersion of the observed values about the regression line.

F-value: The F-value is used as a test of the relationship between the dependent variable and the set of independent variables.

F = Regression Mean Square/Residual Mean Square. (C.3)

The range of difference (df) between the actual and predicted values was calculated for each model within the confidence interval of 0.95. This means that there is a probability of 95% of the difference between the actual and the predicted values fall within a range of ±df, thus, the actual values equal to predicted values ± df.

Independent Variables:

The following variables are selected (using Equation C.1) to be as the independent variables according to the case of study:

a. Diffusion coefficient of chloride D_a:
   1- D_a was computed according to section 3.
   2- *w/cm* ratio.
   3- Temperature of exposure to chloride environment, T.
   As following Equation:

$$D_a = \left(1.3889 + 18.3333\ \frac{w}{cm} + 0.3\ T\right) 10^{-12} \quad (7.1)$$

The correlation coefficient (R) was 0.9384 and all correlations were statistically significant at the P= 0.0017 level .

b. Crack factor of chloride penetration $f_{c4(W)}$ by according to Equation 7.19.
   1- $f_{c4(W)}$ is the proportion of diffusion coefficient in the cracked sample ($D_{a(cracked)}$) to diffusion coefficient in the un-cracked sample ($D_{a(un\text{-}cracked)}$).
   2- W_c is crack width.

$$f_{c4(W)} = 0.934W_c^2 + 0.974W_c + 1 \quad (7.2)$$

The correlation coefficient (R) was 0.956 and all correlations were statistically significant at the P= 0.000 level.

c. Temperature dependence on D_{CO2}, $f_{c2(T)}$ according to Equation 7.45.
   1- $f_{c2(W)}$ is the proportion of DoC at interest temperature, ($DoC_{(T)}$) to DoC at reference temperature (273 K), ($DoC_{(Tref)}$).
   2- Temperature

$$f_{c2}(T) = exp(b) * [\frac{U_c}{R}(\frac{1}{T_{ref}} - \frac{1}{T})] \quad (7.45)$$

where:

b is an adjustment factor (0.322).

The correlation coefficient (R) was 0.87 and all correlations were statistically significant at the P= 0.000 level confidence 95% (alpha 0.005)

d. Crack factor of CO_2 penetration $f_{c4(W)}$ *by* using Equation C.1 according to Equation 7.47.
   3- $f_{c4(W)}$ is the the proportion of DoC in the cracked sample ($DoC_{(cracked)}$) to DoC in the un-cracked sample ($DoC_{(un\text{-}cracked)}$).
   4- *W* is crack width.

$$f_{c3(W)} = (11.4\sqrt{W_c} + 1) \quad (7.47)$$

The correlation coefficient (R) was 0. 85 and all correlations were statistically significant at the P= 0.000 level and level confidence 95% (alpha 0.05)

C- 2 X-ray diffraction analysis (XRD)

This instrumental technique is used to identify other crystalline phases of materials and minerals. XRD is mainly helpful for recognizing fine-grained mixtures and minerals or intergrowths of minerals that cannot lend themselves to study by other techniques. If the sample is a combination of minerals, XRD analysis can be used to find the mix proportion of these different minerals present. In addition, this technique can determine the degree of crystalline of the mineral(s) present and the structural state of the minerals. Within sealed tube is generated X-rays, by applying current that heats a filament within the tube. The greater number of electrons is emitted from the filament. This production of electrons is similar to generation the electrons in a television picture tube. Bragg's Law by (Maroliya, 2012) can measure the procedure of X-ray scan is X-ray beam hits specimen and is diffracted, the distances between the planes of the atoms mat constitute of the sample:

$$ή\ \lambda = 2\ d \sin\theta \qquad (C.1)$$

where: $ή$= the positive integer of the diffracted beam, λ= is the wavelength of the incident X-ray beam, θ = the angle of incidence of the X-ray beam and d = the distance between adjacent planes of atoms called the d-spacings.

C-3 Crack depth, D_{crack}

It was computed by measuring the time of transfer of pulse velocity for the ultrasonic devices according to Equation 3.4 as shown in Figure 3.12 (Al-Samaraai & Raouf -1999).

$$d_{crak} = x\sqrt{\frac{T_{cr}^2}{T_s^2} - 1} \qquad (3.3)$$

Where:

$2x$ is the path length without crack; T_{cr} is travel time around the crack and T_s is surface travel time through sound concrete without a crack (2x).

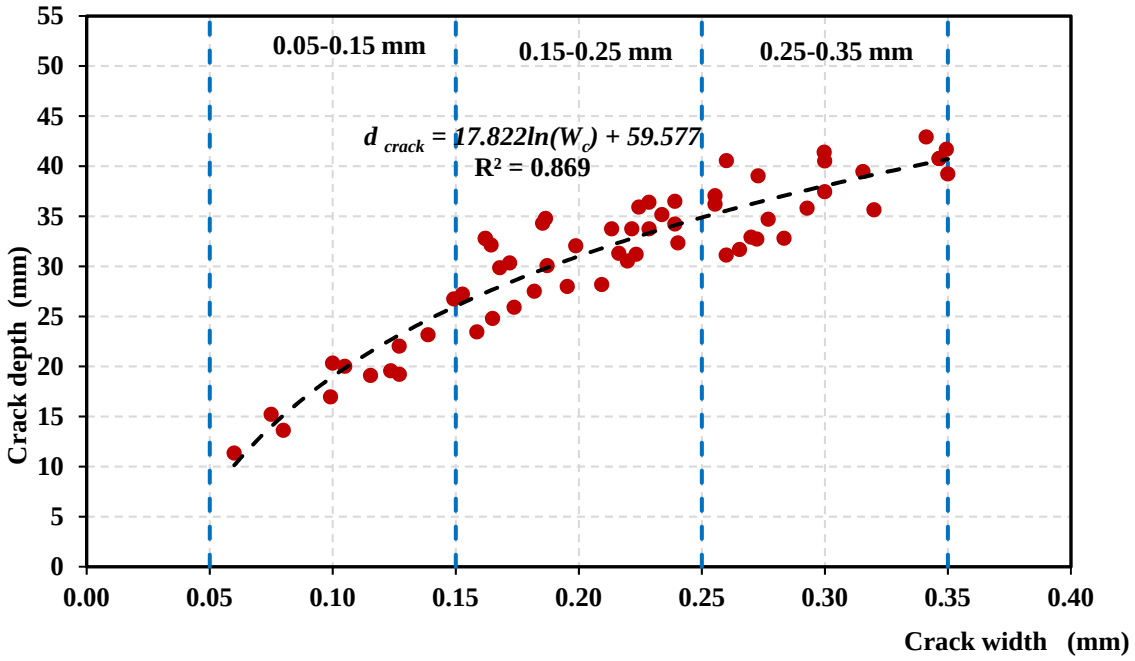

Figure C-3: Relationship of crack width and depth of crack obtained by the experimental programme